

A METAMORPHIC, STRUCTURAL AND GEOPHYSICAL INVESTIGATION
OF THE MOUNT CORMACK SUBZONE, CENTRAL NEWFOUNDLAND

CENTRE FOR NEWFOUNDLAND STUDIES

**TOTAL OF 10 PAGES ONLY
MAY BE XEROXED**

(Without Author's Permission)

STUART WILLIAM DEVEAU, B.Sc.(Hons.)



National Library
of Canada

Bibliothèque nationale
du Canada

Canadian Theses Service

Service des thèses canadiennes

Ottawa, Canada
K1A 0N4

NOTICE

The quality of this microform is heavily dependent upon the quality of the original thesis submitted for microfilming. Every effort has been made to ensure the highest quality of reproduction possible.

If pages are missing, contact the university which granted the degree.

Some pages may have indistinct print especially if the original pages were typed with a poor typewriter ribbon or if the university sent us an inferior photocopy.

Reproduction in full or in part of this microform is governed by the Canadian Copyright Act, R.S.C. 1970, c. C-30, and subsequent amendments.

AVIS

La qualité de cette microforme dépend grandement de la qualité de la thèse soumise au microfilmage. Nous avons tout fait pour assurer une qualité supérieure de reproduction.

S'il manque des pages, veuillez communiquer avec l'université qui a conféré le grade.

La qualité d'impression de certaines pages peut laisser à désirer, surtout si les pages originales ont été dactylographiées à l'aide d'un ruban usé ou si l'université nous a fait parvenir une photocopie de qualité inférieure.

La reproduction, même partielle, de cette microforme est soumise à la Loi canadienne sur le droit d'auteur, SRC 1970, c. C-30, et ses amendements subséquents.

A METAMORPHIC, STRUCTURAL AND GEOPHYSICAL INVESTIGATION
OF THE MOUNT CORMACK SUBZONE, CENTRAL NEWFOUNDLAND

by

Stuart William Deveau, B.Sc.(Hons.)

A Thesis submitted in partial fulfillment
of the requirements for the degree of

Master of Science

Department of Earth Sciences
Memorial University of Newfoundland

May, 1992

St. John's

Newfoundland



National Library
of Canada

Bibliothèque nationale
du Canada

Canadian Theses Service Service des thèses canadiennes

Ottawa, Canada
K1A 0N4

The author has granted an irrevocable non-exclusive licence allowing the National Library of Canada to reproduce, loan, distribute or sell copies of his/her thesis by any means and in any form or format, making this thesis available to interested persons.

The author retains ownership of the copyright in his/her thesis. Neither the thesis nor substantial extracts from it may be printed or otherwise reproduced without his/her permission.

L'auteur a accordé une licence irrévocable et non exclusive permettant à la Bibliothèque nationale du Canada de reproduire, prêter, distribuer ou vendre des copies de sa thèse de quelque manière et sous quelque forme que ce soit pour mettre des exemplaires de cette thèse à la disposition des personnes intéressées.

L'auteur conserve la propriété du droit d'auteur qui protège sa thèse. Ni la thèse ni des extraits substantiels de celle-ci ne doivent être imprimés ou autrement reproduits sans son autorisation.

ISBN 0-315-73299-7

Canada

ABSTRACT

The Mount Cormack Subzone (MCSZ) is located in central Newfoundland and has been interpreted as a tectonic window which exposes rocks of the Gander Zone through the surrounding Dunnage Zone. Structural evidence suggests that three deformation events caused the present geologic pattern. The first deformation was a result of thrusting of an ophiolite on to the Spruce Brook Formation (SBF) causing recumbent isoclinal F_1 folds in the latter; subsequent tectonic shortening during the second deformation caused the formation of large- and small-scale sub-horizontal F_2 folds. Evidence of low-pressure, high-temperature metamorphism suggests that this phase of crustal shortening was followed by widespread crustal extension. This thinning of the crust was accompanied by crustal melting at depth causing high geothermal gradients in the SBF and the development of mineral reactions which have been recorded as reaction isograds. All earlier structures were refolded during the D_3 deformation which rotated the D_2 structures and the isograds and caused a broad doming.

The mineralogy preserved in the metasedimentary rocks of the Mount Cormack Subzone indicates that the regional metamorphic grade increases from greenschist to upper amphibolite facies. The reaction isograds crosscut the large-scale second generation folds in the area consistent with early thrusting (emplacement of oceanic crust of Dunnage Zone over Gander Zone) and shortening, followed by structural and thermal doming. The attitude of the S_2 foliation within the terrane is approximately parallel to the edges of the MCSZ and dips away from the centre, consistent with a broad domal structure.

Five reaction isograds have been mapped within the Mount Cormack Subzone as follows: 1) biotite-muscovite-chlorite isograd; 2) andalusite-biotite-muscovite isograd; 3) sillimanite-biotite-muscovite isograd; 4) sillimanite-K feldspar isograd; and 5) melting isograd defining the beginning of partial melting. Bulk rock compositions lie within the central part of the AFM diagram resulting in cordierite and staurolite being relatively rare.

Mineral assemblages from both sides of the bathogradic reaction:

biotite + garnet + andalusite + vapour \rightleftharpoons

staurolite + muscovite + quartz + sillimanite

occur in rocks of appropriate composition and temperature, indicating a pressure of approximately 3.2 kilobars at the bathograd. This bathograd is approximately coincident with the sillimanite-biotite-muscovite reaction isograd. Pressure increases slightly with increasing metamorphic grade (i.e. higher pressures occur on the high grade side of the isograd), consistent with interpretations that either

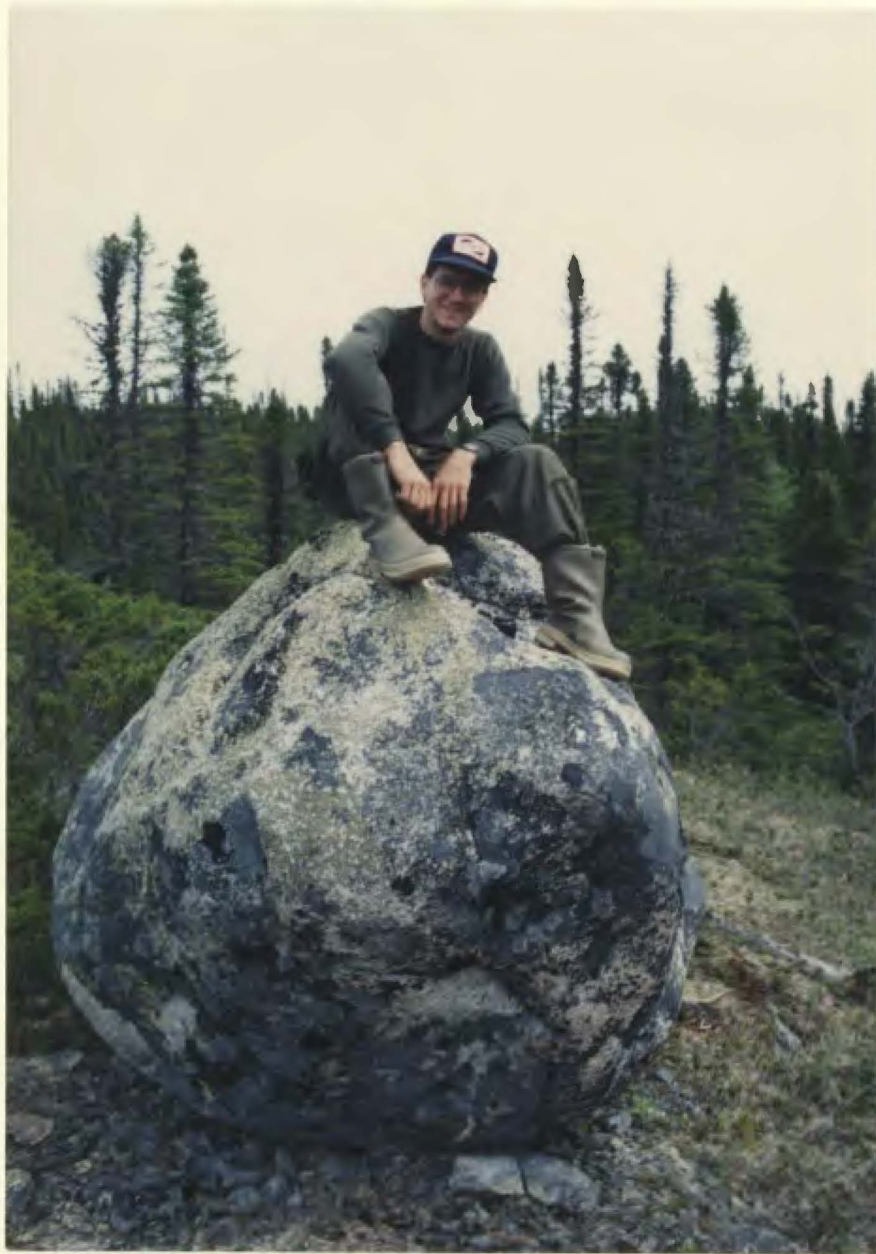
the high-grade areas underwent greater post-metamorphic uplift or that the syn-metamorphic Through Hill Granite dragged up its metamorphic aureole during emplacement.

Results of geothermobarometry from samples from the Mount Cormack terrane indicate that pressure estimates range from 2.5 - 3.5 kilobars and temperature estimates vary from 525 - 600 °C for andalusite-biotite-garnet assemblages, and up to 650 °C for sillimanite-biotite-garnet assemblages. These estimates indicate high geothermal gradients of up to 50 °C/km in the high-grade assemblages. Such high geothermal gradients are consistent with the suggestion that crustal thinning played an important role in the metamorphic development of the Mount Cormack Terrane. P-T vectors from zoned minerals from high-grade rocks are shallow, indicating that the amount of syn-metamorphic uplift and erosion was small. Exhumation must have been delayed until after substantial post-metamorphic cooling, and is not recorded in the mineral assemblages.

Interpretation of gravity and magnetic anomalies in the Mount Cormack Subzone indicates a model for the subsurface geology that is consistent with that observed at the surface. Large magnetic and gravity anomalies are associated with the ophiolitic rocks, and there appears to be little effect from the other units in the study area. The 1985 gravity profile is asymmetric; the anomaly associated with the Coy Pond Complex is much smaller than that associated with the Pipestone Pond Complex, suggesting that the Partridgeberry Hills Granite (or similar low-density body) extends beneath this ophiolite.

The magnetic low directly northwest of the Coy Pond Complex results from the fact that the dip of the ophiolite is similar to the inclination of the overall magnetic field. Small-scale magnetic anomalies within the Mount Cormack Subzone are interpreted as traces of bedding defined by cordierite-magnetite sub-assemblages. The attitude of these features is consistent with structural measurements made at the surface. The magnetic anomaly associated with the high-grade pelites may be due to the breakdown of hematite to form magnetite in the presence of reducing fluids.

Frontispiece



The author perched atop a granite boulder,
approximately 5 kilometres north
of the Through Hill Granite

TABLE OF CONTENTS

| | page |
|---|--------|
| Abstract | ii |
| Frontispiece | iv |
| Table of Contents | v |
| List of Figures | viii |
| List of Plates | xi |
| List of Tables | xiv |
| Acknowledgements | xv |
| CHAPTER 1 INTRODUCTION | 1 |
| 1.1 Appalachian Orogen | 1 |
| 1.2 Dunnage and Gander Zones | 2 |
| 1.3 Location and Geology of the Mount Cormack Subzone | 4 |
| 1.4 Purpose of the Study | 6 |
| 1.5 Location and Access | 7 |
| 1.6 Topography and Exposure | 8 |
| 1.7 Methods | 8 |
| 1.8 Previous Work | 10 |
| 1.9 Geologic Setting | 12 |
| 1.10 Age | 16 |
| CHAPTER 2 LITHOLOGIC UNITS | 18 |
| 2.1 Introduction | 18 |
| 2.2 Metasedimentary Rocks | 18 |
| 2.3 Ophiolitic Rocks | 26 |
| 2.4 Intrusive Rocks | 27 |
| 2.4.1 Felsic Intrusive Rocks (Through Hill Granite and Related Intrusions) | 27 |
| 2.4.2 Cordierite Granodiorite | 33 |
| 2.4.3 Mafic Igneous Rocks | 37 |
| 2.5 Protoliths | 38 |
| CHAPTER 3 STRUCTURAL GEOLOGY | 41 |
| 3.1 Introduction | 41 |
| 3.2 Structural Elements | 42 |
| 3.2.1 Bedding (S_0) - First Cleavage (S_1) | 43 |
| 3.2.2 S_2 Cleavage | 46 |
| 3.2.3 L_2 Intersection Lineations | 48 |
| 3.2.4 F_2 Folds (Axial Planes, Fold Axes) | 48 |
| 3.2.5 D_3 Deformation | 53 |
| 3.2.6 High Strain Fabric | 55 |
| 3.3 Timing of Events | 56 |
| 3.3 Interpretation | 60 |

| | | |
|-----------|--|------------|
| CHAPTER 4 | MINERALOGY, REACTION ISOGRADS AND MINERAL CHEMISTRY | page 62 |
| 4.1 | Introduction | 62 |
| 4.2 | Metamorphic Zones | 63 |
| 4.2.1 | Chlorite-Muscovite Zone | 64 |
| 4.2.2 | Biotite-Muscovite-Chlorite Zone | 66 |
| 4.2.3 | Andalusite-Biotite-Muscovite Zone | 69 |
| 4.2.4 | Sillimanite-Biotite-Muscovite Zone | 77 |
| 4.2.5 | Sillimanite-K Feldspar Zone | 81 |
| 4.3.6 | Zone of Migmatization and Partial Melting | 82 |
| 4.3 | Reaction Isograds | 82 |
| 4.3.1 | Definition of Reaction Isograd | 82 |
| 4.3.2 | Reaction Isograds in the Mount Cormack Subzone | 83 |
| 4.3.2.1 | Biotite-Muscovite Chlorite Reaction Isograd | 85 |
| 4.3.2.2 | Andalusite-Biotite-Muscovite Reaction Isograd | 88 |
| 4.3.2.3 | Sillimanite-Biotite-Muscovite Reaction Isograd | 92 |
| 4.3.2.4 | Sillimanite-K Feldspar Reaction Isograd | 92 |
| 4.3.2.5 | Reactions in the Zone of Partial Melting | 93 |
| 4.4 | Petrogenetic Grid | 96 |
| 4.5 | Metamorphic Bathograds | 96 |
| 4.5.1 | Metamorphic Bathograds in the Mount Cormack Subzone | 98 |
| 4.6 | Metamorphic Microstructures | 102 |
| 4.7 | Mineral Chemistry | 107 |
| 4.7.1 | Analytical Techniques | 107 |
| 4.7.2 | Garnet | 110 |
| 4.7.3 | Feldspars | 117 |
| 4.7.4 | Biotite | 117 |
| 4.7.5 | Cordierite | 122 |
| 4.7.6 | Other Phases | 124 |
| 4.7.7 | Coexisting Phases | 131 |
| CHAPTER 5 | QUANTITATIVE ESTIMATES OF PRESSURE AND TEMPERATURE | 135 |
| 5.1 | Introduction | 135 |
| 5.2 | Methodology | 135 |
| 5.2.1 | Geothermometry | 135 |
| 5.2.2 | Geobarometry | 139 |
| 5.3 | Results of Geothermobarometry | 141 |
| 5.3.1 | Geothermometry Results | 141 |
| 5.3.2 | Geobarometry Results | 146 |
| 5.4 | Pressure-Temperature-Time Path | 151 |
| 5.5 | Activity of Water | 154 |

| | page |
|---|------|
| 5.6 Post-Metamorphic Uplift Conditions | 159 |
| CHAPTER 6 GFOPHYSICS | 163 |
| 6.1 Introduction | 163 |
| 6.2 Methodology | 163 |
| 6.3 Regional Gravity Signature of the MCSZ Area | 169 |
| 6.4 Regional Magnetic Signature of the MCSZ Area | 169 |
| 6.5 1985 Profile | 174 |
| 6.5.1 Gravity Data | 174 |
| 6.5.2 Magnetic Data | 177 |
| 6.6 1988 Profile | 179 |
| 6.6.1 Gravity Data | 179 |
| 6.6.2 Magnetic Data | 182 |
| 6.7 Interpretation | 183 |
| CHAPTER 7 DISCUSSION | 186 |
| 7.1 Introduction | 186 |
| 7.2 Petrogenesis of the Mount Cormack Subzone | 186 |
| 7.3 Conclusions | 195 |
| REFERENCES | 198 |
| APPENDICES | 207 |
| A. Petrographic Descriptions | 207 |
| B. Microprobe Data | 212 |
| B1. Garnet Microprobe Data | 213 |
| B2. Biotite Microprobe Data | 237 |
| B3. Cordierite Microprobe Data | 252 |
| B4. Muscovite Microprobe Data | 254 |
| B5. Plagioclase Microprobe Data | 259 |
| B6. Potassium Feldspar Microprobe Data | 268 |
| B7. Staurolite Microprobe Data | 270 |
| B8. Andalusite Microprobe Data | 273 |
| C. Mixing Models | 275 |
| C1. Exchange Thermometry | 276 |
| C2. Geobarometry | 281 |
| D. Estimate of Activity of Water in Sample G-123-80 | 285 |
| MAPS (in back pocket) | |
| Geological Map | |
| Sample Location Map | |
| Structural Map | |

LIST OF FIGURES

| | page |
|--|------|
| Figure 1-1 Tectonostratigraphic subdivision of central Newfoundland (from Williams et al., 1988) | 3 |
| Figure 1-2 Geology of the Mount Cormack Subzone and surrounding area (from Colman-Sadd, 1985) | 5 |
| Figure 2-1 Streckheisen (1976) plot of the three granitic units and the average modal composition of Elias (1981) | 32 |
| Figure 3-1 Contoured stereonet plots from the Mount Cormack Subzone. a) plot of poles to bedding, Domain A; b) plot of poles to S_2 foliation, Domain A; c) plot of poles to S_2 foliation, Domain B; d) plot of $S_0 \parallel S_1-S_2$ intersection lineations and F_2 fold axes | 47 |
| Figure 3-2 Map of overall synformal structure within the MCSZ | 51 |
| Figure 3-3 Contoured stereonet plots from the MCSZ. a) plot of F_2 fold axes, Domain A; b) plot of F_2 fold axes, Domain B; c) plot of poles to F_2 fold axial planes, Domain A; d) plot of poles to F_2 fold axial planes, Domain B; e) plot of high strain fabric | 52 |
| Figure 3-4 Trends of S_2 foliation throughout the MCSZ | 54 |
| Figure 4-1 Distribution of samples with mineral assemblages appropriate for isograds mapped | 65 |
| Figure 4-2 Location of samples containing garnet, staurolite or cordierite | 73 |
| Figure 4-3 Generalized geological map of the MCSZ area showing the pattern of metamorphic reaction isograds (after Colman-Sadd, 1985) | 84 |
| Figure 4-4 AFM (projected through muscovite) and A'FM (projected through K feldspar) diagrams (Thompson, 1957) from the MCSZ showing the mineralogy of the metamorphic zones and the inferred reactions between each zone | 86 |
| Figure 4-5 Geometry of reaction curves radiating from an invariant point in the modal system albite-orthoclase-muscovite-biotite-quartz-aluminosilicate-vapour | 94 |
| Figure 4-6 P-T grid for the MCSZ showing the location of reactions mentioned in the text along with inferred sample locations | 97 |
| Figure 4-7 P-T phase diagram for part of the MCSZ showing the location of the invariant point on which the bathograd is based | 99 |

| | page |
|---|------|
| Figure 4-8 Map of the MCSZ (modified from Colman-Sadd, 1985) showing the location of samples which define the staurolite-muscovite-quartz-sillimanite bathograd | 101 |
| Figure 4-9 Map of the MCSZ (after Colman-Sadd, 1985) showing the location of samples used in microprobe analyses | 108 |
| Figure 4-10 Types of zoning in garnets from selected samples from the MCSZ | 113 |
| Figure 4-11 AFM plots (Thompson, 1957) of garnets | 114 |
| Figure 4-12 Fe-Mg-Mn ternary atomic percent plot showing zoning patterns of garnets from the MCSZ | 115 |
| Figure 4-13 Plot of feldspar compositions from the MCSZ | 119 |
| Figure 4-14 Plot of biotite compositions from the MCSZ (modified from Deer et al., 1966) | 121 |
| Figure 4-15 AFM diagram (Thompson, 1957) of biotite compositions (projected from muscovite) from the MCSZ | 123 |
| Figure 4-16 AFM plot (Thompson, 1957) of cordierite compositions | 125 |
| Figure 4-17 Plots of muscovite compositions from the MCSZ | 128 |
| Figure 4-18 AFM plot (Thompson, 1957) of staurolite compositions (projected from muscovite) | 130 |
| Figure 4-19 AFM diagrams (Thompson, 1957) projected through muscovite for coexisting biotite-garnet pairs separated on the basis of metamorphic grade | 133 |
| Figure 4-20 AFM diagrams (Thompson, 1957) projected through muscovite for coexisting garnet-biotite-staurolite and garnet-biotite-cordierite | 134 |
| Figure 5-1 Representative temperature-dependent curves from samples from the andalusite-biotite-muscovite zone | 142 |
| Figure 5-2 Representative temperature-dependent curves from samples from the: a) sillimanite-biotite-muscovite zone; b) sillimanite-K feldspar zone; and c) zone of partial melting | 143 |
| Figure 5-3 Temperature-dependent and pressure-dependent curves from sample G-123-80 | 147 |
| Figure 5-4 Representative pressure-dependent curves from selected samples from the MCSZ | 148 |
| Figure 5-5 P-T vectors from selected samples within the MCSZ | 152 |

| | page |
|---|------|
| Figure 5-6 P-T diagram showing the positions of contours of X_{H_2O} ($=a_{H_2O}$) for the $MU + Q = AF + AL + H_2O$ reaction | 157 |
| Figure 6-1 Geologic map of the Mount Cormack Subzone area (after Colman-Sadd, 1985) showing the two geophysical survey lines and the location of Figure 6-2 | 164 |
| Figure 6-2 Magnetic anomaly map of part of the MCSZ area with the two survey lines and gross elements of geology superimposed | 170 |
| Figure 6-3 Part of the magnetic anomaly map with the effect of the ophiolitic rocks removed | 172 |
| Figure 6-4 Two dimensional geological model for the MCSZ area derived from the 1985 gravity and magnetic data | 175 |
| Figure 6-5 Structural map (modified from Colman-Sadd, 1985) combined with trends of the magnetic anomalies (dashed lines) within the MCSZ | 180 |
| Figure 6-6 Two dimensional geological model for the MCSZ area derived from the 1988 gravity and magnetic data | 181 |
| Figure 7-1 Simplified diagram for the closing of the Iapetus Ocean (by continental collision) accompanied by obduction of oceanic crust | 188 |
| Figure 7-2 Typical model for the imbrication of ophiolite | 190 |
| Figure 7-3 Inferred sequence of events in the development of the Mount Cormack Subzone | 192 |

LIST OF PLATES

| | page |
|---|------|
| Plate 1-1 View looking north towards Miguel Mountain (taken from just north of Through Hill) | 9 |
| Plate 1-2 View looking west towards the Pipestone Pond Ophiolite. Gravel in the foreground marks the contact with the MCSZ | 9 |
| Plate 2-1 Typical low-grade rocks from the SBF showing fine-grained nature and original sedimentary structures | 21 |
| Plate 2-2 Samples from the SBF showing increased grain size and biotite porphyroblasts | 21 |
| Plate 2-3 Samples of SBF showing porphyroblasts of andalusite, staurolite and garnet | 22 |
| Plate 2-4 Typical outcrop of SBF containing large (1cm) andalusite porphyroblasts | 22 |
| Plate 2-5 High-grade samples of SBF showing increased grain size and schistosity | 24 |
| Plate 2-6 Typical outcrop of banded gneiss from the SBF | 24 |
| Plate 2-7 Typical samples of high-grade SBF | 25 |
| Plate 2-8 Outcrop of high-grade SBF showing boudinaged melt pods and F_2 folding in sillimanite layers | 25 |
| Plate 2-9 Typical samples of Through Hill Granite and related intrusions (SD-89-328, -156, and -170) | 29 |
| Plate 2-10 Sample SD-89-170 from a small granitic body north of the THG showing coarse ~ euhedral garnet with inclusions of quartz | 29 |
| Plate 2-11 Sample SD-89-096d from shear zone north of Through Hill showing fine grained garnets and foliation defined by muscovite (greenish mineral) | 31 |
| Plate 2-12 Photograph of cordierite granodiorite, sample SD-89-218 showing large K feldspar phenocrysts in a biotite-plagioclase-quartz matrix | 31 |
| Plate 2-13 Large anhedral cordierite grain from the cordierite granodiorite showing abundant pleochroic haloes occurring within the grain | 35 |
| Plate 2-14 Same sample as Plate 2-13, but under cross-polarized light | 35 |
| Plate 2-15 Graphic intergrowth of quartz and K-feldspar from the cordierite granodiorite, sample SD-89-218 | 36 |

| | page |
|------------|---|
| Plate 2-16 | Graphic intergrowth of quartz and plagioclase from the cordierite granodiorite, sample SD-89-218 |
| Plate 2-17 | Photograph of ~ 30 cm wide mafic dyke from the andalusite-biotite-muscovite zone, southeast of Through Hill (sample SD-89-386) |
| Plate 2-18 | Diabase dyke (sample SD-89-386) from the andalusite-biotite-muscovite zone southeast of Through Hill displaying elongate clinopyroxene grains (augite) |
| Plate 3-1 | Photograph of sample SD-89-243 from the chlorite-muscovite zone showing the orientation of two sets of foliation (S_1 parallel to S_0 and S_2 at an angle) |
| Plate 3-2 | Deformed low-strain lozenge of psammite within sillimanite-biotite-muscovite schist |
| Plate 3-3 | Photograph of bedding ($S_0 \parallel S_1$)-cleavage (S_2) intersections from the andalusite-biotite-muscovite zone |
| Plate 3-4 | Photograph of F_2 folds folding bedding (from the andalusite-biotite-muscovite zone) |
| Plate 3-5 | Photograph of shear zone north of Through Hill showing stretched and boudinaged quartz veins |
| Plate 3-6 | High strain fabric in migmatitic gneisses |
| Plate 4-1 | Albite twinning in plagioclase in sample SD-89-325 from the chlorite-muscovite zone |
| Plate 4-2 | Outcrop of schist containing large porphyroblasts of andalusite, southeast of the Through Hill Granite |
| Plate 4-3 | Randomly oriented inclusions in andalusite, sample SD-89-371 |
| Plate 4-4 | Traces of inclusions in andalusite parallel to the external fabric, sample SD-89-097a |
| Plate 4-5 | Inclusion-free andalusite grains adjacent to the Pipestone Pond Ophiolite (sample SD-89-195b) |
| Plate 4-6 | Twinning staurolite grains, sample SD-89-046b |
| Plate 4-7 | Staurolite grains extensively altered to fine grained muscovite, sample SD-89-086 |

| | page |
|---|------|
| Plate 4-8 Cordierite-bearing biotite-muscovite schist from the andalusite-biotite-muscovite zone containing abundant magnetite | 75 |
| Plate 4-9 Sample SD-89-299 containing large porphyroblasts of cordierite and abundant magnetite | 76 |
| Plate 4-10 Outcrop from sillimanite-biotite-muscovite isograd showing coexisting andalusite (large irregular shaped porphyroblasts) and sillimanite (fibrous zones within andalusite) | 76 |
| Plate 4-11 Sample SD-89-362 from the sillimanite-biotite-muscovite isograd showing sillimanite coexisting with andalusite | 78 |
| Plate 4-12 Turbid knots of fibrolitic sillimanite typical of the sillimanite-biotite-muscovite zone (sample SD-89-312) | 78 |
| Plate 4-13 Cordierite from sample G-123-80 from the sillimanite-K feldspar zone | 80 |
| Plate 4-14 Sample SD-89-212 from the zone of partial melting showing pods of melt that have been disrupted by the F ₂ folding | 80 |
| Plate 4-15 Andalusite surrounding staurolite in sample SD-89-366 from the andalusite-biotite-muscovite zone | 91 |

LIST OF TABLES

| | page |
|---|------|
| Table 4-1 Relationship between porphyroblast growth and deformation | 106 |
| Table 4-2 List of minerals analysed and the range of weight percent that were considered acceptable | 109 |
| Table 4-3 Representative analyses of garnets | 111 |
| Table 4-4 Representative analyses of plagioclase and K feldspar | 118 |
| Table 4-5 Representative analyses of biotites | 120 |
| Table 4-6 Representative analyses of cordierite | 126 |
| Table 4-7 Representative analyses of muscovite | 127 |
| Table 4-8 Representative analyses of staurolite and andalusite | 132 |
| Table 5-1 Representative geothermometry results | 144 |
| Table 5-2 Representative geobarometry results | 149 |
| Table 6-1 Gravity and magnetic data | 166 |
| Table 6-2 Geology along the 1985 gravity and magnetic survey | 168 |
| Table 6-3 Geology along the 1988 gravity and magnetic survey | 168 |

ACKNOWLEDGEMENTS

I would like to thank Drs. Toby Rivers and Hugh Miller for their support and for providing me with the opportunity to undertake the present study which was supported by Natural Sciences and Engineering Research Council of Canada operating grants to them. The author also acknowledges the financial support of Memorial University through a Graduate Fellowship.

Special thanks to my field assistant, Glen Lane, for without him life in central Newfoundland during the Summer of 1989 would not have been the same. I also thank the Newfoundland Department of Mines and Energy for the use of equipment during the field season. I am grateful to Bob McKay at Dalhousie University for his assistance and understanding during my trips to the Dalhousie probe lab.

I would like to thank my many friends and colleagues at Memorial, in particular: Adrian Timbal for the enjoyable and rewarding discussions; Kevin Deveau for the use of his computers; Ron Wiseman for producing the high-quality magnetic maps; and, Dr. John Malpas for the use of his many computers, for the opportunity of employment and for his understanding.

Lastly, I would like to thank Melanie for her many years of understanding and support without which this project would not have succeeded. Her belief in me enables me to carry on.

"For My Parents"

CHAPTER 1

INTRODUCTION

1.1 Appalachian Orogen

The Appalachian Orogen, located on the east coast of North America from Alabama to Newfoundland, is a linear belt between ~ 100 and ~ 1000 kilometres in width, composed of rocks that were deformed during the Early and Middle Paleozoic. Its extension to the northeast is exposed in northwest Europe where it is termed the Caledonian Orogen. Most modern tectonic models of the Appalachian-Caledonian system explain the orogen in terms of a Wilson cycle involving opening and closing of an Early Paleozoic Iapetus Ocean (Williams, 1964; Wilson, 1966; Dewey and Bird, 1970).

The Appalachian Orogen in North America has been divided into five zones based on stratigraphic and structural contrasts between Cambrian-Ordovician and older rocks (Williams, 1978; Williams, 1979; Williams and Hatcher, 1982). These are, from west to east, the Humber Zone (ancient eastern margin of North America), Dunnage Zone (relics of Paleozoic ocean crust and associated arcs formed in Iapetus Ocean), Gander Zone (Early Paleozoic continental margin), Avalon Zone (terrane of older Precambrian crust welded on to North America) and Meguma Zone (Paleozoic

western margin of Africa or northeastern margin of South America). The Avalon Zone is also correlated with Africa (Pan-African Orogeny). The four most westerly of these zones are exposed in Newfoundland (Figure 1-1; Williams et al., 1988). This four-fold zonation has been re-examined by recent workers. The work of Williams et al. (1988) has led to a further subdivision of the Dunnage Zone and a redefinition of the Gander Zone.

1.2 Dunnage and Gander Zones

The Dunnage Zone, traceable from Newfoundland into the New England Appalachians (Williams and Hatcher, 1983), is defined by the presence of Ordovician volcanic rocks and ophiolite suites that are inferred to have formed in the Iapetus Ocean. It has been subdivided into the Notre Dame and Exploits Subzones in Newfoundland on the basis of a variety of contrasts including stratigraphy, lithology and structure (Figure 1-1; Williams et al., 1988). The main difference between the two subzones is the presence of Silurian marine greywackes and conglomerates in the Exploits Subzone and their absence in the Notre Dame Subzone (Williams et al., 1988).

The Gander Zone, defined by the presence of Ordovician and earlier (?) metaclastic rocks and the lack of volcanic rocks, is traceable from Newfoundland to Long Island Sound, New York (Williams and Hatcher, 1983).

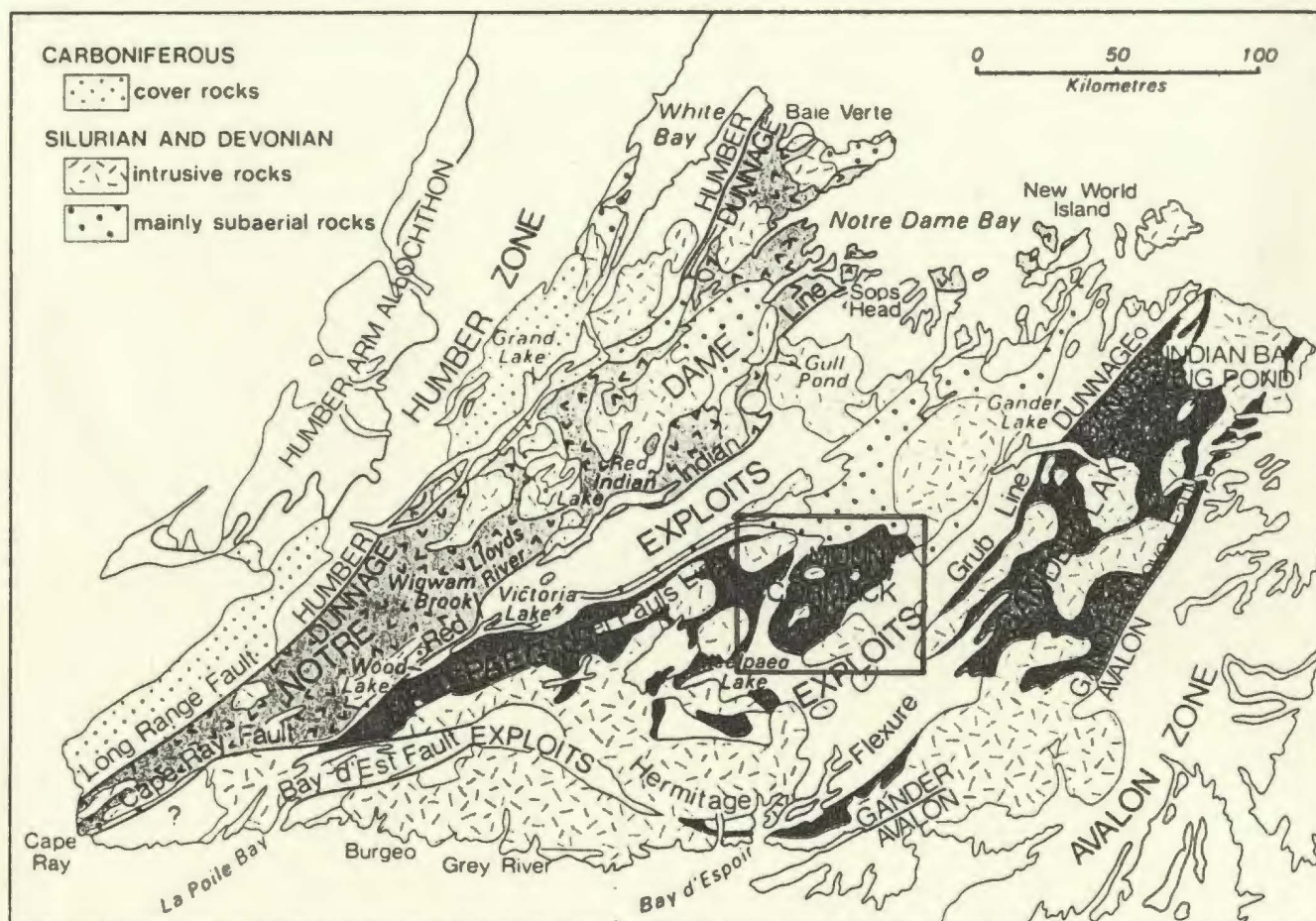


Figure 1-1. Tectonostratigraphic subdivision of central Newfoundland (from Williams et al., 1988). Box shows location of Figure 1-2.

Williams et al. (1988) further subdivided this zone in Newfoundland into the Gander Lake Subzone (the type section), the Mount Cormack Subzone and the Meelpaeg Subzone (Figure 1-1). The western edge of the Gander Lake Subzone is in fault contact with the Exploits Subzone, the Gander River Ultramafic Belt (GRUB) marking the contact. The Mount Cormack Subzone is entirely surrounded by the Exploits Subzone, and the Meelpaeg Subzone is also surrounded by the Exploits Subzone except south of Victoria Lake, where it is in contact with the Notre Dame Subzone (Williams et al., 1988).

1.3 Geology of the Mount Cormack Subzone

Rocks of the Mount Cormack Subzone (MCSZ) consist of metasedimentary units (interbedded quartzite and schist/phyllite, termed the Spruce Brook Formation (SBF) by Colman-Sadd, 1985). The terrane is largely devoid of volcanic lithologies and is intruded by local granitic bodies (Figure 1-2; Colman-Sadd, 1985). The MCSZ is surrounded by ophiolitic and sedimentary rocks of the Exploits Subzone and granite bodies (Partridgeberry Hills Granite and the Mount Peyton Intrusive Suite); the ophiolitic rocks are interpreted to overlie tectonically the SBF. It is on this basis that the SBF is interpreted to be correlative with the Gander Group of the Gander Zone.

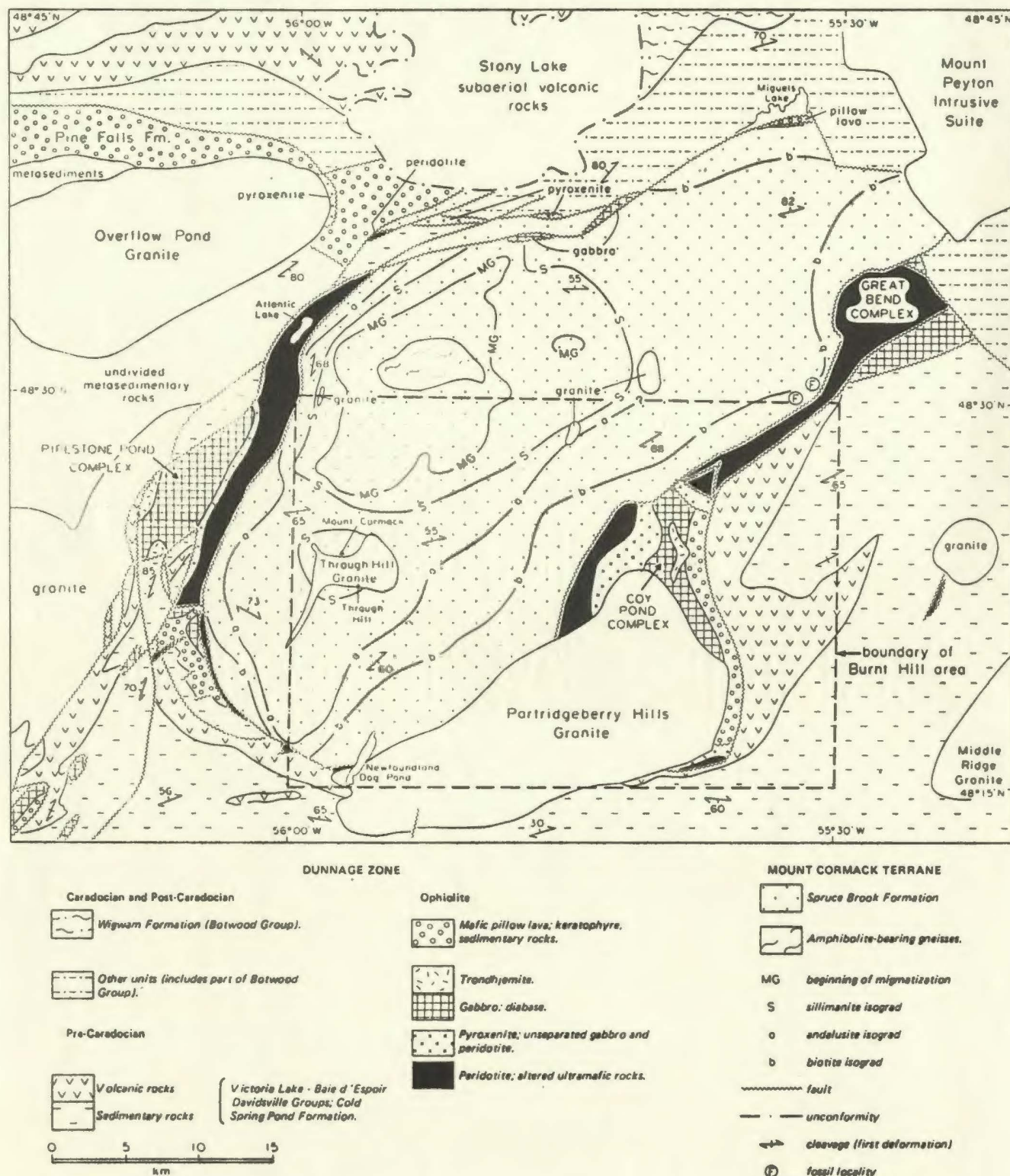


Figure 1-2. Geology of the Mount Cormack Subzone and surrounding area (from Colman-Sadd, 1985).

1.4 Purpose of the Study

Colman-Sadd and Swinden (1984) postulated that during the Lower Paleozoic, emplacement of a major allochthon of oceanic rocks (Dunnage Zone) on to a continental margin sequence (Gander Zone) resulted in a two-layer crust. A possible consequence of this is that the two-layer crust would be thermally and gravitationally unstable, resulting in thermal and structural doming of the lower crust. This has led to modern interpretations which suggest that the MCSZ is a tectonic window through which are exposed rocks of the Gander Zone (Colman-Sadd and Swinden, 1984).

The MCSZ has been mapped by Colman-Sadd (1985) at a scale of 1:50,000. He also described the petrography and structure of the MCSZ and surrounding rocks, with preliminary estimates of pressure and temperature of metamorphism. However, no detailed studies of metamorphic petrology, geothermobarometry or geophysics had been done.

Hence, this study was undertaken to:

- 1) reexamine the petrography of the MCSZ, involving detailed sampling in an attempt to map accurately and characterize the metamorphic reaction isograds occurring within the terrane and characterize the metamorphic field gradient;
- 2) reexamine the structure of the MCSZ to test the model of Colman-Sadd and Swinden (1984);

- 3) conduct detailed geothermobarometric calculations on selected samples in order to determine pressures and temperatures of formation of the MCSZ, and to try to constrain the syn-metamorphic P-T-t path for the MCSZ;
- 4) conduct gravity and magnetic modelling across the MCSZ using data collected during 1985 and 1988 in an attempt to create an acceptable model for the geology at depth; and
- 5) correlate the magnetic signature in the metamorphic rocks with the mineral assemblages present in order to interpret the origin of the first and second order magnetic features.

1.5 Location and Access

The Mount Cormack Subzone is located in central Newfoundland, between latitudes $48^{\circ}15'$ and $48^{\circ}38'$, and longitudes $55^{\circ}24'$ and $56^{\circ}05'$, North and West, respectively. The only road crossing the MCSZ is the Bay d'Espoir Highway which crosses the area in the northeast corner. However, there is a trail following the power line between St. Albans and Grand Falls, which is accessible with a four wheel drive vehicle. The power line runs approximately through the middle of the terrane. Although there are many lakes in the area, they are very shallow and rocky, making access by float plane impossible. The easiest access to the MCSZ is by helicopter.

1.6 Topography and Exposure

The MCSZ is characterized by gently rolling hills which reach an average elevation of 250 m (Plates 1-1 and 1-2). Mount Cormack and Through Hill are the exceptions to this, rising to nearly 400 m in elevation. The only area of low elevation is the Northwest Gander River, which is at approximately 130 m. Vegetation consists of large open bogs with sparse spruce forest in the high grade part of the MCSZ, and dense spruce forest with a few bogs in the low-grade part of the zone. These bogs are sources for water which drains into the Northwest Gander River via a system of tributaries.

Outcrop in the area is variable, with plentiful exposure in the high grade parts of the terrane, and sparse exposure in the lower grade areas.

1.7 Methods

The field work which provides the background for this study was done by the author and his assistant during the summer of 1989, using, as base maps, colour aerial photographs (scale 1:12,500) published by the Newfoundland Department of Lands and Forests. Most of the southwestern part of the MCSZ was mapped at that time (see Geological Map and Sample Location Map in pocket at back). In total, two-hundred-twenty-three samples were collected during the summer of 1989, representing the different rock types found



Plate 1-1. View looking north towards Miguel Mountain (taken from just north of Through Hill).



Plate 1-2. View looking west towards the Pipestone Pond Ophiolite. Gravel in the foreground marks the contact with the MCSZ.

in the area. Sample localities are well distributed throughout the study area (see Sample Location Map), and, when combined with those of Colman-Sadd (1985), provide quite dense coverage of the area.

One-hundred-seventy-four samples were selected for thin sectioning, including five from the granitic rocks, one from the Pipestone Pond Complex, one from a mafic dyke within the SBF, and the remainder from the metasedimentary rocks of the SBF. Petrographic data are presented in Chapter 4 as well as in Appendix A. In addition, mineral analyses were done on twenty-two samples from the MCSZ. These analyses are used in thermobarometric calculations presented in Chapter 5. Gravity surveys (not conducted by the author) were done during the summers of 1985 and 1988. These data were used with modelling packages to interpret the subsurface geology.

1.8 Previous Work

The first recorded geologic observations in the MCSZ and surrounding area were made by W.E. Cormack (Cormack, 1823), after whom Mount Cormack is named. He reported the presence of ultramafic rocks (Pipestone Pond Complex) to the west of the MCT, and noted the presence of slates and granites. In 1876, J.P. Howley traversed from the west side of the island (Murray and Howley, 1881) and followed the Northwest Gander River to Burnt Hill. He noted

the presence of ultramafic rocks (Coy Pond Complex), the northeastern edge of the Partridgeberry Hills Granite and also that the rocks downstream from the Coy Pond Complex consisted of slate, diorite, quartzite and "brecciated trap".

In the 1950's, Wolofsky (1951) and Slipp (1952), described the metamorphic rocks of the SBF. They noted the presence of andalusite-bearing schists within the SBF. In addition, the Through Hill Granite was described by Wolofsky, and Slipp examined the southwestern contact of the SBF, tracing the faulted contact of ophiolitic rocks from west of Newfoundland Dog Pond northwestward to the Pipestone Pond Complex. Grady (1952, 1953) mapped the ultramafic rocks of the Coy Pond Complex. He noted that to the west and northwest of the ophiolitic rocks, shales and sandstones occur, which are tightly folded and striking northeast.

The Through Hill and Partridgeberry Hills Granites were studied as part of the Bay d'Espoir granite project (Colman-Sadd, et al., 1981; Elias, 1981; Elias and Strong, 1982). Elias and Strong (1982) concluded that the Through Hill and Partridgeberry Hills Granites were derived from partial melting of a heterogeneous crust, with mantle convection, magma intrusion, frictional heating and crustal thickening as possible heat sources for the formation of the this melt.

Colman-Sadd (1981) mapped the Burnt Hill area (2D/5) and noted an increase in metamorphic grade towards the Through Hill Granite. Swinden and Collins (1982) mapped the Great Burnt Lake (12A/8)- Cold Spring Pond (12A/1) areas and reported the presence of quartzite and mature greywacke interbedded with fine grained clastic sedimentary rocks. They stated that these rocks were the westward equivalent of the SBF in the MCT. In 1984, Colman-Sadd and Swinden suggested that the Mount Cormack Subzone may be a tectonic window exposing Gander Zone rocks through the Dunnage Zone (Colman-Sadd and Swinden, 1984).

Colman-Sadd (1985) described in detail the SBF, noting the presence of a bull's-eye pattern of metamorphic isograds around two metamorphic culminations, one surrounding the Through Hill Granite and the other around a zone of "migmatization" north of Through Hill.

During the summers of 1985 and 1988, two gravity surveys were conducted, the data from which are used in the present investigation. Most recently, in 1991, the Lithoprobe East Transect was conducted across Newfoundland, passing just south of the Mount Cormack Subzone.

1.9 Geologic Setting

Recent mapping in central Newfoundland has indicated that certain Cambro-Ordovician volcanic and plutonic rocks of the Dunnage Zone with ophiolitic

affinities, overlie Ordovician metasedimentary rocks of continental origin (Colman-Sadd and Swinden, 1984). This has been interpreted to indicate the presence of a two-layer upper crust in which the ophiolite and overlying sedimentary and volcanic rocks of the Dunnage Zone are allochthonous and structurally overlie the metasedimentary rocks of the SBF, interpreted as equivalent to the Gander Group. The Gander Group, the type section of the Gander Zone, has been interpreted as a continental margin sequence that lies upon a basement of unknown affinity (possibly Avalon Zone). This has also been upheld by a recent LITHOPROBE EAST offshore deep marine seismic profiling study (Keen *et al.*, 1986) which interpreted the existence of a two-layer crust under the Dunnage Zone.

Three ophiolite complexes surround the MCT; the Pipestone Pond Complex to the west, the Great Bend Complex to the northeast and the Coy Pond Complex to the east. To the north, the MCT is in fault contact with sedimentary rocks (sandstone, siltstone and shale) of the Bay d'Espoir Group (Salmon River Dam Formation), as well as sandstone and siltstone which appears to be correlative with the Wigwam Formation of the Botwood Group (Colman-Sadd and Russell, 1982). To the south and southwest, sedimentary and volcanic rocks of the Bay d'Espoir Group are faulted against the MCT. The sedimentary rocks consist of dark green phyllite and psammite, and the felsic volcanic rocks consist of

predominantly two lithologies; massive pale green rhyolitic flows and ash flows, and a more "mafic looking" rock consisting of a pale grey, siliceous groundmass with feldspar and quartz phenocrysts. Rhyolitic agglomerate and/or volcanic breccia is also present (Swinden and Collins, 1982).

Two large intrusive bodies appear to cut the boundary of the MCT. The Partridgeberry Hills Granite, formally named by Colman-Sadd (1980), is in contact with the southeastern boundary of the MCT and has been divided into three phases by Colman-Sadd (1985). The main phase consists of a medium to coarse grained, chloritized and sericitized, perthitic microcline, biotite granite; the marginal phase is a strongly foliated, fine to medium grained, chloritized and sericitized biotite granite; and the high silica phase is a medium grained muscovite-biotite granite (Colman-Sadd, 1985). The contact with the MCT has not been mapped. However, Colman-Sadd et al. (in press) interpret the contact to be intrusive.

The Mount Peyton Intrusive Suite, in contact with the extreme northeast boundary of the MCT, consists of two main phases; a pyroxene gabbro and a younger granite phase which intrudes the gabbro (Strong, 1979). The granite phase is in contact with the MCT.

Several smaller intrusions occur within the MCT, the largest of which has been termed the Through Hill

Granite by Colman-Sadd (1985). It occurs in the south-central part of the MCT, with other related intrusions occurring in the extreme western and eastern parts of the area. The mineralogy consists of quartz and feldspar with muscovite as the dominant mica (biotite only occurs at the contacts with the country rock), and garnet and tourmaline as accessory phases. This mineralogy indicates that these smaller intrusions are S-type granites which probably formed from melting of rocks of sedimentary origin.

Granitoid intrusions occur locally within the high grade part of the MCT north of Through Hill. These are dominantly medium grained, unfoliated, biotite-rich granitoids containing modal cordierite and abundant inclusions of psammitic SBF, and are thought to originate from melting of the metasedimentary rock during metamorphism (i.e. syn-metamorphic; T. Rivers, pers. comm., 1989). These intrusions are interpreted as products of partial melting of the metasedimentary rocks of the SBF.

Metasedimentary rocks of the SBF are metamorphosed from greenschist to upper amphibolite facies, culminating in the formation of migmatite and gneiss in the central part of the area (Colman-Sadd, 1985). The SBF consists of pelites and psammities, and is devoid of volcanic lithologies. It is on this basis that it is correlated with the Gander Group of the Gander Zone.

The above noted evidence indicates that a two-layer crust exists in the Mount Cormack Subzone area, and this two-layer crust rests on basement of unknown affinity. The ophiolitic rocks, along with their carapace of sedimentary and volcanic rocks, form the upper plate, and the metasedimentary rocks of the MCT form the lower plate. The small intrusive bodies within the MCT are formed as a result of partial melting of the metasedimentary rocks.

1.10 Age

The age of the metasedimentary rocks of the SBF had been previously determined from two fossil localities on the eastern margin of the terrane (F on Figure 1-2). Colman-Sadd and Russell (1982) collected samples from limestone conglomerate which yielded brachiopods (and other fossils) that indicate an age of Llanvirn-Llandeilo. However, the contacts of this unit are unexposed, and provenance studies by Colman-Sadd et al. (in press) have shown that the limestone contains clasts of metasedimentary rocks (interpreted to be SBF) as well as detrital chromite grains from the ophiolitic units surrounding the MCT. Therefore, rocks of the SBF are older than the Llanvirn-Llandeilo age originally assigned to them, but no specific age has been determined.

The age of the ophiolitic rocks surrounding the MCT has been determined from plagiogranite associated with

the Coy Pond and Pipestone Pond Complexes. Dunning and Krogh (1985) obtained U-Pb zircon ages of $493.9 \pm 2.5/-1.9$ Ma for the Pipestone Pond Complex and 489 Ma (minimum) for the Coy Pond Complex. The authors suggested that since the age of the Coy Pond Complex was determined from only one analysis that is significantly discordant, the two ophiolite complexes could be equivalent in age.

The Through Hill Granite (THG) has yielded a U/Pb age of $464 \pm 4/-3$ Ma from fine-grained needles of zircon (Colman-Sadd et al., in press). In addition, the "migmatitic" or partially melted metasedimentary rocks have been dated (from monazites in the leucosome) and have yielded an age of 465 ± 2 Ma. Since the THG and the "migmatite" are interpreted as having formed by partial melting of the metasedimentary rocks of the SBF, then this age can be correlated with the metamorphic event that caused the partial melting. Although the THG shows cross-cutting relationships with the SBF (implying that it formed at depth and was emplaced at its present level), the age equivalence with the "migmatite" implies that it formed during the same metamorphic event.

The age of the Partridgeberry Hills Granite is determined from zircon grains which indicate an age of 474 ± 4 Ma (Colman-Sadd et al., in press).

CHAPTER 2

LITHOLOGIC UNITS

2.1 Introduction

There are three gross lithologic units that occur in the MCSZ area; metasedimentary rocks, ophiolitic rocks and intrusive rocks (see Geological Map in back pocket). This chapter includes descriptions of these units along with an assessment of their protoliths; emphasis is paid to the metasedimentary and intrusive units (THG and related intrusions) which were mapped during this study. Where samples were collected, petrographic descriptions are given; where no samples were collected, descriptions are taken from the literature. Mineral modal abundances were determined from thin section analysis; all samples were stained for the presence of K feldspar following the method of Hutchison (1974). The mineralogy of the metasedimentary rocks is described in detail in Chapter 4.

2.2 Metasedimentary Rocks

As previously stated, the SBF consists of pelites and psammites at various grades of metamorphism from greenschist to upper amphibolite facies, culminating in the formation of migmatite and gneiss in the central part of the

area (Colman-Sadd, 1985). Amphibolite-bearing gneisses occur in the highest grade part of the MCSZ, but occur outside the area mapped during this study. Rocks of the SBF consist of variable amounts of slate, phyllite, schist and quartzite. Quartzite layers are typically 30 cm thick but occur locally up to 2 m; these are light grey in colour and weather white. At low metamorphic grade, these layers preserve original sedimentary structures. In some areas along Spruce Brook, complete Bouma sequences were observed in sandstone, with sharp bases and fining upward sequences. In most outcrops, quartz veins cut the quartzite layers; these increase in abundance near the contact with the Coy Pond Complex.

Quartzites are separated by layers of slate and phyllite which occur on scales from a few centimetres to several metres. These are dark grey to black in colour and become lighter with increasing grain size. These layers typically display fine-grained laminae defined by alternating quartz-rich and muscovite/chlorite-rich layers. Like the quartzites, they also preserve original sedimentary structures such as parallel lamination. Schists from the SBF contain evidence of two structural fabrics, an early fabric S_1 sub-parallel to bedding and a later fabric that folds the S_0/S_1 surfaces.

At low grades of metamorphism, the rocks of the SBF are typically light to medium grey and weather to a tan

colour (Plate 2-1). They are very fine grained with an average grain size of 0.05 mm. Bedding, where evident, is generally fine scale (< 0.5 mm), but ranges in thickness up to 10's of cm. It is defined by alternating quartz-rich (quartzite) and muscovite-rich (slate/phyllite) layers. As metamorphic grade increases, grain size increases and in some cases porphyroblasts of biotite and chlorite are visible in hand sample. These rocks are light grey and weather to a tan colour (Plate 2-2). Pseudomorphs of cordierite also occur locally.

Original sedimentary structures are locally well preserved in this zone, especially along Spruce Brook. In this area, original sedimentary layering is visible, with quartzite beds ranging in thickness from 10 cm up to 2 m. The quartzite beds are separated by phyllite and slate units ranging in thickness up to 2 m, with individual beds ranging from 1 mm to 5 cm. These are commonly parallel laminated, although cross-lamination is also present.

At still higher metamorphic grade, grain size increases and the rocks are typically light grey and weather to a tan colour (Plate 2-3). Porphyroblast growth in the pelitic layers begins to obscure original sedimentary structures (Plate 2-4). The main porphyroblast phases include andalusite, garnet and staurolite, but cordierite pseudomorphs are also present.



Plate 2-1. Typical low-grade rocks from the SBF showing fine-grained nature and original sedimentary structures.



Plate 2-2. Samples from the SBF showing increased grain size and biotite porphyroblasts (sample SD-89-256). Note cordierite pseudomorphs in sample SD-89-267..

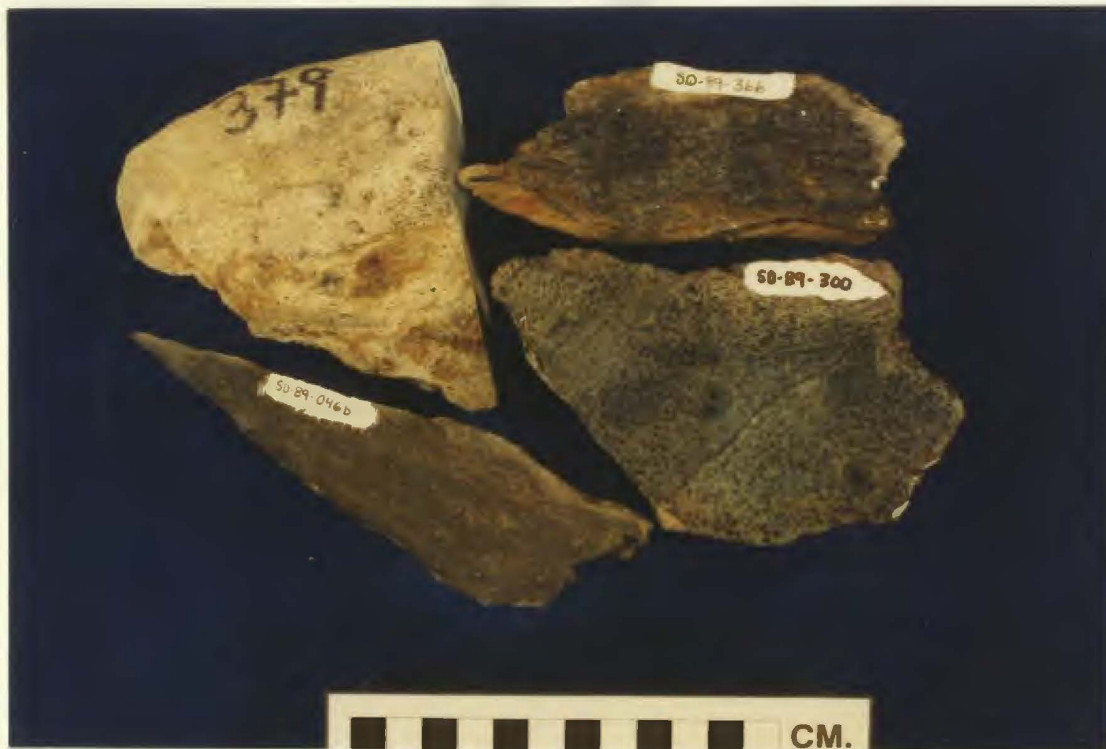


Plate 2-3. Samples of SBF showing porphyroblasts of andalusite, staurolite and garnet.



Plate 2-4. Typical outcrop of SBF containing large (1 cm) andalusite porphyroblasts. Original bedding can be seen between pelite and psammite layers. Sample SD-89-379.

At higher metamorphic grades, sillimanite replaces andalusite and the rocks are medium to dark grey in colour and weather to light grey (Plate 2-5). These rocks are dominantly schists, although some psammitic layers are present which preserve original bedding. This bedding becomes erratic and disrupted as metamorphic grade (and probably strain) increases and, in most cases, the only evidence of original bedding is in disrupted slabs of psammite which are up to several metres in length. In the higher grade parts of this zone, bedding is transposed into the main foliation and banded gneisses are developed (Plate 2-6). In some locations, mylonites are formed in which quartz aggregates are stretched and boudinaged, and reach lengths of up to 7 cm.

Quartzite layers occur locally, but appear to be disrupted slabs with no consistency in the attitude of bedding. In the more pelitic layers, schists also display evidence of partial melting. In these areas, the rocks are typically dark grey on a fresh surface (Plate 2-7) and weather to a light grey (Plate 2-8). In one location, where cordierite-bearing granodiorite can be mapped as a separate unit (see Geological Map and Section 2.4.2), it is interpreted to have been formed from partial melting of the metasedimentary rocks. A large part of the area mapped as "migmatite" may in fact be cordierite-bearing granodiorite that is full of inclusions of the metasedimentary rocks.



Plate 2-5. High grade samples of SBF showing increased grain size and schistosity.



Plate 2-6. Typical outcrop of banded gneiss from the SBF. Note pod of melt just below lens cap. ~ 140 m west of sample SD-89-008.



Plate 2-7. Typical samples of high-grade SBF. Grey patches in SD-89-145 are sillimanite retrogressed to muscovite.



Plate 2-8. Outcrop of high-grade SBF showing boudinaged melt pods and F_2 folding in sillimanite layers (lower right). Also note large boudin of psammite in lower left of photograph. ~ 275 m west of sample SD-89-127.

Distinction between the two is difficult without good exposure.

2.3 Ophiolitic Rocks

These units were not examined during this study and the information has been taken from the literature. Three ophiolite complexes surround the MCSZ; the Pipestone Pond Complex to the west, the Great Bend Complex to the northeast and the Coy Pond Complex to the east. These ophiolites preserve enough stratigraphy to indicate their facing directions, which in each case is upwards and outwards from the MCSZ (Colman-Sadd and Swinden, 1984; Williams et al., 1988).

The Pipestone Pond Complex displays a complete ophiolite stratigraphy consisting of peridotite at the base grading upwards into pyroxenite, gabbro, diabase, pegmatitic gabbro and trondhjemite, mafic pillow lava and scattered sedimentary rocks. This sequence is, however, disrupted by much internal faulting so that no single section through the sequence traverses the complete stratigraphic section (Swinden and Collins, 1982).

The Great Bend Complex also displays a near complete ophiolite sequence, with internal faulting disrupting the stratigraphy. According to Zwicker and Strong (1986) the sequence consists of serpentized peridotite grading into serpentine schist, pyroxenite,

peridotite altered to talc-magnesite schist, gabbro and diabase. Colman-Sadd and Swinden (1984) proposed that the Great Bend and Coy Pond Complexes were continuous with one another, although Zwicker and Strong (1986) were not in accord with this interpretation.

The Coy Pond Complex was mapped by Colman-Sadd (1985) as a complete ophiolite sequence from harzburgite through serpentinite, pyroxenite, gabbro and diabase, trondhjemite and keratophyre, mafic pillow lava and sedimentary rocks. However, mapping by A. Timbal during the summer of 1989 has indicated that the Coy Pond Complex is not a complete ophiolite sequence, but consists of at least two thrust slices, separated by zones of tectonic *mélange*. The tectonic *mélange* units consist of ophiolitic and minor metasedimentary blocks and fragments in a sheared serpentinite and/or magnesite matrix (A. Timbal and T. Rivers, pers. comm., 1989).

2.4 Intrusive Rocks

2.4.1 Felsic Intrusive Rocks (Through Hill Granite and Related Intrusions)

Isolated localities of felsic intrusive rocks occur within the MCSZ (Colman-Sadd, 1985; unit 4 on Geological Map). These units are of similar mineralogy to the Through Hill Granite (THG), which is described below.

The THG is located in the southwest portion of the MCSZ (see Geological Map). It covers an area of about sixteen square kilometres and contains xenoliths of sillimanite grade metasedimentary rocks within it. It consists of approximately equal proportions of medium-grained rock and coarse pegmatite, the latter usually occurring as segregations rather than veins (Colman-Sadd, 1985). In hand sample (SD-89-328), the granite is coarse-grained and light tan in colour (Plate 2-9).

The mineralogy (thin section) consists of ~ 45 % plagioclase, 30 % quartz, 15 % K feldspar and lesser amounts of muscovite and garnet. Plagioclase, K feldspar and quartz are anhedral; the two feldspars are very coarse grained, ranging up to 10 mm in size, and quartz fills the spaces between them. Minor sericitization occurs in the feldspars. Primary muscovite occurs as large (> 5 mm) grains which form books and are visible in hand sample. Secondary muscovite is relatively fine grained (~1 mm) and occurs along fracture surfaces. Garnet is euhedral and commonly fine grained (with respect to the other minerals) ranging from 1 mm to 3 mm in size (Plate 2-10).

Another body of this unit outcrops ~ 7.5 km due north of the THG (see Geological Map). It is milky white in colour, with fine grained garnets throughout and a greenish tinge due to muscovite. A foliation is developed and is

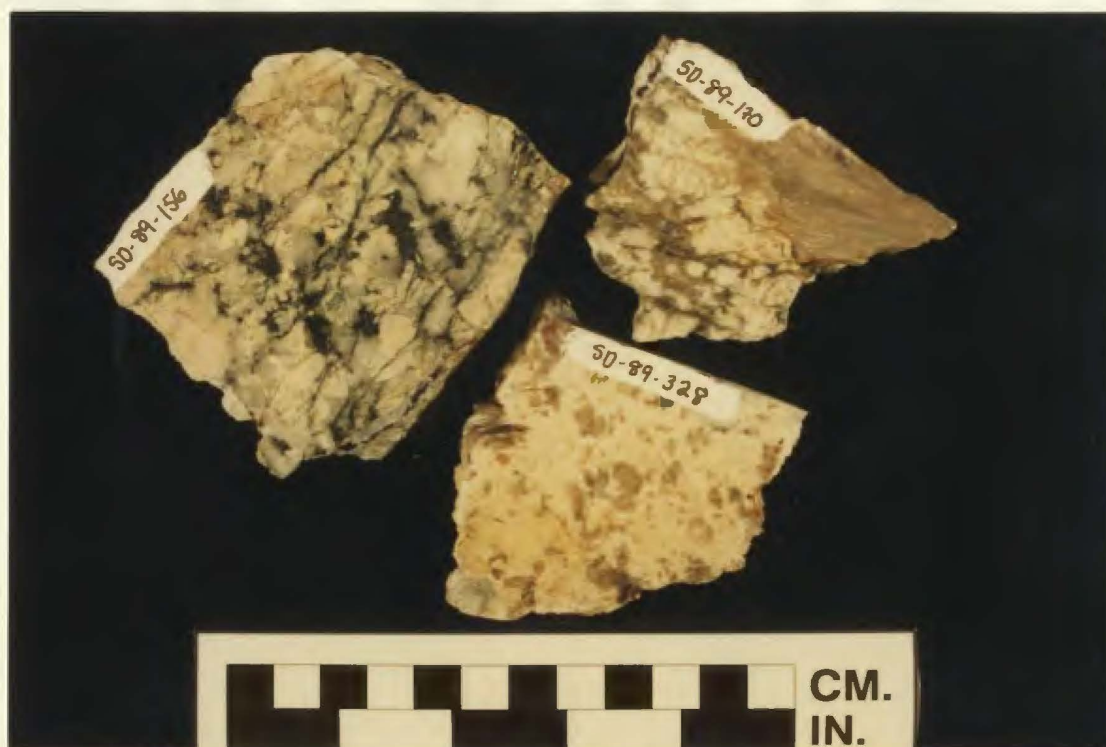


Plate 2-9. Typical samples of Through Hill Granite and related intrusions (SD-89-328, -156, and -170) showing coarse grained feldspar, quartz and garnet phenocrysts.

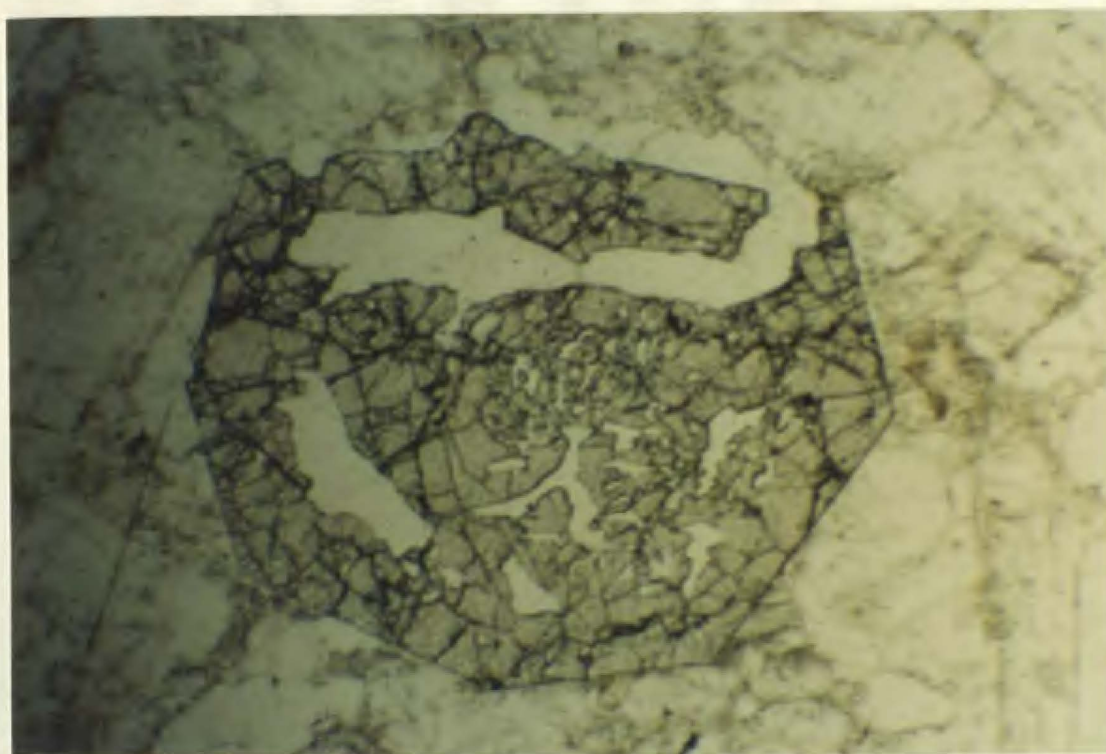


Plate 2-10. Sample SD-89-170 from a small granitic body north of the THG showing coarse ~ euhedral garnet with inclusions of quartz. Ppl., garnet is 6 mm in width.

defined by the muscovite (Plate 2-11) which is variable in grain size and locally reaches 20 mm in size.

In thin section, the unit consists of 35 % quartz, 30 % plagioclase, 20 % K feldspar, 10 % muscovite and 5 % garnet; hematite is an accessory phase. Quartz is fine grained, surrounds the two feldspars and is often recrystallized. Plagioclase consists of anhedral grains which range in size up to 1 mm, but are commonly ~ 0.3 mm in size, and show well developed albite twins. These twins are typically offset along fractures within the grains. K feldspar is also anhedral and shows poorly developed cross-hatched twinning. The grains average 0.5 mm in size but range up to 2 mm. Muscovite is commonly fine grained (< 0.2 mm) and defines a foliation. However, as mentioned above, large muscovite grains also occur within this unit. Garnet occurs as small (0.4 mm) euhedral grains.

The mineralogy of the felsic intrusive rocks is typical of S-type granites (Barker, 1983; White and Chappell, 1983) and is interpreted to have formed from the partial melting of metasedimentary rocks.

A Streckeisen (1976) modal plot (Figure 2-1) of these three granitic units indicates that two of them (samples SD-89-170 and SD-89-328) fall within the granodiorite field, although SD-89-170 is more quartz-rich, and the plagioclase/K feldspar ratio is higher than the others, so that it plots near the boundary between the

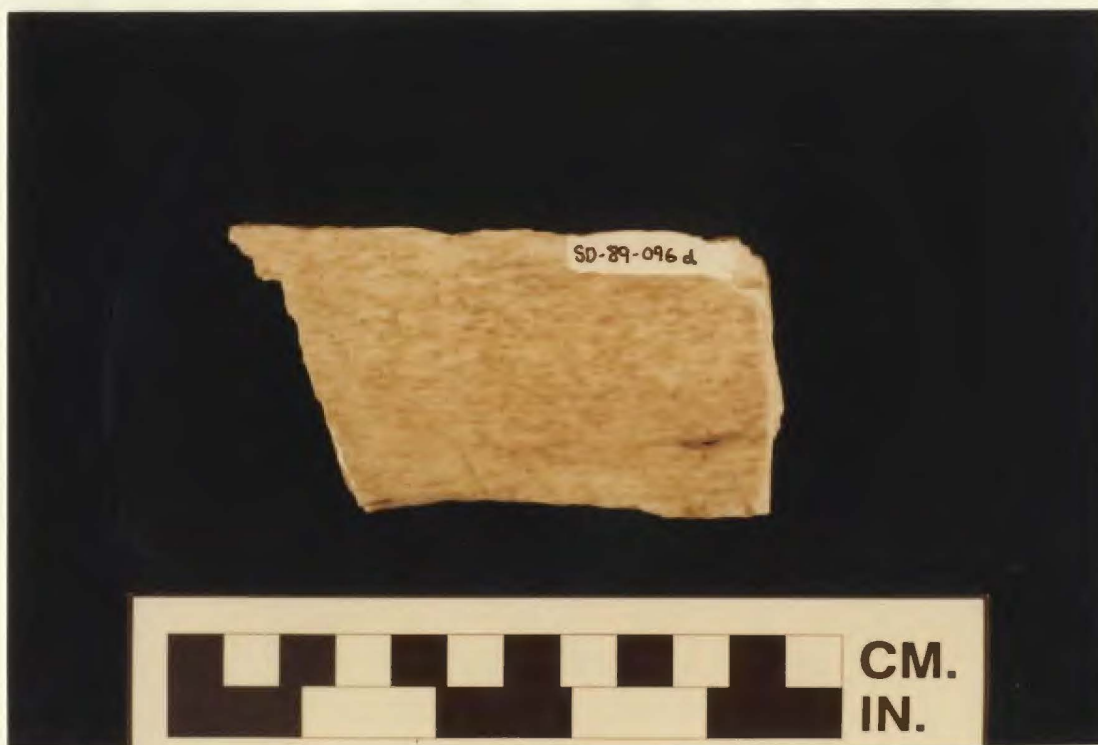


Plate 2-11. Sample SD-89-096d from a granite within a shear zone north of the Through Hill Granite showing fine grained garnets and foliation defined by muscovite (greenish mineral).



Plate 2-12. Photograph of cordierite granodiorite, sample SD-89-218 showing large K feldspar phenocrysts in a biotite-plagioclase-quartz matrix.

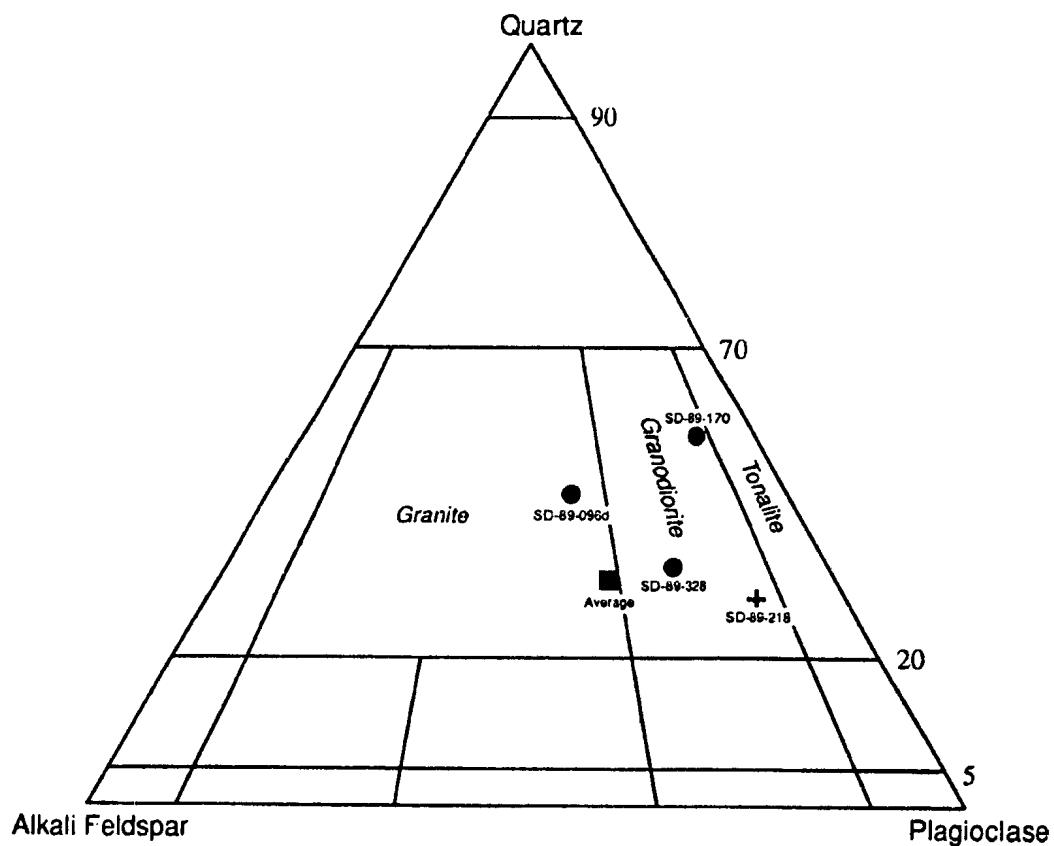


Figure 2-1. Modal quartz-alkali feldspar-plagioclase plot (after Streck-eisen, 1976) of the three granitoid units and the average modal composition of the Through Hill Granite (square box) as determined by Elias (1981). The location of sample SD-89-218 is also shown (cross) and is discussed further under Section 2.4.2.

granodiorite and tonalite fields (Figure 2-1). Only sample SD-89-096d plots within the granite field, near the granite/granodiorite boundary. An average modal composition for the THG (calculated by Elias, 1981, from fifteen samples) also plots near this boundary (box on Figure 2-1).

2.4.2 Cordierite Granodiorite

Although many of the samples collected from the high grade zones (> sillimanite-biotite-muscovite isograd) contain appreciable amounts of "granitoid" melt due to partial melting, there is one location where "granitoid" material is mapped as a separate unit (see Geological Map). It shows a crosscutting relationship with the metasedimentary rocks surrounding it, and also contains abundant xenoliths of the surrounding rocks. This unit is distinct from the other granitic intrusive rocks in that it contains no garnet, but instead contains modal cordierite.

In hand sample (SD-89-218; Plate 2-12), this unit is coarse grained and contains phenocrysts of K feldspar. The sample is light grey in colour and weathers to light brown. In terms of modal mineralogy, the sample consists of 30 % plagioclase, 20 % biotite, 15 % quartz, 15 % cordierite, 10 % muscovite, 5 % K feldspar with lesser amounts of sillimanite, chlorite, opaque minerals and accessory zircon. Plagioclase is sub- to euhedral and averages 2 mm in grain size. Albite twinning is dominant, although some grains display "comb-style" twinning. The

grains are relatively unaltered, with only minor amounts of sericitization present.

Biotite grains range up to 2 mm in size (average 1 mm) and are subhedral. They are relatively inclusion free, with only a few zircon grains included. Quartz grains are anhedral, ~ 2 mm in size and display undulose extinction.

Cordierite grains are also anhedral and average 2 mm in size, although they range up to 5 mm. They contain abundant yellow pleochroic haloes surrounding zircon and apatite (Plate 2-13), which facilitate their optical identification. Fine grained muscovite typically occurs along cracks and fractures (Plate 2-14).

Muscovite occurs as primary subhedral grains which average 0.5 mm in size, and as mentioned above, as secondary fine grains along fractures in cordierite. K feldspar occurs as anhedral grains up to 3 mm in size (averaging 2 mm). They show well developed cross-hatched twinning typical of this mineral. Graphic intergrowths of quartz with K feldspar (Plate 2-15) and quartz with plagioclase are also present (Plate 2-16) indicating that the quartz and feldspars crystallized together. Sillimanite occurs as prismatic needles with no preferred orientation. Chlorite is present not as a primary phase but occurs locally as a replacement mineral on biotite grains. Fe(-Ti) oxides are anhedral grains that average 3 mm in size.

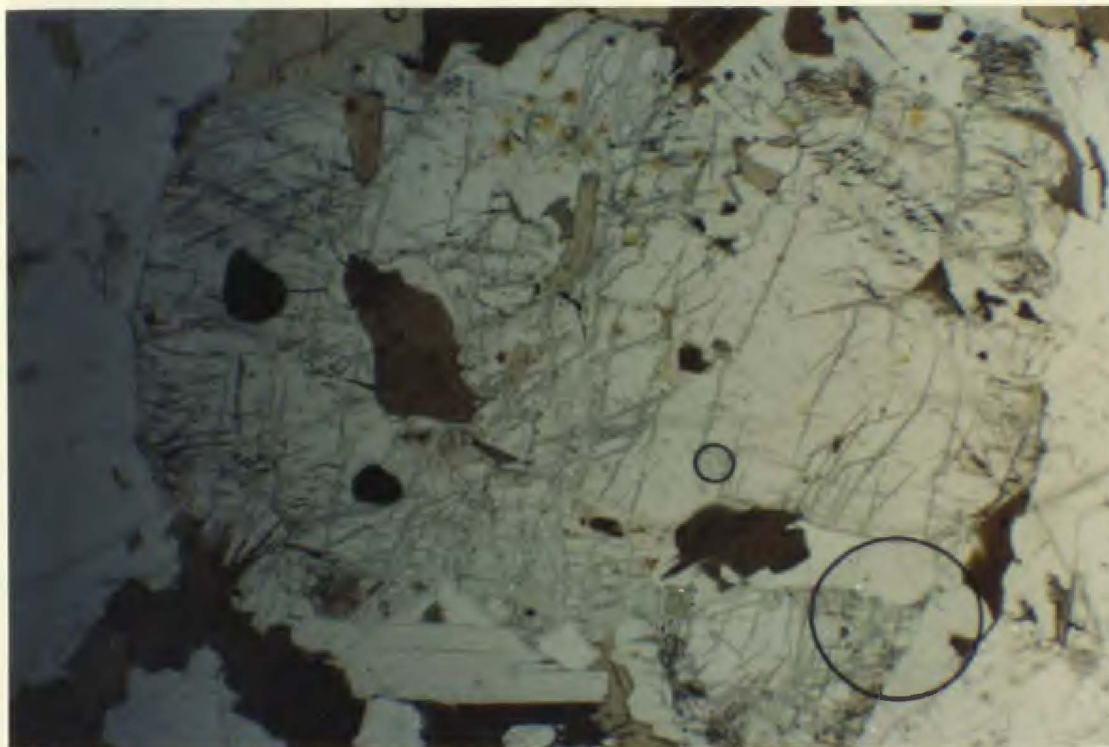


Plate 2-13. Large anhedral cordierite grain from the cordierite granodiorite showing abundant pleochroic haloes occurring within the grain. Ppl., cordierite grain is ~ 8 mm in width.

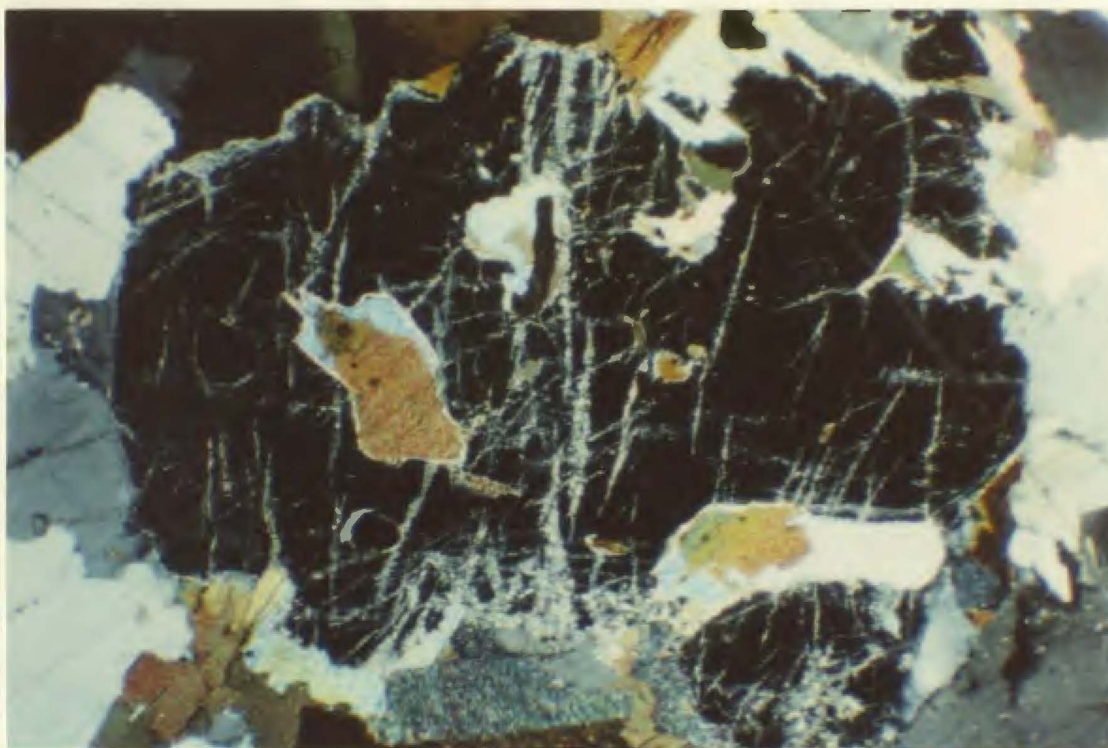


Plate 2-14. Same sample as Plate 2-13, but under cross polarized light. Notice the fine grained muscovite along cracks and fractures.

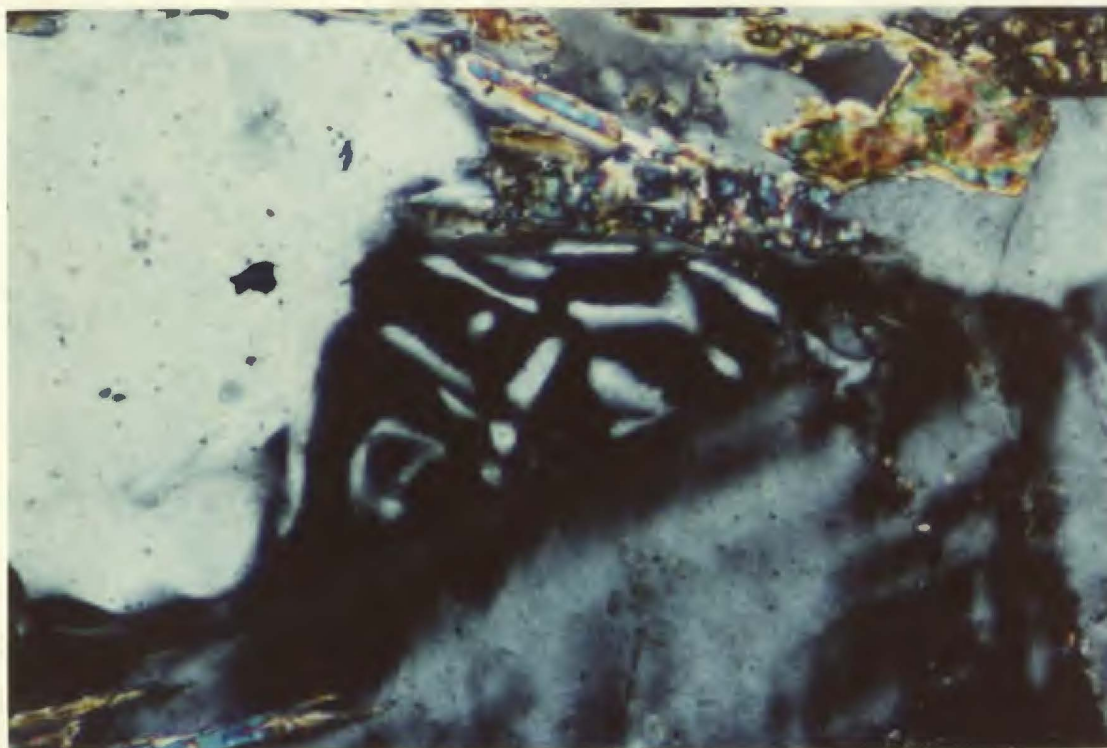


Plate 2-15. Graphic intergrowth of quartz and K-feldspar from the cordierite granodiorite, sample SD-89-218. Xpl., photo is 1.2 mm wide.

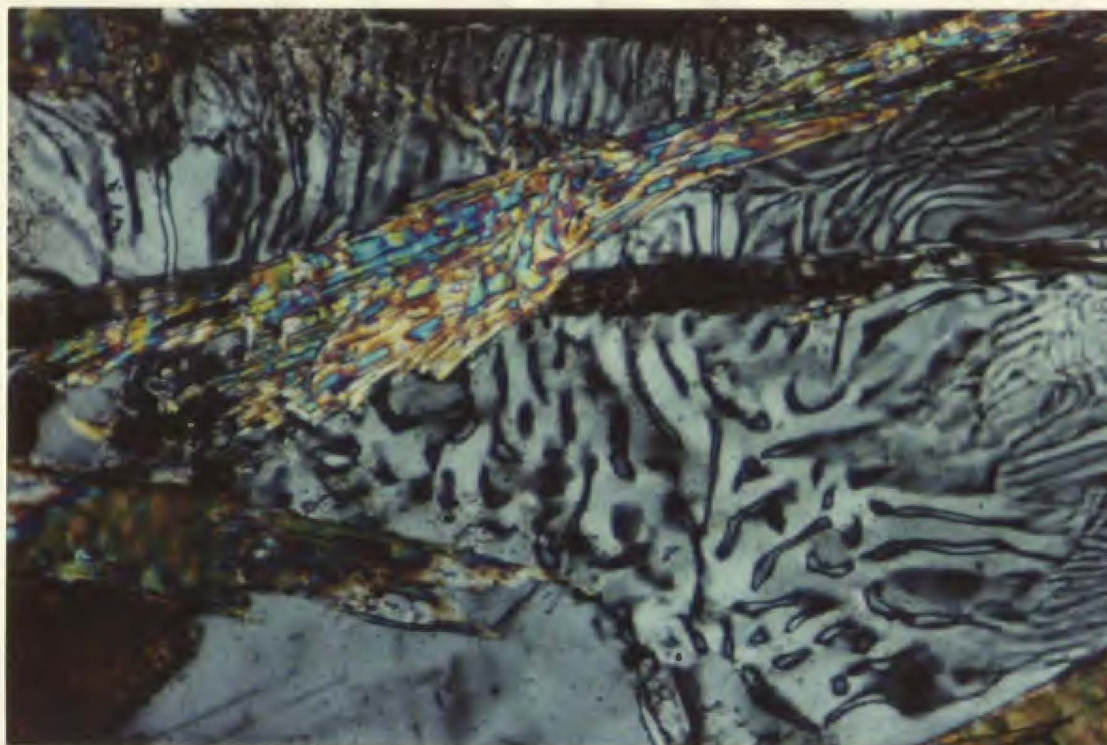


Plate 2-16. Graphic intergrowth of quartz and plagioclase from the cordierite granodiorite, sample SD-89-218. Xpl., photo is 1.2 mm wide.

When this unit is plotted on a Streckeisen (1976) diagram with the other granitic units (Figure 2-1), it plots near the other units within the granodiorite field. It is also interpreted to have formed from partial melting of the metasedimentary rocks. However, as this unit contains cordierite, it is interpreted to have formed at a higher level (lower pressure) than the THG (and related intrusions) which contains garnet. Also, the THG and related intrusions cross-cut the structures in the SBF suggesting that they have intruded the SBF.

2.4.3 Mafic Igneous Rocks

Occurring within the metasedimentary rocks of the MCSZ are isolated outcrops of mafic igneous rocks. These are interpreted as dykes, although in one case (Sample SD-89-246b) no clear boundary could be seen between the igneous phase and the local metasedimentary unit (quartzite). At this locality (within the biotite-muscovite-chlorite zone), the unit is dark grey-green in colour and predominantly equigranular, although small pyroxene phenocrysts are visible in places. In thin section, the mineralogy consists of approximately 70 % pyroxene (both clinopyroxene [augite] and orthopyroxene, with the former being more abundant), 15 % plagioclase, 10 % epidote, and lesser amounts of opaque minerals (pyrite visible in outcrop) and chlorite. The rock is a diabase and is equigranular and fine grained, with the grains ranging from 0.05 mm to 0.20 mm (average 0.1 mm).

However, some of the clinopyroxene grains are up to 1.0 mm in length.

A second outcrop of the unit occurs within the andalusite-biotite-muscovite zone, southeast of the THG (Sample SD-89-386). Unlike the above unit, the boundaries of this body are well constrained (Plate 2-17). It is a mafic dyke, ~ 30 cm in thickness, with an orientation of 062/85 NW. It is dark grey-green in colour and contains visible pyrite and carbonate. In this case, the mineralogy consists of 60 % clinopyroxene, 15 % carbonate, 15 % chlorite and lesser amounts of opaque minerals, plagioclase and quartz (Plate 2-18). This sample is a fine- to medium-grained, inequigranular diabase. Carbonate grains in the diabase are xenoblastic, ~ 2 mm in size (average) and appear to be filling holes or pockets within the matrix.

2.5 Protoliths

The metasedimentary rocks of the SBF are equivalent to the rocks of the Gander Zone which are derived from "... a monotonous sedimentary succession (that) is characterised by quartz-rich sandstones that have an apparent continental provenance." (Colman-Sadd et al., in press). At low grades of metamorphism, the original sedimentary nature of the SBF is preserved and it consists of a sequence of medium- to thick-bedded sandstone and shales with interbedded siltstone and fine-grained sandstone



Plate 2-17. Photograph of ~ 30 cm wide diabase dyke from the andalusite-biotite-muscovite zone, southeast of the Through Hill Granite (sample SD-89-386) .

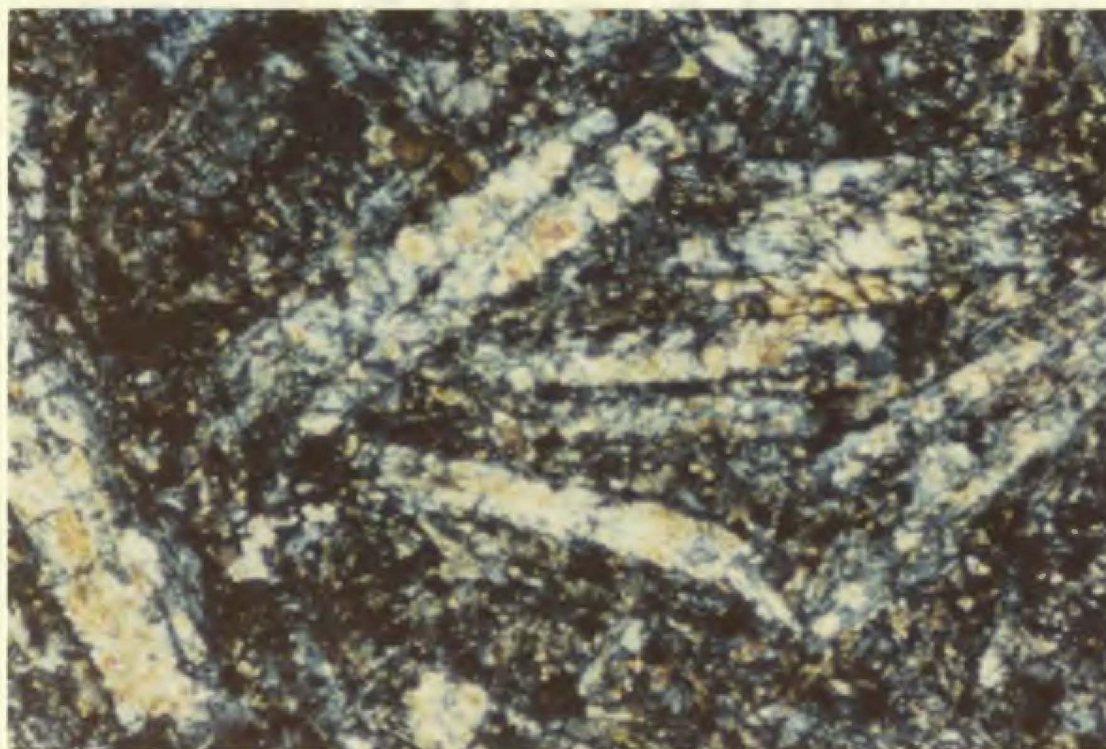


Plate 2-18. Diabase dyke (sample SD-89-386) from the andalusite-biotite-muscovite zone southeast of the Through Hill Granite displaying elongate clinopyroxene grains (augite). Xpl., photo is 3 mm wide.

(Colman-Sadd and Swinden, 1984). Studies of the quartzite indicate that it is most likely derived from continental plutonic and metamorphic rocks (Colman-Sadd et al., in press) and was deposited on the eastern margin of the Iapetus Ocean.

The ophiolitic rocks that surround the MCSZ are interpreted as part of the allochthonous Dunnage Zone or Iapetus Ocean. Analyses of chromite grains from the three ophiolite complexes (Malpas and Strong, 1975; Colman-Sadd et al., in press) show that they have high Cr[#]/Mg[#] ratios and low TiO₂ contents. These data are characteristic of "Type III" alpine peridotites, i.e. those found in arc-related volcanic and intrusive rocks (Dick and Bullen, 1984; Hébert and Laurent, 1987). Jenner and Swinden (1989), on the basis of geochemical analyses, interpreted the Pipestone Pond Complex to record rifting of an island arc.

CHAPTER 3

STRUCTURAL GEOLOGY

3.1 Introduction

The first modern structural mapping of the study area by S.P. Colman-Sadd and H.S. Swinden showed that the Mount Cormack Subzone comprises an oval area of metasedimentary rocks surrounded by ophiolite. In their synthesis paper (Colman-Sadd and Swinden, 1984), they interpreted the presence of a structural dome, with the core of the dome being occupied by metasedimentary rocks of variable metamorphic grade and the flanks by low-grade rocks of ophiolitic affinity. From this interpretation, it followed that the ophiolitic and associated rocks of the Dunnage Zone overlie the metasedimentary rocks of Gander Zone affinity, and thus that there is a two-layer upper crust in this region. Prior to this, rocks of the Dunnage Zone were considered to be underlain by oceanic crust and mantle.

Colman-Sadd's (1985) structural map of the MCSZ shows that the planar fabrics in the metasedimentary rocks (considered to be bedding, S_0 by Colman-Sadd) are folded into a large, map-scale synform plunging towards the southwest in the southeastern part of the MCSZ, but

elsewhere a distinctive large-scale fold pattern was not recognized. However, Colman-Sadd (1981) noted that facing directions in the metasedimentary rocks (determined mainly from grading) were not consistent across the major southwest-plunging fold and he postulated the existence of an earlier phase of deformation, although he could find no evidence for it in the field. Colman-Sadd (1985) noted that the large synform predated the establishment of the isograds in the MCSZ, as the latter are not folded.

As part of this study, a structural analysis was undertaken to determine the cause of the conflicting structural interpretations of Colman-Sadd (1981; 1985) by collecting measurements of structural elements including bedding, cleavage, bedding-cleavage intersection lineations, foliations, high strain fabrics, F_2 fold axial planes and fold axes. These are shown on the Structural Map in the pocket at the back of this thesis. These and other data are used to constrain the structural model, and to resolve some of the associated problems.

3.2 Structural Elements

Evidence of at least two major phases and one more cryptic phase of deformation has been found in this study of the Mount Cormack Subzone. Bedding, S_0 , is defined in the SBF by alternating quartz-rich (psammitic) and mica-rich (pelitic) layers, ranging in thickness from a few

centimetres to several metres. No evidence of the first cleavage, S_1 , was found in the field; however, from petrographic work, especially on samples from the chlorite-muscovite zone, a bedding-parallel fabric (Plate 3-1) was defined that is folded around the large southwest-plunging fold described above. This indicates that the first deformation formed isoclinal folds, although no large-scale F_1 isoclinal folds were mapped, implying that F_1 structures were of small scale.

S_2 (originally termed S_1 by Colman-Sadd, 1985) is defined by a penetrative cleavage in low-grade pelitic beds, and a schistosity at higher grades of metamorphism. In the high grade rocks, $S_0 \parallel S_1$ is locally present in disrupted low-strain augen of psammite, but becomes transposed into the S_2 foliation (Plate 3-2) in zones of high strain. S_1 foliation within the Mount Cormack Subzone has been subdivided into two domains on the basis of orientation (see Structural Map in pocket at back and Section 3.2.2).

Numerous outcrop and larger-scale folds occur throughout the Mount Cormack Subzone at various grades of metamorphism. These are interpreted to be F_2 structures.

3.2.1 Bedding (S_0) - First Cleavage (S_1)

Bedding (S_0) in the Mount Cormack Subzone is most evident in low-grade rocks although it is locally preserved in high-grade rocks. All of the S_0 measurements are from

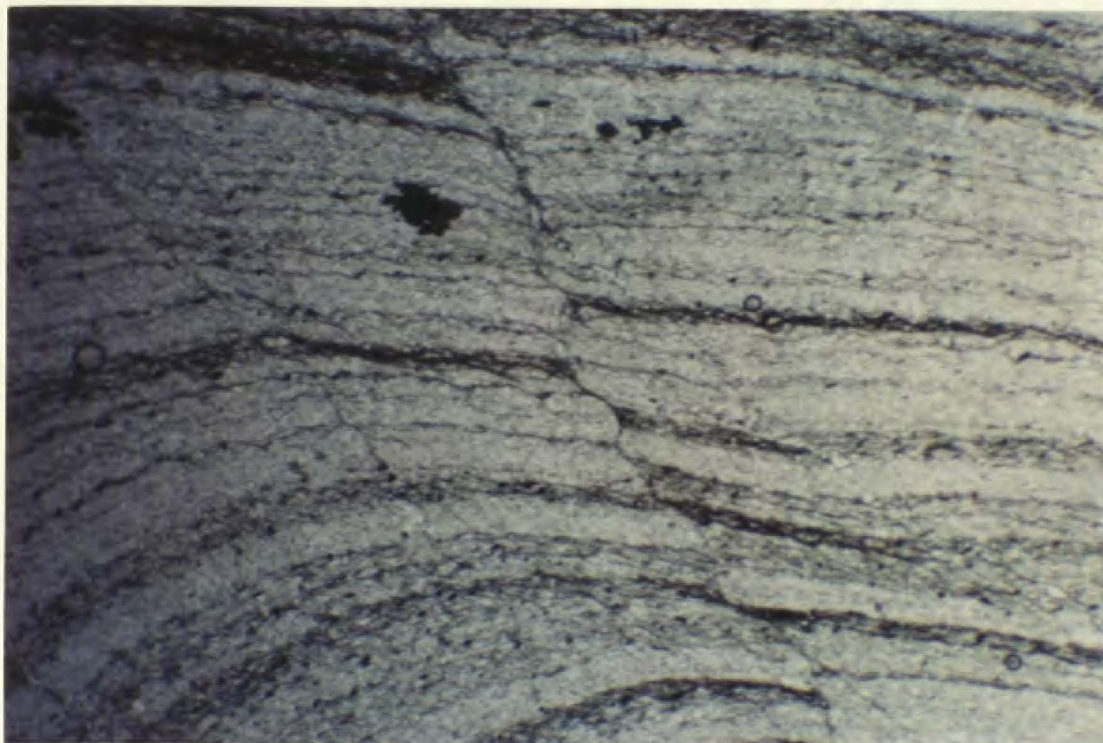


Plate 3-1. Photograph of sample SD-89-243 from the chlorite-muscovite zone showing the orientation of two sets of foliation (S_1 parallel to S_0 and S_2 at an angle). Xpl., photo is 1.5 mm wide.



Plate 3-2. Deformed low-strain lozenge of psammite within a sillimanite-biotite-muscovite schist displaying original fabric ($S_0 \parallel S_1$) and transposition of this fabric into S_2 at high grades. ~125 m SE of sample SD-89-034.

areas where S_0 and S_1 are subparallel, presumably limb regions of F_1 folds. S_1 is defined by the alignment of fine-grained muscovite and chlorite. In the low-grade rocks, $S_0 \parallel S_1$ is usually sub-parallel to the second cleavage (S_2). In Domain A, $S_0 \parallel S_1$ has a general northeast-southwest orientation and is steeply dipping to both the northwest and southeast. A contoured stereonet plot of poles to bedding in Domain A (Figure 3-1a, $n=82$) shows two point maxima; the plane to the first point maxima has an orientation of 054/84 SE and the plane to the second is orientated at 075/80 SE indicating that there is some variation in orientation, presumably due to later folding. In Domain B, $S_0 \parallel S_1$, when present, is generally disrupted by the S_2 foliation, so few measurements were taken.

3.2.2 S_2 Cleavage

S_2 cleavage is defined by the alignment of platy minerals (i.e. muscovite and biotite). In rocks of Domain A, S_2 foliation is orientated northeast-southwest and is steeply dipping to the northwest and southeast, nearly parallel to $S_0 \parallel S_1$ (Figure 3-1b). The point maximum of poles to S_2 foliation indicates that the overall trend of S_2 is 063/79° SE. Although the point maximum is nearly identical to that of the $S_0 \parallel S_1$, individual pairs of $S_0 \parallel S_1$ - S_2 measurements commonly have a small angle between them so

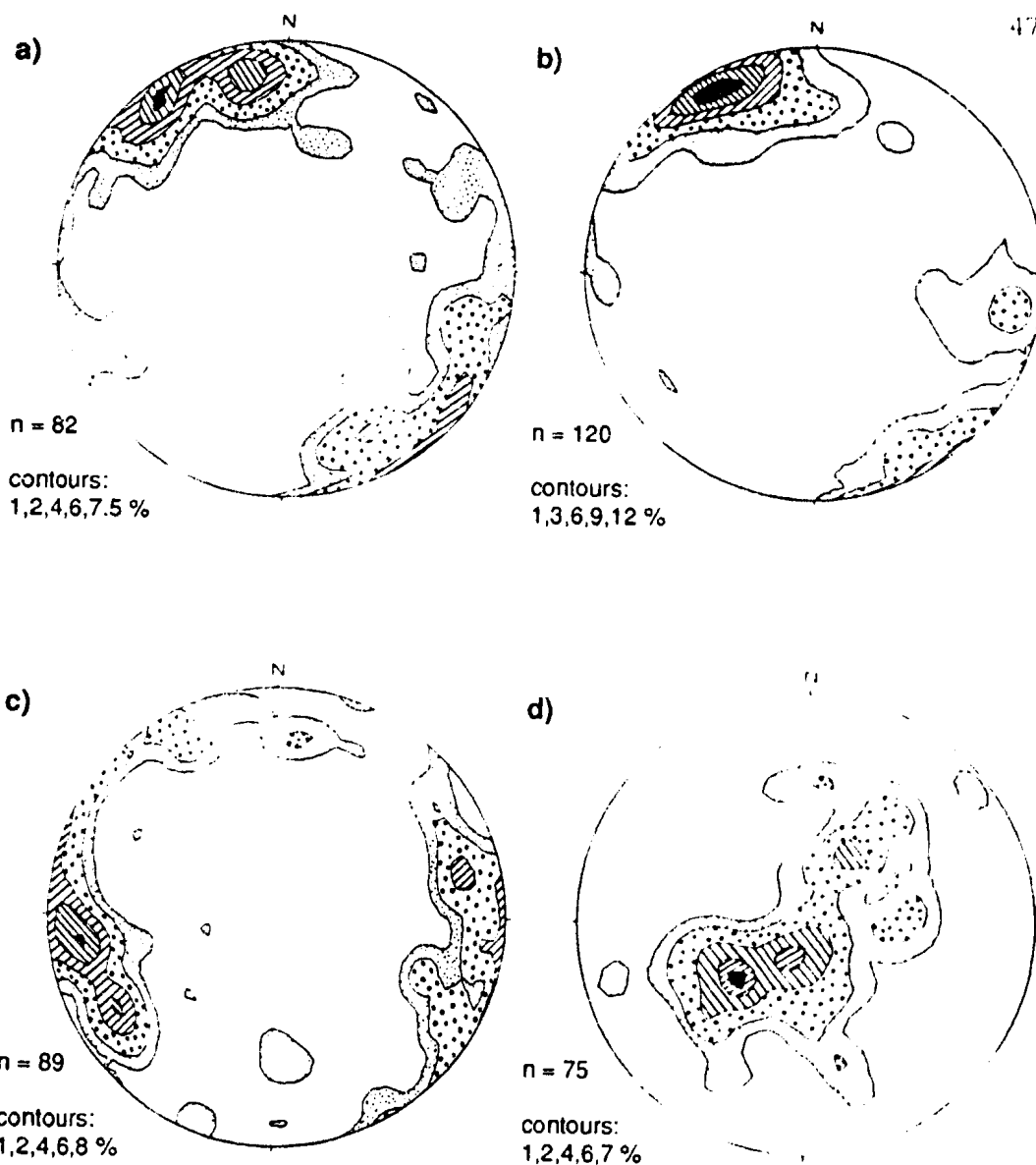


Figure 3-1. Contoured equal area stereonet plots from the Mount Cormack Subzone. a) plot of poles to bedding (Domain A); b) plot of poles to foliation (S_1 , Domain A); c) plot of poles to foliation (S_2 , Domain B); d) plot of $S_6 | S_1-S_2$ intersection lineations (Domain A).

that the sense of vergence and orientation of intersection lineations can be determined (see next section).

In Domain B, the orientation of the S_2 foliation is more erratic (Figure 3-1c). The main point maximum indicates an overall foliation orientation of $173/74^\circ$ E with another possible maximum of $165/80^\circ$ NNE). This is significantly different than Domain A and is interpreted to imply folding between the domains (see below).

3.2.3 L_2 Intersection Lineations

L_2 intersection lineations were determined from the intersection of $S_0 \parallel S_1$ and S_2 from Domain A. These data are shown in Figure 3-1d. Plate 3-3 is a field photograph showing the configuration of S_0 , S_1 and S_2 . The L_2 lineations lie in a steep northeast-southwest trending plane, and the majority plunge towards the southwest moderately to steeply; they yielded two point maxima, one orientated at $232^\circ/57^\circ$ and the other at $210^\circ/75^\circ$. These are in general agreement with the information of Colman-Sadd (1985).

3.2.4 F_2 Folds (Fold Axes, Axial Planes)

F_2 folds are abundant and occur throughout the area. At low-medium grades of metamorphism, F_2 folds fold bedding and the sub-parallel S_1 foliation and commonly have wavelengths of less than five metres (Plate 3-4), although larger-scale folds are interpreted on the basis of

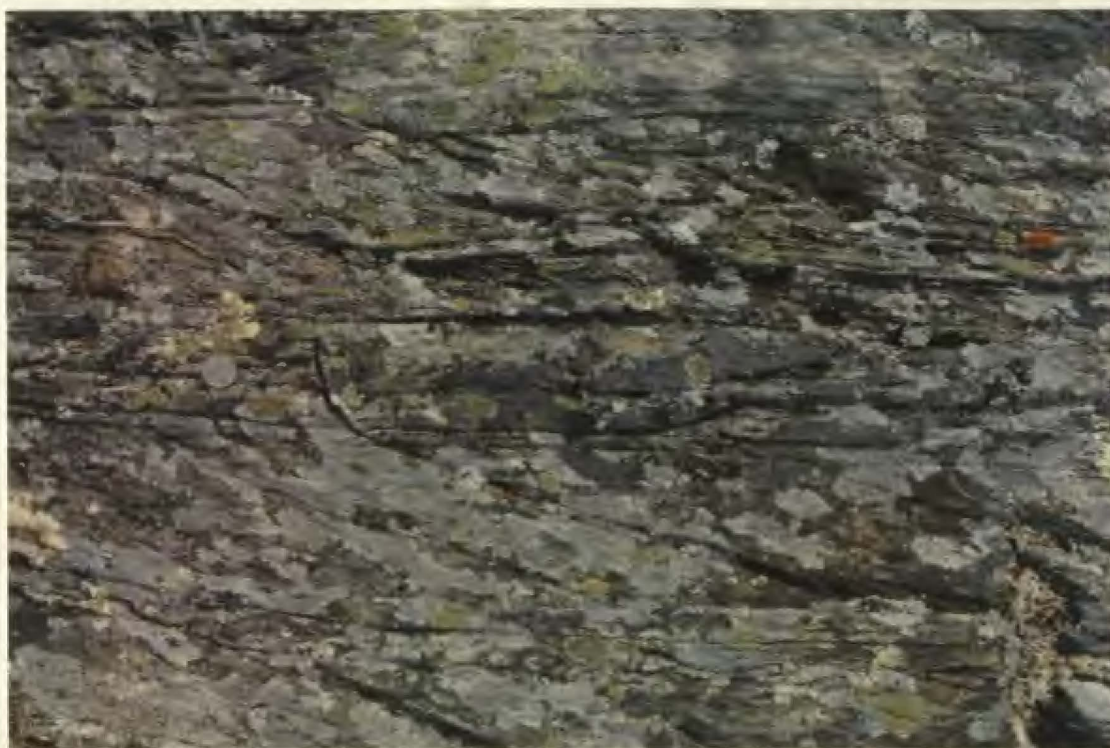


Plate 3-3. Photograph showing intersection between S_0 , S_1 and S_2 from the andalusite-biotite-muscovite zone. The $S_0 \parallel S_1-S_2$ intersection lineation has an orientation of $221^\circ/40^\circ$. Note displacement of $S_0 \parallel S_1$ along S_2 at top of photo and distinction of S_0 and S_1 on F_1 fold limb (quarter for scale). Location SD-89-382.



Plate 3-4. Photograph of F_2 folds folding $S_0 \parallel S_1$ (from the andalusite-biotite-muscovite zone). Location SD-89-012.

intersections between $S_0 \parallel S_1$ and S_2 . Figure 3-2 shows the large-scale F_2 folds defined on the basis of vergence of small-scale structures. At higher metamorphic grade, the F_2 folds are generally of smaller scale than those at lower grade, with wavelengths on the order of one metre and vergence is not consistent, so no larger fold structure has been interpreted.

Figure 3-3a is a plot of F_2 fold axes from Domain A and indicates that they are moderately to steeply plunging to the west-southwest; the point maximum has an orientation of $251^\circ/44^\circ$. F_2 fold axes from Domain B are also moderately to steeply plunging, but to the north-northeast and south-southwest; they display two maxima, one with an orientation of $034^\circ/61^\circ$, and a second with a possible orientation of $200^\circ/75^\circ$. These lie within the same great circle and may represent variable plunge in the same axial plane, or could possibly be explained by refolding.

The orientation of F_2 fold axial surfaces is shown in Figures 3-3c and 3-3d. Again, as with the fold axes, there is a significant change in orientation of the fold axial planes between the two domains. In Domain A (Figure 3-3c), the mean orientation of the axial surface is $079/74$ SE. The comparable orientation is $019/69$ SE in Domain B (Figure 3-3d).

In Domain A, the orientation of F_2 folds and sense of vergence from $S_0 \parallel S_1$ - S_2 intersections indicates that a

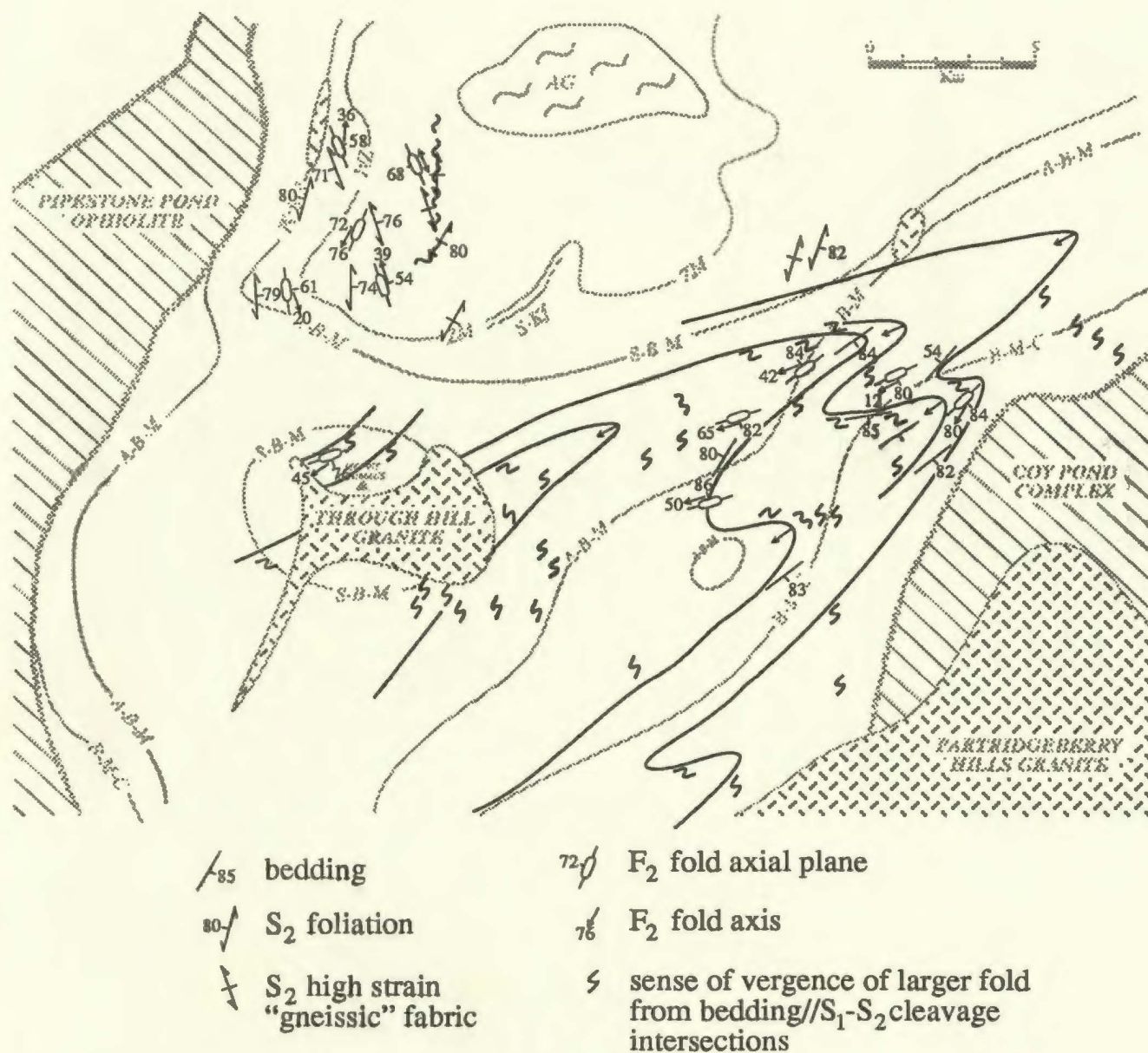


Figure 3-2. Map of large synformal structure (modified from Colman-Sadd, 1985) within the MCSZ (determined from bedding \parallel S_1 - S_2 cleavage intersections and vergence of F_2 fold axes). Measurements from Domain B are shown for comparison. Plunge direction given by arrows in fold hinges. Plunge varies from about 80-40° to the southwest.

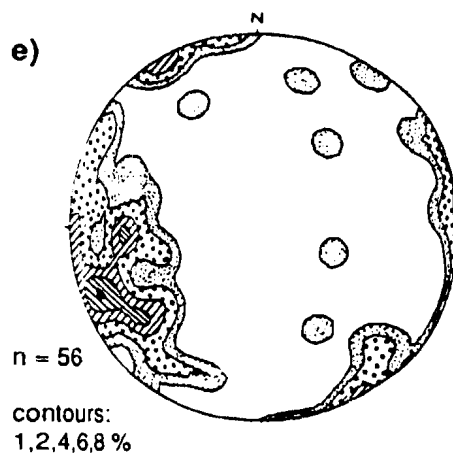
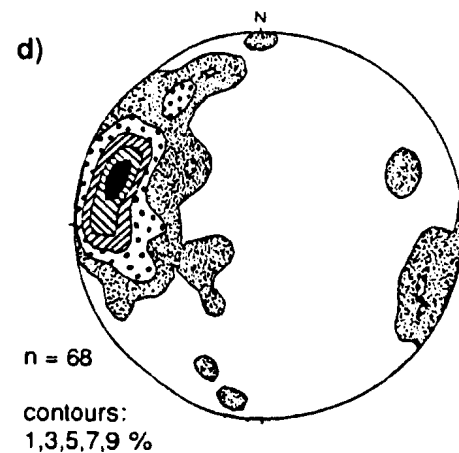
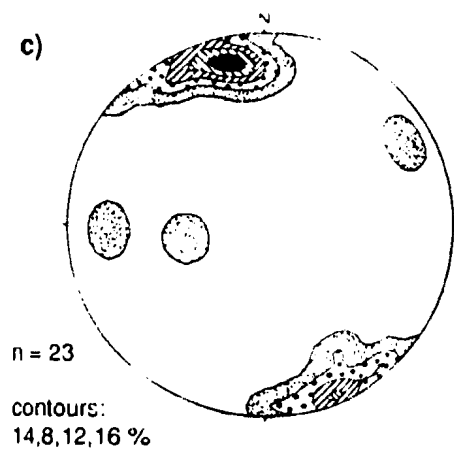
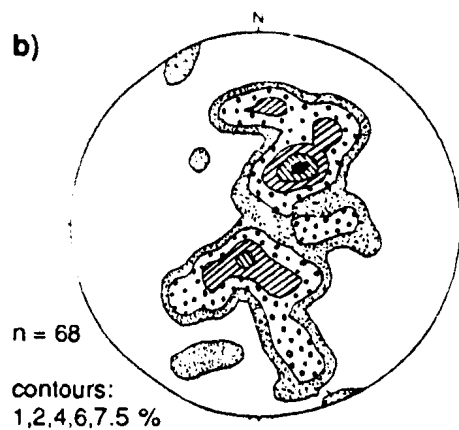
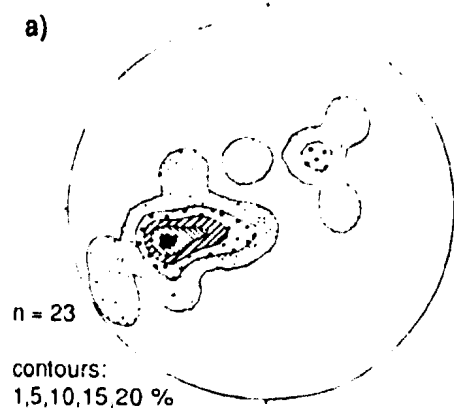


Figure 3-3. Contoured equal area stereonet plots from the MCSZ. a) plot of F_1 fold axes (Domain A); b) plot of F_2 fold axes (Domain B); c) plot of poles to F_2 fold axial planes (Domain A); d) plot of poles to F_2 fold axial planes (Domain B); e) plot of high strain fabric (Domain B).

large-scale synform occurs in this area (Figure 3-2) collaborating the interpretation of Colman-Sadd (1985).

3.2.5 D₁ Deformation

Figure 3-4 shows the trends of S₁ foliation and F₁ fold axes throughout the MCSZ obtained from tracing form lines; S₁ form lines are axial planar to the large F₁ synform just discussed, and are approximately parallel to the boundaries of the subzone. Dips of S₁ are steep and mostly outwards toward the boundary. Representative orientations of F₁ fold axes indicate a plunge reversal of F₁ folds between the southwestern and northeastern parts of the MCSZ. This implies that the MCSZ has an overall domal form, in agreement with the observations of Colman-Sadd (1985). Formation of the dome post-dated the S₁ foliation. In detail, it is clear that the S₁ form lines are truncated at the boundary of the MCSZ in several locations, implying the existence of late (post-S₁ foliation) faulting around the margins.

Just northwest of the THG, traces of S₁ foliation appear to intersect near the boundary of the subzone (Figure 3-4). The reason for this was not defined during the present study. If the interpretation of the trend lines is correct, it may imply the existence of a fault, or alternatively it may be due to tightening of the S₁

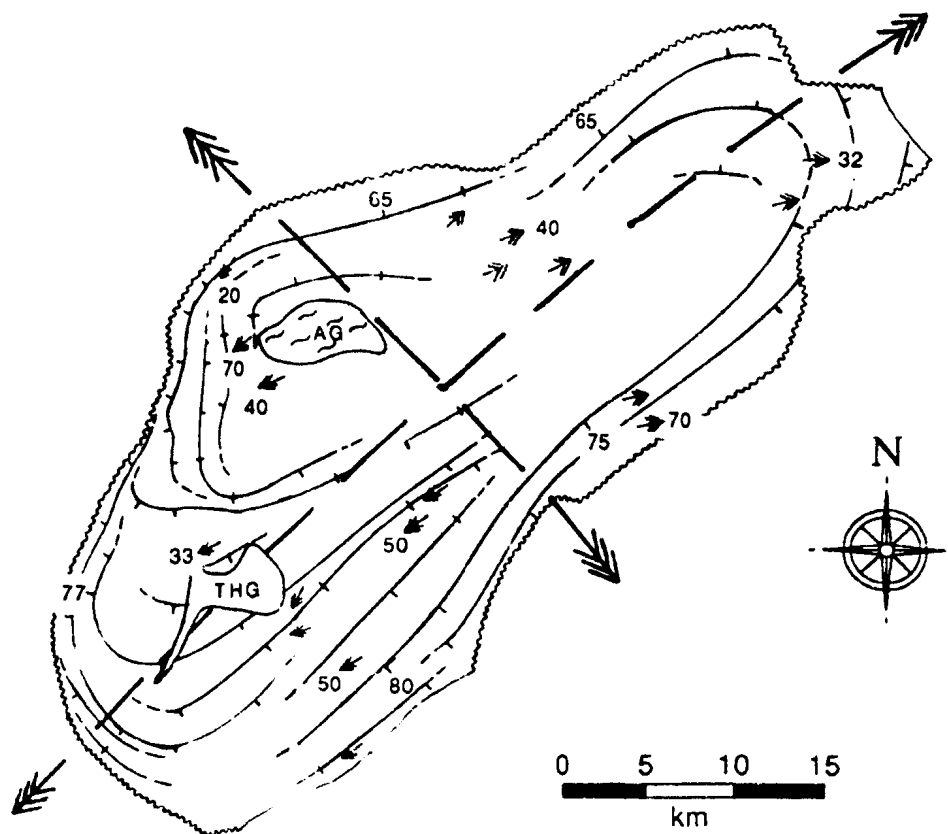


Figure 3-4. Trends of S_2 foliation from the MCSZ with dip direction, along with F_2 fold axes (double arrows). The majority of measurements of S_2 dip outward and are concentric around the centre of the terrane. Measurements taken from the present study and: Colman-Sadd and Russell, 1981; Colman-Sadd, 1982; 1985; and Swinden, 1988. Triple arrows are schematic F_3 fold axes.

foliation, which is known to occur just north of this area (see next section).

The dome shape defined by the S_2 form lines implies that S_2 was originally sub-horizontal and that post- F_2 folding about axes shown schematically on Figure 3-4 (triple arrows) has given rise to the dome. Evidence of this was not seen in small-scale structures in the field, and it is interpreted only on the basis of the orientation of S_2 surfaces. No fabric was seen that could be associated with the late doming.

3.2.6 High Strain Fabric

This fabric, defined by the alignment of platy minerals (i.e. muscovite and biotite) and flattening of others, is interpreted to be equivalent to the S_2 fabric mapped in Domain B, but is developed in areas of greater strain. The main occurrence is in a large north-trending vertical shear zone north of the Through Hill Granite (Figure 3-2) which outcrops over a strike length of about five kilometres. This ductile shear or mylonite zone is up to ~ 200 m wide in the north. To the south, the orientation of this shear zone changes, becoming more east-west. It is in this area that a syn-metamorphic granite (described in Chapter 2) occurs (see Geological Map). This granite is foliated, and contains recrystallized quartz and fractured feldspar grains indicating that it formed prior to or during

the deformation that caused the shearing. Abundant quartz veining is also present and the veins are commonly stretched and boudinaged (Plate 3-5).

On a contoured stereonet plot of poles to high strain fabrics (Figure 3-3e), the pattern is approximately the same as that of S_2 foliation from Domain B (Figure 3-1c). Although the point maximum is more diffuse than that in Figure 3-1c, it is similar in orientation, indicating that the high strain fabric has an overall orientation of ~ north-south and dips steeply to the east (Figure 3-3e and Plate 3-6).

3.3 Timing of Events

The first phase of deformation (D_1) formed small-scale F_1 isoclinal folds in the SBF and a penetrative S_1 -cleavage sub-parallel to bedding (S_0). It is inferred that these structures formed during the initial thrusting event which emplaced the ophiolitic rocks of the Dunnage Zone on to the SBF, although there is no conclusive evidence of this.

The second phase of deformation (D_2) formed small- and large-scale folds throughout the SBF and an S_2 -cleavage inclined to the D_1 structures. The orientation of F_2 folds was probably initially sub-horizontal and their formation was probably also related to the ophiolite emplacement and subsequent thickening of the two-layer crust in response to



Plate 3-5. Photograph of shear zone north of the Through Hill Granite showing stretched and boudinaged quartz veins. Location SD-89-096.



Plate 3-6. High strain fabric in migmatitic gneisses (knife handle is 10 cm in length). Note lenses of low strain with sigmoidal S-fabric surrounded by higher strain C-surfaces. Location SD-89-033.

continued shortening. D_1 and D_2 may have formed part of a single progressive deformational event.

A third stage of deformation (D_3) caused the observed pattern of S_2 structures throughout the MCSZ (i.e. structural doming). Second deformation structural data from the present study have been separated into two domains on the basis of orientation (see Structural Map). D_3 structures (i.e. F_2 folds, F_2 fold axes, S_2 foliation and L_2 intersection lineations) of Domain A show an overall northeast-southwest orientation whereas those of Domain B are orientated approximately north-south. These two structural domains appear to lie on opposite sides of a major elongate structural dome.

The overall domal pattern of S_2 foliation shown in Figure 3-4 may have developed in either two separate events, or a single event with subhorizontal shortening in two directions. No evidence was found in this study to discriminate between these two possibilities. However, tightening of S_2 (and formation of high strain gneisses) in the northwest of the study area may have been a result of this deformation event. The fact that the S_2 structures are truncated by the ophiolites suggests that the contact between the two became reactivated, possibly during this third stage of deformation (or during later extension).

Granite emplacement within the SBF occurred after the D_1 deformational phase and may have been associated with

or post-dated the D_2 deformation. The small granite body within the shear zone north of the Through Hill Granite was probably pre-or syn- D_2 as it displays evidence of deformation. The Through Hill Granite (THG and associated intrusions) is a relatively undeformed granite which post-dates D_2 since it cross-cuts the deformed D_2 structures. The cordierite granodiorite, inferred to have formed from partial melting of the SBF, is also undeformed indicating crystallization after D_2 . However, other areas in the SBF show zones of partial melting that have been deformed. Hence, partial melting within the SBF is inferred to have occurred during the D_2 phase of deformation, with crystallization in the latter stages or immediately following this event. Partial melting of the THG occurred deeper than the present erosion level, whereas for the cordierite granodiorite and migmatites, partial melting was approximately at the present erosion level.

3.4 Interpretation

The overall domal pattern of the MCSZ developed during three stages of deformation. F_1 folds are rare and the D_1 event is typically defined by a fine-scale foliation (S_1) nearly parallel to bedding (S_0). D_1 may have been associated with obduction of the tectonically overlying ophiolite.

The second stage of deformation, as mentioned above, may have occurred during continued shortening and thickening of the two-layer crust in response to the shortening. A penetrative S_2 foliation is axial planar to small- and large-scale F_2 folds. Subsequently, a third stage of deformation caused structural, and probably associated thermal, doming of the SBF resulting in the observed domal pattern. This may have also caused reactivation of the thrust contact between the SBF and the ophiolite as the D_2 structures are truncated along the boundary of the MCSZ.

In the following chapter, metamorphic reaction isograds are discussed; these cross-cut the D_2 structures in the SBF and are possibly related to thermal doming after the D_2 deformation.

CHAPTER 4

MINERALOGY, REACTION ISOGRADS AND MINERAL CHEMISTRY

4.1 Introduction

This chapter includes descriptions of the mineralogy (stable mineral assemblages) of each metamorphic zone within the Mount Cormack Subzone (MCSZ) and interpretation of the reactions occurring at (and between) each metamorphic isograd. This is followed by an examination of the mineral chemistry (where available, from microprobe analyses) of the metasedimentary rocks within the MCSZ. Petrographic descriptions of each metamorphic zone are given (with representative sample descriptions), and the remainder of the sample descriptions are listed in Appendix A. In all cases, the samples were stained for K feldspar by the method of Hutchison (1974). In addition to the author's descriptions, sample descriptions of Colman-Sadd (1985) are referred to, where necessary, either to corroborate the author's data or to give information on areas not sampled during this study.

The approximate location in P-T space of each reaction can be plotted (from published literature), along with locations of samples with appropriate assemblages; this information leads to a qualitative P-T grid as well as

defining the approximate range of P-T conditions within the MCSZ. In addition to defining specific metamorphic reaction isograds, other reactions are used to define metamorphic bathograds to determine the depth of formation of the metasedimentary rocks (and, hence, the amount of post-metamorphic uplift).

The main emphasis of the following descriptions is on the prograde assemblages. However, there is a rather pervasive partial retrogression to chlorite, muscovite, quartz, \pm feldspar at all metamorphic grades.

4.2 Metamorphic Zones

Rocks of the MCSZ are divided into metamorphic zones on the basis of mineral assemblage. Colman-Sadd (1985) defined these zones on the basis of individual indicator minerals, i.e. chlorite zone, biotite zone, garnet-staurolite-andalusite zone and sillimanite zone, culminating in a zone of melting (migmatization) and the formation of gneisses.

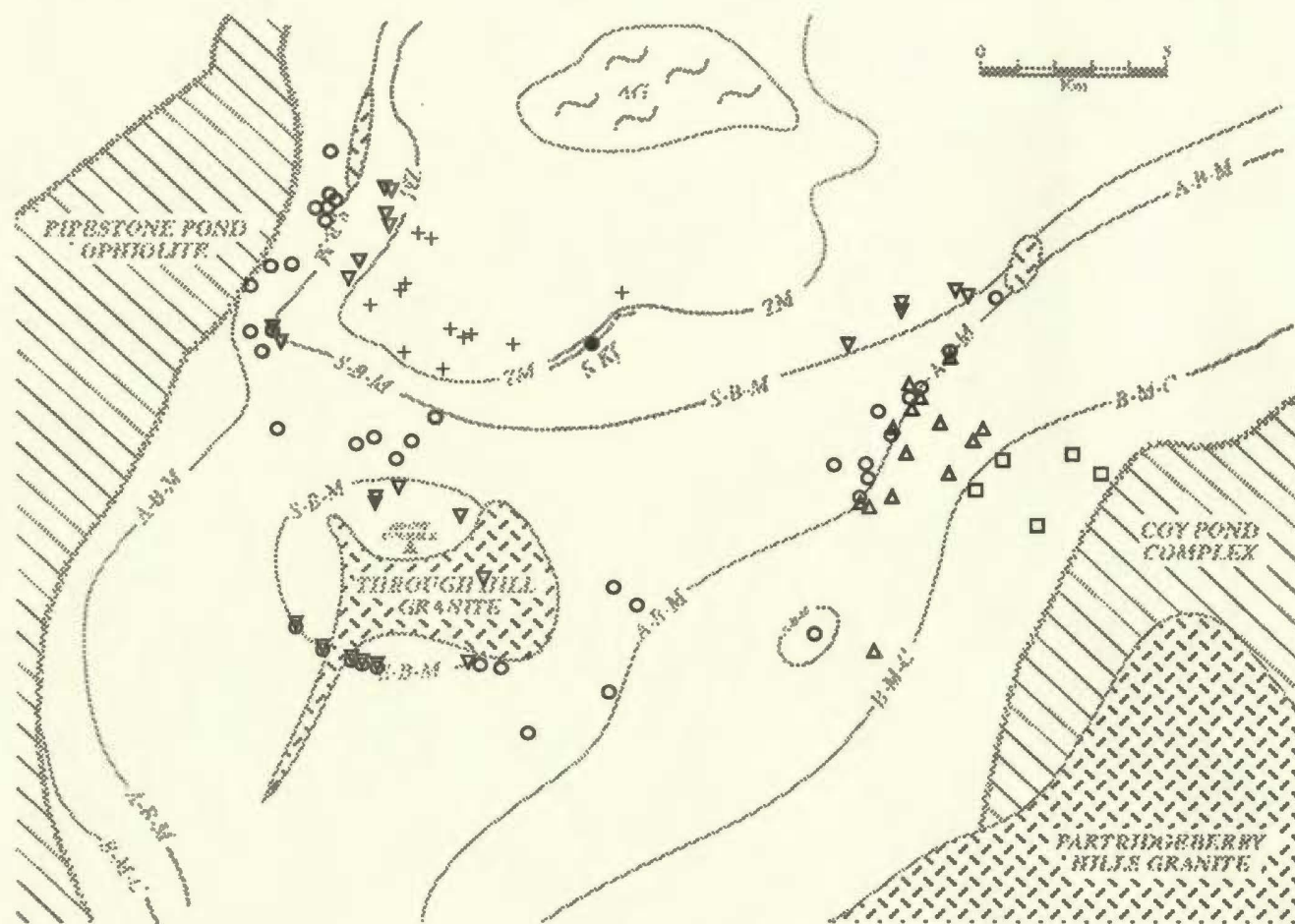
In this study, each metamorphic zone has been defined by the stable mineral assemblage within it. Following this scheme, the metamorphic zones within the MCSZ are, with increasing metamorphic grade; the chlorite-muscovite zone, the biotite-muscovite-chlorite zone, the andalusite-biotite-muscovite zone, the sillimanite-biotite-muscovite zone, the sillimanite-K feldspar zone and the zone

of melting (partial melting and the formation of migmatite). The boundary of each zone is indicated by a reaction isograd defined by a specific metamorphic reaction. The locations of the reaction isograds, which are shown on Figure 4-1 (along with location of samples used to define them), are only slightly modified from the locations of the "first appearance" isograds of Colman-Sadd (1985) and are examined in detail in Section 4.3.

4.2.1 Chlorite-Muscovite Zone

Rocks of the chlorite-muscovite zone are the lowest-grade rocks in the area. They occur along the northeastern, eastern and southern margins of the MCSZ but are absent from the western margin, where biotite and andalusite grade rocks are in contact with the Pipestone Pond Complex (Figure 4-1).

In terms of mineralogy, the stable mineral assemblage within the pelitic portion of the SBF in this zone is quartz-muscovite-chlorite±plagioclase. The samples consist of approximately equal amounts of quartz and muscovite (~ 40 % each), 15 % chlorite, 5 % Fe(-Ti) oxides and/or graphite, plagioclase (minor when present) and accessory zircon, epidote and tourmaline. Discrimination between quartz and plagioclase in these fine grained rocks is difficult, although in some cases (samples SD-89-320 and -325), plagioclase with well developed albite twinning



mineral assemblages

- | | |
|---------------------------------------|---|
| □ chlorite-muscovite-quartz | ▽ sillimanite-biotite-muscovite-quartz |
| ▲ biotite-chlorite-muscovite-quartz | ● sillimanite-K-feldspar-biotite-quartz |
| ○ andalusite-biotite-muscovite-quartz | + leucosome in metasedimentary rocks |

Figure 4-1. Distribution of samples with mineral assemblages appropriate for reaction isograds mapped. Where no samples were taken, the isograds are taken from Colman-Sadd, 1985. B-M-C = biotite-muscovite-chlorite reaction isograd; A-B-M = andalusite-biotite-muscovite reaction isograd; S-B-M = sillimanite-biotite-muscovite reaction isograd; S-Kf = sillimanite-K feldspar reaction isograd; ZM = zone of partial melting; and AG = amphibolite-bearing gneisses.

occurs as 0.05 mm xenoblastic grains (Plate 4-1). Many of these grains (i.e. quartz and plagioclase in Plate 4-1) appear to be detrital in origin.

4.2.2 Biotite-Muscovite-Chlorite Zone

Rocks of the biotite-muscovite-chlorite zone define an area that is nearly concentric with the margin of the MCSZ except to the west where the zone is cut off by rocks of the Pipestone Pond Complex (Figure 4-1). This zone is widest in the east reaching a maximum width of nearly five kilometres.

The mineralogy of the pelitic units is similar to the chlorite-muscovite zone except that biotite is present, and chlorite is reduced in abundance. Detrital quartz and feldspar can still be recognized. Garnet appears locally, but is not sufficiently widespread to define a separate garnet zone. Five stable mineral assemblages are represented in different samples (all with quartz and muscovite):

- biotite-chlorite
- biotite-garnet
- chlorite-garnet
- biotite-chlorite-garnet
- plagioclase

This last assemblage is rare occurring in only one of sixteen samples. The rocks consist of approximately equal amounts of quartz/plagioclase and muscovite (30 % and 35 % respectively), 25 % biotite, 5 % chlorite, and 5 % opaque

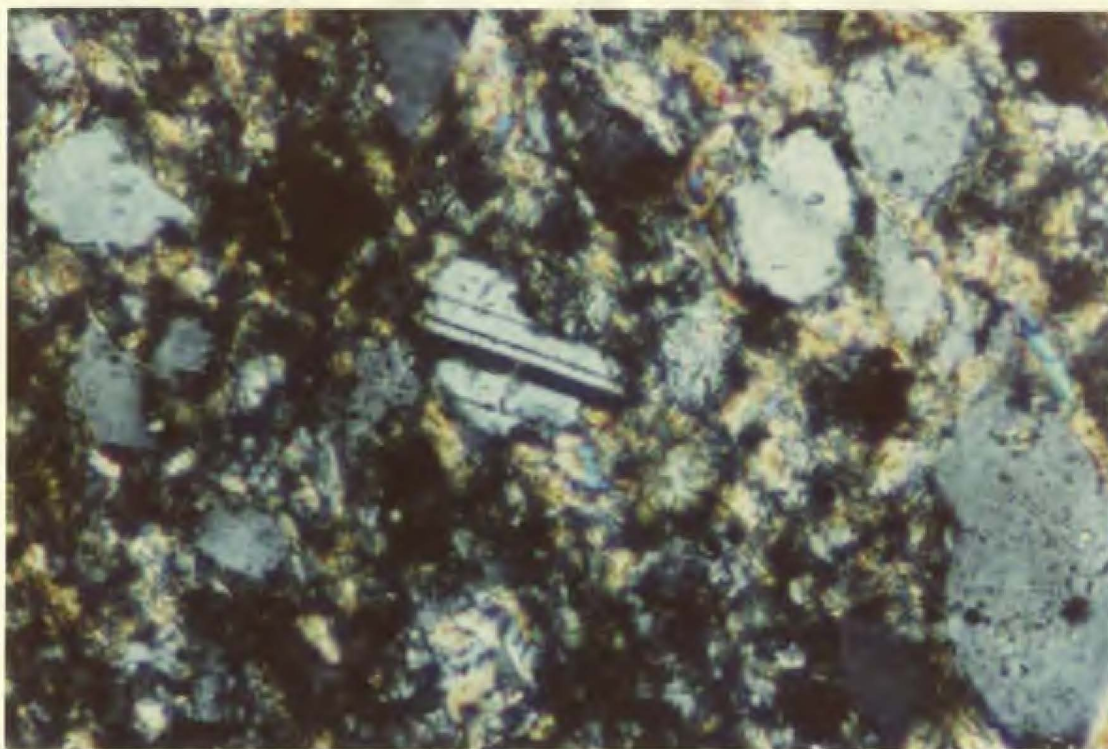


Plate 4-1. Albite twinning in plagioclase in sample SD-89-325 from the chlorite-muscovite zone. Xpl., plagioclase grain is 0.1 mm across.



Plate 4-2. Outcrop of schist containing large porphyroblasts of andalusite, southeast of the Through Hill Granite (sample SD-89-379).

minerals. Biotite commonly occurs as subidioblastic porphyroblasts ranging in size up to 5 mm. The opaque minerals consist of two phases; subidioblastic grains of magnetite up to 1 mm in size, and minute (0.01 mm) xenoblastic grains which are probably graphite. Tourmaline, zircon and apatite form accessory phases. Although plagioclase is almost certainly present in all samples, in only two samples (SD-89-244 and -246a) does it show albite twinning. K feldspar was noted in one sample (SD-89-272).

Garnet occurs in two samples (SD-89-252 and -272), the latter of which is located just above the biotite-muscovite-chlorite reaction isograd. This is lower grade than reported by Colman-Sadd (1985), who stated that the first appearance of garnet occurs "... in the higher grade part of the biotite zone, southeast of the andalusite isograd." Garnet in sample SD-89-272 consists of 0.2 mm subidioblastic porphyroblasts which have a poikilitic texture. These grains comprise about 1-2 % (by volume) of the sample. In contrast, sample SD-89-252 contains approximately 5 % garnet consisting of 0.05 mm idioblastic grains which are free of inclusions. These are stable with biotite, quartz and muscovite.

Pseudomorphs of cordierite have been found in sample SD-89-267 from the high grade part of this zone, northeast of the Through Hill Granite. They occur in a biotite-chlorite-garnet-quartz-muscovite assemblage. In

this sample, the pseudomorphs are green, elongate and have an ovoid structure in three dimensions. In thin section they consist of fine grained aggregates of muscovite, quartz, chlorite and opaque minerals.

4.2.3 Andalusite-Biotite-Muscovite Zone

A number of stable mineral assemblages is represented in this zone, with individual samples commonly consisting of more than one equilibrium assemblage on account of compositional layering. The following is a list of stable mineral assemblages (all with quartz and muscovite):

- andalusite-biotite
- andalusite-biotite-garnet
- andalusite-biotite-staurolite
- andalusite-staurolite
- biotite-staurolite-garnet
- biotite-garnet
- biotite
- biotite-plagioclase
- cordierite-biotite-chlorite-magnetite

These rocks typically contain a groundmass of quartz and plagioclase (25-40 %) and muscovite (15-30 %); the quartz and plagioclase consist of 0.1 mm xenoblastic grains and muscovite occurs as 0.2 mm subidioblastic grains. However, quartz also forms veins up to 5 mm in thickness, and muscovite locally occurs as xenoblastic grains up to 2 mm in size. Biotite typically occurs as 0.1 mm xenoblastic grains (15-30 %), but also as subidioblastic porphyroblasts up to 5 mm in size. These contain inclusions of zircon and

opaque minerals. Chlorite is present (up to 15 % in some samples) and is retrograde after biotite.

Porphyroblast growth is quite extensive in this zone, with the porphyroblasts occurring predominantly in the pelitic and semipelitic layers (Colman-Sadd, 1985). Andalusite porphyroblasts are commonly xenoblastic and up to 1 cm long in cross section, but also occur as prismatic grains up to 3 cm in length (Plate 4-2). Poikiloblastic texture is common, with inclusions of quartz, muscovite, biotite, garnet and graphite. Some andalusite grains contain randomly oriented inclusions (Plate 4-3) whereas others contain inclusions which appear to be continuous with the external fabric (Plate 4-4). In some cases, the porphyroblasts are free of inclusions (Plate 4-5).

Garnet occurs locally as subidioblastic porphyroblasts up to 2 mm in size that contain inclusions of quartz, biotite and opaque minerals. In hand sample, garnets are bright red in colour. They are commonly wrapped by muscovite and have pressure shadows of muscovite, biotite and retrograde chlorite. As in the biotite-muscovite-chlorite zone, garnet is not extensive enough to map as a separate zone (Figure 4-2). Staurolite is locally present and forms idioblastic porphyroblasts up to 1 cm in size, which are poikiloblastic and commonly twinned (Plate 4-6). The inclusion minerals are quartz, biotite, Fe(-Ti) oxides and garnet. Like andalusite, these porphyroblasts also show

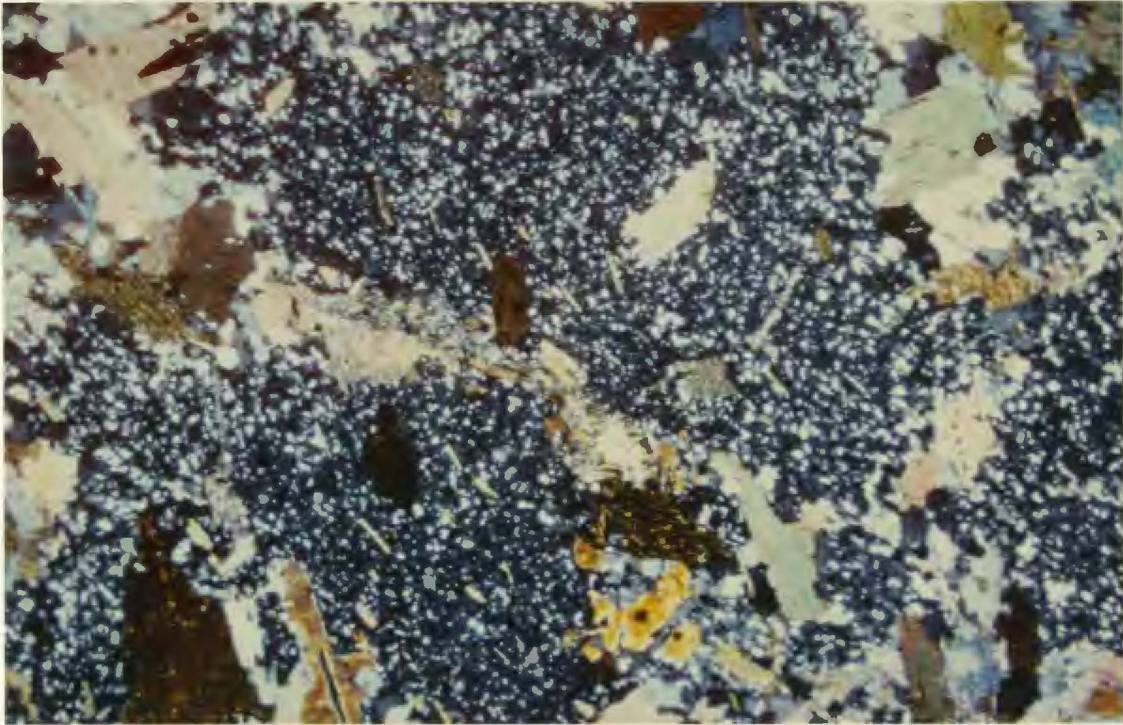


Plate 4-3. Randomly oriented inclusions in andalusite, sample SD-89-371. Xpl., photo is 6 mm wide.



Plate 4-4. Traces of inclusions in andalusite parallel to the external fabric, sample SD-89-097a. Xpl., photo is 6 mm wide.

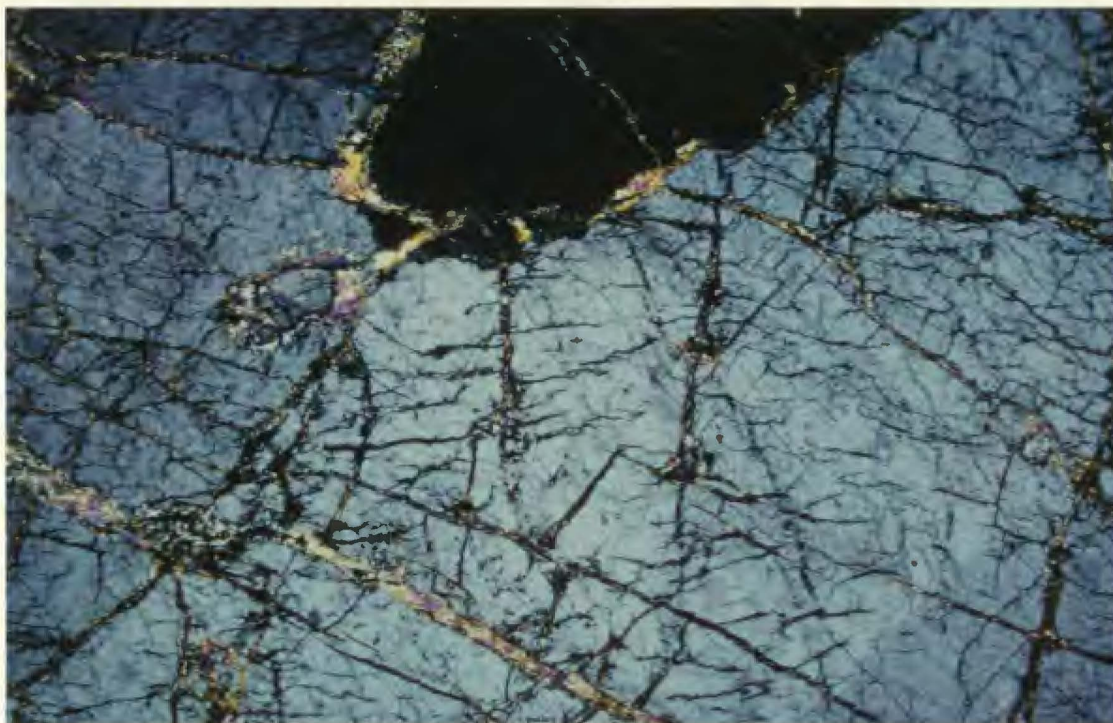


Plate 4-5. Inclusion-free andalusite grains adjacent to the Pipestone Pond Ophiolite (sample SD-89-195b). Xpl., photo is 6 mm wide.

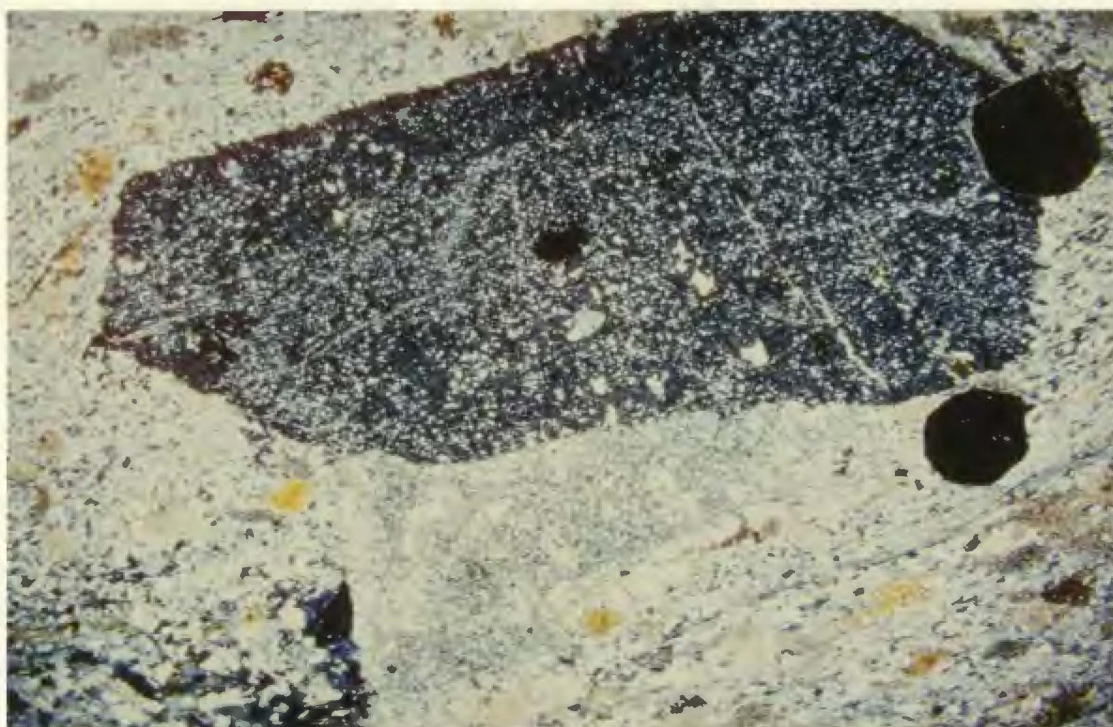
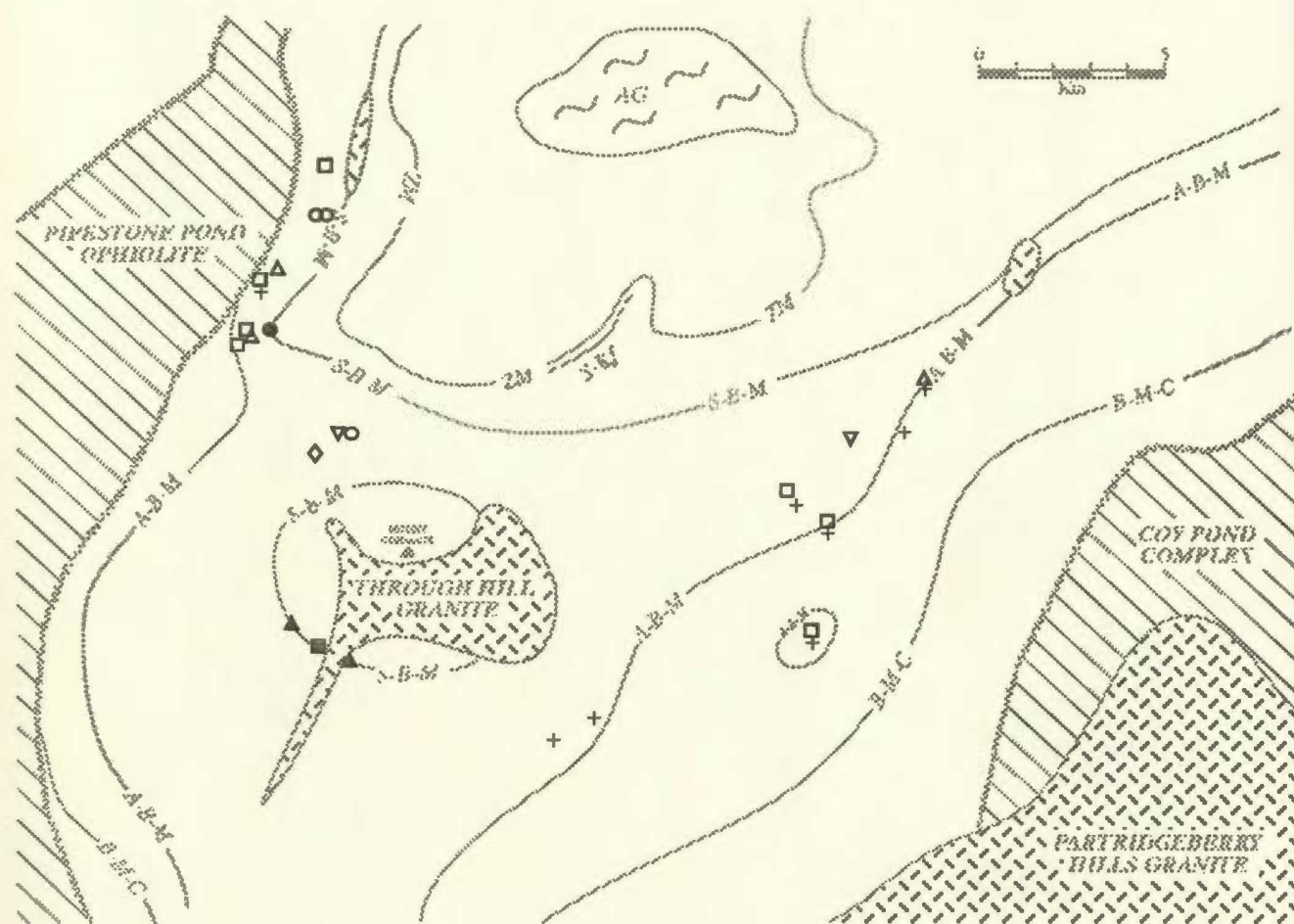


Plate 4-6. Twinned staurolite grains, sample SD-89-046b. Xpl., staurolite grain in extinction is 8 mm in length.



mineral assemblages (+ biotite + muscovite + quartz)

* filled symbols indicate sillimanite present in assemblage

- | | |
|--------------------------------|---------------------------|
| □ andalusite-garnet | ▽ garnet-staurolite |
| △ andalusite-staurolite | ◇ staurolite |
| ○ andalusite-staurolite-garnet | + cordierite pseudomorphs |

Figure 4-2. Location of samples containing garnet, staurolite or cordierite (with or without an aluminosilicate phase). Cordierite pseudomorphs occur in biotite-muscovite-quartz schists which invariably contain andalusite, staurolite and/or garnet.

evidence of overprinting an earlier deformational event. Staurolite typically alters to fine grained muscovite and, in some cases, this alteration is quite extensive (Plate 4-7). Like garnet, staurolite is also limited in abundance and a separate staurolite zone was not mapped.

Relict cordierite is found in four locations in the andalusite-biotite-muscovite zone: northeast of the Through Hill Granite; adjacent to the Pipestone Pond Complex (northwest of the Through Hill Granite); and southeast and east of the Through Hill Granite (Figure 4-2). In all locations it appears to be spatially associated with the andalusite-biotite-muscovite reaction isograd. In most cases, the relict cordierite porphyroblasts are xenoblastic and have been completely replaced by quartz, muscovite and chlorite (Plate 4-8). However, in two locations, minor amounts of cordierite were found in the centres of the porphyroblasts. In these cases, the porphyroblasts are dark green in hand sample (Plate 4-9) and preserve the pseudo-hexagonal crystal form typical of cordierite (Deer et al., 1966).

In some of the samples, cordierite porphyroblasts preserve a pseudo-zoning defined by the distribution of the replacement minerals (see Plate 2-2, sample SD-89-267); the centres consist of fine grained muscovite and quartz and the rims consist of coarser grained quartz, muscovite and chlorite. These porphyroblasts occur in schists with an

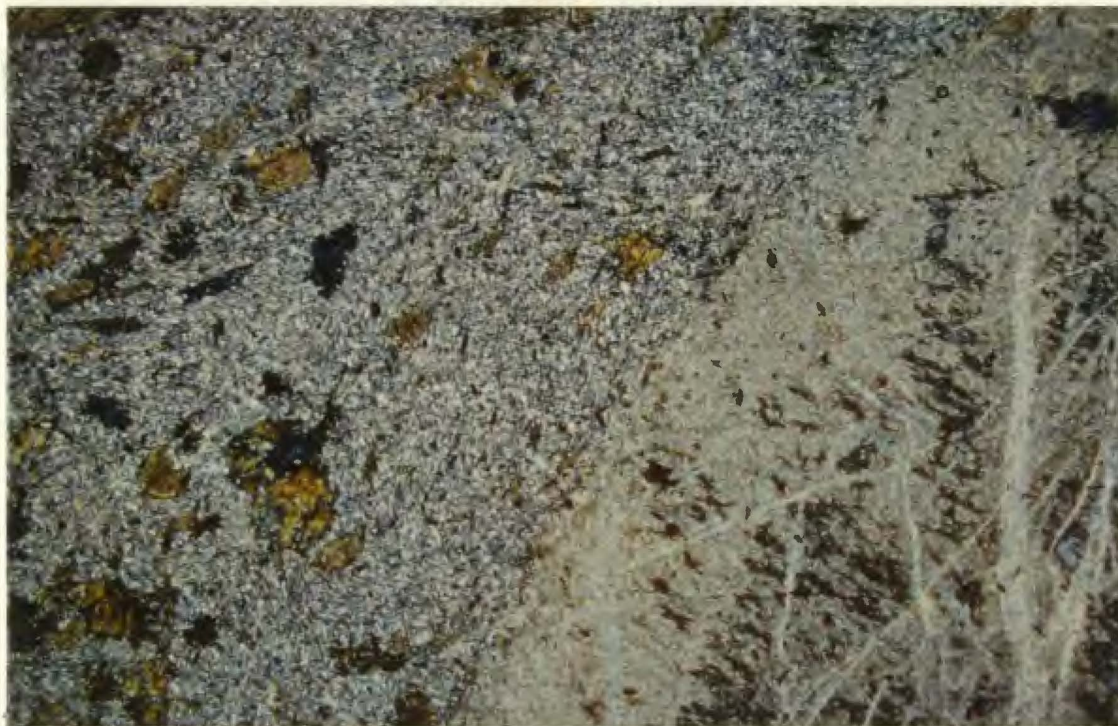


Plate 4-7. Staurolite (right side of photo) extensively altered to fine grained muscovite, sample SD-89-086. Xpl., photo is 6 mm wide.



Plate 4-8. Cordierite-bearing biotite-muscovite-quartz-magnetite schist from the andalusite-biotite-muscovite zone. Sample SD-89-388.



Plate 4-9. Sample SD-89-299 containing large poikiloblasts of cordierite and abundant magnetite.



Plate 4-10. Outcrop from sillimanite-biotite-muscovite isograd showing coexisting andalusite (large irregular shaped porphyroblasts) and sillimanite (Si) (fibrous zones within andalusite). Sample SD-89-371.

elevated content of magnetite in the matrix (Plate 4-9) which gives rise to local magnetic anomalies (Chapter 6).

Opaque minerals occur throughout the andalusite-biotite-muscovite zone (generally less than 5 %) and typically consist of more than one phase. Graphite occurs in the matrix as xenoblastic grains up to 0.02 mm in size, reaching 0.1 mm where they form inclusions in andalusite. Subidioblastic grains of ilmenite are common throughout the zone (qualitative SEM identification). In addition, as mentioned above, magnetite occurs in association with cordierite (where it comprises up to 10 % of the sample) and typically forms idioblastic grains up to 2 mm in size.

4.2.4 Sillimanite-Biotite-Muscovite Zone

Rocks of the sillimanite-biotite-muscovite zone occur in two areas; a small area surrounding the Through Hill Granite and a larger area to the north.

The stable mineral assemblages preserved in rocks of this zone are (all with quartz and muscovite):

- sillimanite-biotite-plagioclase
- sillimanite-biotite
- sillimanite-biotite-garnet-plagioclase
- sillimanite-biotite-garnet-plagioclase-staurolite
- biotite-garnet-plagioclase
- biotite

Sillimanite and andalusite are stable together at the reaction isograd (Plates 4-10 and 4-11). In terms of mineralogy, the rocks consist of three main phases. Quartz occurs as 0.5 mm xenoblastic grains which comprise 20-40 %

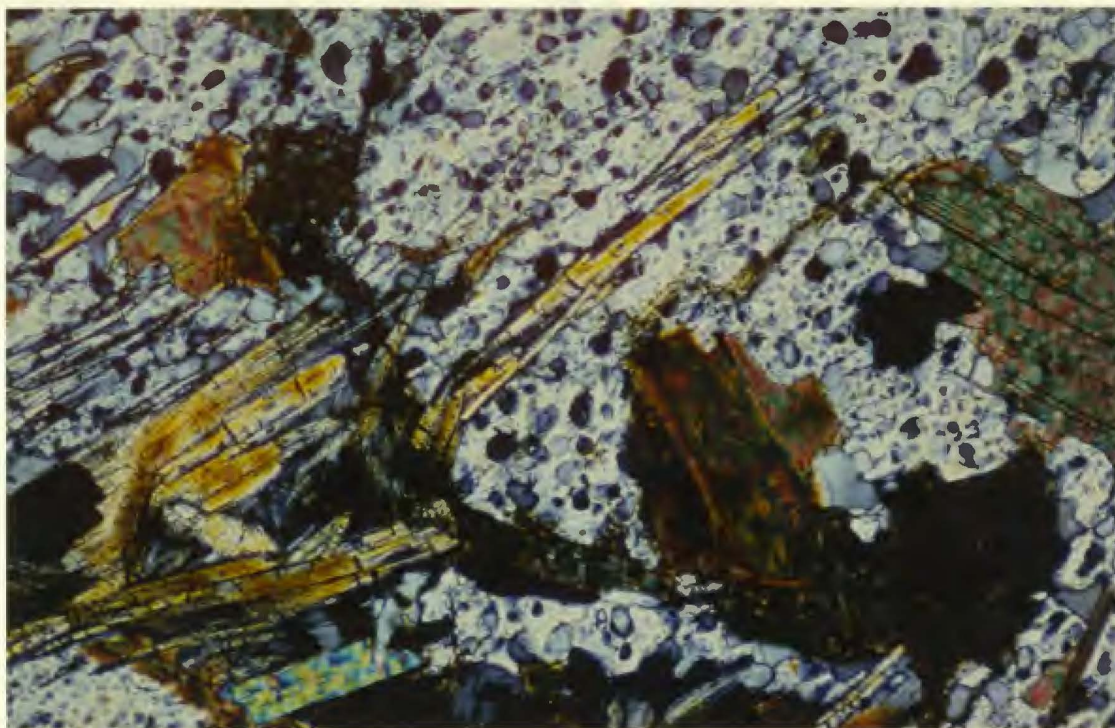


Plate 4-11. Sample SD-89-362 from the sillimanite-biotite-muscovite isograd showing prismatic sillimanite coexisting with andalusite. Xpl., photo is 6 mm across.

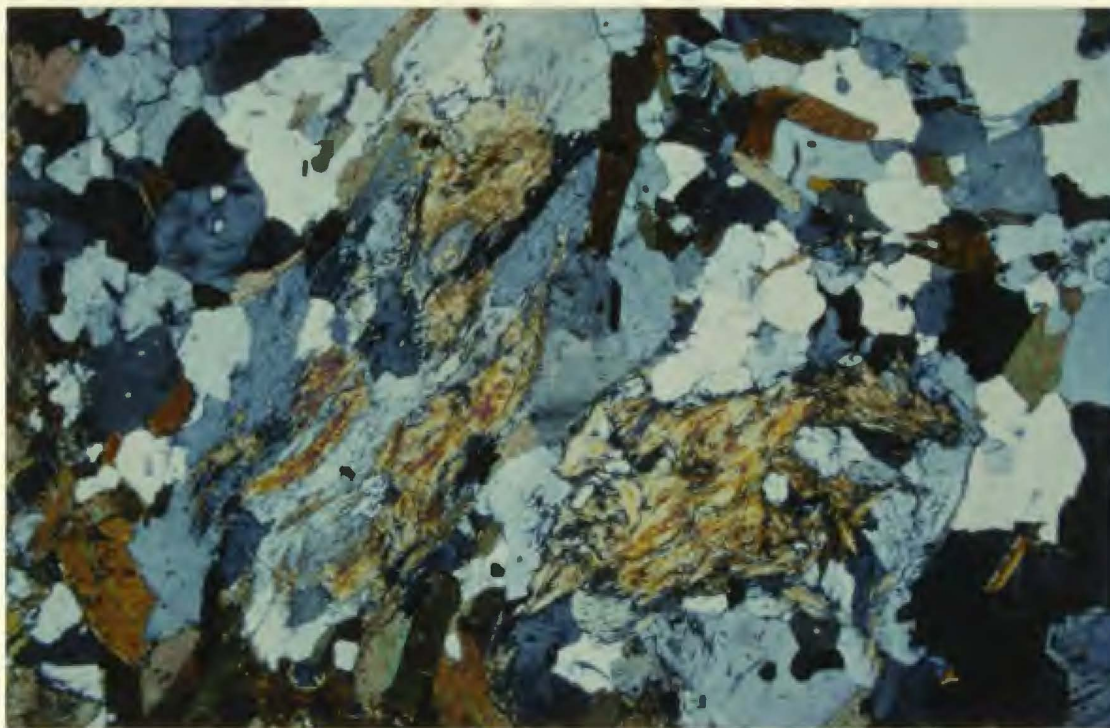


Plate 4-12. Turbid knots of fibrolitic sillimanite typical of the sillimanite-biotite-muscovite zone (sample SD-89-312). Xpl., photo is 6 mm wide. Other phases include quartz, plagioclase, biotite and an opaque phase (ilmenite?).

of the samples. Biotite comprises 15-30 % and consists of xenoblastic grains up to 1 mm in size. Minor chlorite is present (1-3 %) and is retrograde after biotite. Muscovite makes up 10-25 % of the samples and consists of elongate idioblastic grains up to 0.5 mm in length which define the foliation.

Garnet is present in approximately one third of the samples (in amounts < 10 %) as subidioblastic grains up to 3 mm in size. Sillimanite, comprising 5-15 % of the samples where present, occurs as either prismatic crystals or turbid knots of fibrolite (or both), the latter being more common (Plate 4-12). Opaque minerals are present in minor amounts (< 3 %) and occur as three phases: ilmenite (most common) which forms xenoblastic grains up to 0.5 mm; graphite, which forms xenoblastic grains up to 0.2 mm in size; and magnetite which forms idioblastic grains up to 2 mm in size. Cordierite, although not abundant in this zone, occurs as xenoblastic grains up to 5 mm in size, which are commonly pinitized (Plate 4-13) and characteristically display well developed yellow pleochroic haloes around inclusions of zircon. In some cases, cordierite shows evidence of reaction to sillimanite.

Plagioclase is relatively rare (< 10 % in isolated samples) in the lower grade part of this zone, but increases in abundance (> 20 %) as the metamorphic grade increases. This increase in plagioclase content may be due to bulk rock



Plate 4-13. Sillimanite nucleating on cordierite from sample G-123-80 from the sillimanite-K feldspar zone. Ppl., photo is 1.5 mm wide.



Plate 4-14. Sample SD-89-212 from the zone of partial melting showing pods of melt that have been disrupted by the F_2 folding.

compositional changes, or due to partial melting of the metasedimentary rocks. Plagioclase generally forms xenoblastic grains about 0.2 mm in size which increase to ~ 0.5 mm blocky grains at higher grades. Albite twinning is common, and evidence of sericite alteration occurs at higher grades. Sillimanite inclusions have been observed in plagioclase locally. Staurolite is stable in the lowest-grade part of the sillimanite-biotite-muscovite zone in the western part of the map area just south of a small granitic intrusion (Figure 4-1). It is restricted to within 200 metres of the sillimanite-biotite-muscovite reaction isograd.

4.2.5 Sillimanite-K Feldspar Zone

The mineralogy of this zone is equivalent to the previous zone with the exception that primary muscovite is removed from the mineral assemblage and replaced by K feldspar and sillimanite. Secondary muscovite is present, however, and often preserves a foliation. At one location (sample G-123-80), primary muscovite coexists with K feldspar, cordierite, sillimanite, garnet and quartz. The stable mineral assemblages are (plus quartz and K feldspar):

sillimanite-biotite-plagioclase-garnet
sillimanite-biotite-cordierite-
garnet-plagioclase-muscovite.

4.2.6 Zone of Migmatization and Partial Melting

In the highest grade rocks above the sillimanite-biotite-muscovite zone, metamorphism has caused partial melting of the metasedimentary rocks and the formation of leucosomes, granitic pods and veins. Plate 4-14 shows a sample from this zone which displays layers of leucosome that have become deformed due to the F_1 folding.

In terms of mineralogy, the leucosomes are composed mainly of quartz and K feldspar with lesser amounts of plagioclase and biotite. In one location, partial melting has produced a dispersed cordierite granodiorite containing abundant inclusions of the unmelted (quartz-rich) schist. The mineralogy of this granodiorite (see Chapter 2) is consistent with derivation from the metasedimentary rocks that surround it. The schist consists of similar mineralogy to the sillimanite-biotite-muscovite zone.

4.3 Reaction Isograds

4.3.1 Definition of Reaction Isograd

Traditionally, a metamorphic isograd was defined on the basis of "first appearance" of certain metamorphic indicator minerals, which were generally porphyroblastic phases. Colman-Sadd (1985) used this approach in defining the isograds in the MCSZ. Carmichael (1970) defined *reaction isograds* from the spatial distribution of metamorphic mineral assemblages that represent the reactants

and products of balanced metamorphic reactions. This approach is used in this study to determine the specific reaction (or reactions) that define these metamorphic isograds within the MCSZ. The reaction isograds are named for the stable mineral assemblages on the high grade side of the reaction isograd.

4.3.2 Reaction Isograds in the Mount Cormack Subzone

Five reaction isograds have been defined which sub-divide the metamorphic gradient within the MCSZ (Figure 4-3). In order of increasing grade, they are; the biotite-muscovite-chlorite reaction isograd, the andalusite-biotite-muscovite reaction isograd, the sillimanite-biotite-muscovite reaction isograd, the sillimanite-K feldspar reaction isograd (defining the disappearance of prograde muscovite) and the "melting" isograd, or migmatization isograd that marks the start of partial melting. There are two spatially separate sillimanite-biotite-muscovite reaction isograds, one surrounding the Through Hill Granite and the other to the north surrounding the amphibolite-bearing gneisses.

In the following section, the reactions which occurred at each reaction isograd are evaluated. With the exception of the biotite-muscovite-chlorite reaction isograd (see below), mineral assemblages from both sides of the reaction isograds (and, where possible, directly from the

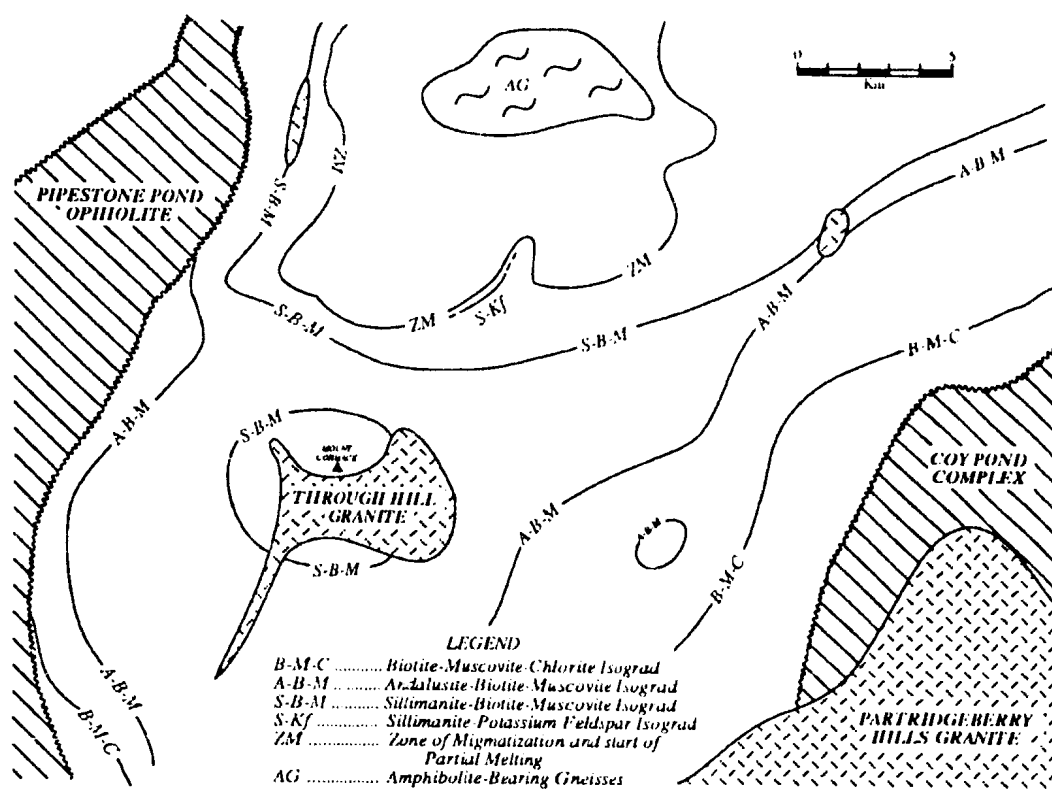
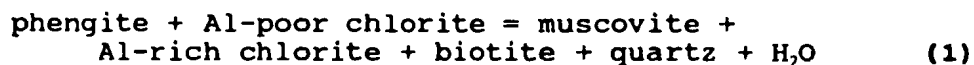


Figure 4-3. Generalized geological map of the MCSZ area showing the pattern of metamorphic reaction isograds (modified from Colman-Sadd, 1985).

reaction isograd) were examined to determine the nature of the reaction(s) that caused the change in mineralogy.

4.3.2.1 Biotite-Muscovite-Chlorite Reaction Isograd

The biotite-muscovite-chlorite reaction isograd (Figure 4-3) separates the chlorite-muscovite and biotite-muscovite-chlorite zones (Figure 4-4a,b). The main mineralogy of the chlorite-muscovite zone is chlorite-quartz-muscovite, with accessory Fe(-Ti) oxides; that of the biotite-muscovite-chlorite zone is biotite-chlorite-quartz-muscovite, also with accessory Fe(-Ti) oxides. The reaction isograd was not analyzed in detail in this study because the fine grain size of most minerals rendered them inaccessible under the electron microprobe system used. According to Colman-Sadd (1985), the biotite isograd is defined by the first appearance of biotite as an incipient replacement product of matrix chlorite. However, chlorite porphyroblasts are still stable. He inferred that if the matrix chlorite and porphyroblasts were of different composition, then a possible reaction for the appearance of biotite would be similar to that proposed by Kamineni and Carrara (1973):



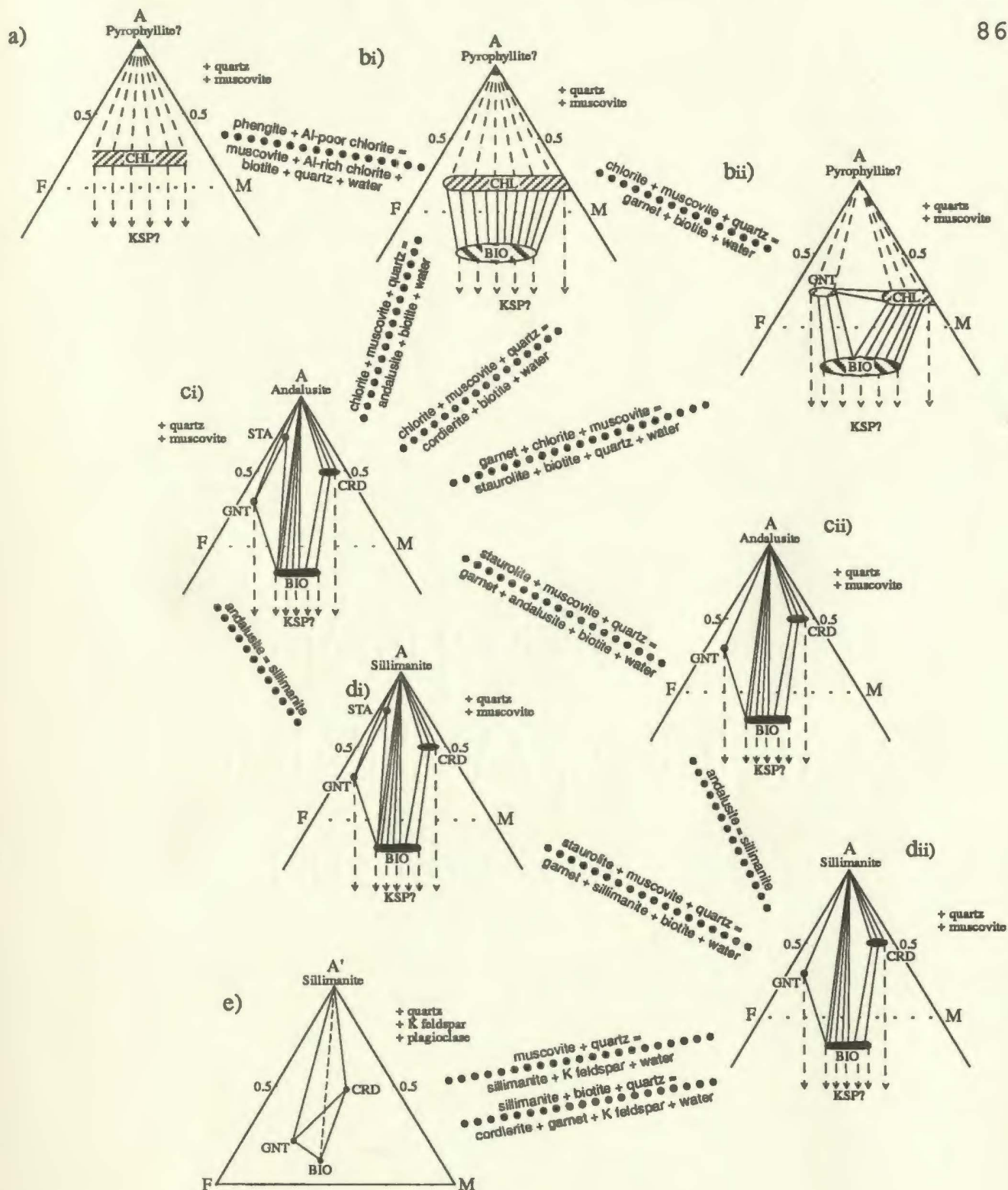


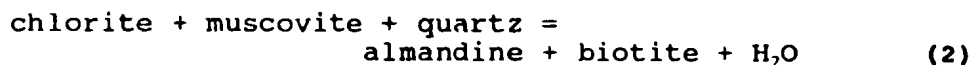
Figure 4-4. AFM (projected through muscovite) and A'FM (projected through K feldspar) diagrams (Thompson, 1957) for observed assemblages from the MCSZ showing the mineralogy of the metamorphic zones and the inferred reactions between each zone. Dashed lines indicate inferred phases (except in e).

Such an origin seems reasonable, but was not tested in this study.

Formation of Garnet

Garnet was found below the andalusite-biotite-muscovite reaction isograd in two locations (sample SD-89-252 and SD-89-272). The first of these samples occurs just below the andalusite-biotite-muscovite reaction isograd and the latter just above the biotite-muscovite-chlorite reaction isograd. In both cases the garnet appears to be unstable breaking down to a combination of biotite, muscovite, chlorite and quartz.

According to Colman-Sadd (1985), in the northern and central parts of the MCSZ, garnet occurs in the higher grade part of the biotite-muscovite-chlorite zone, just below the andalusite-biotite-muscovite reaction isograd. It is inferred that garnet formed in these samples because they are Fe-rich. The stable mineralogy is quartz, chlorite, muscovite, biotite, garnet and possibly feldspar. Thompson and Norton (1968) suggested the reaction:

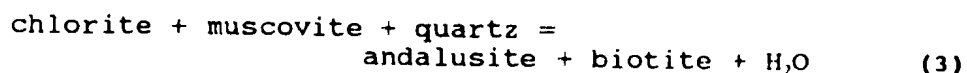


which may explain the occurrences in the study area (Figure 4-4bii).

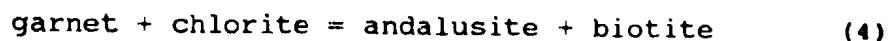
4.3.2.2 Andalusite-Biotite-Muscovite Reaction

Isograd

The andalusite-biotite-muscovite reaction isograd separates biotite-muscovite-chlorite grade rocks from andalusite-biotite-muscovite grade rocks (Figure 4-3). It is approximately concentric around the MCSZ but is truncated on the western boundary by the Pipestone Pond Complex. According to Colman-Sadd (1985), this isograd corresponds to the disappearance of prograde chlorite. This was substantiated in this study, as all chlorite present above the andalusite-biotite-muscovite reaction isograd is retrograde after biotite. The reaction:



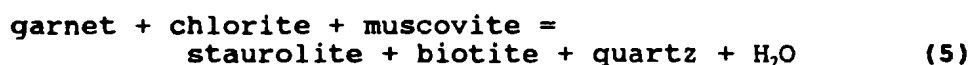
which was inferred by Colman-Sadd (1985), thus appears to be representative of the reaction isograd (Figure 4-4ci). The mineralogy of the andalusite-biotite-muscovite zone is shown in Figure 4-4ci and 4-4cii. As the andalusite-biotite tie line migrates to more Mg-rich compositions with increasing T, chlorite breaks down and is replaced by biotite and andalusite. However, if the assemblage was derived from Figure 4-4bii, the garnet-chlorite tie line would be broken, and the reaction



would have taken place.

Staurolite Forming Reaction

Staurolite first appears north of Spruce Brook, just upgrade from the andalusite-biotite-muscovite reaction isograd. It locally contains inclusions of garnet, biotite, muscovite and quartz; hence it is inferred to have formed in Fe-rich rocks that originally contained garnet (Figure 4-4bii) by the following reaction (Winkler, 1979):

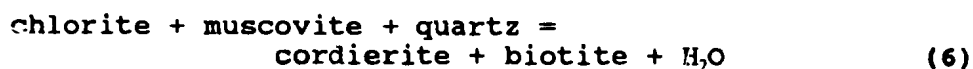


The resulting garnet-staurolite-biotite assemblage is shown in Figure 4-4ci.

Staurolite is present in rocks of the SBF in two areas, north of Spruce Brook, and in the area north of the Through Hill Granite. It also occurs as inclusions in andalusite just southwest of the Through Hill Granite.

Cordierite Forming Reaction

Cordierite occurs just upgrade from the andalusite-biotite-muscovite reaction isograd in a cordierite-biotite-chlorite-magnetite-quartz-muscovite schist and is associated with a marked increase in the concentration of magnetite. Chlorite is restricted to cordierite and is inferred to be retrograde. One possible reaction to explain this occurrence is:



Cordierite occurs in a narrow band and the cordierite porphyroblasts (and poikiloblasts) are full of inclusions of quartz, muscovite, biotite and magnetite, and, in most cases, are nearly completely altered to aggregates of muscovite, quartz and chlorite. The presence of this cordierite-magnetite sub-assemblage is interpreted to be a function of a higher oxidation state than elsewhere in the pelites. Oxidation of some Fe^{2+} to Fe^{3+} resulted in the formation of abundant magnetite, leaving a low Fe^{2+}/Mg ratio in the silicates that favoured the stability of cordierite. The presence of the cordierite-magnetite sub-assemblage in a narrow band suggests that the oxidation may have been a primary feature of the pelites.

Staurolite Breakdown Reaction

The breakdown of staurolite can be attributed to both continuous and discontinuous reactions. Southwest of the Through Hill Granite, in samples SD-89-361 and -366, staurolite is absent from the matrix but occurs as inclusions in andalusite (Plate 4-15). This implies that the continuous reaction



had taken place. Labotka (1981) documented such an occurrence of staurolite in a low-pressure metamorphic aureole in California.

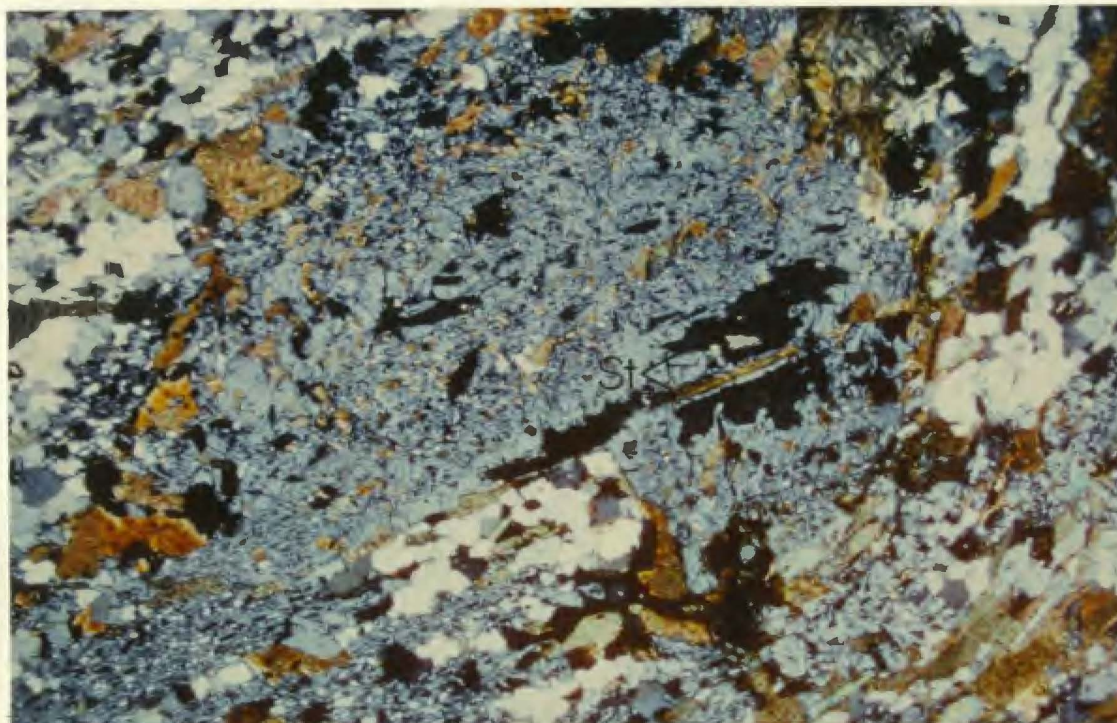
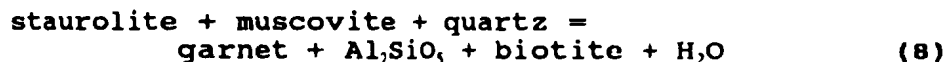


Plate 4-15. Andalusite with staurolite inclusions (St) in sample SD-89-366 from the andalusite-biotite-muscovite zone. Xpl., photo is 6 mm across.

In addition, the discontinuous reaction



also occur in rocks north of the Through Hill Granite. Both andalusite and sillimanite occur as products of the staurolite breakdown reactions since staurolite is stable in a quartz-muscovite-plagioclase-staurolite-biotite-garnet-sillimanite schist within the sillimanite-biotite-muscovite zone (sample G-147-80).

4.3.2.3 Sillimanite-Biotite-Muscovite Reaction

Isograd

The sillimanite-biotite-muscovite reaction isograd is easily mapped in the field (Figure 4-3) and marks the polymorphic transformation of andalusite to sillimanite. In thin section, sillimanite can be seen to occur within, or in close proximity to, andalusite grains suggesting that the reaction



proceeded without the participation of any other phases. This transformation causes no change in AFM topology (i.e. Figure 4-4ci to 4-4di).

4.3.2.4 Sillimanite-K Feldspar Reaction Isograd

This reaction isograd is defined by the

coexistence of sillimanite and K feldspar and the removal of prograde muscovite from the mineral assemblage. Sillimanite appears to be forming from the breakdown of muscovite, as it typically forms within muscovite grains. K feldspar, on the other hand, contains no inclusions, although it is in contact with sillimanite and displays abundant cross-hatched twinning. The isograd is represented by the reaction defining the disappearance of prograde muscovite:



4.3.2.5 Reactions in the Zone of Partial Melting (labelled ZM on Figure 4-3)

This reaction isograd occurs just upgrade from the sillimanite-K feldspar reaction isograd (Figure 4-3). The mineralogy of melt-absent schists within this zone is sillimanite-biotite-plagioclase-quartz-K feldspar. Leucosome-bearing rocks are composed of quartz-plagioclase-K feldspar-biotite, implying that melting occurred first in bulk composition undersaturated in alumina. Numerous melting reactions have been proposed by others and the work of St-Onge (1984) appears to be particularly appropriate to the rocks of the study area. In the modal system albite-orthoclase-muscovite-biotite-quartz-aluminosilicate-vapour, St-Onge showed the arrangement of seven melt and dehydration reactions radiating from an invariant point (Figure 4-5).

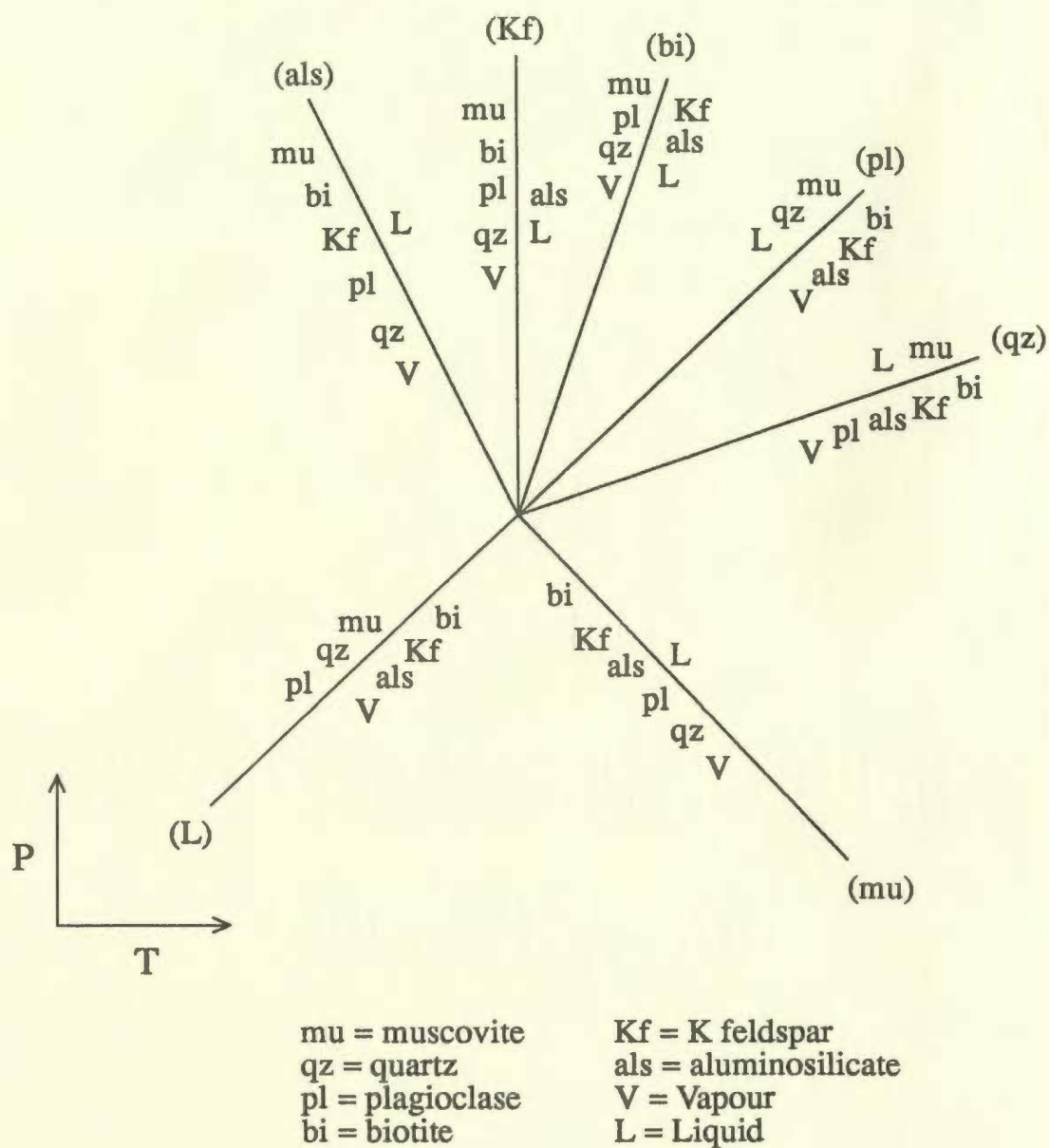
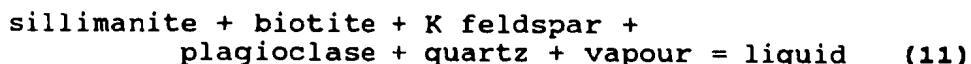


Figure 4-5. Geometry of reaction curves radiating from an invariant point in the modal system albite-orthoclase-muscovite-biotite-quartz-aluminosilicate-vapour (modified from St-Onge, 1984). Minerals in parentheses are absent from the reaction represented by the curve.

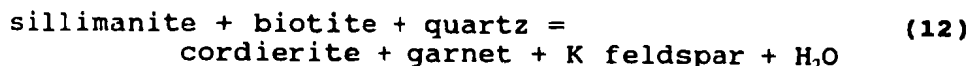
However, six of these reactions involve muscovite on the reactant side; since the sillimanite-K feldspar reaction isograd occurs at a lower grade than the melting isograd, muscovite would not be present to participate in the melting reaction. Thus it seems likely that the melt isograd, which marks the beginning of partial melting of the metasedimentary rocks, is defined by the reaction of Piwinskii (1968)



in the MCSZ.

High-Grade Cordierite Forming Reactions

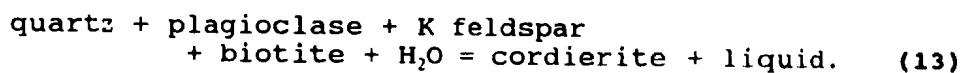
Cordierite occurs in high grade rocks associated with garnet and with granitoid melt. Cordierite and garnet coexist in pelites just upgrade from the first indications of melting (Colman-Sadd, 1985) although there is no evidence of melting in the cordierite-garnet bearing rocks. The breakdown of the sillimanite-biotite tie line and its replacement by the stable assemblage garnet-cordierite implies that the reaction



has taken place. A similar reaction has also been recorded by Ashworth and Chinner (1978) in migmatitic rocks of the Scottish Caledonides.

A second reaction involving cordierite occurs in a

cordierite granodiorite (sample SD-89-218). This isolated outcrop occurs north of the Through Hill Granite, within the zone of migmatization. Large xenoblastic porphyroblasts of cordierite occur with quartz, feldspar, biotite and minor sillimanite. The presence of these minerals indicates that the granite may have formed from partial melting of the metasedimentary rocks by a reaction of the type:

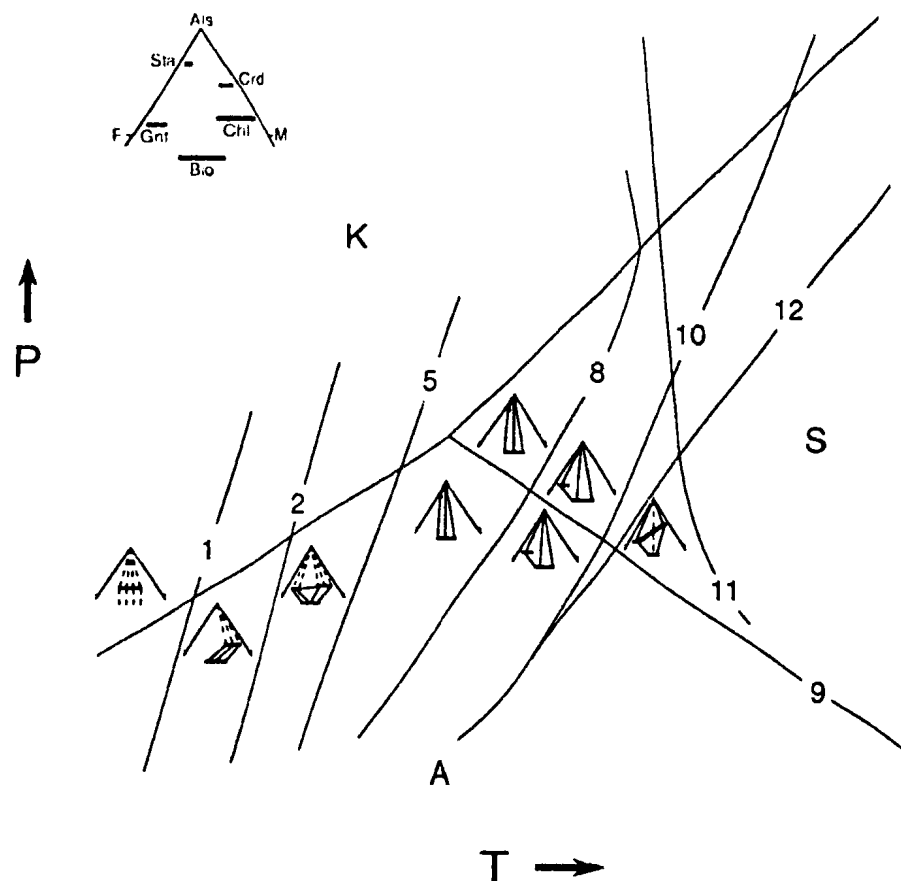


4.4 Petrogenetic Grid

Figure 4-6 is a schematic P-T diagram for the MCSZ showing the locations of reactions that occur in the rocks. Most of the reactions on the grid are at least divariant in the expanded seven-component system $\text{K}_2\text{O}-\text{FeO}-\text{Na}_2\text{O}-\text{MgO}-\text{Al}_2\text{O}_3-\text{SiO}_2-\text{H}_2\text{O}$ (KFMASH) system, so that the positions of the curves is only fixed by fixing the X_{Mg} for all the phases and $X_{\text{H}_2\text{O}}$ for the system. The approximate range of the metamorphic field gradient is also shown along with specific sample locations. The inferred metamorphic field gradient indicates that metamorphism was relatively low-pressure (< 4 kilobars) and nearly isobaric.

4.5 Metamorphic Bathograds

A metamorphic bathograd is a special type of reaction isograd that is sensitive to pressure and takes



Reactions

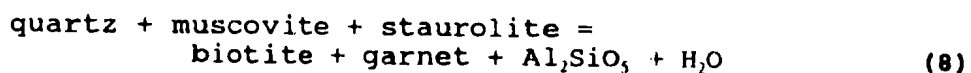
- (1) phengite + Al-poor chlorite = muscovite + Al-rich chlorite +
biotite + quartz + water (Kamineni and Carrara, 1973)
- (2) chlorite + muscovite + quartz = almandine + biotite + water (Thompson and Norton, 1968)
- (5) garnet + chlorite + muscovite = staurolite + biotite + quartz + water (Winkler, 1979)
- (8) staurolite + muscovite + quartz = garnet + Al_2SiO_5 + biotite + water
(Carmichael, 1978)
- (9) andalusite = sillimanite (Holdaway, 1971)
- (10) muscovite + quartz = sillimanite + K feldspar + water (Kerrick, 1972)
- (11) sillimanite + biotite + K-feldspar + plagioclase + quartz + vapour = liquid
(Kerrick, 1972)
- (12) sillimanite + biotite + quartz = cordierite + garnet + K feldspar + water
(Ashworth and Chinner, 1978)

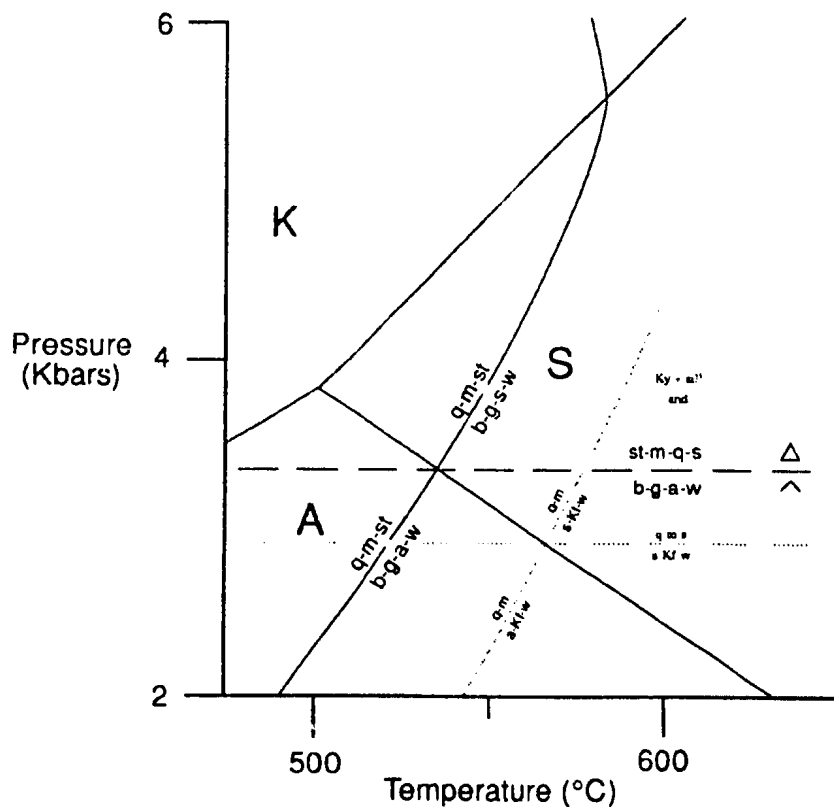
Figure 4-6. Schematic P-T grid for metamorphic mineral assemblages in the MCSZ showing the location of reactions mentioned in the text along with AFM projections of mineral assemblages.

place within a limited range of temperature. Carmichael (1978) defined a bathograd as "... the mappable line that separates occurrences of a higher-P assemblage from occurrences of a lower-P assemblage." The line is defined by an invariant reaction involving all phases stable at the invariant point. In P-T space, bathograds are defined by horizontal lines which extend from the intersection (invariant point) of two univariant reactions.

4.5.1 Metamorphic Bathograds in the Mount Cormack Subzone

Mineral assemblages that occur in rocks of appropriate composition and temperature higher grade than the andalusite-biotite-muscovite reaction isograd define a bathograd based on the six-component system $K_2O-FeO-MgO-Al_2O_3-SiO_2-H_2O$ (KFMASH). The individual phases involved are: quartz, muscovite, biotite, staurolite, garnet, andalusite and sillimanite. Only the andalusite-sillimanite transition is observed, implying that pressure was less than the triple point in the Al_2SiO_5 system (Figure 4-7). The bathograd passes through the invariant point defined by the intersection of the reactions,





Reactions

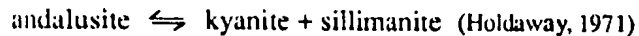
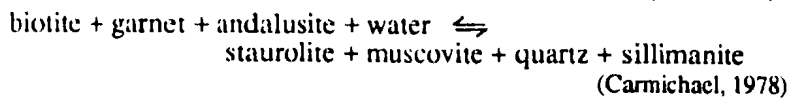
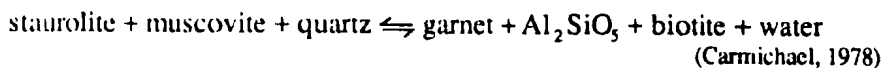


Figure 4-7. P-T phase diagram for part of the MCSZ showing the location of the invariant point on which the bathograd is based. The diagnostic mineral assemblages that constrain the bathograd are labelled on the appropriate side of the isobaric line extending from the invariant point. A lower pressure constraint is provided by the second reaction (in grey) and an upper pressure constraint by the third reaction (also in grey).

and the invariant bathogradic reaction can be written as;



This reaction separates the higher-pressure staurolite-muscovite-quartz-sillimanite assemblage from the lower-pressure biotite-garnet-andalusite assemblage.

Figure 4-7 is a P-T diagram showing that the bathograd occurs at a pressure of about 3.3 kilobars (after Carmichael, 1978), assuming that $P_{\text{fluid}} = P_{\text{total}}$ and $P_{\text{fluid}} = P_{\text{H}_2\text{O}}$. Kerrick (1972) showed that, as this is a dehydration reaction, decreasing the mole fraction of H_2O in the vapour phase (i.e. lowering $X_{\text{H}_2\text{O}}$) would lower the temperature of the reaction, thus shifting the invariant point to higher pressure. However, decreasing the $X_{\text{H}_2\text{O}}$ from 1.0 to 0.5 would increase the pressure by less than 0.5 kilobars.

Figure 4-8 is a map showing the locations of samples with assemblages appropriate to the bathograd which define the location of the bathograd. The bathograd appears to coincide with the sillimanite-biotite-muscovite reaction isograd, with the high-pressure bathogradic assemblage occurring on the high-temperature side of the reaction isograd (i.e. positive correlation between P and T locally). This could indicate that the high grade areas underwent greater post-metamorphic uplift or, in the Through Hill area at least, that the syn-metamorphic Through Hill Granite

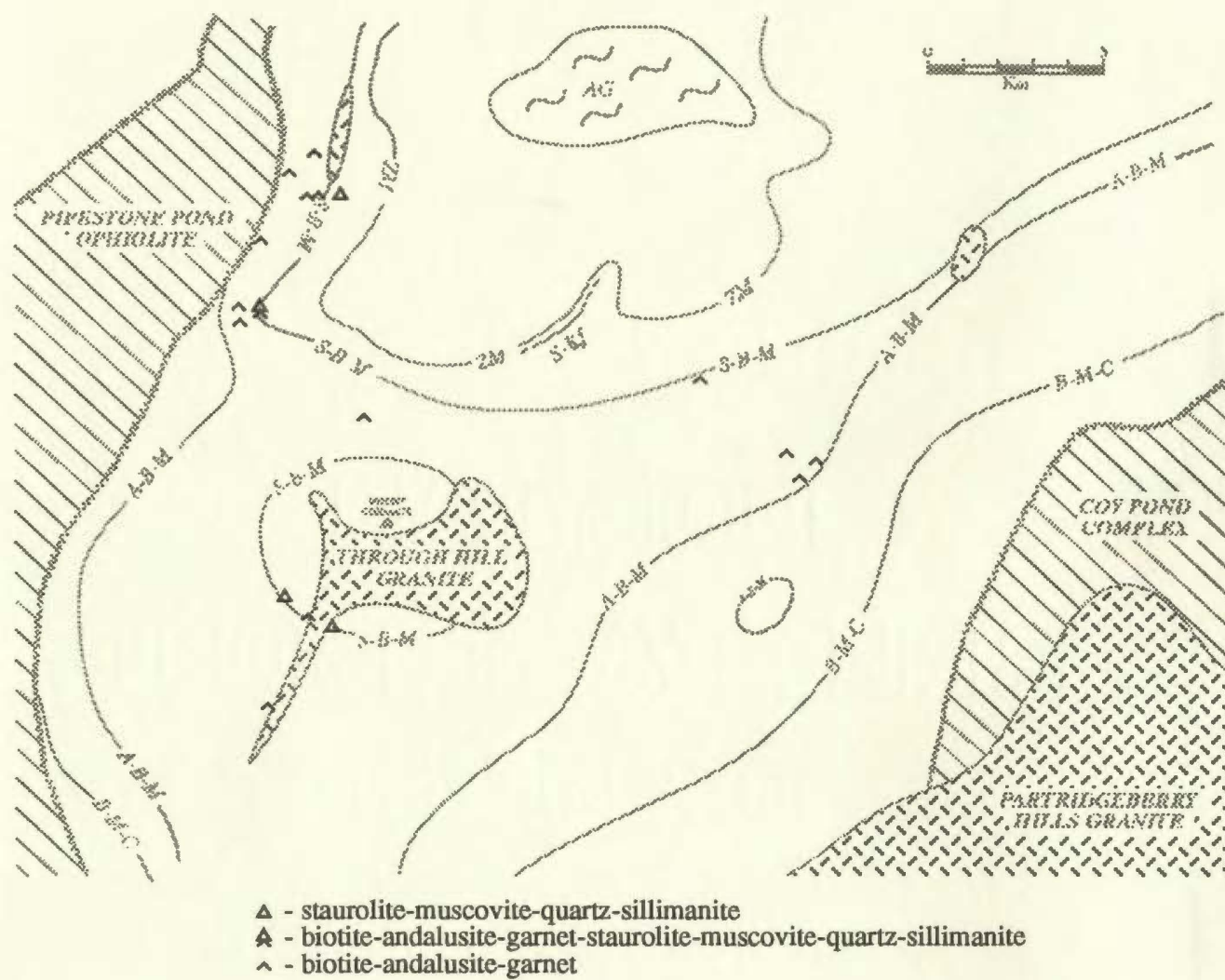


Figure 4-8. Map of part of the MCSZ showing the location of samples which define the staurolite-muscovite-quartz-sillimanite bathograd.

dragged up its metamorphic aureole during emplacement as the map pattern indicates that it is surrounded by its own sillimanite-biotite-muscovite reaction isograd. However, the THG is not symmetrically related to either the sillimanite-biotite-muscovite reaction isograd or to the bathograd. Flood and Vernon (1978) suggested that the Cooma Granodiorite of Australia may have dragged up its metamorphic aureole during emplacement; however, although such an origin appears feasible for the area adjacent to the THG, there is no granitoid body associated with the much larger sillimanite-biotite-muscovite reaction isograd in the north of the study area.

4.6 Metamorphic Microstructures

Microstructural evidence preserved within rocks of the SBF suggests that mineral growth occurred prior to, during and after the second deformation (D_2).

Andalusite porphyroblasts commonly show evidence of pre- and post-tectonic growth (with respect to D_2). In most cases, inclusion minerals (commonly quartz and biotite) preserve a fabric which is approximately parallel to the external fabric (i.e. Plate 4-4) indicating a post-tectonic origin. However, in some cases, inclusion minerals are randomly orientated (i.e. Plate 4-3) suggesting that these porphyroblasts grew prior to the deformation. Although the inclusions in these porphyroblasts appear to be randomly

orientated, they are approximately continuous with those in the external fabric, indicating that they overgrew this fabric. In these samples, deformation may not have been very extensive as the minerals in the matrix show no preferred orientation. In some samples, there appear to be two generations of andalusite. The first generation contains fine-grained inclusions of the matrix minerals which display no preferred orientation, possibly indicating that they are pre-tectonic. In the second generation, the matrix minerals (especially biotite) are coarser grained and are aligned parallel to the deformation fabric. In this case, the andalusite porphyroblasts are probably syn- or post-tectonic.

Staurolite porphyroblasts developed prior to D_2 deformation as indicated by the fact that inclusions show no preferred orientation (Plate 4-6) and the porphyroblasts are commonly wrapped by the deformation fabric. However, some staurolite porphyroblasts display rims altered to biotite; this reaction occurred after deformation as these biotite grains are random in orientation and often cross-cut the deformation fabric. Staurolite also developed prior to andalusite since it locally occurs as xenoblastic inclusions in andalusite porphyroblasts (reaction 7; Plates 4-4, 4-15).

Garnets, at least at low and medium grades, are inferred to be pre- D_2 since they occur as rotated porphyroblasts which are typically wrapped by the

deformation fabric within the rock. However, garnet appears sporadically at low, medium and high grades, so timing of growth is not expected to be the same for all parageneses. Also, garnet occurs as inclusions in andalusite, staurolite (Plate 4-6) and cordierite. Although most garnets contain few inclusions (typically quartz), some contain inclusions of biotite along with quartz and these are randomly orientated. At low grades (i.e. below the sillimanite-biotite-muscovite isograd) garnets are typically idioblastic to subidioblastic; upgrade from the sillimanite-biotite-muscovite isograd, garnets are typically subidioblastic to xenoblastic.

In the low-grade rocks (i.e. from the biotite-muscovite-chlorite zone), fine-grained biotite appears to have developed prior to the D₂ deformation as it locally occurs as xenoblastic grains that have been flattened by the deformation and which are wrapped by the deformation fabric. However, biotite porphyroblasts have overgrown the deformation fabric indicating post-D₂ development. This latter statement is also true of biotites from higher grades, especially within the andalusite-biotite-muscovite zone, where they have overgrown a fabric defined by fine-grained muscovite.

Cordierite porphyroblasts in the low-grade rocks of the SBF are inferred to have developed after the formation of garnet (they locally contain garnet

inclusions). These porphyroblasts invariably preserve the pseudo-hexagonal shape typical of cordierite (Deer et al., 1966). However, they are nearly completely pseudomorphed by muscovite-chlorite-quartz assemblages; in only a few cases, primary cordierite is preserved in the cores. In some cases, cordierite pseudomorphs are deformed and flattened parallel to the deformation fabric. These are inferred to have formed prior to the deformation; however, the pseudomorphing minerals are aligned approximately parallel to the external fabric, inferring that these cordierite porphyroblasts were pseudomorphed during the deformation. At higher grades (i.e. within the zone of partial melting), cordierite is inferred to be post-tectonic, although it occurs in rocks that display little effect of deformation and the porphyroblasts contain few inclusions. These grains also show evidence of reaction to sillimanite (Plate 4-13).

Sillimanite grains are inferred to be both pre- and post-tectonic. In some cases, prismatic sillimanite grains are folded by small scale folds, or, are aligned parallel to the deformation fabric, as in the mylonite zone north of the Through Hill Granite. In other cases, fibrous sillimanite (fibrolite) appears to have formed from the breakdown of biotite, muscovite and/or cordierite; the fibres show no preferred orientation, although, in the case of biotite, the fibres appear to have grown parallel to the long axis of the grains.

The previous discussion has centred on the prograde mineral assemblages. However, as mentioned earlier, there is a pervasive retrogression within the rocks of the SBF defined by chlorite, muscovite and quartz (\pm feldspar). Some andalusite porphyroblasts are completely replaced by fine-grained muscovite; staurolite also shows evidence of retrograde reaction to fine-grained muscovite (i.e. Plate 4-7). In some cases, garnet and biotite show evidence of retrograde reaction to chlorite.

Structural evidence given in Chapter 3 indicates that the metamorphic reaction isograds developed after the D_2 deformation as they cut the D_2 structures (see Figure 3-2). In most samples that show evidence of deformation, the S_2 fabric is dominant and there is little evidence of S_0 or S_1 . In some of these samples, though, evidence of the first deformation fabric is preserved in small-scale folds between zones of S_2 foliation. Table 4-1 shows the relationship between porphyroblast growth and deformation. Porphyroblast minerals are listed in the inferred order of development.

Table 4-1. Mineral growth in relation to deformation in metapelites from the MCSZ

| | D_1 | D_2 | | |
|-------------|-------|-------|-------|-------|
| | | Pre- | Syn- | Post- |
| biotite | | _____ | ----- | _____ |
| garnet | | _____ | | |
| staurolite | | _____ | | |
| andalusite | | _____ | ----- | _____ |
| cordierite | | _____ | ----- | _____ |
| sillimanite | | _____ | ----- | _____ |

4.7 Mineral Chemistry

4.7.1 Analytical Techniques

Semi-quantitative and quantitative analyses were conducted on twenty-three polished thin sections of pelites from the SBF higher grade than the andalusite-biotite-muscovite reaction isograd in order to obtain independent estimates of pressure and temperature and to attempt to reconstruct the P-T-t path (Figure 4-9). The semi-quantitative analyses were done at Memorial University using a Hitachi S570 Scanning Electron Microscope (SEM). The SEM, with a Tracor Northern energy dispersive system, was used to determine the compositions of opaque phases (ie. ilmenite, magnetite, graphite) and to locate unzoned plagioclase grains for the future microprobe work.

The majority of the quantitative microprobe analyses were conducted at the Regional Electron Microprobe Laboratory, Dalhousie University, using a JEOL 733 Superprobe. Limited work was done at Memorial University (sample G-123-80 only) using a JEOL JXA-50A Electron Probe Microanalyzer. A wavelength dispersive set up was used with both instruments, involving up to four simultaneous analyses and automated spectrometer drive, to obtain analyses of ten major elements (Si, Ti, Al, Cr, Fe, Mg, Mn, Ca, Na, K; in the case of staurolite, Zn was also analyzed). An accelerating voltage of 15 kV, a probe current of 5 nA and a beam diameter of approximately 1×10^{-6} m were used. For the

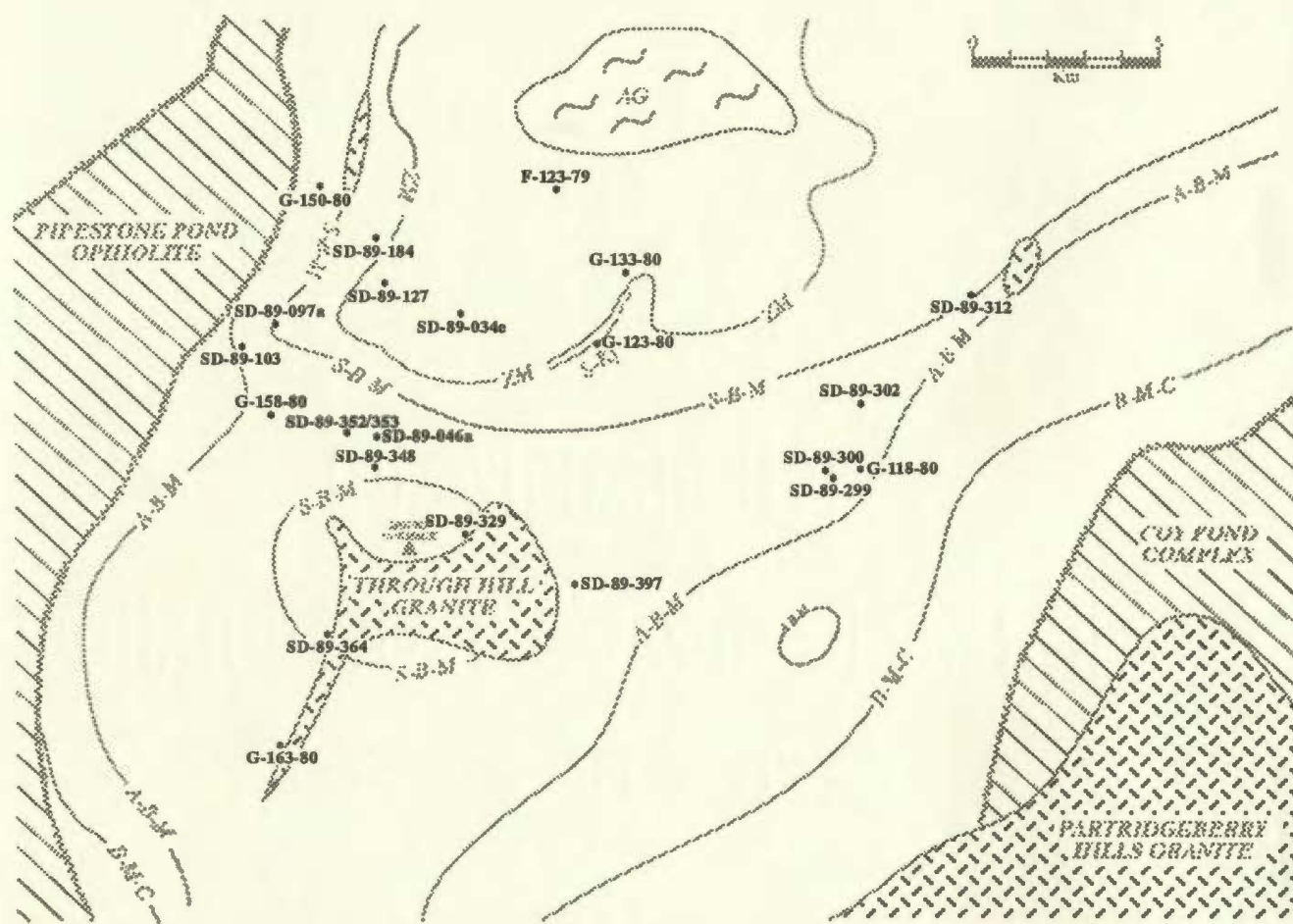


Figure 4-9. Map of part of the MCSZ showing location of samples used in microprobe analyses. Samples prefixed SD were collected in this study; those prefixed F & G were collected by Colman-Sadd in 1979 and 1980 respectively.

JEOL 733, the data reduction (conversion of raw counts per second to corrected weight percent of oxides) was done using Tracor Northern ZAF software. For the JEOL JXA-50A, the Bence-Albee correction procedures were used. In total, 808 analyses were carried out of which 553 are considered acceptable (approximately 70 % of total). Table 4-2 lists the minerals analysed and the ranges of weight percent oxides that were considered acceptable for the analyses, taking into account the error in the instrument and the fact that H₂O, CO₂, and F were not analysed:

Table 4-2

| <u>Mineral</u> | <u>Approximate range of Weight Percent Oxides</u> |
|----------------|---|
| plagioclase | 99 - 101% |
| garnet | 99 - 101% |
| K feldspar | 99 - 101% |
| cordierite | 98 - 100% |
| andalusite | 98 - 100% |
| staurolite | 96 - 98% |
| biotite | 94 - 96% |
| muscovite | 94 - 96% |
| chlorite | 87 - 90% |

In addition to the weight percent total, the stoichiometry of each analysis was compared with the ideal stoichiometry and with published data in order to weed out analyses of poor quality.

In each sample, the mineral compositions required for thermodynamic calculations (garnet, plagioclase, K feldspar, biotite, cordierite) were analyzed along with

other coexisting phases (ie. muscovite, chlorite, staurolite, andalusite). Representative analyses are given in the text and the remainder are listed in Appendix B.

4.7.2 Garnet

Probe traverses across garnet indicate that the majority of the garnets are unzoned. Zoning is present in some samples, however. The majority of garnets is composed of almandine-spessartine-rich mixtures, with almandine 60 to 70 mol %, spessartine 15 to 30 mol %, pyrope 5 to 10 mol % and grossular 2 to 4 mol %. However, sample G-133-80 contains almandine-pyrope garnets; they are unzoned and an average of eighteen analyses shows that they consist of 81 mol % almandine, 12 mol % pyrope, 3 mol % grossular and 4 mol % spessartine components. Table 4-3 lists some representative garnet analyses.

An indication of the amount of Fe^{3+} substituting for Al in garnet (i.e. the amount of andradite) can be gauged from an examination of the stoichiometry. Ideally, in garnet, the M_1 site contains 3 divalent atoms per formula unit (PFU) and the M_2 site contains 2 trivalent atoms PFU. If, with the assumption of all Fe as Fe^{2+} , the M_1 site contains more than 3 atoms PFU, and the M_2 site contains less than 2 atoms PFU, there may be Fe^{3+} substitution. From 180 garnet analyses, the number of atoms in the M_1 site ranges from 2.58 - 3.13 (averaging 3.037 atoms PFU) and the

Table 4-3
Representative analyses of garnets

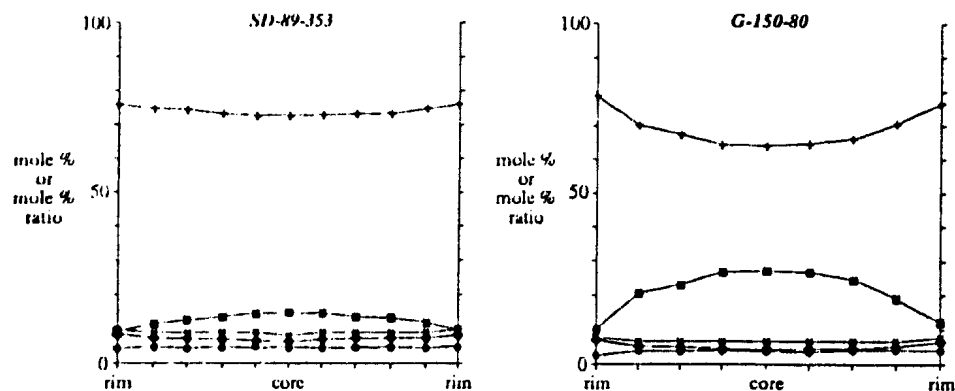
| | <i>SD-89-300</i> (unzoned - A-B-M Zone) | | | <i>SD-89-353</i> (prograde zoning - A-B-M Zone) | | | <i>SD-89-127</i> (retrograde zoning - ZM) | | |
|---|--|--------|-------|--|--------|-------|--|--------|-------|
| | (rim) | (core) | (rim) | (rim) | (core) | (rim) | (rim) | (core) | (rim) |
| SiO ₂ | 36.66 | 36.36 | 36.57 | 36.48 | 36.53 | 36.58 | 36.55 | 36.70 | 36.25 |
| TiO ₂ | 0.02 | 0.08 | 0.11 | 0.03 | 0.03 | 0.03 | 0.04 | 0.01 | 0.06 |
| Al ₂ O ₃ | 21.02 | 20.57 | 20.56 | 21.15 | 20.74 | 20.96 | 20.87 | 21.16 | 20.65 |
| Cr ₂ O ₃ | 0.06 | 0.03 | 0.05 | 0.03 | 0.00 | 0.04 | 0.04 | 0.06 | 0.00 |
| FeO | 29.33 | 28.80 | 29.33 | 34.35 | 32.24 | 34.06 | 25.90 | 27.94 | 25.42 |
| MnO | 8.78 | 9.39 | 8.77 | 4.35 | 6.49 | 4.37 | 14.23 | 11.07 | 15.01 |
| MgO | 2.42 | 2.33 | 2.46 | 2.16 | 1.68 | 2.07 | 1.12 | 2.31 | 1.12 |
| CaO | 1.48 | 1.52 | 1.58 | 1.60 | 1.60 | 1.72 | 0.93 | 0.76 | 1.00 |
| Na ₂ O | 0.15 | 0.05 | 0.04 | 0.04 | 0.05 | 0.02 | 0.01 | 0.04 | 0.03 |
| K ₂ O | 0.06 | 0.02 | 0.02 | 0.01 | 0.01 | 0.02 | 0.02 | 0.02 | 0.03 |
| Total | 99.98 | 99.15 | 99.48 | 100.21 | 99.38 | 99.88 | 99.72 | 100.05 | 99.56 |
| <i>number of cations on the basis of 12 oxygens</i> | | | | | | | | | |
| Si | 2.97 | 2.98 | 2.98 | 2.96 | 2.99 | 2.98 | 2.99 | 2.98 | 2.98 |
| Ti | 0.00 | 0.00 | 0.01 | 0.00 | 0.00 | 0.00 | 0.00 | 0.00 | 0.00 |
| Al | 2.01 | 1.99 | 1.98 | 2.02 | 2.00 | 2.01 | 2.02 | 2.02 | 2.00 |
| Cr | 0.00 | 0.00 | 0.00 | 0.00 | 0.00 | 0.00 | 0.00 | 0.00 | 0.00 |
| Fe | 1.99 | 1.97 | 2.00 | 2.33 | 2.21 | 2.32 | 1.77 | 1.90 | 1.75 |
| Mn | 0.60 | 0.65 | 0.61 | 0.30 | 0.45 | 0.30 | 0.99 | 0.76 | 1.05 |
| Mg | 0.29 | 0.28 | 0.30 | 0.26 | 0.21 | 0.25 | 0.14 | 0.28 | 0.14 |
| Ca | 0.13 | 0.13 | 0.14 | 0.14 | 0.14 | 0.15 | 0.08 | 0.07 | 0.09 |
| Na | 0.02 | 0.01 | 0.01 | 0.01 | 0.01 | 0.00 | 0.00 | 0.01 | 0.00 |
| K | 0.01 | 0.00 | 0.00 | 0.00 | 0.00 | 0.00 | 0.00 | 0.00 | 0.00 |
| Total | 8.03 | 8.03 | 8.02 | 8.03 | 8.01 | 8.02 | 8.00 | 8.01 | 8.02 |
| Almandine | 66.01 | 64.85 | 65.73 | 76.92 | 73.51 | 76.75 | 59.54 | 63.15 | 57.90 |
| Pyrope | 9.71 | 9.35 | 9.82 | 8.62 | 6.83 | 8.31 | 4.59 | 9.30 | 4.55 |
| Grossular | 4.27 | 4.39 | 4.54 | 4.59 | 4.67 | 4.97 | 2.74 | 2.20 | 2.92 |
| Spessartine | 20.01 | 21.42 | 19.91 | 9.87 | 14.99 | 9.97 | 33.13 | 25.34 | 34.63 |
| A | 30.38 | 30.49 | 30.00 | 28.04 | 29.29 | 28.06 | 34.45 | 31.69 | 34.57 |
| F | 0.87 | 0.87 | 0.87 | 0.90 | 0.82 | 0.90 | 0.93 | 0.87 | 0.93 |
| M | 0.13 | 0.13 | 0.13 | 0.10 | 0.08 | 0.10 | 0.07 | 0.13 | 0.07 |
| ΣMg, Fe, Mn, Ca | 3.01 | 3.03 | 3.05 | 3.03 | 3.01 | 3.02 | 2.98 | 3.01 | 3.03 |
| ΣFe, Mg, Mn | 2.89 | 2.91 | 2.91 | 2.89 | 2.86 | 2.87 | 2.90 | 2.93 | 2.93 |
| Fe/Fe+Mg+Mn | 68.95 | 67.82 | 68.86 | 80.62 | 77.12 | 80.76 | 61.22 | 64.57 | 59.65 |
| Mn/Fe+Mg+Mn | 20.91 | 22.40 | 20.85 | 10.34 | 15.72 | 10.49 | 34.07 | 25.91 | 35.67 |
| Mg/Fe+Mg+Mn | 10.14 | 9.78 | 10.29 | 9.03 | 7.16 | 8.75 | 4.72 | 9.51 | 4.68 |

M₂ site ranges from 1.87 - 2.09 atoms PFU (averaging 1.994 atoms), suggesting the presence of a minor andradite component (0.2 - 1.2 mol %).

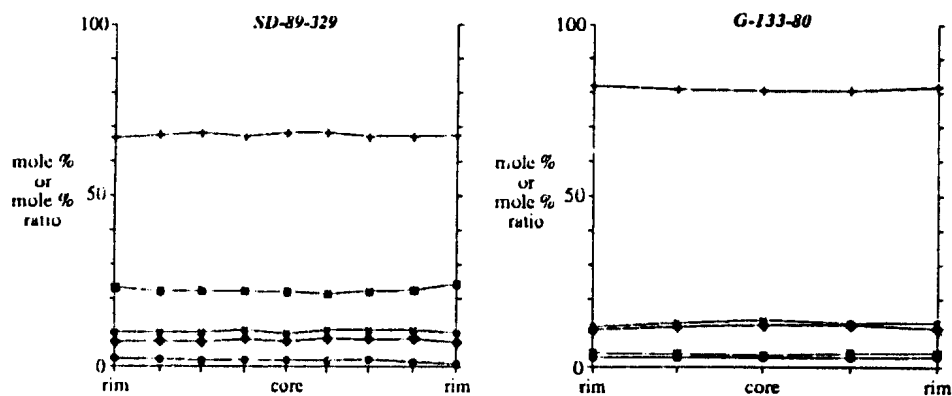
Of seventeen samples analysed, four contained zoned garnets. This zoning is reflected by changes in the Fe, Mg and Mn contents from core to rim (Figure 4-10) as well as changes in Al content (Figure 4-11). This change in Al content may be due to Fe³⁺ substitution (see above). In Figure 4-11b, prograde growth in a garnet from sample G-150-80 displays a nearly constant F/M ratio and shows that the andradite component increases with growth. Figure 4-11c shows a retrograde zoned garnet from sample SD-89-127 which indicates a slight reduction in andradite component and a reduction in the pyrope:almandine ratio from core to rim.

Garnets in two of the samples (SD-89-353 and G-150-80, both from the andalusite-biotite-muscovite zone) display prograde zoning (ie. core to rim increase in Mg and decrease in Mn; Tuccillo et al., 1990 and references therein; Figure 4-12). This decrease in Mn is on the order of 50 % but in some cases Mn decreases by 2.5 times that in the core (27 -> 11 mol % spessartine component). There is also an increase in the Fe and Mg contents in the rim, with Fe increasing by approximately 10-20 % (65 -> 80 mol %) and Mg by about 15-25 % (6.5 -> 8 mol %). The grossular component remains relatively unchanged at 4-5 mol %.

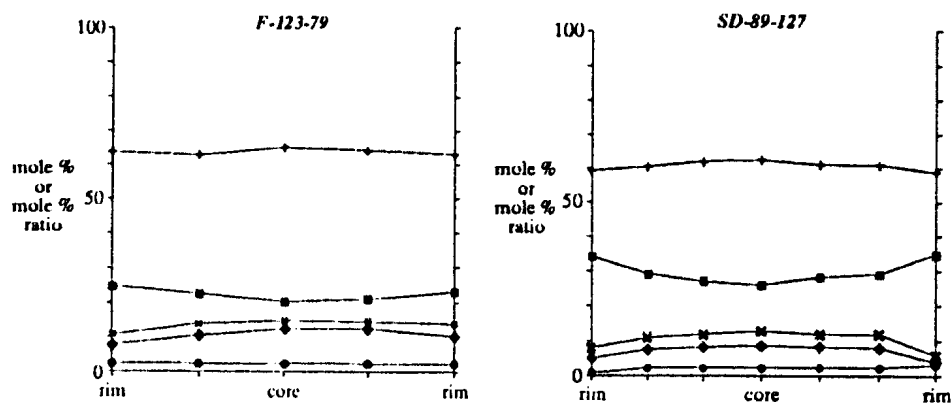
a) Prograde (Growth) Zoning in Garnet (andalusite-biotite-muscovite zone)



b) Unzoned Garnets (sillimanite-biotite-muscovite zone)



c) Retrograde Zoning in Garnet (zone of partial melting)



■ - Mn; ♦ - Mg; ● - Ca; + - Fe; × - Mg/Mg+Fe

Figure 4-10. Types of zoning in garnets from selected samples from the MCSZ (samples prefixed with F & G collected by S.P. Colman-Sadd).

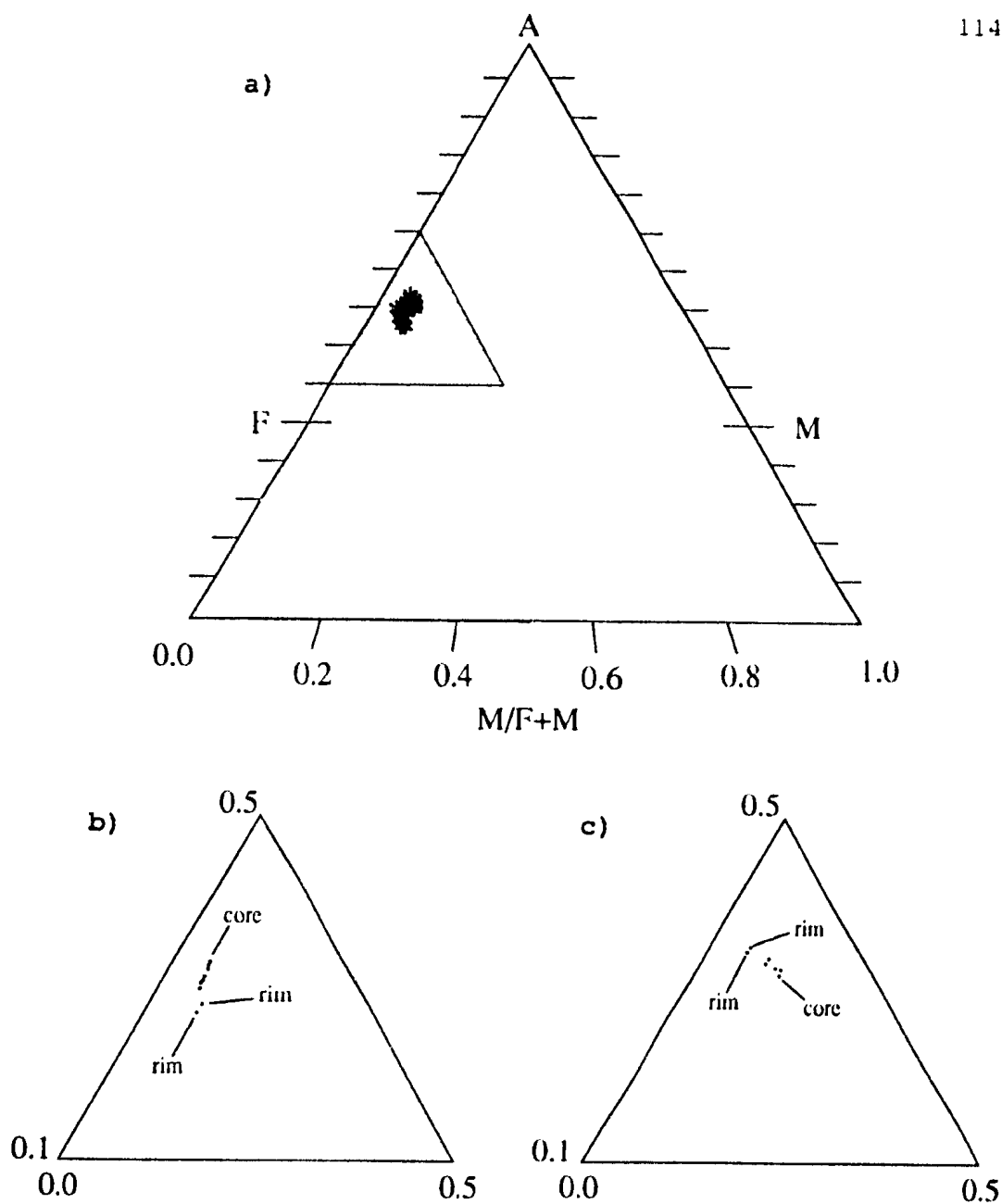


Figure 4-11. AFM plots (Thompson, 1957) of garnet compositions. a) unzoned garnet compositions ($n = 122$); b) prograde zoning in garnet from the andalusite-biotite-muscovite zone (sample G-150-80, $n = 9$); and c) retrograde zoning in garnet from the zone of partial melting (sample SD-89-127, $n = 7$).

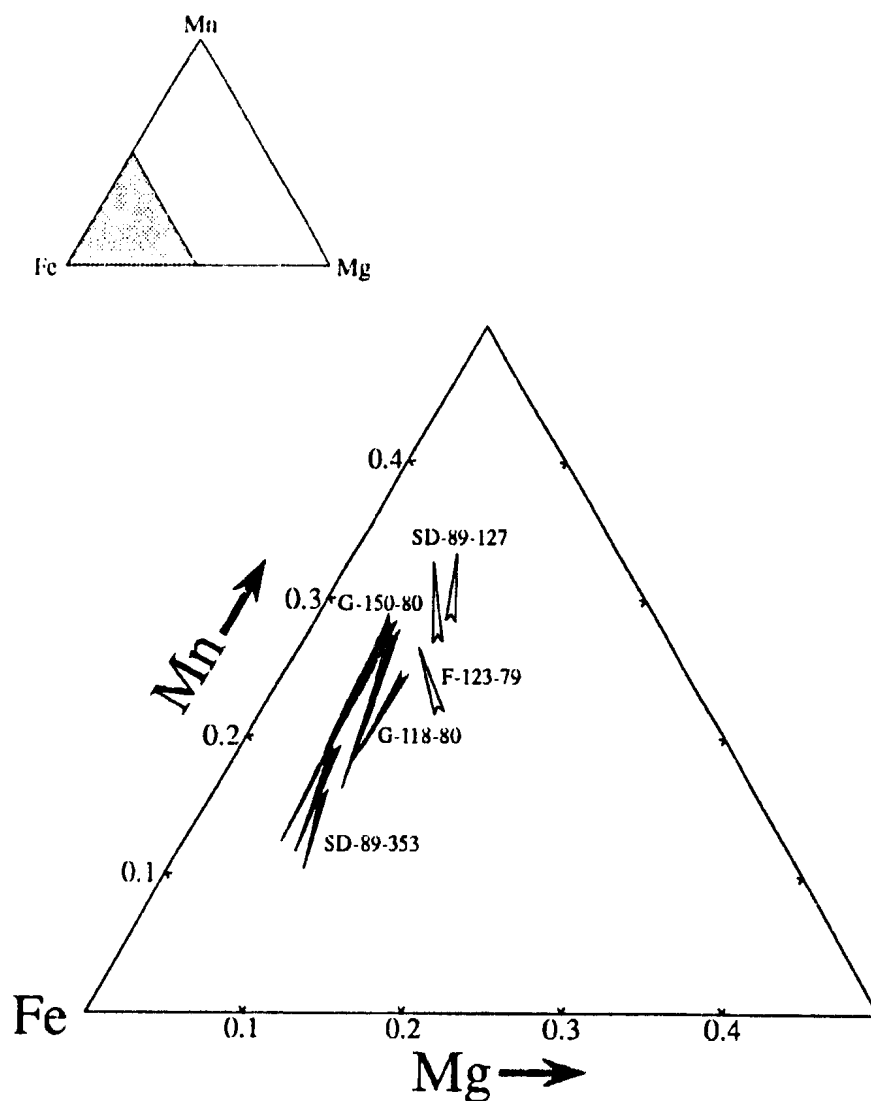


Figure 4-12. Fe-Mg-Mn ternary atomic percent plot showing zoning patterns of garnets from the MCSZ. Arrows point from core to rim compositions. Filled arrows are samples from the andalusite-biotite-muscovite zone; empty arrows are samples from the zone of partial melting.

Garnets in two samples from the zone of partial melting display retrograde zoning (F-123-79 and SD-89-127; Figure 4-12). These garnets display core to rim increases in Mn (25 to 33 mol %), decrease in Fe (63 to 60 mol %) and decrease in Mg by 50 % (in one case, the Mg content drops from 9.2 to 4.6 mole %). Ca remains relatively unchanged.

The zoning patterns in these garnets are consistent with other published data on zoned garnets (see Tracy, 1982 for a summary of zoning patterns in garnet). Woodsworth (1977) suggested that above ~ 600 °C, growth histories of garnets are lost and homogenization occurs. Lepezin and Korolyuk (1985) documented that with increasing metamorphism, the occurrence of garnets with prograde (growth) zoning decreases, and those with retrograde zoning increase in number. As discussed by Tuccillo et al. (1990 and references therein), retrograde zoning is due to retrograde diffusion processes. During resorption (assuming equilibrium with biotite), garnet will become depleted in Mg relative to Fe, and Mn will be incorporated into garnet since it is not easily incorporated into cordierite or biotite. Yardley (1977) suggested that diffusion begins between 615° and 665°C, although this process is dependent upon kinetic factors, so a precise temperature is not especially meaningful.

4.7.3 Feldspars

Both plagioclase and K feldspar were analyzed to determine their compositions and for use in thermodynamic calculations.

Analyses of nineteen plagioclase grains indicate that zoning is negligible, but the compositional range between samples is extensive ($An_{4.31}$). K feldspar was analysed in one sample from the sillimanite-biotite zone (G-123-80). The analyses indicate that the average composition (exclusive of the albite-rich rims) is $Or_{80.1}$, $Ab_{19.8}$ and $An_{0.1}$. Table 4-4 contains some representative analyses of the two feldspars and Figure 4-13 is a plot of feldspar compositions.

4.7.4 Biotite

Two textural groups of biotites were analyzed; those near garnets and those in the matrix away from garnets. The analyses indicate that there is negligible difference between the two (Table 4-5). All Fe was assumed to be Fe^{2+} since the Fe^{3+} in garnet is low. All biotites typically have an iron-magnesium ratio of 3:2, and Al^{VI} ranges from 0.6-0.99 atoms PFU with an average of 0.83 atoms PFU. Minor sodium was detected (< 0.14 atoms PFU) and minor manganese (less than 0.07 atoms PFU) and titanium (0.15-0.38 atoms PFU) are present. Figure 4-14 is a plot of biotite compositions with respect to Mg/Fe and Al^{VI} variations. All

Table 4-4
Representative analyses of
plagioclase and K feldspar

| | <i>SD-89-184</i> (plagioclase - S-B-M Zone) | | | <i>SD-89-329</i> (plagioclase - S-B-M Zone) | | | <i>G-123-80</i> (K feldspar - S-Kf Zone) | | |
|--|--|--------|--------|--|--------|--------|---|-------|-------|
| | (rim) | (core) | (rim) | (rim) | (core) | (rim) | | | |
| SiO ₂ | 63.86 | 64.05 | 64.59 | 66.22 | 66.34 | 65.48 | 65.48 | 65.19 | 65.22 |
| TiO ₂ | 0.00 | 0.00 | 0.00 | 0.00 | 0.00 | 0.00 | 0.02 | 0.04 | 0.04 |
| Al ₂ O ₃ | 22.99 | 23.03 | 22.68 | 21.62 | 21.45 | 21.93 | 19.50 | 19.34 | 19.00 |
| Cr ₂ O ₃ | 0.00 | 0.00 | 0.03 | 0.00 | 0.00 | 0.00 | 0.00 | 0.00 | 0.02 |
| FeO | 0.08 | 0.00 | 0.01 | 0.19 | 0.00 | 0.00 | 0.04 | 0.04 | 0.04 |
| MnO | 0.00 | 0.00 | 0.00 | 0.00 | 0.00 | 0.00 | 0.00 | 0.00 | 0.00 |
| MgO | 0.00 | 0.00 | 0.00 | 0.00 | 0.00 | 0.00 | 0.00 | 0.00 | 0.00 |
| CaO | 4.01 | 3.79 | 3.49 | 1.68 | 1.81 | 2.30 | 0.03 | 0.02 | 0.00 |
| Na ₂ O | 9.23 | 9.48 | 9.20 | 10.35 | 10.66 | 10.41 | 1.29 | 3.02 | 2.30 |
| K ₂ O | 0.09 | 0.05 | 0.06 | 0.09 | 0.16 | 0.12 | 13.82 | 11.80 | 13.14 |
| Total | 100.25 | 100.39 | 100.09 | 100.15 | 100.41 | 100.23 | 100.20 | 99.46 | 99.78 |
| <i>number of cations on the basis of 8 oxygens</i> | | | | | | | | | |
| Si | 2.81 | 2.81 | 2.84 | 2.90 | 2.90 | 2.87 | 2.98 | 2.98 | 2.99 |
| Ti | 0.00 | 0.00 | 0.00 | 0.00 | 0.00 | 0.00 | 0.00 | 0.00 | 0.00 |
| Al | 1.19 | 1.19 | 1.18 | 1.12 | 1.11 | 1.13 | 1.05 | 1.04 | 1.03 |
| Cr | 0.00 | 0.00 | 0.00 | 0.00 | 0.00 | 0.00 | 0.00 | 0.00 | 0.00 |
| Fe | 0.00 | 0.00 | 0.00 | 0.01 | 0.00 | 0.00 | 0.00 | 0.00 | 0.00 |
| Mn | 0.00 | 0.00 | 0.00 | 0.00 | 0.00 | 0.00 | 0.00 | 0.00 | 0.00 |
| Mg | 0.00 | 0.00 | 0.00 | 0.00 | 0.00 | 0.00 | 0.00 | 0.00 | 0.00 |
| Ca | 0.19 | 0.18 | 0.16 | 0.08 | 0.08 | 0.11 | 0.00 | 0.00 | 0.00 |
| Na | 0.79 | 0.81 | 0.78 | 0.88 | 0.90 | 0.89 | 0.11 | 0.27 | 0.20 |
| K | 0.01 | 0.00 | 0.00 | 0.01 | 0.01 | 0.01 | 0.80 | 0.69 | 0.77 |
| Total | 4.99 | 5.00 | 4.97 | 4.98 | 5.00 | 5.01 | 4.95 | 4.98 | 4.99 |
| Albite | 80.22 | 81.67 | 82.38 | 91.29 | 90.60 | 88.52 | 12.40 | 27.98 | 21.01 |
| Anorthite | 19.26 | 18.04 | 17.27 | 8.19 | 8.50 | 10.51 | 0.16 | 0.10 | 0.00 |
| Orthoclase | 0.51 | 0.28 | 0.35 | 0.52 | 0.89 | 0.67 | 87.44 | 71.92 | 78.99 |
| ΣCa+Na+K | 0.99 | 0.99 | 0.94 | 0.97 | 0.99 | 1.01 | 0.91 | 0.96 | 0.97 |
| ΣSi+Al | 4.00 | 4.00 | 4.02 | 4.02 | 4.01 | 4.00 | 4.03 | 4.02 | 4.02 |

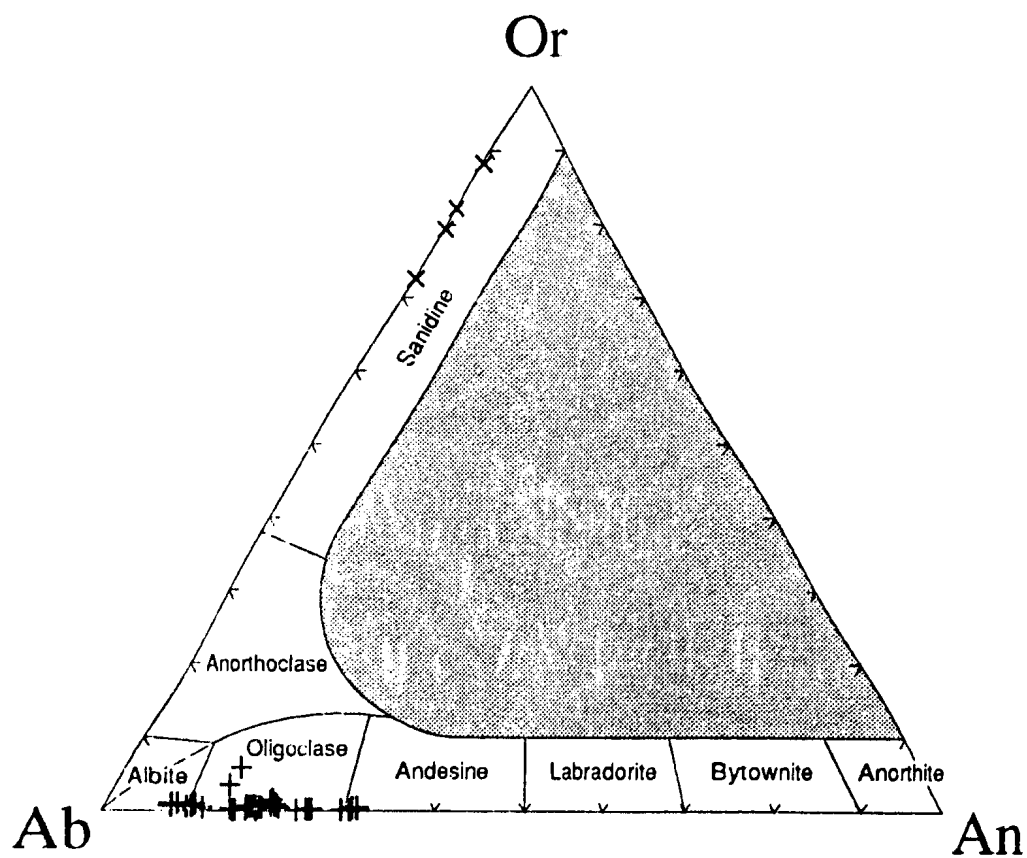


Figure 4-13. Plot of high-grade feldspar compositions from the MCSZ.

Table 4-5
Representative analyses of biotites
(all Fe assumed to be Fe²⁺)

| | ----- matrix ----- | | | | ----- near garnet ----- | | | | no garnet | |
|---|--------------------|------------------|--------|--------|-------------------------|------------------|--------|--------|------------------|--------|
| | <i>SD-89-097A</i> | <i>SD-89-312</i> | | | <i>SD-89-097A</i> | <i>SD-89-312</i> | | | <i>SD-89-299</i> | |
| | (S-B-M Zone) | | | | (S-B-M Zone) | | | | (A-B-M Zone) | |
| SiO ₂ | 34.79 | 34.89 | 34.21 | 34.61 | 34.67 | 34.75 | 34.64 | 34.36 | 36.11 | 35.99 |
| TiO ₂ | 2.23 | 2.35 | 3.13 | 3.33 | 2.55 | 2.37 | 3.22 | 2.82 | 1.44 | 1.50 |
| Al ₂ O ₃ | 19.94 | 19.82 | 19.30 | 19.12 | 20.06 | 19.94 | 18.93 | 18.49 | 18.82 | 18.68 |
| Cr ₂ O ₃ | 0.00 | 0.00 | 0.05 | 0.05 | 0.00 | 0.00 | 0.00 | 0.04 | 0.00 | 0.02 |
| FeO | 22.21 | 22.06 | 21.17 | 20.57 | 22.00 | 22.18 | 20.96 | 21.67 | 16.05 | 16.05 |
| MnO | 0.26 | 0.16 | 0.48 | 0.52 | 0.19 | 0.18 | 0.33 | 0.35 | 0.29 | 0.32 |
| MgO | 7.00 | 7.00 | 7.38 | 7.58 | 7.06 | 6.98 | 7.70 | 7.76 | 12.34 | 12.65 |
| CaO | 0.00 | 0.00 | 0.00 | 0.00 | 0.00 | 0.00 | 0.00 | 0.00 | 0.00 | 0.00 |
| Na ₂ O | 0.19 | 0.20 | 0.25 | 0.25 | 0.11 | 0.12 | 0.23 | 0.13 | 0.17 | 0.15 |
| K ₂ O | 8.68 | 8.60 | 9.06 | 9.20 | 8.62 | 8.69 | 9.39 | 9.29 | 9.02 | 9.03 |
| Total | 95.36 | 95.23 | 95.24 | 95.21 | 95.27 | 95.22 | 95.41 | 94.91 | 94.26 | 93.99 |
| <i>number of cations on the basis of 22 oxygens</i> | | | | | | | | | | |
| Si | 5.35 | 5.37 | 5.30 | 5.32 | 5.32 | 5.34 | 5.33 | 5.33 | 5.45 | 5.40 |
| Ti | 0.26 | 0.27 | 0.36 | 0.38 | 0.29 | 0.27 | 0.37 | 0.33 | 0.16 | 0.17 |
| Al | 3.61 | 3.59 | 3.50 | 3.46 | 3.63 | 3.61 | 3.43 | 3.38 | 3.35 | 3.34 |
| Cr | 0.00 | 0.00 | 0.01 | 0.01 | 0.00 | 0.00 | 0.00 | 0.00 | 0.00 | 0.00 |
| Fe | 2.85 | 2.84 | 2.73 | 2.64 | 2.82 | 2.85 | 2.70 | 2.81 | 2.03 | 2.04 |
| Mn | 0.03 | 0.02 | 0.06 | 0.07 | 0.02 | 0.02 | 0.04 | 0.05 | 0.04 | 0.04 |
| Mg | 1.60 | 1.60 | 1.69 | 1.74 | 1.61 | 1.60 | 1.76 | 1.79 | 2.78 | 2.86 |
| Ca | 0.00 | 0.00 | 0.00 | 0.00 | 0.00 | 0.00 | 0.00 | 0.00 | 0.00 | 0.00 |
| Na | 0.06 | 0.06 | 0.07 | 0.07 | 0.03 | 0.04 | 0.07 | 0.04 | 0.05 | 0.04 |
| K | 1.70 | 1.69 | 1.78 | 1.80 | 1.69 | 1.70 | 1.84 | 1.84 | 1.74 | 1.75 |
| Total | 15.47 | 15.44 | 15.51 | 15.50 | 15.43 | 15.45 | 15.54 | 15.58 | 15.60 | 15.65 |
| Fe/Fe+Mg | 0.64 | 0.64 | 0.62 | 0.60 | 0.64 | 0.64 | 0.60 | 0.61 | 0.42 | 0.42 |
| Al ^{VI} | 0.96 | 0.96 | 0.80 | 0.78 | 0.95 | 0.96 | 0.76 | 0.72 | 0.81 | 0.74 |
| Al ^{IV} | 2.65 | 2.63 | 2.70 | 2.68 | 2.68 | 2.66 | 2.67 | 2.67 | 2.55 | 2.60 |
| A | -20.11 | -19.81 | -26.21 | -28.58 | -19.26 | -20.25 | -30.69 | -30.16 | -24.05 | -24.11 |
| F | 0.64 | 0.64 | 0.62 | 0.60 | 0.64 | 0.64 | 0.60 | 0.61 | 0.42 | 0.42 |
| M | 0.36 | 0.36 | 0.38 | 0.40 | 0.36 | 0.36 | 0.40 | 0.39 | 0.58 | 0.58 |

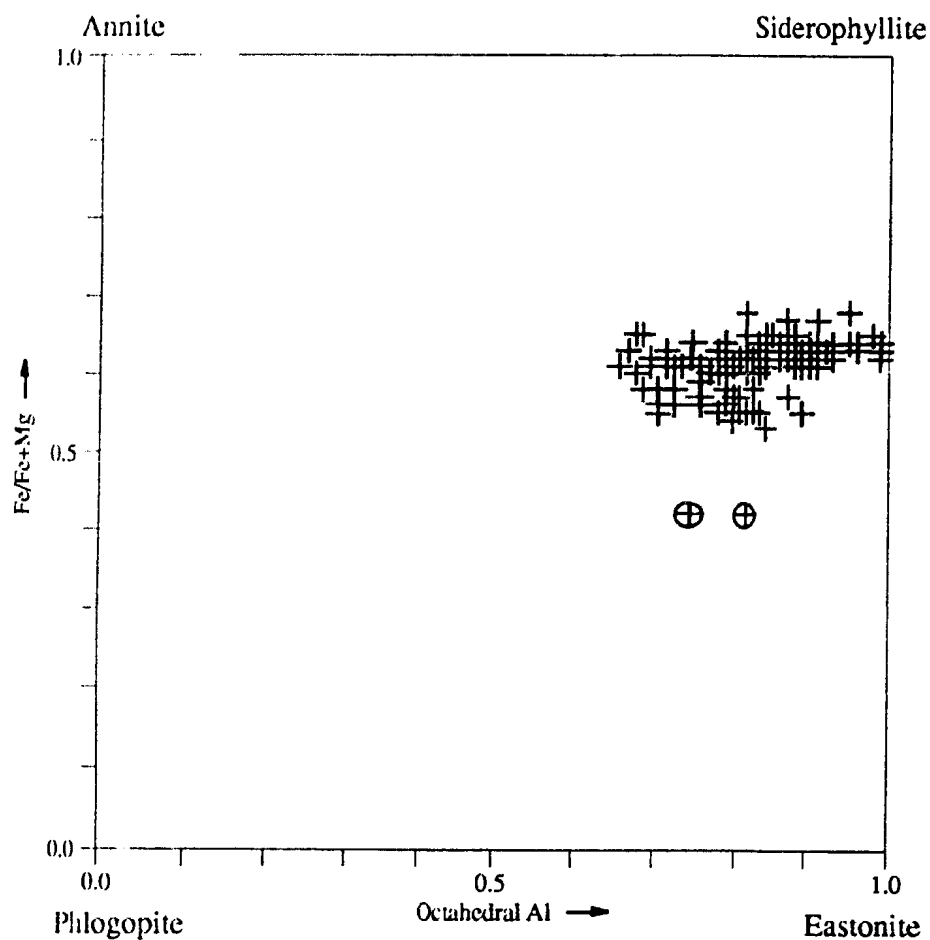


Figure 4-14. Plot of biotite compositions from the MCSZ (andalusite-biotite-muscovite zone and higher grade) modified from Deer *et al.*, 1966. The two circled analyses are from sample SD-89-299 (from the andalusite-biotite-muscovite zone) which contains cordierite and abundant magnetite.

of the compositions plot within the biotite field of Deer et al. (1966) and have a considerable siderophyllite/eastonite component. Figure 4-15 is an AFM plot of biotite compositions which also indicates the substantial variation in Al content between analyses.

4.7.5 Cordierite

Cordierite was analyzed in two samples; one from the sillimanite-biotite zone (G-123-80) and the other (SD-89-299) from a cordierite-magnetite sub-assemblage within the andalusite-biotite-muscovite zone. They are of very different compositions. In the first sample, cordierite is relatively unaltered, and six analyses indicate that it is virtually anhydrous with oxide totals near 100 %. These cordierites contain minor Mn (0.05 atoms PFU) substituting for Mg and Fe and have an average molar Mg:Fe ratio of 1:0.78. They also contain minor Na (0.06 atoms PFU) which, according to Deer et al. (1966), is probably located in axial channels.

In the other sample, the oxide totals are approximately 96 %. These cordierites also contain minor Mn (0.07 atoms PFU) substituting for Mg and Fe. However, the molar Mg:Fe ratio is 1:0.38 (less than half of that in the other sample) and Na is elevated, averaging 0.27 atoms PFU. These low totals may be due to the fact that these cordierites contain H₂O or CO₂ in the axial channel. In

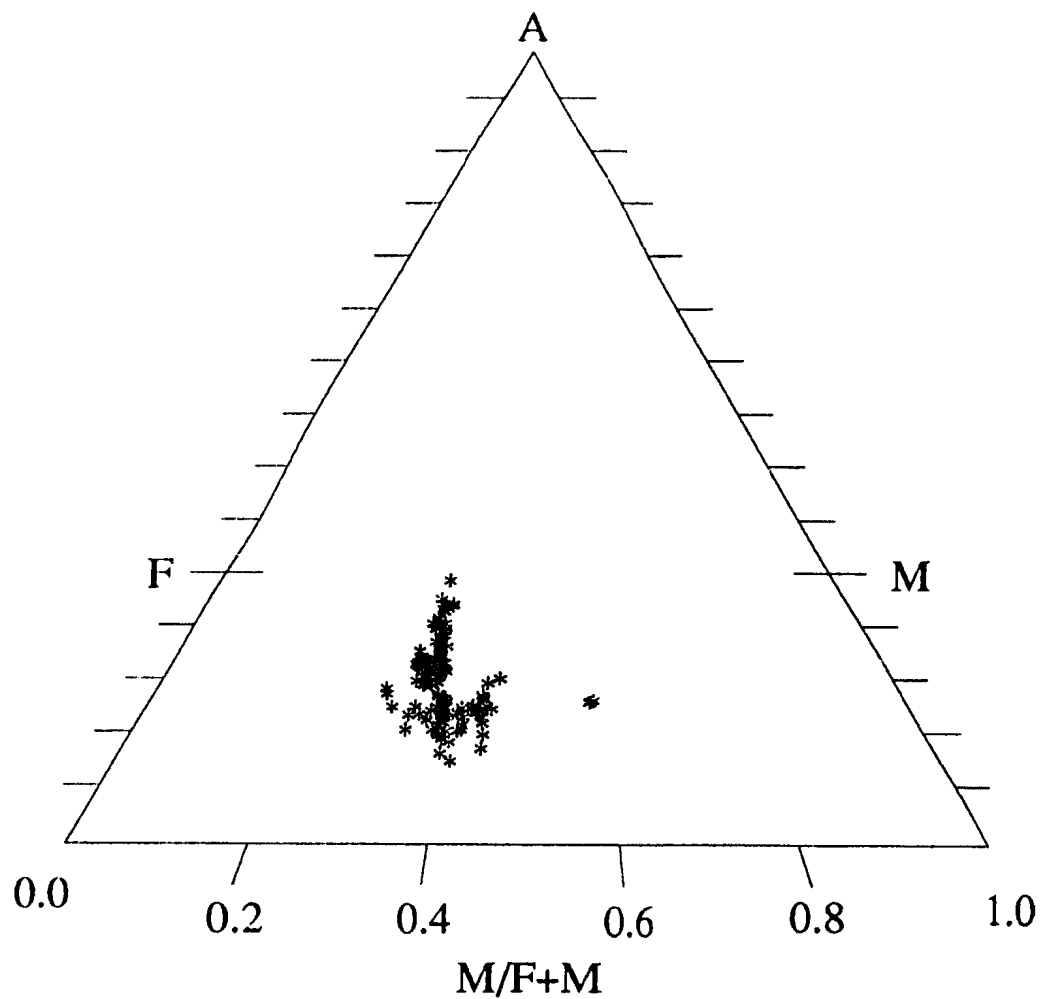


Figure 4-15. AFM diagram (Thompson, 1957) of biotite compositions (projected from muscovite) from the MCSZ. The two high-Mg compositions are from sample SD-89-299, which contains cordierite and abundant magnetite.

addition, these cordierites are extensively pinitized; chlorite present in pinite may have been analysed, causing the observed low totals. However, an examination of the stoichiometry of these analyses indicates that there is a deficiency in the M site; the reason for this is not known. Figure 4-16 is an AFM diagram of cordierite compositions and representative cordierite analyses are listed in Table 4-6.

4.7.6 Other Phases

Muscovite was analysed in fifteen samples from the andalusite-biotite-muscovite and sillimanite-biotite-muscovite zones (Table 4-7 lists some representative muscovite analyses). In all cases, larger grains were analysed and not the fine grained muscovite occurring in the matrix. All of the muscovites analysed contained 10 to 20 % paragonite component (~ 1 wt. % Na_2O) with no measurable margarite component (Figure 4-17a). Octahedral and tetrahedral aluminum are typically present in a 2:1 ratio (Table 4-7), indicating that phengite contents are low. However, minor Mg and Fe are present and substitute for Al^{VI} . In addition, Si content varies from 2.99 mol % to 3.30 mol % (averaging 3.09 mol %), indicating that minor phengite substitution has occurred in these muscovites. Figure 4-17b shows an inverse correlation between $(\text{Fe}+\text{Mg}+\text{Mn}+\text{Ti}+\text{Si})$ and $\text{Al}^{\text{IV}}+\text{Al}^{\text{VI}}$, which also indicates phengite substitution. However, this substitution is not

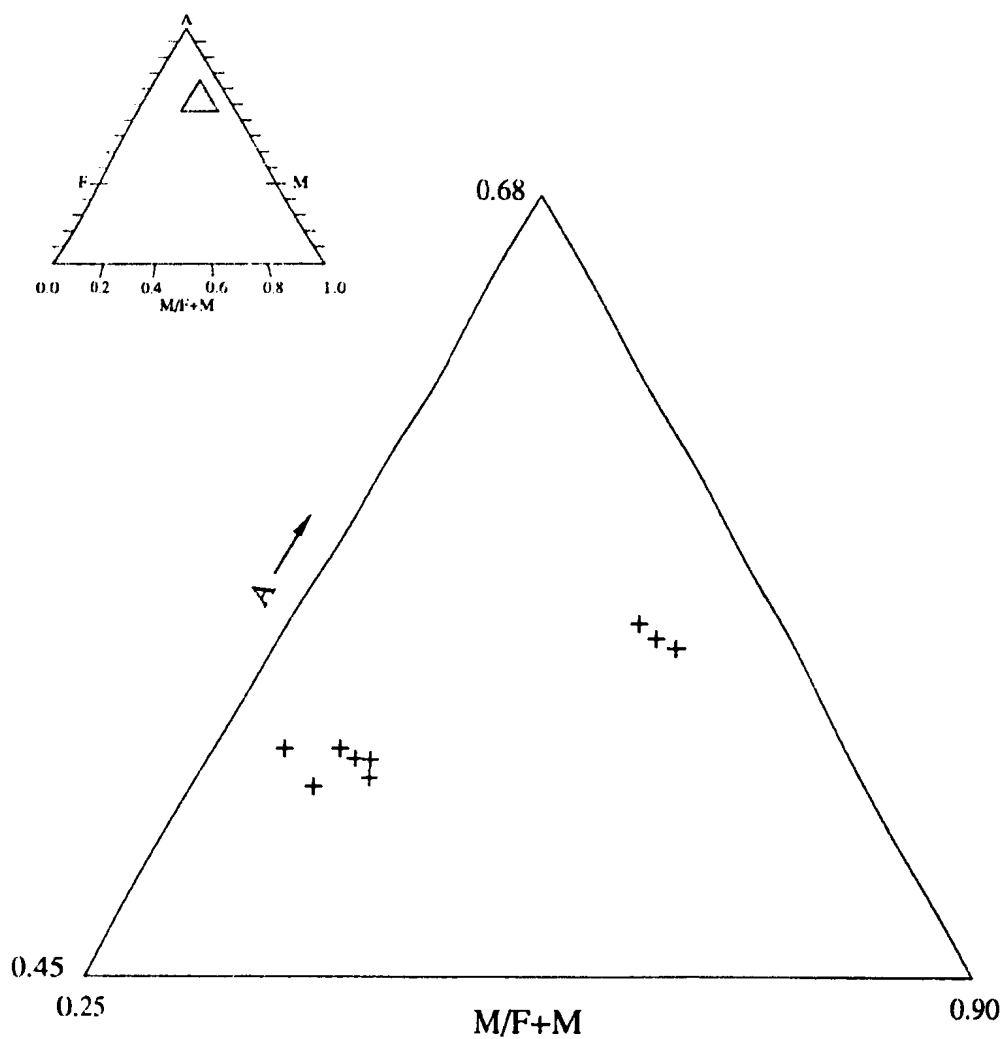


Figure 4-16. AFM plot (Thompson, 1957) of cordierite compositions. The three magnesium-rich compositions are from sample SD-89-299, which contains abundant magnetite.

Table 4-6
Representative analyses of cordierite

| | <i>G-123-80</i> (S-Kf Zone) | | | | | | <i>SD-89-299</i> (A-B-M Zone) | | |
|---|--------------------------------|--------|-------|-------|-------|-------|----------------------------------|-------|-------|
| SiO ₂ | 46.80 | 48.83 | 48.20 | 48.42 | 48.43 | 48.43 | 48.29 | 48.53 | 48.08 |
| TiO ₂ | 0.00 | 0.00 | 0.01 | 0.05 | 0.03 | 0.03 | 0.00 | 0.00 | 0.00 |
| Al ₂ O ₃ | 33.09 | 33.69 | 33.71 | 33.17 | 32.77 | 32.77 | 32.93 | 32.67 | 32.69 |
| Cr ₂ O ₃ | 0.01 | 0.04 | 0.03 | 0.00 | 0.00 | 0.00 | 0.00 | 0.02 | 0.01 |
| FeO | 9.52 | 9.89 | 9.61 | 10.07 | 9.80 | 9.80 | 5.23 | 5.19 | 5.47 |
| MnO | 0.60 | 0.54 | 0.58 | 0.48 | 0.59 | 0.59 | 0.76 | 0.83 | 0.70 |
| MgO | 7.33 | 7.22 | 7.33 | 6.64 | 6.92 | 6.92 | 7.70 | 8.01 | 7.79 |
| CaO | 0.00 | 0.00 | 0.02 | 0.00 | 0.01 | 0.01 | 0.00 | 0.00 | 0.00 |
| Na ₂ O | 0.31 | 0.32 | 0.25 | 0.17 | 0.36 | 0.36 | 1.39 | 1.29 | 1.36 |
| K ₂ O | 0.00 | 0.00 | 0.01 | 0.00 | 0.00 | 0.01 | 0.06 | 0.00 | 0.02 |
| Total | 99.46 | 100.53 | 99.77 | 99.04 | 99.69 | 99.69 | 96.37 | 96.54 | 96.13 |
| <i>number of cations on the basis of 18 oxygens</i> | | | | | | | | | |
| Si | 4.99 | 4.96 | 4.94 | 5.00 | 5.00 | 5.00 | 5.03 | 5.05 | 5.03 |
| Ti | 0.00 | 0.00 | 0.00 | 0.00 | 0.00 | 0.00 | 0.00 | 0.00 | 0.00 |
| Al | 4.00 | 4.04 | 4.07 | 4.03 | 3.99 | 3.99 | 4.05 | 4.01 | 4.03 |
| Cr | 0.00 | 0.00 | 0.00 | 0.00 | 0.00 | 0.00 | 0.00 | 0.00 | 0.00 |
| Fe | 0.82 | 0.84 | 0.82 | 0.87 | 0.85 | 0.85 | 0.46 | 0.45 | 0.48 |
| Mn | 0.05 | 0.05 | 0.05 | 0.04 | 0.05 | 0.05 | 0.07 | 0.07 | 0.06 |
| Mg | 1.12 | 1.09 | 1.12 | 1.02 | 1.07 | 1.07 | 1.20 | 1.24 | 1.21 |
| Ca | 0.00 | 0.00 | 0.00 | 0.00 | 0.00 | 0.00 | 0.00 | 0.00 | 0.00 |
| Na | 0.06 | 0.06 | 0.05 | 0.03 | 0.07 | 0.07 | 0.28 | 0.26 | 0.28 |
| K | 0.00 | 0.00 | 0.00 | 0.00 | 0.00 | 0.00 | 0.01 | 0.00 | 0.00 |
| Total | 11.04 | 11.05 | 11.05 | 11.00 | 11.03 | 11.03 | 11.09 | 11.08 | 11.09 |
| A | 50.81 | 51.06 | 51.15 | 51.63 | 51.07 | 51.07 | 54.90 | 54.19 | 54.30 |
| F | 0.42 | 0.43 | 0.42 | 0.46 | 0.44 | 0.44 | 0.28 | 0.27 | 0.28 |
| M | 0.58 | 0.57 | 0.58 | 0.54 | 0.56 | 0.56 | 0.72 | 0.73 | 0.72 |
| ΣMg+Fe+Mn | 1.99 | 1.98 | 1.99 | 1.93 | 1.97 | 1.97 | 1.73 | 1.76 | 1.75 |

Table 4-7
Representative analyses of muscovite

| | <i>SD-89-184</i> | | <i>SD-89-329</i> | | <i>SD-89-353</i> | | <i>SD-89-364</i> | |
|--------------------------------|------------------|-------|------------------|-------|------------------|-------|------------------|-------|
| | (S-B-M Zone) | | (S-B-M Zone) | | (A-B-M Zone) | | (S-B-M Zone) | |
| SiO ₂ | 46.81 | 47.86 | 48.25 | 47.81 | 48.25 | 47.66 | 47.34 | 47.76 |
| TiO ₂ | 0.61 | 0.52 | 0.50 | 0.50 | 0.28 | 0.22 | 0.67 | 0.82 |
| Al ₂ O ₃ | 35.61 | 35.81 | 35.70 | 35.72 | 37.08 | 36.23 | 36.10 | 35.94 |
| Cr ₂ O ₃ | 0.00 | 0.01 | 0.00 | 0.04 | 0.00 | 0.00 | 0.00 | 0.00 |
| FeO | 1.65 | 1.45 | 1.41 | 1.45 | 0.80 | 1.08 | 0.81 | 0.95 |
| MnO | 0.00 | 0.00 | 0.00 | 0.00 | 0.00 | 0.00 | 0.00 | 0.00 |
| MgO | 0.45 | 0.53 | 0.60 | 0.59 | 0.38 | 0.64 | 0.42 | 0.55 |
| CaO | 0.00 | 0.00 | 0.00 | 0.00 | 0.00 | 0.00 | 0.00 | 0.00 |
| Na ₂ O | 0.75 | 0.86 | 0.80 | 0.82 | 1.23 | 0.95 | 0.76 | 0.79 |
| K ₂ O | 8.79 | 8.77 | 8.70 | 8.53 | 8.31 | 7.59 | 8.42 | 8.12 |
| Total | 94.67 | 95.81 | 95.96 | 95.46 | 96.33 | 94.37 | 94.58 | 94.93 |

number of cations on the basis of 22 oxygens

| | | | | | | | | |
|-------------------------------------|-------|-------|-------|-------|-------|-------|-------|-------|
| Si | 6.21 | 6.26 | 6.29 | 6.26 | 6.24 | 6.27 | 6.24 | 6.26 |
| Ti | 0.06 | 0.05 | 0.05 | 0.05 | 0.03 | 0.02 | 0.07 | 0.08 |
| Al | 5.57 | 5.52 | 5.49 | 5.52 | 5.65 | 5.62 | 5.61 | 5.55 |
| Cr | 0.00 | 0.00 | 0.00 | 0.00 | 0.00 | 0.00 | 0.00 | 0.00 |
| Fe | 0.18 | 0.16 | 0.15 | 0.16 | 0.09 | 0.12 | 0.09 | 0.10 |
| Mn | 0.00 | 0.00 | 0.00 | 0.00 | 0.00 | 0.00 | 0.00 | 0.00 |
| Mg | 0.09 | 0.10 | 0.12 | 0.12 | 0.07 | 0.13 | 0.08 | 0.11 |
| Ca | 0.00 | 0.00 | 0.00 | 0.00 | 0.00 | 0.00 | 0.00 | 0.00 |
| Na | 0.19 | 0.22 | 0.20 | 0.21 | 0.31 | 0.24 | 0.19 | 0.20 |
| K | 1.49 | 1.46 | 1.45 | 1.43 | 1.37 | 1.27 | 1.42 | 1.36 |
| Total | 13.79 | 13.77 | 13.74 | 13.74 | 13.75 | 13.66 | 13.70 | 13.66 |
| Al ^{IV} | 1.79 | 1.74 | 1.71 | 1.74 | 1.74 | 1.73 | 1.76 | 1.74 |
| Al ^{VI} | 3.78 | 3.78 | 3.78 | 3.78 | 3.91 | 3.89 | 3.85 | 3.81 |
| Fe+Mg+Mn+Ti | 0.33 | 0.31 | 0.32 | 0.32 | 0.19 | 0.27 | 0.24 | 0.29 |
| K/K+Na+Ca | 0.89 | 0.87 | 0.88 | 0.87 | 0.82 | 0.84 | 0.88 | 0.87 |
| Na/K+Na+Ca | 0.11 | 0.13 | 0.12 | 0.13 | 0.18 | 0.16 | 0.12 | 0.13 |
| Ca/K+Na+Ca | 0.00 | 0.00 | 0.00 | 0.00 | 0.00 | 0.00 | 0.00 | 0.00 |
| Al ^{IV} + Al ^{VI} | 5.57 | 5.52 | 5.49 | 5.52 | 5.65 | 5.62 | 5.61 | 5.55 |
| Fe+Mg+Mn+Ti+Si | 6.54 | 6.57 | 6.61 | 6.58 | 6.43 | 6.54 | 6.48 | 6.55 |

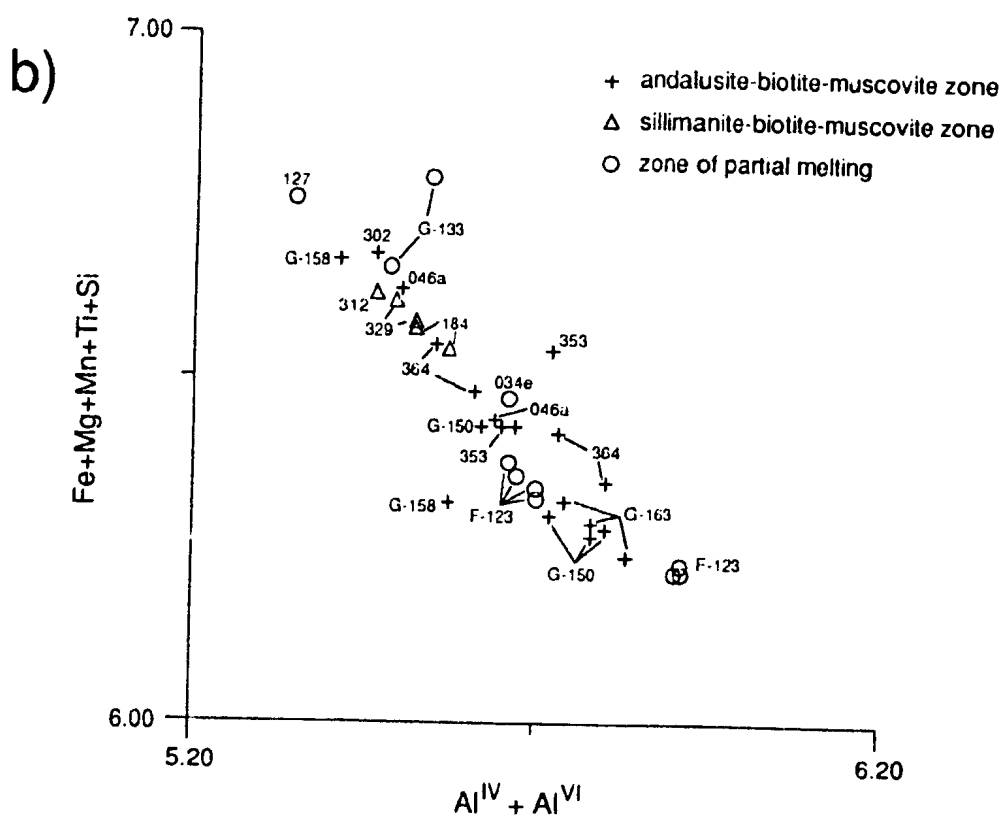
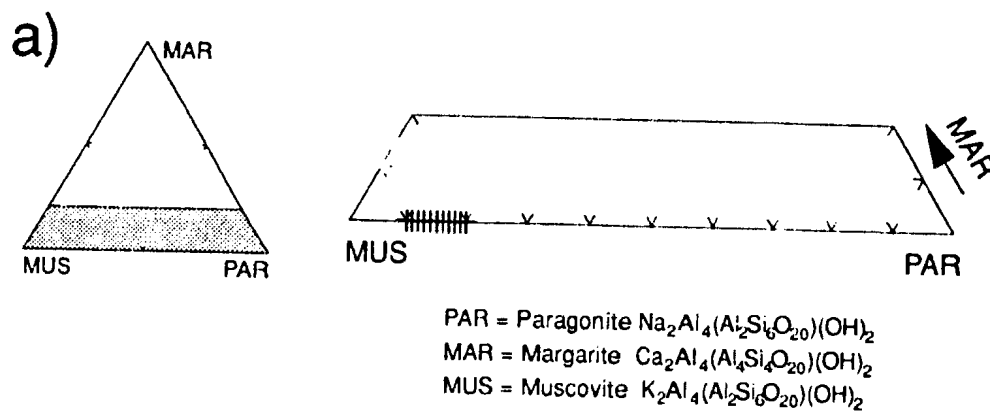


Figure 4-17. Plots of muscovite compositions from the MCSZ.

directly related to temperature and pressure as there is no correlation between amount of substitution and metamorphic grade (Figure 4-17b). Other factors (i.e. activities of solid components) must have accounted for the degree of substitution. For example, the activities of certain components are undefined in some samples; Al_2O_3 would be maximized in muscovites coexisting with an aluminosilicate phase, but an aluminosilicate phase is not present in the mineral assemblage of some samples. Also, if a Ti-bearing phase such as ilmenite were absent from the mineral assemblage, the activity of Ti would be undefined, which would affect its concentration in muscovite at any given T.

Staurolite was analysed in six samples from the andalusite-biotite-muscovite zone. In nineteen analyses, it shows a restricted range in Fe/Fe+Mg ratio (0.81-0.91, averaging 0.88), although there is some variation in aluminum content (Figure 4-18); this variation may be due to Fe^{3+} substituting for Al. This is unlikely, however, since Al is in excess (> 9 cations PFU) and the metal cations are depleted. This implies that either Al substitutes for Si (Si is slightly depleted), Al substitutes for the metal ions (Fe, Mg, Mn, Zn), or both. The analyses show that staurolite contains less than 2 wt. % ZnO (average of 0.78 %). No analyses were performed for lithium, but the wt% totals of ~ 97.5 suggest that it is not a significant component.

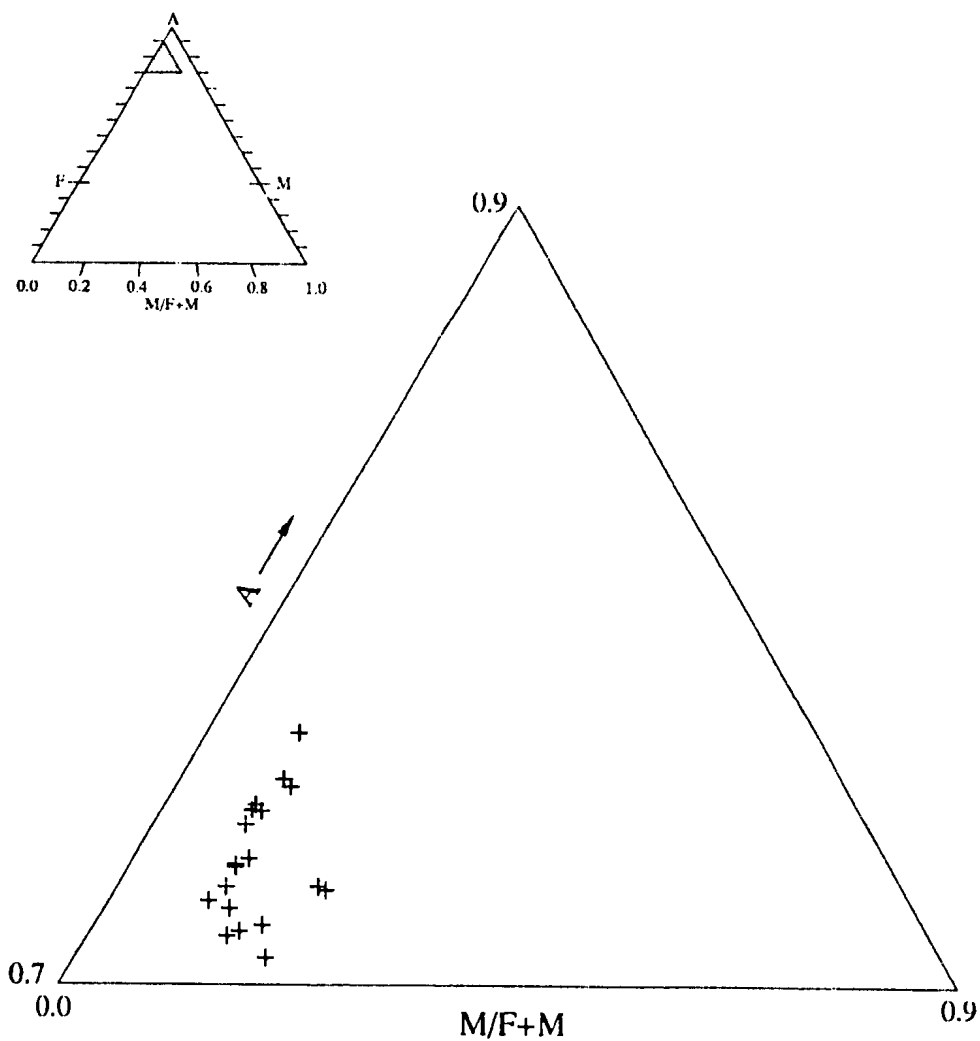


Figure 4-18. AFM plot (Thompson, 1957) of staurolite compositions (projected from muscovite).

Andalusite analyses indicate the presence of minor iron (< 0.2 wt.%), which according to Deer *et al.* (1966) is likely to be ferric. Table 4-8 shows some representative analyses of staurolite and andalusite.

4.7.7 Coexisting Phases

Results of probe analyses from coexisting garnet-biotite, garnet-biotite-staurolite and garnet-biotite-cordierite assemblages are plotted on AFM diagrams in Figures 4-19 and 4-20. Biotite-garnet pairs (Figure 4-19) display a restricted range in composition with respect to the AFM components. However, biotites tend to increase slightly in Fe-content with increasing metamorphic grade (Figure 4-19b and c). This pattern changes at the sillimanite-K feldspar reaction isograd where biotite is slightly more Mg-rich (Figure 4-20b). This increase in Mg content should be expected since the rocks in this area contain abundant cordierite.

The majority of tie lines shown on Figures 4-19 and 4-20 are approximately parallel implying that, at least in the samples analysed, the minerals were in equilibrium when they formed.

Table 4-8
Representative analyses of staurolite and andalusite

| | <i>staurolite</i> | | | | <i>andalusite</i> | | | |
|---|-----------------------------------|-------|----------------------------------|-------|---|-------|----------------------------------|--------|
| | <i>SD-89-097A</i> (S-B-M Zone) | | <i>SD-89-353</i> (A-B-M Zone) | | <i>SD-89-353</i> (A-B-M Zone) | | <i>SD-89-364</i> (S-B-M Zone) | |
| SiO ₂ | 27.33 | 27.37 | 26.98 | 26.75 | SiO ₂ | 35.72 | 35.94 | 35.94 |
| TiO ₂ | 0.54 | 0.54 | 0.47 | 0.45 | TiO ₂ | 0.00 | 0.00 | 0.00 |
| Al ₂ O ₃ | 55.60 | 55.51 | 55.06 | 56.09 | Al ₂ O ₃ | 63.90 | 63.41 | 64.01 |
| Cr ₂ O ₃ | 0.00 | 0.00 | 0.00 | 0.00 | Cr ₂ O ₃ | 0.01 | 0.00 | 0.00 |
| FeO | 12.14 | 12.06 | 13.89 | 13.37 | FeO | 0.19 | 0.16 | 0.20 |
| MnO | 0.46 | 0.46 | 0.23 | 0.26 | MnO | 0.00 | 0.00 | 0.00 |
| MgO | 0.68 | 0.78 | 1.06 | 0.78 | MgO | 0.04 | 0.02 | 0.03 |
| CaO | 0.00 | 0.00 | 0.00 | 0.00 | CaO | 0.00 | 0.00 | 0.00 |
| Na ₂ O | 0.02 | 0.02 | 0.00 | 0.00 | Na ₂ O | 0.02 | 0.01 | 0.00 |
| K ₂ O | 0.00 | 0.00 | 0.00 | 0.00 | K ₂ O | 0.01 | 0.00 | 0.01 |
| ZnO | 0.54 | 0.62 | 0.17 | 0.28 | Total | 99.89 | 99.54 | 100.19 |
| Total | 97.32 | 97.36 | 97.78 | 97.97 | | | | |
| <i>number of cations on the basis of 24 oxygens</i> | | | | | <i>number of cations on the basis of 5 oxygens</i> | | | |
| Si | 3.96 | 3.96 | 3.91 | 3.86 | Si | 0.97 | 0.98 | 0.97 |
| Ti | 0.06 | 0.06 | 0.05 | 0.05 | Ti | 0.00 | 0.00 | 0.00 |
| Al | 9.49 | 9.47 | 9.41 | 9.55 | Al | 2.04 | 2.03 | 2.04 |
| Cr | 0.00 | 0.00 | 0.00 | 0.00 | Cr | 0.00 | 0.00 | 0.00 |
| Fe | 1.47 | 1.46 | 1.67 | 1.62 | Fe | 0.00* | 0.00* | 0.00* |
| Mn | 0.06 | 0.06 | 0.03 | 0.03 | Mn | 0.00 | 0.00 | 0.00 |
| Mg | 0.15 | 0.17 | 0.23 | 0.17 | Mg | 0.00* | 0.00* | 0.00* |
| Ca | 0.00 | 0.00 | 0.00 | 0.00 | Ca | 0.00 | 0.00 | 0.00 |
| Na | 0.01 | 0.01 | 0.00 | 0.00 | Na | 0.00 | 0.00 | 0.00 |
| K | 0.00 | 0.00 | 0.00 | 0.00 | K | 0.00 | 0.00 | 0.00 |
| Zn | 0.06 | 0.07 | 0.02 | 0.03 | Total | 3.01 | 3.01 | 3.01 |
| Total | 15.24 | 15.25 | 15.33 | 15.31 | | | | |
| A | 74.59 | 74.42 | 71.21 | 72.81 | * Average of nine analyses shows that andalusite contains minor amounts of Fe (0.0043) and Mg (0.0013) cations. | | | |
| F | 0.91 | 0.90 | 0.88 | 0.91 | | | | |
| M | 0.09 | 0.10 | 0.12 | 0.09 | | | | |
| ΣMg+Fe+Mn | 1.68 | 1.69 | 1.93 | 1.82 | | | | |
| ΣMg+Fe+Mn+Zn | 1.74 | 1.76 | 1.95 | 1.85 | | | | |

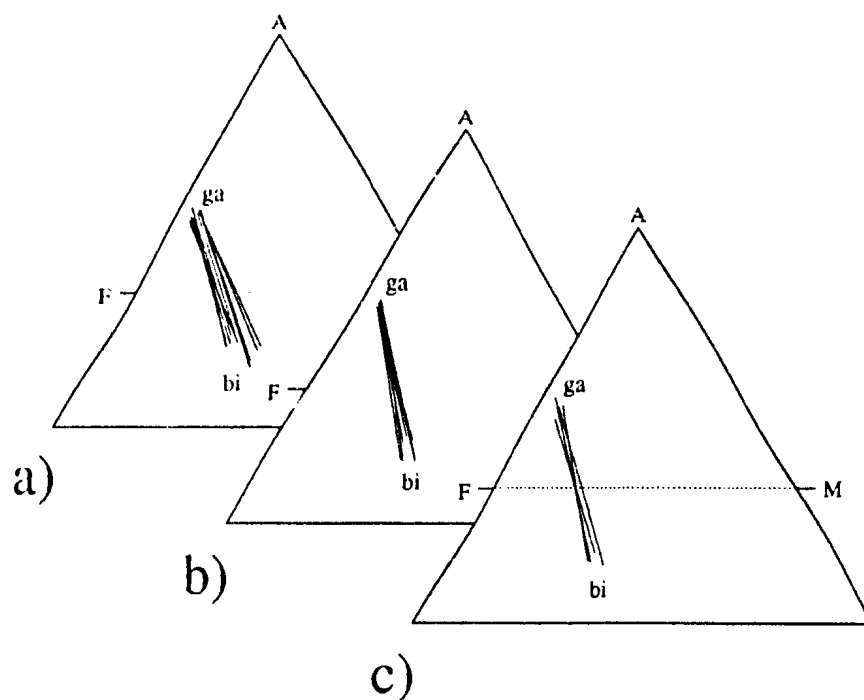


Figure 4-19. AFM diagrams (Thompson, 1957) projected through muscovite for coexisting biotite-garnet pairs separated on the basis of metamorphic grade. a) andalusite-biotite-muscovite zone; b) sillimanite-biotite-muscovite zone; and c) zone of partial melting.

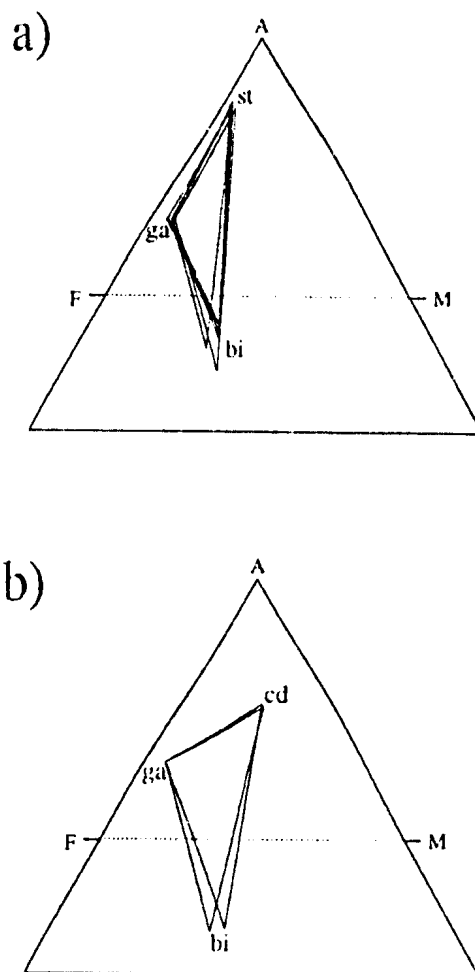


Figure 4-20. AFM diagrams (Thompson, 1957) projected through muscovite for: a) coexisting garnet-biotite-staurolite (from the andalusite-biotite-muscovite and sillimanite-biotite-muscovite zones); and b) garnet-biotite-cordierite (from the sillimanite-K feldspar zone).

CHAPTER 5

QUANTITATIVE ESTIMATION OF PRESSURE AND TEMPERATURE

5.1 Introduction

One of the objectives of this study is to estimate quantitatively the metamorphic pressure and temperature conditions within the MCSZ from compositions of coexisting minerals in selected samples. These P-T estimates are derived from experimentally calibrated geothermobarometric expressions. This chapter includes a description of the methodology used in the thermobarometric calculations along with the P-T results obtained from those calculations. Temperatures and pressures are listed in the text. Where zoning is present, the P-T vectors (Mengel and Rivers, 1989) have been determined, which represent sections of the P-T-t path for individual samples. In addition, in one sample with favourable mineralogy, an estimate of $a_{\text{H}_2\text{O}}$ is determined from which the local mole fraction of water in the fluid phase can be estimated (with certain assumptions; see Section 5.5).

5.2 Methodology

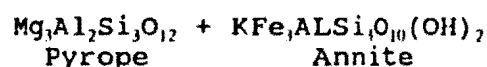
5.2.1 Geothermometry

Temperature estimates have been determined from selected samples within the MCSZ on the basis of Fe-Mg

exchange between coexisting garnet-biotite and garnet-cordierite pairs utilizing the thermometers of Ferry and Spear (1978; with corrections by Hodges and Spear, 1982) for garnet-biotite and Perchuk et al. (1985) for garnet-cordierite.

The assemblage garnet-biotite is stable throughout the andalusite-biotite-muscovite and sillimanite-biotite-muscovite zones. In addition, sample G-123-80 from the sillimanite-K feldspar zone (just below or concurrent with the beginning of melting) contains the equilibrium assemblage garnet-biotite-cordierite-sillimanite-plagioclase-K feldspar. These assemblages allow for the comparison of the two mineralogical thermometers.

The garnet-biotite thermometer of Ferry and Spear (1978) is based on the partitioning of Fe and Mg between the two phases. The cation exchange reaction is:



Ferry and Spear (1978) conducted experiments on synthetic garnet and biotite, but the method is considered to be applicable to natural assemblages with compositions in the interval $0.80 > \text{Fe}/(\text{Fe} + \text{Mg}) < 1.00$ in which Mg and Fe in garnet and biotite are inferred to mix ideally. However, they also suggested that caution be used when applying their

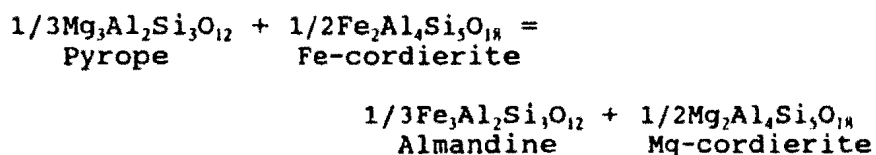
results to systems that contain appreciable amounts of Ca, Mn or Ti. The analyses in the present study indicate that titanium is low in biotite (average of 124 analyses, $\text{TiO}_2 = 2.05 \text{ wt } \%$), calcium is negligible in garnet, but the garnets contain a high proportion of manganese ($X_{\text{Mn}} = 0.20$ or greater).

In order to extend the useful compositional range of the geothermometer, Hodges and Spear (1982) included formulations for mixing models in the solid phases in a revised version of the geothermometer. They suggested that Fe-Mg mixing in garnet is non-ideal (Appendix C1), but that Fe-Mn solutions mix approximately ideally. They accounted for the non-ideality in garnet solid solutions by introducing the non-ideal activity-composition relations (activity coefficients) into the equilibrium constant expression. However, the differences in temperature utilizing their revised model are minimal (less than 10°C) when compared to the accuracy of the thermometer ($\pm 50^\circ \text{C}$) for the compositions used in this study. Nevertheless, in this study, the model of Ferry and Spear (1978) with Hodges and Spear (1982) corrections for non-ideal mixing is followed.

Coexisting garnet and biotite were analyzed in nineteen samples. In each sample, matrix biotite as well as biotite near garnet was analyzed, and probe traverses were done across garnets to determine whether or not they were

zoned. The computer program PTCALC (written by F. Mengel, Memorial University), into which the Ferry and Spear (1978) and Hodges and Spear (1982) calibrations are programmed, was used to calculate temperatures of formation for selected analyses, combining garnet cores with matrix biotites and garnet rims with adjacent biotites. An assumption is made that all garnets analyzed are true cross-sections (through the core) and that matrix biotites are separate from any garnets (at least in the plane of the thin section). If the garnet sections are not through the core, the measured zoning profile will exhibit a less extreme compositional range than the real profile and thus the results will tend to understate the range of temperature.

The garnet-cordierite thermometer is also based on the exchange of Fe and Mg between the phases. The exchange reaction (from Perchuk et al., 1985) is:



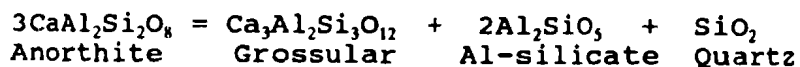
Mixing of Fe and Mg is assumed to be ideal in both phases, at the metamorphic grades in this study. However, this assumption may not hold true at higher temperatures. In a recent paper by Bhattacharya et al. (1988), data were presented from granulite facies rocks which indicate that Fe-Mg mixing in cordierite is approximated by a symmetric

regular solution in the temperature range of 620-860 °C. They showed that Fe-Mg substitution displays positive deviation from ideality at these temperatures.

5.2.2 Geobarometry

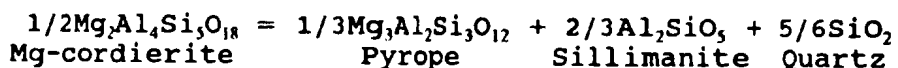
Pressure estimates have been determined from appropriate assemblages using the garnet-plagioclase- Al_2SiO_5 -quartz geobarometer of Newton and Haselton (1981) and the garnet-cordierite-sillimanite-quartz geobarometer of Perchuk *et al.* (1985).

The calibration of the plagioclase-garnet- Al_2SiO_5 -quartz barometer (Newton and Haselton, 1981) is based on the volume change of the reaction:



as Ca-plagioclase breaks down and the Ca is partitioned into the garnet.

The garnet-cordierite-sillimanite-quartz geobarometer (Perchuk *et al.*, 1985) utilizes the volume change of the reaction:



as Mg-garnet (pyrope) breaks down and the Mg is partitioned into the cordierite (Appendix C2).

Analytical results were entered into PTCALC for the first barometer; pressures from the second geobarometer

were calculated manually. For the garnet-plagioclase-sillimanite-quartz geobarometer, a pair of curves was generated for zoned samples by combining garnet and plagioclase core analyses and then utilizing rim analyses from the same pairs. In all samples containing an aluminosilicate phase, sillimanite was the species present.

For each assemblage, a family of temperature-dependent curves was developed by solving the thermodynamic expressions for the appropriate thermometer over a pressure range of 0-10 kilobars. Similarly, pressure-dependent curves were generated by solving the appropriate barometric expressions over a temperature range of 0-1000 °C (subsequently reduced to 450-750 °C since the temperature-dependent curves fall within this range over the specified pressure range).

Assuming that the barometer and thermometer closed at the same time and under the same P-T conditions, we can combine the temperature- and pressure-dependent curves from the same sample, and define a unique P-T point. Where zoned minerals are used in the calculations, curves for core and rim compositions are plotted, resulting in the definition of a P-T vector (i.e. a line joining P-T estimates of core and rim in samples with zoned phases; Mengel and Rivers, 1989). P-T vectors can outline part of the P-T path followed during subsequent erosion and uplift (Mengel and Rivers, 1989; Hodges and Royden, 1984; Royden and Hodges, 1984). However,

if the assumptions about closure conditions were incorrect, and the thermometer continued to re-equilibrate after the barometer closed, spurious P-T paths would result (i.e. Selverstone and Chamberlain, 1990).

5.3 Results of Geothermobarometry

5.3.1 Geothermometry Results

Some of the temperature-dependent curves resulting from the garnet-biotite thermometer are plotted on P-T diagrams (Figures 5-1 and 5-2) and listed in Table 5-1. The majority of the results plot within the 550-700 °C temperature range, over a pressure change of 0-10 kilobars. However, some curves from selected samples showed a wide variation in temperature (in one case, more than 300 °C). These curves were omitted from further calculations on the basis that the minerals used in the calculations are in textural disequilibrium (garnet not stable with biotite).

The most striking feature of the temperature-dependent curves shown in Figures 5-1 and 5-2 is that most of the estimated rim temperatures indicate closure temperatures of about 575 °C (± 25 °C) for the thermometers (at a pressure of ~ 3 kbar). Also, core temperatures are approximately constant at about 610 °C (± 15 °C). There appears to be no difference between metamorphic zones. A notable exception to this is sample G-133-80 from the zone of partial melting. Temperature-dependent curves in this

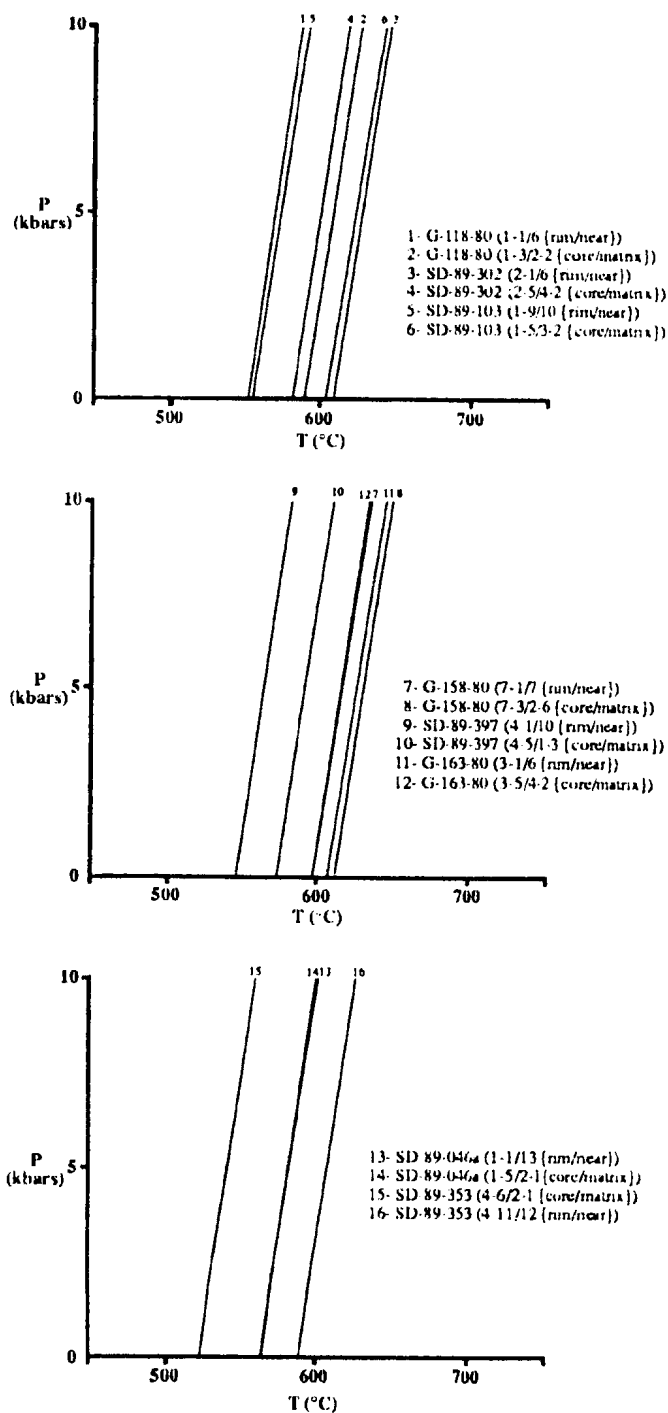


Figure 5-1. Representative temperature-dependent curves from samples from the andalusite-biotite-muscovite zone. Those prefixed with G collected by S.P. Colman-Sadd.

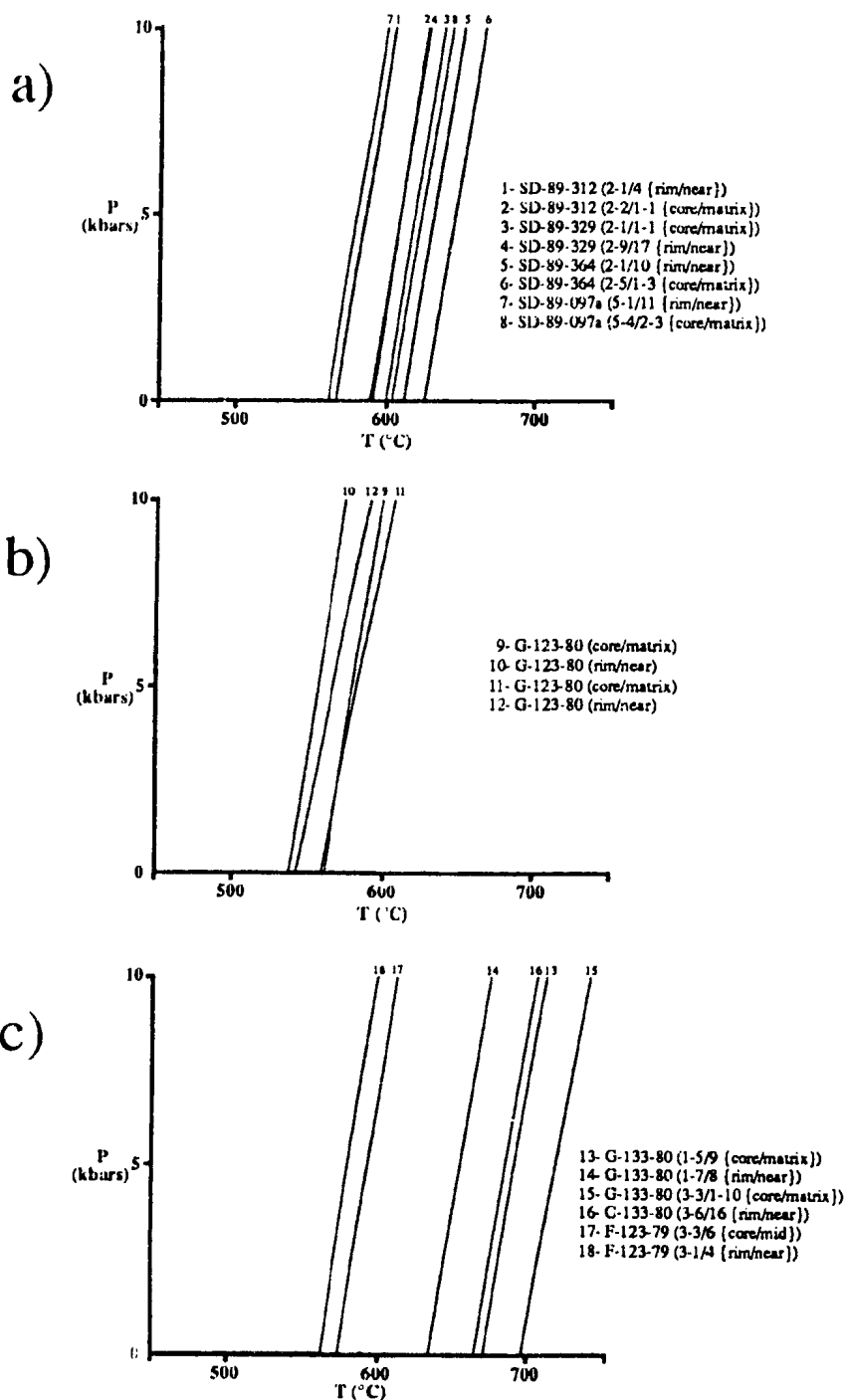


Figure 5-2. Representative temperature-dependent curves from samples from the: a) sillimanite-biotite-muscovite zone; b) sillimanite-K feldspar zone; and c) the zone of partial melting. Those prefixed F and G collected by S.P. Colman-Sadd.

Table 5-1. Results of Garnet-Biotite Thermometry

T1 = Ferry & Spear (1978); T2 = Ferry and Spear (1978) with corrections by
Hodges & Spear (1982)

rim = garnet rim with adjacent biotite; core = garnet core with matrix biotite
Temperatures in °C

| F-123-79 (ZM) | | | | | | | | |
|------------------|------|-----|-------|-----|-------|-----|-------|-----|
| P (Kbar) | rim1 | | rim2 | | core1 | | core2 | |
| | T1 | T2 | T1 | T2 | T1 | T2 | T1 | T2 |
| 2 | 749 | 760 | 571 | 582 | 753 | 763 | 577 | 587 |
| 4 | 758 | 769 | 579 | 589 | 762 | 772 | 585 | 595 |
| 6 | 768 | 778 | 586 | 597 | 771 | 782 | 592 | 603 |
| 8 | 777 | 788 | 594 | 604 | 780 | 791 | 600 | 610 |
| 10 | 786 | 797 | 602 | 612 | 790 | 800 | 608 | 618 |
| G-133-80 (ZM) | | | | | | | | |
| P (Kbar) | rim1 | | rim2 | | core1 | | core2 | |
| | T1 | T2 | T1 | T2 | T1 | T2 | T1 | T2 |
| 2 | 590 | 603 | 630 | 643 | 693 | 706 | 667 | 679 |
| 4 | 598 | 610 | 638 | 651 | 701 | 714 | 675 | 688 |
| 6 | 606 | 618 | 646 | 659 | 710 | 723 | 684 | 696 |
| 8 | 614 | 626 | 655 | 667 | 719 | 732 | 692 | 704 |
| 10 | 621 | 634 | 663 | 676 | 728 | 740 | 701 | 713 |
| SD-89-312 (S) | | | | | | | | |
| P (Kbar) | rim1 | | rim2 | | core1 | | core2 | |
| | T1 | T2 | T1 | T2 | T1 | T2 | T1 | T2 |
| 2 | 565 | 575 | 535 | 544 | 587 | 598 | 595 | 604 |
| 4 | 573 | 582 | 543 | 551 | 595 | 605 | 603 | 612 |
| 6 | 580 | 590 | 550 | 558 | 602 | 613 | 610 | 619 |
| 8 | 588 | 597 | 557 | 565 | 610 | 621 | 618 | 627 |
| 10 | 596 | 605 | 565 | 573 | 618 | 628 | 626 | 635 |
| SD-89-329 (S) | | | | | | | | |
| P (kbar) | rim1 | | rim2 | | core1 | | core2 | |
| | T1 | T2 | T1 | T2 | T1 | T2 | T1 | T2 |
| 2 | 593 | 597 | 622 | 632 | 598 | 607 | 624 | 634 |
| 4 | 601 | 605 | 631 | 640 | 606 | 615 | 633 | 642 |
| 6 | 609 | 613 | 639 | 648 | 614 | 623 | 641 | 650 |
| 8 | 616 | 620 | 647 | 656 | 622 | 631 | 649 | 658 |
| 10 | 624 | 628 | 655 | 664 | 630 | 638 | 657 | 667 |
| SD-89-097a (A-S) | | | | | | | | |
| P (Kbar) | rim1 | | rim2 | | core1 | | core2 | |
| | T1 | T2 | T1 | T2 | T1 | T2 | T1 | T2 |
| 2 | 666 | 686 | 501 | 511 | 615 | 635 | 597 | 612 |
| 4 | 674 | 695 | 508 | 518 | 623 | 643 | 605 | 620 |
| 6 | 683 | 703 | 515 | 525 | 631 | 651 | 613 | 628 |
| 8 | 691 | 712 | 522 | 532 | 640 | 659 | 621 | 636 |
| 10 | 700 | 720 | 529 | 539 | 648 | 667 | 629 | 644 |
| SD-89-364 (A-S) | | | | | | | | |
| P (Kbar) | rim1 | | core1 | | | | | |
| | T1 | T2 | T1 | T2 | | | | |
| 2 | 602 | 620 | 615 | 634 | | | | |
| 4 | 609 | 628 | 623 | 642 | | | | |
| 6 | 617 | 636 | 632 | 650 | | | | |
| 8 | 625 | 644 | 640 | 658 | | | | |
| 10 | 633 | 652 | 648 | 666 | | | | |
| SD-89-397 (A) | | | | | | | | |
| P (Kbar) | rim1 | | rim2 | | core1 | | core2 | |
| | T1 | T2 | T1 | T2 | T1 | T2 | T1 | T2 |
| 2 | 561 | 568 | 548 | 553 | 576 | 586 | 573 | 581 |
| 4 | 568 | 576 | 554 | 561 | 583 | 594 | 580 | 588 |
| 6 | 576 | 583 | 561 | 568 | 591 | 601 | 588 | 596 |
| 8 | 583 | 591 | 568 | 575 | 599 | 609 | 596 | 603 |
| 10 | 591 | 598 | 576 | 583 | 606 | 617 | 603 | 611 |
| G-163-80 (A) | | | | | | | | |
| P (Kbar) | rim1 | | rim2 | | core1 | | core2 | |
| | T1 | T2 | T1 | T2 | T1 | T2 | T1 | T2 |
| 2 | 606 | 615 | 607 | 618 | 594 | 610 | 588 | 605 |
| 4 | 614 | 623 | 615 | 626 | 601 | 618 | 595 | 612 |
| 6 | 622 | 631 | 623 | 634 | 609 | 626 | 603 | 620 |
| 8 | 630 | 639 | 631 | 642 | 617 | 634 | 611 | 628 |
| 10 | 638 | 647 | 639 | 650 | 625 | 642 | 619 | 635 |
| SD-89-103 (A) | | | | | | | | |
| P (Kbar) | rim1 | | rim2 | | core1 | | core2 | |
| | T1 | T2 | T1 | T2 | T1 | T2 | T1 | T2 |
| 2 | 601 | 614 | 552 | 562 | 619 | 634 | 598 | 612 |
| 4 | 609 | 622 | 560 | 570 | 627 | 642 | 606 | 620 |
| 6 | 617 | 630 | 567 | 577 | 636 | 650 | 614 | 628 |
| 8 | 625 | 637 | 575 | 584 | 644 | 658 | 622 | 636 |
| 10 | 633 | 645 | 582 | 592 | 652 | 666 | 630 | 644 |
| G-158-80 (A) | | | | | | | | |
| P (Kbar) | rim1 | | rim2 | | core1 | | core2 | |
| | T1 | T2 | T1 | T2 | T1 | T2 | T1 | T2 |
| 2 | 596 | 613 | 588 | 605 | 609 | 627 | 601 | 620 |
| 4 | 604 | 621 | 596 | 613 | 617 | 635 | 609 | 628 |
| 6 | 612 | 629 | 604 | 621 | 625 | 643 | 617 | 636 |
| 8 | 619 | 637 | 612 | 628 | 633 | 651 | 625 | 643 |
| 10 | 627 | 644 | 620 | 636 | 641 | 659 | 633 | 651 |
| SD-89-353 (A) | | | | | | | | |
| P (Kbar) | rim1 | | rim2 | | core1 | | core2 | |
| | T1 | T2 | T1 | T2 | T1 | T2 | T1 | T2 |
| 2 | 589 | 607 | 579 | 598 | 513 | 531 | 498 | 516 |
| 4 | 596 | 615 | 587 | 606 | 520 | 538 | 505 | 523 |
| 6 | 604 | 623 | 595 | 613 | 527 | 545 | 512 | 530 |
| 8 | 612 | 630 | 602 | 621 | 534 | 552 | 519 | 537 |
| 10 | 620 | 638 | 610 | 628 | 541 | 559 | 526 | 544 |
| SD-89-046a (A) | | | | | | | | |
| P (Kbar) | rim1 | | core1 | | rim1 | | core1 | |
| | T1 | T2 | T1 | T2 | T1 | T2 | T1 | T2 |
| 2 | 562 | 571 | 552 | 571 | 560 | 569 | 596 | 613 |
| 4 | 569 | 579 | 559 | 578 | 567 | 577 | 604 | 621 |
| 6 | 577 | 586 | 567 | 585 | 575 | 584 | 612 | 629 |
| 8 | 584 | 594 | 574 | 593 | 582 | 592 | 620 | 637 |
| 10 | 592 | 602 | 582 | 600 | 590 | 599 | 628 | 644 |
| G-118-80 (A) | | | | | | | | |
| P (Kbar) | rim1 | | core1 | | rim1 | | core1 | |
| | T1 | T2 | T1 | T2 | T1 | T2 | T1 | T2 |
| 2 | 596 | 616 | 561 | 580 | | | | |
| 4 | 604 | 623 | 568 | 588 | | | | |
| 6 | 612 | 631 | 576 | 595 | | | | |
| 8 | 620 | 639 | 583 | 603 | | | | |
| 10 | 628 | 647 | 591 | 610 | | | | |
| SD-89-302 (A) | | | | | | | | |
| P (Kbar) | rim1 | | core1 | | | | | |
| | T1 | T2 | T1 | T2 | | | | |
| 2 | 596 | 616 | 561 | 580 | | | | |
| 4 | 604 | 623 | 568 | 588 | | | | |
| 6 | 612 | 631 | 576 | 595 | | | | |
| 8 | 620 | 639 | 583 | 603 | | | | |
| 10 | 628 | 647 | 591 | 610 | | | | |

sample indicate closure temperatures at about 650 °C. Garnets in this sample also record some of the highest core temperatures in this study (~ 700 °C) and have the most Fe-rich compositions (greater than 80% almandine component). The reason for this difference is not readily apparent. However, local factors (i.e. strain, activity of solid and fluid phases) may have influenced the closure temperature. Also, $a_{\text{H}_2\text{O}}$ may have been very low, as all H_2O previously in equilibrium with solid phases may have been incorporated into the melt phase. Low $a_{\text{H}_2\text{O}}$ would be compatible with slow transport of elements between phases (presumably by diffusion).

The majority of the results indicates decreasing temperature following peak metamorphic conditions (i.e. garnet rims are lower T than garnet cores). However, three of the fifteen samples plotted (G-163-80, SD-89-353 and SD-89-302) from the andalusite-biotite-muscovite zone show rim temperatures higher than core temperatures. A possible explanation for this is that these garnets never reached a high enough temperature to cause homogenization. Garnets from the first two samples display prograde (or growth) zoning; garnets in SD-89-353 are idioblastic and show no evidence of resorption. The cores, therefore, would preserve temperatures at the time of formation, not peak metamorphic conditions (i.e. peak temperature) as with homogenized and retrograde zoned garnets. As temperature

increased, garnet would continue to grow, and the rims would preserve these elevated temperatures. Sample SD-89-302 shows evidence of retrograde metamorphism (biotite altering to chlorite). Elevated rim temperatures may be due to re-equilibration with chlorite, which occurs approximately 2 mm from the garnet.

One sample in this study contains garnet, biotite and cordierite (sample G-123-80). Temperature estimates using the garnet-biotite and garnet-cordierite geothermometers yield nearly identical results with a limited temperature range of $< 25^{\circ}\text{C}$ (Figure 5-3a).

5.3.2 Geobarometry Results

Calculated pressure-dependent curves have been plotted on Figure 5-3b and Figure 5-4 and representative pressure estimates are listed in Table 5-2. The slope of the garnet-cordierite-quartz-sillimanite reaction (Figure 5-3b; $dP/dT = 0.4 \text{ bars}/^{\circ}\text{C}$) is much lower than that of the garnet-plagioclase-sillimanite-quartz reaction ($dP/dT = 12.2 \text{ bars}/^{\circ}\text{C}$). The estimated pressure-dependent curves for the former reaction are nearly isobaric at $\sim 3 \text{ kbar}$ between 500 and 700 $^{\circ}\text{C}$; those of the latter reaction vary from ~ 0.5 to $\sim 3 \text{ kbar}$ in the same temperature range. This difference in pressure between the two reactions is approximately 1.5 kbar at the calculated temperatures in sample G-123-80; the latter pressure is lower than the majority of the calculated pressures from the other samples (Figure 5-4).

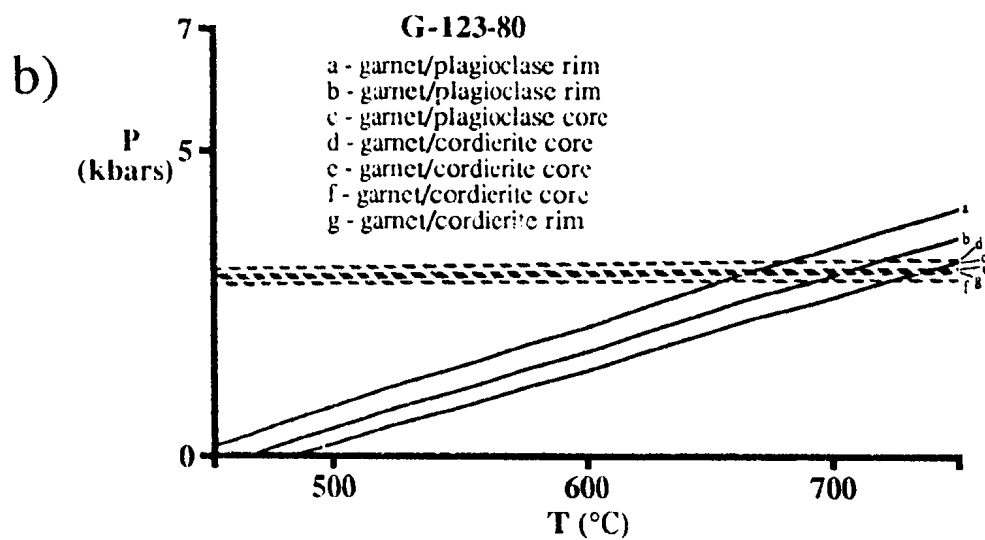
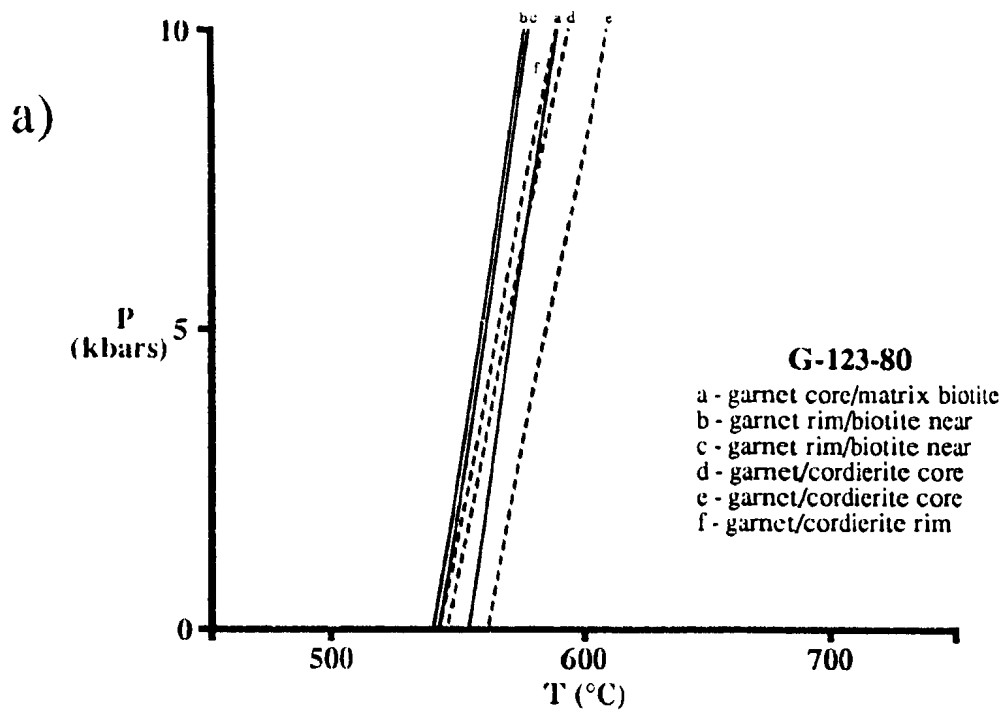


Figure 5-3. Temperature-dependent and pressure-dependent curves from sample G-123-80 from the sillimanite-K feldspar reaction isograd. Dashed lines are garnet-cordierite-biotite-sillimanite-quartz assemblages, solid lines are garnet-biotite-plagioclase-sillimanite-quartz assemblages.

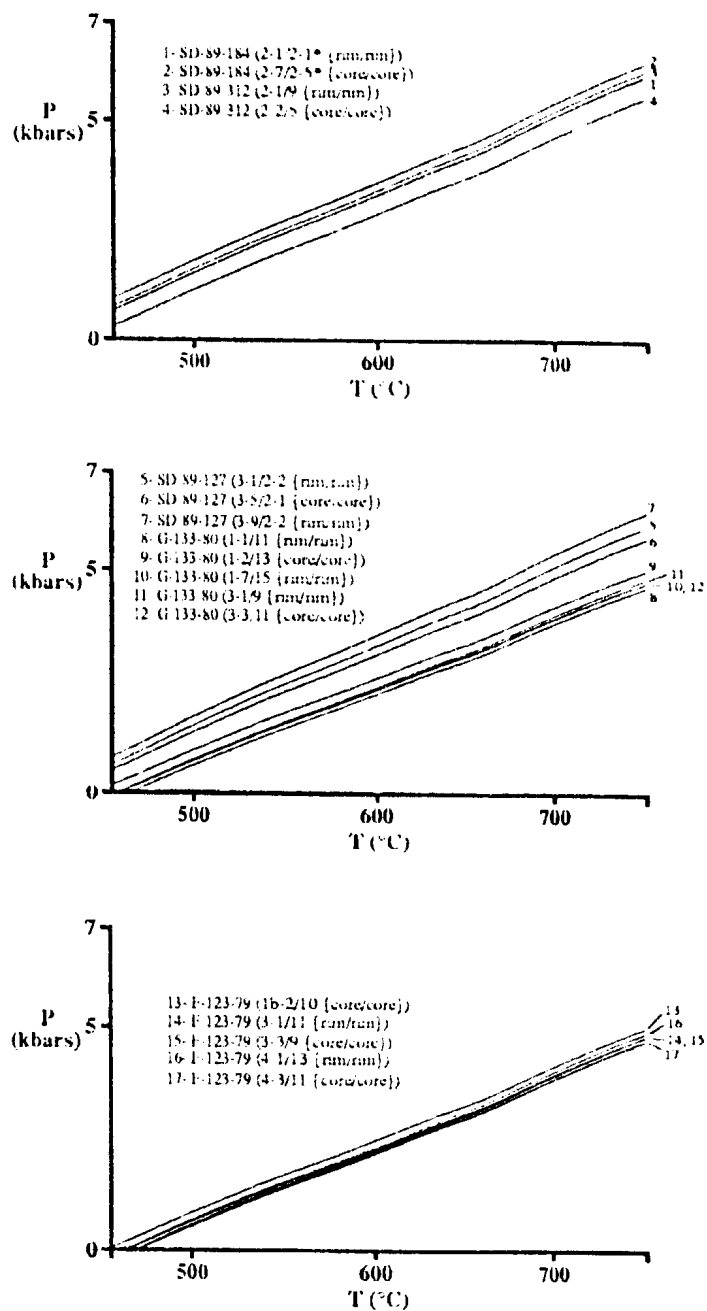


Figure 5-4. Representative pressure-dependent curves using the garnet-plagioclase-sillimanite-quartz barometer from selected samples from the MCSZ (higher grade than the sillimanite-biotite-muscovite reaction isograd). Those prefixed F and G collected by S.P. Colman-Sadd.

**Table 5-2. Results of Garnet-Sillimanite-
Plagioclase- Quartz Barometry**

Newton and Haselton, 1981

rim = garnet rim/plagioclase rim; core = garnet core/plagioclase core
Pressure in kilobars

| F-123-79 (ZM) | | | | | | |
|---------------|------------|-----------|-----------|------------|-----------|------------|
| T (°C) | core1 P | rim1 P | rim2 P | core2 P | rim3 P | core3 P |
| 200 | -4.1 | -4.1 | -4.4 | -4.4 | -4.3 | -4.3 |
| 400 | -0.8 | -0.8 | -1.0 | -1.1 | -1.0 | -1.1 |
| 600 | 2.5 | 2.6 | 2.3 | 2.3 | 2.4 | 2.2 |
| 800 | 5.8 | 6.0 | 5.6 | 5.6 | 5.7 | 5.5 |
| 1000 | 9.1 | 9.4 | 8.9 | 8.9 | 9.1 | 8.7 |

| G-133-80 (ZM) | | | | | | |
|---------------|-----------|-----------|-----------|------------|------------|------------|
| T (°C) | rim1 P | rim2 P | rim3 P | core1 P | core2 P | core3 P |
| 200 | -4.2 | -4.1 | -4.1 | -4.0 | -4.2 | -4.1 |
| 400 | -1.0 | -0.9 | -0.9 | -0.7 | -1.0 | -0.9 |
| 600 | 2.2 | 2.3 | 2.4 | 2.5 | 2.2 | 2.3 |
| 800 | 5.4 | 5.5 | 5.6 | 5.8 | 5.4 | 5.5 |
| 1000 | 8.6 | 8.7 | 8.9 | 9.0 | 8.6 | 8.7 |

| SD-89-312 (S) | | | | |
|---------------|-----------|-----------|------------|------------|
| T (°C) | rim1 P | rim2 P | core1 P | core2 P |
| 200 | -3.8 | -4.9 | -4.1 | -4.2 |
| 400 | -0.2 | -1.8 | -0.6 | -0.8 |
| 600 | 3.4 | 1.3 | 2.9 | 2.7 |
| 800 | 7.0 | 4.5 | 6.4 | 6.1 |
| 1000 | 10.6 | 7.6 | 9.8 | 9.6 |

| SD-89-184 (S) | | SD-89-127 (ZM) | |
|---------------|----------|----------------|----------|
| T (°C) | rim P | core P | rim P |
| 200 | -3.9 | -3.6 | -3.9 |
| 400 | -0.3 | 0.0 | -0.4 |
| 600 | 3.3 | 3.6 | 3.1 |
| 800 | 6.9 | 7.2 | 6.6 |
| 1000 | 10.5 | 10.7 | 10.2 |

The pressures estimates determined using the latter reaction are interpreted to be erroneous, possibly due to disequilibrium (garnet not in equilibrium with plagioclase). P-T estimates from the reactions suggest that this sample occurs at approximately 3 kbar and 575 °C (using the reaction data of Holdaway, 1971, and Ashworth and Chinner, 1978). These estimates are also corroborated by probe data of cordierite and garnet from this sample; Aranovich and Podlesskii (1983) calculated isopleths of $Mg/(Mg + Fe)$ for coexisting garnet and cordierite compositions. Average compositions from probe data of garnet and cordierite from sample G-123-80 (Appendix B) indicate that $X_{Mg}^{garnet} = 0.10$ and $X_{Mg}^{cordierite} = 0.56$, suggesting a pressure and temperature of ~ 3 kbar and 570 °C (see Aranovich and Podlesskii, 1983, Figure 10). Therefore, in the case of this sample, the barometer of Perchuk et al. (1985) is used.

Figure 5-4 shows representative pressure-dependent curves calculated for other samples in the MCSZ. The majority of curves plots within a pressure range of < 2 kilobars; within each sample, however, the range is restricted to less than 0.5 kilobars. Within zoned minerals, the analyses show both core to rim decreases and increases in pressure, although both are small.

5.4 Pressure-Temperature-time (P-T-t) Path

By combining the temperature- and pressure-dependent curves from the geothermometers and geobarometers for individual zoned grains, P-T vectors can be plotted. In all cases, garnet cores yielded higher temperature than rims, and the majority also indicate a slightly higher pressure (two vectors have negative slope). Figure 5-5 shows the resulting P-T vectors. In most cases, vectors from individual samples are nearly isobaric and imply cooling of 25-40 °C (Figure 5-5). Although the pressure and temperature differences implied by the vectors are small (less than the error of the estimates themselves), the sense of temperature displacement is consistent implying that it is likely meaningful. From Figure 5-5, it is clear that although the samples display similar vector orientations, the cores of same mineral pairs record lower P-T conditions than the rims of other pairs. Although the P-T vectors are of very different orientation, a similar pattern was reported for the Torngat orogen in the Saglek area of northern Labrador by Mengel and Rivers (1989), who interpreted that the closure time of individual pairs of grains was a function of temperature, strain and other local factors (i.e. variations in a_{H_2O}) leading to a concept of domainal equilibrium.

Using the interpretation of Mengel and Rivers (1989), these samples define part of the P-T-t path that

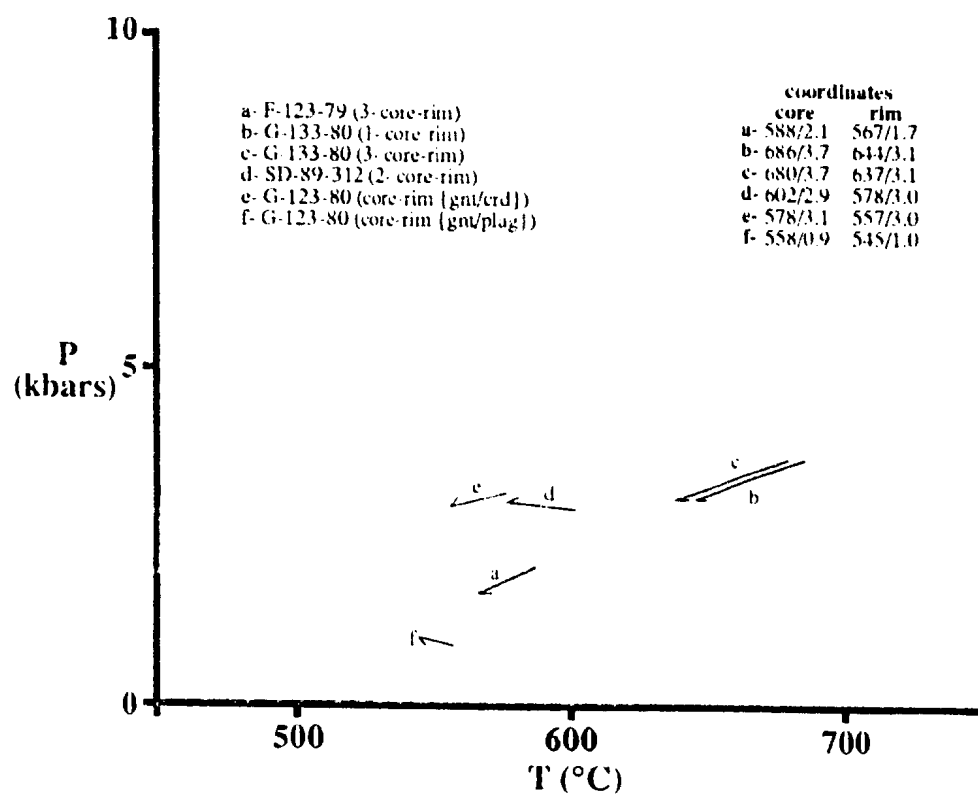


Figure 5-5. P-T vectors from selected samples within the MCSZ. Those prefixed F and G collected by S.P. Colman-Sadri.

ranges from 3.5 kilobars and 680 °C to 2.3 kilobars and 560 °C. These low pressures and high temperatures suggest that a very high geothermal gradient of 50-60°C/km was present in the MCSZ during metamorphism and that uplift was rather slow (no rapid change in pressure with temperature).

The P-T range as defined above is also equivalent to that inferred from analyses of the metamorphic reactions that occur in the MCSZ (Figure 4-5). Since all the samples used in the calculation of the P-T vectors occur upgrade from the sillimanite-biotite-muscovite isograd, then these vectors define only the retrograde part of the P-T-t path (i.e. the post-peak metamorphic conditions) for the high-grade rocks.

In addition, the garnets used in the calculations showed effects of retrograde zoning. This is consistent with interpretations that increasing temperature tends to homogenize garnet and ultimately cause retrograde diffusion to occur under decreasing temperature (see Section 4.5.2). Metamorphic rocks most commonly preserve mineral assemblages that occur at, or after, the peak pressure and temperature corresponding to the lower half or retrograde part of the P-T-t loop. Therefore, the P-T vectors calculated for the MCSZ represent post-peak metamorphic conditions.

The data in Figure 5-5 are compatible with a clockwise P-T-t path, but indicate that the P-T-t path followed by rocks within the MCSZ was probably quite shallow

(in P-T space) in that pressure remained nearly constant as temperature dropped following peak metamorphic conditions. Nearly isobaric cooling paths have also been reported from granulite terranes in the Adirondacks (Bohlen et al., 1985), although they are much higher pressure than that observed in the SBF. Bohlen et al. (1985) inferred that intrusion of magmas and subsequent decay of the high geothermal gradients occurred prior to unloading. The nearly isobaric cooling path reported for the MCSZ suggests that a similar process may apply for the MCSZ, although there is no evidence of large-scale magma intrusion.

5.5 Activity of Water

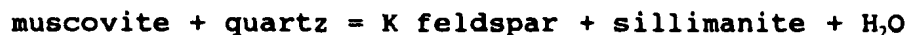
It is possible to estimate a_{H_2O} if the P, T and other variables in a balanced chemical dehydration reaction are known. In this study, the activity of water can be determined locally within the MCSZ. By definition (Wood and Fraser, 1986), the activity of component h in phase i (μ_h^i) reflects the difference in the chemical potential of h in phase i under given conditions of P,T and composition, compared to μ_h^0 in the standard state (at P^0 , T^0). If a standard state at the P-T of interest is chosen, it reflects the difference in thermodynamic concentration (μ) of the component in the mixed substance and in the pure end member.

The complete thermodynamic expression used is

$$\Delta G = \Delta H - T\Delta S + (P-1)\Delta V + RT\ln K_i + RT\ln f_{H_2O} + RT\ln a_{\text{water}}^{\text{fluid}}$$

where $RT \ln f = RT \ln P + RT \ln \Gamma$ (Γ is the fugacity coefficient) and $RT \ln a = RT \ln X + RT \ln \gamma$ (γ is the activity coefficient). Assuming ideal mixing between H_2O and other (unknown) components of fluid phases, $\gamma = 1$ so the latter term is reduced to $RT \ln X$. $RT \ln K$, is the equilibrium constant for the solid phases; it involves an X and γ term for each solid phase. If an assumption of ideal mixing is made, the γ terms again drop out leaving terms for mole fractions of components in the solid phases.

Sample G-123-80 contains the assemblage garnet-biotite-muscovite-sillimanite-cordierite-quartz which are interpreted to be in equilibrium. The presence of coexisting sillimanite and K feldspar with quartz and muscovite in sample G-123-80 indicates that the upper stability of muscovite and quartz has been reached, but not surpassed, and the reaction (univariant in the KASH system)



has not gone to completion. The presence of sillimanite indicates that the sample lies within the sillimanite field on the aluminosilicate phase diagram.

Firstly, the position of this reaction boundary was calculated for $X_{H_2O} = 1$, assuming that all solid phases are pure. However, the P and T of formation of this sample have been independently calculated using the garnet-biotite thermometer and the garnet-cordierite-sillimanite-quartz

barometer. By utilizing the independent estimates of pressure and temperature from sample G-123-80, the X_{H_2O} for the assemblage in that sample can be determined. Assuming that the minerals are in equilibrium at the same temperature and pressure as that calculated for the sample (from thermometry and barometry), then the muscovite + quartz breakdown reaction boundary must pass through the same point. Substituting these values of P and T into the expression for ΔG allows the equation to be solved for a_{H_2O} .

Powell (1978) showed how the position of the muscovite + quartz reaction boundary changes in P-T space as a result of changes in X_{H_2O} (Figure 5-6). Figure 5-6 only applies to assemblages containing pure muscovite ($KAl_3Si_3O_{10}(OH)_2$) and pure K feldspar ($KAlSi_3O_8$). In natural assemblages, however, muscovite may contain paragonite ($NaAl_3Si_3O_{10}(OH)_2$) and margarite ($CaAl_4Si_2O_{10}(OH)_2$) in solid solution, and alkali feldspar can contain albite and anorthite in solid solution. This would have the effect of lowering the temperature, at a particular pressure and X_{H_2O} , thus moving the reaction boundaries to the left (Powell, 1978). Although no analyses of muscovite were carried out on G-123-80, a reasonable estimate can be made by comparison with other muscovites analyzed from the sillimanite-biotite-muscovite zone and higher grade. From these other analyses ($n = 12$), X_K in muscovite is estimated at 0.87 ± 0.03 ; X_K in K feldspar in this sample is 0.80 ± 0.08 from an average of

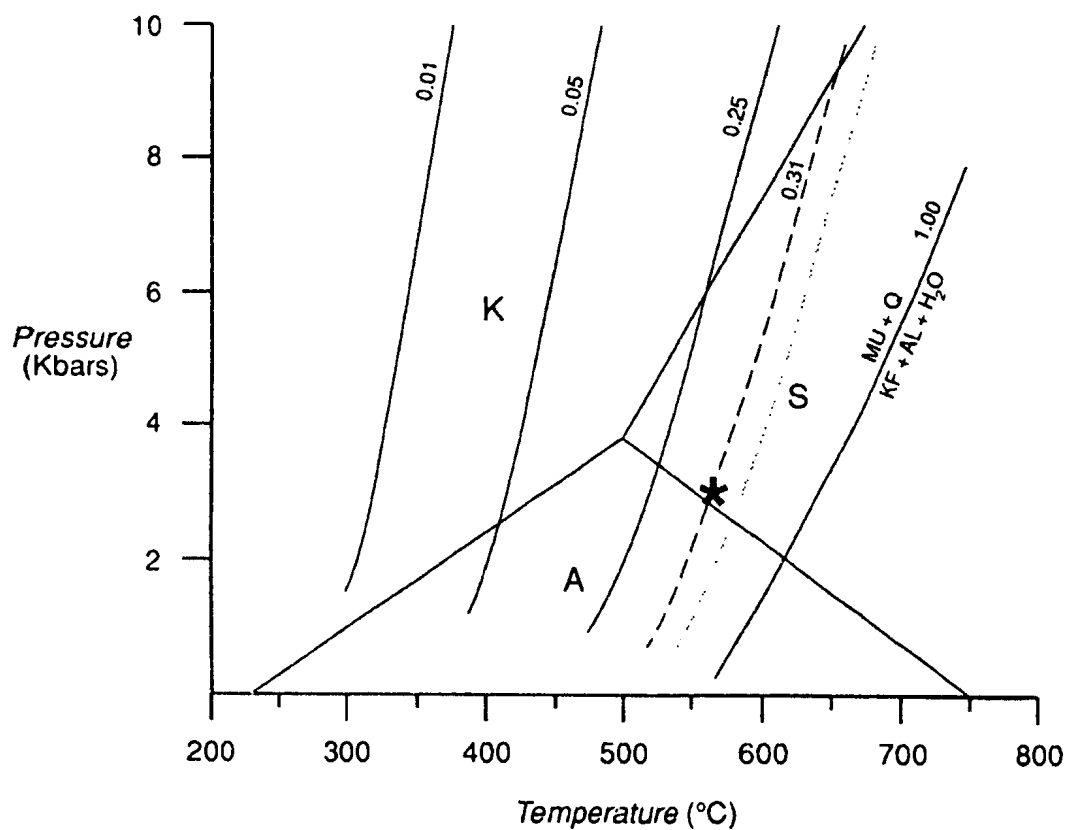


Figure 5-6. P-T diagram (after Powell, 1978) showing the positions of isopleths of X_{H_2O} ($= a_{H_2O}$) for the $MU + Q = KF + ALS + H_2O$ reaction, with the independently estimated P-T location of sample G-123-80 (*). Black dashed line is value of X_{H_2O} calculated for garnet rim composition; grey dashed line is value of X_{H_2O} calculated for garnet core composition. Aluminosilicate triple point is from Holdaway (1971).

four analyses. As shown in the calculations in Appendix D, this has the effect of raising the X_{H_2O} slightly, if pressure and temperature remain constant. If we assume ideal mixing in the fluid, then $X_{H_2O} = a_{H_2O}$.

From Figure 5-6 and the thermodynamic data of Powell (1978), along with the compositional data and independent P-T estimates ($P = 2.95$ kbar; $T = 565$ °C) of this study, the X_{H_2O} value is determined at 0.31 (see Appendix D). With the assumption of ideal mixing with another (unknown) component, a_{H_2O} also equals 0.31. The P-T estimate shown on Figure 5-6 (*) is from a garnet rim and adjacent biotite, although little change would occur with a garnet core and matrix biotite (increase T by 20°C and P by 0.1 kbar; grey line on Figure 5-6). Error estimates are given in Appendix D. With correlation of errors in P and T, the error in estimated a_{H_2O} is $0.31^{+0.08}_{-0.09}$. Since the curves are quite steep, the error on the thermometer (± 12 °C) has more of an effect than the error on the barometer (± 1 kbar).

The low calculated value of X_{H_2O} suggests that the metamorphic fluid consisted of H_2O diluted by one or more other components. The most likely component is CO_2 , as metamorphic fluids are usually considered to be H_2O - CO_2 mixtures (Powell, 1978). Also, evidence for light (organic) carbon has been found in magnesite in the structurally overlying Coy Pond Complex that was most likely derived from the SBF (A. Timbal, pers. com., 1991).

Such a low value of X_{H_2O} from just below the zone of partial melting implies that melting did not occur under water saturated, minimum melt conditions. Similar low values of X_{H_2O} have been reported from migmatites in South Brittany in France (Triboulet and Audren, 1985). These authors found that at low temperatures (550-600°C), X_{H_2O} values were low, but that this value increased with increasing temperature. Further work should be undertaken to better document the X_{H_2O} values throughout the MCSZ. Although muscovite-quartz-sillimanite-K feldspar rocks are rare, muscovite-quartz-andalusite/sillimanite-plagioclase rocks are more widespread, which would allow the use of the sodium analogue of the reaction in which the paragonite component in muscovite breaks down to albite + aluminosilicate, if suitable mixing models were available.

5.6 Post-Metamorphic Uplift Conditions

P-T conditions within the SBF are typical of andalusite-sillimanite facies series metamorphism (Miyashiro, 1961). Maximum pressures recorded within the SBF reach only 3.5 kbar at ~ 700°C. These pressures correspond to a depth of ~13 km and indicate very high lower crustal geothermal gradients of 50-60°C/km.

The majority of the P-T vectors shown in Figure 5-5 indicate decompression on the order of 0.5 kilobars associated with cooling of approximately 50 °C. The nearly

isobaric P-T trajectories also indicate that the amount of post-peak metamorphic uplift and erosion was very small, or was long delayed from the time of the metamorphic event. A possible explanation for this is that since the rocks were not buried to a great depth, isostatic equilibrium was not a powerful driving force.

The Trois Seigneurs Massif of the Hercynian Pyrenees is typical of low-pressure metamorphic terranes within the Pyrenees. Wickham and Oxburgh (1987) suggested that low-pressure metamorphism in the Pyrenees may have been associated with rifting and intrusion of mafic material. This may explain the high geothermal gradient observed in the Trois Seigneurs Massif which locally reaches >100 °C/km (Wickham and Oxburgh, 1987). High geothermal gradients have also been reported from the Basin and Range Province of the western U.S. (i.e. Lachenbruch and Sass, 1978). The authors suggested that the high geothermal gradients are related to crustal extension rather than injection of magma. However, as high grade metamorphic rocks typically remove all evidence of the prograde metamorphic path (due to re-equilibration), intrusion of magmas into the base of the crust and raising the base of the lithosphere during thinning would leave similar thermal signatures (Thompson and Ridley, 1987).

In New South Wales, Australia, Flood and Vernon (1978) suggested the presence of high geothermal gradients

associated with the Cooma Granodiorite, which they inferred formed from partial melting of the metasedimentary rocks that surround it. They further suggested that basaltic magma injection was an unlikely cause of the high geothermal gradients (since there is no evidence of mafic intrusive rocks) or that, if this were a factor, it occurred at a much deeper level than that of the Cooma Granodiorite.

In contrast, England and Thompson (1984) examined P-T-t paths of regionally metamorphosed tectonically thickened crust and found that kyanite-sillimanite facies series metamorphism will occur in the lower crust as a response to crustal thickening by a factor of two or more. Such metamorphism could cause partial melting and, as the melts move upward, removal of heat via thermal convection, resulting in lower pressure metamorphism in the upper crust. They also stated that andalusite-sillimanite facies metamorphism, such as that within the MCSZ, can occur as a result of regional granitic intrusion, or could develop from kyanite-sillimanite facies metamorphism via rapid uplift or tectonic unroofing. However, there is no evidence of higher-pressure metamorphic facies in the rocks of the MCSZ. Regional plutonism is also unlikely as only isolated localities of volumetrically subordinate plutonic rocks (THG and related intrusions) occur within the SBF.

Thompson and Ridley (1987) suggested that crustal thickening followed by extension can lead to the development

of low-pressure metamorphic terrains. Extension would result in thinning of the crust and could produce high geothermal gradients such as are inferred for low-pressure metamorphic terrains. This seems a likely scenario for the MCSZ; limited crustal thickening, as a result of thrusting and emplacement of the oceanic rocks of the Dunnage Zone on to the continental margin sequence of the Gander Zone, was followed by crustal extension causing thinning and the development of high geothermal gradients. This extension must have been pre-peak metamorphism and followed by post-metamorphic cooling to account for the pattern reported earlier and to get the high geothermal gradient. However, very little field evidence for extension within the MCSZ was found in this study with the exception of a small amount of SBF observed to structurally overlie the CPC (A. Timbal, pers. com., 1991).

CHAPTER 6

GEOPHYSICS

6.1 Introduction

During the summers of 1985 and 1988, two gravity surveys were conducted across the Mount Cormack Subzone in an attempt to decipher the geology at depth. These two survey lines traverse parts of the 2D/5 and 12A/8 map areas (Figure 6-1). In each survey, gravity measurements were carried out at approximately 2.5 kilometre station intervals, and rock samples collected by the Newfoundland Department of Mines and Energy were analysed for density and magnetic susceptibility. Limited work was done on these data until the present project was undertaken in the fall of 1988.

Geophysical modelling of gravity and aeromagnetic data was done by the author using computer programs (both commercial and written at Memorial University), and has resulted in a model of the subsurface geology beneath the Mount Cormack Subzone. This model provides some new constraints on the geology at depth.

6.2 Methodology

Two gravity surveys were conducted across the Mount Cormack Subzone, that in 1985 running east-west, and

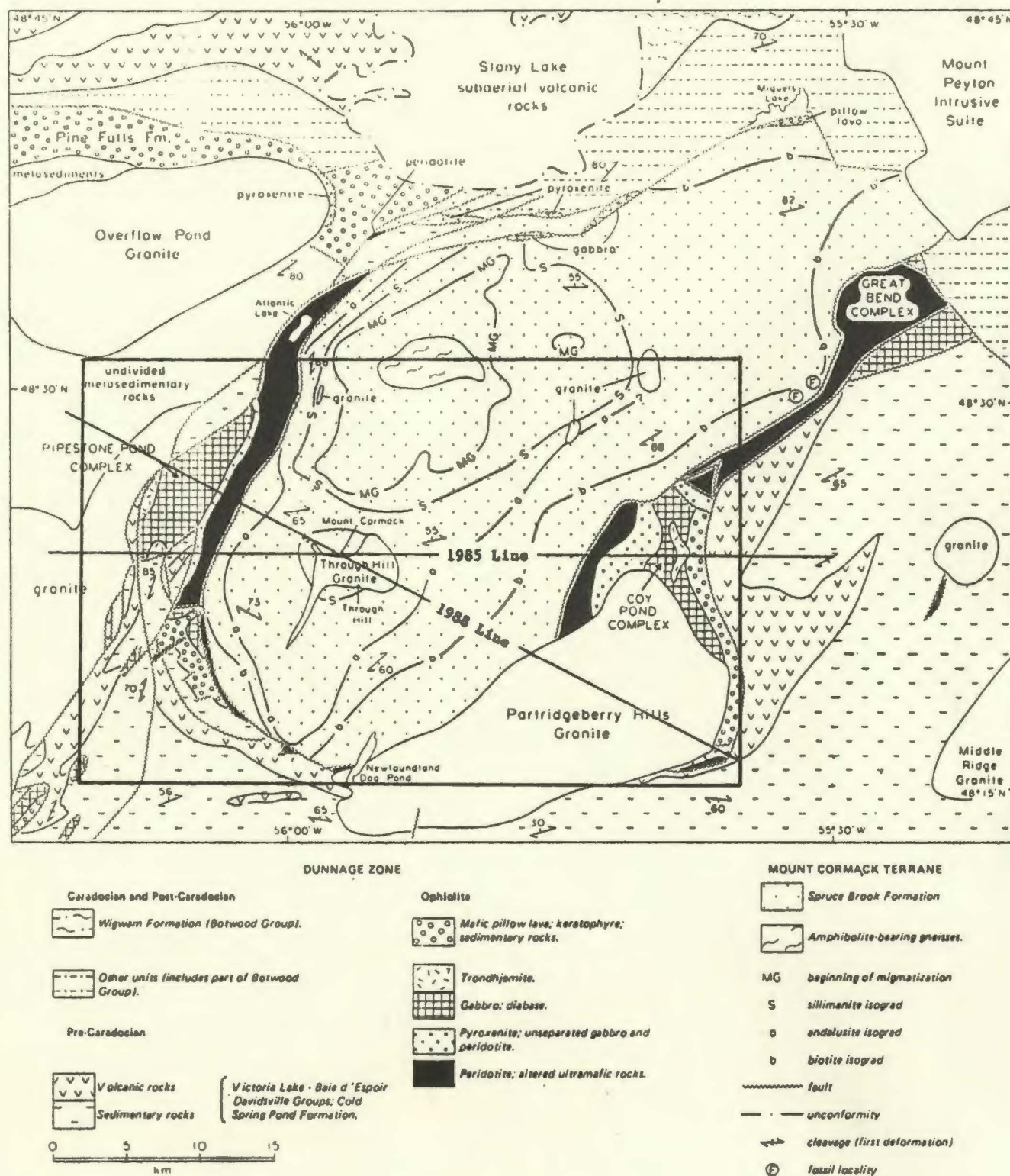


Figure 6-1. Geologic map of the Mount Cormack Subzone area (after Colman-Sadd, 1985) showing the location of the two geophysical survey lines and the location of Figure 6-2.

that in 1988 being orientated approximately northwest-southeast. These two surveys intersect at Mount Cormack, just north of the Through Hill Granite (Figure 6-1).

The gravity data were collected at approximately 2.5 kilometre station spacing using a LaCoste and Romberg land gravity meter. The survey was tied to elevation and gravity control at the Northwest Gander River Bridge, with the gravity base tied to the Canadian National Gravity Network. These data were subsequently reduced to Bouguer anomalies using the 1967 international gravity formula, the IGSN71 (Morelli et al., 1971) base system with a crustal density of $2.67 \text{ g}\cdot\text{cm}^3$. No corrections for Earth tide effects or for terrain effects were applied to the calculated anomalies.

Rock samples collected from the Mount Cormack Subzone area by S.P. Colman-Sadd and others of the Newfoundland Department of Mines and Energy were analysed for density and magnetic susceptibility. Table 6-1 shows the average densities, density contrasts and magnetic susceptibilities for the geological units in the area. Density contrast is calculated as the difference between the measured density of the samples and a mean crustal density of $2.67 \text{ g}\cdot\text{cm}^3$. These data were used to construct the geological model presented here.

Magnetic profiles along the two survey lines were taken from 1:63,360 scale GSC aeromagnetic maps for the

Table 6-1
GRAVITY AND MAGNETIC DATA
 (Standard Deviations given in brackets)

| <u>Rock Type</u> | <u>Density</u> (g*cm ⁻³) | <u>Density Contrast</u> | <u>Magnetic Susceptibility</u> (*10 ⁻³ emu) |
|--|---|-------------------------|---|
| Metasedimentary rocks (SBF and equivalent; n=50) | 2.70 (0.04) | 0.03 (0.04) | 0.03 (0.05) |
| Granite (THG, PHG and unnamed granite; n=23) | 2.63 (0.05) | -0.04 (0.05) | 0.01 (0.01) |
| <i>Coy Pond & Pipestone Pond Ophiolites</i> | | | |
| Gabbro (n=10) | 2.77 (0.09) | 0.10 (0.09) | 1.00 (2.81) |
| Meta-Pyroxenite (n=7) | 2.86 (0.19) | 0.19 (0.19) | 3.00 (2.19) |
| Meta-Peridotite (n=4) | 2.68 (0.20) | 0.01 (0.20) | 4.00 (1.83) |
| <i>Baie d'Espoir Formation</i> | | | |
| Volcanic rocks (n=15) | 2.66 (0.07) | -0.01 (0.07) | 0.01 (0.01) |
| Sedimentary Rocks (n=2) | 2.65 (0.02) | -0.02 (0.02) | 0.01 (0.01) |

(Abbreviations used: SBF -> Spruce Brook Formation; THG -> Through Hill Granite; PHG -> Partridgeberry Hills Granite; n -> number of analyses)

Mount Cormack Subzone. The station localities for the two surveys lie on or near the respective profile lines. Gridded map data were extracted from the GSC digital gridded data set for Canada with a grid interval of 200 metres. These data were used to examine the magnetic signature of the MCSZ and to plot maps that were produced at Memorial University by R. Wiseman using the computer program Geosoft.

Both the gravity and magnetic modelling were conducted using two-dimensional modelling packages written at Memorial University. The surface geology is from 1:50,000 scale geologic maps of the 2D/5 (Colman-Sadd, 1985) and 12A/8 (Swinden, 1981) map areas, as modified in this study. Tables 6-2 and 6-3 list the surface geology along the 1985 and 1988 survey lines, with the zero points located at the western and northwestern extremities, respectively.

The modelling programs involve calculating the gravity and magnetic effects of blocks representing the geologic units mapped at the surface, as well as those interpreted to exist at depth. Each block was assigned a shape based on the inferred geological model, and a specific density contrast and magnetic susceptibility according to the rock sample analyses. By manipulating the size and shape of each block, a close match may be obtained between the calculated and observed anomaly. The model obtained is consistent with all the available geological and geophysical information.

Table 6-2
GEOLOGY ALONG THE 1985 GRAVITY AND MAGNETIC LINE

| <u>DISTANCE</u> <u>(from west)</u> | <u>ROCK TYPE</u> |
|---------------------------------------|--|
| 0.00-1.55 | granodiorite (m.g., grey, bio, porphyritic/equigranular) |
| 1.55-2.70 | metasedimentary rocks (psammite/pelite) |
| 2.70-4.35 | granite (megacrystic, pink, bio, strongly foliated) |
| 4.35-4.60 | metasedimentary rocks (psammite/pelite) |
| 4.60-5.35 | granite (same as above) |
| 5.35-6.25 | mafic pillow lavas, massive basalt, pillow breccia |
| 6.25-9.10 | gabbro (coarse to medium grained) |
| 9.10-9.80 | sedimentary rocks (psammite/siltstone, conglomerate) |
| 9.80-10.7 | pyroxenite (coarse to medium grained) |
| 10.7-12.1 | peridotite (f.g., pyroxene crystals & diss. chromite) |
| 12.1-17.8 | metasedimentary rocks (psammite/pelite) |
| 17.8-18.4 | granite (pegmatite, gt-tour-mu [Through Hill]) |
| 18.4-21.3 | metasedimentary rocks (psammite/pelite) |
| 21.3-23.0 | granite (Through Hill) |
| 23.0-36.4 | metasedimentary rocks (psammite/pelite) |
| 36.4-37.5 | harzburgite |
| 37.5-37.9 | sheared serpentinite |
| 37.9-40.2 | pyroxenite |
| 40.2-42.3 | gabbro |
| 42.3-43.3 | trondhjemite |
| 43.3-44.3 | mafic pillow lava |
| 44.3-47.8 | felsic/intermediate flows and crystal/lithic tuffs |
| 47.8-53.3 | conglomerate, sandstone, siltstone, phyllite |

Table 6-3
GEOLOGY ALONG THE 1988 GRAVITY AND MAGNETIC LINE

| <u>DISTANCE</u> <u>(from n. west)</u> | <u>ROCK TYPE</u> |
|--|---|
| 0.00-6.75 | metased. rocks (psammite/pelite, mafic dykes) |
| 6.75-8.50 | granite (megacrystic, pink, bio, strongly foliated) |
| 8.50-12.8 | gabbro (coarse to medium grained) |
| 12.8-14.6 | pyroxenite (coarse to medium grained) |
| 14.6-22.9 | metasedimentary rocks (psammite/pelite) |
| 22.9-26.1 | granite (pegmatite, gt-tour-mu [Through Hill]) |
| 26.1-36.4 | metasedimentary rocks (psammite/pelite) |
| 36.4-50.2 | granite (Partridgeberry Hills) |
| 50.2-53.2 | gabbro |
| 53.2- | volcanics |

(Abbreviations used: m.g. -> medium grained; bio -> biotite; f.g. -> fine grained; diss. -> disseminated; gt -> garnet; tour -> tourmaline; mu -> muscovite)

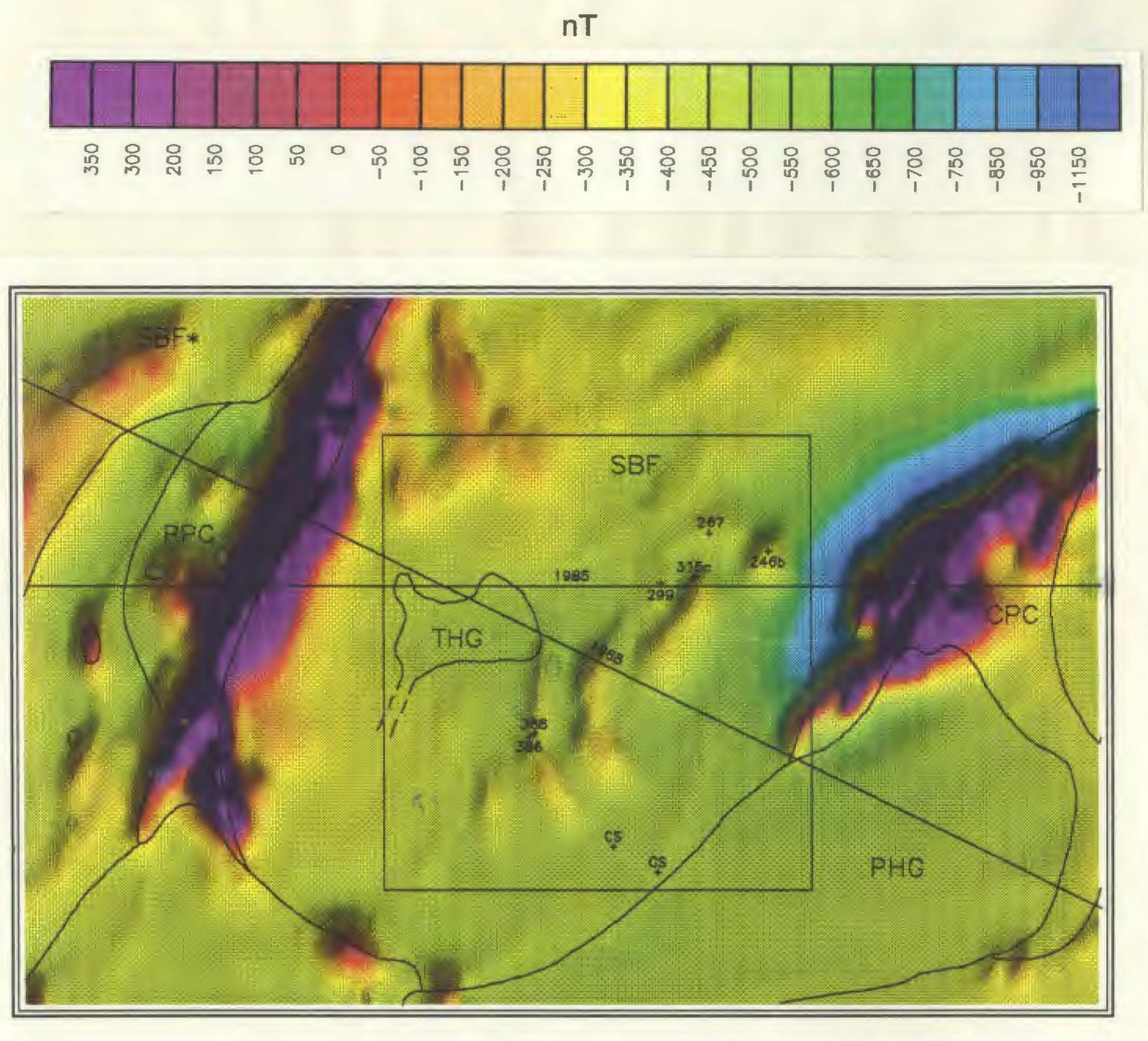
The first profile calculated was the 1988 gravity profile. Once a geologically suitable model had been obtained for the 1988 gravity data, the density contrasts were replaced by magnetic susceptibilities and the model was transferred to the 1988 magnetic data. The same was done for the 1985 data, first calculating the gravity profile and then the magnetic profile.

6.3 Regional Gravity Signature of the MCSZ Area

The majority of the gravity data stations within the MCSZ lie on or near the two survey lines. Only a few regional gravity stations (at a spacing of 13 kilometres) lie within the study area, and a map produced using these few data points and the survey data would contain little additional information specific to the MCSZ. Therefore, the gravity signature of the MCSZ area is taken from the two survey lines and is discussed in Sections 6.5.1 and 6.6.1.

6.4 Regional Magnetic Signature of the MCSZ Area

Figure 6-2 is a magnetic anomaly map of the MCSZ area with the gross elements of geology superimposed. The most prominent features on the map are the large positive magnetic anomalies associated with the ophiolitic rocks of the Coy Pond Complex (CPC) and Pipestone Pond Complex (PPC) with the other units composing a relative background. Smaller positive anomalies located at the southern contact



Abbreviations used in Figures 6-2 and 6-3:

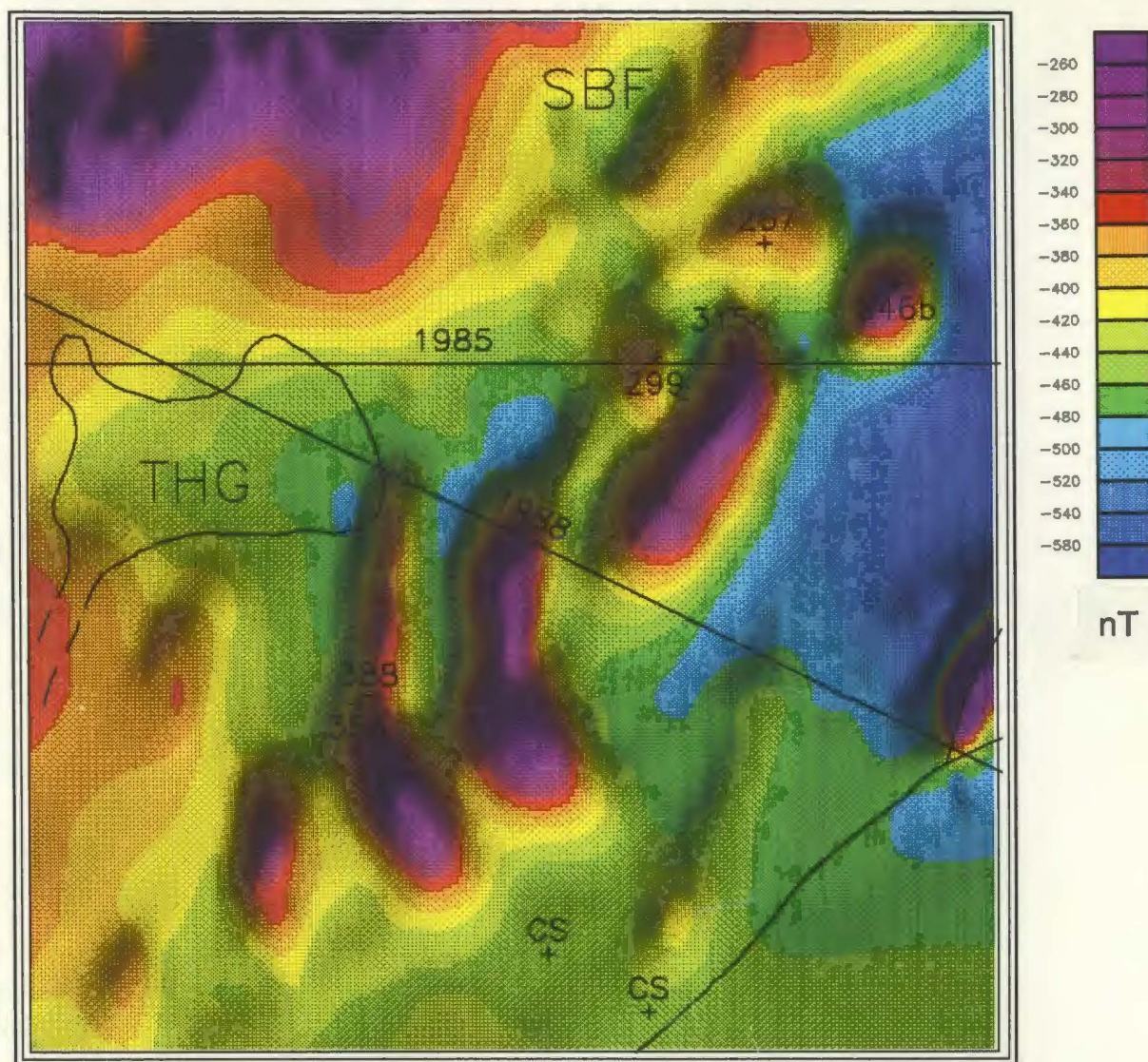
| | |
|------------------------------------|-----------------------------------|
| THG - Through Hill Granite | CPC - Coy Pond Complex |
| PHG - Partridgeberry Hills Granite | SBF - Spruce Brook Formation |
| PPC - Pipestone Pond Complex | SBF* - SBF equivalent |
| G - Granite | CS - Colman-Sadd sample locations |

Figure 6-2. Magnetic anomaly map of part of the MCSZ with the two survey lines and gross elements of geology superimposed. Sample numbers are referred to in text. Box shows location of Figure 6-3.

of the MCSZ and to the west of the PPC are due to the presence of ultramafic rocks (serpentinite and peridotite, respectively) which outcrop in these areas.

The magnetic signature of the CPC is asymmetric with a large magnetic low immediately to the northwest, and the anomaly associated with the PPC is displaced to the east compared with the surface geology (Figure 6-2). The low immediately northwest of the CPC is an artifact of the interaction between the present magnetic field and the dip of the CPC; the CPC dips to the east which is the same direction as the overall present magnetic field. The magnetic low is termed an "edge effect" and occurs when the dip of a body and the magnetic field are in the same direction. The reason that the magnetic anomaly occurs to the east of the surface geology of the PPC is possibly due to ophiolite occurring at depth beneath the surface expression of the anomaly (see Section 6.6.2).

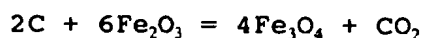
Another important feature of the regional magnetic anomaly map (Figure 6-2) is that there is an increase in the strength of the magnetic anomaly approximately coincident with the regional increase in metamorphic grade in the MCSZ. The highest-grade rocks (i.e. within the zone of partial melting) appear to be more magnetic than lower-grade rocks. This becomes even more evident when the effect of the ophiolites is removed (Figure 6-3). A possible explanation for this increased anomaly is that sedimentary organic



1:147 500

Figure 6-3. Part of the magnetic anomaly map with the effect of the ophiolitic rocks removed. Symbols and sample numbers are the same as Figure 6-2.

carbon became mobilized in the highest grade rocks; this carbon would have reacted with local hematite (see below) to form magnetite by a reaction such as



The CO_2 produced by this reaction would have migrated through the SBF (and overlying CPC) as an intergranular fluid through microscopic ephemeral cracks and fractures. Indirect evidence to support this theory is present in the CPC which, from C-isotope work (A. Timbal, pers. com., 1991), contains light carbon in magnesite that was most likely derived from the SBF. This would also account for the observation that hematite is present in the low-grade rocks, but absent from those at high grade. Also, the local activity of water (as determined from sample G-123-80) is very low, possibly indicating that a CO_2 -rich fluid was present.

When the effect of the ophiolitic rocks is removed (Figure 6-3), other features within the MCSZ become apparent. East and southeast of the THG, small positive magnetic anomalies are plainly visible. These smaller anomalies are approximately linear features which trend north-south and northeast-southwest; these features are sub-parallel to the trace of bedding in the folded SBF and are interpreted to be due to the presence of magnetite, as it is abundant in the four samples (SD-89-388, -315, -299 and -267) collected from this area.

The mafic dyke rocks appear to have little magnetic effect. In two localities mapped by S.P. Colman-Sadd (Unit 13 of Colman-Sadd, 1985; labelled CS on Figure 6-3) they appear to have no magnetic signature. Whether the two mafic dykes mapped by the author do have an effect on the map pattern is not clear. This is because sample SD-89-386, a 30 cm mafic dyke, occurs within a larger anomaly due to the cordierite-magnetite sub-assemblage. Sample SD-89-246b was taken from an outcrop which occurs within a small positive magnetic anomaly northeast of the other anomalies associated with the cordierite-magnetite sub-assemblage (Figure 6-3). This magnetic anomaly is most likely due to an extension of the cordierite-magnetite sub-assemblage which follows the trace of bedding in the area. At the scale of the map, and given the fact that the dykes are < 1 metre in width, it is unlikely that they would have much of a magnetic signature (assuming they do not widen significantly at depth).

6.5 1985 Survey

6.5.1 Gravity Data

Gravity modelling of the 1985 data has led to the inference of geological features previously unmapped in the area of the Mount Cormack Subzone. Figure 6-4a shows the gravity data (crosses) along the 1985 survey, as well as the calculated gravity anomaly (solid line) from the geologic

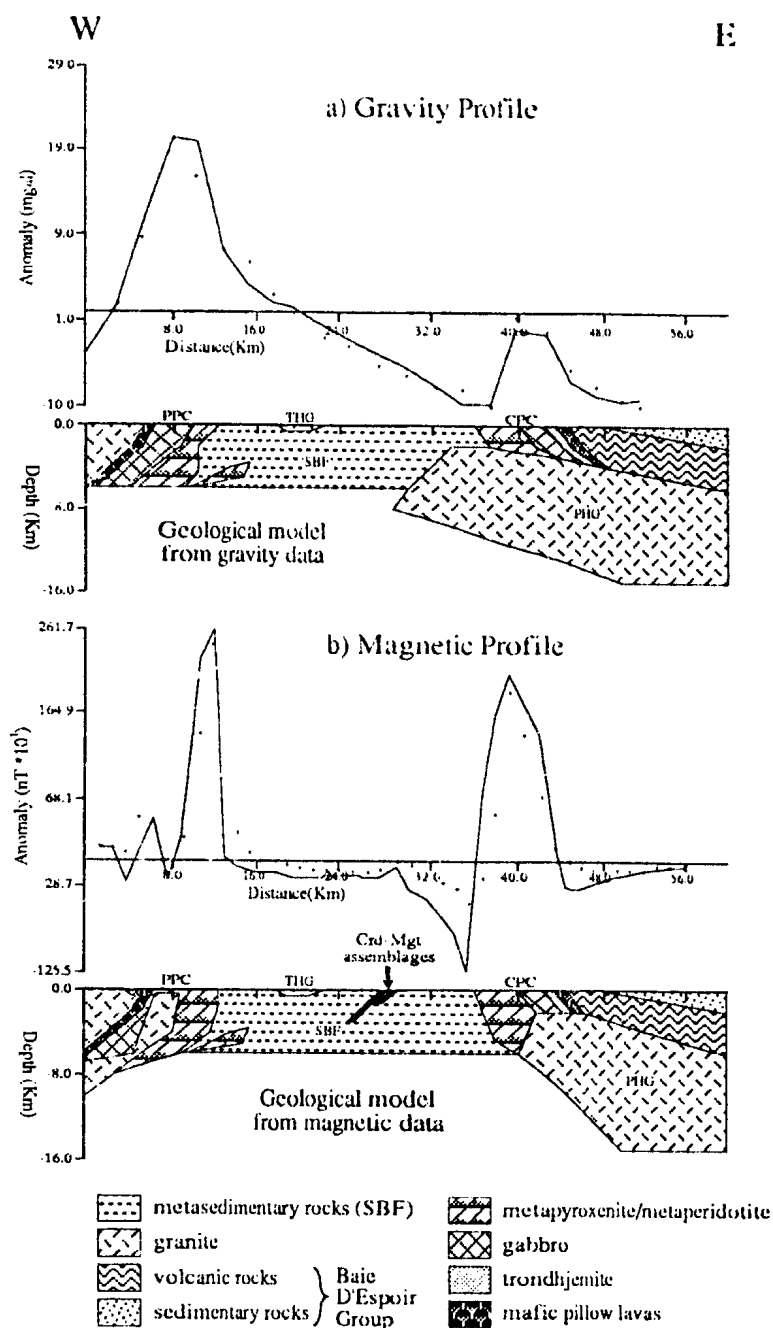


Figure 6-4. Two dimensional geological model for the MCSZ area derived from the 1985 gravity (a) and magnetic (b) data. Crosses are data points; lines are profiles calculated from geological model. See text for discussion of the two models. No density or magnetic susceptibility was assigned to the white areas beneath the models.

model at the bottom of the figure. Positive gravity anomalies are associated with the mafic and ultramafic rocks, negative gravity anomalies are related to the granitic bodies, and there is little effect from the metasedimentary and volcanic rocks.

One point of particular interest is that the gravity anomaly due to the western PPC is much larger than that due to the eastern CPC (Figure 6-4a). This implies that there is either a low density body at depth below the CPC or that there is a smaller volume of ophiolitic rocks in the CPC (according to the inferred model, either of these could be correct). The Partridgeberry Hills Granite (PHG) outcrops just south of the profile line (Figure 6-1), and is interpreted to extend north beneath the CPC. The size of the negative anomaly makes it necessary to extend the PHG, or a body of equivalent density (SBF and/or basement to SBF), to a depth of nearly sixteen kilometres. The nature of the contact between the PHG and the CPC in the field, and the implications of the depth extent of the PHG are discussed in Section 6.7.

The THG has been mapped as a pegmatitic granite by Colman-Sadd (1985) who interpreted it as an irregularly shaped body. Since it has little effect on the gravity data, the interpretation of Colman-Sadd (1985) is maintained in the present model (Figure 6-4a).

When the gravity model is compared to that

calculated from the magnetic data (see next section and Figure 6-4b), some notable differences emerge. The most prominent is the size differential of the PHG. In the gravity profile, the PHG is modelled to extend beneath the CPC and the Spruce Brook Formation (SBF). As noted above this is necessary to accommodate the gravity low observed in this area. However, the models are restrictive in that only the geology at depth below the two survey lines is incorporated in the calculated anomaly. If we assume that a low density body exists to the east, then this would have the effect of lowering the calculated anomaly if the PHG were reduced to the size in Figure 6-4b. A granitic body does occur to the east of the profile line (H. Miller, pers. comm., 1992) and this is interpreted to contribute to the gravity low in the area.

Figure 6-4b shows a subsurface granitic body intruding the PPC. This was inferred due to a small magnetic low in the observed anomaly, just west of the large positive magnetic anomaly due to the PPC. The body was interpreted as granitic since granite outcrops to the west; however, it could be of any composition of equally low magnetic susceptibility. Additional work is required to refine the geology at depth.

6.5.2 Magnetic Data

Figure 6-4b shows the extracted magnetic data along the 1985 profile line and the calculated anomaly from

the geologic model shown. The calculated anomaly assumes a background magnetic anomaly of 950 nT which has been subtracted from the observed magnetic data. As expected, there are high magnetic anomalies associated with the two ophiolite bodies and little effect from the other units. The PHG is again interpreted to extend beneath the CPC (Figure 6-4b), but it has little effect on the magnetic anomaly pattern since it has a very small magnetic signature (see Table 6-1).

However, there are two small magnetic anomalies located approximately five and twenty-nine kilometres from the western extent of the profile (Figure 6-4b). These can also be seen on the magnetic anomaly map of the area (Figure 6-2). The first of these small anomalies is due to the presence of peridotite which outcrops in the area. The size and nature of the anomaly (Figure 6-2) suggests that it is not extensive at depth and that it may be part of the dismembered PPC. Swinden (1981) inferred that this unit is in fault contact with the surrounding units.

The second anomaly is located east of the THG and shows up as a series of small elongate curvilinear north-south to northeast-southwest trending anomalies on the magnetic anomaly map of the area (Figure 6-3). The area is predominantly underlain by SBF, with subordinate (< 1%) mafic dykes. The anomaly may be due in part to the presence of the mafic dykes, but appears to be at least in part due

to the presence of abundant magnetite in the SBF locally (part of a sub-assemblage with cordierite, See Chapter 4).

Not only is it possible to pinpoint the surface location of this cordierite-magnetite sub-assemblage, but the dip can also be estimated. It is shown in Figure 6-4b as dipping approximately 60° to the west; by combining the magnetic and structural data (Figures 6-4 and 3-5), a good correlation is achieved between small-scale bedding measurements taken in these areas and the large-scale measurements inferred from the magnetic anomalies (Figure 6-5). However, there are places where the trend of the magnetic anomalies does not easily fit with form lines of major structures (i.e. southern extent of the middle two trends on Figure 6-5). If the anomaly is due to original chemical (Eh) differences in the sediments, it is not clear why it is not more extensive.

6.6 1988 Profile

6.6.1 Gravity Data

The most prominent feature of the 1988 gravity data is the presence of a positive gravity anomaly associated with the PPC. The ophiolite is modelled as quite extensive, reaching a maximum stratigraphic thickness of nearly ten kilometres (Figure 6-6a). Such a conclusion is a result of using a reasonable value of density contrast (0.20 g*cm³ for the ultramafic part of the ophiolite, and 0.10

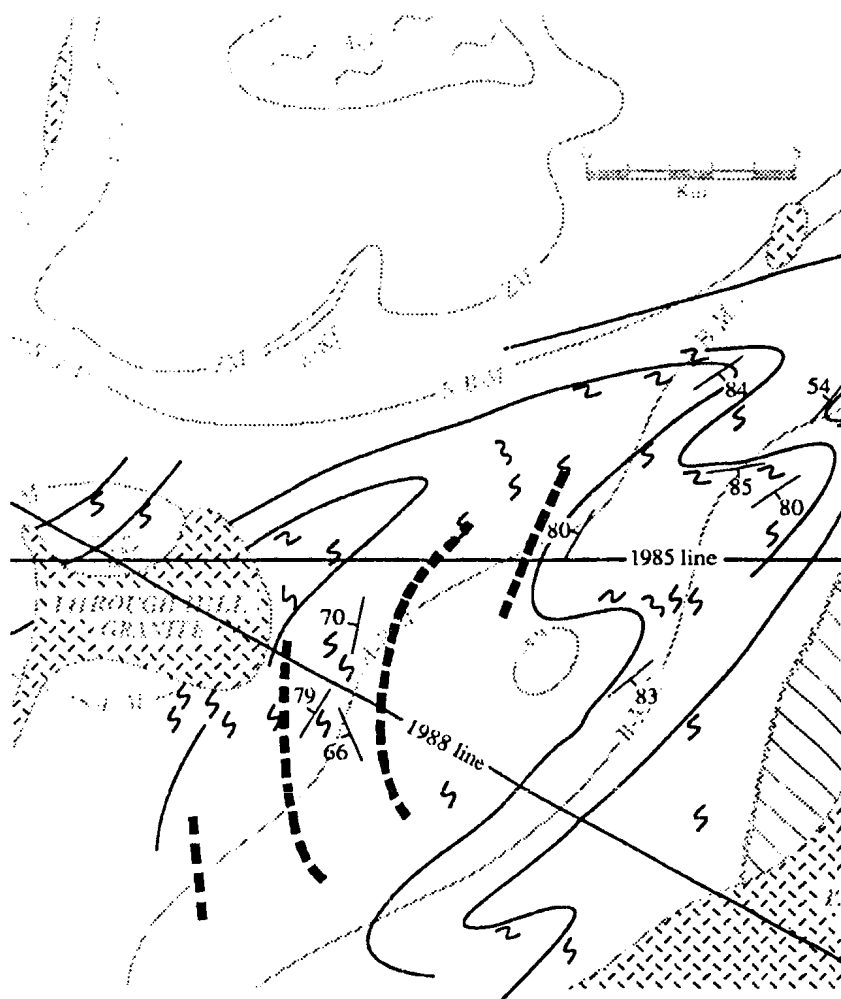


Figure 6-5. Structural map (modified from Colman-Sadd, 1985) combined with trends of the magnetic anomalies (dashed lines) within the MCSZ. Straight lines are gravity survey lines. The inferred dip of the anomalies (see text) correlates well with field measurements although the trend does not always fit well with the structures inferred from form lines (i.e. bottom of two middle anomalies).

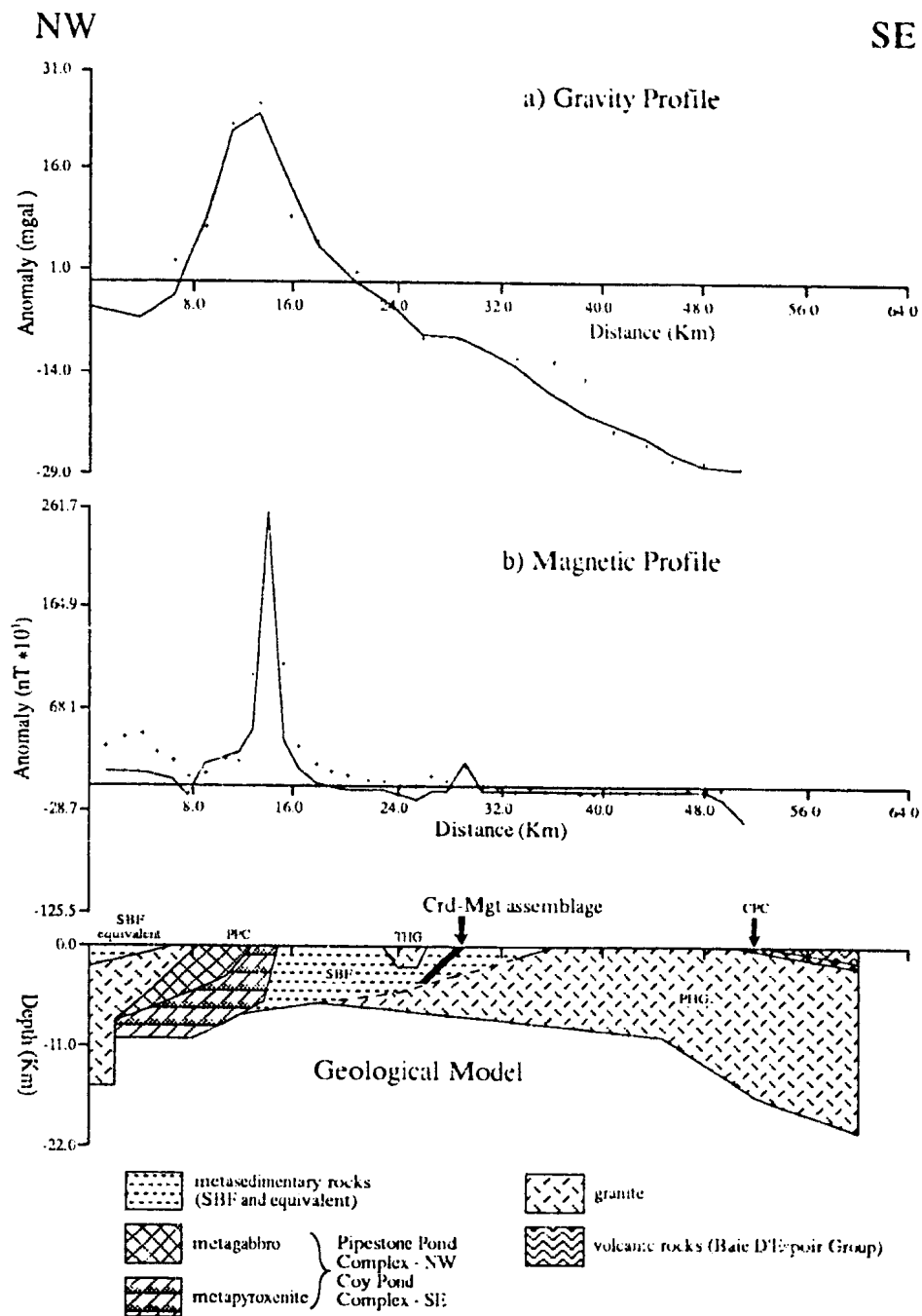


Figure 6-6. Two dimensional geological model for the MCSZ area derived from the 1988 gravity and magnetic data. Crosses are data points; lines are profiles calculated from geological model at bottom. No density or susceptibility was assigned to the white area beneath the model.

$g \cdot \text{cm}^3$ for the gabbro), and may be explained by imbrication of thrust slices.

The CPC only occurs in the extreme southeastern part of the profile, and has little effect on the gravity anomaly (Figure 6-6a). The PHG is the main unit in the southeastern half of the profile, modelled as extending to a depth of approximately twenty kilometres to account for the large, negative gravity anomaly in the area. However, rocks of comparable density could explain the observed profile. This negative gravity anomaly is known to extend further to the southeast (G. Kilfoil, pers. comm., 1989), suggesting that the PHG or a similar low-density body has a large subsurface extent.

The THG displays a small negative effect on the gravity profile (Figure 6-6a). It is modelled as somewhat thicker than on the 1985 profile, since the 1988 profile passes nearer the centre of the body (Figure 6-2).

6.6.2 Magnetic Data

The magnetic anomaly profile for the 1988 data is shown in Figure 6-6b. As with the 1985 data, a background anomaly of 950 nT was removed from the observed magnetic data. Like the gravity profile, there is a large magnetic anomaly due to the high susceptibility ophiolitic rocks of the PPC, with little effect from the other units.

However, in the northwest part of the profile, metasedimentary rocks (psammites and pelites) equivalent to

the SBF display a slightly positive magnetic anomaly (Figure 6-6b). This is uncharacteristic of metasedimentary rocks in general, which typically have low or negligible magnetic susceptibilities (Telford et al., 1987). However, this unit has been intruded by mafic dykes (Swinden, 1981), and this is interpreted as the cause of the anomaly. These metasedimentary rocks were assigned a slightly higher magnetic susceptibility (0.005 emu) to account for the presence of the mafic dykes.

Also, a small magnetic anomaly occurs approximately twenty-nine kilometres from the northwestern edge of the profile (Figure 6-6b). As in the 1985 profile, this is interpreted as due to the cordierite-magnetite sub-assemblage in the SBF which has been mapped at this location. The dip of the anomaly is consistent with the 1985 data, and again indicates that in this location, bedding appears to dip approximately 60° to the west, in general agreement with the structural measurements from this area (Figure 6-5).

6.7 Interpretation

A model for the subsurface geology of the Mount Cormack Subzone and surrounding area is inferred from the gravity and magnetic modelling of the 1985 and 1988 data sets. This model is not significantly different from that proposed by Colman-Sadd and Swinden (1984), but adds some

thickness and depth constraints and indicates the presence of the PHG (or similar low density/magnetic susceptibility body) and the effect of the cordierite-magnetite sub-assembly.

The PHG is interpreted to extend north beneath the CPC and northwest beneath the SBF. This interpretation is necessary to accommodate the large negative gravity anomalies in the eastern and southeastern portions of the two surveys (Figures 6-4a and 6-6a). However, since the PHG and the SBF are similar in density and magnetic susceptibility (see Table 6-1), some of the material inferred to be PHG may in fact be SBF.

Colman-Sadd (1985) and Colman-Sadd et al. (in press) reported that the PHG is in intrusive contact with the CPC. They noted that the granite cross-cuts the banding in the ophiolite, that it contains xenoliths of serpentinite and is cut by numerous quartz veins. The gravity data suggest that a low density body extends beneath the SBF (Figure 6-6a), which is interpreted as an extension of the PHG. However, some of this low density unit (interpreted as the PHG) may be SBF itself (or its basement) since the standard deviations (Table 6-1) are as large or larger than the density contrasts used for these two units. If this were the case, the model would not change significantly but the spatial extent of the units would change.

The size of the negative gravity anomaly

associated with the PHG is also of importance. The anomaly, which reaches a peak of -10.9 milligals on the 1985 profile (Figure 6-4a) and -27.7 milligals on the 1988 profile (Figure 6-6a), illustrates the necessity of extending a low-density body to a depth of approximately fifteen kilometres beneath the 1985 profile and twenty kilometres beneath the 1988 profile. If correct, this model suggests that the PHG (or similar body) is rooted in the crust. However, as stated above, this is not conclusive since some of this unit may be SBF.

The most prominent features of the magnetic data are the presence of the ophiolitic units (sharp, positive magnetic anomalies), and the low magnetic signature of the other units. These data also indicate that the ophiolitic units dip outward from the MCSZ. The work of Stuckless (1975) indicated an angle of dip of these units. He determined that the PPC dips 60° to the west and the CPC dips 80° to the east. These conclusions are approximately correct; however, his determination was strictly mathematical and assumed that the ophiolitic units were dyke-like and of infinite length.

The smaller-scale magnetic anomalies which occur within the MCSZ are interpreted as traces of bedding of units bearing unusual amounts of magnetite; the depth configuration of these anomalies is consistent with structural measurements made in these areas (Figure 6-5).

CHAPTER 7

DISCUSSION AND CONCLUSIONS

7.1 Introduction

This chapter brings together the results from the previous pages in an attempt to refine the tectonic model for the evolution of the Mount Cormack Subzone (MCSZ). This is not intended as an exhaustive analysis; the model presented is consistent with the information reported herein, but it is not a unique interpretation. Other possible models are briefly alluded to in the text.

7.2 Petrogenesis of the Mount Cormack Subzone

As discussed previously, the Mount Cormack Subzone consists of metasedimentary rocks of Gander Zone affinity (Spruce Brook Formation), surrounded by ophiolitic rocks of the Dunnage Zone; this configuration has led others to interpret the Mount Cormack Subzone as a tectonic window which exposes Gander Zone rocks through rocks of the Dunnage Zone (i.e. Colman-Sadd and Swinden, 1984).

Rocks of the Spruce Brook Formation (SBF) consist of metamorphosed equivalents of a continental margin sequence (sandstone, siltstone and shale); the sediments were derived from continental plutonic and metamorphic rocks

and were deposited on the Gondwanan eastern margin of Iapetus (Colman-Sadd *et al.*, in press). However, it is still not clear which continent the sediments were shed from (i.e. Africa or South America). This continent is, therefore, referred to as Gondwana. No precise age has been assigned to the SBF, but it is older than Llanvirn-Llandeilo (see Section 1.10 for reasoning). Figure 7-1a shows a schematic section of a typical continental margin on the eastern side of an ocean (i.e. Iapetus).

At some point in the Lower Paleozoic, the Iapetus Ocean began to close. Subduction of Iapetus ocean crust occurred in the early stages of closure (Figure 7-1b). The change from subduction to obduction (Figure 7-1b to 7-1c) may have been the result of the proximity of the North American craton. van Staal (1987) suggested that in the Miramichi Highlands of New Brunswick, a back-arc basin developed (eastward of Iapetus) in response to east-directed subduction. During final closure of the Iapetus Ocean, a new west-dipping subduction zone developed in the back-arc basin. An analogous situation may have occurred in Newfoundland; the Pipestone Pond Complex has been interpreted to have formed from rifting of a volcanic arc (Jenner and Swinden, 1989). If this were the case, Figure 7-1c would then show the latest stages of this "westward" subduction, which resulted in obduction of oceanic crust on to the Gondwana margin. Figure 7-1d shows the final stages

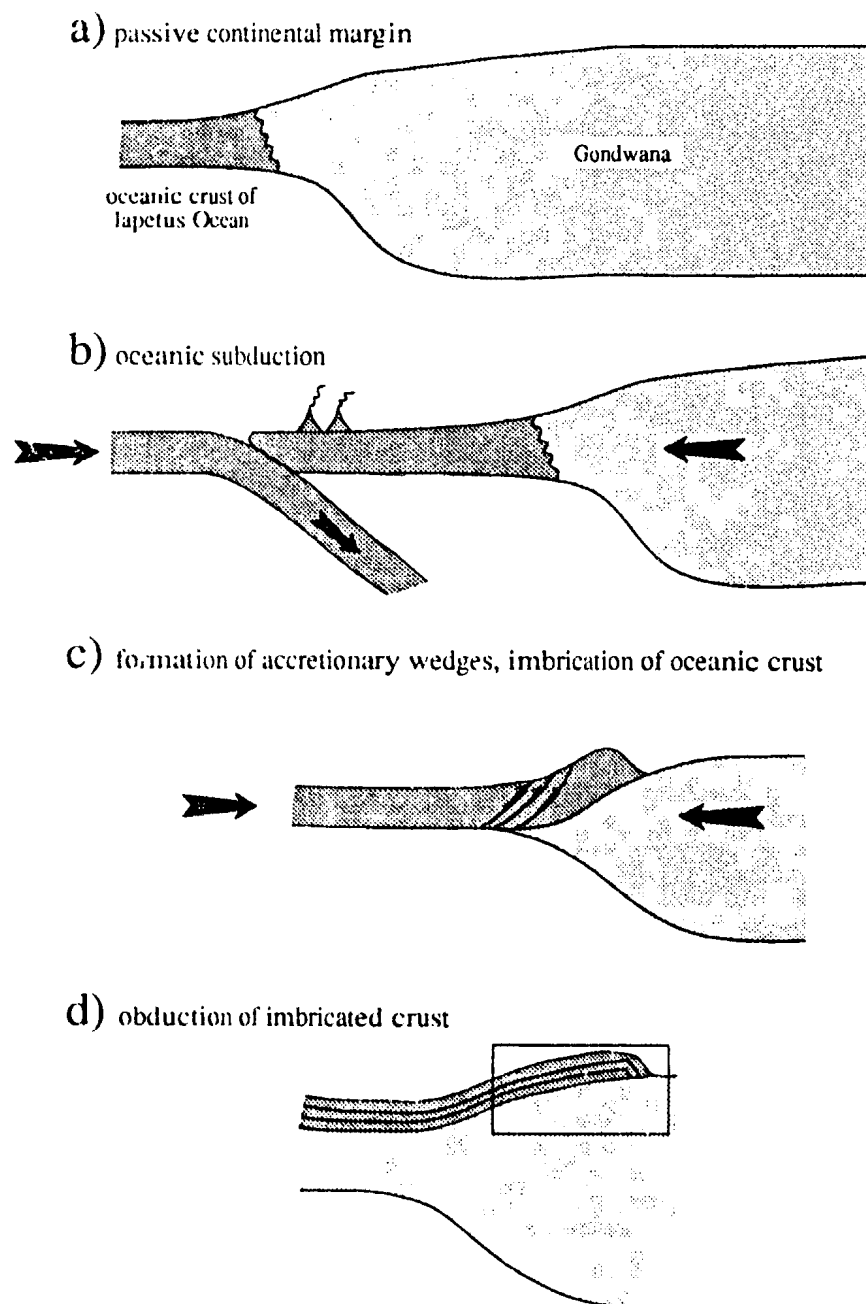


Figure 7-1. Simplified diagram for the closure of the Iapetus Ocean (by continental collision) accompanied by obduction of oceanic crust. The oceanic crust becomes imbricated by thrusting at c) and also at d). Box shows location of Figure 7-3. See text for discussion.

of ophiolite obduction; emplacement of imbricated oceanic crust of the Dunnage Zone on to the eastern margin of Gondwana. Imbrication of the ophiolitic rocks in the MCSZ area is inferred from the fact that major shear zones occur within the Coy Pond Complex (CPC) (Rivers et al., 1990). Figure 7-2 illustrates the process of imbrication. The age of ophiolite emplacement can be inferred from fossils within black shales which are interpreted to unconformably overlie the CPC. This gives a maximum age for emplacement of late Arenig (~490-480 Ma, Tucker et al., 1990; Williams et al., in press). Colman-Sadd et al. (in press) inferred a minimum age of emplacement of 474 Ma, the age of the Partridgeberry Hills Granite (PHG) which is interpreted to intrude both the CPC and the SBF. This is also consistent with the minimum age constraint that can be inferred from the age of the Through Hill Granite (THG) (464 Ma; Colman-Sadd et al., in press) which is interpreted to be due to partial melting of the SBF. However, the THG is discordant into the SBF and, hence, did not form at the present level of erosion. Melting at depth could have taken place at a (slightly) different time to metamorphism at the current level of erosion. However, high-grade migmatites from north of the THG are of equivalent age (465 ± 2 Ma; Colman-Sadd et al., in press) suggesting they formed at the same time as the peak of metamorphism.

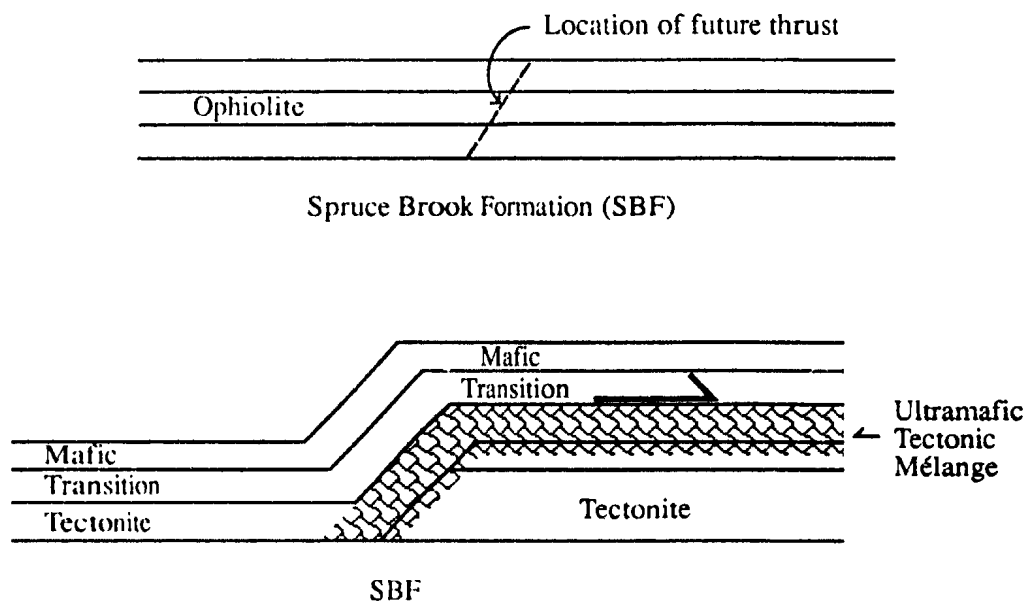


Figure 7-2. Model for the imbrication of ophiolite (Rivers et al., 1990). The ultramafic tectonic mélange is a shear zone in which blocks of ultramafic lithologies "float" in a serpentine matrix.

If we now look at the right (eastern) side of Figure 7-1d, we can examine the model for the development of the MCSZ in greater detail. Figure 7-3 shows an inferred sequence of events leading to the present surface geology in the MCSZ. During emplacement of the imbricated ophiolite and the development of the two-layer crust, simultaneous deformation (D_1) is inferred to have occurred in the SBF and was expressed by isoclinal folds (Figure 7-3a) which have been inferred from petrographic observation of $S_0 \parallel S_1$ (see Chapter 3). Following this, the second deformational event occurred causing sub-horizontal folding in the SBF accompanied by shortening and thickening of the two-layer crust (Figure 7-3b).

Following formation of the F_1 folds, a period of crustal thinning in an extensional environment is proposed. Evidence for such an event is circumstantial and comes from the inference of a high geothermal gradient in the MCSZ. No structures associated with such an extensional event have been identified, but Thompson and England (1984) and Thompson and Ridley (1987) suggested that low-pressure metamorphic terrains (i.e. andalusite-sillimanite facies series of Miyashiro, 1961) are characterized by crustal extension and it appears to be a suitable model in this area also, as is illustrated in Figure 7-3c. The extension would have been associated with formation of *in situ* anatectic melts in the SBF (THG and associated plutons, the cordierite

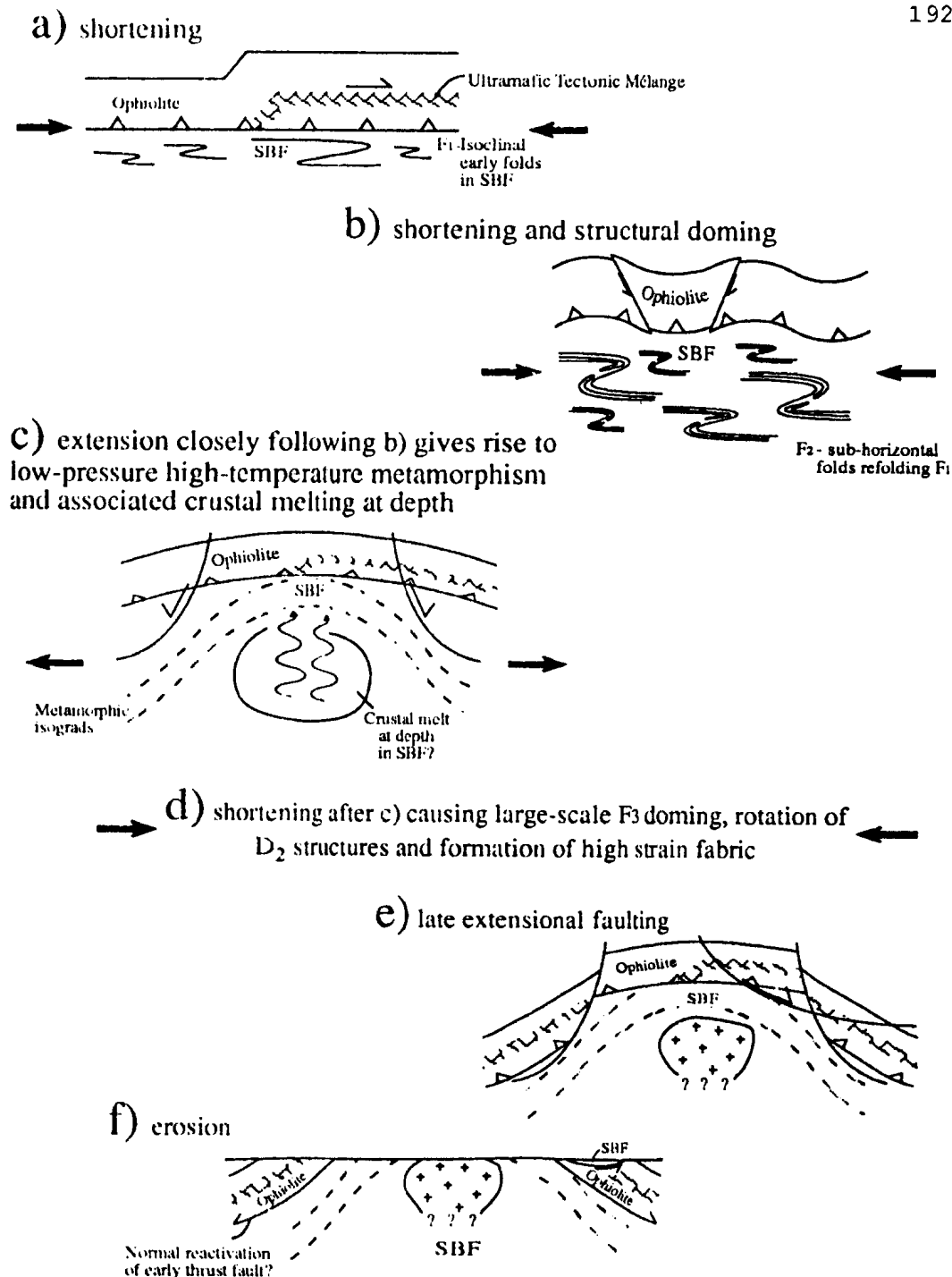


Figure 7-3. Inferred sequence of events in the development of the Mount Cormack Subzone (modified from Rivers et al., 1990). No attempt is made to include the Partridgeberry Hills Granite.

granodiorite), and by extensive migmatization in the highest-grade rocks.

The geometry of the two-layer crust at that time was probably gravitationally unstable, with low-density hot metasedimentary rocks underlying higher-density cooler ultramafic/mafic rocks. Crustal melting at depth (associated with crustal thinning) could have facilitated thermal doming of the two-layer crust, which would have accompanied partial melting in the SBF and the development of metamorphic isograds in a rising thermal front (Figure 7-3c). Assuming the THG and cordierite granodiorite formed in response to partial melting of the SBF, and since they are relatively undeformed, this dates the end (or climax) of metamorphism at ~465 Ma. Since the reaction isograds are approximately parallel to the boundaries of the MCSZ, they probably developed in response to the thermal doming and prior to (or during) the mechanical doming related to the third stage of deformation (D_3). This third stage of deformation was probably non-penetrative and caused rotation of the sub-horizontal S_2 fabric along with the reaction isograds (Figure 7-3d) as a result of gravitational rise of the hot SBF and enclosed magmatic rocks.

Gravitational or diapiric rise has also been suggested for the origin of the Cooma Granodiorite, New South Wales, Australia. Flood and Vernon (1978) suggested that the Cooma Granodiorite is a diapiric intrusion formed

by *in situ* crustal melting and intrusion of a pluton that dragged up its thermal aureole during emplacement, causing the layers around the diapir to undergo thinning. The THG may also be such a diapiric intrusion as it cross-cuts the structures in the metasedimentary rocks and is encircled by its own sillimanite-biotite-muscovite isograd. However, in places it also cross-cuts the isograd indicating that final emplacement occurred at a later time.

As a response to the gravitational instability, renewed extensional faulting may have occurred in the MCSZ. This second phase of extension would have been long delayed from metamorphism (the post-peak metamorphic cooling path was nearly isobaric), and is indicated by the truncation of the foliation at the margins of the MCSZ. In addition, mapping by A. Timbal has indicated the presence of slices of SBF structurally overlying the CPC; this evidence has been incorporated into Figures 7-3e and 7-3f.

This sequence of events does not take into account the PHG. Its radiometric age places it as pre-THG and the fact that it is relatively undeformed (except in the southeast; Colman-Sadd, 1985) may indicate that it closely followed the thickening and shortening of the double crust depicted in Figure 7-3b.

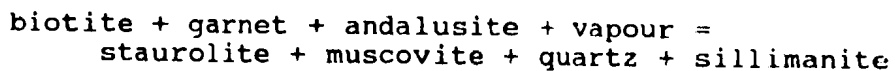
7.3 Conclusions

The present investigation has yielded much new information about the development of the Mount Cormack Subzone. The main conclusions are summarized below.

1) The structural data indicate an overall domal structure within the MCSZ. First deformation structures are preserved as foliations parallel to bedding (S_0) implying the presence of isoclinal folds. The second deformation, associated with shortening and thickening of the two-layer crust, formed a large-scale synformal structure in the low-grade units of the SBF. D_1 deformation within the SBF rotated the D_2 structures along with the reaction isograds into a major domal structure.

2) Five reaction isograds have been defined within the Mount Cormack Subzone as follows: i) biotite-muscovite-chlorite isograd; ii) andalusite-biotite-muscovite isograd; iii) sillimanite-biotite-muscovite isograd; iv) sillimanite-potassium feldspar isograd; and v) melting isograd defining the beginning of partial melting. These isograds crosscut the large-scale second generation folds in the area, consistent with an evolution of early thrusting and shortening, followed by structural and thermal doming.

3) Mineral assemblages from both sides of the bathogradic reaction,



occur in rocks of appropriate composition and temperature indicating a pressure of 3.2 kilobars at the bathograd. Pressure increases slightly with increasing metamorphic grade (the bathograd approximately coincides with the sillimanite-biotite-muscovite reaction isograd), consistent with interpretations that either the high-grade areas underwent greater post-metamorphic uplift or that the syn-metamorphic Through Hill Granite (which is surrounded by its own sillimanite-biotite-muscovite isograd) dragged up its metamorphic aureole during emplacement.

5) Results of geothermobarometry have confirmed the estimates of the P-T conditions within the high-grade part of the Mount Cormack Subzone; pressure estimates range from 2.5 - 3.5 kilobars and temperature estimates range from 525 - 600 °C from andalusite-biotite-garnet assemblages up to 650 °C from sillimanite-biotite-garnet assemblages. No estimates were obtained from the low-grade units.

6) P-T vectors from rocks upgrade from the sillimanite-biotite-muscovite isograd are shallow indicating that the rocks underwent principally isobaric cooling initially.

7) Gravity and magnetic modelling have been employed to produce a model for the geology beneath the MCSZ. This model is consistent with structural information from surface outcrops and suggests that the ophiolites dip outward and away from the MCSZ, and the Coy Pond Complex is underlain by

a low-density body (perhaps the Partridgeberry Hills Granite or Spruce Brook Formation).

8) The small-scale magnetic anomalies within the MCSZ southeast of the Through Hill Granite are due to cordierite-magnetite assemblages which are interpreted as traces of folded bedding surfaces. The dip of this bedding estimated from magnetic modelling ($\sim 45^\circ$) is consistent with structural measurements.

References

- Aranovich, L. Ya. and Podlesskii, K.K. 1983. The cordierite-garnet-sillimanite-quartz equilibrium: Experiments and applications. In: Kinetics and Equilibrium in Mineral Reactions. Edited by S.K. Saxena. New York: Springer-Verlag, pp. 173-198.
- Ashworth, J.R. and Chinner, G.A. 1978. Coexisting garnet and cordierite in migmatites from the Scottish Caledonides. Contributions to Mineralogy and Petrology, 65: 379-394.
- Barker, D. S. 1983. Igneous Rocks. New Jersey: Prentice-Hall, Inc., pp. 292-293.
- Bhattacharya, A., Mazumdar, A.C. and Sen, S.K. 1988. Fe-Mg mixing in cordierite: Constraints from natural data and implications for cordierite-garnet geothermometry in granulites. American Mineralogist, 73: 336-344.
- Fohlen, S.R., Valley, J.W. and Essene, E.R. 1985. Metamorphism in the Adirondacks. I. Petrology, pressure and temperature. Journal of Petrology, 26: 971-992.
- Burnham, C.W., Hollaway, J.R. Davis, N.F. 1969. Thermodynamic properties of water to 1,000°C and 10,000 bars. Geological Society of America, Special Paper, 132: 96p.
- Carmichael, D.M. 1970. Intersecting isograds in the Whetstone Lake area, Ontario. Journal of Petrology, 11: 147-181.
- Carmichael, D.M. 1978. Metamorphic bathozones and bathograds: A measure of the depth of post-metamorphic uplift and erosion on the regional scale. American Journal of Science, 278: 769-797.
- Colman-Sadd, S.P. 1980. Geology of parts of the Burnt Hill area (2D/5), Newfoundland. In: Current Research. Edited by C.F. O'Driscoll and R.V. Gibbons. Newfoundland Department of Mines and Energy, Mineral Development Division, Report 80-1: 44-49.

- 1981. Geology of the Burnt Hill map area (2D/5), Newfoundland. In: Current Research. Edited by C.F. O'Driscoll and R.V. Gibbons. Newfoundland Department of Mines and Energy, Mineral Development Division, Report 81-1: 40-49.
- 1982. Geology of the western part of the West Gander Rivers area. Newfoundland Department of Mines and Energy, Mineral Development Division, Map 82-59 (Open File).
- 1985. Geology of the Burnt Hill map area (2D/5), Newfoundland. Newfoundland Department of Mines and Energy, Mineral Development Division, Report 85-3, 94p.
- Colman-Sadd, S.P. and Russell, H.A.J. 1982. Geology of the Miguels Lake map area (2D/12), Newfoundland. In: Current Research. Edited by C.F. O'Driscoll and R.V. Gibbons. Newfoundland Department of Mines and Energy, Mineral Development Division, Report 82-1: 30-50.
- Colman-Sadd, S.P. and Swinden, H.S. 1984. A tectonic window in central Newfoundland? Geological evidence that the Appalachian Dunnage Zone may be allochthonous. Canadian Journal of Earth Sciences, 21: 1349-1367.
- Colman-Sadd, S.P., Dickson, W.L., Elias, P. and Davenport, P.H. 1981. Rock geochemical data from the plutonic intrusions of south-central Newfoundland. Newfoundland Department of Mines and Energy, Mineral Development Division, Open File Newfoundland 1157.
- Colman-Sadd, S.P., Dunning, G.R. and Dec, T. In press. Dunnage-Gander relationships and Ordovician orogeny in central Newfoundland: A sediment provenance and U/Pb age study. American Journal of Science.
- Cormack, W.E. 1823. Account of a journey across the island of Newfoundland. Edinburgh Philosophical Journal. Volume 10.
- Deer, W.A., Howie, R.A. and Zussman, J. 1966. An Introduction to the Rock Forming Minerals. Hong Kong: Commonwealth Printing Press Ltd., 528p.

- Dewey, J.F. and Bird, J.M. 1970. Mountain belts and the new global tectonics. *Journal of Geophysical Research*, 75: 2625-2647.
- Dick, H.J.B. and Bullen, T. 1984. Chromian spinel as a petrogenetic indicator in abyssal and alpine-type peridotites and spatially associated lavas. *Contributions to Mineralogy and Petrology*, 86: 54-76.
- Dunning, G.R. and Krogh, T.E. 1985. Geochronology of ophiolites of the Newfoundland Appalachians. *Canadian Journal of Earth Sciences*, 22: 1659-1670.
- Elias, P. 1981. Geochemistry and petrology of granitoid rocks of the Gander Zone, Bay d'Espoir area, Newfoundland. Unpublished M.Sc. thesis, Memorial University of Newfoundland, 271p.
- Elias, P. and Strong, D.F. 1982. Paleozoic granitoid plutonism of southern Newfoundland: contrasts in timing, tectonic setting and level of emplacement. *Transactions of the Royal Society of Edinburgh: Earth Sciences*, 73: 43-57.
- England, P.C. and Thompson, A.B. 1984. Pressure-temperature-time paths of regional metamorphism I. Heat transfer during the evolution of regions of thickened continental crust. *Journal of Petrology*, 25: 894-928.
- Ferry, J.M. and Spear, F.S. 1978. Experimental calibration of the partitioning of Fe and Mg between biotite and garnet. *Contributions to Mineralogy and Petrology*, 66: 113-117.
- Flood, R.H. and Vernon, R.H. 1978. The Cooma Granodiorite, Australia: An example of in situ crustal anatexis? *Geology*, 6: 81-84.
- Ganguly, J. and Kennedy, G.C. 1974. The energetics of natural garnet solid solution: I. Mixing of the aluminosilicate end-members. *Contributions to Mineralogy and Petrology*, 48: 137-148.
- Grady, J.C. 1952. Preliminary report on the ultrabasic rocks of the Upper Gander River. Newfoundland Department of Mines and Resources, Mines Branch, Geology Section, 5p.

- 1953. The geology of the southern half of the serpentinite belt in east-central Newfoundland. Geological Survey of Newfoundland report, 63p. [2D/11 (5)]
- Hébert, R. and Laurent, R. 1990. Mineral chemistry of the plutonic section of the Troodos ophiolite: New constraints for genesis of arc-related ophiolites. In: *Ophiolites: Oceanic Crustal Analogues, Proceedings of the Symposium "Troodos 1987"*. Edited by J. Malpas, E. Moores, A. Panayiotou and C. Xenophontos. Cyprus: SOGEK Printers, pp. 149-163.
- Hodges, K.V. and Royden, L. 1984. Geologic thermobarometry of retrograded metamorphic rocks: An indication of the uplift trajectory of a portion of the northern Scandinavian Caledonides. *Journal of Geophysical Research*, **89**: 7077-7090.
- Hodges, K.V. and Spear, F.S. 1982. Geothermometry, geobarometry and the Al_2SiO_5 triple point at Mt. Moosilauke, New Hampshire. *American Mineralogist*, **67**: 1118-1134.
- Holdaway, M.J. 1971. Stability of andalusite and the aluminum silicate phase diagram. *American Journal of Science*, **271**: 97-131.
- Hutchison, C.S. 1974. Laboratory Handbook of Petrographic Techniques. New York: Wiley, 551p.
- Jenner, G.A. and Swinden, H.S. 1989. Trace element and isotope geochemistry of the Pipestone Pond Complex, Newfoundland: Complex magmatism in an eastern dunnage zone ophiolite. In: *Geological Association of Canada/ Mineralogical Association of Canada Program With Abstracts*, p. A96.
- Kamineni, D.C. and Carrara, A. 1973. Comparison of the composition of porphyroblastic and fabric-forming biotite in two metamorphic rocks. *Canadian Journal of Earth Sciences*, **10**: 948-953.
- Keen, C.E., Keen, M.J., Nichols, B., Reid, I., Stockmal, G.S., Colman-Sadd, S.P., O'Brien, S.J., Miller, H., Quinlan, G., Williams, H. and Wright, J. 1986. Deep seismic reflection profile across the northern Appalachians. *Geology*, **14**: 141-145.

- Kerrick, D.M. 1972. Experimental determination of muscovite + quartz stability with $P_{H_2O} < P_{total}$. *American Journal of Science*, 272: 946-958.
- Labotka, T.C. 1981. Petrology of an andalusite-type regional metamorphic terrane, Panamint Mountains, California. *Journal of Petrology*, 22: 261-296.
- Lachenbruch, A. and Sass, J.H. 1978. Models of an extending lithosphere and heat flow in the Basin and Range Province. In: *Cenozoic Tectonics and Regional Geophysics of the Western Cordillera*. Edited by: R.B. Smith and G.P. Eaton. Geological Society of America, Memoir 152: 209-250.
- Lepezin, G.G. and Korolyuk, V.N. 1985. Types of zoning in garnets. *Soviet Geology and Geophysics*, 26: 71-79.
- Malpas, J. and Strong, D.F. 1975. A comparison of chrome-spinels in ophiolites and mantle diapirs of Newfoundland. *Geochimica et Cosmochimica Acta*, 39: 1045-1060.
- Mengel, F. and Rivers, T. 1989. Thermotectonic evolution of Proterozoic and reworked Archaean terranes along the Nain-Churchill boundary in the Saglek area, northern Labrador. In: *Evolution of Metamorphic Belts*. Edited by J.S. Daly, R.A. Cliff and B.W.D. Yardley. Geological Society Special Publication, 43: 319-324.
- Miyashiro, A. 1961. Evolution of metamorphic belts. *Journal of Petrology*, 2: 277-311.
- Morelli, C., Gantar, C., Honkasalo, T., McConnell, R.K., Szabo, B., Tanner, J.G., Uotila, U. and Whelan, T. 1971. The international standardization gravity net (IGSN71). International Association of Geodesy, Paris, France, Special Bulletin 4.
- Murray, A. and Howley, J.P. 1881. *Geological Survey of Newfoundland*. Edward Stanford, London, 536 p.
- Newton, R.C. and Haselton, H.T. 1981. Thermodynamics of the garnet-plagioclase- Al_2SiO_5 -quartz geobarometer. In: *Thermodynamics of Minerals and Melts*. Edited by R.C. Newton, A. Navrotsky and B.J. Wood. New York: Springer-Verlag, pp. 131-147.

- Perchuk, L.L. and Lavrent'eva, I.V. 1983. Experimental investigation of exchange equilibria in the system cordierite-garnet-biotite. *In: Kinetics and Equilibrium in Mineral Reactions. Edited by S.K. Saxena. New York: Springer-Verlag, pp. 199-239.*
- Perchuk, L.L., Aranovich, L. Ya., Podlesskii, K.K., Lavrant'eva, I.V., Gerasimov, V. Yu., Fed'kin, V.V., Kitsul, V.I., Karsakov, L.P. and Berdnikov, N.V. 1985. Precambrian granulites of the Aldan Shield, eastern Siberia, USSR. *Journal of Metamorphic Geology*, 3: 265-310.
- Piwinskii, A.J. 1968. Experimental studies of igneous rock series, Central Sierra Nevada Batholith, California. *Journal of Geology*, 76: 548-570.
- Powell, R. 1978. Equilibrium Thermodynamics in Petrology: An Introduction. London: Harper & Row, Publishers, 284p.
- Rivers, T., Deveau, S., Timbal, A. and Colman-Sadd, S. 1990. Mount Cormack Terrane: An Appalachian example of a metamorphic core complex? *In: Lithoprobe East, Report of Transect Meeting. Edited by: J. Hall. Lithoprobe East Transect, Report No. 13: 153-158.*
- Royden, L. and Hodges, K.V. 1984. A technique for analyzing the thermal and uplift histories of eroding orogenic belts: A Scandinavian example. *Journal of Geophysical Research*, 89: 7091-7106.
- Silverstone, J. and Chamberlain, C.P. 1990. Apparent isobaric cooling paths from granulites: Two counterexamples from British Columbia and New Hampshire. *Geology*, 18: 307-310.
- Slipp, R.M. 1952. The geology of the Round Pond map area, Newfoundland. Unpublished M.Sc. thesis, McGill University, 79p. [Nfld. (96)]
- St-Onge, M.R. 1984. The muscovite-melt bathograd and low-P isograd suites in north-central Wopmay Orogen, Northwest Territories, Canada. *Journal of Metamorphic Geology*, 2: 315-326.
- Streckeisen, A. 1976. To each plutonic rock its proper name. *Earth Science Review*, 12: 1-33.
- Strong, D.F. 1979. The Mount Peyton Batholith, central Newfoundland: A bimodal calc-alkaline suite. *Journal of Petrology*, 20: 119-138.

- Stuckless, S.K. 1975. Aeromagnetic expression of rocks of the Eastern half of the mobile belt of Newfoundland with special reference to the ultramafics. Unpublished B.Sc. thesis, Memorial University, 39p.
- Swinden, H.S. 1981. Geology of the Great Burnt Lake area. Newfoundland Department of Mines and Energy, Mineral Development Division, Maps 81-113, 81-114, 81-115 (Open File).
- Swinden, H.S. 1988. Geology of the Pipestone Pond area. Newfoundland Department of Mines and Energy, Mineral Development Division, Map 88-51 (Open File).
- Swinden, H.S. and Collins, W.T. 1982. Geology and economic potential of the Great Burnt Lake area, central Newfoundland. In: Current Research. Edited by C.F. O'Driscoll and R.V. Gibbons. Newfoundland Department of Mines and Energy, Mineral Development Division, Report 82-1: 188-207.
- Telford, W.M., Geldart, L.P., Sheriff, R.E. and Keys, D.A. 1987. Applied Geophysics, New York: Cambridge University Press, 860p.
- Thompson, A.B. and Ridley, J.R. 1987. Pressure-temperature-time (P-T-t) histories of orogenic belts. Philosophical Transactions of the Royal Society of London, A 321: 27-45.
- Thompson, J.B. Jr. 1957. The graphical analysis of mineral assemblages in pelitic schists. American Mineralogist, 42: 842-858.
- Thompson, J.B. and Norton, S.A. 1968. Paleozoic regional metamorphism in New England and adjacent areas. In: Studies of Appalachian Geology, Northern and Maritime. Edited by: E-An Zen, W.S. White, J.B. Hadley and J.B. Thompson, Jr. Interscience Publishers, New York, pp. 319-327.
- Tracy, R.J. 1982. Compositional zoning and inclusions in metamorphic minerals. In: Characterization of metamorphism through Mineral Equilibria; Mineralogical Society of America Reviews in Mineralogy Volume 10. Edited by: John M. Ferry. Chelsea: Michigan, Bookcrafters, Inc., 397p.

- Triboulet, C. and Audren, C. 1985. Continuous reactions between biotite, garnet, staurolite, kyanite-sillimanite-andalusite and P-T-time-deformation path in mica-schists from the estuary of the river Vilaine, South Brittany, France. *Journal of Metamorphic Geology*, 3: 91-105.
- Tuccillo, M.E., Essene, E.J. and van der Pluijm, B.A. 1990. Growth and retrograde zoning in garnets from high-grade metapelites: Implications for pressure-temperature paths. *Geology*, 18: 839-842.
- Tucker, R.D., Krogh, T.E., Ross, R.J.Jr. and Williams, S.H. 1990. Time-scale calibration by high-precision U-Pb zircon dating of interstratified volcanic ashes in the Ordovician and Lower Silurian stratotypes of Britain. *Earth and Planetary Science Letters*, 100: 51-58.
- van Staal, C.R. 1987. Tectonic setting of the Tetagouche Group in northern New Brunswick: Implications for plate tectonic models of the northern Appalachians. *Canadian Journal of Earth Sciences*, 24: 1329-1351.
- White, A.J.R. and Chappell, B.W. 1983. Granitoid types and their distribution in the Lachlan Fold Belt, southeastern Australia. In: *Circum-Pacific Plutonic Terranes*. Edited by: J.A. Roddick. Geological Society of America, Memoir 159: 21-34.
- Wickham, S.M. and Oxburgh, E.R. 1987. Low-pressure regional metamorphism in the Pyrenees and its implications for the thermal evolution of rifted continental crust. *Philosophical Transactions of the Royal Society of London*, A 321: 219-242.
- Williams, H. 1964. The Appalachians in northeastern Newfoundland - a two-sided symmetrical system. *American Journal of Science*, 262: 1137-1158.
- Williams, H. 1978. Geological Development of the northern Appalachians: Its bearing on the evolution of the British Isles. In: *Crustal evolution in northwestern Britain and adjacent regions*. Edited by: D.R. Bowes and B.E. Leake. *Geological Journal Special Issue No. 10*: 1-22.
- Williams, H. 1979. Appalachian Orogen in Canada. *Canadian Journal of Earth Sciences*, 16: 792-807.

- Williams, H. and Hatcher, R.D. Jr. 1982. Suspect terranes and accretionary history of the Appalachian Orogen. *Geology*, 10: 530-536.
- Williams, H. and Hatcher, R.D. Jr. 1983. Appalachian suspect terranes. In: Contributions to the tectonics and geophysics of mountain chains. Edited by R.D. Hatcher, H. Williams and I. Zietz. Geological Society of America, Memoir 158: 33-53.
- Williams, S.H., Boyce, W.D. and Colman-Sadd, S.P. In press. A new Lower Ordovician (Arenig) fauna from the Coy Pond Complex, central Newfoundland, and its implications in understanding the closure of the Iapetus Ocean. *Transactions of the Royal Society of Edinburgh*.
- Williams, H., Colman-Sadd, S.P. and Swinden, H.S. 1988. Tectonic-stratigraphic subdivisions of central Newfoundland. In: Current Research, Part B, Geological Survey of Canada, Paper 88-1A: 91-98.
- Wilson, J.T. 1966. Did the Atlantic close and then reopen? *Nature*, 211: 676-681.
- Winkler, H.G. 1979. Petrogenesis of Metamorphic Rocks, Fifth Edition. New York: Springer-Verlag, 348p.
- Wolofsky, L. 1951. Geology of the Sitdown Pond area, central Newfoundland. Unpublished B.A. thesis, Queen's University, 47p. [12A/8 (95)]
- Wood, B.J. and Fraser, D.G. 1986. Elementary Thermodynamics for Geologists. Great Britain: Thomson Litho Ltd., 303p.
- Woodsworth, G.J. 1977. Homogenization of zoned garnets from pelitic schists. *Canadian Mineralogist*, 15: 230-242.
- Yardley, B.W.D. 1977. An empirical study of diffusion in garnet. *American Mineralogist*, 62: 793-800.
- Zwicker, E.J. and Strong, D.F. 1986. The Great Bend ophiolite, eastern Newfoundland: field investigations. In: Current Research, Part A, Geological Survey of Canada, Paper 86-1A: 393-397.

APPENDIX A:
Petrographic Descriptions

Petrographic Sample Descriptions

208

(Abbreviations listed on Page 211)

| Sample # | Mineralogy | | | | | | | | | | | | | | Accessory Phases | | | | | | | | Zone |
|------------|------------|----|----|----|-------|-------|----|----|----|----|----|----|----|----|------------------|----|----|---|----|---|---|-----|------|
| | Q | P | K | B | M | Ch | G | A | S | Cd | St | Px | Cc | Cz | Op | Ap | Z | H | Ti | T | E | | |
| SD-89-002 | 40 | 30 | 5 | 25 | <1 | | | | | | | | | | | | | | | | | ZM | |
| SD-89-003a | 15 | 45 | | 20 | 15 | 5(r) | <1 | | | | | | | | <1 | | | | | | | ZM | |
| SD-89-003b | 25 | 5 | | 10 | 5 | 3(r) | 30 | | | | | 10 | 1 | 5 | 2 | 1 | 2 | | 1 | | | ZM | |
| SD-89-004 | 35 | 30 | | 20 | 12 | 2(r) | 1 | | | | | | | | | | | | | | | ZM | |
| SD-89-011 | 30 | 25 | 10 | 15 | 15 | 1(r) | | | | | | | | | 1 | | | | | | | S | |
| SD-89-012 | 45 | 20 | | 25 | 10 | 1(r) | | | | | | | | | 1 | 2 | | | | | | S | |
| SD-89-015 | 30 | 20 | | 15 | 20 | 5(r) | 8 | | | | | | | | 2 | | | | | | | S | |
| SD-89-020 | 35 | 20 | | 15 | 5 | 5(r) | <1 | | 20 | | | | | | | | | | | | | ZM | |
| SD-89-025a | 40 | 20 | | 20 | 15 | | | | | | | | | | 3 | | | | | | | ZM | |
| SD-89-025b | 40 | 15 | | 15 | 17 | | | | 10 | | | | | | 2 | | | | | | | ZM | |
| SD-89-028 | 50 | | | 40 | 5(r) | | | | 3 | | | | | | 1 | | | | | | | ZM | |
| SD-89-030 | 40 | 20 | | 25 | 15 | | | | | | | | | | | | | | | | | ZM | |
| SD-89-033 | 35 | 20 | | 20 | 15 | 5(r) | | | 5 | 1 | | | | | 1 | | | | | | | ZM | |
| SD-89-034a | 35 | 25 | | 20 | 17 | 2(r) | 5 | | | | | | | | 1 | | | | | | | ZM | |
| SD-89-034b | 40 | 10 | | 30 | 15 | 2(r) | 3 | | | | | | | | 1 | | | | | | | ZM | |
| SD-89-034c | 25 | 20 | | 30 | 20 | 2(r) | 5 | | | | | | | | 1 | | | | | | | ZM | |
| SD-89-034d | 25 | 20 | | 30 | 15 | 1(r) | 8 | | | | | | | | 1 | | | | | | | ZM | |
| SD-89-034e | 35 | 20 | | 20 | 15 | 2(r) | 5 | | | | | | | | 1 | | | | | | | ZM | |
| SD-89-043 | 40 | | | 30 | 30 | | | | | | 1 | | | | 1 | | | | | | | A | |
| SD-89-046a | 25 | | | 30 | 33 | 3 | | | | 7 | | | | | 2 | | | 1 | | | | A | |
| SD-89-046b | 35 | | | 30 | 20 | 2(r) | 4 | | | 10 | | | | | 2 | | | | | | | A | |
| SD-89-048 | 25 | | | 5 | 40 | 25(r) | | | | 5 | | | | | 1 | | | | | | | A | |
| SD-89-067 | 30 | 15 | | 30 | 20 | | | | 5 | | | | | | 2 | | | | | | | ZM | |
| SD-89-076a | 30 | 10 | 25 | 25 | 5 | | | | <5 | | | | | | 1 | | | | | | | ZM | |
| SD-89-076b | 40 | 15 | 10 | 20 | 15 | | | | | | | | | | 1 | | | | | | | ZM | |
| SD-89-077 | 25 | 10 | | 15 | 35 | 5(r) | | | | | | | | | | | | | | | | ZM | |
| SD-89-079 | 10 | 10 | 20 | 35 | 15 | 1(r) | | | | | | | | | 5 | | | | | | | S | |
| SD-89-085 | 20 | | | 15 | 60 | 5(r) | 5 | | | | | | | | 2 | | | 5 | | | | A | |
| SD-89-085a | 30 | | 1 | 50 | 10 | | | | | | | | | | 1 | | <1 | 5 | | 1 | | A | |
| SD-89-086 | 30 | | | 15 | 25 | 15(r) | | | | | 10 | | | | <5 | | | | | | | A | |
| SD-89-087 | 40 | | | 15 | 30 | 5(r) | 5 | | | | | | | | <5 | | | | | | | A | |
| SD-89-091a | 40 | 20 | | 25 | 10 | 2(r) | | | 1 | | | | | | 1 | | | | | | | ZM | |
| SD-89-091b | 15 | | | 5 | 55 | 15(r) | | | 10 | | | | | | <5 | | | | | | | ZM | |
| SD-89-096 | 45 | 10 | | 7 | 35 | 3(r) | | | | | | | | | 1 | | | | | | | ZM | |
| SD-89-096d | 35 | 30 | 20 | | 10 | 5 | | | | | | | | | | | | | | | | ZM | |
| SD-89-097a | 30 | | | 30 | 20 | 5 | <5 | 10 | | | <1 | | | | 1 | | | | | | | A-S | |
| SD-89-097b | 20 | | | 20 | 50 | | 5 | 2 | | | <1 | | | | 2 | | | | | | | A-S | |
| SD-89-102a | 25 | | | 25 | 40 | | 10 | | | | <1 | | | | 1 | | | | | | | A | |
| SD-89-102b | 45 | | | 25 | 15 | <1 | 10 | | | | | | | | <5 | | | | | | | A | |
| SD-89-103 | 50 | | | 20 | 20 | 3 | 5 | | | | | | | | 2 | | | | | | | A | |
| SD-89-104a | 55 | | | 30 | 10(r) | 1? | | | | | | | | | 4 | | | 1 | | | | A | |
| SD-89-104b | 40 | | | 2 | 40 | 10(r) | | | | | | | | | 3 | | | 2 | | | | A | |
| SD-89-107 | 40 | 1 | | 15 | 25 | 3 | | | 15 | | | | | | 1 | | | | | | | S | |
| SD-89-110 | 45 | 10 | 15 | 15 | 2 | 3(r) | <1 | | 10 | | | | | | 1 | | | | | | | S | |
| SD-89-112 | 40 | 5 | | 15 | 20 | 1 | | | 15 | | | | | | 2 | | | | | | | S | |
| SD-89-114 | 25 | 20 | | 35 | 15 | | | | 5 | | | | | | 1 | | | | | | | S | |
| SD-89-116 | 45 | 10 | | 10 | 25 | 3(r) | 1 | | 5 | | | | | | 1 | | | | | | | S | |
| SD-89-127 | 30 | 5 | | 30 | 25 | 2 | | | 6 | | | | | | 2 | | | | | | | ZM | |
| SD-89-128 | 25 | | | 40 | 25 | 2 | | | 7 | | | | | | 1 | | | | | | | ZM | |
| SD-89-143 | 30 | | | 20 | 25 | 2(r) | 3 | | 15 | | | | | | 5 | | | | 1 | | | ZM | |
| SD-89-145a | 50 | 15 | | 5 | 30 | | | | | | | | | | | | | | | | | S | |
| SD-89-145b | 23 | 5 | | 40 | 15 | | | | 15 | | | | | | 2 | | | | 2 | | | S | |
| SD-89-155 | 50 | 20 | | 20 | 10 | | | | | | | | | | 2 | | | | | | | ZM | |
| SD-89-156 | 45 | 25 | 20 | | 4 | 3(r) | | | | | | | | | <1 | | | | | | | ZM | |
| SD-89-160 | 30 | | | 30 | 20 | 10(r) | 5 | | 5 | | | | | | 1 | | | | | | | ZM | |

Petrographic Sample Descriptions

209

| Sample # | Mineralogy | | | | | | | | | | | | | | Accessory Phases | | | | | | | Zone |
|------------|------------|----|----|----|------|-------|----|----|----|-------|----|----|----|----|------------------|----|----|----|----|----|----|------|
| | Q | P | K | B | M | Ch | G | A | S | Cd | St | Px | Cc | Cz | Op | Ap | Z | H | Ti | T | E | |
| SD-89-160a | 45 | 20 | 1 | 20 | 10 | | | | | | | | | | 2 | <1 | <1 | | | | | ZM |
| SD-89-161 | 15 | 45 | | 20 | 15 | 5(r) | 1 | | | | | | | | 1 | | | | | | | ZM |
| SD-89-162 | 25 | 5 | | 10 | 5 | 3(r) | 30 | | | | | | | | | | | | | | | ZM |
| SD-89-170 | 35 | 35 | 5 | | 20 | 1(r) | 1 | | | | | | | | | | | | | | | G |
| SD-89-171 | 25 | | | 30 | 35 | 2(r) | 2 | | | | | | | | 1 | | | 1 | | | | A |
| SD-89-174 | 35 | | | 15 | 40 | 3(r) | 5 | | | | | | | | 2 | | | | | | | A |
| SD-89-175 | 30 | | | 30 | 15 | 3(r) | <1 | 15 | | | 2 | | | | 2 | | | | | | | A |
| SD-89-176 | 35 | | | 15 | 25 | 5(r) | 1 | 5 | | | 5 | | | | 3 | | | | | | | A |
| SD-89-178 | 35 | | | 10 | 50 | 5(r) | 5 | | | | | | | | 2 | | | | | | | A |
| SD-89-182 | 60 | 20 | 1 | 10 | 5 | 1(r) | 1 | | | | | | | | 2 | | | | | | | S |
| SD-89-184 | 35 | 3 | | 35 | 20 | 3(r) | 2 | | 2 | | | | | | | | | | | | | S |
| SD-89-186 | 40 | 2 | | 20 | 30 | 1(r) | | | 5 | | | | | | 2 | | | | | 1 | | S |
| SD-89-187 | 20 | | | 25 | 10 | 1(r) | 40 | | | | | | | | 2 | | | | | | | A |
| SD-89-188 | 20 | | | 20 | 40 | 5(r) | 10 | | | | | | | | 3 | | | 1 | | | | A |
| SD-89-190a | 50 | | | 20 | 15 | 3(r) | 5 | | | | 5 | | | | 2 | | | | | | | A |
| SD-89-190b | 50 | | | 25 | 10 | 3(r) | 5 | | | | 5 | | | | 2 | | | | | | | A |
| SD-89-195a | 30 | | | 20 | 35 | 5(r) | 1 | 2 | | 2(p) | | | | | 3 | | | | | | | A |
| SD-89-195b | <1 | <1 | | 15 | 5(r) | 75 | | | | | | | | | 2 | | | | | | | A |
| SD-89-200 | 45 | 20 | | 20 | 5 | | 3 | | <1 | | | | | | 3 | | 2 | | | | | S |
| SD-89-201a | 40 | 30 | | 20 | 5 | 1(r) | | | | | | | | | 2 | | <1 | | | | | S |
| SD-89-201b | 20 | 10 | | 30 | 15 | 10(r) | | | 10 | | | | | | 5 | | 1 | | | 1 | | S |
| SD-89-209a | 16 | 12 | 20 | 35 | 10 | | | | 5 | | | | | | | | <1 | <1 | | <1 | | S |
| SD-89-209b | 30 | 2 | 20 | 30 | 15 | | 1 | | 2 | | | | | | 1 | | <1 | | | | | S |
| SD-89-212 | 25 | 15 | | 35 | 20 | | 5 | | | | | | | | <1 | | | <1 | | <1 | | ZM |
| SD-89-213 | 45 | 2 | | 25 | 25 | | 1 | | | | | | | | 1 | <1 | | <1 | | | | ZM |
| SD-89-218 | 15 | 30 | 5 | 20 | 10 | 2(r) | | | | 15 | | | | | 2 | | <1 | | | | | G |
| SD-89-220 | 25 | | | | | | 15 | | | | | | | 35 | | | | | | | 25 | ZM |
| SD-89-221 | 35 | 30 | | 15 | 10 | 5(r) | | | | | | | | | 5 | | | 1 | | | | ZM |
| SD-89-227 | 25 | 5 | | 25 | 35 | | 5 | | 5 | | | | | | <1 | | | | | | | S |
| SD-89-229 | 55 | 2 | | 10 | 25 | 2(r) | 2 | <1 | | | | | | | 3 | | | <1 | | <1 | | A |
| SD-89-235 | 30 | | | 25 | 35 | | | | 5 | | | | | | | | <1 | <1 | | 5 | | A |
| SD-89-236 | 30 | | | 20 | 35 | 2(r) | | <1 | | | | | | | <1 | | | | | 10 | | A |
| SD-89-237 | 40 | 1 | | 25 | 20 | 5(r) | | | | | | | | | 3 | | | | | 5 | | A |
| SD-89-243 | 50 | | | | 25 | 20 | | | | | | | | | 5 | | | 1 | | | | C |
| SD-89-244 | 40 | 5 | | 10 | 35 | 5 | | | | | | | | | 3 | | <1 | 1 | | 1 | | B |
| SD-89-246a | 60 | 5 | 2 | | | 10 | | | | | | | | | 3 | <1 | | | | | 20 | B |
| SD-89-246b | | 15 | | | | 2 | | | | | 70 | | | | 5 | | | | | | 10 | B |
| SD-89-247 | 40 | | | 10 | 40 | 5 | | | | | | | | | 5 | | | | | | | B |
| SD-89-252 | 40 | | | 10 | 40 | 5 | <1 | | | | | | | | 2 | | | | | | | B |
| SD-89-256 | 30 | | | 20 | 40 | 5 | | | | | | | | | 3 | | | | | | | B |
| SD-89-259 | 60 | | | 15 | 15 | 10 | | | | | | | | | 1 | | | | | | | B |
| SD-89-260 | 25 | | | 45 | 20 | 5(r) | | 5 | | | | | | | 1 | | | | | | | A |
| SD-89-261 | 20 | | | 35 | 40 | 5 | | | | | | | | | | | | | | | | B |
| SD-89-262 | 25 | | | 25 | 35 | 10(r) | 2 | | | | 1 | | | | | | | | | | | A |
| SD-89-266 | 30 | | | 15 | 45 | 5(r) | 2 | | | | | | | | | | | | | | | A |
| SD-89-267 | 40 | | | 15 | 25 | 10 | 5 | | | 10(p) | | | | | 5 | | | | | 1 | | B |
| SD-89-268 | 25 | | | 15 | 50 | 2 | | | | | | | | | 7 | | | | | | | B |
| SD-89-272 | 80 | | 2 | | 10 | 5 | 2 | | | | | | | | 2 | <1 | <1 | 1 | | | | B |
| SD-89-276 | 35 | <1 | | 15 | 25 | 10(r) | 5 | 5 | | 10(p) | | | | | 5 | | | | | | | A |
| SD-89-277 | 60 | | | 15 | 15 | 2(r) | 5 | | | | | | | | 1 | | | | | | | A |
| SD-89-278 | 25 | | | 5 | 35 | 20 | 5 | 1 | | 1(p) | | | | | 3 | | | 1 | | | | A-B |
| SD-89-280 | 40 | | | 15 | 30 | 15 | | | | | | | | | 2 | | | | | | | B |
| SD-89-281 | 40 | | | 20 | 30 | 5 | | | | | | | | | 3 | | | | | | | B |
| SD-89-282 | 40 | | | 20 | 30 | 5 | | | | | | | | | 3 | | | | | | | B |
| SD-89-284 | 60 | | | 15 | 20 | 1(r) | | 5 | | | | | | | 4 | | | | <1 | | | A |

Petrographic Sample Descriptions

| Sample # | Mineralogy | | | | | | | | | | | | | | Accessory Phases | | | | | | | Zone |
|------------|------------|----|----|----|-------|-------|----|----|------|------|----|----|----|----|------------------|----|----|----|----|----|----|------|
| | Q | P | K | B | M | Ch | G | A | S | Cd | St | Px | Cc | Cz | Op | Ap | Z | H | Ti | T | E | |
| SD-89-285 | 40 | | | 20 | 15 | 10(r) | | | 3 | | 7 | | | | 2 | 1 | | | | | | A |
| SD-89-287 | 35 | | | 30 | 30 | 3(r) | | | 5(r) | | | | | | 1 | | | | | | | A |
| SD-89-288 | 35 | | | 30 | 20 | 4(r) | | | 5 | 5(p) | 4 | | | | 1 | | | | | | | A |
| SD-89-289 | 30 | | | 25 | 35 | 2(r) | | | 5(r) | | 1 | | | | 2 | | | | | | | A |
| SD-89-291 | 70 | | | 10 | 10 | 5 | | | | | | | | | 2 | | <1 | | | <1 | | B |
| SD-89-294 | 45 | | | 20 | 20 | 10 | | | | | | | | | 3 | | | | | | | B |
| SD-89-295a | 75 | | | 10 | 15 | 5(r) | | | | | | | | | 2 | | | | | | | A |
| SD-89-295b | 25 | | | 25 | 35 | 10(r) | 3 | | | | | | | | 2 | | | | | | | A |
| SD-89-295c | 25 | 5 | | 40 | 20(r) | | | | | | | | | | 10 | 1 | <1 | | | | | A |
| SD-89-296 | 25 | | | 25 | 25 | 15(r) | | 7 | | | | | | | 3 | | | | | | | A |
| SD-89-297 | 70 | 1 | | 10 | 10 | 3(r) | 5 | | | | | | | | 2 | | | | | | | A |
| SD-89-298 | 30 | | | 30 | 35 | 5(r) | | | | | | | | | 1 | | | | | | | A |
| SD-89-299 | 30 | | | 10 | 25 | 5(r) | | | | 20 | | | | | 10 | | 2 | | | | | A |
| SD-89-300 | 25 | | | 20 | 20 | 5(r) | 5 | 20 | | | | | | | 5 | | 1 | | | | | A |
| SD-89-302 | 55 | 1 | | 5 | 25 | 10(r) | 3 | | | | | | | | 2 | | | | | | | A |
| SD-89-304 | 40 | 2 | | 40 | 10 | 2(r) | 1 | | 5 | | | | | | 1 | | 1 | | | | | S |
| SD-89-306 | 20 | | | 5 | 45 | 15(r) | | | | 10 | | | | | 1 | | 2 | | 1 | | | S |
| SD-89-307 | 40 | 10 | 5 | 20 | 5 | | | | 10 | | | | | | 1 | | 1 | 5 | | | | S |
| SD-89-310 | 25 | 2 | 2 | 20 | 40 | 5(r) | | | 5 | | | | | | 1 | | | | | | | S |
| SD-89-312 | 50 | 5 | | 20 | 10 | | 5 | | 10 | | | | | | | | 1 | | 1 | | | S |
| SD-89-313 | 40 | 2 | 5 | 35 | 10 | | | | | | | | | | 2 | 1 | | | | | 5 | B |
| SD-89-315c | 10 | 5 | | | 65 | | | | | | | | | | 5 | | | | | | 15 | B |
| SD-89-315d | 40 | | | 15 | 30 | 10 | | | | | | | | | 5 | | <1 | | | | | B |
| SD-89-319 | 35 | | | 15 | 45 | 1 | | | | | | | | | 3 | | <1 | | | | | B |
| SD-89-320 | 40 | 5 | | 45 | | | | | | | | | 5 | | 3 | | <1 | | | | | C |
| SD-89-325 | 50 | 20 | | 25 | 2 | | | | | | | | <1 | | | | <1 | | | | | C |
| SD-89-327 | 50 | | | 30 | 15 | | | | | | | | 5 | | 1 | 1 | | | | <1 | | C |
| SD-89-328 | 30 | 45 | 15 | | 7 | | 2 | | | | | | | | | | | | | | | G |
| SD-89-329 | 15 | 5 | | 35 | 25 | | 10 | | 10 | | | | | | | | <1 | <1 | | <1 | | S |
| SD-89-331 | 30 | 1 | | 35 | 20 | 2(r) | | | 10 | | | | | | | | | <1 | | <1 | | S |
| SD-89-334 | 35 | 5 | | 25 | 20 | 1(r) | | | 10 | | | | | | 1 | | 1 | | | | | S |
| SD-89-344 | 60 | 10 | | 15 | 15 | 1(r) | | | | | | | | | 1 | | | | | | | S |
| SD-89-347 | 35 | 3 | | 10 | 25 | 15(r) | | | 5 | | | | | | 1 | | 1 | | 5 | | | S |
| SD-89-348 | 35 | 1 | | 15 | 40 | 5(r) | 5 | | | | | | | | 2 | | | | | | | A |
| SD-89-349 | 10 | | | 25 | 15 | | | 25 | 15 | | | | | | 2 | | | | | | | A-S |
| SD-89-350 | 55 | 1 | | 30 | 10 | | 1 | | | | | | | | | | | | | | | A |
| SD-89-351 | 80 | 1 | | 10 | 8 | <1(r) | | | | | | | | | 1 | | | | | | | A |
| SD-89-352 | 30 | | | 25 | 35 | 2(r) | 5 | | | | 2 | | | | 1 | | | | | | | A |
| SD-89-353 | 25 | 1 | | 25 | 30 | 1(r) | 3 | 10 | | | 2 | | | | 3 | | | | | | | A |
| SD-89-354 | 15 | | | 15 | 30 | 15(r) | | | | | 20 | | | | 5 | | | | | | | A |
| SD-89-356 | 55 | 2 | 1 | 15 | 20(r) | | | | 10 | | | | | | 1 | | | | | | | S |
| SD-89-357 | 45 | 5 | | 25 | 10 | 10(r) | | | 5 | | | | | | | | | | | | | S |
| SD-89-361 | 45 | | | 20 | 20 | 1(r) | | 3 | 10 | | 1 | | | | 1 | | | | | | | A-S |
| SD-89-362 | 20 | | | 30 | 10 | | | 30 | 10 | | | | | | 1 | | | | | | | A-S |
| SD-89-364 | 25 | | | 15 | 10 | | 5 | 40 | 5 | | | | | | 1 | | | | | | | A-S |
| SD-89-366 | 35 | | | 25 | 20 | | | 15 | 1 | | 2 | | | | 1 | | | | | | | A-S |
| SD-89-367 | 40 | | | 25 | 15 | | | 20 | 1 | | | | | | 1 | | | | | | | A-S |
| SD-89-369 | 30 | | | 30 | 15 | 5(r) | | 20 | 1 | | | | | | 1 | | | | | | | A-S |
| SD-89-370 | 30 | | | 30 | 20 | | | 15 | 3 | | | | | | 1 | | | | | | | A-S |
| SD-89-371 | 20 | | | 35 | 10 | | | 30 | 5 | | | | | | 1 | | | | | | | A-S |
| SD-89-373 | 60 | | | 10 | 15 | | | | | 10 | | | | | 1 | 1 | | | | | | S |
| SD-89-374 | 25 | | | 30 | 35 | | | 10 | | | | | | | | | <1 | | | | | A |
| SD-89-375 | 50 | | | 25 | 15 | | 5 | | 5 | | | | | | | | | | | | | S |
| SD-89-377 | 40 | | | 35 | 20 | | | | | | | | | | 1 | | | | | | | A |
| SD-89-379 | 15 | | | 20 | 10 | 5(r) | | | 50 | | | | | | 2 | | | | | | | A |

Petrographic Sample Descriptions

211

| Sample # | Mineralogy | | | | | | | | | | | | | | Accessory Phases | | | | | | | Zone | |
|-----------|------------|---|---|----|----|-------|---|----|---|-------|----|----|----|----|------------------|----|---|---|----|---|---|------|---|
| | Q | P | K | B | M | Ch | G | A | S | Cd | St | Px | Cc | Cz | Op | Ap | Z | H | Ti | T | E | | |
| SD-89-382 | 25 | | | 30 | 30 | 10(r) | 1 | | | | | | | | 2 | | | 1 | | | | | A |
| SD-89-386 | 10 | 5 | | | | 15 | | | | | | 65 | | | 5 | | | | | | | | A |
| SD-89-387 | 55 | | | 15 | 15 | 10(r) | 3 | | | | | | | | 2 | | | | | | | | A |
| SD-89-388 | 10 | | | 15 | 50 | 10(r) | | | | 5 | | | | | 10 | | | | | | | | A |
| SD-89-392 | 25 | | | 15 | 30 | 15(r) | | | | 10(p) | | | | | 3 | | | | | | | | A |
| SD-89-393 | 65 | 5 | | 20 | 10 | | | | | | | | | | 1 | | | | | | | | A |
| SD-89-394 | 25 | | | 35 | 25 | 2(r) | | 10 | | | | | | | 1 | | | | | | | | A |
| SD-89-395 | 35 | | | 30 | 25 | 5(r) | | 2 | | | | | | | 1 | | | | | | | | A |
| SD-89-396 | 35 | | | 30 | 30 | | | 3 | | | | | | | 1 | | | | | | | | A |
| SD-89-397 | 55 | | | 20 | 15 | 2(r) | 5 | | | | | | | | 3 | | | | | 2 | | | A |

Abbreviations Used:

| | | | |
|-----------------|------------------------|------------------------|-------------------|
| Q - quartz | P - plagioclase | K - potassium feldspar | B - biotite |
| M - muscovite | Ch - chlorite | G - garnet | A - andalusite |
| S - sillimanite | Cd - cordierite | St - staurolite | Px - pyroxene |
| Cc - carbonate | Cz - clinozoisite | Op - opaque | Ap - apatite |
| Z - zircon | H - hematite | Ti - titanite | T - tourmaline |
| E - epidote | (r) - retrograde phase | (rt) - relict phase | (p) - pseudomorph |

Zone Abbreviations:

C - chlorite-muscovite zone
 B - biotite-muscovite-chlorite zone
 A-B - andalusite-biotite-muscovite isograd
 A - andalusite-biotite-muscovite zone
 A-S - sillimanite-biotite-muscovite isograd
 S - sillimanite-biotite-muscovite zone
 ZM - zone of partial melting
 G - granite

APPENDIX B:
Microprobe Data

APPENDIX B1:
Garnet Microprobe Analyses

Garnet

| | SD-89-329-4 | | | | | | SD-89-329-2 | | | |
|--------------------------------|-------------|--------|--------|--------|--------|-------|-------------|-------|--------|--------|
| | (core) | (rim) | (mid) | (mid) | (rim) | (mid) | (mid) | (mid) | (core) | (mid) |
| SiO ₂ | 36.68 | 36.75 | 36.86 | 36.73 | 36.56 | 36.74 | 36.70 | 36.86 | 36.66 | 36.66 |
| TiO ₂ | 0.00 | 0.03 | 0.01 | 0.00 | 0.00 | 0.00 | 0.00 | 0.00 | 0.00 | 0.01 |
| Al ₂ O ₃ | 20.75 | 20.95 | 20.59 | 20.66 | 20.96 | 20.28 | 20.77 | 20.72 | 20.52 | 21.06 |
| Cr ₂ O ₃ | 0.04 | 0.03 | 0.07 | 0.04 | 0.05 | 0.06 | 0.05 | 0.00 | 0.07 | 0.00 |
| FeO | 30.74 | 29.84 | 30.41 | 30.79 | 29.74 | 29.66 | 30.43 | 29.62 | 30.50 | 30.00 |
| MnO | 9.11 | 9.72 | 9.42 | 9.22 | 10.27 | 9.66 | 9.93 | 9.83 | 9.85 | 9.48 |
| MgO | 2.13 | 2.00 | 2.17 | 2.21 | 1.88 | 1.94 | 1.88 | 2.06 | 1.96 | 2.08 |
| CaO | 0.82 | 0.79 | 0.80 | 0.77 | 0.84 | 0.75 | 0.70 | 0.73 | 0.74 | 0.65 |
| Na ₂ O | 0.02 | 0.04 | 0.00 | 0.03 | 0.03 | 0.00 | 0.01 | 0.02 | 0.01 | 0.04 |
| K ₂ O | 0.00 | 0.02 | 0.02 | 0.01 | 0.00 | 0.01 | 0.01 | 0.00 | 0.02 | 0.02 |
| Total | 100.29 | 100.15 | 100.34 | 100.46 | 100.33 | 99.10 | 100.49 | 99.84 | 100.33 | 100.00 |

number of cations on the basis of 12 oxygens

| | | | | | | | | | | |
|-------------|-------|-------|-------|-------|-------|-------|-------|-------|-------|-------|
| Si | 2.98 | 2.99 | 2.99 | 2.98 | 2.97 | 3.02 | 2.98 | 3.00 | 2.99 | 2.98 |
| Ti | 0.00 | 0.00 | 0.00 | 0.00 | 0.00 | 0.00 | 0.00 | 0.00 | 0.00 | 0.00 |
| Al | 1.99 | 2.01 | 1.97 | 1.98 | 2.01 | 1.96 | 1.99 | 1.99 | 1.97 | 2.02 |
| Cr | 0.00 | 0.00 | 0.00 | 0.00 | 0.00 | 0.00 | 0.00 | 0.00 | 0.00 | 0.00 |
| Fe | 2.09 | 2.03 | 2.07 | 2.09 | 2.02 | 2.04 | 2.07 | 2.02 | 2.08 | 2.04 |
| Mn | 0.63 | 0.67 | 0.65 | 0.63 | 0.71 | 0.67 | 0.68 | 0.68 | 0.68 | 0.65 |
| Mg | 0.26 | 0.24 | 0.26 | 0.27 | 0.23 | 0.24 | 0.23 | 0.25 | 0.24 | 0.25 |
| Ca | 0.07 | 0.07 | 0.07 | 0.07 | 0.07 | 0.07 | 0.06 | 0.06 | 0.06 | 0.06 |
| Na | 0.00 | 0.01 | 0.00 | 0.00 | 0.00 | 0.00 | 0.00 | 0.00 | 0.00 | 0.01 |
| K | 0.00 | 0.00 | 0.00 | 0.00 | 0.00 | 0.00 | 0.00 | 0.00 | 0.00 | 0.00 |
| Total | 8.02 | 8.01 | 8.02 | 8.03 | 8.02 | 8.00 | 8.02 | 8.00 | 8.03 | 8.01 |
| Fe/FMCM* | 68.60 | 67.42 | 67.81 | 68.34 | 66.73 | 67.62 | 68.02 | 67.04 | 67.90 | 67.96 |
| Mg/FMCM* | 8.47 | 8.05 | 8.62 | 8.74 | 7.52 | 7.88 | 7.49 | 8.31 | 7.78 | 8.40 |
| Ca/FMCM* | 2.34 | 2.29 | 2.29 | 2.19 | 2.41 | 2.19 | 2.00 | 2.12 | 2.11 | 1.89 |
| Mn/FMCM* | 20.59 | 22.24 | 21.28 | 20.73 | 23.34 | 22.31 | 22.48 | 22.53 | 22.21 | 21.75 |
| Si+Al | 4.97 | 4.99 | 4.97 | 4.96 | 4.98 | 4.98 | 4.97 | 4.99 | 4.96 | 5.00 |
| Fe+Mg+Ca+Mn | 3.05 | 3.01 | 3.05 | 3.06 | 3.03 | 3.01 | 3.04 | 3.01 | 3.06 | 3.00 |
| Fe/(Fe+Mg) | 0.89 | 0.89 | 0.89 | 0.89 | 0.90 | 0.90 | 0.90 | 0.89 | 0.90 | 0.89 |
| A | 29.75 | 30.59 | 29.68 | 29.51 | 30.87 | 30.12 | 30.20 | 30.49 | 29.78 | 30.51 |
| F | 0.89 | 0.89 | 0.89 | 0.89 | 0.90 | 0.90 | 0.90 | 0.89 | 0.90 | 0.89 |
| M | 0.11 | 0.11 | 0.11 | 0.11 | 0.10 | 0.10 | 0.10 | 0.11 | 0.10 | 0.11 |
| Fe+Mg+Mn | 2.98 | 2.94 | 2.98 | 2.99 | 2.96 | 2.95 | 2.98 | 2.95 | 3.00 | 2.95 |
| Fe/Fe+Mg+Mn | 70.24 | 69.00 | 69.40 | 69.87 | 68.38 | 69.14 | 69.42 | 68.49 | 69.37 | 69.27 |
| Mn/Fe+Mg+Mn | 21.08 | 22.76 | 21.77 | 21.19 | 23.92 | 22.81 | 22.94 | 23.02 | 22.69 | 22.17 |
| Mg/Fe+Mg+Mn | 8.67 | 8.24 | 8.83 | 8.94 | 7.70 | 8.06 | 7.64 | 8.49 | 7.94 | 8.56 |

*FMCM=Fe+Mg+Ca+Mn

Garnet

| | SD-89-329-2 | | | | SD-89-300-1 | | | |
|--------------------------------|-------------|--------|--------|-------|-------------|--------|-------|-------|
| | (mid) | (mid) | (rim) | (rim) | (mid) | (core) | (mid) | (rim) |
| SiO ₂ | 36.73 | 36.75 | 36.76 | 36.66 | 36.59 | 36.36 | 36.70 | 36.57 |
| TiO ₂ | 0.00 | 0.00 | 0.01 | 0.02 | 0.07 | 0.08 | 0.08 | 0.11 |
| Al ₂ O ₃ | 20.89 | 21.16 | 21.07 | 21.02 | 20.63 | 20.57 | 20.76 | 20.56 |
| Cr ₂ O ₃ | 0.05 | 0.01 | 0.02 | 0.06 | 0.03 | 0.03 | 0.09 | 0.05 |
| FeO | 29.99 | 29.68 | 29.49 | 29.33 | 28.92 | 28.80 | 28.91 | 29.35 |
| MnO | 9.93 | 9.93 | 10.67 | 8.78 | 8.91 | 9.39 | 9.13 | 8.77 |
| MgO | 2.09 | 2.09 | 1.81 | 2.42 | 2.43 | 2.33 | 2.34 | 2.46 |
| CaO | 0.75 | 0.62 | 0.33 | 1.48 | 1.45 | 1.52 | 1.67 | 1.58 |
| Na ₂ O | 0.00 | 0.01 | 0.01 | 0.15 | 0.06 | 0.05 | 0.01 | 0.04 |
| K ₂ O | 0.01 | 0.02 | 0.00 | 0.06 | 0.03 | 0.02 | 0.01 | 0.02 |
| Total | 100.45 | 100.28 | 100.15 | 99.98 | 99.13 | 99.15 | 99.70 | 99.48 |

number of cations on the basis of 12 oxygens

| | | | | | | | | |
|-------------|-------|-------|-------|-------|-------|-------|-------|-------|
| Si | 2.98 | 2.98 | 2.99 | 2.97 | 2.99 | 2.98 | 2.98 | 2.98 |
| Ti | 0.00 | 0.00 | 0.00 | 0.00 | 0.00 | 0.00 | 0.00 | 0.01 |
| Al | 2.00 | 2.02 | 2.02 | 2.01 | 1.99 | 1.99 | 1.99 | 1.98 |
| Cr | 0.00 | 0.00 | 0.00 | 0.00 | 0.00 | 0.00 | 0.01 | 0.00 |
| Fe | 2.04 | 2.01 | 2.01 | 1.99 | 1.98 | 1.97 | 1.97 | 2.00 |
| Mn | 0.68 | 0.68 | 0.73 | 0.60 | 0.62 | 0.65 | 0.63 | 0.61 |
| Mg | 0.25 | 0.25 | 0.22 | 0.29 | 0.30 | 0.28 | 0.28 | 0.30 |
| Ca | 0.07 | 0.05 | 0.03 | 0.13 | 0.13 | 0.13 | 0.15 | 0.14 |
| Na | 0.00 | 0.00 | 0.00 | 0.02 | 0.01 | 0.01 | 0.00 | 0.01 |
| K | 0.00 | 0.00 | 0.00 | 0.01 | 0.00 | 0.00 | 0.00 | 0.00 |
| Total | 8.02 | 8.01 | 8.00 | 8.03 | 8.02 | 8.03 | 8.01 | 8.02 |
| Fe/FMCM* | 67.04 | 67.06 | 67.11 | 66.01 | 65.53 | 64.85 | 65.02 | 65.73 |
| Mg/FMCM* | 8.33 | 8.42 | 7.34 | 9.71 | 9.81 | 9.35 | 9.38 | 9.82 |
| Ca/FMCM* | 2.15 | 1.79 | 0.96 | 4.27 | 4.21 | 4.39 | 4.81 | 4.54 |
| Mn/FMCM* | 22.48 | 22.73 | 24.59 | 20.01 | 20.45 | 21.42 | 20.80 | 19.91 |
| Si+Al | 4.98 | 5.00 | 5.01 | 4.98 | 4.98 | 4.97 | 4.98 | 4.96 |
| Fe+Mg+Ca+Mn | 3.04 | 3.00 | 2.99 | 3.01 | 3.02 | 3.04 | 3.02 | 3.04 |
| Fe/(Fe+Mg) | 0.89 | 0.89 | 0.90 | 0.87 | 0.87 | 0.87 | 0.87 | 0.87 |
| A | 30.36 | 30.80 | 31.22 | 30.38 | 30.33 | 30.49 | 30.63 | 30.00 |
| F | 0.89 | 0.89 | 0.90 | 0.87 | 0.87 | 0.87 | 0.87 | 0.87 |
| M | 0.11 | 0.11 | 0.10 | 0.13 | 0.13 | 0.13 | 0.13 | 0.13 |
| Fe+Mg+Mn | 2.97 | 2.95 | 2.96 | 2.89 | 2.89 | 2.91 | 2.88 | 2.91 |
| Fe/Fe+Mg+Mn | 68.51 | 68.29 | 67.76 | 68.95 | 68.41 | 67.82 | 68.50 | 68.86 |
| Mn/Fe+Mg+Mn | 22.98 | 23.14 | 24.83 | 20.91 | 21.35 | 22.40 | 21.85 | 20.85 |
| Mg/Fe+Mg+Mn | 8.51 | 8.57 | 7.41 | 10.14 | 10.24 | 9.78 | 9.65 | 10.29 |

*FMCM=Fe+Mg+Ca+Mn

Garnet

SD-89-127-3

| | (rim) | (mid) | (mid) | (core) | (mid) | (mid) | (rim) | (rim) | (mid) | (mid) |
|--------------------------------|-------|-------|--------|--------|--------|--------|-------|-------|--------|--------|
| SiO ₂ | 36.55 | 36.79 | 36.77 | 36.86 | 36.70 | 36.78 | 36.25 | 36.39 | 36.96 | 36.82 |
| TiO ₂ | 0.04 | 0.00 | 0.01 | 0.00 | 0.01 | 0.01 | 0.06 | 0.05 | 0.01 | 0.00 |
| Al ₂ O ₃ | 20.87 | 20.94 | 20.93 | 21.14 | 21.16 | 21.26 | 20.65 | 20.90 | 20.96 | 20.87 |
| Cr ₂ O ₃ | 0.04 | 0.05 | 0.06 | 0.02 | 0.06 | 0.04 | 0.00 | 0.03 | 0.02 | 0.04 |
| FeO | 25.90 | 26.54 | 27.62 | 28.08 | 27.94 | 27.47 | 25.42 | 25.62 | 26.59 | 27.40 |
| MnO | 14.23 | 12.47 | 12.02 | 11.43 | 11.07 | 11.73 | 15.01 | 14.60 | 12.83 | 11.98 |
| MgO | 1.12 | 1.87 | 2.22 | 2.32 | 2.31 | 2.29 | 1.12 | 1.34 | 1.94 | 2.16 |
| CaO | 0.93 | 0.79 | 0.80 | 0.80 | 0.76 | 0.80 | 1.00 | 0.39 | 0.83 | 0.76 |
| Na ₂ O | 0.01 | 0.00 | 0.04 | 0.03 | 0.04 | 0.05 | 0.03 | 0.02 | 0.01 | 0.00 |
| K ₂ O | 0.02 | 0.01 | 0.02 | 0.01 | 0.02 | 0.00 | 0.03 | 0.02 | 0.03 | 0.02 |
| Total | 99.77 | 99.46 | 100.49 | 100.69 | 100.05 | 100.43 | 99.56 | 99.37 | 100.20 | 100.04 |

number of cations on the basis of 12 oxygens

| | | | | | | | | | | |
|-------------|-------|-------|-------|-------|-------|-------|-------|-------|-------|-------|
| Si | 2.99 | 3.00 | 2.98 | 2.98 | 2.98 | 2.97 | 2.98 | 2.99 | 3.00 | 2.99 |
| Ti | 0.00 | 0.00 | 0.00 | 0.00 | 0.00 | 0.00 | 0.00 | 0.00 | 0.00 | 0.00 |
| Al | 2.02 | 2.01 | 2.00 | 2.01 | 2.02 | 2.03 | 2.00 | 2.02 | 2.00 | 2.00 |
| Cr | 0.00 | 0.00 | 0.00 | 0.00 | 0.00 | 0.00 | 0.00 | 0.00 | 0.00 | 0.00 |
| Fe | 1.77 | 1.81 | 1.87 | 1.90 | 1.90 | 1.86 | 1.75 | 1.76 | 1.80 | 1.86 |
| Mn | 0.99 | 0.86 | 0.82 | 0.78 | 0.76 | 0.80 | 1.05 | 1.02 | 0.88 | 0.82 |
| Mg | 0.14 | 0.23 | 0.27 | 0.28 | 0.28 | 0.28 | 0.14 | 0.16 | 0.23 | 0.26 |
| Ca | 0.08 | 0.07 | 0.07 | 0.07 | 0.07 | 0.07 | 0.09 | 0.03 | 0.07 | 0.07 |
| Na | 0.00 | 0.00 | 0.01 | 0.00 | 0.01 | 0.01 | 0.00 | 0.00 | 0.00 | 0.00 |
| K | 0.00 | 0.00 | 0.00 | 0.00 | 0.00 | 0.00 | 0.00 | 0.00 | 0.00 | 0.00 |
| Total | 8.00 | 7.99 | 8.02 | 8.02 | 8.01 | 8.02 | 8.02 | 8.00 | 8.00 | 8.01 |
| Fe/FMCM* | 59.54 | 60.99 | 61.69 | 62.66 | 63.15 | 61.79 | 57.90 | 59.18 | 60.29 | 61.77 |
| Mg/FMCM* | 4.59 | 7.66 | 8.84 | 9.22 | 9.30 | 9.18 | 4.55 | 5.52 | 7.84 | 8.68 |
| Ca/FMCM* | 2.74 | 2.33 | 2.29 | 2.29 | 2.20 | 2.31 | 2.92 | 1.15 | 2.41 | 2.20 |
| Mn/FMCM* | 33.13 | 29.02 | 27.19 | 25.83 | 25.34 | 26.72 | 34.63 | 34.15 | 29.46 | 27.35 |
| Si+Al | 5.01 | 5.02 | 4.98 | 4.99 | 5.00 | 5.00 | 4.98 | 5.01 | 5.00 | 4.99 |
| Fe+Mg+Ca+Mn | 2.98 | 2.97 | 3.03 | 3.03 | 3.00 | 3.01 | 3.02 | 2.97 | 2.99 | 3.01 |
| Fe/(Fe+Mg) | 0.93 | 0.89 | 0.87 | 0.87 | 0.87 | 0.87 | 0.93 | 0.91 | 0.88 | 0.88 |
| A | 34.45 | 33.03 | 31.78 | 31.59 | 31.69 | 32.20 | 34.57 | 34.40 | 32.86 | 31.94 |
| F | 0.93 | 0.89 | 0.87 | 0.87 | 0.87 | 0.87 | 0.93 | 0.91 | 0.88 | 0.88 |
| H | 0.07 | 0.11 | 0.13 | 0.13 | 0.13 | 0.13 | 0.07 | 0.09 | 0.12 | 0.12 |
| Fe+Mg+Mn | 2.90 | 2.90 | 2.96 | 2.96 | 2.93 | 2.94 | 2.93 | 2.94 | 2.92 | 2.95 |
| Fe/Fe+Mg+Mn | 61.22 | 62.44 | 63.13 | 64.12 | 64.57 | 63.25 | 59.65 | 59.87 | 61.78 | 63.16 |
| Mn/Fe+Mg+Mn | 34.07 | 29.72 | 27.83 | 26.44 | 25.91 | 27.35 | 35.67 | 34.55 | 30.19 | 27.97 |
| Mg/Fe+Mg+Mn | 4.72 | 7.84 | 9.04 | 9.44 | 9.51 | 9.40 | 4.68 | 5.58 | 8.03 | 8.87 |

*FMCM=Fe+Mg+Ca+Mn

Garnet

| | SD-89-127-3 | | | | | SD-89-502-2 | | | | |
|--|-------------|--------|--------|-------|--------|-------------|-------|-------|--------|--|
| | (core) | (mid) | (mid) | (rim) | (rim) | (mid) | (mid) | (mid) | (core) | |
| SiO ₂ | 36.27 | 36.95 | 36.97 | 36.45 | 36.95 | 36.70 | 36.62 | 36.62 | 36.73 | |
| TiO ₂ | 0.00 | 0.00 | 0.00 | 0.02 | 0.02 | 0.05 | 0.05 | 0.04 | 0.00 | |
| Al ₂ O ₃ | 20.85 | 20.95 | 21.04 | 20.80 | 20.88 | 20.81 | 20.73 | 20.86 | 20.90 | |
| Cr ₂ O ₃ | 0.06 | 0.07 | 0.06 | 0.03 | 0.07 | 0.05 | 0.07 | 0.00 | 0.06 | |
| FeO | 27.42 | 27.12 | 26.90 | 25.29 | 29.44 | 28.66 | 28.63 | 28.66 | 28.43 | |
| MnO | 11.69 | 12.35 | 12.70 | 14.58 | 9.26 | 9.46 | 9.29 | 9.03 | 9.61 | |
| MgO | 2.20 | 2.17 | 1.99 | 0.99 | 2.29 | 2.25 | 2.17 | 2.30 | 2.17 | |
| CaO | 0.76 | 0.82 | 0.80 | 1.04 | 1.63 | 1.76 | 1.75 | 1.78 | 1.69 | |
| Na ₂ O | 0.01 | 0.01 | 0.00 | 0.03 | 0.04 | 0.04 | 0.00 | 0.05 | 0.05 | |
| K ₂ O | 0.01 | 0.00 | 0.00 | 0.03 | 0.02 | 0.00 | 0.03 | 0.01 | 0.00 | |
| Total | 99.27 | 100.44 | 100.46 | 99.26 | 100.62 | 99.77 | 99.32 | 99.34 | 99.66 | |
| number of cations on the basis of 12 oxygens | | | | | | | | | | |
| Si | 2.97 | 2.99 | 2.99 | 3.00 | 2.98 | 2.98 | 2.99 | 2.99 | 2.99 | |
| Ti | 0.00 | 0.00 | 0.00 | 0.00 | 0.00 | 0.00 | 0.00 | 0.00 | 0.00 | |
| Al | 2.01 | 2.00 | 2.01 | 2.02 | 1.99 | 1.99 | 2.00 | 2.00 | 2.00 | |
| Cr | 0.00 | 0.00 | 0.00 | 0.00 | 0.00 | 0.00 | 0.00 | 0.00 | 0.00 | |
| Fe | 1.88 | 1.84 | 1.82 | 1.74 | 1.99 | 1.95 | 1.95 | 1.95 | 1.93 | |
| Mn | 0.81 | 0.85 | 0.87 | 1.02 | 0.63 | 0.65 | 0.64 | 0.62 | 0.66 | |
| Mg | 0.27 | 0.26 | 0.24 | 0.12 | 0.28 | 0.27 | 0.26 | 0.28 | 0.26 | |
| Ca | 0.07 | 0.07 | 0.07 | 0.09 | 0.14 | 0.15 | 0.15 | 0.16 | 0.15 | |
| Na | 0.00 | 0.00 | 0.00 | 0.00 | 0.01 | 0.01 | 0.00 | 0.01 | 0.01 | |
| K | 0.00 | 0.00 | 0.00 | 0.00 | 0.00 | 0.00 | 0.00 | 0.00 | 0.00 | |
| Total | 8.02 | 8.01 | 8.00 | 8.00 | 8.02 | 8.02 | 8.01 | 8.01 | 8.01 | |
| Fe/FMCM* | 62.10 | 60.88 | 60.68 | 58.60 | 65.40 | 64.40 | 64.85 | 64.86 | 64.31 | |
| Mg/FMCM* | 8.88 | 8.68 | 8.00 | 4.09 | 9.07 | 9.01 | 8.76 | 9.28 | 8.75 | |
| Ca/FMCM* | 2.21 | 2.36 | 2.31 | 3.09 | 4.70 | 5.07 | 5.08 | 5.16 | 4.90 | |
| Mn/FMCM* | 26.82 | 28.08 | 29.01 | 34.22 | 20.84 | 21.53 | 21.31 | 20.70 | 22.04 | |
| Si+Al | 4.99 | 4.99 | 5.00 | 5.02 | 4.97 | 4.98 | 4.98 | 4.99 | 4.99 | |
| Fe+Mg+Ca+Mn | 3.03 | 3.01 | 3.00 | 2.97 | 3.04 | 3.03 | 3.01 | 3.01 | 3.01 | |
| Fe/(Fe+Mg) | 0.87 | 0.88 | 0.88 | 0.93 | 0.88 | 0.88 | 0.88 | 0.87 | 0.88 | |
| A | 31.89 | 32.27 | 32.75 | 35.04 | 30.44 | 30.99 | 30.92 | 30.94 | 31.32 | |
| F | 0.87 | 0.88 | 0.88 | 0.93 | 0.88 | 0.88 | 0.88 | 0.87 | 0.88 | |
| M | 0.13 | 0.12 | 0.12 | 0.07 | 0.12 | 0.12 | 0.12 | 0.13 | 0.12 | |
| Fe+Mg+Mn | 2.96 | 2.94 | 2.93 | 2.88 | 2.90 | 2.87 | 2.86 | 2.86 | 2.86 | |
| Fe/Fe+Mg+Mn | 63.50 | 62.35 | 62.11 | 60.47 | 68.63 | 67.83 | 68.32 | 68.59 | 67.63 | |
| Mn/Fe+Mg+Mn | 27.42 | 28.76 | 29.70 | 35.31 | 21.86 | 22.68 | 22.45 | 21.83 | 23.18 | |
| Mg/Fe+Mg+Mn | 9.08 | 8.89 | 8.19 | 4.22 | 9.51 | 9.49 | 9.23 | 9.78 | 9.20 | |

*FMCM=Fe+Mg+Ca+Mn

Garnet

| | SD-89-312-2 | | | SD-89-312-3 | | | SD-89-312-5 | | |
|--|-------------|--------|-------|-------------|--------|--------|-------------|--------|-------|
| | (rim) | (core) | (rim) | (rim) | (core) | (rim) | (rim) | (core) | (rim) |
| SiO ₂ | 36.92 | 36.61 | 36.50 | 36.58 | 36.74 | 36.76 | 36.34 | 36.35 | 36.47 |
| TiO ₂ | 0.01 | 0.02 | 0.02 | 0.00 | 0.00 | 0.02 | 0.00 | 0.00 | 0.02 |
| Al ₂ O ₃ | 20.62 | 20.38 | 20.32 | 20.87 | 20.58 | 20.69 | 20.62 | 20.69 | 20.69 |
| Cr ₂ O ₃ | 0.07 | 0.02 | 0.00 | 0.07 | 0.04 | 0.07 | 0.04 | 0.07 | 0.07 |
| FeO | 26.68 | 26.51 | 27.02 | 26.93 | 27.27 | 27.38 | 26.39 | 26.95 | 26.15 |
| MnO | 13.08 | 12.72 | 12.85 | 12.81 | 12.79 | 13.05 | 13.31 | 13.09 | 13.34 |
| MgO | 1.68 | 1.85 | 1.63 | 1.64 | 1.81 | 1.62 | 1.57 | 1.75 | 1.56 |
| CaO | 0.79 | 0.90 | 0.77 | 0.68 | 0.76 | 0.71 | 0.90 | 0.74 | 0.62 |
| Na ₂ O | 0.00 | 0.04 | 0.02 | 0.00 | 0.00 | 0.00 | 0.01 | 0.03 | 0.00 |
| K ₂ O | 0.00 | 0.03 | 0.02 | 0.04 | 0.01 | 0.03 | 0.00 | 0.03 | 0.00 |
| Total | 99.85 | 99.07 | 99.15 | 99.62 | 100.00 | 100.33 | 99.18 | 99.70 | 98.90 |
| number of cations on the basis of 12 oxygens | | | | | | | | | |
| Si | 3.01 | 3.01 | 3.01 | 2.99 | 3.00 | 2.99 | 2.99 | 2.98 | 3.00 |
| Ti | 0.00 | 0.00 | 0.00 | 0.00 | 0.00 | 0.00 | 0.00 | 0.00 | 0.00 |
| Al | 1.98 | 1.97 | 1.97 | 2.01 | 1.98 | 1.99 | 2.00 | 2.00 | 2.01 |
| Cr | 0.00 | 0.00 | 0.00 | 0.00 | 0.00 | 0.00 | 0.00 | 0.00 | 0.00 |
| Fe | 1.82 | 1.82 | 1.86 | 1.84 | 1.86 | 1.86 | 1.82 | 1.85 | 1.80 |
| Mn | 0.90 | 0.89 | 0.90 | 0.89 | 0.88 | 0.90 | 0.93 | 0.91 | 0.93 |
| Mg | 0.20 | 0.23 | 0.20 | 0.20 | 0.22 | 0.20 | 0.19 | 0.21 | 0.19 |
| Ca | 0.07 | 0.08 | 0.07 | 0.06 | 0.07 | 0.06 | 0.08 | 0.06 | 0.05 |
| Na | 0.00 | 0.01 | 0.00 | 0.00 | 0.00 | 0.00 | 0.00 | 0.00 | 0.00 |
| K | 0.00 | 0.00 | 0.00 | 0.00 | 0.00 | 0.00 | 0.00 | 0.00 | 0.00 |
| Total | 7.99 | 8.01 | 8.01 | 8.00 | 8.01 | 8.01 | 8.01 | 8.02 | 7.99 |
| Fe/FMCM* | 60.73 | 60.47 | 61.51 | 61.63 | 61.39 | 61.68 | 60.22 | 60.87 | 60.48 |
| Mg/FMCM* | 6.81 | 7.52 | 6.61 | 6.69 | 7.26 | 6.50 | 6.38 | 7.04 | 6.43 |
| Ca/FMCM* | 2.30 | 2.63 | 2.25 | 1.99 | 2.19 | 2.05 | 2.63 | 2.14 | 1.84 |
| Mn/FMCM* | 30.15 | 29.38 | 29.63 | 29.69 | 29.16 | 29.77 | 30.76 | 29.94 | 31.25 |
| Si+Al | 4.99 | 4.98 | 4.98 | 5.00 | 4.98 | 4.98 | 4.99 | 4.98 | 5.01 |
| Fe+Mg+Ca+Mn | 3.00 | 3.01 | 3.02 | 2.99 | 3.03 | 3.02 | 3.02 | 3.03 | 2.98 |
| Fe/(Fe+Mg) | 0.90 | 0.89 | 0.90 | 0.90 | 0.89 | 0.90 | 0.90 | 0.90 | 0.90 |
| A | 32.88 | 32.41 | 32.30 | 32.87 | 32.20 | 32.41 | 33.24 | 32.56 | 33.51 |
| F | 0.90 | 0.89 | 0.90 | 0.90 | 0.89 | 0.90 | 0.90 | 0.90 | 0.90 |
| M | 0.10 | 0.11 | 0.10 | 0.10 | 0.11 | 0.10 | 0.10 | 0.10 | 0.10 |
| Fe+Mg+Mn | 2.93 | 2.93 | 2.96 | 2.93 | 2.96 | 2.96 | 2.94 | 2.97 | 2.92 |
| Fe/Fe+Mg+Mn | 62.16 | 62.10 | 62.93 | 62.88 | 62.76 | 62.97 | 61.85 | 62.20 | 61.61 |
| Mn/Fe+Mg+Mn | 30.87 | 30.18 | 30.31 | 30.29 | 29.81 | 30.40 | 31.59 | 30.60 | 31.84 |
| Mg/Fe+Mg+Mn | 6.97 | 7.72 | 6.76 | 6.82 | 7.42 | 6.64 | 6.56 | 7.20 | 6.55 |

*FMCM=Fe+Mg+Ca+Mn

Garnet

| | SD-89-046a-1 | | | | | | SD-89-046a-1 | | |
|--------------------------------|--------------|-------|-------|-------|--------|-------|--------------|--------|-------|
| | (rim) | (mid) | (mid) | (mid) | (core) | (mid) | (mid) | (mid) | (rim) |
| SiO ₂ | 36.53 | 36.69 | 36.64 | 36.51 | 36.43 | 36.76 | 36.55 | 36.56 | 36.40 |
| TiO ₂ | 0.00 | 0.05 | 0.04 | 0.03 | 0.04 | 0.05 | 0.05 | 0.03 | 0.00 |
| Al ₂ O ₃ | 21.00 | 21.04 | 21.00 | 20.77 | 20.85 | 20.87 | 20.95 | 20.86 | 20.88 |
| Cr ₂ O ₃ | 0.03 | 0.03 | 0.00 | 0.02 | 0.01 | 0.05 | 0.04 | 0.06 | 0.06 |
| FeO | 34.84 | 33.84 | 33.51 | 33.11 | 33.73 | 33.43 | 33.85 | 34.31 | 35.34 |
| MnO | 4.48 | 4.61 | 5.18 | 5.15 | 5.16 | 4.98 | 4.87 | 4.72 | 4.28 |
| MgO | 2.11 | 2.03 | 1.85 | 1.87 | 1.86 | 1.92 | 1.98 | 2.00 | 2.07 |
| CaO | 0.83 | 1.56 | 1.71 | 1.61 | 1.63 | 1.62 | 1.53 | 1.51 | 0.69 |
| Na ₂ O | 0.05 | 0.05 | 0.04 | 0.04 | 0.05 | 0.04 | 0.05 | 0.04 | 0.04 |
| K ₂ O | 0.00 | 0.00 | 0.01 | 0.02 | 0.00 | 0.00 | 0.03 | 0.02 | 0.03 |
| Total | 99.86 | 99.90 | 99.97 | 99.14 | 99.78 | 99.70 | 99.89 | 100.11 | 99.79 |

number of cations on the basis of 12 oxygens

| | | | | | | | | | |
|-------------|-------|-------|-------|-------|-------|-------|-------|-------|-------|
| Si | 2.98 | 2.98 | 2.98 | 2.99 | 2.97 | 2.99 | 2.98 | 2.98 | 2.97 |
| Ti | 0.00 | 0.00 | 0.00 | 0.00 | 0.00 | 0.00 | 0.00 | 0.00 | 0.00 |
| Al | 2.02 | 2.02 | 2.01 | 2.01 | 2.01 | 2.00 | 2.01 | 2.00 | 2.01 |
| Cr | 0.00 | 0.00 | 0.00 | 0.00 | 0.00 | 0.00 | 0.00 | 0.00 | 0.00 |
| Fe | 2.37 | 2.30 | 2.28 | 2.27 | 2.30 | 2.28 | 2.31 | 2.33 | 2.42 |
| Mn | 0.31 | 0.32 | 0.36 | 0.36 | 0.36 | 0.34 | 0.34 | 0.33 | 0.30 |
| Mg | 0.26 | 0.25 | 0.22 | 0.23 | 0.23 | 0.23 | 0.24 | 0.24 | 0.25 |
| Ca | 0.07 | 0.14 | 0.15 | 0.14 | 0.14 | 0.14 | 0.13 | 0.13 | 0.06 |
| Na | 0.01 | 0.01 | 0.01 | 0.01 | 0.01 | 0.01 | 0.01 | 0.01 | 0.01 |
| K | 0.00 | 0.00 | 0.00 | 0.00 | 0.00 | 0.00 | 0.00 | 0.00 | 0.00 |
| Total | 8.02 | 8.01 | 8.01 | 8.01 | 8.02 | 8.00 | 8.02 | 8.02 | 8.02 |
| Fe/FMCM* | 78.82 | 76.69 | 75.74 | 75.73 | 76.04 | 76.03 | 76.46 | 76.95 | 79.87 |
| Mg/FMCM* | 8.51 | 8.20 | 7.45 | 7.62 | 7.47 | 7.78 | 7.97 | 7.99 | 8.34 |
| Ca/FMCM* | 2.41 | 4.53 | 4.95 | 4.72 | 4.71 | 4.72 | 4.43 | 4.34 | 2.00 |
| Mn/FMCM* | 10.27 | 10.58 | 11.86 | 11.93 | 11.78 | 11.47 | 11.14 | 10.72 | 9.80 |
| Si+Al | 4.99 | 5.00 | 4.99 | 5.00 | 4.98 | 5.00 | 4.99 | 4.98 | 4.97 |
| Fe+Mg+Ca+Mn | 3.01 | 3.00 | 3.01 | 3.00 | 3.03 | 2.99 | 3.02 | 3.03 | 3.02 |
| Fe/(Fe+Mg) | 0.90 | 0.90 | 0.91 | 0.91 | 0.91 | 0.91 | 0.91 | 0.91 | 0.91 |
| A | 27.72 | 28.36 | 28.65 | 28.59 | 28.40 | 28.53 | 28.22 | 27.90 | 27.29 |
| F | 0.90 | 0.90 | 0.91 | 0.91 | 0.91 | 0.91 | 0.91 | 0.91 | 0.91 |
| M | 0.10 | 0.10 | 0.09 | 0.09 | 0.09 | 0.09 | 0.09 | 0.09 | 0.09 |
| Fe+Mg+Mn | 2.94 | 2.86 | 2.86 | 2.86 | 2.89 | 2.85 | 2.88 | 2.90 | 2.96 |
| Fe/Fe+Mg+Mn | 80.77 | 80.33 | 79.68 | 79.48 | 79.80 | 79.79 | 80.00 | 80.44 | 81.50 |
| Mn/Fe+Mg+Mn | 10.52 | 11.08 | 12.48 | 12.52 | 12.36 | 12.04 | 11.66 | 11.21 | 10.00 |
| Mg/Fe+Mg+Mn | 8.72 | 8.59 | 7.84 | 8.00 | 7.84 | 8.17 | 8.34 | 8.36 | 8.51 |

*FMCM=Fe+Mg+Ca+Mn

Garnet

| | | SD-89-034e-3 | | | | SD-89-184-2 | | | |
|--------------------------------|-------|--------------|--------|-------|-------|-------------|-------|-------|-------|
| | | (core) | (core) | | | (rim) | (mid) | (mid) | |
| SiO ₂ | 37.18 | 37.60 | 37.01 | 37.51 | 37.23 | 37.21 | 36.17 | 36.25 | 36.62 |
| TiO ₂ | 0.00 | 0.02 | 0.00 | 0.01 | 0.00 | 0.00 | 0.01 | 0.00 | 0.00 |
| Al ₂ O ₃ | 21.12 | 21.39 | 21.31 | 21.38 | 21.54 | 21.16 | 20.95 | 20.94 | 20.88 |
| Cr ₂ O ₃ | 0.05 | 0.06 | 0.03 | 0.00 | 0.00 | 0.00 | 0.03 | 0.06 | 0.00 |
| FeO | 33.90 | 34.00 | 34.07 | 33.90 | 34.30 | 33.95 | 28.58 | 30.35 | 30.48 |
| MnO | 2.91 | 1.25 | 1.18 | 1.24 | 1.28 | 1.39 | 10.94 | 8.89 | 8.65 |
| MgO | 2.60 | 4.03 | 4.32 | 3.96 | 3.95 | 3.88 | 1.75 | 2.33 | 2.39 |
| CaO | 1.37 | 1.44 | 1.30 | 1.40 | 1.49 | 1.46 | 0.85 | 0.87 | 0.87 |
| Na ₂ O | 0.02 | 0.02 | 0.02 | 0.01 | 0.00 | 0.02 | 0.01 | 0.02 | 0.00 |
| K ₂ O | 0.01 | 0.01 | 0.01 | 0.02 | 0.00 | 0.00 | 0.02 | 0.01 | 0.02 |
| Total | 99.17 | 99.81 | 99.26 | 99.42 | 99.79 | 99.07 | 99.30 | 99.72 | 99.91 |

number of cations on the basis of 12 oxygens

| | | | | | | | | | |
|-------------|-------|-------|-------|-------|-------|-------|-------|-------|-------|
| Si | 3.02 | 3.00 | 2.98 | 3.01 | 2.98 | 3.00 | 2.97 | 2.96 | 2.98 |
| Ti | 0.00 | 0.00 | 0.00 | 0.00 | 0.00 | 0.00 | 0.00 | 0.00 | 0.00 |
| Al | 2.02 | 2.01 | 2.02 | 2.02 | 2.03 | 2.01 | 2.03 | 2.02 | 2.00 |
| Cr | 0.00 | 0.00 | 0.00 | 0.00 | 0.00 | 0.00 | 0.00 | 0.00 | 0.00 |
| Fe | 2.30 | 2.27 | 2.29 | 2.27 | 2.30 | 2.29 | 1.96 | 2.07 | 2.07 |
| Mn | 0.20 | 0.08 | 0.08 | 0.08 | 0.09 | 0.09 | 0.76 | 0.61 | 0.60 |
| Mg | 0.31 | 0.48 | 0.52 | 0.47 | 0.47 | 0.47 | 0.21 | 0.28 | 0.29 |
| Ca | 0.12 | 0.12 | 0.11 | 0.12 | 0.13 | 0.13 | 0.07 | 0.08 | 0.08 |
| Na | 0.00 | 0.00 | 0.00 | 0.00 | 0.00 | 0.00 | 0.00 | 0.00 | 0.00 |
| K | 0.00 | 0.00 | 0.00 | 0.00 | 0.00 | 0.00 | 0.00 | 0.00 | 0.00 |
| Total | 7.98 | 7.99 | 8.01 | 7.98 | 8.00 | 7.99 | 8.02 | 8.03 | 8.02 |
| Fe/FMCM* | 78.41 | 76.76 | 76.34 | 77.03 | 77.00 | 76.91 | 65.15 | 68.02 | 68.32 |
| Mg/FMCM* | 10.72 | 16.21 | 17.25 | 16.04 | 15.80 | 15.66 | 7.11 | 9.31 | 9.55 |
| Ca/FMCM* | 4.06 | 4.17 | 3.73 | 4.08 | 4.29 | 4.24 | 2.48 | 2.50 | 2.50 |
| Mn/FMCM* | 6.82 | 2.86 | 2.68 | 2.85 | 2.91 | 3.19 | 25.26 | 20.18 | 19.64 |
| Si+Al | 5.04 | 5.02 | 5.00 | 5.03 | 5.02 | 5.01 | 5.00 | 4.98 | 4.98 |
| Fe+Mg+Ca+Mn | 2.93 | 2.96 | 3.00 | 2.95 | 2.98 | 2.98 | 3.01 | 3.05 | 3.04 |
| Fe/(Fe+Mg) | 0.88 | 0.83 | 0.82 | 0.83 | 0.83 | 0.83 | 0.90 | 0.88 | 0.88 |
| A | 27.84 | 26.77 | 26.42 | 26.84 | 26.86 | 26.74 | 31.71 | 29.93 | 29.69 |
| F | 0.88 | 0.83 | 0.82 | 0.83 | 0.83 | 0.83 | 0.90 | 0.88 | 0.88 |
| M | 0.12 | 0.17 | 0.18 | 0.17 | 0.17 | 0.17 | 0.10 | 0.12 | 0.12 |
| Fe+Mg+Mn | 2.81 | 2.84 | 2.89 | 2.83 | 2.86 | 2.85 | 2.94 | 2.97 | 2.90 |
| Fe/Fe+Mg+Mn | 81.73 | 80.10 | 79.30 | 80.31 | 80.45 | 80.31 | 66.81 | 69.76 | 70.07 |
| Mn/Fe+Mg+Mn | 7.11 | 2.98 | 2.78 | 2.98 | 3.04 | 3.33 | 25.90 | 20.70 | 20.14 |
| Mg/Fe+Mg+Mn | 11.17 | 16.92 | 17.92 | 16.72 | 16.51 | 16.36 | 7.29 | 9.54 | 9.79 |

*FMCM=Fe+Mg+Ca+Mn

Garnet

| | (mid) | (mid) | (mid) | (core) | SD-89-184-2 | | (mid) | (mid) | (mid) | (rim) |
|--------------------------------|--------|--------|--------|--------|-------------|-------|--------|--------|-------|-------|
| SiO ₂ | 36.78 | 36.90 | 36.82 | 36.52 | 36.92 | 36.64 | 37.10 | 37.12 | 36.67 | 36.55 |
| TiO ₂ | 0.00 | 0.00 | 0.01 | 0.00 | 0.00 | 0.00 | 0.01 | 0.01 | 0.00 | 0.00 |
| Al ₂ O ₃ | 21.02 | 21.14 | 20.97 | 21.20 | 21.12 | 20.94 | 21.18 | 21.07 | 21.01 | 20.79 |
| Cr ₂ O ₃ | 0.05 | 0.04 | 0.05 | 0.04 | 0.04 | 0.05 | 0.02 | 0.03 | 0.04 | 0.00 |
| FeO | 31.18 | 31.12 | 31.40 | 31.57 | 31.28 | 31.45 | 31.89 | 31.69 | 31.17 | 26.21 |
| MnO | 8.13 | 7.54 | 7.20 | 6.84 | 6.89 | 6.70 | 6.75 | 6.99 | 7.70 | 14.65 |
| MgO | 2.61 | 2.68 | 2.84 | 2.85 | 2.92 | 2.90 | 3.00 | 2.85 | 2.57 | 0.98 |
| CaO | 0.91 | 0.89 | 0.85 | 0.81 | 0.80 | 0.80 | 0.75 | 0.68 | 0.87 | 1.01 |
| Na ₂ O | 0.02 | 0.00 | 0.02 | 0.02 | 0.04 | 0.04 | 0.00 | 0.04 | 0.00 | 0.02 |
| K ₂ O | 0.03 | 0.01 | 0.02 | 0.00 | 0.00 | 0.02 | 0.02 | 0.02 | 0.02 | 0.02 |
| Total | 100.74 | 100.31 | 100.20 | 99.86 | 100.02 | 99.54 | 100.71 | 100.51 | 99.94 | 99.98 |

number of cations on the basis of 12 oxygens

| | | | | | | | | | | |
|-------------|-------|-------|-------|-------|-------|-------|-------|-------|-------|-------|
| Si | 2.97 | 2.98 | 2.98 | 2.96 | 2.98 | 2.98 | 2.98 | 2.99 | 2.98 | 2.97 |
| Ti | 0.00 | 0.00 | 0.00 | 0.00 | 0.00 | 0.00 | 0.00 | 0.00 | 0.00 | 0.00 |
| Al | 2.00 | 2.01 | 2.00 | 2.03 | 2.01 | 2.01 | 2.01 | 2.00 | 2.01 | 2.01 |
| Cr | 0.00 | 0.00 | 0.00 | 0.00 | 0.00 | 0.00 | 0.00 | 0.00 | 0.00 | 0.00 |
| Fe | 2.10 | 2.10 | 2.12 | 2.14 | 2.11 | 2.14 | 2.14 | 2.13 | 2.11 | 1.80 |
| Mn | 0.56 | 0.52 | 0.49 | 0.47 | 0.47 | 0.46 | 0.46 | 0.48 | 0.53 | 1.02 |
| Mg | 0.31 | 0.32 | 0.34 | 0.34 | 0.35 | 0.35 | 0.36 | 0.34 | 0.31 | 0.12 |
| Ca | 0.08 | 0.08 | 0.07 | 0.07 | 0.07 | 0.07 | 0.06 | 0.06 | 0.08 | 0.09 |
| Na | 0.00 | 0.00 | 0.00 | 0.00 | 0.01 | 0.01 | 0.00 | 0.01 | 0.00 | 0.00 |
| K | 0.00 | 0.00 | 0.00 | 0.00 | 0.00 | 0.00 | 0.00 | 0.00 | 0.00 | 0.00 |
| Total | 8.03 | 8.01 | 8.02 | 8.02 | 8.01 | 8.02 | 8.02 | 8.01 | 8.02 | 8.02 |
| Fe/FMCM* | 68.93 | 69.66 | 70.02 | 70.76 | 70.31 | 70.79 | 70.81 | 70.86 | 69.72 | 59.45 |
| Mg/FMCM* | 10.28 | 10.69 | 11.29 | 11.38 | 11.70 | 11.63 | 11.87 | 11.56 | 10.28 | 5.99 |
| Ca/FMCM* | 2.58 | 2.55 | 2.43 | 2.33 | 2.30 | 2.31 | 2.13 | 1.95 | 2.59 | 2.99 |
| Mn/FMCM* | 18.20 | 17.09 | 16.26 | 15.53 | 15.69 | 15.27 | 15.18 | 15.83 | 17.50 | 33.66 |
| Si+Al | 4.97 | 4.99 | 4.98 | 4.99 | 5.00 | 4.99 | 4.99 | 4.99 | 4.99 | 4.99 |
| Fe+Mg+Ca+Mn | 3.05 | 3.02 | 3.03 | 3.03 | 3.01 | 3.02 | 3.03 | 3.01 | 3.03 | 3.03 |
| Fe/(Fe+Mg) | 0.87 | 0.87 | 0.86 | 0.86 | 0.86 | 0.86 | 0.86 | 0.86 | 0.87 | 0.79 |
| A | 29.16 | 29.30 | 28.78 | 28.96 | 28.98 | 28.66 | 28.56 | 28.71 | 29.28 | 34.52 |
| F | 0.87 | 0.87 | 0.86 | 0.86 | 0.86 | 0.86 | 0.86 | 0.86 | 0.87 | 0.79 |
| M | 0.13 | 0.13 | 0.14 | 0.14 | 0.14 | 0.14 | 0.14 | 0.14 | 0.13 | 0.06 |
| Fe+Mg+Mn | 2.97 | 2.94 | 2.96 | 2.96 | 2.94 | 2.95 | 2.96 | 2.95 | 2.95 | 2.96 |
| Fe/Fe+Mg+Mn | 70.76 | 71.49 | 71.77 | 72.45 | 71.97 | 72.46 | 72.36 | 72.27 | 71.51 | 61.25 |
| Mn/Fe+Mg+Mn | 18.69 | 17.54 | 16.67 | 15.90 | 16.06 | 15.63 | 15.51 | 16.15 | 17.95 | 34.67 |
| Mg/Fe+Mg+Mn | 10.55 | 10.97 | 11.57 | 11.65 | 11.97 | 11.91 | 12.13 | 11.58 | 10.54 | 4.08 |

*FMCM=Fe+Mg+Ca+Mn

Garnet

| | SD-89-397-2 | | | | | | SD-89-397-4 | | | |
|--------------------------------|-------------|-------|-------|--------|-------|-------|-------------|--------|--------|-------|
| | (rim) | (mid) | (mid) | (core) | (mid) | (mid) | (rim) | (rim) | (mid) | (mid) |
| SiO ₂ | 36.46 | 36.54 | 36.83 | 36.41 | 36.62 | 36.62 | 36.79 | 36.94 | 33.92 | 36.60 |
| TiO ₂ | 0.04 | 0.04 | 0.04 | 0.05 | 0.07 | 0.06 | 0.06 | 0.05 | 4.23 | 0.08 |
| Al ₂ O ₃ | 20.79 | 20.63 | 20.82 | 20.76 | 20.65 | 20.78 | 20.64 | 20.55 | 19.27 | 20.70 |
| Cr ₂ O ₃ | 0.07 | 0.03 | 0.07 | 0.00 | 0.06 | 0.04 | 0.00 | 0.05 | 0.02 | 0.04 |
| FeO | 28.45 | 28.42 | 28.66 | 28.66 | 28.61 | 28.32 | 28.29 | 28.32 | 29.36 | 28.81 |
| MnO | 10.57 | 10.48 | 10.30 | 10.15 | 10.50 | 10.75 | 11.19 | 11.37 | 10.56 | 10.42 |
| MgO | 2.43 | 2.50 | 2.41 | 2.33 | 2.40 | 2.40 | 2.15 | 2.24 | 2.12 | 2.44 |
| CaO | 0.65 | 0.71 | 0.79 | 0.88 | 0.74 | 0.70 | 0.63 | 0.62 | 0.60 | 0.67 |
| Na ₂ O | 0.00 | 0.04 | 0.04 | 0.05 | 0.65 | 0.00 | 0.02 | 0.04 | 0.04 | 0.03 |
| K ₂ O | 0.01 | 0.02 | 0.02 | 0.02 | 0.00 | 0.01 | 0.03 | 0.03 | 0.03 | 0.02 |
| Total | 99.49 | 99.42 | 99.98 | 99.33 | 99.70 | 99.68 | 99.79 | 100.22 | 100.61 | 99.80 |

number of cations on the basis of 12 oxygens

| | | | | | | | | | | |
|-------------|-------|-------|-------|-------|-------|-------|-------|-------|-------|-------|
| Si | 2.98 | 2.99 | 2.99 | 2.98 | 2.97 | 2.98 | 3.00 | 3.00 | 2.79 | 2.98 |
| Ti | 0.00 | 0.00 | 0.00 | 0.00 | 0.00 | 0.00 | 0.00 | 0.00 | 0.26 | 0.00 |
| Al | 2.00 | 1.99 | 1.99 | 2.00 | 1.98 | 2.00 | 1.98 | 1.97 | 1.87 | 1.99 |
| Cr | 0.00 | 0.00 | 0.00 | 0.00 | 0.00 | 0.00 | 0.00 | 0.00 | 0.00 | 0.00 |
| Fe | 1.94 | 1.94 | 1.95 | 1.96 | 1.94 | 1.93 | 1.93 | 1.92 | 2.02 | 1.96 |
| Mn | 0.73 | 0.73 | 0.71 | 0.70 | 0.72 | 0.74 | 0.77 | 0.78 | 0.74 | 0.72 |
| Mg | 0.30 | 0.30 | 0.29 | 0.28 | 0.29 | 0.29 | 0.26 | 0.27 | 0.26 | 0.30 |
| Ca | 0.06 | 0.06 | 0.07 | 0.08 | 0.06 | 0.06 | 0.06 | 0.05 | 0.05 | 0.06 |
| Na | 0.00 | 0.01 | 0.01 | 0.01 | 0.10 | 0.00 | 0.00 | 0.01 | 0.01 | 0.00 |
| K | 0.00 | 0.00 | 0.00 | 0.00 | 0.00 | 0.00 | 0.00 | 0.00 | 0.00 | 0.00 |
| Total | 8.02 | 8.02 | 8.01 | 8.02 | 8.08 | 8.01 | 8.01 | 8.02 | 8.01 | 8.02 |
| Fe/FMCM* | 64.19 | 64.01 | 64.55 | 64.81 | 64.34 | 63.81 | 63.91 | 63.47 | 65.83 | 64.64 |
| Mg/FMCM* | 9.77 | 10.03 | 9.67 | 9.39 | 9.62 | 9.64 | 8.66 | 8.95 | 8.47 | 9.76 |
| Ca/FMCM* | 1.88 | 2.05 | 2.28 | 2.55 | 2.13 | 2.02 | 1.82 | 1.78 | 1.72 | 1.93 |
| Mn/FMCM* | 24.16 | 23.91 | 23.50 | 23.25 | 23.91 | 24.53 | 25.61 | 25.81 | 23.98 | 23.68 |
| Si+Al | 4.98 | 4.97 | 4.98 | 4.98 | 4.95 | 4.98 | 4.98 | 4.97 | 4.67 | 4.97 |
| Fe+Mg+Mn+Ca | 3.03 | 3.03 | 3.01 | 3.03 | 3.02 | 3.02 | 3.02 | 3.03 | 3.07 | 3.04 |
| Fe/(Fe+Mg) | 0.87 | 0.86 | 0.87 | 0.87 | 0.87 | 0.87 | 0.88 | 0.88 | 0.89 | 0.87 |
| A | 30.86 | 30.60 | 30.74 | 30.77 | 30.68 | 30.97 | 31.07 | 30.85 | 28.97 | 30.49 |
| F | 0.87 | 0.86 | 0.87 | 0.87 | 0.87 | 0.87 | 0.88 | 0.88 | 0.89 | 0.87 |
| M | 0.13 | 0.14 | 0.13 | 0.13 | 0.13 | 0.13 | 0.12 | 0.12 | 0.11 | 0.13 |
| Fe+Mg+Mn | 2.97 | 2.97 | 2.95 | 2.95 | 2.96 | 2.96 | 2.96 | 2.98 | 3.02 | 2.98 |
| Fe/Fe+Mg+Mn | 65.42 | 65.35 | 66.06 | 66.51 | 65.74 | 65.13 | 65.10 | 64.62 | 66.98 | 65.91 |
| Mn/Fe+Mg+Mn | 24.62 | 24.41 | 24.04 | 23.86 | 24.44 | 25.04 | 26.08 | 26.28 | 24.40 | 24.14 |
| Mg/Fe+Mg+Mn | 9.96 | 10.24 | 9.90 | 9.64 | 9.83 | 9.84 | 8.82 | 9.11 | 8.62 | 9.95 |

*FMCM = Fe+Mg+Ca+Mn

Garnet

| | SD-89-397-4 | | | SD-89-397-4 | | | SD-89-364-2 | | |
|--------------------------------|-------------|--------|--------|-------------|-------|-------|-------------|--------|-------|
| | (mid) | (core) | (mid) | (mid) | (rim) | (rim) | (mid) | (mid) | (mid) |
| SiO ₂ | 36.53 | 36.69 | 36.82 | 36.48 | 36.70 | 36.81 | 36.73 | 36.50 | 36.82 |
| TiO ₂ | 0.04 | 0.06 | 0.06 | 0.04 | 0.03 | 0.00 | 0.01 | 0.03 | 0.03 |
| Al ₂ O ₃ | 20.71 | 20.50 | 20.86 | 20.76 | 20.73 | 20.68 | 21.12 | 20.79 | 20.95 |
| Cr ₂ O ₃ | 0.05 | 0.03 | 0.05 | 0.04 | 0.04 | 0.07 | 0.06 | 0.03 | 0.00 |
| FeO | 28.82 | 28.87 | 28.92 | 28.39 | 28.79 | 27.41 | 28.96 | 29.28 | 29.81 |
| MnO | 10.74 | 10.46 | 10.50 | 10.50 | 10.53 | 12.35 | 9.39 | 9.07 | 8.68 |
| MgO | 2.40 | 2.44 | 2.44 | 2.40 | 2.32 | 1.81 | 1.83 | 2.06 | 2.12 |
| CaO | 0.65 | 0.68 | 0.67 | 0.66 | 0.65 | 0.67 | 1.56 | 1.13 | 1.34 |
| Na ₂ O | 0.00 | 0.03 | 0.06 | 0.03 | 0.04 | 0.01 | 0.02 | 0.05 | 0.02 |
| K ₂ O | 0.03 | 0.02 | 0.01 | 0.00 | 0.02 | 0.04 | 0.02 | 0.01 | 0.01 |
| Total | 99.97 | 99.79 | 100.41 | 99.30 | 99.85 | 99.75 | 99.78 | 100.18 | 99.77 |

number of cations on the basis of 12 oxygens

| | | | | | | | | | | |
|-------------|-------|-------|-------|-------|-------|-------|-------|-------|-------|-------|
| Si | 2.98 | 2.99 | 2.98 | 2.98 | 2.99 | 3.00 | 2.99 | 2.99 | 2.98 | 2.99 |
| Ti | 0.00 | 0.00 | 0.00 | 0.00 | 0.00 | 0.00 | 0.00 | 0.00 | 0.00 | 0.00 |
| Al | 1.99 | 1.97 | 1.99 | 2.00 | 1.99 | 1.99 | 2.02 | 1.99 | 2.01 | 2.01 |
| Cr | 0.00 | 0.00 | 0.00 | 0.00 | 0.00 | 0.00 | 0.00 | 0.00 | 0.00 | 0.00 |
| Fe | 1.96 | 1.97 | 1.96 | 1.94 | 1.96 | 1.87 | 1.97 | 2.06 | 2.04 | 2.03 |
| Mn | 0.74 | 0.72 | 0.72 | 0.73 | 0.73 | 0.85 | 0.65 | 0.62 | 0.62 | 0.60 |
| Mg | 0.29 | 0.30 | 0.29 | 0.29 | 0.28 | 0.22 | 0.22 | 0.25 | 0.24 | 0.26 |
| Ca | 0.06 | 0.06 | 0.06 | 0.06 | 0.06 | 0.06 | 0.14 | 0.10 | 0.11 | 0.12 |
| Na | 0.00 | 0.00 | 0.01 | 0.00 | 0.01 | 0.00 | 0.00 | 0.01 | 0.01 | 0.00 |
| K | 0.00 | 0.00 | 0.00 | 0.00 | 0.00 | 0.00 | 0.00 | 0.00 | 0.00 | 0.00 |
| Total | 8.03 | 8.02 | 8.02 | 8.01 | 8.02 | 8.01 | 8.00 | 8.02 | 8.02 | 8.00 |
| Fe/FMCM* | 64.32 | 64.61 | 64.61 | 64.31 | 64.81 | 62.29 | 66.22 | 67.92 | 67.51 | 67.60 |
| Mg/FMCM* | 9.54 | 9.73 | 9.71 | 9.69 | 9.31 | 7.33 | 7.46 | 8.23 | 8.06 | 8.57 |
| Ca/FMCM* | 1.86 | 1.95 | 1.92 | 1.92 | 1.87 | 1.95 | 4.57 | 3.25 | 3.80 | 3.87 |
| Mn/FMCM* | 24.28 | 23.71 | 23.76 | 24.09 | 24.01 | 28.43 | 21.75 | 20.60 | 20.62 | 19.94 |
| Si+Al | 4.97 | 4.96 | 4.97 | 4.99 | 4.98 | 4.99 | 5.01 | 4.98 | 4.99 | 5.00 |
| Fe+Mg+Mn+Ca | 3.05 | 3.05 | 3.03 | 3.02 | 3.03 | 3.01 | 2.97 | 3.03 | 3.02 | 3.00 |
| Fe/(Fe+Mg) | 0.87 | 0.87 | 0.87 | 0.87 | 0.87 | 0.89 | 0.90 | 0.89 | 0.89 | 0.89 |
| A | 30.51 | 30.25 | 30.62 | 30.94 | 30.67 | 32.10 | 31.53 | 30.12 | 30.47 | 30.50 |
| F | 0.87 | 0.87 | 0.87 | 0.87 | 0.87 | 0.89 | 0.90 | 0.89 | 0.89 | 0.89 |
| M | 0.13 | 0.13 | 0.13 | 0.13 | 0.13 | 0.11 | 0.10 | 0.11 | 0.11 | 0.11 |
| Fe+Mg+Mn | 3.00 | 2.99 | 2.97 | 2.96 | 2.97 | 2.95 | 2.84 | 2.93 | 2.90 | 2.88 |
| Fe/Fe+Mg+Mn | 65.54 | 65.89 | 65.87 | 65.56 | 66.05 | 63.53 | 69.40 | 70.19 | 70.18 | 70.54 |
| Mn/Fe+Mg+Mn | 24.74 | 24.18 | 24.22 | 24.56 | 24.47 | 28.99 | 22.79 | 21.50 | 21.44 | 20.74 |
| Mg/Fe+Mg+Mn | 9.73 | 9.92 | 9.90 | 9.88 | 9.48 | 7.48 | 7.81 | 8.51 | 8.58 | 8.91 |

*FMCM = Fe+Mg+Ca+Mn

Garnet

| | SD-89-364-2 | | | | | F-123-79-1 | | |
|--------------------------------|-------------|-------|--------|-------|--------|------------|--------|-------|
| | (core) | (mid) | (mid) | (mid) | (rim) | (Rim) | (Core) | (Rim) |
| SiO ₂ | 36.57 | 36.63 | 36.58 | 36.86 | 36.63 | 36.53 | 36.67 | 36.32 |
| TiO ₂ | 0.22 | 0.01 | 0.00 | 0.01 | 0.02 | 0.02 | 0.02 | 0.03 |
| Al ₂ O ₃ | 20.95 | 21.07 | 21.02 | 20.92 | 20.79 | 20.62 | 20.74 | 20.59 |
| Cr ₂ O ₃ | 0.00 | 0.05 | 0.04 | 0.03 | 0.00 | 0.00 | 0.00 | 0.00 |
| FeO | 29.94 | 29.37 | 30.14 | 29.71 | 29.60 | 29.45 | 29.08 | 28.83 |
| MnO | 8.39 | 8.50 | 8.61 | 8.59 | 9.79 | 8.03 | 7.97 | 9.36 |
| MgO | 2.12 | 2.17 | 2.12 | 2.07 | 1.89 | 3.35 | 3.33 | 2.47 |
| CaO | 1.57 | 1.82 | 1.86 | 1.77 | 1.35 | 0.88 | 0.86 | 0.92 |
| Na ₂ O | 0.03 | 0.04 | 0.03 | 0.04 | 0.02 | 0.01 | 0.03 | 0.00 |
| K ₂ O | 0.03 | 0.02 | 0.00 | 0.00 | 0.02 | 0.00 | 0.00 | 0.00 |
| Total | 99.83 | 99.68 | 100.40 | 99.99 | 100.11 | 98.89 | 98.69 | 98.54 |

number of cations on the basis of 12 oxygens

| | | | | | | | | |
|-------------|-------|-------|-------|-------|-------|-------|-------|-------|
| Si | 2.97 | 2.98 | 2.96 | 2.99 | 2.98 | 2.98 | 2.99 | 2.99 |
| Ti | 0.01 | 0.00 | 0.00 | 0.00 | 0.00 | 0.00 | 0.00 | 0.00 |
| Al | 2.01 | 2.02 | 2.01 | 2.00 | 2.00 | 1.99 | 2.00 | 2.00 |
| Cr | 0.00 | 0.00 | 0.00 | 0.00 | 0.00 | 0.00 | 0.00 | 0.00 |
| Fe | 2.04 | 2.00 | 2.04 | 2.02 | 2.02 | 2.01 | 1.98 | 1.98 |
| Mn | 0.58 | 0.59 | 0.59 | 0.59 | 0.68 | 0.56 | 0.55 | 0.65 |
| Mg | 0.26 | 0.26 | 0.26 | 0.25 | 0.23 | 0.41 | 0.41 | 0.30 |
| Ca | 0.14 | 0.16 | 0.16 | 0.15 | 0.12 | 0.08 | 0.08 | 0.08 |
| Na | 0.00 | 0.01 | 0.00 | 0.01 | 0.00 | 0.00 | 0.00 | 0.00 |
| K | 0.00 | 0.00 | 0.00 | 0.00 | 0.00 | 0.00 | 0.00 | 0.00 |
| Total | 8.01 | 8.01 | 8.03 | 8.01 | 8.02 | 8.02 | 8.01 | 8.01 |
| Fe/FMCM* | 67.70 | 66.48 | 66.95 | 66.96 | 66.35 | 65.91 | 65.81 | 65.69 |
| Mg/FMCM* | 8.54 | 8.75 | 8.39 | 8.31 | 7.55 | 13.36 | 13.43 | 10.03 |
| Ca/FMCM* | 4.55 | 5.28 | 5.29 | 5.11 | 3.88 | 2.52 | 2.49 | 2.69 |
| Mn/FMCM* | 19.21 | 19.49 | 19.37 | 19.61 | 22.23 | 18.20 | 18.27 | 21.60 |
| Si+Al | 4.98 | 5.00 | 4.97 | 4.99 | 4.98 | 4.97 | 4.99 | 4.99 |
| Fe+Mg+Mn+Ca | 3.01 | 3.00 | 3.05 | 3.01 | 3.04 | 3.05 | 3.02 | 3.02 |
| Fe/(Fe+Mg) | 0.89 | 0.88 | 0.89 | 0.89 | 0.90 | 0.83 | 0.83 | 0.87 |
| A | 30.36 | 30.82 | 30.40 | 30.63 | 30.70 | 29.09 | 29.45 | 30.40 |
| F | 0.89 | 0.88 | 0.89 | 0.89 | 0.90 | 0.83 | 0.83 | 0.87 |
| M | 0.11 | 0.12 | 0.11 | 0.11 | 0.10 | 0.17 | 0.17 | 0.13 |
| Fe+Mg+Mn | 2.87 | 2.85 | 2.89 | 2.86 | 2.92 | 2.97 | 2.94 | 2.94 |
| Fe/Fe+Mg+Mn | 70.92 | 70.19 | 70.69 | 70.57 | 69.02 | 67.62 | 67.49 | 67.50 |
| Mn/Fe+Mg+Mn | 20.13 | 20.57 | 20.45 | 20.67 | 23.12 | 18.67 | 18.74 | 22.20 |
| Mg/Fe+Mg+Mn | 8.95 | 9.24 | 8.86 | 8.76 | 7.85 | 13.71 | 13.77 | 10.31 |

*FMCM = Fe+Mg+Ca+Mn

Garnet

| | F-123-79-3 | | | F-123-79-4 | | | | |
|--------------------------------|------------|-------|--------|------------|-------|--------|-------|-------|
| | (Rim) | (Mid) | (Core) | (Rim) | (Mid) | (Core) | (Mid) | (Rim) |
| SiO ₂ | 36.26 | 36.28 | 36.02 | 36.09 | 36.26 | 36.13 | 36.52 | 36.09 |
| TiO ₂ | 0.03 | 0.01 | 0.07 | 0.03 | 0.00 | 0.04 | 0.01 | 0.02 |
| Al ₂ O ₃ | 20.56 | 20.62 | 20.64 | 20.46 | 20.42 | 20.65 | 20.88 | 20.62 |
| Cr ₂ O ₃ | 0.00 | 0.00 | 0.00 | 0.00 | 0.00 | 0.00 | 0.00 | 0.00 |
| FeO | 27.92 | 29.72 | 28.13 | 28.34 | 28.50 | 29.34 | 28.93 | 28.13 |
| MnO | 10.66 | 8.70 | 11.08 | 10.92 | 10.12 | 9.10 | 9.36 | 10.29 |
| MgO | 2.12 | 2.59 | 2.05 | 1.97 | 2.69 | 2.96 | 2.91 | 2.54 |
| CaO | 0.90 | 0.89 | 0.90 | 0.90 | 0.86 | 0.85 | 0.89 | 0.89 |
| Na ₂ O | 0.00 | 0.00 | 0.01 | 0.02 | 0.00 | 0.00 | 0.01 | 0.00 |
| K ₂ O | 0.00 | 0.00 | 0.00 | 0.00 | 0.00 | 0.00 | 0.00 | 0.00 |
| Total | 98.44 | 98.82 | 98.91 | 98.72 | 98.86 | 99.06 | 99.50 | 98.58 |

number of cations on the basis of 12 oxygens

| | | | | | | | | |
|-------------|-------|-------|-------|-------|-------|-------|-------|-------|
| Si | 2.99 | 2.98 | 2.97 | 2.98 | 2.98 | 2.96 | 2.97 | 2.97 |
| Ti | 0.00 | 0.00 | 0.00 | 0.00 | 0.00 | 0.00 | 0.00 | 0.00 |
| Al | 2.00 | 2.00 | 2.01 | 1.99 | 1.98 | 2.00 | 2.00 | 2.00 |
| Cr | 0.00 | 0.00 | 0.00 | 0.00 | 0.00 | 0.00 | 0.00 | 0.00 |
| Fe | 1.93 | 2.04 | 1.94 | 1.96 | 1.96 | 2.01 | 1.97 | 1.94 |
| Mn | 0.75 | 0.61 | 0.77 | 0.76 | 0.70 | 0.63 | 0.65 | 0.72 |
| Mg | 0.26 | 0.32 | 0.25 | 0.24 | 0.33 | 0.36 | 0.35 | 0.31 |
| Ca | 0.08 | 0.08 | 0.08 | 0.08 | 0.08 | 0.07 | 0.08 | 0.08 |
| Na | 0.00 | 0.00 | 0.00 | 0.00 | 0.00 | 0.00 | 0.00 | 0.00 |
| K | 0.00 | 0.00 | 0.00 | 0.00 | 0.00 | 0.00 | 0.00 | 0.00 |
| Total | 8.01 | 8.02 | 8.02 | 8.02 | 8.03 | 8.04 | 8.04 | 8.02 |
| Fe/FMCM* | 63.97 | 67.11 | 63.70 | 64.32 | 63.84 | 65.32 | 64.67 | 63.62 |
| Mg/FMCM* | 8.66 | 10.42 | 8.27 | 7.97 | 10.74 | 11.74 | 11.59 | 10.24 |
| Ca/FMCM* | 2.64 | 2.57 | 2.61 | 2.62 | 2.47 | 2.42 | 2.55 | 2.58 |
| Mn/FMCM* | 24.74 | 19.90 | 25.41 | 25.10 | 22.96 | 20.52 | 21.19 | 23.57 |
| Si+Al | 4.99 | 4.98 | 4.97 | 4.97 | 4.96 | 4.96 | 4.98 | 4.98 |
| Fe+Mg+Mn+Ca | 3.01 | 3.04 | 3.04 | 3.04 | 3.07 | 3.08 | 3.05 | 3.05 |
| Fe/(Fe+Mg) | 0.88 | 0.87 | 0.89 | 0.89 | 0.86 | 0.85 | 0.85 | 0.86 |
| A | 31.37 | 29.74 | 31.40 | 31.17 | 30.18 | 29.60 | 30.14 | 30.80 |
| F | 0.88 | 0.87 | 0.89 | 0.89 | 0.86 | 0.85 | 0.85 | 0.86 |
| M | 0.12 | 0.13 | 0.11 | 0.11 | 0.14 | 0.15 | 0.15 | 0.14 |
| Fe+Mg+Mn | 2.93 | 2.96 | 2.96 | 2.96 | 2.99 | 3.00 | 2.97 | 2.97 |
| Fe/Fe+Mg+Mn | 65.70 | 68.88 | 65.41 | 66.04 | 65.45 | 66.94 | 66.36 | 65.50 |
| Mn/Fe+Mg+Mn | 25.41 | 20.42 | 26.09 | 25.77 | 23.54 | 21.03 | 21.75 | 24.19 |
| Mg/Fe+Mg+Mn | 8.89 | 10.70 | 8.49 | 8.18 | 11.01 | 12.03 | 11.89 | 10.51 |

*FMCM = Fe+Mg+Ca+Mn

Garnet

| | G-118-80-1 | | | | G-163-80-3 | | | | | |
|--------------------------------|------------|-------|--------|-------|------------|-------|-------|-------|-------|--------|
| | (Rim) | (Mid) | (Core) | (Mid) | (Rim) | (Rim) | (Mid) | (Mid) | (Mid) | (Core) |
| SiO ₂ | 36.20 | 35.92 | 36.11 | 36.16 | 36.01 | 35.97 | 39.95 | 36.04 | 35.74 | 35.21 |
| TiO ₂ | 0.04 | 0.10 | 0.08 | 0.03 | 0.05 | 0.03 | 0.07 | 0.06 | 0.09 | 0.06 |
| Al ₂ O ₃ | 20.02 | 19.99 | 20.04 | 20.24 | 20.22 | 20.54 | 20.56 | 20.29 | 20.57 | 20.44 |
| Cr ₂ O ₃ | 0.00 | 0.00 | 0.00 | 0.00 | 0.00 | 0.00 | 0.00 | 0.00 | 0.00 | 0.00 |
| FeO | 31.95 | 29.83 | 29.10 | 29.78 | 31.84 | 32.80 | 32.01 | 31.44 | 31.72 | 31.51 |
| MnO | 7.88 | 9.33 | 9.90 | 9.97 | 8.08 | 7.08 | 7.62 | 7.94 | 8.45 | 8.20 |
| MgO | 2.06 | 1.98 | 2.00 | 2.01 | 2.09 | 2.01 | 2.00 | 2.00 | 1.96 | 1.87 |
| CaO | 0.84 | 1.41 | 1.42 | 1.23 | 0.92 | 0.81 | 0.95 | 0.97 | 1.13 | 1.46 |
| Na ₂ O | 0.01 | 0.01 | 0.02 | 0.00 | 0.00 | 0.02 | 0.02 | 0.03 | 0.05 | 0.03 |
| K ₂ O | 0.00 | 0.00 | 0.00 | 0.00 | 0.00 | 0.00 | 0.00 | 0.00 | 0.00 | 0.00 |
| Total | 99.00 | 98.57 | 98.68 | 99.42 | 99.20 | 99.25 | 99.18 | 98.78 | 99.72 | 98.77 |

number of cations on the basis of 12 oxygens

| | | | | | | | | | | |
|-------------|-------|-------|-------|-------|-------|-------|-------|-------|-------|-------|
| Si | 2.99 | 2.98 | 2.99 | 2.98 | 2.97 | 2.96 | 3.12 | 2.98 | 2.94 | 2.93 |
| Ti | 0.00 | 0.01 | 0.00 | 0.00 | 0.00 | 0.00 | 0.00 | 0.00 | 0.01 | 0.00 |
| Al | 1.95 | 1.95 | 1.95 | 1.96 | 1.97 | 2.00 | 1.89 | 1.98 | 2.00 | 2.00 |
| Cr | 0.00 | 0.00 | 0.00 | 0.00 | 0.00 | 0.00 | 0.00 | 0.00 | 0.00 | 0.00 |
| Fe | 2.21 | 2.07 | 2.01 | 2.05 | 2.20 | 2.26 | 2.09 | 2.17 | 2.18 | 2.19 |
| Mn | 0.55 | 0.66 | 0.69 | 0.69 | 0.56 | 0.49 | 0.50 | 0.56 | 0.59 | 0.58 |
| Mg | 0.25 | 0.24 | 0.25 | 0.25 | 0.26 | 0.25 | 0.23 | 0.25 | 0.24 | 0.23 |
| Ca | 0.07 | 0.13 | 0.13 | 0.11 | 0.08 | 0.07 | 0.08 | 0.09 | 0.10 | 0.13 |
| Na | 0.00 | 0.00 | 0.00 | 0.00 | 0.00 | 0.00 | 0.00 | 0.00 | 0.01 | 0.00 |
| K | 0.00 | 0.00 | 0.00 | 0.00 | 0.00 | 0.00 | 0.00 | 0.00 | 0.00 | 0.00 |
| Total | 8.03 | 8.04 | 8.03 | 8.04 | 8.04 | 8.04 | 7.93 | 8.03 | 8.06 | 8.07 |
| Fe/FMCM* | 71.51 | 66.86 | 65.38 | 66.13 | 70.87 | 73.56 | 71.92 | 70.99 | 70.15 | 69.99 |
| Mg/FMCM* | 8.22 | 7.91 | 8.01 | 7.95 | 8.29 | 8.03 | 8.01 | 8.05 | 7.72 | 7.40 |
| Ca/FMCM* | 2.41 | 4.05 | 4.09 | 3.50 | 2.62 | 2.33 | 2.73 | 2.81 | 3.20 | 4.16 |
| Mn/FMCM* | 17.86 | 21.18 | 22.53 | 22.42 | 18.22 | 16.08 | 17.34 | 18.16 | 18.93 | 18.45 |
| Si+Al | 4.94 | 4.93 | 4.94 | 4.94 | 4.94 | 4.96 | 5.01 | 4.96 | 4.94 | 4.93 |
| Fe+Mg+Mn+Ca | 3.09 | 3.10 | 3.08 | 3.10 | 3.10 | 3.07 | 2.91 | 3.06 | 3.11 | 3.13 |
| Fe/(Fe+Mg) | 0.90 | 0.89 | 0.89 | 0.89 | 0.90 | 0.90 | 0.90 | 0.90 | 0.90 | 0.90 |
| A | 28.37 | 29.69 | 30.19 | 29.95 | 28.61 | 28.47 | 28.94 | 29.01 | 29.17 | 29.25 |
| F | 0.90 | 0.89 | 0.89 | 0.89 | 0.90 | 0.90 | 0.90 | 0.90 | 0.90 | 0.90 |
| M | 0.10 | 0.11 | 0.11 | 0.11 | 0.10 | 0.10 | 0.10 | 0.10 | 0.10 | 0.10 |
| Fe+Mg+Mn | 3.01 | 2.97 | 2.95 | 2.99 | 3.02 | 3.00 | 2.83 | 2.98 | 3.01 | 3.00 |
| Fe/Fe+Mg+Mn | 73.28 | 69.68 | 68.16 | 68.52 | 72.78 | 75.31 | 73.94 | 73.04 | 72.47 | 73.03 |
| Mn/Fe+Mg+Mn | 18.30 | 22.07 | 23.49 | 23.24 | 18.71 | 16.46 | 17.83 | 18.68 | 19.55 | 19.25 |
| Mg/Fe+Mg+Mn | 8.42 | 8.24 | 8.35 | 8.24 | 8.51 | 8.22 | 8.23 | 8.28 | 7.98 | 7.72 |

*FMCM = Fe+Mg+Ca+Mn

Garnet

| | SD-89-353-4 | | | | | | SD-89-353-4 | | | |
|--------------------------------|-------------|--------|--------|--------|--------|--------|-------------|--------|--------|-------|
| | (rim) | (mid) | (mid) | (mid) | (mid) | (core) | (mid) | (mid) | (mid) | (mid) |
| SiO ₂ | 36.48 | 37.02 | 36.68 | 36.72 | 36.56 | 36.53 | 36.71 | 36.76 | 36.77 | 36.78 |
| TiO ₂ | 0.03 | 0.02 | 0.05 | 0.05 | 0.02 | 0.03 | 0.03 | 0.06 | 0.04 | 0.04 |
| Al ₂ O ₃ | 21.15 | 21.03 | 20.68 | 20.95 | 20.82 | 20.74 | 20.88 | 21.02 | 21.02 | 20.75 |
| Cr ₂ O ₃ | 0.03 | 0.05 | 0.03 | 0.08 | 0.05 | 0.00 | 0.05 | 0.06 | 0.05 | 0.00 |
| FeO | 34.35 | 33.50 | 33.41 | 32.99 | 32.76 | 32.24 | 32.64 | 32.87 | 33.20 | 33.52 |
| MnO | 4.35 | 5.20 | 5.67 | 6.07 | 6.47 | 6.49 | 6.49 | 6.02 | 5.90 | 5.21 |
| MgO | 2.16 | 1.95 | 1.83 | 1.78 | 1.73 | 1.68 | 1.77 | 1.85 | 1.93 | 1.93 |
| CaO | 1.60 | 1.67 | 1.58 | 1.67 | 1.68 | 1.60 | 1.60 | 1.62 | 1.66 | 1.66 |
| Na ₂ O | 0.04 | 0.04 | 0.04 | 0.00 | 0.02 | 0.05 | 0.04 | 0.05 | 0.05 | 0.04 |
| K ₂ O | 0.01 | 0.02 | 0.02 | 0.01 | 0.01 | 0.01 | 0.02 | 0.02 | 0.02 | 0.02 |
| Total | 100.21 | 100.52 | 100.00 | 100.33 | 100.12 | 99.38 | 100.22 | 100.35 | 100.59 | 99.74 |

number of cations on the basis of 12 oxygens

| | | | | | | | | | | |
|-------------|-------|-------|-------|-------|-------|-------|-------|-------|-------|-------|
| Si | 2.96 | 2.99 | 2.99 | 2.98 | 2.98 | 2.99 | 2.98 | 2.98 | 2.98 | 3.00 |
| Ti | 0.00 | 0.00 | 0.00 | 0.00 | 0.00 | 0.00 | 0.00 | 0.00 | 0.00 | 0.00 |
| Al | 2.02 | 2.00 | 1.99 | 2.00 | 2.00 | 2.00 | 2.00 | 2.01 | 2.01 | 1.99 |
| Cr | 0.00 | 0.00 | 0.00 | 0.01 | 0.00 | 0.00 | 0.00 | 0.00 | 0.00 | 0.00 |
| Fe | 2.33 | 2.26 | 2.28 | 2.24 | 2.23 | 2.21 | 2.22 | 2.23 | 2.25 | 2.27 |
| Mn | 0.30 | 0.36 | 0.39 | 0.42 | 0.45 | 0.45 | 0.45 | 0.41 | 0.40 | 0.36 |
| Mg | 0.26 | 0.23 | 0.22 | 0.22 | 0.21 | 0.21 | 0.21 | 0.22 | 0.23 | 0.23 |
| Ca | 0.14 | 0.14 | 0.14 | 0.15 | 0.15 | 0.14 | 0.14 | 0.14 | 0.14 | 0.14 |
| Na | 0.01 | 0.01 | 0.01 | 0.00 | 0.00 | 0.01 | 0.01 | 0.01 | 0.00 | 0.01 |
| K | 0.00 | 0.00 | 0.00 | 0.00 | 0.00 | 0.00 | 0.00 | 0.00 | 0.00 | 0.00 |
| Total | 8.03 | 8.01 | 8.02 | 8.01 | 8.02 | 8.01 | 8.02 | 8.01 | 8.02 | 8.01 |
| Fe/FMCM* | 76.92 | 75.48 | 75.18 | 74.22 | 73.54 | 73.51 | 73.48 | 74.13 | 74.20 | 75.65 |
| Mg/FMCM* | 8.62 | 7.83 | 7.34 | 7.14 | 6.92 | 6.83 | 7.10 | 7.44 | 7.69 | 7.79 |
| Ca/FMCM* | 4.59 | 4.82 | 4.56 | 4.81 | 4.83 | 4.67 | 4.62 | 4.68 | 4.75 | 4.82 |
| Mn/FMCM* | 9.87 | 11.87 | 12.92 | 13.83 | 14.71 | 14.99 | 14.80 | 13.75 | 13.56 | 11.95 |
| Si+Al | 4.99 | 5.00 | 4.98 | 4.99 | 4.98 | 4.99 | 4.98 | 4.99 | 4.98 | 4.99 |
| Fe+Mg+Mn+Ca | 3.03 | 3.00 | 3.03 | 3.02 | 3.03 | 3.00 | 3.02 | 3.01 | 3.03 | 3.01 |
| Fe/(Fe+Mg) | 0.90 | 0.91 | 0.91 | 0.91 | 0.91 | 0.92 | 0.91 | 0.91 | 0.91 | 0.91 |
| A | 28.04 | 28.55 | 28.38 | 28.96 | 29.02 | 29.29 | 29.07 | 29.00 | 28.75 | 28.60 |
| F | 0.90 | 0.91 | 0.91 | 0.91 | 0.91 | 0.92 | 0.91 | 0.91 | 0.91 | 0.91 |
| M | 0.10 | 0.09 | 0.09 | 0.09 | 0.09 | 0.08 | 0.09 | 0.09 | 0.09 | 0.09 |
| Fe+Mg+Mn | 2.89 | 2.86 | 2.89 | 2.87 | 2.89 | 2.86 | 2.88 | 2.87 | 2.88 | 2.86 |
| Fe/Fe+Mg+Mn | 80.62 | 79.31 | 78.77 | 77.97 | 77.27 | 77.12 | 77.04 | 77.77 | 77.91 | 79.27 |
| Mn/Fe+Mg+Mn | 10.34 | 12.47 | 13.54 | 14.53 | 15.46 | 15.72 | 15.51 | 14.43 | 14.02 | 12.55 |
| Mg/Fe+Mg+Mn | 9.03 | 8.23 | 7.69 | 7.50 | 7.27 | 7.16 | 7.44 | 7.80 | 8.07 | 8.15 |

*FMCM = Fe+Mg+Ca+Mn

Garnet

| | SD-89-353-4 | | SD-89-353-5 | | | | | | SD-89-353-5 | |
|--------------------------------|-------------|--------|-------------|-------|-------|-------|-------|--------|-------------|--------|
| | (rim) | (rim) | (rim) | (mid) | (mid) | (mid) | (mid) | (mid) | (mid) | (core) |
| SiO ₂ | 36.58 | 36.45 | 36.62 | 36.82 | 36.44 | 36.21 | 36.02 | 36.53 | 36.86 | 36.85 |
| TiO ₂ | 0.03 | 0.06 | 0.03 | 0.06 | 0.03 | 0.06 | 0.04 | 0.03 | 0.05 | 0.05 |
| Al ₂ O ₃ | 20.96 | 20.94 | 20.89 | 20.86 | 21.00 | 20.93 | 20.75 | 20.98 | 21.00 | 20.85 |
| Cr ₂ O ₃ | 0.04 | 0.04 | 0.05 | 0.00 | 0.05 | 0.00 | 0.07 | 0.07 | 0.00 | 0.04 |
| FeO | 34.06 | 34.00 | 34.22 | 32.98 | 32.64 | 32.41 | 31.63 | 31.80 | 31.17 | 31.07 |
| MnO | 4.37 | 5.22 | 4.68 | 5.63 | 6.29 | 6.52 | 7.18 | 7.67 | 8.10 | 8.28 |
| MgO | 2.07 | 1.96 | 2.03 | 1.88 | 1.79 | 1.65 | 1.65 | 1.64 | 1.55 | 1.48 |
| CaO | 1.72 | 1.67 | 1.61 | 1.64 | 1.62 | 1.68 | 1.63 | 1.58 | 1.60 | 1.69 |
| Na ₂ O | 0.02 | 0.04 | 0.04 | 0.04 | 0.06 | 0.09 | 0.03 | 0.04 | 0.02 | 0.04 |
| K ₂ O | 0.02 | 0.02 | 0.00 | 0.02 | 0.01 | 0.04 | 0.03 | 0.01 | 0.03 | 0.03 |
| Total | 99.88 | 100.33 | 100.17 | 99.93 | 99.93 | 99.59 | 99.02 | 100.35 | 100.38 | 100.37 |

number of cations on the basis of 12 oxygens

| | | | | | | | | | | |
|-------------|-------|-------|-------|-------|-------|-------|-------|-------|-------|-------|
| Si | 2.98 | 2.96 | 2.98 | 2.99 | 2.97 | 2.97 | 2.97 | 2.97 | 2.99 | 2.99 |
| Ti | 0.00 | 0.00 | 0.00 | 0.00 | 0.00 | 0.00 | 0.00 | 0.00 | 0.00 | 0.00 |
| Al | 2.01 | 2.01 | 2.00 | 2.00 | 2.02 | 2.02 | 2.02 | 2.01 | 2.01 | 2.00 |
| Cr | 0.00 | 0.00 | 0.00 | 0.00 | 0.00 | 0.00 | 0.00 | 0.00 | 0.00 | 0.00 |
| Fe | 2.32 | 2.31 | 2.33 | 2.24 | 2.23 | 2.22 | 2.18 | 2.16 | 2.11 | 2.11 |
| Mn | 0.30 | 0.36 | 0.32 | 0.39 | 0.43 | 0.45 | 0.50 | 0.53 | 0.56 | 0.57 |
| Mg | 0.25 | 0.24 | 0.25 | 0.23 | 0.22 | 0.20 | 0.20 | 0.20 | 0.19 | 0.18 |
| Ca | 0.15 | 0.15 | 0.14 | 0.14 | 0.14 | 0.15 | 0.14 | 0.14 | 0.14 | 0.15 |
| Na | 0.00 | 0.01 | 0.01 | 0.01 | 0.01 | 0.01 | 0.00 | 0.01 | 0.00 | 0.01 |
| K | 0.00 | 0.00 | 0.00 | 0.00 | 0.00 | 0.00 | 0.00 | 0.00 | 0.00 | 0.00 |
| Total | 8.02 | 8.03 | 8.02 | 8.01 | 8.02 | 8.03 | 8.02 | 8.02 | 8.01 | 8.01 |
| Fe/FMCM* | 76.75 | 75.69 | 76.66 | 74.73 | 73.72 | 73.48 | 72.00 | 71.44 | 70.54 | 70.20 |
| Mg/FMCM* | 8.31 | 7.78 | 8.10 | 7.59 | 7.20 | 6.67 | 6.69 | 6.57 | 6.25 | 5.96 |
| Ca/FMCM* | 4.97 | 4.76 | 4.62 | 4.76 | 4.69 | 4.88 | 4.75 | 4.55 | 4.64 | 4.89 |
| Mn/FMCM* | 9.97 | 11.77 | 10.62 | 12.92 | 14.39 | 14.97 | 16.55 | 17.45 | 18.57 | 18.95 |
| Si+Al | 4.99 | 4.97 | 4.98 | 4.99 | 4.99 | 4.99 | 4.98 | 4.98 | 5.00 | 4.99 |
| Fe+Mg+Mn+Ca | 3.02 | 3.05 | 3.03 | 3.00 | 3.02 | 3.02 | 3.03 | 3.03 | 3.00 | 3.01 |
| Fe/(Fe+Mg) | 0.90 | 0.91 | 0.90 | 0.91 | 0.91 | 0.92 | 0.91 | 0.92 | 0.92 | 0.92 |
| A | 28.06 | 28.18 | 28.01 | 28.75 | 29.20 | 29.31 | 29.63 | 29.83 | 30.27 | 30.26 |
| F | 0.90 | 0.91 | 0.90 | 0.91 | 0.91 | 0.92 | 0.91 | 0.92 | 0.92 | 0.92 |
| M | 0.10 | 0.09 | 0.10 | 0.09 | 0.09 | 0.08 | 0.09 | 0.08 | 0.08 | 0.08 |
| Fe+Mg+Mn | 2.87 | 2.91 | 2.89 | 2.86 | 2.88 | 2.87 | 2.88 | 2.89 | 2.86 | 2.86 |
| Fe/Fe+Mg+Mn | 80.76 | 79.48 | 80.37 | 78.46 | 77.35 | 77.25 | 75.59 | 74.84 | 73.97 | 73.81 |
| Mn/Fe+Mg+Mn | 10.49 | 12.36 | 11.13 | 13.57 | 15.10 | 15.74 | 17.38 | 18.28 | 19.47 | 19.92 |
| Mg/Fe+Mg+Mn | 8.75 | 8.16 | 8.50 | 7.97 | 7.56 | 7.01 | 7.03 | 6.88 | 6.56 | 6.27 |

*FMCM = Fe+Mg+Ca+Mn

Garnet

| | G-133-80-1 | | | | G-133-80-2 | | | | G-123-80 | |
|--------------------------------|------------|--------|--------|--------|------------|--------|-------|--------|----------|--------|
| | (Rim) | (Core) | (Rim) | (Mid) | (Core) | (Mid) | (Rim) | (Rim) | (Mid) | (Core) |
| SiO ₂ | 36.50 | 36.49 | 36.62 | 36.81 | 36.65 | 36.73 | 36.56 | 36.83 | 37.42 | 36.56 |
| TiO ₂ | 0.00 | 0.00 | 0.02 | 0.02 | 0.01 | 0.01 | 0.03 | 0.00 | 0.00 | 0.04 |
| Al ₂ O ₃ | 20.78 | 20.87 | 20.77 | 20.95 | 20.58 | 20.74 | 20.74 | 20.96 | 20.91 | 20.83 |
| Cr ₂ O ₃ | 0.00 | 0.00 | 0.00 | 0.00 | 0.00 | 0.00 | 0.00 | 0.07 | 0.01 | 0.04 |
| FeO | 37.04 | 36.05 | 36.96 | 36.83 | 36.83 | 36.45 | 36.62 | 31.60 | 30.56 | 31.43 |
| MnO | 1.93 | 1.85 | 2.03 | 1.87 | 1.83 | 1.89 | 1.91 | 9.02 | 8.90 | 9.21 |
| MgO | 2.51 | 3.13 | 2.85 | 3.19 | 3.01 | 3.10 | 2.82 | 1.95 | 1.90 | 1.96 |
| CaO | 1.07 | 1.13 | 1.08 | 1.09 | 1.06 | 1.08 | 1.12 | 0.52 | 0.61 | 0.61 |
| Na ₂ O | 0.00 | 0.02 | 0.00 | 0.00 | 0.00 | 0.00 | 0.00 | 0.00 | 0.00 | 0.00 |
| K ₂ O | 0.00 | 0.00 | 0.00 | 0.00 | 0.00 | 0.00 | 0.00 | 0.00 | 0.00 | 0.00 |
| Total | 99.83 | 99.53 | 100.33 | 100.75 | 99.97 | 100.01 | 99.79 | 101.00 | 100.11 | 100.54 |

number of cations on the basis of 12 oxygens

| | | | | | | | | | | |
|-------------|-------|-------|-------|-------|-------|-------|-------|-------|-------|-------|
| Si | 2.97 | 2.97 | 2.97 | 2.96 | 2.98 | 2.98 | 2.97 | 2.98 | 3.03 | 2.96 |
| Ti | 0.00 | 0.00 | 0.00 | 0.00 | 0.00 | 0.00 | 0.00 | 0.00 | 0.00 | 0.00 |
| Al | 2.00 | 2.00 | 1.98 | 1.99 | 1.97 | 1.98 | 1.99 | 2.00 | 2.00 | 2.00 |
| Cr | 0.00 | 0.00 | 0.00 | 0.00 | 0.00 | 0.00 | 0.00 | 0.00 | 0.00 | 0.00 |
| Fe | 2.52 | 2.45 | 2.51 | 2.48 | 2.50 | 2.47 | 2.49 | 2.14 | 2.06 | 2.14 |
| Mn | 0.13 | 0.13 | 0.14 | 0.13 | 0.13 | 0.13 | 0.13 | 0.62 | 0.61 | 0.64 |
| Mg | 0.30 | 0.38 | 0.34 | 0.38 | 0.36 | 0.37 | 0.34 | 0.24 | 0.23 | 0.24 |
| Ca | 0.09 | 0.10 | 0.09 | 0.09 | 0.09 | 0.09 | 0.10 | 0.05 | 0.05 | 0.05 |
| Na | 0.00 | 0.00 | 0.00 | 0.00 | 0.00 | 0.00 | 0.00 | 0.00 | 0.00 | 0.00 |
| K | 0.00 | 0.00 | 0.00 | 0.00 | 0.00 | 0.00 | 0.00 | 0.00 | 0.00 | 0.00 |
| Total | 8.03 | 8.03 | 8.04 | 8.04 | 8.04 | 8.03 | 8.03 | 8.02 | 7.97 | 8.03 |
| Fe/FMCM* | 82.61 | 80.20 | 81.27 | 80.41 | 81.11 | 80.51 | 81.35 | 70.41 | 69.73 | 69.79 |
| Mg/FMCM* | 9.98 | 12.41 | 11.17 | 12.41 | 11.81 | 12.20 | 11.16 | 7.74 | 7.78 | 7.76 |
| Ca/FMCM* | 3.06 | 3.22 | 3.04 | 3.05 | 2.99 | 3.06 | 3.19 | 1.48 | 1.79 | 1.74 |
| Mn/FMCM* | 4.36 | 4.17 | 4.52 | 4.13 | 4.08 | 4.23 | 4.30 | 20.36 | 20.70 | 20.71 |
| Si+Al | 4.97 | 4.97 | 4.95 | 4.95 | 4.95 | 4.96 | 4.96 | 4.98 | 5.02 | 4.96 |
| Fe+Mg+Mn+Ca | 3.06 | 3.06 | 3.08 | 3.09 | 3.09 | 3.07 | 3.06 | 3.04 | 2.95 | 3.07 |
| Fe/(Fe+Mg) | 0.89 | 0.87 | 0.88 | 0.87 | 0.87 | 0.87 | 0.88 | 0.90 | 0.90 | 0.90 |
| A | 26.08 | 26.11 | 25.83 | 25.78 | 25.58 | 25.83 | 25.98 | 25.59 | 30.40 | 29.59 |
| F | 0.89 | 0.87 | 0.88 | 0.87 | 0.87 | 0.87 | 0.88 | 0.90 | 0.90 | 0.90 |
| M | 0.11 | 0.13 | 0.12 | 0.13 | 0.13 | 0.13 | 0.12 | 0.10 | 0.10 | 0.10 |
| Fe+Mg+Mn | 2.96 | 2.96 | 2.99 | 2.99 | 2.99 | 2.98 | 2.97 | 3.00 | 2.90 | 3.02 |
| Fe/Fe+Mg+Mn | 85.21 | 82.87 | 83.82 | 82.93 | 83.61 | 83.05 | 84.03 | 71.33 | 71.03 | 70.86 |
| Mn/Fe+Mg+Mn | 4.50 | 4.31 | 4.66 | 4.26 | 4.21 | 4.36 | 4.44 | 20.67 | 21.03 | 21.19 |
| Mg/Fe+Mg+Mn | 10.29 | 12.82 | 11.52 | 12.80 | 12.18 | 12.59 | 11.53 | 8.00 | 7.93 | 7.95 |

*FMCM = Fe+Mg+Ca+Mn

Garnet

| | G-133-80-3 | | | | | G-133-80-3a | | |
|--------------------------------|------------|-------|--------|-------|-------|-------------|--------|-------|
| | (Rim) | (Mid) | (Core) | (Mid) | (Rim) | (Rim) | (Core) | (Rim) |
| SiO ₂ | 36.77 | 36.71 | 36.74 | 36.90 | 36.57 | 36.84 | 36.58 | 36.47 |
| TiO ₂ | 0.00 | 0.04 | 0.02 | 0.02 | 0.00 | 0.02 | 0.01 | 0.03 |
| Al ₂ O ₃ | 20.73 | 20.83 | 20.77 | 20.74 | 20.78 | 20.91 | 20.82 | 20.88 |
| Cr ₂ O ₃ | 0.00 | 0.00 | 0.00 | 0.00 | 0.00 | 0.00 | 0.00 | 0.00 |
| FeO | 36.42 | 36.21 | 35.75 | 36.24 | 36.49 | 36.36 | 36.28 | 36.66 |
| MnO | 1.68 | 1.67 | 1.66 | 1.77 | 1.77 | 1.70 | 1.69 | 1.79 |
| MgO | 2.77 | 3.08 | 3.14 | 3.14 | 2.93 | 3.05 | 3.01 | 2.71 |
| CaO | 1.09 | 1.07 | 1.07 | 1.09 | 1.07 | 1.07 | 1.06 | 1.07 |
| Na ₂ O | 0.00 | 0.00 | 0.01 | 0.02 | 0.00 | 0.00 | 0.02 | 0.00 |
| K ₂ O | 0.00 | 0.00 | 0.00 | 0.00 | 0.00 | 0.00 | 0.00 | 0.00 |
| Total | 99.46 | 99.62 | 99.17 | 99.91 | 99.62 | 99.94 | 99.48 | 99.61 |

number of cations on the basis of 12 oxygens

| | | | | | | | | |
|-------------|-------|-------|-------|-------|-------|-------|-------|-------|
| Si | 2.99 | 2.98 | 2.99 | 2.99 | 2.98 | 2.98 | 2.98 | 2.97 |
| Ti | 0.00 | 0.00 | 0.00 | 0.00 | 0.00 | 0.00 | 0.00 | 0.00 |
| Al | 1.99 | 1.99 | 1.99 | 1.98 | 1.99 | 2.00 | 2.00 | 2.01 |
| Cr | 0.00 | 0.00 | 0.00 | 0.00 | 0.00 | 0.00 | 0.00 | 0.00 |
| Fe | 2.48 | 2.46 | 2.43 | 2.45 | 2.48 | 2.46 | 2.47 | 2.50 |
| Mn | 0.12 | 0.11 | 0.11 | 0.12 | 0.12 | 0.12 | 0.12 | 0.12 |
| Mg | 0.34 | 0.37 | 0.38 | 0.38 | 0.36 | 0.37 | 0.37 | 0.33 |
| Ca | 0.10 | 0.09 | 0.09 | 0.09 | 0.09 | 0.09 | 0.09 | 0.09 |
| Na | 0.00 | 0.00 | 0.00 | 0.00 | 0.00 | 0.00 | 0.00 | 0.00 |
| K | 0.00 | 0.00 | 0.00 | 0.00 | 0.00 | 0.00 | 0.00 | 0.00 |
| Total | 8.01 | 8.02 | 8.01 | 8.02 | 8.03 | 8.02 | 8.02 | 8.02 |
| Fe/FMCM* | 81.93 | 80.90 | 80.52 | 80.49 | 81.32 | 81.00 | 81.14 | 82.06 |
| Mg/FMCM* | 11.10 | 12.26 | 12.60 | 12.43 | 11.64 | 12.11 | 12.00 | 10.81 |
| Ca/FMCM* | 3.14 | 3.06 | 3.09 | 3.10 | 3.05 | 3.05 | 3.04 | 3.07 |
| Mn/FMCM* | 3.83 | 3.78 | 3.79 | 3.98 | 3.99 | 3.84 | 3.83 | 4.06 |
| Si+Al | 4.98 | 4.98 | 4.99 | 4.97 | 4.97 | 4.98 | 4.98 | 4.98 |
| Fe+Mg+Mn+Ca | 3.03 | 3.04 | 3.02 | 3.05 | 3.06 | 3.04 | 3.04 | 3.04 |
| Fe/(Fe+Mg) | 0.88 | 0.87 | 0.86 | 0.87 | 0.87 | 0.87 | 0.87 | 0.88 |
| A | 26.11 | 26.04 | 26.15 | 25.89 | 25.99 | 26.07 | 26.06 | 26.18 |
| f | 0.88 | 0.87 | 0.86 | 0.87 | 0.87 | 0.87 | 0.87 | 0.88 |
| M | 0.12 | 0.13 | 0.14 | 0.13 | 0.13 | 0.13 | 0.13 | 0.12 |
| Fe+Mg+Mn | 2.93 | 2.95 | 2.93 | 2.95 | 2.96 | 2.95 | 2.95 | 2.95 |
| Fe/Fe+Mg+Mn | 84.58 | 83.45 | 83.09 | 83.07 | 83.88 | 83.55 | 83.68 | 84.66 |
| Mn/Fe+Mg+Mn | 3.95 | 3.90 | 3.91 | 4.11 | 4.12 | 3.96 | 3.95 | 4.19 |
| Mg/Fe+Mg+Mn | 11.46 | 12.65 | 13.00 | 12.83 | 12.00 | 12.49 | 12.37 | 11.15 |

*FMCM = Fe+Mg+Ca+Mn

Garnet

| | G-133-80-4 | | | G-150-80-1 | | | | | | |
|--------------------------------|------------|--------|-------|------------|-------|-------|-------|--------|-------|-------|
| | (Rim) | (Core) | (Rim) | (Rim) | (Mid) | (Mid) | (Mid) | (Core) | (Mid) | (Mid) |
| SiO ₂ | 36.46 | 36.67 | 36.80 | 36.29 | 35.90 | 36.04 | 35.87 | 36.12 | 36.05 | 36.00 |
| TiO ₂ | 0.02 | 0.01 | 0.00 | 0.16 | 0.03 | 0.05 | 0.07 | 0.04 | 0.07 | 0.07 |
| Al ₂ O ₃ | 20.62 | 20.65 | 20.65 | 20.35 | 20.39 | 20.41 | 20.31 | 20.26 | 20.31 | 20.31 |
| Cr ₂ O ₃ | 0.00 | 0.00 | 0.00 | 0.00 | 0.00 | 0.00 | 0.00 | 0.00 | 0.00 | 0.00 |
| FeO | 36.77 | 36.03 | 36.96 | 35.22 | 30.71 | 29.53 | 27.97 | 27.79 | 27.87 | 28.87 |
| MnO | 1.90 | 1.68 | 2.05 | 5.05 | 8.88 | 10.16 | 11.67 | 11.82 | 11.57 | 10.80 |
| MgO | 2.39 | 2.90 | 2.30 | 1.80 | 1.34 | 1.29 | 1.16 | 1.13 | 1.15 | 1.14 |
| CaO | 1.11 | 1.09 | 1.07 | 0.95 | 1.41 | 1.39 | 1.41 | 1.37 | 1.33 | 1.52 |
| Na ₂ O | 0.02 | 0.00 | 0.00 | 0.00 | 0.00 | 0.03 | 0.03 | 0.02 | 0.02 | 0.01 |
| K ₂ O | 0.00 | 0.00 | 0.00 | 0.00 | 0.00 | 0.00 | 0.00 | 0.00 | 0.00 | 0.00 |
| Total | 99.28 | 99.04 | 99.83 | 99.82 | 98.67 | 98.91 | 98.50 | 98.56 | 98.36 | 98.72 |

number of cations on the basis of 12 oxygens

| | | | | | | | | | | |
|-------------|-------|-------|-------|-------|-------|-------|-------|-------|-------|-------|
| Si | 2.99 | 3.00 | 3.00 | 2.98 | 2.98 | 2.98 | 2.98 | 3.00 | 3.00 | 2.99 |
| Ti | 0.00 | 0.00 | 0.00 | 0.01 | 0.00 | 0.00 | 0.00 | 0.00 | 0.00 | 0.00 |
| Al | 1.99 | 1.99 | 1.98 | 1.97 | 1.99 | 1.99 | 1.99 | 1.98 | 1.99 | 1.99 |
| Cr | 0.00 | 0.00 | 0.00 | 0.00 | 0.00 | 0.00 | 0.00 | 0.00 | 0.00 | 0.00 |
| Fe | 2.52 | 2.46 | 2.52 | 2.42 | 2.13 | 2.04 | 1.95 | 1.93 | 1.94 | 2.00 |
| Mn | 0.13 | 0.12 | 0.14 | 0.35 | 0.62 | 0.71 | 0.82 | 0.83 | 0.81 | 0.76 |
| Mg | 0.29 | 0.35 | 0.28 | 0.22 | 0.17 | 0.16 | 0.14 | 0.14 | 0.14 | 0.14 |
| Ca | 0.10 | 0.10 | 0.09 | 0.08 | 0.13 | 0.12 | 0.13 | 0.12 | 0.12 | 0.14 |
| Na | 0.00 | 0.00 | 0.00 | 0.00 | 0.00 | 0.00 | 0.00 | 0.00 | 0.00 | 0.00 |
| K | 0.00 | 0.00 | 0.00 | 0.00 | 0.00 | 0.00 | 0.00 | 0.00 | 0.00 | 0.00 |
| Total | 8.02 | 8.01 | 8.01 | 8.03 | 8.02 | 8.02 | 8.02 | 8.01 | 8.01 | 8.02 |
| Fe/FMCM* | 82.86 | 81.34 | 83.05 | 78.69 | 69.96 | 67.27 | 64.06 | 63.84 | 64.30 | 65.93 |
| Mg/FMCM* | 9.60 | 11.67 | 9.21 | 7.17 | 5.44 | 5.24 | 4.73 | 4.63 | 4.73 | 4.64 |
| Ca/FMCM* | 3.20 | 3.15 | 3.08 | 2.72 | 4.12 | 4.06 | 4.14 | 4.03 | 3.93 | 4.45 |
| Mn/FMCM* | 4.34 | 3.84 | 4.67 | 11.43 | 20.49 | 23.44 | 27.07 | 27.50 | 27.04 | 24.98 |
| Si+Al | 4.98 | 4.98 | 4.98 | 4.95 | 4.97 | 4.97 | 4.97 | 4.98 | 4.99 | 4.97 |
| Fe+Mg+Mn+Ca | 3.04 | 3.03 | 3.03 | 3.07 | 3.05 | 3.04 | 3.04 | 3.02 | 3.01 | 3.04 |
| Fe/(Fe+Mg) | 0.90 | 0.87 | 0.90 | 0.92 | 0.93 | 0.93 | 0.93 | 0.93 | 0.93 | 0.93 |
| A | 26.16 | 26.11 | 26.17 | 27.18 | 30.28 | 31.13 | 32.28 | 32.39 | 32.36 | 31.66 |
| F | 0.90 | 0.87 | 0.90 | 0.92 | 0.93 | 0.93 | 0.93 | 0.93 | 0.93 | 0.93 |
| M | 0.10 | 0.13 | 0.10 | 0.08 | 0.07 | 0.07 | 0.07 | 0.07 | 0.07 | 0.07 |
| Fe+Mg+Mn | 2.94 | 2.93 | 2.94 | 2.99 | 2.92 | 2.92 | 2.91 | 2.90 | 2.89 | 2.90 |
| Fe/Fe+Mg+Mn | 85.60 | 83.99 | 85.68 | 80.89 | 72.96 | 70.11 | 66.82 | 66.52 | 66.73 | 67.00 |
| Mn/Fe+Mg+Mn | 4.48 | 3.97 | 4.81 | 11.75 | 21.37 | 24.43 | 28.24 | 28.66 | 28.14 | 24.14 |
| Mg/Fe+Mg+Mn | 9.92 | 12.05 | 9.50 | 7.37 | 5.67 | 5.46 | 4.94 | 4.82 | 4.92 | 4.86 |

*FMCM = Fe+Mg+Ca+Mn

Garnet

| | G-150-80-1 | | G-158-80-4 | | | | G-150-80-4 | | | |
|--------------------------------|------------|-------|------------|-------|-------|--------|------------|-------|-------|--------|
| | (Mid) | (Rim) | (Rim) | (Mid) | (Mid) | (Core) | (Rim) | (Mid) | (Mid) | (Core) |
| SiO ₂ | 36.02 | 36.27 | 36.01 | 36.20 | 36.05 | 36.05 | 36.19 | 35.95 | 35.68 | 35.75 |
| TiO ₂ | 0.05 | 0.03 | 0.02 | 0.06 | 0.03 | 0.05 | 0.04 | 0.06 | 0.06 | 0.09 |
| Al ₂ O ₃ | 20.56 | 20.50 | 20.36 | 20.33 | 20.41 | 20.32 | 20.63 | 20.44 | 20.44 | 20.48 |
| Cr ₂ O ₃ | 0.00 | 0.00 | 0.00 | 0.00 | 0.00 | 0.00 | 0.00 | 0.00 | 0.00 | 0.00 |
| FeO | 30.60 | 33.70 | 34.11 | 33.39 | 33.08 | 33.16 | 31.88 | 29.85 | 28.76 | 27.90 |
| MnO | 8.43 | 5.50 | 4.38 | 4.96 | 5.39 | 5.41 | 6.71 | 9.07 | 10.86 | 11.13 |
| MgO | 1.34 | 1.70 | 2.29 | 2.36 | 2.23 | 2.19 | 1.93 | 1.71 | 1.52 | 1.45 |
| CaO | 1.45 | 1.40 | 1.48 | 1.47 | 1.54 | 1.51 | 1.66 | 1.51 | 1.40 | 1.45 |
| Na ₂ O | 0.05 | 0.00 | 0.03 | 0.01 | 0.03 | 0.03 | 0.50 | 0.00 | 0.03 | 0.02 |
| K ₂ O | 0.00 | 0.00 | 0.00 | 0.00 | 0.00 | 0.00 | 0.00 | 0.00 | 0.00 | 0.00 |
| Total | 98.50 | 99.10 | 98.67 | 98.78 | 98.76 | 98.72 | 99.10 | 98.59 | 98.75 | 98.28 |

number of cations on the basis of 12 oxygens

| | | | | | | | | | | |
|-------------|-------|-------|-------|-------|-------|-------|-------|-------|-------|-------|
| Si | 2.98 | 2.99 | 2.97 | 2.98 | 2.97 | 2.98 | 2.97 | 2.98 | 2.96 | 2.97 |
| Ti | 0.00 | 0.00 | 0.00 | 0.00 | 0.00 | 0.00 | 0.00 | 0.00 | 0.00 | 0.01 |
| Al | 2.01 | 1.99 | 1.98 | 1.97 | 1.98 | 1.98 | 2.00 | 1.99 | 2.00 | 2.01 |
| Cr | 0.00 | 0.00 | 0.00 | 0.00 | 0.00 | 0.00 | 0.00 | 0.00 | 0.00 | 0.00 |
| Fe | 2.12 | 2.32 | 2.36 | 2.30 | 2.28 | 2.29 | 2.19 | 2.07 | 2.00 | 1.94 |
| Mn | 0.59 | 0.38 | 0.31 | 0.35 | 0.38 | 0.38 | 0.47 | 0.64 | 0.76 | 0.78 |
| Mg | 0.17 | 0.21 | 0.28 | 0.29 | 0.27 | 0.27 | 0.24 | 0.21 | 0.19 | 0.18 |
| Ca | 0.13 | 0.12 | 0.13 | 0.13 | 0.14 | 0.13 | 0.15 | 0.13 | 0.12 | 0.13 |
| Na | 0.01 | 0.00 | 0.00 | 0.00 | 0.00 | 0.00 | 0.00 | 0.00 | 0.00 | 0.00 |
| K | 0.00 | 0.00 | 0.00 | 0.00 | 0.00 | 0.00 | 0.00 | 0.00 | 0.00 | 0.00 |
| Total | 8.01 | 8.02 | 8.04 | 8.03 | 8.03 | 8.03 | 8.02 | 8.02 | 8.04 | 8.02 |
| Fe/FMCM* | 70.53 | 76.43 | 76.61 | 75.03 | 74.36 | 74.56 | 71.91 | 67.81 | 64.98 | 63.97 |
| Mg/FMCM* | 5.50 | 6.87 | 9.17 | 9.45 | 8.93 | 8.77 | 7.96 | 6.92 | 6.12 | 5.92 |
| Ca/FMCM* | 4.28 | 4.07 | 4.26 | 4.23 | 4.44 | 4.35 | 4.80 | 4.40 | 4.05 | 4.26 |
| Mn/FMCM* | 19.68 | 12.63 | 9.96 | 11.29 | 12.27 | 12.32 | 15.33 | 20.87 | 24.85 | 25.85 |
| Si+Al | 4.99 | 4.98 | 4.96 | 4.96 | 4.96 | 4.95 | 4.97 | 4.97 | 4.96 | 4.98 |
| Fe+Mg+Mn+Ca | 3.01 | 3.04 | 3.07 | 3.07 | 3.07 | 3.07 | 3.05 | 3.05 | 3.07 | 3.03 |
| Fe/(Fe+Mg) | 0.93 | 0.92 | 0.89 | 0.89 | 0.89 | 0.89 | 0.90 | 0.91 | 0.91 | 0.92 |
| A | 30.52 | 28.23 | 27.31 | 27.60 | 27.97 | 27.87 | 29.11 | 30.46 | 31.40 | 32.14 |
| F | 0.93 | 0.92 | 0.89 | 0.89 | 0.89 | 0.89 | 0.90 | 0.91 | 0.91 | 0.92 |
| M | 0.07 | 0.08 | 0.11 | 0.11 | 0.11 | 0.11 | 0.10 | 0.09 | 0.09 | 0.08 |
| Fe+Mg+Mn | 2.88 | 2.91 | 2.94 | 2.94 | 2.93 | 2.94 | 2.90 | 2.91 | 2.95 | 2.90 |
| Fe/Fe+Mg+Mn | 73.69 | 79.67 | 80.02 | 78.35 | 77.81 | 77.95 | 75.54 | 70.93 | 67.72 | 66.82 |
| Mn/Fe+Mg+Mn | 20.56 | 13.17 | 10.41 | 11.79 | 12.84 | 12.88 | 16.10 | 21.83 | 25.90 | 27.00 |
| Mg/Fe+Mg+Mn | 5.75 | 7.16 | 9.57 | 9.87 | 9.35 | 9.17 | 8.36 | 7.24 | 6.38 | 6.19 |

*FMCM = Fe+Mg+Ca+Mn

Garnet

| | G-150-80-4 | | | | G-158-80-7 | | SD 89-552-2 | | | |
|--------------------------------|------------|-------|-------|-------|------------|--------|-------------|-------|-------|-------|
| | (Mid) | (Mid) | (Rim) | (Rim) | (Mid) | (Core) | (Mid) | (Rim) | (Mid) | (Mid) |
| SiO ₂ | 35.90 | 36.08 | 36.08 | 36.07 | 35.94 | 36.05 | 36.05 | 36.13 | 35.89 | 35.99 |
| TiO ₂ | 0.06 | 0.04 | 0.04 | 0.09 | 0.05 | 0.09 | 0.04 | 0.04 | 0.04 | 0.03 |
| Al ₂ O ₃ | 20.49 | 20.44 | 20.62 | 20.40 | 20.29 | 20.46 | 20.40 | 20.49 | 20.64 | 20.51 |
| Cr ₂ O ₃ | 0.00 | 0.00 | 0.00 | 0.00 | 0.00 | 0.00 | 0.00 | 0.00 | 0.00 | 0.00 |
| FeO | 28.75 | 30.82 | 33.54 | 34.03 | 33.75 | 33.06 | 33.20 | 33.66 | 32.96 | 33.11 |
| MnO | 9.99 | 8.71 | 5.28 | 4.55 | 4.81 | 5.08 | 4.96 | 5.17 | 5.93 | 5.99 |
| MgO | 1.54 | 1.66 | 2.12 | 2.27 | 2.37 | 2.29 | 2.30 | 2.47 | 2.50 | 2.36 |
| CaO | 1.46 | 1.46 | 1.39 | 1.43 | 1.47 | 1.61 | 1.47 | 1.51 | 1.63 | 1.61 |
| Na ₂ O | 0.04 | 0.02 | 0.00 | 0.02 | 0.03 | 0.03 | 0.01 | 0.00 | 0.02 | 0.04 |
| K ₂ O | 0.00 | 0.00 | 0.00 | 0.00 | 0.00 | 0.00 | 0.00 | 0.00 | 0.00 | 0.00 |
| Total | 98.23 | 99.22 | 99.08 | 98.86 | 98.70 | 98.67 | 98.45 | 99.47 | 99.59 | 98.44 |

number of cations on the basis of 12 oxygens

| | | | | | | | | | | |
|-------------|-------|-------|-------|-------|-------|-------|-------|-------|-------|-------|
| Si | 2.98 | 2.97 | 2.97 | 2.97 | 2.97 | 2.97 | 2.98 | 2.96 | 2.94 | 3.14 |
| Ti | 0.00 | 0.00 | 0.00 | 0.01 | 0.00 | 0.01 | 0.00 | 0.00 | 0.00 | 0.00 |
| Al | 2.01 | 1.99 | 2.00 | 1.98 | 1.98 | 1.99 | 1.99 | 1.98 | 1.99 | 2.09 |
| Cr | 0.00 | 0.00 | 0.00 | 0.00 | 0.00 | 0.00 | 0.00 | 0.00 | 0.00 | 0.00 |
| Fe | 2.00 | 2.12 | 2.31 | 2.35 | 2.33 | 2.28 | 2.29 | 2.31 | 2.26 | 1.69 |
| Mn | 0.70 | 0.61 | 0.37 | 0.32 | 0.34 | 0.35 | 0.35 | 0.36 | 0.41 | 0.64 |
| Mg | 0.19 | 0.20 | 0.26 | 0.28 | 0.29 | 0.28 | 0.28 | 0.30 | 0.31 | 0.31 |
| Ca | 0.13 | 0.13 | 0.12 | 0.13 | 0.13 | 0.14 | 0.13 | 0.13 | 0.14 | 0.15 |
| Na | 0.01 | 0.00 | 0.00 | 0.00 | 0.00 | 0.00 | 0.00 | 0.00 | 0.00 | 0.01 |
| K | 0.00 | 0.00 | 0.00 | 0.00 | 0.00 | 0.00 | 0.00 | 0.00 | 0.00 | 0.00 |
| Total | 8.02 | 8.03 | 8.03 | 8.03 | 8.04 | 8.03 | 8.03 | 8.05 | 8.06 | 7.82 |
| Fe/FMCM* | 66.12 | 69.30 | 75.46 | 76.45 | 75.46 | 74.55 | 75.10 | 74.42 | 72.64 | 65.20 |
| Mg/FMCM* | 6.31 | 6.65 | 8.50 | 9.09 | 9.44 | 9.20 | 9.27 | 9.73 | 9.79 | 11.86 |
| Ca/FMCM* | 4.30 | 4.21 | 4.01 | 4.12 | 4.21 | 4.65 | 4.26 | 4.28 | 4.56 | 5.82 |
| Mn/FMCM* | 23.27 | 19.84 | 12.03 | 10.35 | 10.89 | 11.60 | 11.36 | 11.58 | 13.20 | 17.12 |
| Si+Al | 4.99 | 4.96 | 4.97 | 4.95 | 4.94 | 4.96 | 4.97 | 4.94 | 4.94 | 5.23 |
| Fe+Mg+Mn+Ca | 3.02 | 3.07 | 3.06 | 3.07 | 3.09 | 3.06 | 3.06 | 3.10 | 3.12 | 2.58 |
| Fe/(Fe+Mg) | 0.91 | 0.91 | 0.90 | 0.89 | 0.89 | 0.89 | 0.89 | 0.88 | 0.88 | 0.85 |
| A | 31.44 | 29.90 | 28.03 | 27.41 | 27.36 | 27.97 | 27.82 | 27.51 | 28.00 | 34.39 |
| F | 0.91 | 0.91 | 0.90 | 0.89 | 0.89 | 0.89 | 0.89 | 0.88 | 0.88 | 0.85 |
| M | 0.09 | 0.09 | 0.10 | 0.11 | 0.11 | 0.11 | 0.11 | 0.12 | 0.12 | 0.15 |
| Fe+Mg+Mn | 2.89 | 2.94 | 2.94 | 2.94 | 2.96 | 2.92 | 2.92 | 2.97 | 2.98 | 2.43 |
| Fe/Fe+Mg+Mn | 69.09 | 72.35 | 78.61 | 79.73 | 78.77 | 78.18 | 78.45 | 77.74 | 75.91 | 69.23 |
| Mn/Fe+Mg+Mn | 24.32 | 20.71 | 12.53 | 10.80 | 11.37 | 12.17 | 11.87 | 12.09 | 13.83 | 18.17 |
| Mg/Fe+Mg+Mn | 6.59 | 6.94 | 8.85 | 9.48 | 9.86 | 9.65 | 9.68 | 10.17 | 10.26 | 12.60 |

*FMCM = Fe+Mg+Ca+Mn

Garnet

| | SD-89-352-2 | | | | | | SD-89-103-1 | | | |
|--------------------------------|-------------|-------|-------|-------|-------|-------|-------------|--------|--------|-------|
| | (Core) | (Mid) | (Mid) | (Rim) | (Rim) | (Mid) | (Mid) | (Mid) | (Core) | (Mid) |
| SiO ₂ | 36.05 | 36.04 | 35.99 | 36.00 | 36.16 | 36.03 | 35.97 | 36.31 | 36.15 | 36.06 |
| TiO ₂ | 0.03 | 0.06 | 0.03 | 0.07 | 0.04 | 0.09 | 0.06 | 0.08 | 0.08 | 0.05 |
| Al ₂ O ₃ | 20.25 | 20.42 | 20.42 | 20.30 | 20.47 | 20.57 | 20.70 | 20.71 | 20.62 | 20.39 |
| Cr ₂ O ₃ | 0.00 | 0.00 | 0.00 | 0.00 | 0.00 | 0.00 | 0.00 | 0.00 | 0.00 | 0.00 |
| FeO | 32.19 | 32.46 | 32.78 | 33.62 | 32.67 | 32.60 | 32.10 | 32.45 | 32.38 | 32.24 |
| MnO | 6.22 | 5.95 | 5.72 | 5.15 | 7.14 | 6.75 | 7.00 | 7.15 | 7.01 | 6.66 |
| MgO | 2.04 | 2.20 | 2.09 | 2.18 | 2.00 | 2.14 | 2.16 | 2.17 | 2.09 | 2.18 |
| CaO | 1.70 | 1.58 | 1.53 | 1.53 | 1.05 | 1.15 | 1.21 | 1.26 | 1.21 | 1.23 |
| Na ₂ O | 0.04 | 0.03 | 0.03 | 0.01 | 0.03 | 0.01 | 0.02 | 0.02 | 0.05 | 0.03 |
| K ₂ O | 0.00 | 0.00 | 0.00 | 0.00 | 0.00 | 0.00 | 0.00 | 0.00 | 0.00 | 0.00 |
| Total | 98.50 | 98.75 | 98.59 | 98.87 | 99.56 | 99.33 | 99.21 | 100.14 | 99.59 | 98.86 |

number of cations on the basis of 12 oxygens

| | | | | | | | | | | |
|-------------|-------|-------|-------|-------|-------|-------|-------|-------|-------|-------|
| Si | 2.98 | 2.97 | 2.97 | 2.97 | 2.97 | 2.96 | 2.96 | 2.96 | 2.96 | 2.97 |
| Ti | 0.00 | 0.00 | 0.00 | 0.00 | 0.00 | 0.01 | 0.00 | 0.00 | 0.00 | 0.00 |
| Al | 1.98 | 1.99 | 1.99 | 1.98 | 1.98 | 1.99 | 2.01 | 1.99 | 1.99 | 1.98 |
| Cr | 0.00 | 0.00 | 0.00 | 0.00 | 0.00 | 0.00 | 0.00 | 0.00 | 0.00 | 0.00 |
| Fe | 2.23 | 2.24 | 2.27 | 2.32 | 2.24 | 2.24 | 2.21 | 2.21 | 2.22 | 2.22 |
| Mn | 0.44 | 0.42 | 0.40 | 0.36 | 0.50 | 0.47 | 0.49 | 0.49 | 0.49 | 0.47 |
| Mg | 0.25 | 0.27 | 0.26 | 0.27 | 0.24 | 0.26 | 0.26 | 0.26 | 0.26 | 0.27 |
| Ca | 0.15 | 0.14 | 0.14 | 0.14 | 0.09 | 0.10 | 0.11 | 0.11 | 0.11 | 0.11 |
| Na | 0.01 | 0.00 | 0.00 | 0.00 | 0.00 | 0.00 | 0.00 | 0.00 | 0.01 | 0.00 |
| K | 0.00 | 0.00 | 0.00 | 0.00 | 0.00 | 0.00 | 0.00 | 0.00 | 0.00 | 0.00 |
| Total | 8.03 | 8.03 | 8.03 | 8.04 | 8.04 | 8.04 | 8.04 | 8.04 | 8.04 | 8.03 |
| Fe/FMCM* | 72.66 | 73.06 | 74.07 | 75.24 | 72.91 | 72.89 | 71.99 | 71.84 | 72.35 | 72.54 |
| Mg/FMCM* | 8.21 | 8.82 | 8.42 | 8.69 | 7.95 | 8.53 | 8.63 | 8.56 | 8.32 | 8.74 |
| Ca/FMCM* | 4.92 | 4.56 | 4.43 | 4.39 | 3.00 | 3.29 | 3.48 | 3.57 | 3.46 | 3.55 |
| Mn/FMCM* | 14.22 | 13.56 | 13.09 | 11.67 | 16.14 | 15.29 | 15.90 | 16.03 | 15.86 | 15.18 |
| Si+Al | 4.96 | 4.96 | 4.96 | 4.95 | 4.95 | 4.96 | 4.96 | 4.95 | 4.96 | 4.96 |
| Fe+Mg+Mn+Ca | 3.07 | 3.07 | 3.06 | 3.08 | 3.08 | 3.07 | 3.07 | 3.08 | 3.07 | 3.07 |
| Fe/(Fe+Mg) | 0.90 | 0.89 | 0.90 | 0.90 | 0.90 | 0.90 | 0.89 | 0.89 | 0.90 | 0.89 |
| A | 28.49 | 28.35 | 28.28 | 27.61 | 28.48 | 28.48 | 28.87 | 28.67 | 28.70 | 28.46 |
| F | 0.90 | 0.89 | 0.90 | 0.90 | 0.90 | 0.90 | 0.89 | 0.89 | 0.90 | 0.89 |
| M | 0.10 | 0.11 | 0.10 | 0.10 | 0.10 | 0.10 | 0.11 | 0.11 | 0.10 | 0.11 |
| Fe+Mg+Mn | 2.91 | 2.93 | 2.92 | 2.95 | 2.99 | 2.97 | 2.96 | 2.97 | 2.96 | 2.96 |
| Fe/Fe+Mg+Mn | 76.42 | 76.54 | 77.50 | 78.70 | 75.16 | 75.38 | 74.58 | 74.50 | 74.95 | 75.20 |
| Mn/Fe+Mg+Mn | 14.95 | 14.21 | 13.70 | 12.21 | 16.64 | 15.81 | 16.47 | 16.63 | 16.43 | 15.73 |
| Mg/Fe+Mg+Mn | 8.63 | 9.24 | 8.81 | 9.09 | 8.20 | 8.82 | 8.94 | 8.88 | 8.62 | 9.06 |

*FMCM = Fe+Mg+Ca+Mn

Garnet

| | SD-89-103-1 | | | | SD-89-097a-5 | | | | | |
|--------------------------------|-------------|-------|-------|-------|--------------|-------|--------|-------|--------|--------|
| | (Mid) | (Mid) | (Rim) | (Rim) | (Mid) | (Mid) | (Core) | (Mid) | (Mid) | (Rim) |
| SiO ₂ | 35.90 | 35.93 | 36.00 | 36.16 | 36.51 | 36.39 | 36.28 | 36.47 | 36.43 | 36.19 |
| TiO ₂ | 0.06 | 0.05 | 0.04 | 0.04 | 0.03 | 0.02 | 0.04 | 0.03 | 0.03 | 0.05 |
| Al ₂ O ₃ | 20.63 | 20.53 | 20.52 | 20.56 | 20.69 | 20.73 | 20.67 | 20.58 | 20.63 | 20.74 |
| Cr ₂ O ₃ | 0.00 | 0.00 | 0.00 | 0.00 | 0.00 | 0.00 | 0.00 | 0.00 | 0.00 | 0.00 |
| FeO | 32.40 | 32.80 | 33.21 | 31.07 | 31.67 | 30.93 | 31.44 | 31.05 | 31.45 | 31.73 |
| MnO | 6.99 | 6.74 | 7.04 | 8.88 | 8.08 | 7.77 | 7.75 | 8.01 | 8.22 | 9.16 |
| MgO | 2.11 | 2.02 | 1.76 | 1.43 | 1.90 | 1.99 | 1.92 | 1.89 | 1.85 | 1.50 |
| CaO | 1.13 | 1.12 | 0.87 | 0.91 | 1.31 | 1.40 | 1.29 | 1.28 | 1.21 | 0.95 |
| Na ₂ O | 0.02 | 0.03 | 0.06 | 0.03 | 0.02 | 0.01 | 0.03 | 0.03 | 0.04 | 0.00 |
| K ₂ O | 0.00 | 0.00 | 0.00 | 0.00 | 0.00 | 0.00 | 0.00 | 0.00 | 0.00 | 0.00 |
| Total | 99.24 | 99.22 | 99.49 | 99.08 | 100.20 | 99.24 | 99.41 | 99.35 | 100.04 | 100.11 |

number of cations on the basis of 12 oxygens

| | | | | | | | | | | |
|-------------|-------|-------|-------|-------|-------|-------|-------|-------|-------|-------|
| Si | 2.96 | 2.96 | 2.97 | 2.98 | 2.98 | 2.98 | 2.98 | 2.99 | 2.98 | 2.97 |
| Ti | 0.00 | 0.00 | 0.00 | 0.00 | 0.00 | 0.00 | 0.00 | 0.00 | 0.00 | 0.00 |
| Al | 2.00 | 1.99 | 1.99 | 2.00 | 1.99 | 2.00 | 2.00 | 1.99 | 1.99 | 2.00 |
| Cr | 0.00 | 0.00 | 0.00 | 0.00 | 0.00 | 0.00 | 0.00 | 0.00 | 0.00 | 0.00 |
| Fe | 2.23 | 2.26 | 2.29 | 2.14 | 2.16 | 2.12 | 2.16 | 2.13 | 2.15 | 2.18 |
| Mn | 0.49 | 0.47 | 0.49 | 0.62 | 0.56 | 0.54 | 0.54 | 0.56 | 0.57 | 0.64 |
| Mg | 0.26 | 0.25 | 0.22 | 0.18 | 0.23 | 0.24 | 0.23 | 0.23 | 0.22 | 0.16 |
| Ca | 0.10 | 0.10 | 0.08 | 0.08 | 0.11 | 0.12 | 0.11 | 0.11 | 0.11 | 0.08 |
| Na | 0.00 | 0.00 | 0.01 | 0.00 | 0.00 | 0.00 | 0.00 | 0.00 | 0.01 | 0.00 |
| K | 0.00 | 0.00 | 0.00 | 0.00 | 0.00 | 0.00 | 0.00 | 0.00 | 0.00 | 0.00 |
| Total | 8.04 | 8.04 | 8.04 | 8.01 | 8.03 | 8.01 | 8.02 | 8.02 | 8.03 | 8.03 |
| Fe/FMCM* | 72.50 | 73.44 | 74.48 | 70.97 | 70.51 | 70.07 | 70.87 | 70.50 | 70.54 | 71.38 |
| Mg/FMCM* | 8.41 | 8.05 | 7.03 | 5.82 | 7.54 | 8.03 | 7.71 | 7.62 | 7.51 | 5.20 |
| Ca/FMCM* | 3.24 | 3.21 | 2.50 | 2.66 | 3.74 | 4.06 | 3.73 | 3.71 | 3.68 | 2.65 |
| Mn/FMCM* | 15.84 | 15.29 | 15.99 | 20.54 | 18.22 | 17.83 | 17.69 | 18.57 | 18.67 | 20.84 |
| Si+Al | 4.96 | 4.96 | 4.96 | 4.99 | 4.96 | 4.99 | 4.97 | 4.98 | 4.97 | 4.97 |
| Fe+Mg+Mn+Ca | 3.08 | 3.08 | 3.07 | 3.02 | 3.06 | 3.03 | 3.04 | 3.03 | 3.05 | 3.05 |
| Fe/(Fe+Mg) | 0.90 | 0.90 | 0.91 | 0.92 | 0.90 | 0.90 | 0.90 | 0.90 | 0.91 | 0.93 |
| A | 28.68 | 28.45 | 28.47 | 30.12 | 29.38 | 29.77 | 29.47 | 29.65 | 29.52 | 30.04 |
| F | 0.90 | 0.90 | 0.91 | 0.92 | 0.90 | 0.90 | 0.90 | 0.90 | 0.91 | 0.93 |
| M | 0.10 | 0.10 | 0.09 | 0.08 | 0.10 | 0.10 | 0.10 | 0.10 | 0.09 | 0.07 |
| Fe+Mg+Mn | 2.98 | 2.98 | 2.99 | 2.94 | 2.95 | 2.90 | 2.93 | 2.92 | 2.94 | 2.97 |
| Fe/Fe+Mg+Mn | 74.93 | 75.88 | 76.39 | 72.91 | 73.24 | 73.04 | 73.61 | 73.01 | 73.08 | 73.24 |
| Mn/Fe+Mg+Mn | 16.37 | 15.79 | 16.40 | 21.11 | 18.93 | 18.58 | 18.38 | 19.08 | 19.35 | 21.41 |
| Mg/Fe+Mg+Mn | 8.70 | 8.33 | 7.21 | 5.98 | 7.83 | 8.37 | 8.01 | 7.97 | 7.58 | 5.35 |

*FMCM = Fe+Mg+Ca+Mn

Garnet

SD-89-097a-4

| | (Rim) | (Mid) | (Mid) | (Core) | (Mid) | (Mid) | (Rim) |
|--------------------------------|-------|-------|-------|--------|--------|-------|--------|
| SiO ₂ | 36.32 | 36.43 | 36.24 | 36.43 | 36.60 | 36.46 | 36.60 |
| TiO ₂ | 0.03 | 0.03 | 0.02 | 0.03 | 0.01 | 0.04 | 0.01 |
| Al ₂ O ₃ | 20.77 | 20.79 | 20.73 | 20.48 | 20.83 | 20.71 | 20.87 |
| Cr ₂ O ₃ | 0.00 | 0.00 | 0.00 | 0.00 | 0.00 | 0.00 | 0.00 |
| FeO | 31.17 | 31.53 | 31.86 | 32.56 | 32.68 | 32.02 | 32.03 |
| MnO | 6.98 | 6.65 | 6.40 | 6.31 | 6.49 | 6.71 | 6.95 |
| MgO | 1.93 | 2.01 | 2.06 | 2.09 | 2.14 | 2.09 | 2.03 |
| CaO | 1.70 | 1.80 | 1.70 | 1.66 | 1.51 | 1.48 | 1.59 |
| Na ₂ O | 0.03 | 0.02 | 0.02 | 0.02 | 0.01 | 0.01 | 0.03 |
| K ₂ O | 0.00 | 0.00 | 0.00 | 0.00 | 0.00 | 0.00 | 0.00 |
| Total | 98.92 | 99.26 | 99.03 | 99.59 | 100.28 | 99.53 | 100.10 |

number of cations on the basis of 12 oxygens

| | | | | | | | |
|---------------|-------|-------|-------|-------|-------|-------|-------|
| Si | 2.98 | 2.98 | 2.98 | 2.98 | 2.97 | 2.98 | 2.98 |
| Ti | 0.00 | 0.00 | 0.00 | 0.00 | 0.00 | 0.00 | 0.00 |
| Al | 2.01 | 2.01 | 2.01 | 1.98 | 2.00 | 2.00 | 2.00 |
| Cr | 0.00 | 0.00 | 0.00 | 0.00 | 0.00 | 0.00 | 0.00 |
| Fe | 2.14 | 2.16 | 2.19 | 2.23 | 2.22 | 2.19 | 2.18 |
| Mn | 0.49 | 0.46 | 0.45 | 0.44 | 0.45 | 0.46 | 0.48 |
| Mg | 0.24 | 0.25 | 0.25 | 0.25 | 0.26 | 0.25 | 0.25 |
| Ca | 0.15 | 0.16 | 0.15 | 0.15 | 0.13 | 0.13 | 0.14 |
| Na | 0.00 | 0.00 | 0.00 | 0.00 | 0.00 | 0.00 | 0.00 |
| K | 0.00 | 0.00 | 0.00 | 0.00 | 0.00 | 0.00 | 0.00 |
| Total | 8.01 | 8.02 | 8.02 | 8.03 | 8.03 | 8.02 | 8.02 |
| Fe/FMCM* | 71.07 | 71.41 | 72.10 | 72.68 | 72.62 | 72.06 | 71.62 |
| Mg/FMCM* | 7.84 | 8.11 | 8.31 | 8.31 | 8.47 | 8.38 | 8.09 |
| Ca/FMCM* | 4.97 | 5.22 | 4.93 | 4.75 | 4.30 | 4.27 | 4.55 |
| Mn/FMCM* | 16.12 | 15.25 | 14.67 | 14.26 | 14.61 | 15.29 | 15.74 |
| Si+Al | 4.99 | 4.99 | 4.98 | 4.96 | 4.97 | 4.98 | 4.98 |
| Fe+Mg+Mn+Ca | 3.01 | 3.02 | 3.03 | 3.07 | 3.06 | 3.04 | 3.04 |
| Fe/(Fe+Mg) | 0.90 | 0.90 | 0.90 | 0.90 | 0.90 | 0.90 | 0.90 |
| A | 29.73 | 29.44 | 29.14 | 28.46 | 28.69 | 29.00 | 29.21 |
| F | 0.90 | 0.90 | 0.90 | 0.90 | 0.90 | 0.90 | 0.90 |
| M | 0.10 | 0.10 | 0.10 | 0.10 | 0.10 | 0.10 | 0.10 |
| Fe+Mg+Mn | 2.86 | 2.86 | 2.89 | 2.92 | 2.93 | 2.91 | 2.90 |
| Fe/(Fe+Mg+Mn) | 74.79 | 75.35 | 75.83 | 76.30 | 75.88 | 75.27 | 75.04 |
| Mn/(Fe+Mg+Mn) | 16.96 | 16.10 | 15.43 | 14.98 | 15.26 | 15.98 | 16.49 |
| Mg/(Fe+Mg+Mn) | 8.25 | 8.56 | 8.74 | 8.73 | 8.85 | 8.75 | 8.47 |

*FMCM = Fe+Mg+Ca+Mn

APPENDIX B2:
Biotite Microprobe Analyses

Biotite (near)

| | F-123-79-1 | | F-123-79-4 | | G-118-80-1 | |
|--------------------------------|------------|-------|------------|-------|------------|-------|
| SiO ₂ | 34.25 | 33.89 | 34.74 | 34.08 | 34.34 | 34.10 |
| TiO ₂ | 2.48 | 2.01 | 2.68 | 2.81 | 2.94 | 1.48 |
| Al ₂ O ₃ | 19.06 | 17.73 | 19.74 | 18.69 | 19.22 | 18.67 |
| Cr ₂ O ₃ | 0.00 | 0.00 | 0.00 | 0.00 | 0.00 | 0.00 |
| FeO | 20.62 | 22.30 | 18.98 | 20.80 | 20.08 | 21.58 |
| MnO | 0.13 | 0.13 | 0.12 | 0.11 | 0.09 | 0.13 |
| MgO | 8.44 | 8.32 | 8.55 | 8.37 | 8.08 | 8.01 |
| CaO | 0.00 | 0.00 | 0.00 | 0.00 | 0.00 | 0.01 |
| Na ₂ O | 0.14 | 0.06 | 0.22 | 0.18 | 0.25 | 0.12 |
| K ₂ O | 9.63 | 8.83 | 9.81 | 9.33 | 9.35 | 9.69 |
| Total | 94.76 | 93.28 | 94.86 | 94.35 | 94.35 | 93.80 |

number of cations on the basis of 22 oxygens

| | | | | | | |
|-------------|--------|--------|--------|--------|--------|--------|
| Si | 5.30 | 5.36 | 5.32 | 5.30 | 5.31 | 5.36 |
| Ti | 0.29 | 0.24 | 0.31 | 0.33 | 0.34 | 0.18 |
| Al | 3.48 | 3.31 | 3.57 | 3.43 | 3.51 | 3.46 |
| Cr | 0.00 | 0.00 | 0.00 | 0.00 | 0.00 | 0.00 |
| Fe | 2.67 | 2.95 | 2.43 | 2.70 | 2.60 | 2.84 |
| Mn | 0.02 | 0.02 | 0.02 | 0.01 | 0.01 | 0.02 |
| Mg | 1.95 | 1.96 | 1.95 | 1.94 | 1.86 | 1.88 |
| Ca | 0.00 | 0.00 | 0.00 | 0.00 | 0.00 | 0.00 |
| Na | 0.04 | 0.02 | 0.07 | 0.05 | 0.07 | 0.04 |
| K | 1.90 | 1.78 | 1.92 | 1.85 | 1.85 | 1.94 |
| Total | 15.64 | 15.64 | 15.58 | 15.61 | 15.55 | 15.72 |
| Fe/FMCM* | 57.61 | 59.85 | 55.27 | 58.06 | 58.09 | 59.95 |
| Mg/FMCM* | 42.02 | 39.79 | 44.37 | 41.63 | 41.65 | 39.65 |
| Ca/FMCM* | 0.00 | 0.00 | 0.00 | 0.00 | 0.00 | 0.04 |
| Mn/FMCM* | 0.37 | 0.35 | 0.35 | 0.31 | 0.26 | 0.37 |
| Si+Al | 8.78 | 8.67 | 8.89 | 8.72 | 8.82 | 8.83 |
| Fe+Mg+Mn+Ca | 4.63 | 4.93 | 4.40 | 4.66 | 4.47 | 4.74 |
| Fe/(Fe+Mg) | 0.58 | 0.60 | 0.55 | 0.58 | 0.58 | 0.60 |
| Octa Al | 0.78 | 0.67 | 0.89 | 0.72 | 0.82 | 0.83 |
| A | -31.79 | -26.20 | -33.23 | -29.69 | -29.47 | -33.58 |
| F | 0.58 | 0.60 | 0.55 | 0.58 | 0.58 | 0.60 |
| M | 0.42 | 0.40 | 0.45 | 0.42 | 0.42 | 0.40 |

*FMCM = Fe+Mg+Ca+Mn

Biotite (near)

| | G-163-80-3 | | | | G-133-80-1 | | |
|--------------------------------|------------|-------|-------|-------|------------|-------|-------|
| SiO ₂ | 33.29 | 33.49 | 33.67 | 33.34 | 34.72 | 33.61 | 34.06 |
| TiO ₂ | 2.13 | 2.19 | 2.18 | 2.29 | 2.33 | 2.64 | 2.36 |
| Al ₂ O ₃ | 19.34 | 19.54 | 19.37 | 19.75 | 19.17 | 18.72 | 18.80 |
| Cr ₂ O ₃ | 0.00 | 0.00 | 0.00 | 0.00 | 0.00 | 0.00 | 0.00 |
| FeO | 22.74 | 23.09 | 22.74 | 23.20 | 21.52 | 22.49 | 22.35 |
| MnO | 0.14 | 0.10 | 0.13 | 0.12 | 0.08 | 0.12 | 0.09 |
| MgO | 7.02 | 7.25 | 7.18 | 7.07 | 7.83 | 7.93 | 7.97 |
| CaO | 0.00 | 0.01 | 0.00 | 0.00 | 0.01 | 0.00 | 0.00 |
| Na ₂ O | 0.15 | 0.11 | 0.10 | 0.14 | 0.12 | 0.09 | 0.15 |
| K ₂ O | 8.23 | 8.22 | 8.28 | 8.29 | 9.25 | 8.21 | 8.87 |
| Total | 93.04 | 94.01 | 93.66 | 94.21 | 95.03 | 93.81 | 94.64 |

number of cations on the basis of 22 oxygens

| | | | | | | | |
|--------------|--------|--------|--------|--------|--------|--------|--------|
| Si | 5.27 | 5.25 | 5.29 | 5.22 | 5.36 | 5.27 | 5.30 |
| Ti | 0.25 | 0.26 | 0.26 | 0.27 | 0.27 | 0.31 | 0.28 |
| Al | 3.61 | 3.61 | 3.59 | 3.65 | 3.49 | 3.46 | 3.45 |
| Cr | 0.00 | 0.00 | 0.00 | 0.00 | 0.00 | 0.00 | 0.00 |
| Fe | 3.01 | 3.03 | 2.99 | 3.04 | 2.78 | 2.95 | 2.91 |
| Mn | 0.02 | 0.01 | 0.02 | 0.02 | 0.01 | 0.02 | 0.01 |
| Mg | 1.66 | 1.69 | 1.68 | 1.65 | 1.80 | 1.85 | 1.85 |
| Ca | 0.00 | 0.00 | 0.00 | 0.00 | 0.00 | 0.00 | 0.00 |
| Na | 0.05 | 0.03 | 0.03 | 0.04 | 0.04 | 0.03 | 0.05 |
| K | 1.66 | 1.64 | 1.66 | 1.66 | 1.82 | 1.64 | 1.76 |
| Total | 15.53 | 15.53 | 15.51 | 15.54 | 15.56 | 15.53 | 15.60 |
| Fe/FMCM* | 64.25 | 63.92 | 63.76 | 64.59 | 60.51 | 61.21 | 60.99 |
| Mg/FMCM* | 35.35 | 35.76 | 35.87 | 35.07 | 39.23 | 38.46 | 38.76 |
| Ca/FMCM* | 0.00 | 0.04 | 0.00 | 0.00 | 0.04 | 0.00 | 0.00 |
| Mn/FMCM* | 0.40 | 0.28 | 0.37 | 0.34 | 0.23 | 0.33 | 0.25 |
| Si+Al | 8.88 | 8.86 | 8.87 | 8.87 | 8.84 | 8.73 | 8.75 |
| Fe+Mg+Mn+Ca | 4.69 | 4.73 | 4.68 | 4.70 | 4.59 | 4.82 | 4.77 |
| Fe/(Fe+Mg) | 0.65 | 0.64 | 0.64 | 0.65 | 0.61 | 0.61 | 0.61 |
| Octahedral A | 0.88 | 0.86 | 0.87 | 0.87 | 0.84 | 0.73 | 0.75 |
| A | -17.31 | -16.26 | -17.51 | -16.42 | -27.52 | -18.02 | -23.88 |
| F | 0.65 | 0.64 | 0.64 | 0.65 | 0.61 | 0.61 | 0.61 |
| M | 0.35 | 0.36 | 0.36 | 0.35 | 0.39 | 0.39 | 0.39 |

*FMCM = Fe+Mg+Ca+Mn

Biotite (near)

| | G-133-80-4 | | | | G-150-80-1 | | | G-150-80-4 | | |
|--------------------------------|------------|-------|-------|-------|------------|-------|-------|------------|-------|-------|
| SiO ₂ | 34.56 | 34.31 | 34.27 | 33.65 | 32.95 | 33.25 | 32.98 | 33.05 | 33.97 | 33.08 |
| TiO ₂ | 2.44 | 2.01 | 2.51 | 1.42 | 1.51 | 1.46 | 1.59 | 1.44 | 1.61 | 1.48 |
| Al ₂ O ₃ | 18.90 | 19.06 | 18.59 | 19.18 | 19.24 | 19.48 | 19.67 | 19.85 | 19.31 | 19.68 |
| Cr ₂ O ₃ | 0.00 | 0.00 | 0.00 | 0.00 | 0.00 | 0.00 | 0.00 | 0.00 | 0.00 | 0.00 |
| FeO | 21.60 | 22.28 | 22.00 | 22.99 | 24.24 | 23.31 | 23.53 | 22.89 | 23.19 | 23.13 |
| MnO | 0.10 | 0.07 | 0.11 | 0.08 | 0.07 | 0.06 | 0.07 | 0.07 | 0.06 | 0.05 |
| MgO | 8.16 | 8.14 | 8.04 | 7.61 | 8.01 | 8.06 | 7.91 | 8.00 | 7.50 | 7.89 |
| CaO | 0.00 | 0.00 | 0.00 | 0.04 | 0.00 | 0.00 | 0.00 | 0.00 | 0.00 | 0.00 |
| Na ₂ O | 0.16 | 0.13 | 0.15 | 0.08 | 0.07 | 0.07 | 0.05 | 0.10 | 0.09 | 0.10 |
| K ₂ O | 9.16 | 9.07 | 9.20 | 7.70 | 7.00 | 7.38 | 7.43 | 8.10 | 7.96 | 8.34 |
| Total | 95.09 | 95.07 | 94.88 | 92.75 | 93.09 | 93.08 | 93.25 | 93.50 | 93.68 | 93.76 |

number of cations on the basis of 22 oxygens

| | | | | | | | | | | |
|--------------|--------|--------|--------|--------|-------|-------|-------|--------|--------|--------|
| Si | 5.33 | 5.31 | 5.32 | 5.33 | 5.22 | 5.24 | 5.20 | 5.20 | 5.33 | 5.21 |
| Ti | 0.28 | 0.23 | 0.29 | 0.17 | 0.18 | 0.17 | 0.19 | 0.17 | 0.19 | 0.18 |
| Al | 3.44 | 3.48 | 3.40 | 3.58 | 3.59 | 3.62 | 3.66 | 3.68 | 3.57 | 3.65 |
| Cr | 0.00 | 0.00 | 0.00 | 0.00 | 0.00 | 0.00 | 0.00 | 0.00 | 0.00 | 0.00 |
| Fe | 2.79 | 2.89 | 2.86 | 3.04 | 3.21 | 3.07 | 3.10 | 3.01 | 3.04 | 3.05 |
| Mn | 0.01 | 0.01 | 0.01 | 0.01 | 0.01 | 0.01 | 0.01 | 0.01 | 0.01 | 0.01 |
| Mg | 1.88 | 1.88 | 1.86 | 1.79 | 1.89 | 1.89 | 1.86 | 1.88 | 1.75 | 1.85 |
| Ca | 0.00 | 0.00 | 0.00 | 0.01 | 0.00 | 0.00 | 0.00 | 0.00 | 0.00 | 0.00 |
| Na | 0.05 | 0.04 | 0.05 | 0.02 | 0.02 | 0.02 | 0.02 | 0.03 | 0.03 | 0.03 |
| K | 1.80 | 1.79 | 1.82 | 1.55 | 1.41 | 1.49 | 1.50 | 1.63 | 1.59 | 1.68 |
| Total | 15.59 | 15.63 | 15.62 | 15.51 | 15.53 | 15.52 | 15.53 | 15.61 | 15.51 | 15.64 |
| Fe/FMCM* | 59.60 | 60.45 | 60.38 | 62.67 | 62.82 | 61.78 | 62.42 | 61.50 | 63.33 | 62.11 |
| Mg/FMCM* | 40.12 | 39.36 | 39.32 | 36.97 | 36.99 | 38.06 | 37.39 | 38.31 | 36.50 | 37.75 |
| Ca/FMCM* | 0.00 | 0.00 | 0.00 | 0.14 | 0.00 | 0.00 | 0.00 | 0.00 | 0.00 | 0.00 |
| Mn/FMCM* | 0.28 | 0.19 | 0.31 | 0.22 | 0.18 | 0.16 | 0.19 | 0.19 | 0.17 | 0.14 |
| Si+Al | 8.77 | 8.79 | 8.72 | 8.90 | 8.81 | 8.87 | 8.86 | 8.89 | 8.90 | 8.86 |
| Fe+Mg+Mn+Ca | 4.68 | 4.77 | 4.73 | 4.85 | 5.11 | 4.98 | 4.97 | 4.90 | 4.80 | 4.90 |
| Fe/(Fe+Mg) | 0.60 | 0.61 | 0.61 | 0.63 | 0.63 | 0.62 | 0.63 | 0.62 | 0.63 | 0.62 |
| Octahedral A | 0.77 | 0.79 | 0.72 | 0.90 | 0.81 | 0.87 | 0.86 | 0.89 | 0.90 | 0.86 |
| A | -26.80 | -24.84 | -28.01 | -12.64 | -6.81 | -9.15 | -9.10 | -13.94 | -14.41 | -16.50 |
| F | 0.60 | 0.61 | 0.61 | 0.63 | 0.63 | 0.62 | 0.63 | 0.62 | 0.63 | 0.62 |
| M | 0.40 | 0.39 | 0.39 | 0.37 | 0.37 | 0.38 | 0.37 | 0.38 | 0.37 | 0.38 |

*FMCM = Fe+Mg+Ca+Mn

Biotite (near)

| | | G-158-80-4 | | | | G-158-80-7 | | | SD-89-097a-4 | | |
|--------------------------------|-------|------------|-------|-------|-------|------------|-------|-------|--------------|-------|--|
| SiO ₂ | 33.48 | 32.58 | 31.54 | 33.86 | 31.74 | 33.29 | 33.79 | 34.71 | 34.56 | 34.89 | |
| TiO ₂ | 1.38 | 1.37 | 1.30 | 1.58 | 1.46 | 1.43 | 1.51 | 2.60 | 2.76 | 2.82 | |
| Al ₂ O ₃ | 19.97 | 18.73 | 18.85 | 19.32 | 18.91 | 18.56 | 19.23 | 20.15 | 19.68 | 19.60 | |
| Cr ₂ O ₃ | 0.00 | 0.00 | 0.00 | 0.00 | 0.00 | 0.00 | 0.00 | 0.00 | 0.00 | 0.00 | |
| FeO | 22.26 | 24.15 | 24.17 | 22.88 | 24.67 | 24.03 | 22.28 | 21.51 | 22.64 | 22.70 | |
| MnO | 0.06 | 0.06 | 0.06 | 0.04 | 0.05 | 0.07 | 0.05 | 0.22 | 0.18 | 0.22 | |
| MgO | 7.74 | 8.47 | 8.79 | 7.82 | 8.90 | 7.88 | 7.86 | 6.98 | 6.06 | 6.26 | |
| CaO | 0.02 | 0.00 | 0.06 | 0.00 | 0.00 | 0.00 | 0.00 | 0.00 | 0.01 | 0.00 | |
| Na ₂ O | 0.10 | 0.06 | 0.07 | 0.08 | 0.05 | 0.04 | 0.09 | 0.11 | 0.14 | 0.09 | |
| K ₂ O | 7.64 | 6.77 | 6.58 | 8.30 | 6.73 | 7.54 | 8.60 | 8.59 | 8.80 | 8.95 | |
| Total | 92.64 | 92.20 | 91.42 | 93.88 | 92.52 | 92.84 | 93.40 | 94.87 | 94.55 | 95.31 | |

number of cations on the basis of 22 oxygens

| | | | | | | | | | | | |
|--------------|--------|-------|-------|--------|-------|--------|-------|-------|-------|-------|--|
| Si | 5.28 | 5.21 | 5.10 | 5.30 | 5.08 | 5.30 | 5.32 | 5.34 | 5.34 | 5.38 | |
| Ti | 0.16 | 0.16 | 0.16 | 0.19 | 0.18 | 0.17 | 0.18 | 0.30 | 0.32 | 0.33 | |
| Al | 3.71 | 3.53 | 3.59 | 3.57 | 3.57 | 3.48 | 3.57 | 3.65 | 3.61 | 3.53 | |
| Cr | 0.00 | 0.00 | 0.00 | 0.00 | 0.00 | 0.00 | 0.00 | 0.00 | 0.00 | 0.00 | |
| Fe | 2.94 | 3.23 | 3.27 | 3.00 | 3.30 | 3.20 | 2.93 | 2.77 | 2.94 | 2.93 | |
| Mn | 0.01 | 0.01 | 0.01 | 0.01 | 0.01 | 0.01 | 0.01 | 0.03 | 0.02 | 0.03 | |
| Mg | 1.82 | 2.02 | 2.12 | 1.83 | 2.12 | 1.87 | 1.84 | 1.60 | 1.40 | 1.54 | |
| Ca | 0.00 | 0.00 | 0.01 | 0.00 | 0.00 | 0.00 | 0.00 | 0.00 | 0.00 | 0.00 | |
| Na | 0.03 | 0.02 | 0.02 | 0.02 | 0.02 | 0.01 | 0.03 | 0.03 | 0.04 | 0.03 | |
| K | 1.54 | 1.38 | 1.36 | 1.66 | 1.37 | 1.53 | 1.73 | 1.68 | 1.74 | 1.76 | |
| Total | 15.49 | 15.56 | 15.64 | 15.57 | 15.65 | 15.56 | 15.60 | 15.40 | 15.43 | 15.62 | |
| Fe/FMCM* | 61.60 | 61.44 | 60.47 | 62.08 | 60.79 | 63.00 | 61.31 | 62.95 | 62.51 | 66.61 | |
| Mg/FMCM* | 38.17 | 38.40 | 39.19 | 37.81 | 39.08 | 36.81 | 38.55 | 36.40 | 32.11 | 32.73 | |
| Ca/FMCM* | 0.07 | 0.00 | 0.19 | 0.00 | 0.00 | 0.00 | 0.00 | 0.00 | 0.04 | 0.00 | |
| Mn/FMCM* | 0.17 | 0.15 | 0.15 | 0.11 | 0.12 | 0.19 | 0.14 | 0.65 | 0.54 | 0.65 | |
| Si+Al | 8.99 | 8.74 | 8.69 | 8.87 | 8.65 | 8.78 | 8.88 | 8.99 | 8.66 | 8.91 | |
| Fe+Mg+Mn+Ca | 4.76 | 5.26 | 5.41 | 4.83 | 5.43 | 5.07 | 4.78 | 4.39 | 4.37 | 4.40 | |
| Fe/(Fe+Mg) | 0.62 | 0.62 | 0.61 | 0.62 | 0.61 | 0.63 | 0.61 | 0.63 | 0.68 | 0.67 | |
| Octahedral A | 0.99 | 0.74 | 0.69 | 0.87 | 0.65 | 0.78 | 0.88 | 0.99 | 0.95 | 0.91 | |
| A | -10.43 | -6.20 | -4.65 | -17.10 | -5.39 | -12.31 | 20.31 | 19.14 | 25.06 | 25.16 | |
| F | 0.62 | 0.62 | 0.61 | 0.62 | 0.61 | 0.63 | 0.61 | 0.63 | 0.68 | 0.67 | |
| M | 0.38 | 0.38 | 0.39 | 0.38 | 0.39 | 0.37 | 0.39 | 0.37 | 0.34 | 0.33 | |

*FMCM = Fe+Mg+Ca+Mn

Biotite (near)

| | | SD-89-097a-5 | | | 034e-3 | SD-89-302-2 | | 312-2 | 312-3 | 312-5 |
|--------------------------------|-------|--------------|-------|-------|--------|-------------|-------|-------|-------|-------|
| SiO ₂ | 34.67 | 34.75 | 34.06 | 34.38 | 34.45 | 34.86 | 34.84 | 34.95 | 34.64 | 34.36 |
| TiO ₂ | 2.55 | 2.37 | 2.45 | 2.90 | 1.96 | 1.75 | 1.53 | 3.31 | 3.22 | 2.82 |
| Al ₂ O ₃ | 20.06 | 19.94 | 20.39 | 18.89 | 18.98 | 17.77 | 18.06 | 19.59 | 18.93 | 18.49 |
| Cr ₂ O ₃ | 0.00 | 0.00 | 0.00 | 0.00 | 0.06 | 0.00 | 0.00 | 0.07 | 0.00 | 0.04 |
| FeO | 22.00 | 22.18 | 22.48 | 23.69 | 20.98 | 21.81 | 21.17 | 19.98 | 20.96 | 21.67 |
| MnO | 0.19 | 0.18 | 0.18 | 0.16 | 0.08 | 0.20 | 0.21 | 0.31 | 0.33 | 0.35 |
| MgO | 7.06 | 6.98 | 6.82 | 6.30 | 8.88 | 8.77 | 9.00 | 7.12 | 7.70 | 7.76 |
| CaO | 0.00 | 0.00 | 0.00 | 0.00 | 0.00 | 0.00 | 0.00 | 0.02 | 0.00 | 0.00 |
| Na ₂ O | 0.11 | 0.12 | 0.08 | 0.06 | 0.12 | 0.03 | 0.08 | 0.31 | 0.23 | 0.13 |
| K ₂ O | 8.62 | 8.69 | 8.17 | 8.58 | 9.15 | 9.66 | 9.13 | 9.10 | 9.39 | 9.29 |
| Total | 95.27 | 95.22 | 94.62 | 94.97 | 94.64 | 94.85 | 94.01 | 94.75 | 95.41 | 94.91 |

number of cations on the basis of 22 oxygens

| | | | | | | | | | | |
|--------------|--------|--------|--------|--------|--------|--------|--------|--------|--------|--------|
| Si | 5.32 | 5.34 | 5.27 | 5.35 | 5.33 | 5.42 | 5.43 | 5.37 | 5.33 | 5.33 |
| Ti | 0.29 | 0.27 | 0.28 | 0.34 | 0.23 | 0.20 | 0.18 | 0.38 | 0.37 | 0.33 |
| Al | 3.63 | 3.61 | 3.72 | 3.47 | 3.46 | 3.26 | 3.32 | 3.55 | 3.43 | 3.38 |
| Cr | 0.00 | 0.00 | 0.00 | 0.00 | 0.01 | 0.00 | 0.00 | 0.31 | 0.00 | 0.00 |
| Fe | 2.82 | 2.85 | 2.91 | 3.08 | 2.71 | 2.84 | 2.76 | 2.57 | 2.70 | 2.81 |
| Mn | 0.02 | 0.02 | 0.02 | 0.02 | 0.01 | 0.03 | 0.03 | 0.04 | 0.04 | 0.05 |
| Mg | 1.61 | 1.60 | 1.57 | 1.46 | 2.05 | 2.03 | 2.09 | 1.63 | 1.76 | 1.79 |
| Ca | 0.00 | 0.00 | 0.00 | 0.00 | 0.00 | 0.00 | 0.00 | 0.00 | 0.00 | 0.00 |
| Na | 0.03 | 0.04 | 0.02 | 0.02 | 0.04 | 0.01 | 0.02 | 0.09 | 0.07 | 0.04 |
| K | 1.69 | 1.70 | 1.61 | 1.70 | 1.80 | 1.92 | 1.82 | 1.78 | 1.84 | 1.84 |
| Total | 15.43 | 15.45 | 15.41 | 15.44 | 15.63 | 15.71 | 15.65 | 15.41 | 15.54 | 15.58 |
| Fe/FMCM* | 63.27 | 63.73 | 64.57 | 67.53 | 56.88 | 57.94 | 56.57 | 60.53 | 59.86 | 60.44 |
| Mg/FMCM* | 36.18 | 35.74 | 34.91 | 32.00 | 42.90 | 41.52 | 42.86 | 38.44 | 39.19 | 38.57 |
| Ca/FMCM* | 0.00 | 0.00 | 0.00 | 0.00 | 0.00 | 0.00 | 0.00 | 0.08 | 0.00 | 0.00 |
| Mn/FMCM* | 0.55 | 0.52 | 0.52 | 0.46 | 0.22 | 0.54 | 0.57 | 0.95 | 0.95 | 0.99 |
| Si+Al | 8.95 | 8.96 | 8.98 | 8.81 | 8.79 | 8.68 | 8.75 | 8.91 | 8.76 | 8.72 |
| Fe+Mg+Mn+Ca | 4.46 | 4.47 | 4.50 | 4.56 | 4.77 | 4.90 | 4.88 | 4.24 | 4.50 | 4.65 |
| Fe/(Fe+Mg) | 0.64 | 0.64 | 0.65 | 0.68 | 0.57 | 0.58 | 0.57 | 0.61 | 0.60 | 0.61 |
| Octahedral A | 0.95 | 0.96 | 0.98 | 0.81 | 0.79 | 0.68 | 0.75 | 0.91 | 0.76 | 0.72 |
| A | -19.26 | -20.25 | -14.26 | -22.10 | -25.85 | -34.39 | -28.10 | -27.35 | -30.69 | -30.16 |
| F | 0.64 | 0.64 | 0.65 | 0.68 | 0.57 | 0.58 | 0.57 | 0.61 | 0.60 | 0.61 |
| M | 0.36 | 0.36 | 0.35 | 0.32 | 0.43 | 0.42 | 0.43 | 0.39 | 0.40 | 0.39 |

*FMCM = Fe+Mg+Ca+Mn

Biotite (near)

| | 300-1 | 184-2 | 127-3 | 046a-1 | 127-3 | 329-4 | SD-89 | 597-2 | SD-89 | 597-2 |
|--------------------------------|-------|-------|-------|--------|-------|-------|-------|-------|-------|-------|
| SiO ₂ | 34.77 | 33.72 | 34.20 | 34.62 | 33.88 | 34.49 | 34.59 | 33.97 | 34.67 | 34.54 |
| TiO ₂ | 1.54 | 2.22 | 1.95 | 1.68 | 2.31 | 2.07 | 1.68 | 1.70 | 1.72 | 1.75 |
| Al ₂ O ₃ | 18.75 | 18.15 | 18.31 | 20.15 | 18.01 | 20.07 | 19.23 | 18.63 | 19.05 | 19.06 |
| Cr ₂ O ₃ | 0.04 | 0.03 | 0.06 | 0.04 | 0.08 | 0.00 | 0.06 | 0.09 | 0.06 | 0.05 |
| FeO | 20.45 | 23.98 | 23.28 | 22.06 | 22.70 | 22.51 | 19.70 | 20.41 | 20.06 | 20.02 |
| MnO | 0.16 | 0.32 | 0.32 | 0.05 | 0.28 | 0.38 | 0.23 | 0.19 | 0.24 | 0.25 |
| MgO | 9.28 | 7.15 | 7.87 | 7.64 | 7.45 | 7.27 | 9.65 | 9.26 | 9.52 | 9.25 |
| CaO | 0.00 | 0.00 | 0.00 | 0.02 | 0.04 | 0.00 | 0.01 | 0.05 | 0.00 | 0.09 |
| Na ₂ O | 0.13 | 0.09 | 0.13 | 0.18 | 0.16 | 0.32 | 0.11 | 0.10 | 0.16 | 0.15 |
| K ₂ O | 9.34 | 8.98 | 9.28 | 8.38 | 8.75 | 8.76 | 8.61 | 8.78 | 9.25 | 9.30 |
| Total | 94.45 | 94.64 | 95.40 | 94.83 | 93.66 | 95.86 | 93.87 | 93.19 | 94.72 | 94.60 |

number of cations on the basis of 22 oxygens

| | 300-1 | 184-2 | 127-3 | 046a-1 | 127-3 | 329-4 | SD-89 | 597-2 | SD-89 | 597-2 |
|--------------|--------|--------|--------|--------|--------|--------|-------|-------|-------|-------|
| Si | 5.38 | 5.31 | 5.32 | 5.33 | 5.35 | 5.29 | 5.34 | 5.33 | 5.34 | 5.34 |
| Ti | 0.18 | 0.26 | 0.23 | 0.19 | 0.27 | 0.24 | 0.20 | 0.20 | 0.20 | 0.20 |
| Al | 3.42 | 3.37 | 3.36 | 3.66 | 3.35 | 3.63 | 3.50 | 3.44 | 3.45 | 3.47 |
| Cr | 0.00 | 0.00 | 0.01 | 0.00 | 0.01 | 0.00 | 0.01 | 0.01 | 0.01 | 0.01 |
| Fe | 2.65 | 3.16 | 3.03 | 2.84 | 3.00 | 2.89 | 2.54 | 2.68 | 2.58 | 2.59 |
| Mn | 0.02 | 0.04 | 0.04 | 0.01 | 0.04 | 0.05 | 0.03 | 0.03 | 0.03 | 0.03 |
| Mg | 2.14 | 1.68 | 1.83 | 1.75 | 1.75 | 1.66 | 2.22 | 2.16 | 2.18 | 2.13 |
| Ca | 0.00 | 0.00 | 0.00 | 0.00 | 0.01 | 0.00 | 0.00 | 0.01 | 0.00 | 0.01 |
| Na | 0.04 | 0.03 | 0.04 | 0.05 | 0.05 | 0.10 | 0.03 | 0.03 | 0.03 | 0.04 |
| K | 1.84 | 1.80 | 1.84 | 1.65 | 1.76 | 1.71 | 1.70 | 1.76 | 1.82 | 1.83 |
| Total | 15.67 | 15.66 | 15.70 | 15.49 | 15.60 | 15.56 | 15.57 | 15.64 | 15.66 | 15.66 |
| Fe/FMCM* | 55.05 | 64.73 | 61.87 | 61.71 | 62.52 | 62.79 | 53.04 | 54.91 | 53.85 | 54.55 |
| Mg/FMCM* | 44.52 | 34.39 | 37.27 | 38.08 | 36.56 | 36.14 | 46.30 | 44.40 | 45.52 | 44.73 |
| Ca/FMCM* | 0.00 | 0.00 | 0.00 | 0.07 | 0.14 | 0.00 | 0.03 | 0.17 | 0.00 | 0.31 |
| Mn/FMCM* | 0.44 | 0.87 | 0.86 | 0.14 | 0.78 | 1.07 | 0.63 | 0.52 | 0.65 | 0.63 |
| Si+Al | 8.80 | 8.68 | 8.69 | 8.99 | 8.71 | 8.92 | 8.84 | 8.77 | 8.79 | 8.81 |
| Fe+Mg+Mn+Ca | 4.81 | 4.88 | 4.90 | 4.60 | 4.80 | 4.60 | 4.80 | 4.87 | 4.80 | 4.76 |
| Fe/(Fe+Mg) | 0.55 | 0.65 | 0.62 | 0.62 | 0.63 | 0.63 | 0.53 | 0.55 | 0.56 | 0.55 |
| Octahedral A | 0.80 | 0.68 | 0.69 | 0.99 | 0.71 | 0.92 | 0.84 | 0.77 | 0.79 | 0.81 |
| A | -28.29 | -26.78 | -28.75 | -16.20 | -25.58 | -19.95 | 19.99 | 23.24 | 26.49 | 27.38 |
| F | 0.55 | 0.65 | 0.62 | 0.62 | 0.63 | 0.63 | 0.53 | 0.55 | 0.56 | 0.55 |
| M | 0.45 | 0.35 | 0.38 | 0.38 | 0.37 | 0.37 | 0.47 | 0.45 | 0.46 | 0.45 |

*FMCM = Fe+Mg+Ca+Mn

Biotite (near)

| | 353-4 | SD-89-353-5 | SD-89-364-2 | 329-2 | G-123-80 | | |
|--------------------------------|-------|-------------|-------------|-------|----------|-------|-------|
| SiO ₂ | 33.59 | 33.26 | 33.28 | 34.10 | 34.11 | 34.43 | 35.44 |
| TiO ₂ | 1.50 | 1.69 | 1.59 | 3.01 | 3.04 | 3.01 | 2.67 |
| Al ₂ O ₃ | 19.27 | 19.06 | 18.85 | 19.70 | 19.51 | 19.24 | 18.83 |
| Cr ₂ O ₃ | 0.08 | 0.06 | 0.04 | 0.06 | 0.06 | 0.00 | 0.05 |
| FeO | 23.89 | 24.22 | 24.30 | 21.95 | 22.21 | 21.78 | 20.93 |
| MnO | 0.11 | 0.11 | 0.00 | 0.25 | 0.34 | 0.41 | 0.22 |
| MgO | 7.94 | 7.80 | 8.00 | 7.07 | 6.83 | 6.98 | 8.77 |
| CaO | 0.00 | 0.03 | 0.00 | 0.00 | 0.00 | 0.00 | 0.00 |
| Na ₂ O | 0.04 | 0.07 | 0.04 | 0.21 | 0.14 | 0.22 | 0.23 |
| K ₂ O | 7.53 | 7.33 | 7.12 | 8.48 | 8.58 | 8.94 | 9.77 |
| Total | 93.93 | 93.63 | 93.23 | 94.85 | 94.83 | 95.00 | 96.93 |

number of cations on the basis of 22 oxygens

| | | | | | | | |
|--------------|--------|-------|-------|--------|--------|--------|--------|
| Si | 5.27 | 5.24 | 5.26 | 5.27 | 5.28 | 5.32 | 5.36 |
| Ti | 0.18 | 0.20 | 0.19 | 0.35 | 0.35 | 0.35 | 0.30 |
| Al | 3.56 | 3.54 | 3.51 | 3.59 | 3.56 | 3.51 | 3.36 |
| Cr | 0.01 | 0.01 | 0.00 | 0.01 | 0.01 | 0.00 | 0.01 |
| Fe | 3.13 | 3.19 | 3.21 | 2.84 | 2.88 | 2.82 | 2.65 |
| Mn | 0.01 | 0.01 | 0.00 | 0.03 | 0.04 | 0.05 | 0.03 |
| Mg | 1.85 | 1.83 | 1.88 | 1.63 | 1.58 | 1.61 | 1.98 |
| Ca | 0.00 | 0.01 | 0.00 | 0.00 | 0.00 | 0.00 | 0.00 |
| Na | 0.01 | 0.02 | 0.01 | 0.06 | 0.04 | 0.07 | 0.07 |
| K | 1.51 | 1.47 | 1.44 | 1.67 | 1.70 | 1.76 | 1.89 |
| Total | 15.53 | 15.53 | 15.51 | 15.45 | 15.45 | 15.49 | 15.63 |
| Fe/FMCM* | 62.62 | 63.29 | 63.03 | 63.07 | 63.96 | 62.89 | 56.90 |
| Mg/FMCM* | 37.09 | 36.32 | 36.97 | 36.20 | 35.05 | 35.91 | 42.49 |
| Ca/FMCM* | 0.00 | 0.10 | 0.00 | 0.00 | 0.00 | 0.00 | 0.00 |
| Mn/FMCM* | 0.29 | 0.29 | 0.00 | 0.73 | 0.99 | 1.20 | 0.61 |
| Si+Al | 8.83 | 8.78 | 8.77 | 8.86 | 8.85 | 8.83 | 8.72 |
| Fe+Mg+Mn+Ca | 5.00 | 5.04 | 5.10 | 4.50 | 4.50 | 4.48 | 4.65 |
| Fe/(Fe+Mg) | 0.63 | 0.64 | 0.63 | 0.64 | 0.65 | 0.64 | 0.57 |
| Octahedral A | 0.83 | 0.78 | 0.77 | 0.86 | 0.85 | 0.83 | 0.72 |
| A | -10.61 | -9.60 | -8.46 | -19.01 | -20.64 | -25.24 | -33.24 |
| F | 0.63 | 0.64 | 0.63 | 0.64 | 0.65 | 0.64 | 0.57 |
| M | 0.37 | 0.36 | 0.37 | 0.36 | 0.35 | 0.36 | 0.43 |

*FMCM = Fe+Mg+Ca+Mn

Biotite (matrix)

| | G-118-80-2 | | G-163-80-1 | | G-163-80-4 | | G-163-80-7 | | G-163-80-2 | |
|--------------------------------|------------|-------|------------|-------|------------|-------|------------|-------|------------|--------|
| SiO ₂ | 33.05 | 33.98 | 33.27 | 34.03 | 33.75 | 33.56 | 33.74 | 32.71 | 33.48 | 32.74 |
| TiO ₂ | 1.37 | 1.39 | 2.21 | 2.18 | 2.29 | 2.20 | 2.24 | 1.97 | 1.97 | 1.95 |
| Al ₂ O ₃ | 18.37 | 18.48 | 19.42 | 19.82 | 19.65 | 19.28 | 19.49 | 19.53 | 19.36 | 19.30* |
| Cr ₂ O ₃ | 0.00 | 0.00 | 0.00 | 0.00 | 0.00 | 0.00 | 0.00 | 0.00 | 0.00 | 0.00 |
| FeO | 23.08 | 22.30 | 23.70 | 22.24 | 22.92 | 22.83 | 23.59 | 23.87 | 22.86 | 23.74 |
| MnO | 0.11 | 0.12 | 0.11 | 0.10 | 0.12 | 0.11 | 0.12 | 0.06 | 0.08 | 0.09 |
| MgO | 8.20 | 8.28 | 7.22 | 7.11 | 7.09 | 7.18 | 7.19 | 8.16 | 7.63 | 7.99* |
| CaO | 0.00 | 0.00 | 0.00 | 0.00 | 0.00 | 0.00 | 0.00 | 0.00 | 0.00 | 0.00 |
| Na ₂ O | 0.04 | 0.08 | 0.15 | 0.19 | 0.10 | 0.08 | 0.16 | 0.07 | 0.05 | 0.06 |
| K ₂ O | 9.34 | 9.59 | 8.29 | 8.74 | 8.47 | 8.33 | 8.12 | 7.28 | 8.16 | 7.00* |
| Total | 93.56 | 94.21 | 94.36 | 94.41 | 94.39 | 93.56 | 94.63 | 92.86 | 93.09 | 93.00* |

number of cations, on the basis of 22 oxygens.

| | | | | | | | | | | |
|-------------|--------|--------|--------|--------|--------|-------|--------|-------|-------|-------|
| Si | 5.26 | 5.34 | 5.22 | 5.29 | 5.26 | 5.28 | 5.26 | 5.18 | 5.28 | 5.19 |
| Ti | 0.16 | 0.16 | 0.26 | 0.26 | 0.27 | 0.26 | 0.26 | 0.18 | 0.19 | 0.17 |
| Al | 3.45 | 3.42 | 3.59 | 3.63 | 3.61 | 3.58 | 3.58 | 3.65 | 3.61 | 3.61 |
| Cr | 0.00 | 0.00 | 0.00 | 0.00 | 0.00 | 0.00 | 0.00 | 0.00 | 0.00 | 0.00 |
| Fe | 3.07 | 2.93 | 3.11 | 2.89 | 2.99 | 3.00 | 3.07 | 3.12 | 3.01 | 3.11 |
| Mn | 0.01 | 0.02 | 0.01 | 0.01 | 0.02 | 0.01 | 0.02 | 0.01 | 0.01 | 0.01 |
| Mg | 1.94 | 1.94 | 1.69 | 1.65 | 1.65 | 1.68 | 1.67 | 1.95 | 1.86 | 1.89* |
| Ca | 0.00 | 0.00 | 0.00 | 0.00 | 0.00 | 0.00 | 0.00 | 0.00 | 0.00 | 0.00 |
| Na | 0.01 | 0.02 | 0.05 | 0.06 | 0.03 | 0.02 | 0.05 | 0.02 | 0.02 | 0.02 |
| K | 1.90 | 1.92 | 1.66 | 1.73 | 1.69 | 1.67 | 1.61 | 1.47 | 1.64 | 1.41 |
| Total | 15.81 | 15.76 | 15.58 | 15.53 | 15.52 | 15.52 | 15.52 | 15.56 | 15.56 | 15.51 |
| Fe/FMCM* | 61.05 | 59.98 | 64.62 | 63.52 | 64.25 | 63.88 | 64.57 | 61.75 | 60.50 | 61.49 |
| Mg/FMCM* | 38.65 | 39.69 | 35.08 | 36.19 | 35.41 | 35.86 | 35.68 | 38.07 | 37.37 | 37.38 |
| Ca/FMCM* | 0.00 | 0.00 | 0.00 | 0.00 | 0.00 | 0.00 | 0.00 | 0.00 | 0.00 | 0.00 |
| Mn/FMCM* | 0.29 | 0.33 | 0.30 | 0.29 | 0.34 | 0.31 | 0.33 | 0.17 | 0.17 | 0.17 |
| Si+Al | 8.71 | 8.76 | 8.81 | 8.93 | 8.88 | 8.86 | 8.84 | 8.83 | 8.84 | 8.84 |
| Fe+Mg+Mn+Ca | 5.03 | 4.89 | 4.81 | 4.55 | 4.65 | 4.70 | 4.76 | 5.06 | 4.86 | 4.91 |
| Fe/(Fe+Mg) | 0.61 | 0.60 | 0.65 | 0.64 | 0.64 | 0.64 | 0.65 | 0.62 | 0.63 | 0.62 |
| Octa Al | 0.71 | 0.76 | 0.81 | 0.93 | 0.88 | 0.86 | 0.86 | 0.83 | 0.84 | 0.84 |
| A | -28.78 | -31.70 | -16.88 | -20.88 | -18.42 | 18.15 | -15.35 | 9.21 | 16.07 | 9.74 |
| F | 0.61 | 0.60 | 0.65 | 0.64 | 0.64 | 0.64 | 0.65 | 0.62 | 0.63 | 0.62 |
| M | 0.39 | 0.40 | 0.35 | 0.36 | 0.36 | 0.36 | 0.35 | 0.38 | 0.37 | 0.37 |

*FMCM = Fe+Mg+Ca+Mn

Biotite (matrix)

| | G-150 80-3 | | | G-158-80-2 | | | G-158 80-5 | | | |
|-------|------------|-------|-------|------------|-------|-------|------------|-------|-------|-------|
| SiO2 | 33.29 | 33.90 | 33.86 | 33.70 | 33.41 | 33.73 | 33.99 | 34.00 | 33.44 | 33.92 |
| TiO2 | 1.43 | 1.52 | 1.60 | 1.59 | 1.63 | 1.52 | 1.72 | 1.50 | 1.52 | 1.65 |
| Al2O3 | 19.66 | 19.38 | 19.35 | 19.17 | 18.74 | 19.85 | 19.53 | 19.33 | 19.01 | 19.38 |
| Cr2O3 | 0.00 | 0.00 | 0.00 | 0.00 | 0.00 | 0.00 | 0.00 | 0.00 | 0.00 | 0.00 |
| FeO | 23.72 | 23.46 | 22.90 | 22.74 | 23.69 | 22.86 | 22.31 | 22.48 | 23.24 | 21.96 |
| MnO | 0.07 | 0.04 | 0.05 | 0.06 | 0.05 | 0.07 | 0.06 | 0.06 | 0.07 | 0.03 |
| MgO | 7.99 | 7.88 | 7.55 | 7.74 | 8.16 | 8.11 | 7.65 | 7.95 | 8.07 | 8.01 |
| CaO | 0.00 | 0.00 | 0.00 | 0.01 | 0.00 | 0.00 | 0.00 | 0.00 | 0.00 | 0.01 |
| Na2O | 0.10 | 0.02 | 0.12 | 0.07 | 0.08 | 0.07 | 0.10 | 0.06 | 0.09 | 0.12 |
| K2O | 8.26 | 7.84 | 8.34 | 7.93 | 7.47 | 7.99 | 8.53 | 8.25 | 7.78 | 8.37 |
| Total | 94.53 | 94.04 | 93.76 | 93.01 | 93.23 | 94.21 | 93.88 | 93.63 | 93.23 | 93.45 |

Number of cations on the basis of 22 oxygens

| | | | | | | | | | | |
|-------|-------|-------|-------|-------|-------|-------|-------|-------|-------|-------|
| Si | 5.21 | 5.30 | 5.31 | 5.32 | 5.28 | 5.25 | 5.31 | 5.33 | 5.28 | 5.32 |
| Ti | 0.17 | 0.18 | 0.19 | 0.19 | 0.19 | 0.18 | 0.20 | 0.18 | 0.18 | 0.19 |
| Al | 3.62 | 3.57 | 3.58 | 3.57 | 3.49 | 3.64 | 3.60 | 3.57 | 3.54 | 3.58 |
| Cr | 0.00 | 0.00 | 0.00 | 0.00 | 0.00 | 0.00 | 0.00 | 0.00 | 0.00 | 0.00 |
| Fe | 3.10 | 3.07 | 3.00 | 3.00 | 3.13 | 2.98 | 2.92 | 2.94 | 3.07 | 2.88 |
| Mn | 0.01 | 0.01 | 0.01 | 0.01 | 0.01 | 0.01 | 0.01 | 0.01 | 0.01 | 0.00 |
| Mg | 1.86 | 1.84 | 1.77 | 1.82 | 1.92 | 1.88 | 1.78 | 1.86 | 1.90 | 1.87 |
| Ca | 0.00 | 0.00 | 0.00 | 0.00 | 0.00 | 0.00 | 0.00 | 0.00 | 0.00 | 0.00 |
| Na | 0.03 | 0.01 | 0.04 | 0.02 | 0.02 | 0.02 | 0.03 | 0.02 | 0.03 | 0.04 |
| K | 1.65 | 1.56 | 1.67 | 1.60 | 1.51 | 1.59 | 1.70 | 1.65 | 1.57 | 1.67 |
| Total | 15.65 | 15.52 | 15.56 | 15.52 | 15.55 | 15.55 | 15.55 | 15.55 | 15.57 | 15.56 |

| | | | | | | | | | | |
|----------|-------|-------|-------|-------|-------|-------|-------|-------|-------|-------|
| Fe/FMCM* | 62.37 | 62.49 | 62.90 | 62.12 | 61.88 | 61.15 | 61.97 | 61.24 | 61.66 | 60.53 |
| Mg/FMCM* | 37.44 | 37.40 | 36.96 | 37.68 | 37.98 | 38.66 | 37.86 | 38.59 | 38.15 | 39.35 |
| Ca/FMCM* | 0.00 | 0.00 | 0.00 | 0.03 | 0.00 | 0.00 | 0.00 | 0.00 | 0.00 | 0.04 |
| Mn/FMCM* | 0.19 | 0.11 | 0.14 | 0.17 | 0.13 | 0.19 | 0.17 | 0.17 | 0.19 | 0.08 |

| | | | | | | | | | | |
|-------------|------|------|------|------|------|------|------|------|------|------|
| Si+Al | 8.83 | 8.87 | 8.89 | 8.88 | 8.77 | 8.90 | 8.91 | 8.89 | 8.82 | 8.90 |
| Fe+Mg+Mn+Ca | 4.97 | 4.91 | 4.78 | 4.83 | 5.06 | 4.87 | 4.71 | 4.81 | 4.98 | 4.75 |
| Fe/(Fe+Mg) | 0.62 | 0.63 | 0.63 | 0.62 | 0.62 | 0.61 | 0.62 | 0.61 | 0.62 | 0.61 |
| Octa Al | 0.83 | 0.87 | 0.89 | 0.88 | 0.77 | 0.90 | 0.91 | 0.89 | 0.82 | 0.90 |

| | | | | | | | | | | |
|---|--------|--------|--------|--------|--------|--------|--------|--------|--------|--------|
| A | -15.32 | -12.88 | -17.62 | -14.53 | -11.31 | -13.00 | -19.06 | -16.73 | -13.26 | -17.87 |
| I | 0.62 | 0.63 | 0.63 | 0.62 | 0.62 | 0.61 | 0.62 | 0.61 | 0.62 | 0.61 |
| M | 0.38 | 0.37 | 0.37 | 0.38 | 0.38 | 0.39 | 0.38 | 0.39 | 0.38 | 0.39 |

*FMCM = Fe+Mg+Ca+Mn

Biotite (matrix)

| | SD-89-103-3 | | | | SD-89-097-2 | | | | | |
|--------------------------------|-------------|-------|-------|-------|-------------|-------|-------|-------|-------|-------|
| SiO ₂ | 33.74 | 33.41 | 33.86 | 31.48 | 34.57 | 34.47 | 34.79 | 34.89 | 34.36 | 34.30 |
| TiO ₂ | 1.60 | 1.70 | 1.70 | 1.24 | 2.32 | 2.38 | 2.23 | 2.35 | 2.26 | 1.97 |
| Al ₂ O ₃ | 19.27 | 19.51 | 19.49 | 20.08 | 19.50 | 19.65 | 19.94 | 19.82 | 19.86 | 18.71 |
| Cr ₂ O ₃ | 0.00 | 0.00 | 0.00 | 0.00 | 0.00 | 0.00 | 0.00 | 0.00 | 0.00 | 0.08 |
| FeO | 22.36 | 23.28 | 22.25 | 23.97 | 22.55 | 22.39 | 22.21 | 22.06 | 21.82 | 21.15 |
| MnO | 0.05 | 0.08 | 0.07 | 0.08 | 0.20 | 0.21 | 0.26 | 0.16 | 0.23 | 0.06 |
| MgO | 7.74 | 7.30 | 7.39 | 8.16 | 7.00 | 7.08 | 7.03 | 7.00 | 6.95 | 8.99 |
| CaO | 0.00 | 0.00 | 0.03 | 0.00 | 0.01 | 0.00 | 0.00 | 0.00 | 0.00 | 0.00 |
| Na ₂ O | 0.09 | 0.06 | 0.11 | 0.05 | 0.16 | 0.17 | 0.19 | 0.20 | 0.09 | 0.11 |
| K ₂ O | 8.54 | 8.39 | 8.78 | 6.51 | 8.70 | 8.49 | 8.68 | 8.60 | 8.75 | 9.32 |
| Total | 93.38 | 93.72 | 93.68 | 91.56 | 95.08 | 94.96 | 95.36 | 95.23 | 94.76 | 95.20 |

number of cations on the basis of 22 oxygens

| | | | | | | | | | | |
|-------|-------|-------|-------|-------|-------|-------|-------|-------|-------|-------|
| Si | 5.31 | 5.26 | 5.31 | 5.06 | 5.35 | 5.33 | 5.35 | 5.37 | 5.37 | 5.36 |
| Ti | 0.19 | 0.20 | 0.20 | 0.15 | 0.27 | 0.28 | 0.26 | 0.27 | 0.26 | 0.23 |
| Al | 3.58 | 3.62 | 3.61 | 3.81 | 3.55 | 3.58 | 3.61 | 3.59 | 3.62 | 3.52 |
| Cr | 0.00 | 0.00 | 0.00 | 0.00 | 0.00 | 0.00 | 0.00 | 0.00 | 0.00 | 0.01 |
| Fe | 2.94 | 3.07 | 2.92 | 3.22 | 2.92 | 2.89 | 2.85 | 2.84 | 2.82 | 2.72 |
| Mn | 0.01 | 0.01 | 0.01 | 0.01 | 0.03 | 0.03 | 0.03 | 0.02 | 0.03 | 0.01 |
| Mg | 1.82 | 1.71 | 1.73 | 1.96 | 1.61 | 1.63 | 1.60 | 1.60 | 1.58 | 1.96 |
| Ca | 0.00 | 0.00 | 0.01 | 0.00 | 0.00 | 0.00 | 0.00 | 0.00 | 0.00 | 0.00 |
| Na | 0.03 | 0.02 | 0.03 | 0.02 | 0.05 | 0.05 | 0.06 | 0.06 | 0.03 | 0.03 |
| K | 1.71 | 1.69 | 1.76 | 1.34 | 1.72 | 1.67 | 1.70 | 1.67 | 1.72 | 1.93 |
| Total | 15.58 | 15.58 | 15.58 | 15.56 | 15.49 | 15.47 | 15.47 | 15.54 | 15.43 | 15.64 |

| | | | | | | | | | | |
|----------|-------|-------|-------|-------|-------|-------|-------|-------|-------|-------|
| Fe/FMCM* | 61.76 | 64.01 | 62.63 | 62.11 | 63.99 | 63.57 | 63.55 | 63.58 | 63.69 | 64.91 |
| Mg/FMCM* | 38.10 | 35.77 | 37.07 | 37.68 | 35.40 | 35.87 | 35.69 | 35.75 | 35.63 | 35.03 |
| Ca/FMCM* | 0.00 | 0.00 | 0.11 | 0.00 | 0.04 | 0.00 | 0.00 | 0.00 | 0.00 | 0.00 |
| Mn/FMCM* | 0.14 | 0.22 | 0.20 | 0.21 | 0.57 | 0.60 | 0.75 | 0.47 | 0.68 | 0.16 |

| | | | | | | | | | | |
|-------------|------|------|------|------|------|------|------|------|------|------|
| Si+Al | 8.89 | 8.88 | 8.92 | 8.87 | 8.90 | 8.91 | 8.96 | 8.96 | 8.99 | 8.79 |
| Fe+Mg+Mn+Ca | 4.77 | 4.79 | 4.66 | 5.19 | 4.56 | 4.55 | 4.49 | 4.66 | 4.63 | 4.79 |
| Fe/(Fe+Mg) | 0.62 | 0.64 | 0.63 | 0.62 | 0.64 | 0.64 | 0.64 | 0.64 | 0.64 | 0.57 |
| Octa Al | 0.89 | 0.88 | 0.92 | 0.87 | 0.90 | 0.91 | 0.96 | 0.96 | 0.99 | 0.79 |

| | | | | | | | | | | |
|---|--------|--------|--------|-------|-------|-------|-------|-------|-------|-------|
| A | -19.74 | -17.66 | -21.86 | -1.97 | 21.36 | 18.95 | 20.11 | 19.81 | 21.51 | 20.33 |
| F | 0.62 | 0.64 | 0.63 | 0.62 | 0.64 | 0.64 | 0.64 | 0.64 | 0.64 | 0.57 |
| M | 0.38 | 0.36 | 0.37 | 0.38 | 0.36 | 0.36 | 0.36 | 0.36 | 0.36 | 0.33 |

*FMCM = Fe+Mg+Ca+Mn

Biotite (matrix)

| | SD-89-034e-1 | | | SD-89-302-4 | | | SD-89-312-1 | | | SD-89-312-6 | |
|--------------------------------|--------------|-------|-------|-------------|-------|-------|-------------|-------|-------|-------------|--|
| SiO ₂ | 34.70 | 34.84 | 35.61 | 34.87 | 35.21 | 34.26 | 34.38 | 34.20 | 34.42 | 34.61 | |
| TiO ₂ | 2.17 | 1.82 | 1.96 | 1.57 | 1.60 | 2.94 | 2.97 | 3.26 | 3.13 | 3.33 | |
| Al ₂ O ₃ | 18.53 | 18.68 | 17.94 | 18.29 | 18.17 | 19.27 | 19.84 | 19.25 | 19.30 | 19.12 | |
| Cr ₂ O ₃ | 0.11 | 0.11 | 0.03 | 0.03 | 0.05 | 0.06 | 0.04 | 0.08 | 0.05 | 0.05 | |
| FeO | 20.92 | 20.75 | 20.89 | 21.08 | 21.35 | 20.85 | 20.68 | 21.06 | 21.17 | 20.57 | |
| MnO | 0.07 | 0.04 | 0.04 | 0.22 | 0.17 | 0.36 | 0.36 | 0.39 | 0.48 | 0.52 | |
| MgO | 9.15 | 9.11 | 9.41 | 9.23 | 9.11 | 7.73 | 7.13 | 7.32 | 7.38 | 7.58 | |
| CaO | 0.02 | 0.01 | 0.02 | 0.02 | 0.04 | 0.00 | 0.04 | 0.02 | 0.00 | 0.00 | |
| Na ₂ O | 0.12 | 0.09 | 0.08 | 0.09 | 0.08 | 0.29 | 0.28 | 0.35 | 0.25 | 0.25 | |
| K ₂ O | 8.97 | 9.06 | 9.38 | 9.07 | 8.95 | 8.93 | 8.90 | 8.82 | 9.06 | 9.20 | |
| Total | 94.75 | 94.50 | 95.37 | 94.48 | 94.73 | 94.70 | 94.62 | 94.73 | 95.24 | 95.21 | |

number of cations on the basis of 22 oxygens

| | | | | | | | | | | | |
|-------|-------|-------|-------|-------|-------|-------|-------|-------|-------|-------|--|
| Si | 5.35 | 5.38 | 5.46 | 5.40 | 5.44 | 5.30 | 5.30 | 5.29 | 5.30 | 5.32 | |
| Ti | 0.25 | 0.21 | 0.23 | 0.18 | 0.19 | 0.34 | 0.34 | 0.38 | 0.36 | 0.58 | |
| Al | 3.37 | 3.40 | 3.24 | 3.34 | 3.31 | 3.51 | 3.61 | 3.51 | 3.50 | 3.46 | |
| Cr | 0.01 | 0.01 | 0.00 | 0.00 | 0.01 | 0.01 | 0.00 | 0.01 | 0.01 | 0.01 | |
| Fe | 2.70 | 2.68 | 2.68 | 2.73 | 2.76 | 2.70 | 2.67 | 2.72 | 2.73 | 2.64 | |
| Mn | 0.01 | 0.01 | 0.01 | 0.03 | 0.02 | 0.05 | 0.05 | 0.05 | 0.06 | 0.07 | |
| Mg | 2.10 | 2.10 | 2.15 | 2.13 | 2.10 | 1.78 | 1.64 | 1.69 | 1.69 | 1.74 | |
| Ca | 0.00 | 0.00 | 0.00 | 0.00 | 0.01 | 0.00 | 0.01 | 0.00 | 0.00 | 0.00 | |
| Na | 0.04 | 0.03 | 0.02 | 0.03 | 0.02 | 0.09 | 0.08 | 0.10 | 0.07 | 0.07 | |
| K | 1.77 | 1.79 | 1.83 | 1.79 | 1.76 | 1.76 | 1.75 | 1.74 | 1.78 | 1.80 | |
| Total | 15.60 | 15.61 | 15.62 | 15.65 | 15.61 | 15.53 | 15.46 | 15.50 | 15.51 | 15.50 | |

| | | | | | | | | | | | |
|----------|-------|-------|-------|-------|-------|-------|-------|-------|-------|-------|--|
| Fe/FMCM* | 56.05 | 56.02 | 55.37 | 55.80 | 56.47 | 59.59 | 61.18 | 61.00 | 60.82 | 59.44 | |
| Mg/FMCM* | 43.69 | 43.83 | 44.45 | 43.54 | 42.94 | 39.37 | 37.59 | 37.78 | 37.78 | 39.03 | |
| Ca/FMCM* | 0.07 | 0.03 | 0.07 | 0.07 | 0.14 | 0.00 | 0.15 | 0.07 | 0.00 | 0.00 | |
| Mn/FMCM* | 0.19 | 0.11 | 0.11 | 0.59 | 0.46 | 1.04 | 1.08 | 1.14 | 1.40 | 1.52 | |

| | | | | | | | | | | | |
|-------------|------|------|------|------|------|------|------|------|------|------|--|
| Si+Al | 8.72 | 8.78 | 8.70 | 8.75 | 8.75 | 8.81 | 8.91 | 8.80 | 8.80 | 8.78 | |
| Fe+Mg+Mn+Ca | 4.82 | 4.78 | 4.84 | 4.90 | 4.88 | 4.52 | 4.36 | 4.46 | 4.48 | 4.45 | |
| Fe/(Fe+Mg) | 0.56 | 0.56 | 0.55 | 0.56 | 0.57 | 0.60 | 0.62 | 0.62 | 0.62 | 0.60 | |
| Octa Al | 0.72 | 0.78 | 0.70 | 0.75 | 0.75 | 0.81 | 0.91 | 0.80 | 0.80 | 0.78 | |

| | | | | | | | | | | | |
|---|--------|--------|--------|--------|--------|--------|--------|--------|--------|--------|--|
| A | -25.08 | -25.72 | -30.58 | -26.51 | -25.65 | -24.67 | -23.63 | -24.06 | -26.21 | -29.58 | |
| F | 0.56 | 0.56 | 0.55 | 0.56 | 0.57 | 0.60 | 0.62 | 0.62 | 0.62 | 0.60 | |
| M | 0.44 | 0.44 | 0.45 | 0.44 | 0.43 | 0.40 | 0.38 | 0.38 | 0.38 | 0.40 | |

*FMCM = Fe+Mg+Ca+Mn

Biotite (matrix)

| | SD-89-184-1 | | SD-89-046a-2 | | 127-1 | SD-89-199-2 | | SD-89-397-1 | | |
|--------------------------------|-------------|-------|--------------|-------|-------|-------------|-------|-------------|-------|-------|
| SiO ₂ | 33.92 | 34.20 | 34.47 | 34.00 | 34.21 | 35.59 | 36.11 | 35.91 | 34.57 | 34.74 |
| TiO ₂ | 2.33 | 2.22 | 1.78 | 1.84 | 2.01 | 1.50 | 1.44 | 1.55 | 1.77 | 1.81 |
| Al ₂ O ₃ | 18.21 | 18.65 | 19.43 | 19.58 | 18.06 | 18.68 | 18.82 | 18.53 | 19.04 | 19.05 |
| Cr ₂ O ₃ | 0.07 | 0.09 | 0.00 | 0.00 | 0.03 | 0.02 | 0.00 | 0.08 | 0.07 | 0.03 |
| FeO | 23.75 | 23.25 | 22.77 | 22.53 | 23.77 | 16.05 | 16.05 | 21.23 | 20.29 | 19.86 |
| MnO | 0.32 | 0.28 | 0.06 | 0.07 | 0.34 | 0.32 | 0.29 | 0.24 | 0.23 | 0.21 |
| MgO | 7.23 | 7.38 | 7.40 | 7.60 | 7.72 | 12.65 | 12.34 | 9.47 | 9.26 | 9.29 |
| CaO | 0.00 | 0.00 | 0.00 | 0.00 | 0.00 | 0.00 | 0.00 | 0.00 | 0.00 | 0.00 |
| Na ₂ O | 0.11 | 0.11 | 0.09 | 0.14 | 0.11 | 0.15 | 0.17 | 0.08 | 0.11 | 0.13 |
| K ₂ O | 9.28 | 9.12 | 8.50 | 8.41 | 9.16 | 9.03 | 9.02 | 8.83 | 8.69 | 9.09 |
| Total | 95.21 | 95.30 | 94.50 | 94.17 | 95.41 | 93.99 | 94.26 | 94.01 | 93.85 | 94.21 |

number of cations on the basis of 22 oxygens

| | | | | | | | | | | |
|-------|-------|-------|-------|-------|-------|-------|-------|-------|-------|-------|
| Si | 5.31 | 5.32 | 5.36 | 5.30 | 5.34 | 5.40 | 5.45 | 5.29 | 5.33 | 5.36 |
| Ti | 0.27 | 0.26 | 0.21 | 0.22 | 0.24 | 0.17 | 0.16 | 0.19 | 0.21 | 0.21 |
| Al | 3.36 | 3.42 | 3.56 | 3.60 | 3.32 | 3.34 | 3.35 | 3.41 | 3.48 | 3.47 |
| Cr | 0.01 | 0.01 | 0.00 | 0.00 | 0.00 | 0.00 | 0.00 | 0.01 | 0.01 | 0.00 |
| Fe | 3.11 | 3.02 | 2.96 | 2.94 | 3.10 | 2.04 | 2.03 | 2.77 | 2.63 | 2.56 |
| Mn | 0.04 | 0.04 | 0.01 | 0.01 | 0.04 | 0.04 | 0.04 | 0.03 | 0.03 | 0.03 |
| Mg | 1.69 | 1.71 | 1.71 | 1.77 | 1.79 | 2.86 | 2.78 | 2.20 | 2.14 | 2.14 |
| Ca | 0.00 | 0.00 | 0.00 | 0.00 | 0.00 | 0.00 | 0.00 | 0.00 | 0.00 | 0.00 |
| Na | 0.03 | 0.03 | 0.03 | 0.04 | 0.03 | 0.04 | 0.05 | 0.02 | 0.03 | 0.04 |
| K | 1.85 | 1.81 | 1.68 | 1.67 | 1.82 | 1.75 | 1.74 | 1.76 | 1.74 | 1.77 |
| Total | 15.68 | 15.63 | 15.51 | 15.54 | 15.69 | 15.65 | 15.60 | 15.62 | 15.59 | 15.60 |

| | | | | | | | | | | |
|----------|-------|-------|-------|-------|-------|-------|-------|-------|-------|-------|
| Fe/FMCM* | 64.26 | 63.38 | 63.22 | 62.33 | 62.77 | 41.24 | 41.87 | 45.36 | 44.81 | 44.11 |
| Mg/FMCM* | 34.86 | 35.85 | 36.61 | 37.47 | 36.33 | 57.92 | 57.36 | 44.11 | 44.57 | 45.74 |
| Ca/FMCM* | 0.00 | 0.00 | 0.00 | 0.00 | 0.00 | 0.00 | 0.00 | 0.00 | 0.00 | 0.00 |
| Mn/FMCM* | 0.88 | 0.77 | 0.17 | 0.20 | 0.91 | 0.83 | 0.77 | 0.63 | 0.63 | 0.59 |

| | | | | | | | | | | |
|-------------|------|------|------|------|------|------|------|------|------|------|
| Si+Al | 8.67 | 8.74 | 8.91 | 8.90 | 8.66 | 8.74 | 8.81 | 8.70 | 8.84 | 8.83 |
| Fe+Mg+Mn+Ca | 4.84 | 4.77 | 4.68 | 4.71 | 4.94 | 4.94 | 4.84 | 5.01 | 4.81 | 4.73 |
| Fe/(Fe+Mg) | 0.65 | 0.64 | 0.63 | 0.62 | 0.63 | 0.42 | 0.42 | 0.56 | 0.55 | 0.55 |
| Octa Al | 0.67 | 0.74 | 0.91 | 0.90 | 0.66 | 0.74 | 0.81 | 0.70 | 0.80 | 0.83 |

| | | | | | | | | | | |
|---|--------|--------|--------|--------|--------|-------|-------|-------|-------|-------|
| A | -29.75 | -26.93 | -19.06 | -17.77 | -28.10 | 24.11 | 24.05 | 23.08 | 21.57 | 21.32 |
| F | 0.65 | 0.64 | 0.63 | 0.62 | 0.63 | 0.42 | 0.42 | 0.56 | 0.55 | 0.55 |
| M | 0.35 | 0.36 | 0.37 | 0.38 | 0.37 | 0.58 | 0.58 | 0.44 | 0.45 | 0.47 |

*FMCM = Fe+Mg+Ca+Mn

Biotite (matrix)

| | SD-89-353-1 | | SD-89-353-2 | | SD-89-364-1 | | | SD-89-329-1 | | G-123-80 |
|--------------------------------|-------------|-------|-------------|-------|-------------|-------|-------|-------------|-------|----------|
| SiO ₂ | 33.86 | 33.61 | 34.15 | 34.03 | 33.97 | 34.25 | 34.19 | 34.23 | 34.63 | 35.43 |
| TiO ₂ | 1.67 | 1.58 | 2.00 | 2.15 | 2.86 | 2.52 | 2.24 | 2.10 | 2.05 | 2.93 |
| Al ₂ O ₃ | 19.43 | 19.22 | 19.62 | 19.25 | 19.09 | 19.30 | 19.98 | 19.63 | 19.88 | 17.89 |
| Cr ₂ O ₃ | 0.03 | 0.08 | 0.04 | 0.08 | 0.04 | 0.08 | 0.05 | 0.04 | 0.04 | 0.08 |
| FeO | 23.08 | 22.71 | 22.55 | 22.49 | 21.71 | 22.25 | 21.72 | 22.24 | 21.56 | 22.33 |
| MnO | 0.11 | 0.12 | 0.13 | 0.16 | 0.30 | 0.29 | 0.23 | 0.25 | 0.31 | 0.28 |
| MgO | 7.98 | 7.95 | 7.87 | 7.68 | 7.16 | 6.94 | 7.55 | 7.35 | 7.16 | 8.14 |
| CaO | 0.00 | 0.06 | 0.00 | 0.00 | 0.02 | 0.00 | 0.00 | 0.00 | 0.00 | 0.01 |
| Na ₂ O | 0.08 | 0.10 | 0.10 | 0.10 | 0.28 | 0.19 | 0.16 | 0.39 | 0.46 | 0.15 |
| K ₂ O | 7.73 | 7.65 | 8.31 | 8.23 | 8.34 | 8.27 | 8.32 | 8.51 | 8.82 | 9.68 |
| Total | 93.96 | 93.07 | 94.76 | 94.16 | 93.77 | 94.08 | 94.44 | 94.73 | 94.91 | 96.92 |

number of cations on the basis of 22 oxygens

| | | | | | | | | | | |
|-------|-------|-------|-------|-------|-------|-------|-------|-------|-------|-------|
| Si | 5.29 | 5.29 | 5.29 | 5.30 | 5.31 | 5.34 | 5.29 | 5.31 | 5.34 | 5.40 |
| Ti | 0.20 | 0.19 | 0.23 | 0.25 | 0.34 | 0.30 | 0.26 | 0.24 | 0.24 | 0.34 |
| Al | 3.58 | 3.57 | 3.58 | 3.54 | 3.52 | 3.55 | 3.64 | 3.59 | 3.62 | 3.21 |
| Cr | 0.00 | 0.01 | 0.00 | 0.01 | 0.00 | 0.01 | 0.01 | 0.00 | 0.00 | 0.01 |
| Fe | 3.01 | 2.99 | 2.92 | 2.93 | 2.84 | 2.90 | 2.81 | 2.88 | 2.78 | 2.85 |
| Mn | 0.01 | 0.02 | 0.02 | 0.02 | 0.04 | 0.04 | 0.03 | 0.03 | 0.04 | 0.04 |
| Mg | 1.86 | 1.87 | 1.82 | 1.78 | 1.67 | 1.61 | 1.74 | 1.70 | 1.65 | 1.85 |
| Ca | 0.00 | 0.01 | 0.00 | 0.00 | 0.00 | 0.00 | 0.00 | 0.00 | 0.00 | 0.00 |
| Na | 0.02 | 0.03 | 0.03 | 0.03 | 0.08 | 0.06 | 0.05 | 0.12 | 0.14 | 0.04 |
| K | 1.54 | 1.54 | 1.64 | 1.64 | 1.66 | 1.64 | 1.64 | 1.68 | 1.74 | 1.88 |
| Total | 15.51 | 15.51 | 15.52 | 15.50 | 15.47 | 15.44 | 15.47 | 15.55 | 15.55 | 15.62 |

| | | | | | | | | | | |
|----------|-------|-------|-------|-------|-------|-------|-------|-------|-------|-------|
| Fe/FMCM* | 61.69 | 61.25 | 61.43 | 61.89 | 62.39 | 63.73 | 61.34 | 62.49 | 62.25 | 60.14 |
| Mg/FMCM* | 38.01 | 38.21 | 38.21 | 37.66 | 36.67 | 35.42 | 38.00 | 36.80 | 36.84 | 39.06 |
| Ca/FMCM* | 0.00 | 0.21 | 0.00 | 0.00 | 0.07 | 0.00 | 0.00 | 0.00 | 0.00 | 0.03 |
| Mn/FMCM* | 0.30 | 0.33 | 0.36 | 0.45 | 0.87 | 0.84 | 0.66 | 0.71 | 0.91 | 0.76 |

| | | | | | | | | | | |
|-------------|------|------|------|------|------|------|------|------|------|------|
| Si+Al | 8.86 | 8.86 | 8.87 | 8.84 | 8.83 | 8.88 | 8.93 | 8.89 | 8.96 | 8.61 |
| Fe+Mg+Mn+Ca | 4.88 | 4.88 | 4.75 | 4.74 | 4.55 | 4.55 | 4.58 | 4.61 | 4.47 | 4.73 |
| Fe/(Fe+Mg) | 0.62 | 0.62 | 0.62 | 0.62 | 0.63 | 0.64 | 0.62 | 0.63 | 0.63 | 0.61 |
| Octa Al | 0.86 | 0.86 | 0.87 | 0.84 | 0.83 | 0.88 | 0.93 | 0.89 | 0.96 | 0.61 |

| | | | | | | | | | | |
|---|--------|--------|--------|--------|--------|--------|--------|--------|--------|--------|
| A | -11.99 | -12.02 | -16.52 | -17.03 | -19.52 | -18.16 | -16.40 | -18.98 | -21.92 | -34.86 |
| F | 0.62 | 0.62 | 0.62 | 0.62 | 0.63 | 0.64 | 0.62 | 0.63 | 0.63 | 0.61 |
| M | 0.38 | 0.38 | 0.38 | 0.38 | 0.37 | 0.36 | 0.38 | 0.37 | 0.37 | 0.39 |

*FMCM = Fe+Mg+Ca+Mn

Biotite (matrix)

| | F-123-79-3 | | | | G-133-80-3 | |
|--------------------------------|------------|-------|-------|-------|------------|-------|
| SiO ₂ | 34.14 | 34.24 | 34.05 | 34.46 | 32.94 | 34.48 |
| TiO ₂ | 2.64 | 2.41 | 2.24 | 3.01 | 1.94 | 2.31 |
| Al ₂ O ₃ | 18.72 | 19.40 | 19.22 | 18.77 | 18.63 | 19.18 |
| Cr ₂ O ₃ | 0.00 | 0.00 | 0.00 | 0.00 | 0.00 | 0.00 |
| FeO | 21.36 | 19.77 | 20.48 | 20.98 | 23.58 | 21.88 |
| MnO | 0.20 | 0.12 | 0.15 | 0.07 | 0.08 | 0.08 |
| MgO | 8.51 | 8.36 | 8.65 | 8.04 | 8.21 | 8.03 |
| CaO | 0.00 | 0.03 | 0.00 | 0.00 | 0.00 | 0.00 |
| Na ₂ O | 0.19 | 0.21 | 0.17 | 0.18 | 0.13 | 0.14 |
| K ₂ O | 9.16 | 9.15 | 9.51 | 9.27 | 7.56 | 8.99 |
| Total | 94.94 | 93.69 | 94.47 | 94.77 | 93.07 | 95.09 |

number of cations on the basis of 22 oxygens

| | | | | | | |
|-------------|--------|--------|--------|--------|--------|-------|
| Si | 5.29 | 5.32 | 5.28 | 5.33 | 5.22 | 5.32 |
| Ti | 0.31 | 0.28 | 0.26 | 0.35 | 0.23 | 0.27 |
| Al | 3.42 | 3.55 | 3.51 | 3.42 | 3.48 | 3.49 |
| Cr | 0.00 | 0.00 | 0.00 | 0.00 | 0.00 | 0.00 |
| Fe | 2.77 | 2.57 | 2.66 | 2.71 | 3.13 | 2.82 |
| Mn | 0.03 | 0.02 | 0.02 | 0.01 | 0.01 | 0.01 |
| Mg | 1.96 | 1.94 | 2.00 | 1.85 | 1.94 | 1.85 |
| Ca | 0.00 | 0.00 | 0.00 | 0.00 | 0.00 | 0.00 |
| Na | 0.06 | 0.06 | 0.05 | 0.05 | 0.04 | 0.04 |
| K | 1.81 | 1.81 | 1.88 | 1.83 | 1.53 | 1.77 |
| Total | 15.63 | 15.56 | 15.67 | 15.55 | 15.59 | 15.57 |
| Fe/FMCM* | 58.16 | 56.77 | 56.82 | 59.30 | 61.58 | 60.32 |
| Mg/FMCM* | 41.29 | 42.78 | 42.76 | 40.50 | 38.21 | 39.45 |
| Ca/FMCM* | 0.00 | 0.11 | 0.00 | 0.00 | 0.00 | 0.00 |
| Mn/FMCM* | 0.55 | 0.35 | 0.42 | 0.20 | 0.21 | 0.22 |
| Si+Al | 8.70 | 8.87 | 8.80 | 8.75 | 8.71 | 8.81 |
| Fe+Mg+Mn+Ca | 4.76 | 4.53 | 4.68 | 4.57 | 5.08 | 4.68 |
| Fe/(Fe+Mg) | 0.58 | 0.57 | 0.57 | 0.59 | 0.62 | 0.60 |
| Octa Al | 0.70 | 0.87 | 0.80 | 0.75 | 0.71 | 0.81 |
| A | -27.00 | -26.51 | -29.68 | -29.21 | -12.24 | 24.20 |
| F | 0.58 | 0.57 | 0.57 | 0.59 | 0.62 | 0.60 |
| M | 0.42 | 0.43 | 0.43 | 0.41 | 0.38 | 0.40 |

*FMCM = Fe+Mg+Ca+Mn

APPENDIX B3:
Cordierite Microprobe Analyses

Cordierite

| | G-123-80 | | | | SC 89 299 2 | | | | SC 89 299 3 |
|--------------------------------|----------|--------|-------|-------|-------------|-------|-------|-------|-------------|
| SiO ₂ | 48.60 | 48.83 | 48.20 | 48.42 | 49.08 | 48.43 | 48.29 | 48.53 | 48.08 |
| TiO ₂ | 0.00 | 0.00 | 0.01 | 0.05 | 0.02 | 0.03 | 0.00 | 0.00 | 0.00 |
| Al ₂ O ₃ | 33.09 | 33.69 | 33.71 | 33.17 | 32.82 | 32.77 | 32.93 | 32.67 | 32.69 |
| Cr ₂ O ₃ | 0.01 | 0.04 | 0.03 | 0.00 | 0.00 | 0.00 | 0.00 | 0.02 | 0.01 |
| FeO | 9.52 | 9.89 | 9.61 | 10.07 | 10.08 | 9.80 | 9.23 | 9.19 | 9.47 |
| MnO | 0.60 | 0.54 | 0.58 | 0.48 | 0.52 | 0.59 | 0.76 | 0.83 | 0.70 |
| MgO | 7.33 | 7.22 | 7.33 | 6.64 | 6.94 | 6.92 | 7.70 | 8.01 | 7.99 |
| CaO | 0.00 | 0.00 | 0.02 | 0.00 | 0.01 | 0.01 | 0.00 | 0.00 | 0.00 |
| Na ₂ O | 0.31 | 0.32 | 0.25 | 0.17 | 0.35 | 0.36 | 1.39 | 1.29 | 1.36 |
| K ₂ O | 0.00 | 0.00 | 0.01 | 0.00 | 0.01 | 0.00 | 0.06 | 0.00 | 0.00 |
| Total | 99.46 | 100.53 | 99.77 | 99.04 | 99.91 | 99.69 | 96.57 | 96.54 | 96.13 |

number of cations on the basis of 18 oxygens

| | | | | | | | | | |
|-------------|-------|-------|-------|-------|-------|-------|-------|-------|-------|
| Si | 4.99 | 4.96 | 4.94 | 5.00 | 5.03 | 5.00 | 5.03 | 5.05 | 5.03 |
| Ti | 0.00 | 0.00 | 0.00 | 0.00 | 0.00 | 0.00 | 0.00 | 0.00 | 0.00 |
| Al | 4.00 | 4.04 | 4.07 | 4.03 | 3.96 | 3.99 | 4.05 | 4.01 | 4.03 |
| Cr | 0.00 | 0.00 | 0.00 | 0.00 | 0.00 | 0.00 | 0.00 | 0.00 | 0.00 |
| Fe | 0.82 | 0.84 | 0.82 | 0.87 | 0.86 | 0.85 | 0.46 | 0.45 | 0.48 |
| Mn | 0.05 | 0.05 | 0.05 | 0.04 | 0.05 | 0.05 | 0.07 | 0.07 | 0.06 |
| Mg | 1.12 | 1.09 | 1.12 | 1.02 | 1.06 | 1.07 | 1.10 | 1.14 | 1.11 |
| Ca | 0.00 | 0.00 | 0.00 | 0.00 | 0.00 | 0.00 | 0.00 | 0.00 | 0.00 |
| Na | 0.06 | 0.06 | 0.05 | 0.03 | 0.07 | 0.07 | 0.28 | 0.26 | 0.28 |
| K | 0.00 | 0.00 | 0.00 | 0.00 | 0.00 | 0.00 | 0.01 | 0.00 | 0.00 |
| Total | 11.04 | 11.05 | 11.05 | 11.00 | 11.03 | 11.03 | 11.09 | 11.08 | 11.09 |
| Fe/FMCM* | 41.05 | 42.44 | 41.27 | 44.98 | 43.85 | 43.09 | 26.52 | 25.56 | 27.17 |
| Mg/FMCM* | 56.33 | 55.21 | 56.10 | 52.85 | 53.80 | 54.22 | 69.58 | 70.50 | 69.11 |
| Ca/FMCM* | 0.00 | 0.00 | 0.11 | 0.00 | 0.06 | 0.06 | 0.00 | 0.00 | 0.00 |
| Mn/FMCM* | 2.62 | 2.35 | 2.52 | 2.17 | 2.29 | 2.63 | 3.90 | 4.14 | 3.55 |
| Si+Al | 8.99 | 9.00 | 9.00 | 9.03 | 8.99 | 8.99 | 9.08 | 9.05 | 9.06 |
| Fe+Mg+Mn+Ca | 1.99 | 1.98 | 1.99 | 1.93 | 1.97 | 1.97 | 1.74 | 1.77 | 1.75 |
| Fe/(Fe+Mg) | 0.42 | 0.43 | 0.42 | 0.46 | 0.45 | 0.44 | 0.28 | 0.27 | 0.29 |
| A | 50.81 | 51.06 | 51.15 | 51.63 | 50.73 | 51.07 | 54.90 | 54.19 | 54.56 |
| F | 0.42 | 0.43 | 0.42 | 0.46 | 0.45 | 0.44 | 0.28 | 0.27 | 0.29 |
| M | 0.58 | 0.57 | 0.58 | 0.54 | 0.55 | 0.56 | 0.72 | 0.73 | 0.72 |

*FMCM = Fe+Mg+Ca+Mn

APPENDIX B4:
Muscovite Microprobe Analyses

Muscovite

| | F-123-79-1 | | F-123-79-1 | | F-123-79-4 | | F-123-80-1 | | F-123-80-1 | |
|--------------------------------|------------|-------|------------|-------|------------|-------|------------|-------|------------|-------|
| SiO ₂ | 45.70 | 45.88 | 46.58 | 46.38 | 44.44 | 43.80 | 43.96 | 44.45 | 45.01 | 46.15 |
| TiO ₂ | 1.12 | 0.87 | 0.42 | 0.32 | 0.01 | 0.04 | 0.03 | 0.51 | 0.56 | 0.50 |
| Al ₂ O ₃ | 36.40 | 36.20 | 36.50 | 36.57 | 36.87 | 36.62 | 36.66 | 36.95 | 37.05 | 36.87 |
| Cr ₂ O ₃ | 0.00 | 0.00 | 0.00 | 0.00 | 0.00 | 0.00 | 0.00 | 0.00 | 0.00 | 0.00 |
| FeO | 0.77 | 0.93 | 0.89 | 0.76 | 0.90 | 1.10 | 0.93 | 0.83 | 0.90 | 0.87 |
| MnO | 0.00 | 0.00 | 0.00 | 0.00 | 0.00 | 0.00 | 0.00 | 0.00 | 0.00 | 0.00 |
| MgO | 0.35 | 0.51 | 0.45 | 0.45 | 0.42 | 0.53 | 0.47 | 0.39 | 0.38 | 0.44 |
| CaO | 0.00 | 0.00 | 0.00 | 0.00 | 0.00 | 0.00 | 0.00 | 0.00 | 0.00 | 0.00 |
| Na ₂ O | 1.09 | 0.98 | 1.11 | 0.73 | 0.98 | 1.07 | 1.09 | 1.05 | 1.05 | 1.05 |
| K ₂ O | 9.49 | 9.72 | 9.75 | 10.19 | 8.90 | 8.80 | 8.85 | 9.45 | 9.47 | 9.36 |
| Total | 94.93 | 95.10 | 95.71 | 95.41 | 92.53 | 91.96 | 91.99 | 94.93 | 94.91 | 94.93 |

number of cations on the basis of 22 oxygens

| | | | | | | | | | | |
|-------------|-------|-------|-------|-------|-------|-------|-------|-------|-------|-------|
| Si | 6.07 | 6.09 | 6.13 | 6.13 | 6.03 | 5.99 | 6.01 | 6.07 | 6.01 | 6.09 |
| Ti | 0.11 | 0.09 | 0.04 | 0.03 | 0.00 | 0.00 | 0.00 | 0.05 | 0.06 | 0.05 |
| Al | 5.70 | 5.66 | 5.67 | 5.70 | 5.90 | 5.91 | 5.91 | 5.78 | 5.83 | 5.74 |
| Cr | 0.00 | 0.00 | 0.00 | 0.00 | 0.00 | 0.00 | 0.00 | 0.00 | 0.00 | 0.00 |
| Fe | 0.09 | 0.10 | 0.10 | 0.08 | 0.10 | 0.13 | 0.11 | 0.09 | 0.10 | 0.10 |
| Mn | 0.00 | 0.00 | 0.00 | 0.00 | 0.00 | 0.00 | 0.00 | 0.00 | 0.00 | 0.00 |
| Mg | 0.07 | 0.10 | 0.09 | 0.09 | 0.08 | 0.11 | 0.10 | 0.08 | 0.08 | 0.09 |
| Ca | 0.00 | 0.00 | 0.00 | 0.00 | 0.00 | 0.00 | 0.00 | 0.00 | 0.00 | 0.00 |
| Na | 0.28 | 0.25 | 0.28 | 0.19 | 0.26 | 0.28 | 0.29 | 0.27 | 0.27 | 0.27 |
| K | 1.61 | 1.65 | 1.64 | 1.72 | 1.54 | 1.54 | 1.54 | 1.60 | 1.61 | 1.58 |
| Total | 13.92 | 13.94 | 13.95 | 13.94 | 13.92 | 13.96 | 13.95 | 13.95 | 13.96 | 13.91 |
| Si+Al | 11.76 | 11.75 | 11.80 | 11.83 | 11.93 | 11.90 | 11.91 | 11.84 | 11.84 | 11.83 |
| Fe+Mg+Mn+Ca | 0.15 | 0.20 | 0.19 | 0.17 | 0.19 | 0.23 | 0.20 | 0.17 | 0.18 | 0.18 |
| Fe/(Fe+Mg) | 0.55 | 0.51 | 0.53 | 0.49 | 0.55 | 0.54 | 0.53 | 0.54 | 0.57 | 0.53 |
| Tetra Al | 1.93 | 1.91 | 1.87 | 1.87 | 1.97 | 2.01 | 1.99 | 1.93 | 1.99 | 1.91 |
| Octa Al | 3.77 | 3.75 | 3.80 | 3.83 | 3.93 | 3.90 | 3.92 | 3.85 | 3.84 | 3.83 |
| Fe+Mg+Ti+Mn | 0.27 | 0.29 | 0.23 | 0.20 | 0.19 | 0.24 | 0.21 | 0.22 | 0.23 | 0.23 |
| K/Na+K+Ca | 0.85 | 0.87 | 0.85 | 0.90 | 0.86 | 0.84 | 0.84 | 0.86 | 0.86 | 0.85 |
| Ca/Na+K+Ca | 0.00 | 0.00 | 0.00 | 0.00 | 0.00 | 0.00 | 0.00 | 0.00 | 0.00 | 0.00 |
| AlIV+AlVI | 5.70 | 5.66 | 5.67 | 5.70 | 5.90 | 5.91 | 5.91 | 5.78 | 5.83 | 5.74 |
| FMTM*+Si | 6.34 | 6.38 | 6.36 | 6.33 | 6.22 | 6.23 | 6.22 | 6.29 | 6.24 | 6.32 |

*FMTM=Fe+Mg+Ti+Mn

| | G-133-80-3 | | | | Muscovite | | | | | |
|--------------------------------|------------|-------|------------|-------|------------|-------|------------|-------|--------|-------|
| | G-133-80-1 | | G-150-80-2 | | G-150-80-3 | | G-158-80-2 | | 0342-2 | 302-2 |
| SiO ₂ | 47.11 | 43.62 | 45.83 | 46.81 | 46.81 | 47.16 | 47.16 | 45.47 | 46.99 | 48.01 |
| TiO ₂ | 0.08 | 0.02 | 0.21 | 0.19 | 0.19 | 0.24 | 0.38 | 0.37 | 0.40 | 0.19 |
| Al ₂ O ₃ | 35.10 | 34.36 | 37.01 | 36.93 | 37.52 | 36.17 | 34.48 | 36.60 | 36.50 | 35.35 |
| Cr ₂ O ₃ | 0.00 | 0.00 | 0.00 | 0.00 | 0.00 | 0.00 | 0.00 | 0.00 | 0.00 | 0.05 |
| FeO | 1.84 | 4.95 | 0.72 | 0.62 | 0.71 | 0.89 | 1.33 | 0.86 | 1.01 | 2.53 |
| MnO | 0.00 | 0.00 | 0.00 | 0.00 | 0.00 | 0.00 | 0.00 | 0.00 | 0.00 | 0.00 |
| MgO | 1.07 | 1.25 | 0.36 | 0.32 | 0.35 | 0.43 | 1.03 | 0.53 | 0.64 | 0.50 |
| CaO | 0.03 | 0.02 | 0.00 | 0.00 | 0.00 | 0.00 | 0.00 | 0.00 | 0.00 | 0.00 |
| Na ₂ O | 0.83 | 1.01 | 1.47 | 1.43 | 1.17 | 0.90 | 0.84 | 1.27 | 0.64 | 0.81 |
| K ₂ O | 9.09 | 8.98 | 8.80 | 8.99 | 9.39 | 9.41 | 9.27 | 8.88 | 8.74 | 8.38 |
| Total | 95.15 | 94.21 | 94.42 | 95.28 | 96.14 | 95.19 | 94.50 | 93.97 | 94.92 | 95.82 |

number of cations on the basis of 22 oxygens

| | | | | | | | | | | |
|-------------|-------|-------|-------|-------|-------|-------|-------|-------|-------|-------|
| Si | 6.24 | 5.97 | 6.09 | 6.15 | 6.11 | 6.22 | 6.28 | 6.08 | 6.19 | 6.29 |
| Ti | 0.01 | 0.00 | 0.02 | 0.02 | 0.02 | 0.02 | 0.04 | 0.04 | 0.04 | 0.02 |
| Al | 5.48 | 5.54 | 5.80 | 5.72 | 5.78 | 5.62 | 5.41 | 5.77 | 5.66 | 5.46 |
| Cr | 0.00 | 0.00 | 0.00 | 0.00 | 0.00 | 0.00 | 0.00 | 0.00 | 0.00 | 0.01 |
| Fe | 0.20 | 0.57 | 0.08 | 0.07 | 0.08 | 0.10 | 0.15 | 0.10 | 0.11 | 0.28 |
| Mn | 0.00 | 0.00 | 0.00 | 0.00 | 0.00 | 0.00 | 0.00 | 0.00 | 0.00 | 0.00 |
| Mg | 0.21 | 0.25 | 0.07 | 0.06 | 0.07 | 0.08 | 0.20 | 0.11 | 0.13 | 0.10 |
| Ca | 0.00 | 0.00 | 0.00 | 0.00 | 0.00 | 0.00 | 0.00 | 0.00 | 0.00 | 0.00 |
| Na | 0.21 | 0.27 | 0.38 | 0.36 | 0.30 | 0.23 | 0.22 | 0.33 | 0.16 | 0.21 |
| K | 1.54 | 1.57 | 1.49 | 1.51 | 1.56 | 1.58 | 1.57 | 1.51 | 1.47 | 1.40 |
| Total | 13.89 | 14.17 | 13.93 | 13.90 | 13.91 | 13.86 | 13.87 | 13.92 | 13.76 | 13.76 |
| Si+Al | 11.71 | 11.51 | 11.88 | 11.88 | 11.89 | 11.84 | 11.69 | 11.84 | 11.85 | 11.75 |
| Fe+Mg+Mn+Ca | 0.42 | 0.82 | 0.15 | 0.13 | 0.15 | 0.18 | 0.35 | 0.20 | 0.24 | 0.37 |
| Fe/(Fe+Mg) | 0.49 | 0.69 | 0.53 | 0.52 | 0.53 | 0.54 | 0.42 | 0.48 | 0.47 | 0.74 |
| Tetra Al | 1.76 | 2.03 | 1.91 | 1.85 | 1.89 | 1.78 | 1.72 | 1.92 | 1.81 | 1.71 |
| Octa Al | 3.72 | 3.51 | 3.89 | 3.87 | 3.89 | 3.84 | 3.69 | 3.85 | 3.85 | 3.75 |
| Fe+Mg+Ti+Mn | 0.42 | 0.82 | 0.17 | 0.15 | 0.16 | 0.21 | 0.39 | 0.24 | 0.28 | 0.39 |
| K/Na+K+Ca | 0.88 | 0.85 | 0.80 | 0.81 | 0.84 | 0.87 | 0.88 | 0.82 | 0.90 | 0.87 |
| Ca/Ca+Na+K | 0.00 | 0.00 | 0.00 | 0.00 | 0.00 | 0.00 | 0.00 | 0.00 | 0.00 | 0.00 |
| AlIV+AlVI | 5.48 | 5.54 | 5.80 | 5.72 | 5.78 | 5.62 | 5.41 | 5.77 | 5.66 | 5.46 |
| FMIM*+Si | 6.66 | 6.79 | 6.28 | 6.30 | 6.27 | 6.43 | 6.67 | 6.32 | 6.47 | 6.68 |

*FMIM=Fe+Mg+Ti+Mn

Muscovite

| | 312-3 | 184-1 | 184-2 | SD-89-046a-2 | 127-1 | 397-4 | 353-1 | SD-89-553-3 | |
|--------------------------------|-------|-------|-------|--------------|-------|-------|-------|-------------|-------|
| SiO ₂ | 47.74 | 46.81 | 47.86 | 47.78 | 47.83 | 47.65 | 49.53 | 48.25 | 47.04 |
| TiO ₂ | 1.26 | 0.61 | 0.52 | 0.33 | 0.32 | 1.11 | 0.40 | 0.28 | 0.50 |
| Al ₂ O ₃ | 35.35 | 35.61 | 35.81 | 36.73 | 35.67 | 34.50 | 51.45 | 57.08 | 56.54 |
| Cr ₂ O ₃ | 0.00 | 0.00 | 0.01 | 0.01 | 0.05 | 0.03 | 0.04 | 0.00 | 0.00 |
| FeO | 1.26 | 1.65 | 1.45 | 0.92 | 1.77 | 2.50 | 2.51 | 0.89 | 0.79 |
| MnO | 0.00 | 0.00 | 0.00 | 0.00 | 0.00 | 0.00 | 0.00 | 0.00 | 0.00 |
| MgO | 0.56 | 0.45 | 0.53 | 0.42 | 0.75 | 0.57 | 1.27 | 0.38 | 0.43 |
| CaO | 0.00 | 0.00 | 0.00 | 0.00 | 0.00 | 0.00 | 0.00 | 0.00 | 0.00 |
| Na ₂ O | 0.70 | 0.75 | 0.86 | 1.17 | 1.07 | 0.69 | 0.68 | 1.23 | 1.05 |
| K ₂ O | 8.63 | 8.79 | 8.77 | 8.23 | 8.24 | 9.11 | 8.00 | 8.31 | 7.81 |
| Total | 95.51 | 94.67 | 95.81 | 95.58 | 95.72 | 96.15 | 93.88 | 96.33 | 94.04 |

number of cations on the basis of 22 oxygens

| | | | | | | | | | |
|--------------|-------|-------|-------|-------|-------|-------|-------|-------|-------|
| Si | 6.25 | 6.21 | 6.26 | 6.23 | 6.26 | 6.26 | 6.60 | 6.24 | 6.21 |
| Ti | 0.12 | 0.06 | 0.05 | 0.03 | 0.03 | 0.11 | 0.04 | 0.03 | 0.05 |
| Al | 5.46 | 5.57 | 5.52 | 5.64 | 5.50 | 5.34 | 4.94 | 5.65 | 5.67 |
| Cr | 0.00 | 0.00 | 0.00 | 0.00 | 0.01 | 0.00 | 0.00 | 0.00 | 0.00 |
| Fe | 0.14 | 0.18 | 0.16 | 0.10 | 0.19 | 0.27 | 0.28 | 0.09 | 0.09 |
| Mn | 0.00 | 0.00 | 0.00 | 0.00 | 0.00 | 0.00 | 0.00 | 0.00 | 0.00 |
| Mg | 0.11 | 0.09 | 0.10 | 0.08 | 0.15 | 0.11 | 0.25 | 0.07 | 0.08 |
| Ca | 0.00 | 0.00 | 0.00 | 0.00 | 0.00 | 0.00 | 0.00 | 0.00 | 0.00 |
| Na | 0.18 | 0.19 | 0.22 | 0.30 | 0.27 | 0.18 | 0.18 | 0.31 | 0.27 |
| K | 1.44 | 1.49 | 1.46 | 1.37 | 1.38 | 1.53 | 1.36 | 1.37 | 1.32 |
| Total | 13.70 | 13.79 | 13.77 | 13.75 | 13.78 | 13.81 | 13.65 | 13.75 | 13.69 |
| Si+Al | 11.71 | 11.78 | 11.78 | 11.87 | 11.76 | 11.61 | 11.54 | 11.89 | 11.88 |
| Fe+Mg+Mn+Ca | 0.25 | 0.27 | 0.26 | 0.18 | 0.34 | 0.39 | 0.53 | 0.16 | 0.17 |
| Fe/(Fe+Mg) | 0.56 | 0.67 | 0.61 | 0.55 | 0.57 | 0.71 | 0.53 | 0.54 | 0.51 |
| Tetra Al | 1.75 | 1.79 | 1.74 | 1.77 | 1.74 | 1.74 | 1.40 | 1.76 | 1.79 |
| Octa Al | 3.71 | 3.78 | 3.78 | 3.87 | 3.76 | 3.60 | 3.54 | 3.89 | 3.88 |
| Fe+Mg+Ti+Mn | 0.37 | 0.33 | 0.31 | 0.21 | 0.37 | 0.50 | 0.57 | 0.19 | 0.22 |
| K/(Na+K+Ca) | 0.89 | 0.89 | 0.87 | 0.82 | 0.84 | 0.90 | 0.89 | 0.82 | 0.83 |
| Ca/(Ca+Na+K) | 0.00 | 0.00 | 0.00 | 0.00 | 0.00 | 0.00 | 0.00 | 0.00 | 0.00 |
| AlIV+AlVI | 5.46 | 5.57 | 5.52 | 5.64 | 5.50 | 5.34 | 4.94 | 5.65 | 5.67 |
| FMTM*+Si | 6.62 | 6.54 | 6.57 | 6.44 | 6.63 | 6.76 | 7.17 | 6.43 | 6.43 |

*FMTM=Fe+Mg+Ti+Mn

Muscovite

| | SD-89-364-1 | | SD-89-364-3 | | 329-1 | 329-2 |
|--------------------------------|-------------|-------|-------------|-------|-------|-------|
| SiO ₂ | 46.07 | 45.73 | 47.34 | 47.76 | 48.25 | 47.81 |
| TiO ₂ | 0.49 | 0.85 | 0.67 | 0.82 | 0.50 | 0.50 |
| Al ₂ O ₃ | 36.89 | 36.11 | 36.10 | 35.94 | 35.70 | 35.72 |
| Cr ₂ O ₃ | 0.06 | 0.04 | 0.00 | 0.00 | 0.00 | 0.04 |
| FeO | 0.88 | 0.85 | 0.81 | 0.95 | 1.41 | 1.45 |
| MnO | 0.01 | 0.00 | 0.00 | 0.00 | 0.00 | 0.00 |
| MgO | 0.32 | 0.43 | 0.42 | 0.55 | 0.60 | 0.59 |
| CaO | 0.00 | 0.00 | 0.00 | 0.00 | 0.00 | 0.00 |
| Na ₂ O | 0.77 | 0.80 | 0.76 | 0.79 | 0.80 | 0.82 |
| K ₂ O | 7.70 | 7.47 | 8.42 | 8.12 | 8.70 | 8.53 |
| Total | 93.18 | 92.27 | 94.58 | 94.93 | 95.96 | 95.46 |

number of cations on the basis of 22 oxygens

| | | | | | | |
|-------------|-------|-------|-------|-------|-------|-------|
| Si | 6.14 | 6.15 | 6.24 | 6.26 | 6.29 | 6.26 |
| Ti | 0.05 | 0.09 | 0.07 | 0.08 | 0.05 | 0.05 |
| Al | 5.80 | 5.73 | 5.61 | 5.55 | 5.49 | 5.52 |
| Cr | 0.01 | 0.00 | 0.00 | 0.00 | 0.00 | 0.00 |
| Fe | 0.10 | 0.10 | 0.09 | 0.10 | 0.15 | 0.16 |
| Mn | 0.00 | 0.00 | 0.00 | 0.00 | 0.00 | 0.00 |
| Mg | 0.06 | 0.09 | 0.08 | 0.11 | 0.12 | 0.12 |
| Ca | 0.00 | 0.00 | 0.00 | 0.00 | 0.00 | 0.00 |
| Na | 0.20 | 0.21 | 0.19 | 0.20 | 0.20 | 0.21 |
| K | 1.31 | 1.28 | 1.42 | 1.36 | 1.45 | 1.43 |
| Total | 13.66 | 13.64 | 13.70 | 13.66 | 13.74 | 13.74 |
| Si+Al | 11.94 | 11.88 | 11.85 | 11.81 | 11.78 | 11.78 |
| Fe+Mg+Mn+Ca | 0.16 | 0.18 | 0.17 | 0.21 | 0.27 | 0.27 |
| Fe/(Fe+Mg) | 0.61 | 0.53 | 0.52 | 0.49 | 0.57 | 0.58 |
| Tetra Al | 1.86 | 1.85 | 1.76 | 1.74 | 1.71 | 1.74 |
| Octa Al | 3.94 | 3.88 | 3.85 | 3.81 | 3.78 | 3.78 |
| Fe+Mg+Ti+Mn | 0.21 | 0.27 | 0.24 | 0.29 | 0.32 | 0.32 |
| K/Na+K+Ca | 0.87 | 0.86 | 0.88 | 0.87 | 0.88 | 0.87 |
| Ca/Na+K+Ca | 0.00 | 0.00 | 0.00 | 0.00 | 0.00 | 0.00 |
| AlIV+AlVI | 5.80 | 5.73 | 5.61 | 5.55 | 5.49 | 5.52 |
| FMIM*+Si | 6.35 | 6.42 | 6.48 | 6.55 | 6.61 | 6.58 |

*FMIM=Fe+Mg+Ti+Mn

APPENDIX B5:
Plagioclase Microprobe Analyses

Plagioclase

| | G-133-80-1 | | | | G-133-80-5 | | | | | |
|--------------------------------|------------|--------|--------|--------|------------|--------|-------|--------|--------|--------|
| | (rim) | (mid) | (core) | (mid) | (rim) | (rim) | (mid) | (core) | (mid) | (rim) |
| SiO ₂ | 60.06 | 60.79 | 60.67 | 60.58 | 60.23 | 59.84 | 60.05 | 60.06 | 60.25 | 60.27 |
| TiO ₂ | 0.00 | 0.00 | 0.00 | 0.00 | 0.00 | 0.00 | 0.00 | 0.00 | 0.00 | 0.00 |
| Al ₂ O ₃ | 25.20 | 25.21 | 25.49 | 25.46 | 25.71 | 25.61 | 25.26 | 25.35 | 25.45 | 25.63 |
| Cr ₂ O ₃ | 0.00 | 0.00 | 0.00 | 0.00 | 0.00 | 0.00 | 0.00 | 0.00 | 0.00 | 0.00 |
| FeO | 0.17 | 0.11 | 0.03 | 0.04 | 0.00 | 0.00 | 0.00 | 0.00 | 0.01 | 0.17 |
| MnO | 0.00 | 0.00 | 0.00 | 0.00 | 0.00 | 0.00 | 0.00 | 0.00 | 0.00 | 0.00 |
| MgO | 0.00 | 0.00 | 0.00 | 0.00 | 0.00 | 0.00 | 0.00 | 0.00 | 0.00 | 0.00 |
| CaO | 6.36 | 6.04 | 6.43 | 6.57 | 6.62 | 6.51 | 6.26 | 6.41 | 6.54 | 6.55 |
| Na ₂ O | 8.03 | 8.43 | 8.26 | 8.05 | 8.07 | 8.36 | 8.32 | 8.13 | 8.22 | 8.34 |
| K ₂ O | 0.00 | 0.00 | 0.00 | 0.00 | 0.00 | 0.00 | 0.00 | 0.00 | 0.00 | 0.00 |
| Total | 99.83 | 100.57 | 100.88 | 100.70 | 100.63 | 100.36 | 99.89 | 99.95 | 100.47 | 100.65 |

number of cations on the basis of 8 oxygen

| | | | | | | | | | | |
|-------|------|------|------|------|------|------|------|------|------|------|
| Si | 2.68 | 2.69 | 2.68 | 2.68 | 2.66 | 2.66 | 2.68 | 2.67 | 2.67 | 2.67 |
| Ti | 0.00 | 0.00 | 0.00 | 0.00 | 0.00 | 0.00 | 0.00 | 0.00 | 0.00 | 0.00 |
| Al | 1.32 | 1.31 | 1.33 | 1.33 | 1.34 | 1.34 | 1.33 | 1.33 | 1.33 | 1.34 |
| Cr | 0.00 | 0.00 | 0.00 | 0.00 | 0.00 | 0.00 | 0.00 | 0.00 | 0.00 | 0.00 |
| Fe | 0.01 | 0.00 | 0.00 | 0.00 | 0.00 | 0.00 | 0.00 | 0.00 | 0.00 | 0.01 |
| Mn | 0.00 | 0.00 | 0.00 | 0.00 | 0.00 | 0.00 | 0.00 | 0.00 | 0.00 | 0.00 |
| Mg | 0.00 | 0.00 | 0.00 | 0.00 | 0.00 | 0.00 | 0.00 | 0.00 | 0.00 | 0.00 |
| Ca | 0.30 | 0.29 | 0.30 | 0.31 | 0.31 | 0.31 | 0.30 | 0.31 | 0.31 | 0.31 |
| Na | 0.69 | 0.72 | 0.71 | 0.69 | 0.69 | 0.72 | 0.72 | 0.70 | 0.71 | 0.72 |
| K | 0.00 | 0.00 | 0.00 | 0.00 | 0.00 | 0.00 | 0.00 | 0.00 | 0.00 | 0.00 |
| Total | 5.01 | 5.02 | 5.01 | 5.01 | 5.01 | 5.03 | 5.00 | 5.01 | 5.00 | 5.02 |

Plagioclase end members

| | | | | | | | | | | |
|------------|-------|-------|-------|-------|-------|-------|-------|-------|-------|-------|
| Albite | 69.56 | 71.64 | 69.92 | 68.92 | 68.81 | 69.91 | 70.65 | 69.65 | 69.65 | 69.65 |
| Anorthite | 30.44 | 28.36 | 30.08 | 31.08 | 31.19 | 30.09 | 29.35 | 30.35 | 30.35 | 30.35 |
| Orthoclase | 0.00 | 0.00 | 0.00 | 0.00 | 0.00 | 0.00 | 0.00 | 0.00 | 0.00 | 0.00 |
| Si+Al | 4.00 | 4.00 | 4.00 | 4.00 | 4.01 | 4.00 | 4.00 | 4.00 | 4.00 | 4.00 |

Plagioclase

| | SD-89-312-2 | | | | | SD-89-312-5 | | | | |
|--------------------------------|-------------|--------|-------|-------|-------|-------------|-------|-------|-------|--------|
| | (core) | (mid) | (mid) | (mid) | (rim) | (core) | (mid) | (mid) | (mid) | (rim) |
| SiO ₂ | 62.64 | 62.98 | 61.70 | 62.59 | 63.20 | 63.39 | 63.00 | 62.95 | 62.41 | 63.27 |
| TiO ₂ | 0.00 | 0.00 | 0.00 | 0.00 | 0.00 | 0.00 | 0.00 | 0.00 | 0.00 | 0.00 |
| Al ₂ O ₃ | 23.57 | 23.53 | 23.36 | 23.45 | 22.92 | 22.90 | 23.19 | 23.49 | 23.36 | 23.49 |
| Cr ₂ O ₃ | 0.01 | 0.02 | 0.00 | 0.00 | 0.03 | 0.01 | 0.00 | 0.02 | 0.00 | 0.00 |
| FeO | 0.00 | 0.00 | 0.00 | 0.00 | 0.01 | 0.00 | 0.00 | 0.00 | 0.00 | 0.00 |
| MnO | 0.00 | 0.00 | 0.00 | 0.00 | 0.00 | 0.00 | 0.00 | 0.00 | 0.00 | 0.00 |
| MgO | 0.00 | 0.00 | 0.00 | 0.00 | 0.00 | 0.00 | 0.00 | 0.00 | 0.00 | 0.00 |
| CaO | 4.50 | 4.66 | 4.65 | 4.60 | 3.88 | 3.98 | 4.23 | 4.50 | 4.52 | 4.64 |
| Na ₂ O | 8.69 | 9.04 | 9.08 | 8.76 | 9.86 | 9.00 | 9.28 | 8.89 | 8.56 | 8.68 |
| K ₂ O | 0.13 | 0.15 | 0.17 | 0.15 | 0.08 | 0.07 | 0.11 | 0.14 | 0.13 | 0.10 |
| Total | 99.55 | 100.38 | 98.96 | 98.55 | 99.98 | 99.36 | 99.82 | 99.99 | 98.99 | 100.19 |

number of cations on the basis of 8 oxygens

| | | | | | | | | | | |
|-------|------|------|------|------|------|------|------|------|------|------|
| Si | 2.78 | 2.78 | 2.76 | 2.78 | 2.80 | 2.81 | 2.79 | 2.78 | 2.78 | 2.79 |
| Ti | 0.00 | 0.00 | 0.00 | 0.00 | 0.00 | 0.00 | 0.00 | 0.00 | 0.00 | 0.00 |
| Al | 1.23 | 1.22 | 1.23 | 1.23 | 1.20 | 1.20 | 1.21 | 1.22 | 1.23 | 1.22 |
| Cr | 0.00 | 0.00 | 0.00 | 0.00 | 0.00 | 0.00 | 0.00 | 0.00 | 0.00 | 0.00 |
| Fe | 0.00 | 0.00 | 0.00 | 0.00 | 0.00 | 0.00 | 0.00 | 0.00 | 0.00 | 0.00 |
| Mn | 0.00 | 0.00 | 0.00 | 0.00 | 0.00 | 0.00 | 0.00 | 0.00 | 0.00 | 0.00 |
| Mg | 0.00 | 0.00 | 0.00 | 0.00 | 0.00 | 0.00 | 0.00 | 0.00 | 0.00 | 0.00 |
| Ca | 0.21 | 0.22 | 0.22 | 0.22 | 0.18 | 0.19 | 0.20 | 0.21 | 0.22 | 0.22 |
| Na | 0.75 | 0.77 | 0.79 | 0.75 | 0.85 | 0.77 | 0.80 | 0.76 | 0.74 | 0.74 |
| K | 0.01 | 0.01 | 0.01 | 0.01 | 0.00 | 0.00 | 0.01 | 0.01 | 0.01 | 0.01 |
| Total | 4.98 | 5.00 | 5.02 | 4.99 | 5.03 | 4.98 | 5.01 | 4.99 | 4.98 | 4.98 |

Plagioclase end members

| | | | | | | | | | | |
|------------|-------|-------|-------|-------|-------|-------|-------|-------|-------|-------|
| Albite | 77.16 | 77.17 | 77.20 | 76.84 | 81.78 | 80.03 | 79.38 | 77.51 | 76.82 | 76.75 |
| Anorthite | 22.08 | 21.98 | 21.85 | 22.30 | 17.78 | 19.56 | 20.00 | 21.68 | 22.42 | 22.67 |
| Orthoclase | 0.76 | 0.84 | 0.95 | 0.87 | 0.44 | 0.41 | 0.62 | 0.80 | 0.77 | 0.58 |
| Si+Al | 4.01 | 4.00 | 4.00 | 4.01 | 3.99 | 4.01 | 4.00 | 4.01 | 4.01 | 4.01 |

Plagioclase

| | 034e-2 | 299-2 | 353-5 | SD-89-329-4 | | SD-89-034e-3 | | SD-89-127-2 | |
|--------------------------------|--------|--------|--------|-------------|--------|--------------|-------|-------------|-------|
| | | | | (core) | (rim) | (core) | (rim) | (core) | (rim) |
| SiO ₂ | 59.89 | 64.40 | 64.12 | 65.78 | 65.49 | 60.62 | 59.79 | 64.28 | 63.48 |
| TiO ₂ | 0.00 | 0.00 | 0.00 | 0.00 | 0.00 | 0.00 | 0.00 | 0.00 | 0.00 |
| Al ₂ O ₃ | 24.44 | 23.35 | 22.72 | 22.00 | 21.72 | 24.88 | 25.07 | 22.91 | 23.05 |
| Cr ₂ O ₃ | 0.00 | 0.00 | 0.01 | 0.02 | 0.00 | 0.02 | 0.03 | 0.00 | 0.00 |
| FeO | 0.03 | 0.23 | 0.38 | 0.00 | 0.10 | 0.02 | 0.00 | 0.04 | 0.03 |
| MnO | 0.00 | 0.00 | 0.00 | 0.00 | 0.00 | 0.00 | 0.00 | 0.00 | 0.00 |
| MgO | 0.00 | 0.01 | 0.00 | 0.00 | 0.00 | 0.00 | 0.00 | 0.00 | 0.00 |
| CaO | 6.40 | 4.30 | 3.68 | 2.59 | 2.18 | 6.43 | 6.34 | 3.86 | 4.10 |
| Na ₂ O | 7.65 | 8.33 | 9.48 | 10.16 | 10.68 | 7.82 | 7.92 | 9.01 | 8.81 |
| K ₂ O | 0.07 | 0.03 | 0.06 | 0.05 | 0.12 | 0.06 | 0.03 | 0.06 | 0.05 |
| Total | 98.48 | 100.65 | 100.40 | 100.59 | 100.28 | 99.85 | 99.18 | 100.16 | 99.52 |

number of cations on the basis of 8 oxygens

| | | | | | | | | | |
|-------|------|------|------|------|------|------|------|------|------|
| Si | 2.70 | 2.82 | 2.82 | 2.87 | 2.87 | 2.70 | 2.68 | 2.83 | 2.81 |
| Ti | 0.00 | 0.00 | 0.00 | 0.00 | 0.00 | 0.00 | 0.00 | 0.00 | 0.00 |
| Al | 1.30 | 1.20 | 1.18 | 1.13 | 1.12 | 1.31 | 1.33 | 1.19 | 1.20 |
| Cr | 0.00 | 0.00 | 0.00 | 0.00 | 0.00 | 0.00 | 0.00 | 0.00 | 0.00 |
| Fe | 0.00 | 0.01 | 0.01 | 0.00 | 0.00 | 0.00 | 0.00 | 0.00 | 0.00 |
| Mn | 0.00 | 0.00 | 0.00 | 0.00 | 0.00 | 0.00 | 0.00 | 0.00 | 0.00 |
| Mg | 0.00 | 0.00 | 0.00 | 0.00 | 0.00 | 0.00 | 0.00 | 0.00 | 0.00 |
| Ca | 0.31 | 0.20 | 0.17 | 0.12 | 0.10 | 0.31 | 0.30 | 0.18 | 0.19 |
| Na | 0.67 | 0.71 | 0.81 | 0.86 | 0.91 | 0.67 | 0.69 | 0.77 | 0.76 |
| K | 0.00 | 0.00 | 0.00 | 0.00 | 0.01 | 0.00 | 0.00 | 0.00 | 0.00 |
| Total | 4.99 | 4.94 | 5.00 | 4.99 | 5.02 | 4.99 | 5.00 | 4.97 | 4.97 |

Plagioclase end members

| | | | | | | | | | |
|------------|-------|-------|-------|-------|-------|-------|-------|-------|-------|
| Albite | 68.10 | 77.66 | 82.06 | 87.40 | 89.27 | 68.52 | 69.21 | 80.57 | 79.31 |
| Anorthite | 31.49 | 22.15 | 17.60 | 12.31 | 10.07 | 31.13 | 30.62 | 19.08 | 20.46 |
| Orthoclase | 0.41 | 0.18 | 0.34 | 0.28 | 0.66 | 0.35 | 0.17 | 0.35 | 0.33 |
| Si+Al | 4.00 | 4.02 | 4.00 | 4.01 | 4.00 | 4.00 | 4.01 | 4.01 | 4.01 |

Plagioclase

| | SD-89-329-2 | | | | | | SD-89-184 | |
|--------------------------------|-------------|-------|-------|--------|--------|--------|-----------|-------|
| | (rim) | (mid) | (mid) | (core) | (mid) | (mid) | (rim) | |
| SiO ₂ | 66.22 | 66.29 | 65.65 | 66.34 | 65.76 | 66.21 | 65.48 | 69.58 |
| TiO ₂ | 0.00 | 0.00 | 0.00 | 0.00 | 0.00 | 0.00 | 0.00 | 0.00 |
| Al ₂ O ₃ | 21.62 | 21.55 | 21.39 | 21.45 | 21.80 | 21.84 | 21.95 | 19.79 |
| Cr ₂ O ₃ | 0.00 | 0.00 | 0.00 | 0.00 | 0.03 | 0.00 | 0.00 | 0.00 |
| FeO | 0.19 | 0.00 | 0.00 | 0.00 | 0.03 | 0.00 | 0.00 | 0.00 |
| MnO | 0.00 | 0.00 | 0.00 | 0.00 | 0.00 | 0.00 | 0.00 | 0.00 |
| MgO | 0.00 | 0.00 | 0.00 | 0.00 | 0.00 | 0.00 | 0.00 | 0.00 |
| CaO | 1.68 | 1.65 | 1.68 | 1.81 | 2.15 | 2.16 | 2.50 | 6.57 |
| Na ₂ O | 10.35 | 10.19 | 10.37 | 10.66 | 10.11 | 9.84 | 10.41 | 9.96 |
| K ₂ O | 0.09 | 0.14 | 0.17 | 0.16 | 0.13 | 0.16 | 0.12 | 0.07 |
| Total | 100.15 | 99.82 | 99.26 | 100.41 | 100.01 | 100.20 | 100.23 | 99.77 |

number of cations on the basis of 8 oxygens

| | | | | | | | | |
|-------|------|------|------|------|------|------|------|------|
| Si | 2.90 | 2.91 | 2.90 | 2.90 | 2.89 | 2.89 | 2.87 | 3.02 |
| Ti | 0.00 | 0.00 | 0.00 | 0.00 | 0.00 | 0.00 | 0.00 | 0.00 |
| Al | 1.12 | 1.11 | 1.11 | 1.11 | 1.13 | 1.13 | 1.13 | 1.01 |
| Cr | 0.00 | 0.00 | 0.00 | 0.00 | 0.03 | 0.00 | 0.00 | 0.00 |
| Fe | 0.01 | 0.00 | 0.00 | 0.00 | 0.00 | 0.00 | 0.00 | 0.00 |
| Mn | 0.00 | 0.00 | 0.00 | 0.00 | 0.00 | 0.00 | 0.00 | 0.00 |
| Mg | 0.00 | 0.00 | 0.00 | 0.00 | 0.00 | 0.00 | 0.00 | 0.00 |
| Ca | 0.08 | 0.08 | 0.08 | 0.08 | 0.10 | 0.10 | 0.11 | 0.02 |
| Na | 0.88 | 0.87 | 0.87 | 0.90 | 0.86 | 0.83 | 0.89 | 0.84 |
| K | 0.01 | 0.01 | 0.01 | 0.01 | 0.01 | 0.01 | 0.01 | 0.00 |
| Total | 4.98 | 4.97 | 4.99 | 5.00 | 4.98 | 4.96 | 5.01 | 4.89 |

Plagioclase end members

| | | | | | | | | |
|------------|-------|-------|-------|-------|-------|-------|-------|-------|
| Albite | 91.29 | 91.03 | 90.88 | 90.60 | 88.81 | 88.34 | 88.52 | 77.15 |
| Anorthite | 8.19 | 8.15 | 8.14 | 8.50 | 10.44 | 10.72 | 10.81 | 22.84 |
| Orthoclase | 0.52 | 0.82 | 0.98 | 0.89 | 0.75 | 0.95 | 0.67 | 0.01 |
| Si+Al | 4.02 | 4.02 | 4.01 | 4.01 | 4.01 | 4.02 | 4.01 | 4.05 |

Plagioclase

SD-89-312-2

| | (rim) | (mid) | (mid) | (mid) | (mid) | (mid) | (core) |
|--------------------------------|-------|-------|-------|-------|-------|--------|--------|
| SiO ₂ | 63.19 | 65.79 | 62.98 | 62.34 | 64.57 | 62.98 | 66.57 |
| TiO ₂ | 0.00 | 0.00 | 0.00 | 0.00 | 0.00 | 0.00 | 0.00 |
| Al ₂ O ₃ | 22.78 | 21.17 | 22.90 | 23.71 | 23.49 | 23.47 | 22.93 |
| Cr ₂ O ₃ | 0.00 | 0.00 | 0.00 | 0.00 | 0.00 | 0.00 | 0.00 |
| FeO | 0.06 | 0.06 | 0.01 | 0.05 | 0.01 | 0.00 | 0.01 |
| MnO | 0.00 | 0.00 | 0.00 | 0.00 | 0.00 | 0.00 | 0.00 |
| MgO | 0.00 | 0.00 | 0.00 | 0.00 | 0.00 | 0.00 | 0.00 |
| CaO | 3.95 | 1.84 | 4.47 | 4.55 | 2.92 | 4.48 | 2.54 |
| Na ₂ O | 9.60 | 10.78 | 8.77 | 9.19 | 8.01 | 9.32 | 7.88 |
| K ₂ O | 0.04 | 0.04 | 0.26 | 0.09 | 0.96 | 0.25 | 0.53 |
| Total | 99.62 | 99.68 | 99.40 | 99.92 | 99.96 | 100.50 | 100.45 |

number of cations on the basis of 8 oxygens

| | | | | | | | |
|-------|------|------|------|------|------|------|------|
| Si | 2.80 | 2.90 | 2.80 | 2.76 | 2.84 | 2.78 | 2.89 |
| Ti | 0.00 | 0.00 | 0.00 | 0.00 | 0.00 | 0.00 | 0.00 |
| Al | 1.19 | 1.10 | 1.20 | 1.24 | 1.22 | 1.22 | 1.17 |
| Cr | 0.00 | 0.00 | 0.00 | 0.00 | 0.00 | 0.00 | 0.00 |
| Fe | 0.00 | 0.00 | 0.00 | 0.00 | 0.00 | 0.00 | 0.00 |
| Mn | 0.00 | 0.00 | 0.00 | 0.00 | 0.00 | 0.00 | 0.00 |
| Mg | 0.00 | 0.00 | 0.00 | 0.00 | 0.00 | 0.00 | 0.00 |
| Ca | 0.19 | 0.09 | 0.21 | 0.22 | 0.14 | 0.21 | 0.12 |
| Na | 0.83 | 0.92 | 0.76 | 0.79 | 0.68 | 0.80 | 0.66 |
| K | 0.00 | 0.00 | 0.01 | 0.01 | 0.05 | 0.01 | 0.03 |
| Total | 5.01 | 5.01 | 4.98 | 5.01 | 4.92 | 5.02 | 4.87 |

Plagioclase end members

| | | | | | | | |
|------------|-------|-------|-------|-------|-------|-------|-------|
| Albite | 81.29 | 91.18 | 76.85 | 78.12 | 78.11 | 77.92 | 81.81 |
| Anorthite | 18.48 | 8.60 | 21.65 | 21.37 | 15.73 | 20.70 | 14.57 |
| Orthoclase | 0.22 | 0.22 | 1.50 | 0.50 | 6.16 | 1.38 | 3.62 |
| Si+Al | 4.00 | 4.00 | 4.00 | 4.00 | 4.05 | 4.00 | 4.06 |

Plagioclase

| | F-123-79-1 | | | | | | | | G-123-80 | |
|--------------------------------|------------|--------|--------|--------|--------|-------|-------|-------|----------|--------|
| | (rim) | (mid) | (mid) | (core) | (mid) | (mid) | (rim) | (rim) | (mid) | (core) |
| SiO ₂ | 61.63 | 61.74 | 62.15 | 61.85 | 61.90 | 61.43 | 61.13 | 63.28 | 62.08 | 61.35 |
| TiO ₂ | 0.00 | 0.00 | 0.00 | 0.00 | 0.00 | 0.00 | 0.00 | 0.05 | 0.00 | 0.05 |
| Al ₂ O ₃ | 24.09 | 24.29 | 24.13 | 24.39 | 24.26 | 24.33 | 24.69 | 22.46 | 22.89 | 23.33 |
| Cr ₂ O ₃ | 0.00 | 0.00 | 0.00 | 0.00 | 0.00 | 0.00 | 0.00 | 0.00 | 0.00 | 0.00 |
| FeO | 0.00 | 0.00 | 0.00 | 0.00 | 0.00 | 0.00 | 0.00 | 0.07 | 0.01 | 0.01 |
| MnO | 0.00 | 0.00 | 0.00 | 0.00 | 0.00 | 0.00 | 0.00 | 0.01 | 0.01 | 0.01 |
| MgO | 0.00 | 0.00 | 0.00 | 0.00 | 0.00 | 0.00 | 0.00 | 0.00 | 0.02 | 0.00 |
| CaO | 5.09 | 5.21 | 5.14 | 5.17 | 5.11 | 5.19 | 5.56 | 4.20 | 4.95 | 5.39 |
| Na ₂ O | 8.80 | 8.88 | 8.68 | 8.93 | 8.93 | 8.83 | 8.56 | 9.00 | 8.56 | 8.65 |
| K ₂ O | 0.00 | 0.00 | 0.00 | 0.00 | 0.00 | 0.00 | 0.00 | 0.14 | 0.12 | 0.22 |
| Total | 99.60 | 100.12 | 100.10 | 100.33 | 100.21 | 99.79 | 99.94 | 99.21 | 98.64 | 98.87 |

number of cations on the basis of 8 oxygens

| | | | | | | | | | | |
|-------------------------|-------|-------|-------|-------|-------|-------|-------|-------|-------|-------|
| Si | 2.74 | 2.73 | 2.75 | 2.73 | 2.74 | 2.73 | 2.71 | 2.82 | 2.78 | 2.75 |
| Ti | 0.00 | 0.00 | 0.00 | 0.00 | 0.00 | 0.00 | 0.00 | 0.00 | 0.00 | 0.00 |
| Al | 1.26 | 1.27 | 1.26 | 1.27 | 1.27 | 1.27 | 1.29 | 1.18 | 1.21 | 1.23 |
| Cr | 0.00 | 0.00 | 0.00 | 0.00 | 0.00 | 0.00 | 0.00 | 0.00 | 0.00 | 0.00 |
| Fe | 0.00 | 0.00 | 0.00 | 0.00 | 0.00 | 0.00 | 0.00 | 0.00 | 0.00 | 0.00 |
| Mn | 0.00 | 0.00 | 0.00 | 0.00 | 0.00 | 0.00 | 0.00 | 0.00 | 0.00 | 0.00 |
| Mg | 0.00 | 0.00 | 0.00 | 0.00 | 0.00 | 0.00 | 0.00 | 0.00 | 0.00 | 0.00 |
| Ca | 0.24 | 0.25 | 0.24 | 0.24 | 0.24 | 0.25 | 0.26 | 0.20 | 0.24 | 0.26 |
| Na | 0.76 | 0.76 | 0.74 | 0.77 | 0.77 | 0.76 | 0.74 | 0.78 | 0.74 | 0.74 |
| K | 0.00 | 0.00 | 0.00 | 0.00 | 0.00 | 0.00 | 0.00 | 0.01 | 0.01 | 0.01 |
| Total | 5.01 | 5.01 | 4.99 | 5.01 | 5.01 | 5.01 | 5.01 | 4.99 | 4.97 | 5.00 |
| Plagioclase end members | | | | | | | | | | |
| Albite | 75.78 | 75.52 | 75.34 | 75.76 | 75.97 | 75.48 | 73.57 | 78.86 | 75.28 | 77.81 |
| Anorthite | 24.22 | 24.48 | 24.66 | 24.24 | 24.03 | 24.52 | 26.41 | 21.14 | 24.72 | 22.19 |
| Orthoclase | 0.00 | 0.00 | 0.00 | 0.00 | 0.00 | 0.00 | 0.00 | 0.00 | 0.00 | 0.00 |
| Si+Al | 4.00 | 4.00 | 4.01 | 4.00 | 4.00 | 4.00 | 4.01 | 4.00 | 4.00 | 4.00 |

APPENDIX B6:
K Feldspar Microprobe Analyses

| K Feldspar G-123-80 | | | | |
|--------------------------------|-------|--------|-------|-------|
| SiO ₂ | 64.44 | 65.48 | 65.19 | 65.22 |
| TiO ₂ | 0.04 | 0.02 | 0.04 | 0.04 |
| Al ₂ O ₃ | 18.02 | 19.50 | 19.34 | 19.00 |
| Cr ₂ O ₃ | 0.00 | 0.00 | 0.00 | 0.02 |
| FeO | 0.05 | 0.04 | 0.04 | 0.04 |
| MnO | 0.03 | 0.00 | 0.00 | 0.00 |
| MgO | 0.00 | 0.00 | 0.00 | 0.00 |
| CaO | 0.00 | 0.03 | 0.02 | 0.00 |
| Na ₂ O | 2.05 | 1.29 | 3.02 | 2.30 |
| K ₂ O | 14.29 | 13.82 | 11.80 | 13.14 |
| Total | 98.92 | 100.20 | 99.46 | 99.78 |

number of cations on the basis of 8 oxygens

| | | | | |
|-------|------|------|------|------|
| Si | 3.00 | 2.98 | 2.98 | 2.99 |
| Ti | 0.00 | 0.00 | 0.00 | 0.00 |
| Al | 0.99 | 1.05 | 1.04 | 1.03 |
| Cr | 0.00 | 0.00 | 0.00 | 0.00 |
| Fe | 0.00 | 0.00 | 0.00 | 0.00 |
| Mn | 0.00 | 0.00 | 0.00 | 0.00 |
| Mg | 0.00 | 0.00 | 0.00 | 0.00 |
| Ca | 0.00 | 0.00 | 0.00 | 0.00 |
| Na | 0.18 | 0.11 | 0.27 | 0.20 |
| K | 0.85 | 0.80 | 0.69 | 0.77 |
| Total | 5.02 | 4.95 | 4.98 | 4.99 |

| Feldspar end members | | | | |
|----------------------|-------|-------|-------|-------|
| Albite | 17.90 | 12.40 | 27.98 | 21.01 |
| Anorthite | 0.00 | 0.16 | 0.10 | 0.00 |
| Orthoclase | 82.10 | 87.44 | 71.92 | 78.99 |
| Si+Al | 3.99 | 4.03 | 4.02 | 4.01 |

APPENDIX B7:
Staurolite Microprobe Analyses

Stauroilite

| | G-118-80-3 | | G-158-80-1 | | G-158-80-3 | | SD 89 | SD 1 | | |
|-------|------------|-------|------------|-------|------------|-------|-------|-------|-------|-------|
| SiO2 | 26.26 | 27.39 | 26.41 | 25.24 | 26.66 | 27.10 | 27.22 | 26.98 | 27.54 | 27.05 |
| TiO2 | 0.32 | 0.37 | 0.42 | 0.37 | 0.46 | 0.70 | 0.66 | 0.44 | 0.54 | 0.48 |
| Al2O3 | 53.65 | 52.69 | 54.13 | 55.53 | 54.42 | 54.12 | 54.78 | 54.41 | 54.58 | 55.23 |
| Cr2O3 | 0.00 | 0.00 | 0.00 | 0.00 | 0.00 | 0.00 | 0.00 | 0.00 | 0.00 | 0.00 |
| FeO | 11.72 | 11.54 | 13.26 | 13.34 | 13.29 | 13.01 | 12.73 | 12.74 | 12.78 | 12.19 |
| MnO | 0.39 | 0.39 | 0.25 | 0.24 | 0.21 | 0.28 | 0.22 | 0.24 | 0.27 | 0.30 |
| MgO | 1.47 | 1.47 | 1.43 | 1.23 | 0.92 | 0.81 | 0.78 | 0.81 | 0.68 | 0.67 |
| CaO | 0.00 | 0.00 | 0.00 | 0.00 | 0.00 | 0.00 | 0.00 | 0.00 | 0.00 | 0.00 |
| Na2O | 0.06 | 0.05 | 0.00 | 0.01 | 0.03 | 0.00 | 0.01 | 0.02 | 0.01 | 0.01 |
| K2O | 0.00 | 0.00 | 0.00 | 0.00 | 0.00 | 0.00 | 0.00 | 0.00 | 0.00 | 0.00 |
| ZnO | 1.70 | 1.72 | 0.24 | 0.38 | 0.57 | 0.38 | 0.54 | 0.41 | 0.62 | 0.77 |
| Total | 95.58 | 95.62 | 96.14 | 96.34 | 96.55 | 96.41 | 96.45 | 96.05 | 96.50 | 96.73 |

number of cations on the basis of 24 oxygens

| | | | | | | | | | | |
|-------------|-------|-------|-------|-------|-------|-------|-------|-------|-------|-------|
| Si | 3.90 | 4.06 | 3.89 | 3.72 | 3.92 | 3.98 | 3.99 | 3.97 | 4.02 | 3.95 |
| Ti | 0.04 | 0.04 | 0.05 | 0.04 | 0.05 | 0.08 | 0.07 | 0.05 | 0.06 | 0.05 |
| Al | 9.40 | 9.20 | 9.41 | 9.66 | 9.43 | 9.36 | 9.37 | 9.43 | 9.39 | 9.50 |
| Cr | 0.00 | 0.00 | 0.00 | 0.00 | 0.00 | 0.00 | 0.00 | 0.00 | 0.00 | 0.00 |
| Fe | 1.46 | 1.43 | 1.63 | 1.65 | 1.63 | 1.60 | 1.56 | 1.57 | 1.50 | 1.62 |
| Mn | 0.05 | 0.05 | 0.03 | 0.03 | 0.03 | 0.03 | 0.03 | 0.03 | 0.03 | 0.04 |
| Mg | 0.33 | 0.32 | 0.31 | 0.27 | 0.20 | 0.18 | 0.17 | 0.18 | 0.15 | 0.15 |
| Ca | 0.00 | 0.00 | 0.00 | 0.00 | 0.00 | 0.00 | 0.00 | 0.00 | 0.00 | 0.00 |
| Na | 0.02 | 0.01 | 0.00 | 0.00 | 0.01 | 0.00 | 0.00 | 0.01 | 0.00 | 0.01 |
| K | 0.00 | 0.00 | 0.00 | 0.00 | 0.00 | 0.00 | 0.00 | 0.00 | 0.00 | 0.00 |
| Zn | 0.19 | 0.19 | 0.03 | 0.04 | 0.06 | 0.04 | 0.06 | 0.04 | 0.07 | 0.08 |
| Total | 15.37 | 15.31 | 15.36 | 15.41 | 15.32 | 15.27 | 15.25 | 15.27 | 15.22 | 15.25 |
| Fe/FMZM* | 72.19 | 71.80 | 81.48 | 82.80 | 84.95 | 86.32 | 85.90 | 86.15 | 85.89 | 84.84 |
| Mg/FMZM* | 16.13 | 16.30 | 15.66 | 13.61 | 10.48 | 9.58 | 9.38 | 9.76 | 8.67 | 8.51 |
| Zn/FMZM* | 9.24 | 9.45 | 1.30 | 2.08 | 3.22 | 2.23 | 3.22 | 2.45 | 3.82 | 4.73 |
| Mn/FMZM* | 2.43 | 2.46 | 1.56 | 1.51 | 1.36 | 1.88 | 1.50 | 1.64 | 1.91 | 2.11 |
| Si+Al | 13.30 | 13.26 | 13.30 | 13.38 | 13.34 | 13.34 | 13.36 | 13.40 | 13.41 | 13.44 |
| Fe+Mg+Zn+Mn | 2.02 | 1.99 | 2.01 | 1.99 | 1.92 | 1.85 | 1.82 | 1.82 | 1.75 | 1.75 |
| Fe/(Fe+Mg) | 0.82 | 0.81 | 0.84 | 0.86 | 0.89 | 0.90 | 0.90 | 0.90 | 0.91 | 0.91 |
| A | 72.51 | 72.40 | 70.70 | 71.59 | 71.98 | 72.52 | 73.04 | 73.00 | 74.03 | 74.41 |
| F | 0.82 | 0.81 | 0.84 | 0.86 | 0.89 | 0.90 | 0.90 | 0.90 | 0.91 | 0.91 |
| M | 0.18 | 0.19 | 0.16 | 0.14 | 0.11 | 0.10 | 0.10 | 0.10 | 0.09 | 0.09 |

*FMZM = Fe+Mg+Zn+Mn

Staurolite

| | SD-89-103-1 | | | SD-89-097a-1 | | | SD-89-353-4 | | |
|--------------------------------|-------------|-------|-------|--------------|-------|-------|-------------|-------|-------|
| SiO ₂ | 25.47 | 26.24 | 25.90 | 27.33 | 27.37 | 26.49 | 26.98 | 27.26 | 26.75 |
| TiO ₂ | 0.30 | 0.27 | 0.30 | 0.54 | 0.54 | 0.43 | 0.47 | 0.53 | 0.45 |
| Al ₂ O ₃ | 56.49 | 55.53 | 55.69 | 55.60 | 55.51 | 55.18 | 55.06 | 55.58 | 56.08 |
| Cr ₂ O ₃ | 0.00 | 0.00 | 0.00 | 0.00 | 0.00 | 0.00 | 0.00 | 0.00 | 0.00 |
| FeO | 11.01 | 11.48 | 11.54 | 12.14 | 12.06 | 13.60 | 13.80 | 12.73 | 13.57 |
| MnO | 0.41 | 0.35 | 0.37 | 0.46 | 0.46 | 0.19 | 0.23 | 0.26 | 0.26 |
| MgO | 0.71 | 0.89 | 0.78 | 0.68 | 0.78 | 1.11 | 1.06 | 0.92 | 0.78 |
| CaO | 0.00 | 0.00 | 0.00 | 0.00 | 0.00 | 0.00 | 0.00 | 0.00 | 0.00 |
| Na ₂ O | 0.07 | 0.07 | 0.04 | 0.02 | 0.02 | 0.00 | 0.00 | 0.00 | 0.00 |
| K ₂ O | 0.00 | 0.00 | 0.00 | 0.00 | 0.00 | 0.00 | 0.00 | 0.00 | 0.00 |
| ZnO | 1.97 | 1.75 | 1.70 | 0.54 | 0.62 | 0.19 | 0.17 | 0.27 | 0.28 |
| Total | 96.42 | 96.58 | 96.32 | 97.32 | 97.36 | 97.20 | 97.78 | 97.55 | 97.97 |

number of cations on the basis of 24 oxygens

| | | | | | | | | | |
|-------------|-------|-------|-------|-------|-------|-------|-------|-------|-------|
| Si | 3.74 | 3.85 | 3.81 | 3.96 | 3.96 | 3.86 | 3.91 | 3.94 | 3.86 |
| Ti | 0.03 | 0.03 | 0.03 | 0.06 | 0.06 | 0.05 | 0.05 | 0.06 | 0.05 |
| Al | 9.78 | 9.60 | 9.66 | 9.49 | 9.47 | 9.49 | 9.41 | 9.47 | 9.55 |
| Cr | 0.00 | 0.00 | 0.00 | 0.00 | 0.00 | 0.00 | 0.00 | 0.00 | 0.00 |
| Fe | 1.35 | 1.41 | 1.42 | 1.47 | 1.46 | 1.66 | 1.67 | 1.54 | 1.62 |
| Mn | 0.05 | 0.04 | 0.05 | 0.06 | 0.06 | 0.02 | 0.03 | 0.03 | 0.03 |
| Mg | 0.16 | 0.19 | 0.17 | 0.15 | 0.17 | 0.24 | 0.23 | 0.20 | 0.17 |
| Ca | 0.00 | 0.00 | 0.00 | 0.00 | 0.00 | 0.00 | 0.00 | 0.00 | 0.00 |
| Na | 0.02 | 0.02 | 0.01 | 0.01 | 0.01 | 0.00 | 0.00 | 0.00 | 0.00 |
| K | 0.00 | 0.00 | 0.00 | 0.00 | 0.00 | 0.00 | 0.00 | 0.00 | 0.00 |
| Zn | 0.21 | 0.19 | 0.18 | 0.06 | 0.07 | 0.02 | 0.02 | 0.03 | 0.03 |
| Total | 15.35 | 15.33 | 15.33 | 15.24 | 15.25 | 15.34 | 15.33 | 15.27 | 15.31 |
| Fe/FMZM* | 76.30 | 76.71 | 77.95 | 84.93 | 83.38 | 85.33 | 85.86 | 85.60 | 87.54 |
| Mg/FMZM* | 8.77 | 10.60 | 9.39 | 8.48 | 9.61 | 12.41 | 11.75 | 11.02 | 9.10 |
| Zn/FMZM* | 12.05 | 10.32 | 10.14 | 3.33 | 3.78 | 1.05 | 0.93 | 1.60 | 1.64 |
| Mn/FMZM* | 2.88 | 2.37 | 2.53 | 3.26 | 3.22 | 1.21 | 1.45 | 1.77 | 1.72 |
| Si+Al | 13.52 | 13.45 | 13.47 | 13.45 | 13.43 | 13.35 | 13.33 | 13.41 | 13.47 |
| Fe+Mg+Zn+Mn | 1.77 | 1.84 | 1.82 | 1.73 | 1.75 | 1.94 | 1.95 | 1.80 | 1.84 |
| Fe/(Fe+Mg) | 0.90 | 0.88 | 0.89 | 0.91 | 0.90 | 0.87 | 0.88 | 0.89 | 0.91 |
| A | 76.43 | 74.97 | 75.22 | 74.59 | 74.42 | 71.40 | 71.21 | 73.16 | 72.81 |
| F | 0.90 | 0.88 | 0.89 | 0.91 | 0.90 | 0.87 | 0.88 | 0.89 | 0.91 |
| M | 0.10 | 0.12 | 0.11 | 0.09 | 0.10 | 0.13 | 0.12 | 0.11 | 0.09 |

*FMZM = Fe+Mg+Zn+Mn

APPENDIX B8:
Andalusite Microprobe Analyses

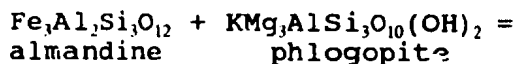
APPENDIX C:
Mixing Models

APPENDIX C1:
Exchange Thermometry

The basis of exchange thermometry lies in the exchange of atoms, either between sites within one mineral (intracrystalline) or between sites within two different minerals (intercrystalline) as a response to changes in T. The present investigation utilizes the intercrystalline exchange of Fe and Mg between biotite and garnet, and between cordierite and garnet. According to Perchuk and Lavrent'eva (1983), increasing temperature will result in the transfer of Mg from the hydrous phase (cordierite and biotite) to the anhydrous phase (garnet), the reverse occurring for Fe.

During metamorphism, cations of similar size and charge are partitioned into one phase over another, due to the chemical potential gradient for the element in question. They diffuse into the phases until the chemical potential gradient is eliminated (i.e. $\Delta\mu = 0$). Therefore, the distribution of cations changes, but the amounts of minerals present do not. Entropy changes are large, whereas volume changes are small for these reactions, and so they are sensitive to temperature, but relatively insensitive to pressure, making them potential thermometers.

The exchange of Fe and Mg between garnet and biotite involves the mass balanced reaction:



Ferry and Spear (1978) suggested an energy balance for this equilibrium can be expressed by:

$$\Delta G^\circ = \Delta H^\circ - T\Delta S^\circ + P\Delta V^\circ + RT\ln K$$

where, for ideal mixing in garnet and biotite,

$$K = \frac{(Mg/Fe)_{gr}}{(Mg/Fe)_{bi}}$$

and ΔH° , ΔS° , and ΔV° values for the reaction of:

$$\Delta H^\circ = 12\,454 \text{ cal}$$

$$\Delta S^\circ = 4.662 \text{ e.u.}$$

$$\Delta V^\circ = 0.057 \text{ cal/bar.}$$

Hodges and Spear (1982) inferred a new equilibrium expression based on the non-ideality of garnet. They assumed ideal mixing in biotite, but suggested caution be applied when Ti is a major component in that phase. Their expression is:

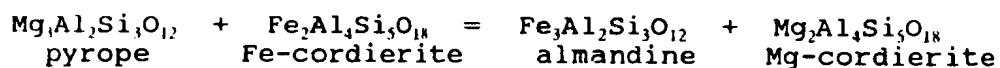
$$K = \frac{(a_{py}^{gr})^3 (a_{ann}^{bi})^3}{(a_{ph}^{bi})^3 (a_{al}^{gr})^3} = \frac{(X_{py}^{gr})^3 (X_{ann}^{bi})^3}{(X_{ph}^{bi})^3 (X_{al}^{gr})^3} \times \frac{(\gamma_{py}^{gr})^3}{(\gamma_{al}^{gr})^3}$$

where a = activity and γ is the activity coefficient; the latter terms account for the non-ideality in garnet. They followed the work of Ganguly and Kennedy (1974) and accounted for mixing in the Fe-Mg-Mn-Ca quaternary garnet system, such that,

$$\frac{(\gamma_{py}^{gr})}{(\gamma_{al}^{gr})} = \exp \left(\frac{[3300 - 1.5T(^{\circ}K)] (X_{gr}^2 + X_{al}X_{gr} + X_{gr}X_{sp} + X_{py}X_{gr})}{RT(^{\circ}K)} + \frac{W_{MgMn} (X_{sp}^2 + X_{gr}X_{sp} + X_{al}X_{sp} + X_{py}X_{sp})}{RT(^{\circ}K)} \right)$$

The W -term is the Margules parameter for the Mg-Mn binary join in the quaternary system. They found that at temperature ranges equivalent to those in the MCSZ, $W_{\text{MgMn}} \sim 0$ indicating that pyrope-spessartine solutions are ideal at those temperatures. Hodges and Spear (1982) suggested an accuracy of ± 50 °C for this thermometer.

The garnet-cordierite thermometer also utilizes the exchange of Fe and Mg between the two phases. It is based on the reaction:



Perchuk et al. (1985) showed that the energy balance for this reaction can be expressed by the following equation:

$$T = \frac{3087 + 0.018P}{\ln K_D + 1.342}$$

$$\text{where } K_D = \frac{X_{\text{Fe}}^{\text{py}} X_{\text{Mg}}^{\text{Mg-crd}}}{X_{\text{Mg}}^{\text{py}} X_{\text{Fe}}^{\text{Fe-crd}}}$$

This equation uses the following thermodynamic parameters:

$$\Delta H^\circ = -6134 \text{ cal}$$

$$\Delta S^\circ = -2.688 \text{ e.u.}$$

$$\Delta V^\circ = -0.03535 \text{ cal/bar}$$

Perchuk et al. (1985) assumed an ideal two-site model for cordierite (Fe-Mg exchange) which takes into account H_2O in the structural channels. This seems reasonable for sample G-123-80 which, from an average of six analyses contains only 0.55 wt% MnO (and 0.29 wt% Na_2O).

For garnet, the authors estimated the activity of the components in the Fe-Mg-Mn-Ca quaternary system as follows (from interaction of the binary bounding systems):

$$RT\ln a_{\text{Gros}} = 3[RT\ln X_{\text{Ca}} + (2404 + 0.258T)X_{\text{Ca}}(2 - X_{\text{Ca}}) \\ + (5704 - 1.242T)X_{\text{Mg}}(1 - X_{\text{Ca}}) \\ - (234 + 0.748T)] + 3PV_{\text{Gros}}^{\text{e}}$$

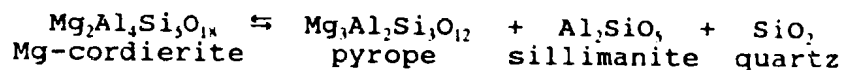
$$RT\ln a_{\text{Alm}} = 3[RT\ln X_{\text{Fe}} + (2404 + 0.258T)X_{\text{Ca}}^2 \\ + (5704 - 1.242T)X_{\text{Ca}}X_{\text{Mg}}]$$

$$RT\ln a_{\text{Pyr}} = 3[RT\ln X_{\text{Mg}} + (3300 - 1.5T)X_{\text{Ca}}^2 \\ + (5704 - 1.242T)X_{\text{Ca}}X_{\text{Fe}}]$$

where $V_{\text{Gros}}^{\text{e}}$ is the partial excess molar volume of the grossular component. Perchuk et al. (1985) suggested an accuracy of ± 12 °C for the geothermometer.

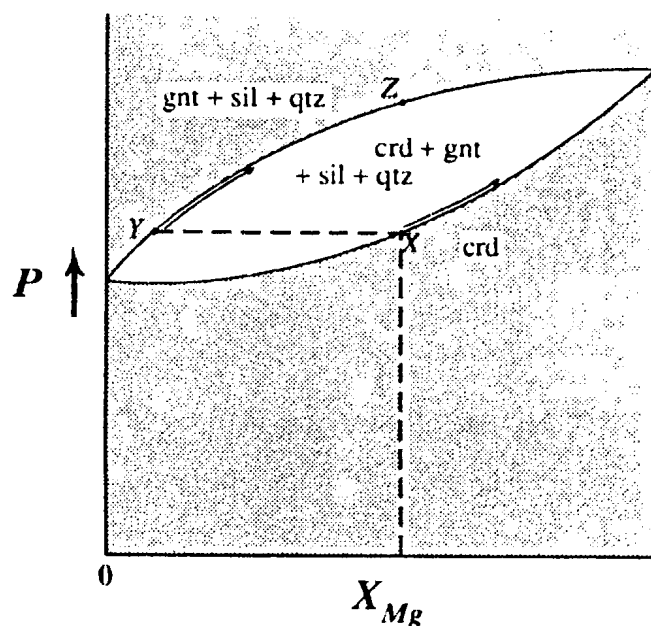
APPENDIX C2:
Geobarometry

The barometer involving cordierite-garnet-sillimanite-quartz (Perchuk et al., 1985) uses the change in volume of the following reaction,



For pure end-members, this reaction takes place at a specific pressure (discontinuous reaction). For intermediate compositions, cordierite of composition X breaks down to garnet of composition Y plus sillimanite and quartz (Figure C2-1). With increasing P , both become more Mg-rich until garnet reaches composition Z , at which time there is no cordierite left.

Figure C2-1. A P - X_{Mg} diagram for the cordierite \rightleftharpoons garnet + sillimanite + quartz reaction.



The thermodynamic parameters of the reaction above are:

$$\Delta H^\circ = 51 \text{ cal}$$

$$\Delta S^\circ = 4.62 \text{ e.u.}$$

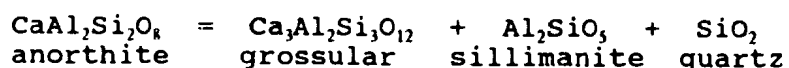
$$\Delta V^\circ = 0.63827 \text{ cal/bar}$$

When these are combined with the activity equations for pyrope and cordierite (see garnet-cordierite mixing model above), Perchuk et al. (1985) obtained the equation:

$$P(\text{bar}) = 2605 + T(7.855 - 4.310 \ln K_{Mg})$$

where $K_{Mg} = X_{Mg} = X_{Mg}^{cd} / X_{Mg}^{gt}$, and T is in °K. Aranovich and Poulesskii (1983) estimated an accuracy of ± 1 kilobar for this barometer.

The second barometer used in this study is the plagioclase-garnet-aluminosilicate-quartz barometer. It involves the volume change as the An-component in plagioclase breaks down to grossular garnet, aluminosilicate and quartz. The relevant end-member reaction is:



In this reaction, the important parameters are the activity (α) of the Ca-component (grossular) in garnet and the Ca-component (anorthite) in plagioclase, and the volume changes for each of the phases. Newton and Haselton (1981) suggested that the pressure for the reaction can be calculated by using the following formula:

$$\Delta P_{[\text{bars}]}^{\circ} = \frac{\left(\Delta P_{[\text{bars}]}^{\circ} \times \Delta V_{\text{A}}^{\circ} [\text{J/deg}] \times -3RT_{[\text{K}]} \times \ln \frac{\alpha_{\text{gr}}^3}{\alpha_{\text{an}}^3} \right)}{V_{[\text{J/bar}]}}$$

Where:

$$R_{[\text{J/deg}]} = 8.314$$

$$\Delta V_{[\text{cm}^3]} = V_{\text{g}} + 2V_{\text{als}} + V_{\text{gr}} - 3V_{\text{an}}$$

$$V_{\text{gr}}_{[\text{cm}^3]} = \frac{(X_{\text{py}} \times V_{\text{gr-py}}) + (X_{\text{alm}} \times V_{\text{gr-alm}})}{(X_{\text{py}} + X_{\text{alm}})}$$

$$V_{\text{gr-py}}_{[\text{cm}^3]} = 125.24 + 0.512(1 - X_{\text{gr}})^2 - 0.418 \times 1 +$$

$$\frac{(1 - X_{\text{gr}} - 0.94)(1 - X_{\text{gr}})}{(0.083)^2} \times \exp\left(\frac{-(1 - X_{\text{gr}} - 0.94)^2}{2(0.066)^2}\right)$$

$$V_{\text{gr-alm}}_{[\text{cm}^3]} = 125.24 + 1.482 \times (1 - X_{\text{gr}})^2 - 0.480 \times 1 +$$

$$\frac{(1 - X_{\text{gr}} - 0.94)(1 - X_{\text{gr}})}{(0.083)^2} \times \exp\left(\frac{-(1 - X_{\text{gr}} - 0.94)^2}{2(0.066)^2}\right)$$

$$\alpha_{\text{gr}}^{\text{ent}} = X_{\text{gr}} \times \exp\left(\frac{(3300 - 1.5 \times T_{[\text{K}]}) (X_{\text{py}}^2 + X_{\text{py}}X_{\text{alm}})}{R_{[\text{cal/deg}]} \times T_{[\text{K}]}}\right)$$

$$\alpha_{\text{an}}^{\text{plag}} = \frac{X_{\text{an}}(1 - X_{\text{an}})^2}{4} \exp\left(\frac{(1 - X_{\text{an}})^2}{R_{[\text{cal/deg}]} \times T_{[\text{K}]}} (2050 + 9392X_{\text{an}})\right)$$

Thermodynamic data for sillimanite are given by Newton and Haselton (1981). These are:

$$V_{\text{sill}} = 44.09 \text{ cm}^3$$

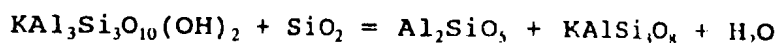
$$\Delta V_{[\text{J/bar}]}^{\circ} = -6.6202$$

$$\Delta P_{(\text{bar})}^{\circ} = -1170 + 23.8 T(^{\circ}\text{C})$$

APPENDIX D:
Estimate of the Activity of Water
in Sample G-123-80

Activity of Water

The breakdown of ideal muscovite (MU) + quartz (Q) to aluminosilicate (AL) + alkali feldspar (AF) + fluid (F) occurs in rocks within the MCSZ at high metamorphic grade. The end-member reaction has the form



This reaction takes place in the upper part of the amphibolite facies (Powell, 1978). The precise P-T conditions are dependent upon the activity of H_2O in the fluid and the composition of the solid phases. In the above reaction, there is typically only minor variation in the composition of the solid phases, but there may be major variations in the composition of the fluid phase.

One sample in particular (G-123-80) contains the four phases (muscovite-quartz-sillimanite-K-feldspar) in equilibrium. Independent estimates of pressure and temperature have been made for this sample and these data can be used to estimate the activity of water in this sample at the time of the muscovite + quartz breakdown reaction. As this is the only sample that contains the appropriate assemblage, this is a local estimate only and extrapolation across a wide area of the MCSZ is not realistic.

Using the thermodynamic data of Powell (1978, Appendix A) for the above reaction, we obtain, for each aluminosilicate phase:

$$\Delta G_{\lambda}^{\circ} = 98.0 - 0.1747T + 0.31P + F_{H_2O}$$

$$\Delta G_{\xi}^{\circ} = 104.3 - 0.1808T + 0.48P + F_{H_2O}$$

$$\Delta G_{\kappa}^{\circ} = 95.0 - 0.1668T + 1.05P + F_{H_2O}$$

where T is temperature in $^{\circ}K$, P is pressure in kilobars, R is the gas constant in kilojoules/ $^{\circ}K$ and F_{H_2O} is equal to $RT \ln f_{H_2O}$, where f_{H_2O} is the fugacity of H_2O at a given P and T . Powell (1978) has tabulated values of F_{H_2O} (using the thermodynamic data of Burnham et al., 1969) for pressures and temperatures of relevance to crustal metamorphism (see Powell 1978, Appendix A). In the case of pure phases, the equilibrium relation is:

$$\Delta G = 0 = \Delta G_{\lambda l}^{\circ} + RT \ln f_{H_2O} + RT \ln X_{H_2O} + RT \ln \gamma_{H_2O}$$

The fugacity term accounts for the fact the H_2O is not an ideal gas; X_{H_2O} is the mol. fraction of H_2O in the fluid during the progress of the reaction and accounts for the possibility that H_2O is mixed with another gas/fluid species; and the activity coefficient term accounts for the possibility of non-ideal mixing between H_2O and the other fluid species. However, since the identity of the other species is unknown, we assume ideal mixing and $\gamma = 1$.

To calculate X_{H_2O} for an assemblage where P and T are known, the equation above can be rearranged to give:

$$\ln X_{H_2O} = \frac{-\Delta G_{\lambda l}^{\circ} - F_{H_2O}}{RT}$$

Since sample G-123-80 contains sillimanite as the aluminosilicate phase,

$$\Delta G_s^\circ = 104.3 - 0.1808T + 0.48P + F_{H_2O} + RT \ln X_{H_2O}$$

The pressure and temperature estimates (2.95 kbar and 565 °C) indicate that (extrapolating between 2 and 4 kbar):

$$F_{H_2O} = -27.4 + 0.0977T$$

The equilibrium becomes:

$$0 = 104.3 - 0.1808T + 0.48P - 27.4 + 0.0977T + RT \ln X_{H_2O}$$

$$\ln X_{H_2O} = \frac{-76.9 + 0.0831(838) - 0.48(2.95)}{(8.3143 \times 10^{-3})(838)}$$

Solving this, $X_{H_2O} = 0.29$. If we assume ideal mixing (since the identity of the other component(s) in the fluid is unknown), the activity of water is also 0.29.

If the phases are not pure, we need to add another $RT \ln X$ term to account for the solid state mixing. From the microprobe analyses of K feldspar, and assuming coupled substitution,

$$X_K^{\text{K feldspar}} = \frac{X_K}{X_K + X_{Na}}$$

$$= 0.80 \pm 0.08$$

Although no analyses were made on muscovite from sample G-123-80, numerous analyses were done on muscovite from other samples. There is little variation (see Appendix B4). An average of 12 analyses from samples from above the sillimanite-biotite-muscovite isograd indicates that,

$$X_K^{\text{muscovite}} = \frac{X_K}{X_K + X_{Na} + X_{Ca}}$$

$$= 0.87 \pm 0.03$$

This value is assumed for sample G-123-80; it is based on an ideal on-site mixing model.

Utilizing these values for the compositions of muscovite and K-feldspar, and assuming ideal mixing (i.e. $\gamma = 1$, not an unreasonable assumption with compositions close to end-member), the activities are equal to mol. fraction. The equilibrium then becomes:

$$0 = 104.3 - 0.1808T + 0.48P - 27.4 + 0.0977T + RT \ln X_K + RT \ln X_{H_2O}$$

where $X_K = X_K^{K\text{-feldspar}} / X_K^{\text{muscovite}} = 0.91$, assuming that quartz and sillimanite are pure phases. By solving this equation, $X_{H_2O} = 0.31$.

Another approach to the calculation of $X_{\text{muscovite}}^{\text{white mica}}$ would be to include mixing on the octahedral and tetrahedral sites in muscovite as well. Mixing on the hydroxyl site is neglected since there is no information on site occupancies. To determine how this effects the activity of water, the muscovite analysis from a sample adjacent to G-123-80, but slightly higher grade, will be used. This analysis yields a formula for muscovite as follows:



To calculate the $X_{\text{muscovite}}^{\text{white mica}}$ we assume ideal on-site mixing and an ideal solution model. Thus,

$$\begin{aligned}
 X_{\text{white mica muscovite}}^{\text{white mica}} &= X_K^A \cdot (X_{\text{Al}}^M)^2 \cdot X_{\text{Al}}^{T4} \cdot (X_{\text{Si}}^{T1-3})^3 \\
 &= \frac{K}{K+Na} \cdot \left(\frac{\text{Al}^A}{\text{Al}^A + \text{Mg} + \text{Fe}} \right)^2 \cdot \left(\frac{\text{Al}^{T4}}{\text{Al}^{T4} + \text{Si}^{T4}} \right) \cdot \left(\frac{\text{Si}^{T1-3}}{\text{Si}^{T1-3}} \right) \\
 &= 0.88 \cdot 0.81 \cdot 0.88 \cdot 1.00 \\
 &= \underline{0.63}
 \end{aligned}$$

Hence, accounting for this mixing, the X_K term becomes

$$\frac{X_{\text{Kfeldspar}}^{\text{feldspar}}}{X_{\text{white mica muscovite}}^{\text{white mica}}} = 1.27$$

By incorporating this into the $RT \ln X_K$ term, the activity of water becomes 0.22. For the assemblage in sample G-123-80, the assumption of ideal solution and ideal on site mixing is used.

We must now calculate the amount of error in the estimation of $a_{\text{H}_2\text{O}}$. By using the published accuracies of the thermometer ($\pm 12^\circ\text{C}$) and barometer (± 1 kilobar) used to calculate T and P, an accuracy of the activity of water can be determined. If both errors are correlated so as to minimize the estimate of $a_{\text{H}_2\text{O}}$, the equilibrium term becomes,

$$0 = 104.3 - 0.1808T + 0.48P - 27.21 + 0.1003T +$$

$$RT \ln X_K + RT \ln X_{\text{H}_2\text{O}}$$

Thus, following the calculations above for ideal on site mixing and ideal solution,

$$\ln X_{\text{H}_2\text{O}} = \frac{-77.09 + 0.0805(850) - 0.48(3.95)}{(8.3143 \times 10^3)(850)}$$

$$X_{\text{H}_2\text{O}} = 0.22.$$

If both estimates are correlated so as to maximize the calculated estimate of $a_{\text{H}_2\text{O}}$, the equilibrium term becomes,

$$0 = 104.3 - 0.1808T + 0.48P - 27.69 + 0.0948T + RT \ln X_k + RT \ln X_{\text{H}_2\text{O}}$$

$$X_{\text{H}_2\text{O}} = 0.39.$$

Therefore, the activity of water equals $0.31^{+0.08}_{-0.09}$. This error range is associated only with the P-T estimates; an estimate of the error associated with the various mixing models cannot easily be made (Powell, 1978). This is also a maximum range since there is no reason to believe that the errors in the P and T estimates should be correlated.

GEOLOGICAL MAP

Cordierite Granodiorite (biotite cordierite muscovite-sillimanite granodiorite)

Through Hill Granite (and related smaller intrusions)
(garnet muscovite (pegmatitic) granite)

Partridgeberry Hills Granite (fine to coarse grained, chloritized and
sericitized, perthitic microcline, muscovite, biotite granite)*

Spruce Brook Formation (interbedded pelites and psammites)

Ophiolite Rocks (pseudotite, serpentinite, pyroxenite, gabbro,
iron, diorite, mafic pillow lava)

Mafic Dyke (fine to medium grained diabase)

Fault

Inferred Contact

Reaction Isograd

Biotite Muscovite Chlorite

Andalusite Biotite Muscovite

Sillimanite Biotite Muscovite

Sillimanite Potassium Feldspar

Zone of Partial Melting

Bedding** (inclined, vertical)

Foliation S (inclined, vertical)

High Strain Fabric (inclined, vertical)

F₁ Fold Axial Plane

F₂ Fold Axis

* Description from Colman, Sadd, 1985

** Bedding is S, however, S is parallel to B.

5

4

3

2

1

85

80

75

70

65

60

55

50

45

40

35

30

25

20

15

10

5

0

35

30

25

20

15

10

5

0

35

30

25

20

15

10

5

0

35

30

25

20

15

10

5

0

35

30

25

20

15

10

5

0

35

30

25

20

15

10

5

0

35

30

25

20

15

10

5

0

35

30

25

20

15

10

5

0

35

30

25

20

15

10

5

0

35

30

25

20

15

10

5

0

35

30

25

20

15

10

5

0

35

30

25

20

15

10

5

0

35

30

25

20

15

10

5

0

35

30

25

20

15

10

5

0

35

30

25

20

15

10

5

0

35

30

25

20

15

10

5

0

35

30

25

20

15

10

5

0

35

30

25

20

15

10

5

0

35

30

25

20

15

10

5

0

35

30

25

20

15

10

5

0

35

30

25

20

15

10

5

0

35

30

25

20

15

10

5

0

35

30

25

20

15

10

5

0

35

30

25

20

15

10

5

0

35

30

25

20

15

10

5

0

35

30

25

20

15

10

5

0

35

30

25

20

15

10

5

0

35

30

25

20

15

10

5

0

35

30

25

20

15

10

5

0

35

30

25

20

15

10

5

0

35

30

25

20

15

10

5

0

35

30

25

20

15

10

5

0

35

30

25

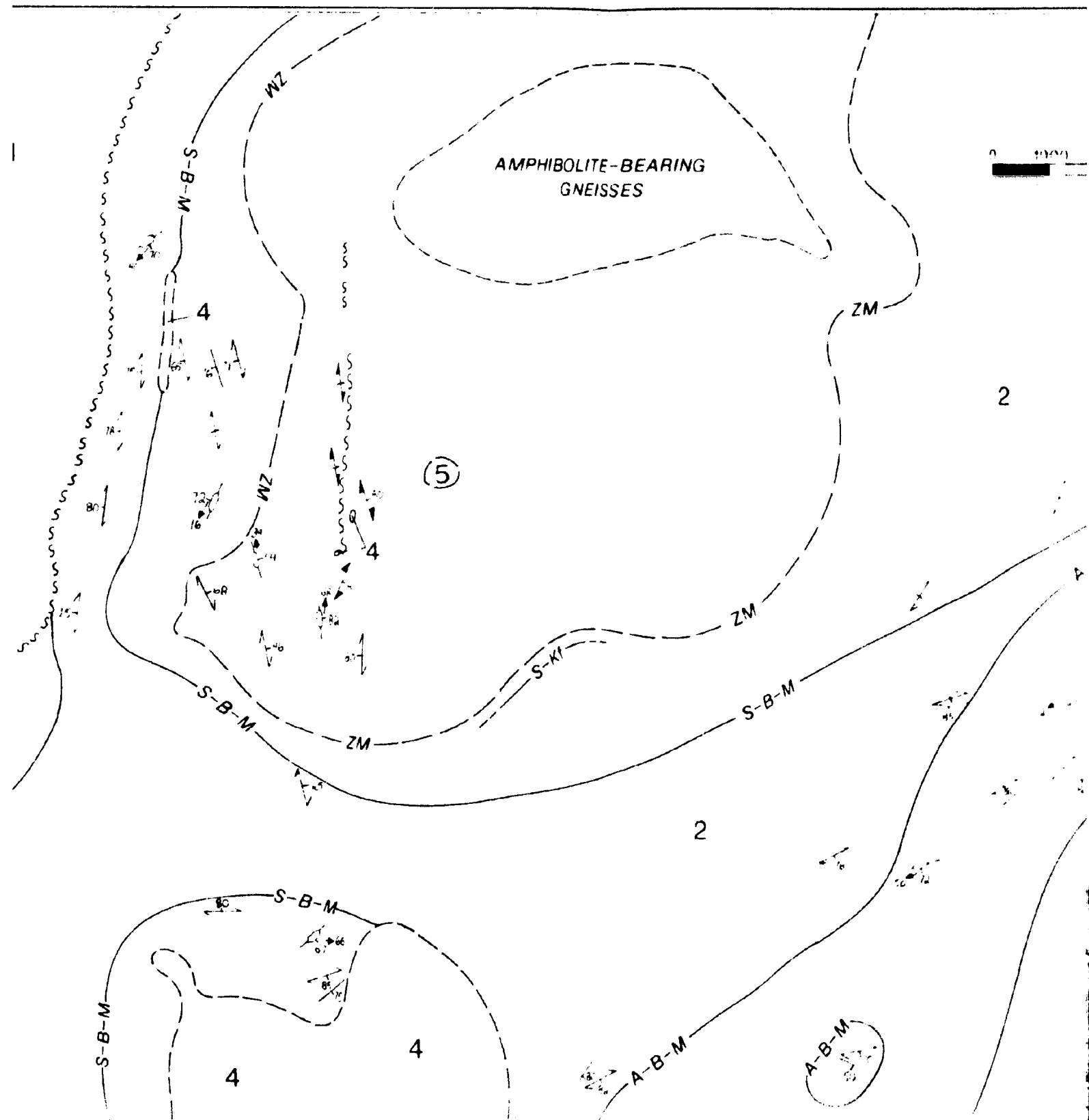
20

15

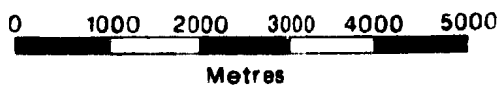
10

5

0



EARING



ZM

2

4

A-B-M

S-B-M

B-M-C

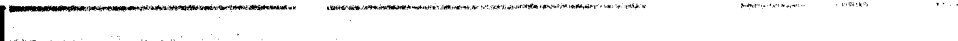
2

1

A-B-M

A-B-M





STRUCTURAL MAP

Fault

Inferred Contact

Reaction Isograds

Biotite-Muscovite-Chlorite

Andalusite-Biotite-Muscovite

Sillimanite-Biotite-Muscovite

Sillimanite-Potassium Feldspar

Zone of Partial Melting

Bedding* (inclined, vertical)

Foliation - S_2 (inclined, vertical)

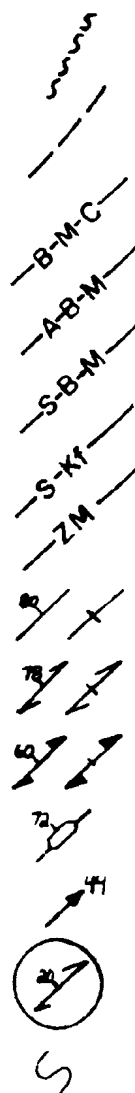
High Strain Fabric (inclined, vertical)

F_2 Fold Axial Plane

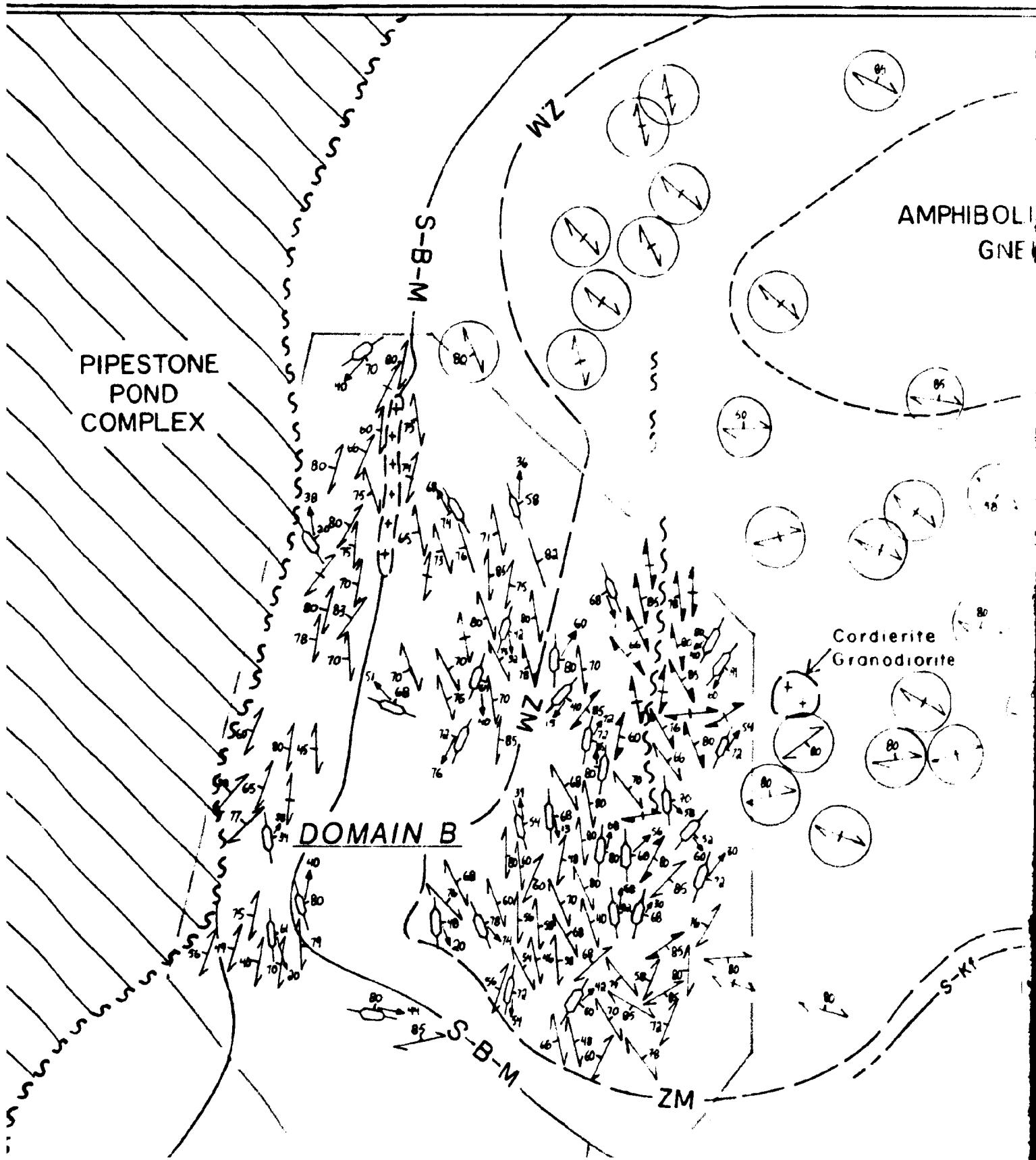
F_2 Fold Axis

Structural Measurements of S.P. Colman-Sadd

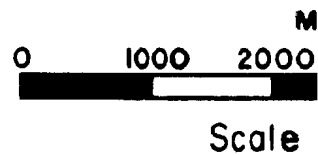
Sense of Vergence of Small-Scale F_2 Folds



* Bedding is S_0 ; however, S_1 is parallel to S_0 .



AMPHIBOLITE-BEARING
GNEISSES



Cordierite
Granodiorite

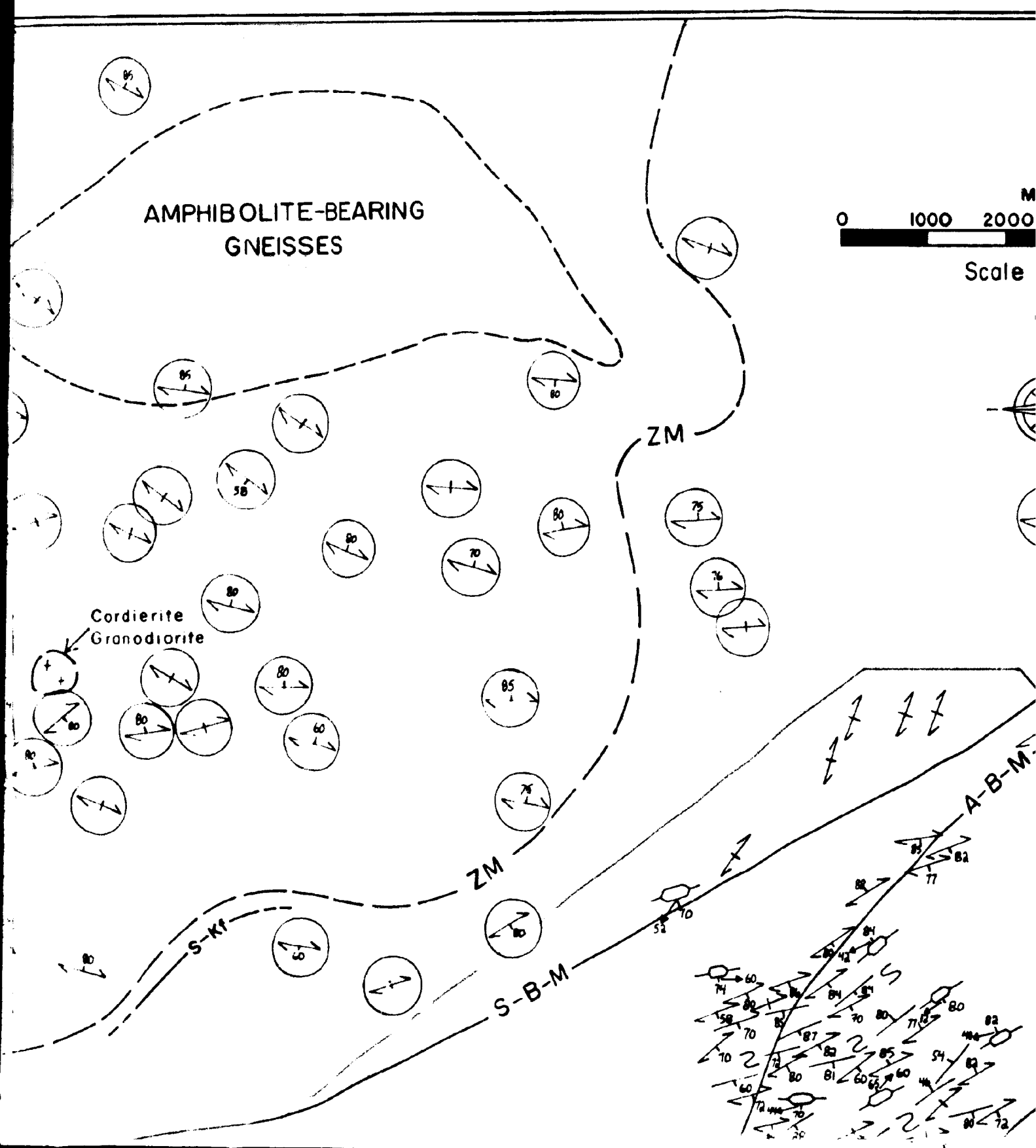
ZM

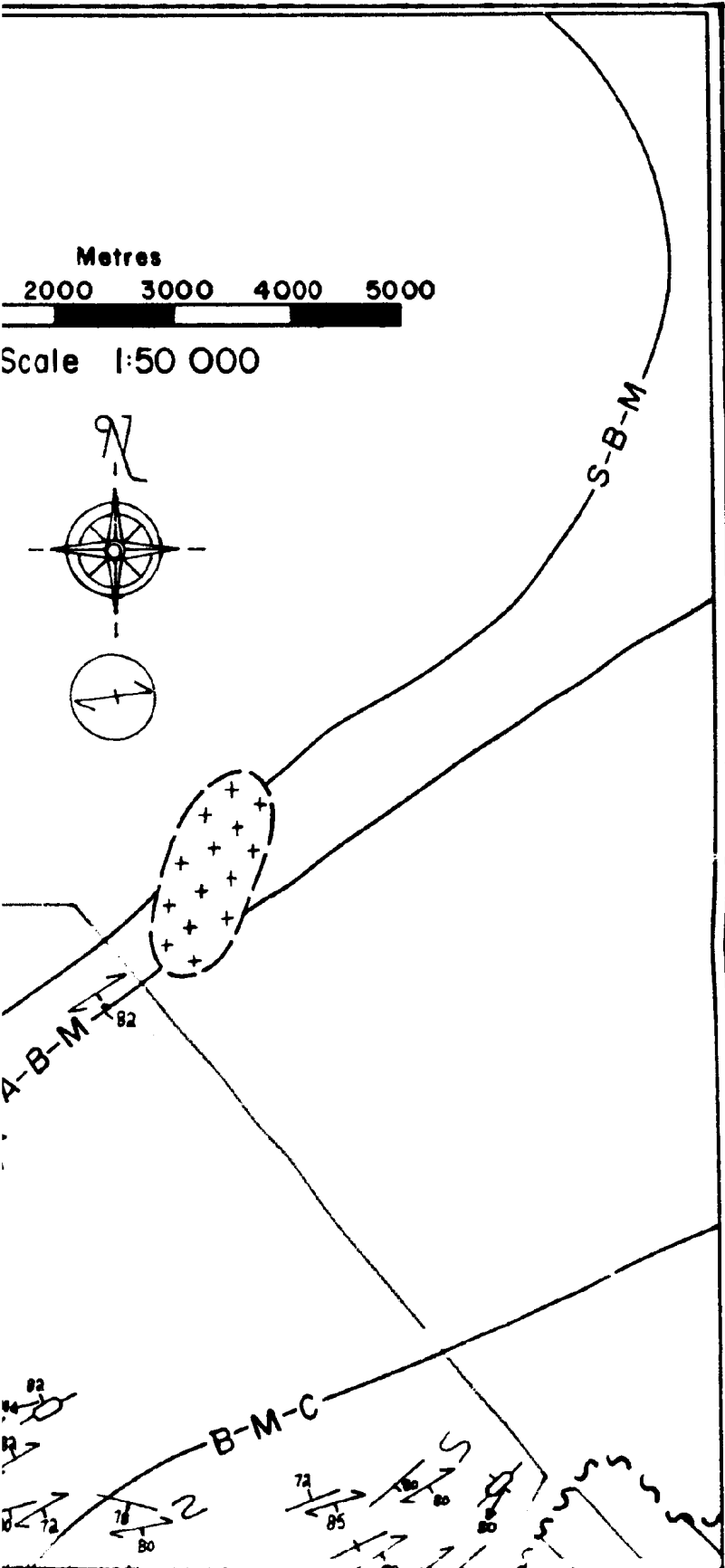
ZM

S-Kf

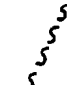

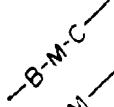
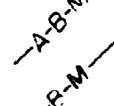
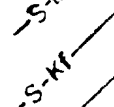
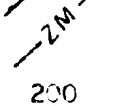


S-B-M

A-B-M

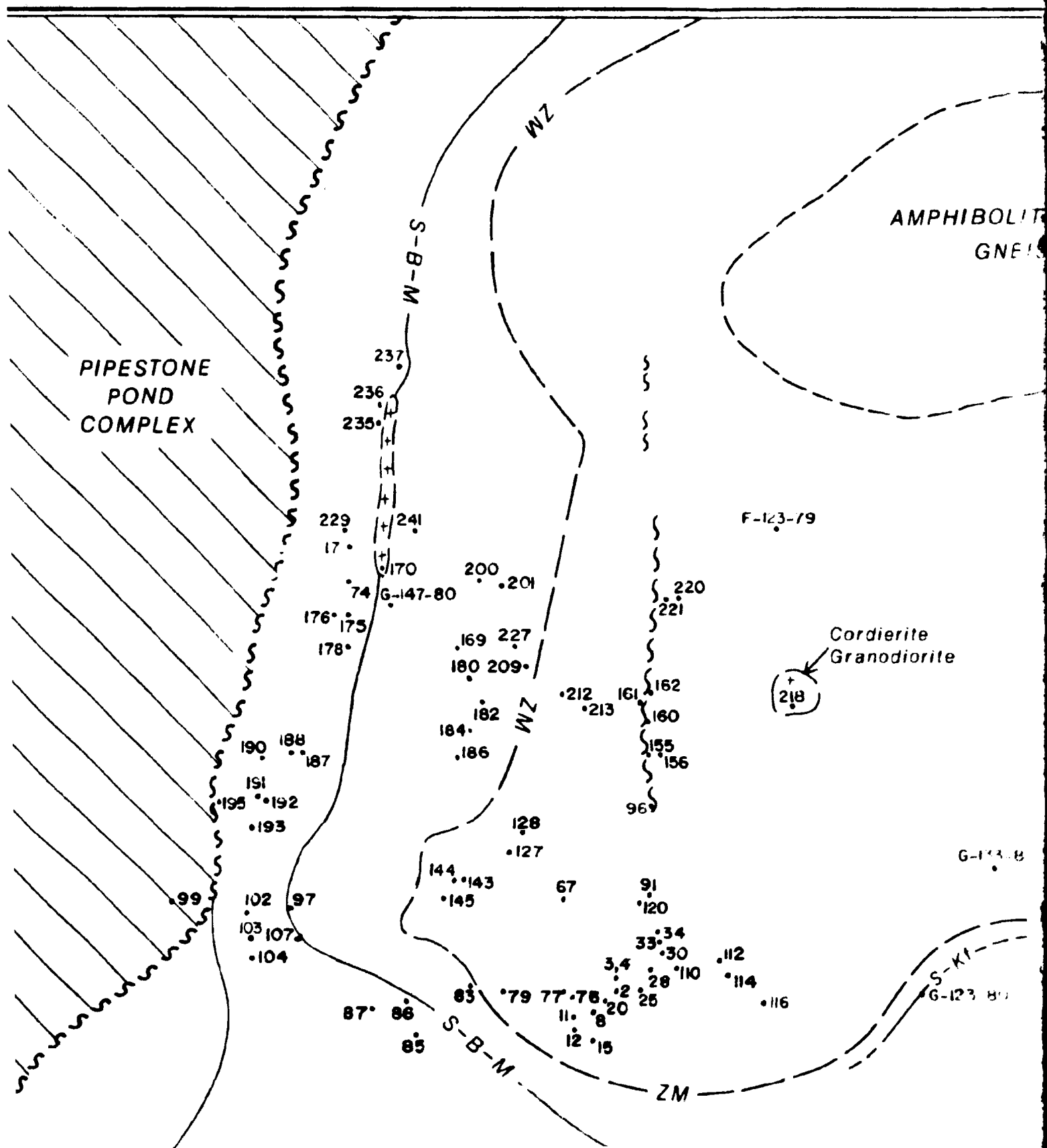




SAMPLE LOCATION MAP

| | |
|---|---|
| Fault |  |
| Inferred Contact |  |
| Reaction Isograds | |
| Biotite-Muscovite-Chlorite |  |
| Andalusite-Biotite-Muscovite |  |
| Sillimanite-Biotite-Muscovite |  |
| Sillimanite-Potassium Feldspar |  |
| Zone of Partial Melting |  |
| Sample Location (corresponds to station number) |  |

* Sample numbers prefixed F- and G- collected by S.P. Colman-Sadd. Others are prefixed SD-89- in the text.



AMPHIBOLITE-BEARING
GNEISSES

0 1000 2000
Scale



F-123-79

Cordierite
Granodiorite

(218)

G-133-80

S-K1
G-123 80

ZM

ZM

S-B-M

A-B-N

307

310

312

306

287, -8, -9

304

285

302

282

284

266

280, 281

267

268

262

252

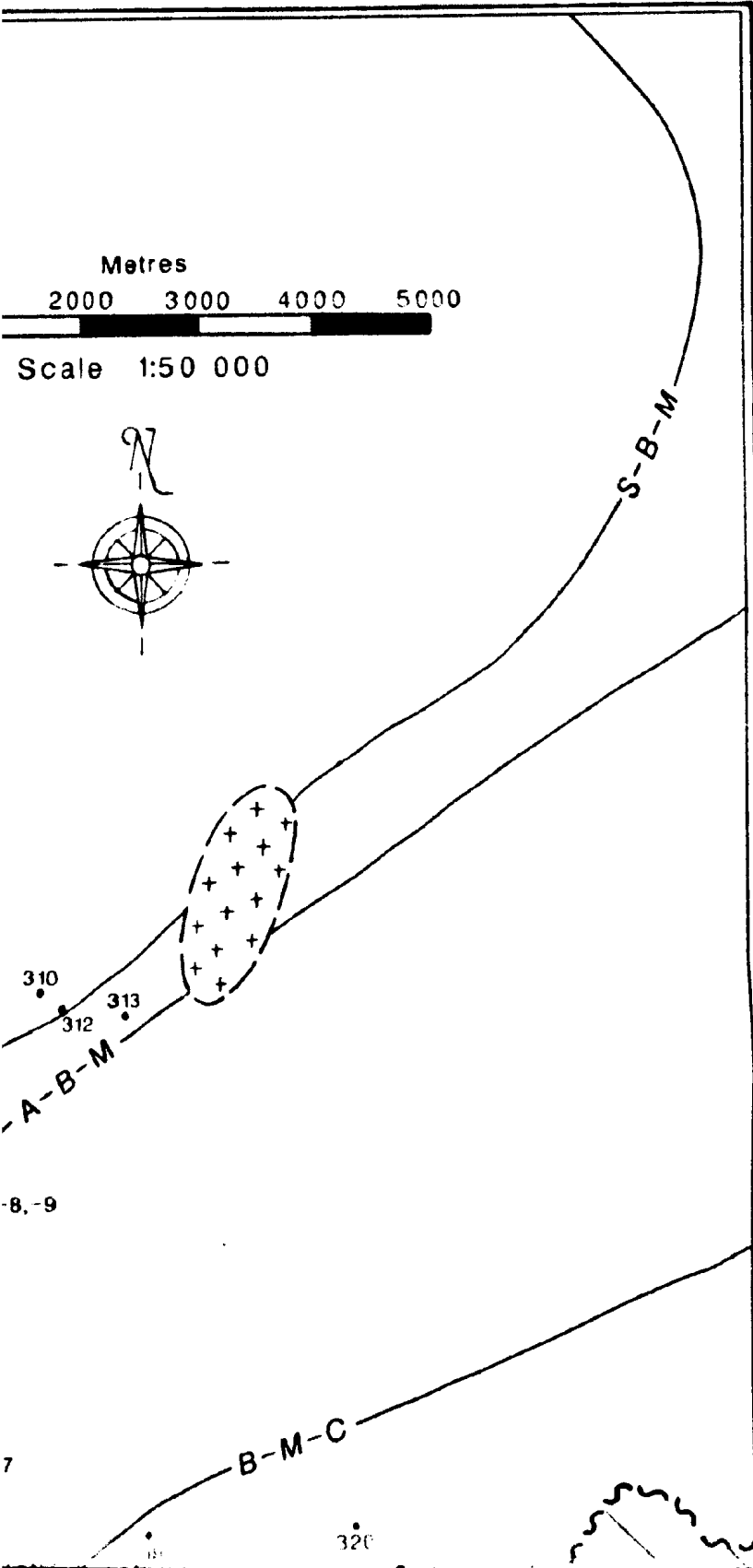
247

261

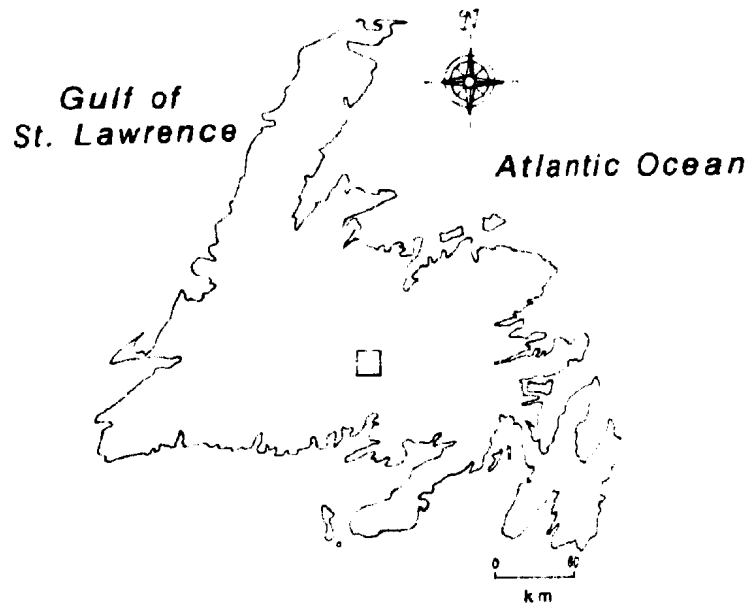
216

116

114

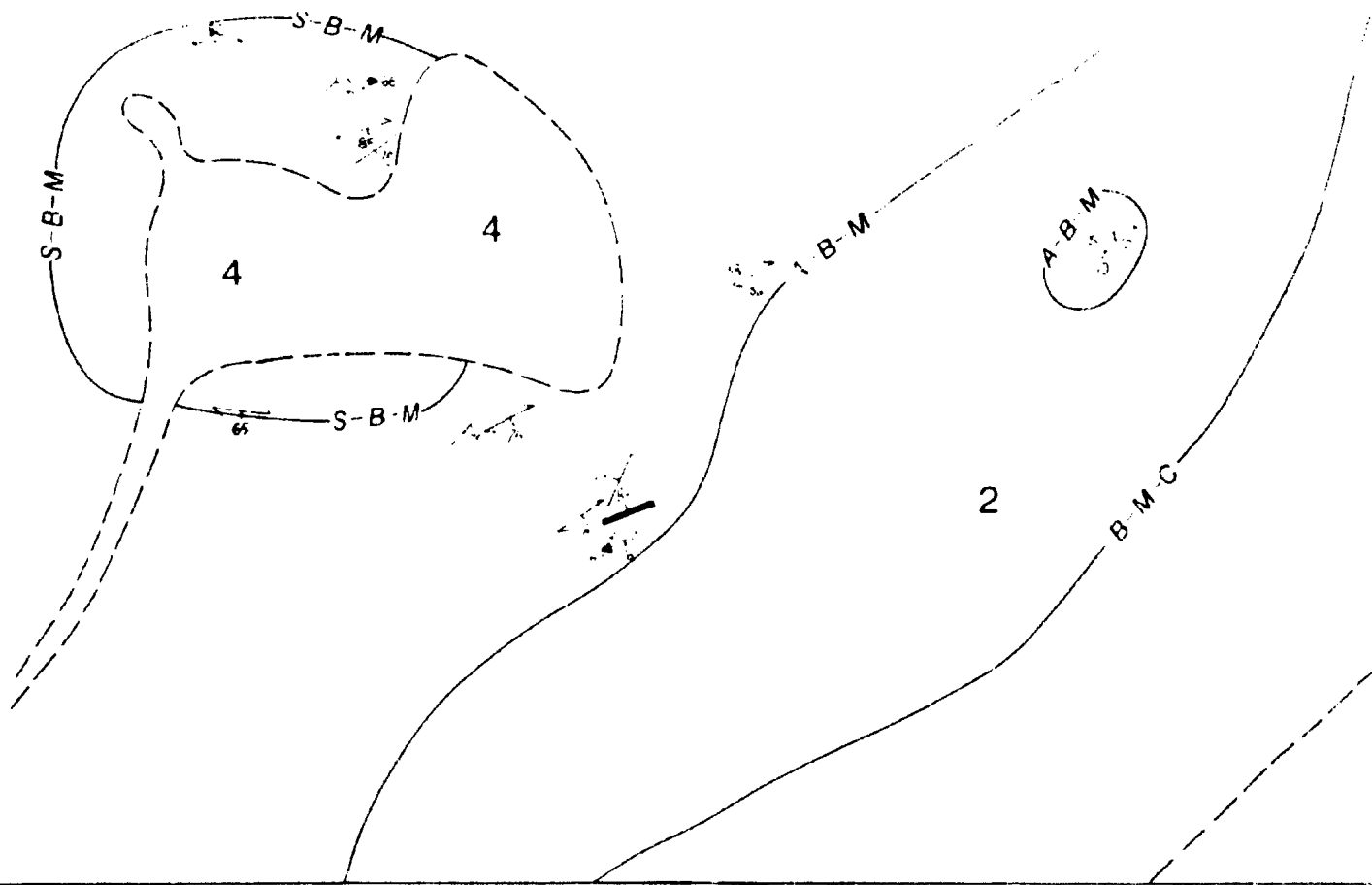


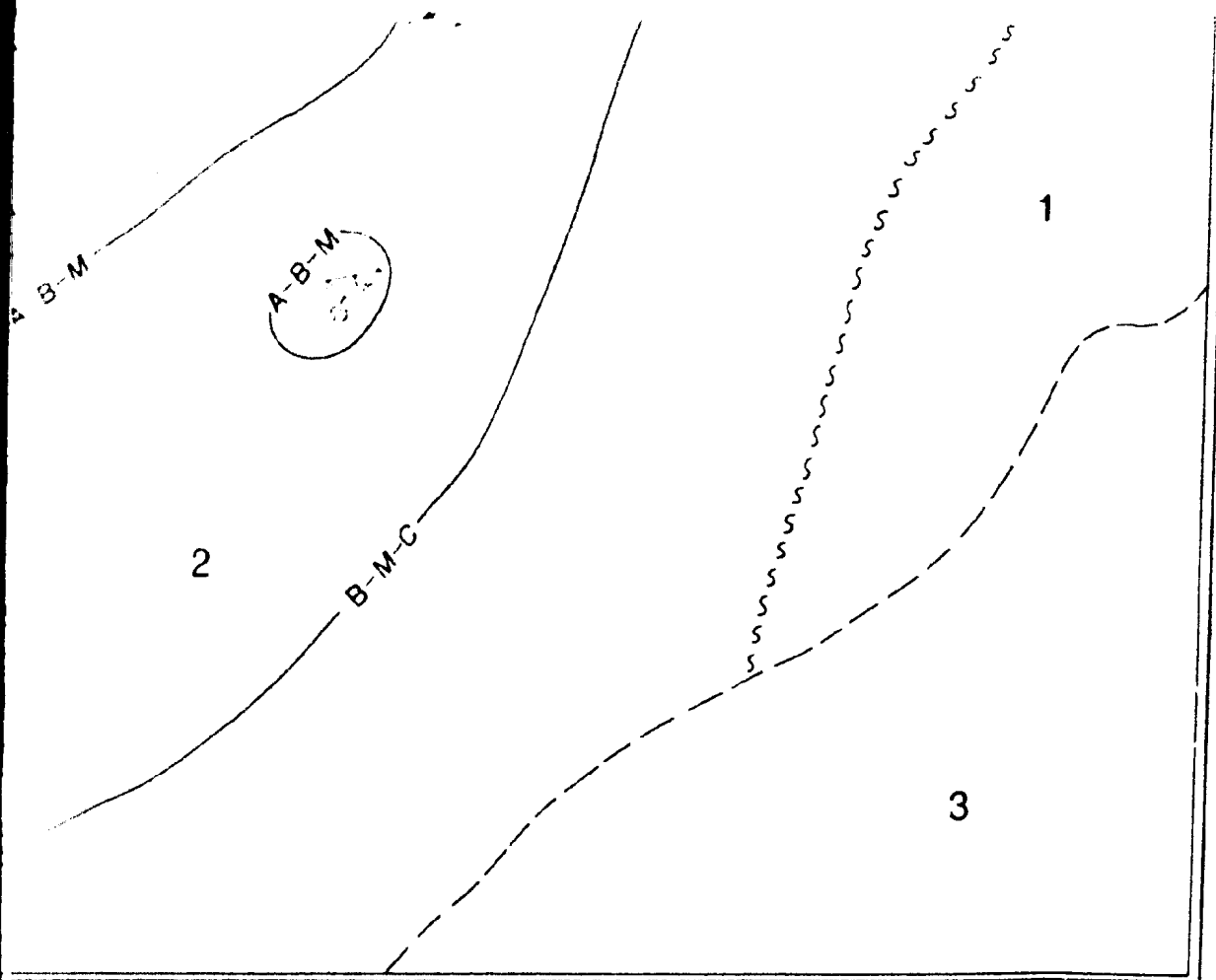
* Diagrams illustrate location of study area
** Diagrams illustrate location of study area



2

S-B-M





F₂ Fold Axis

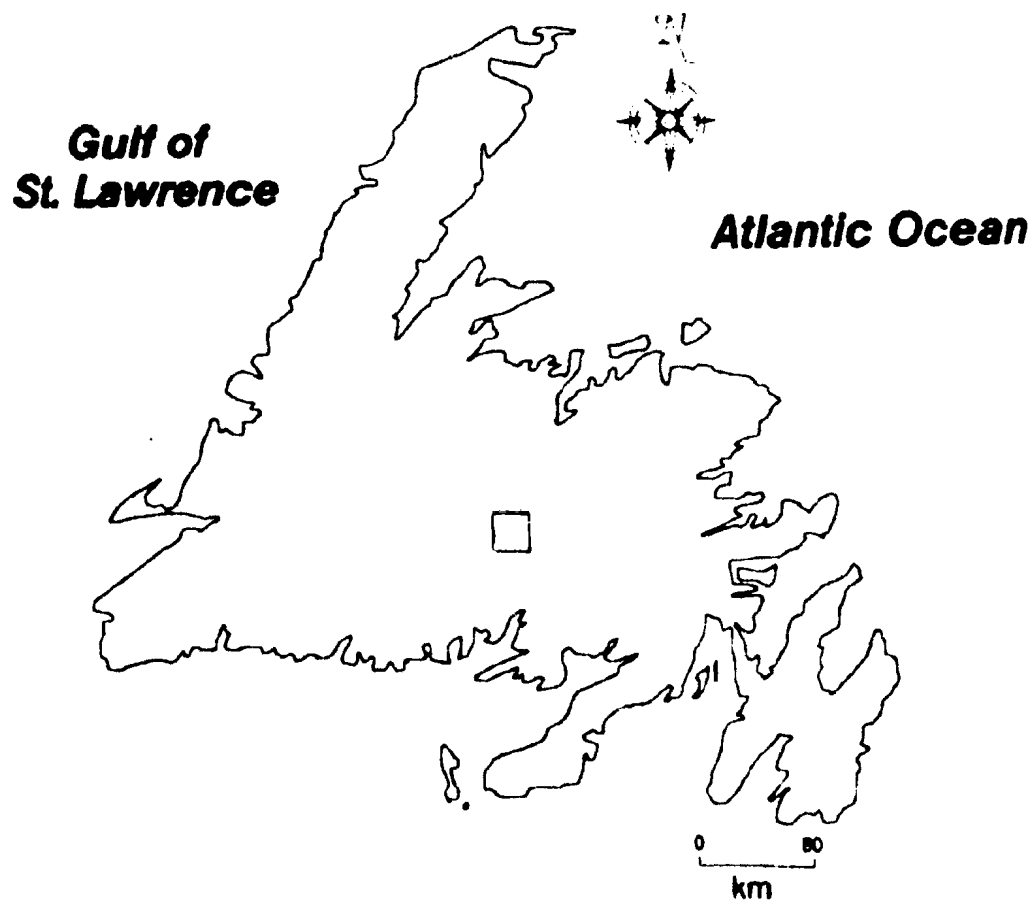
Structural Measurements of S.P. Colman-Sadd

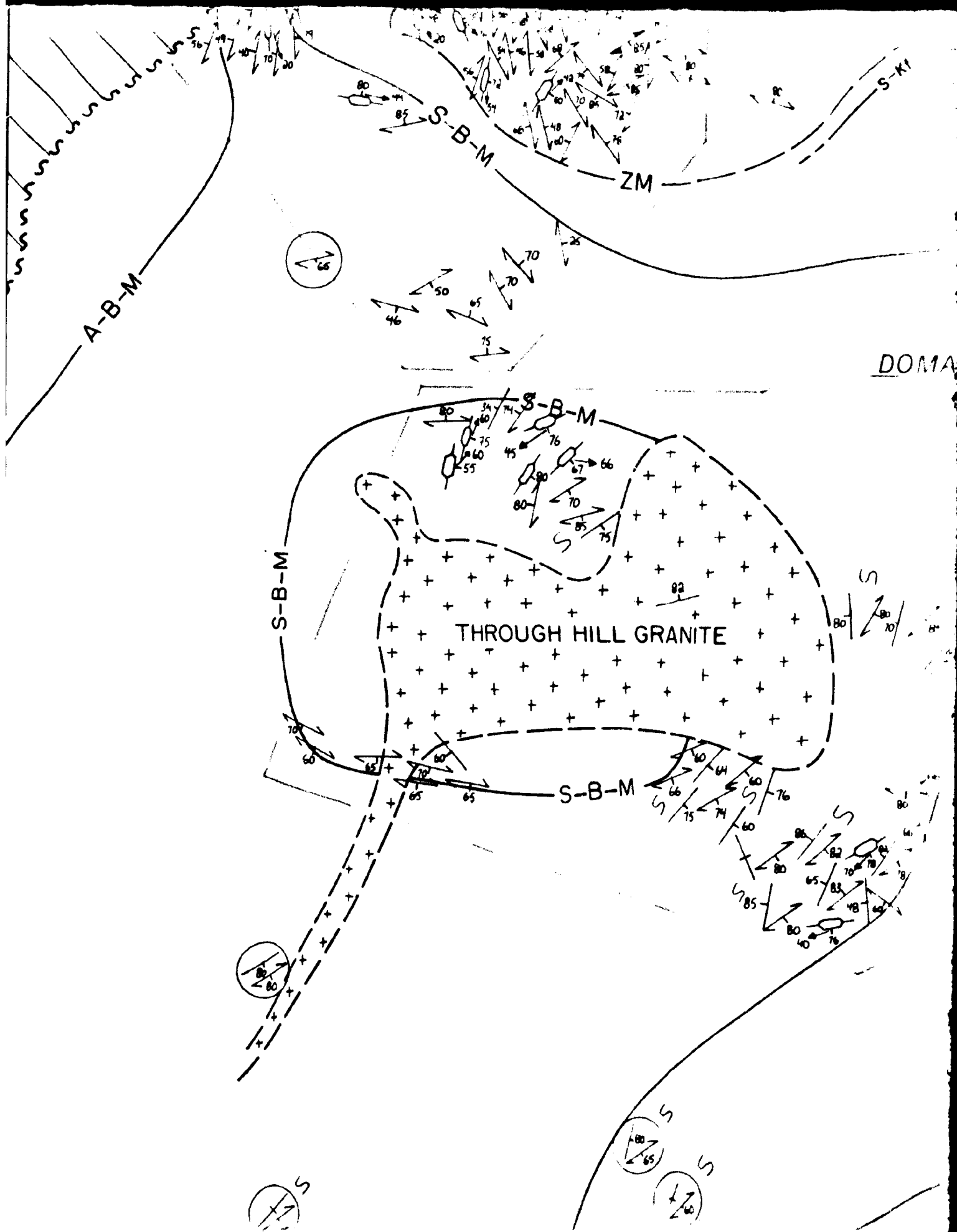


Sense of Vergence of Small-Scale F₂ Folds



* Bedding is S₀; however, S₁ is parallel to S₀.





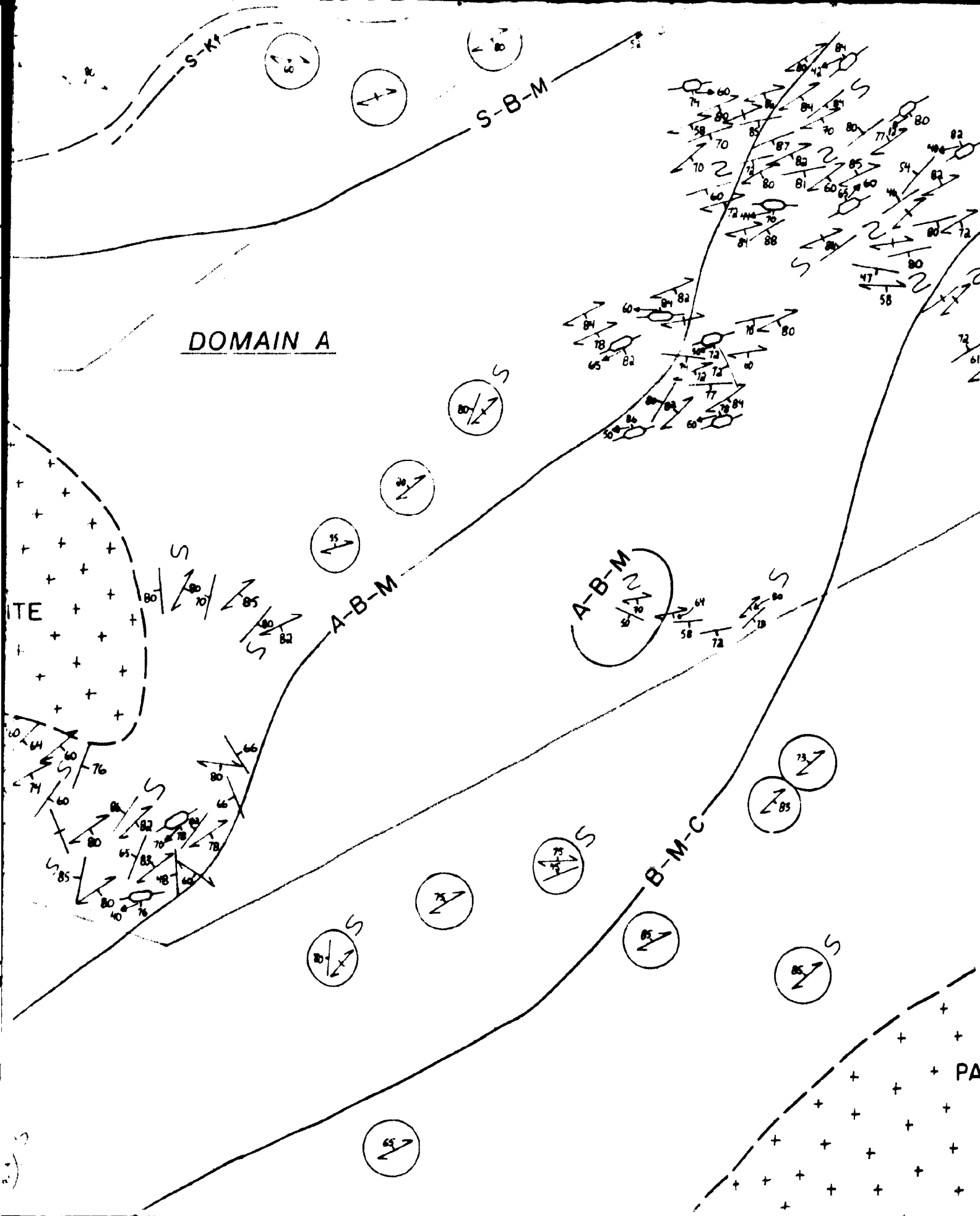
DOMAIN A

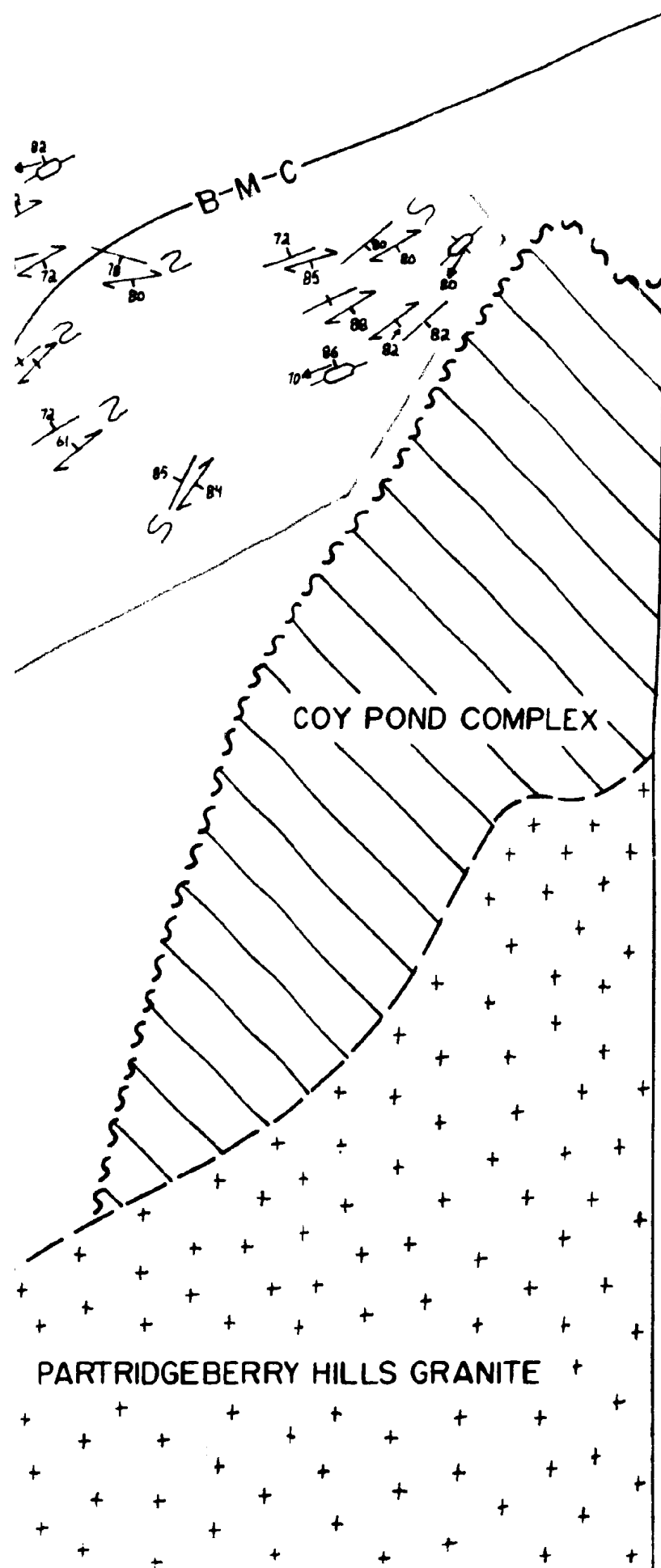
ITE

A-B-M

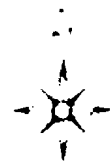
B-M-C

PA

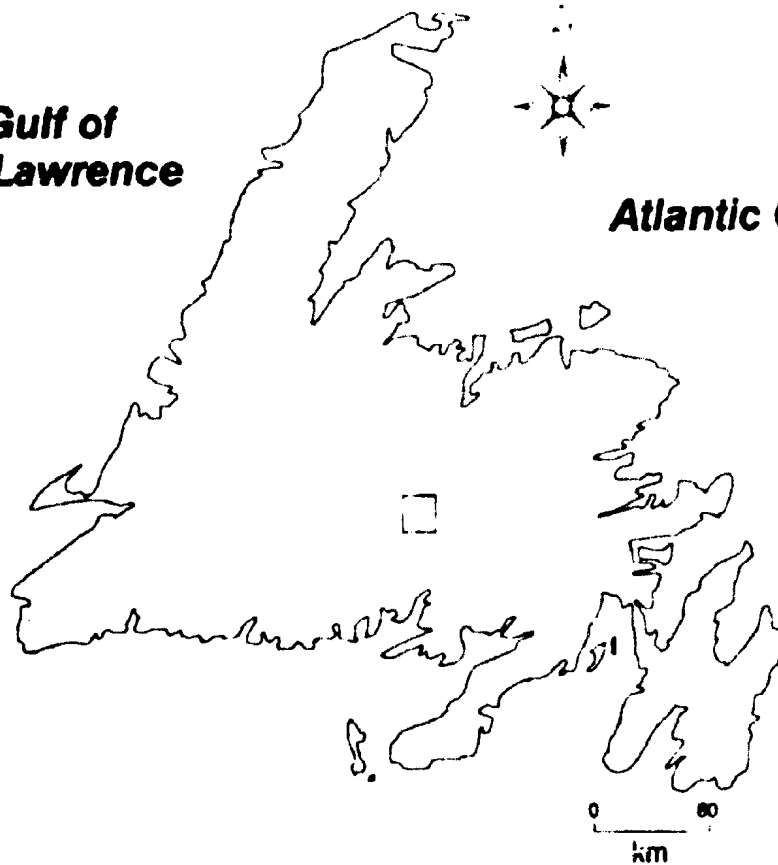


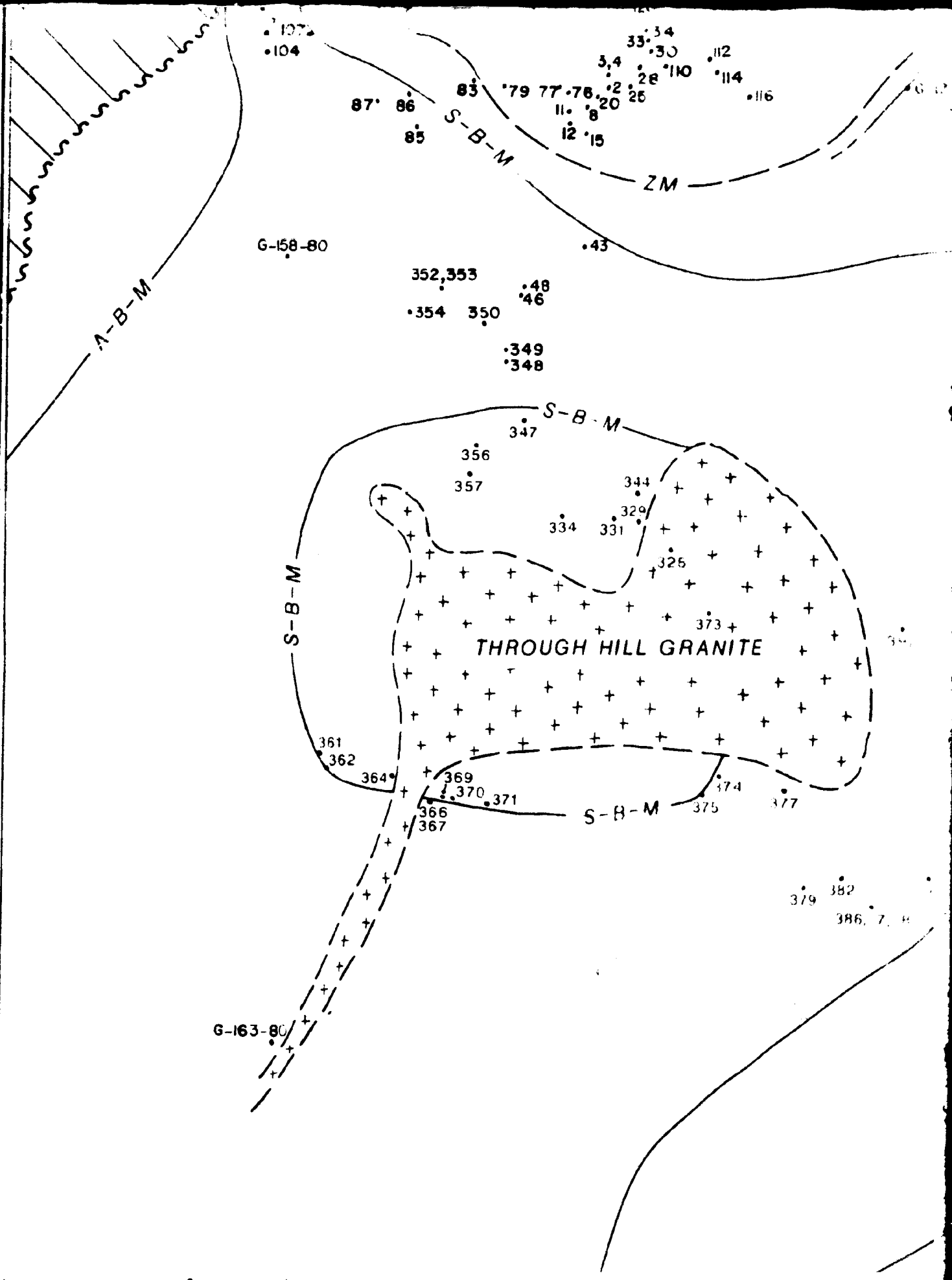


**Gulf of
St. Lawrence**



Atlantic Ocean





14
•116

S-K1
G-123 80

S-B-M

302

285

282

284

265

280, 281

267

268

262

261

252

247

260

246

259

256

244

300

297

296

295

277

278

291

294

G-118-80

315

298

299

327

319

ITE

397

396

395

A-B-M

A-B-M
276

272

394

393

379

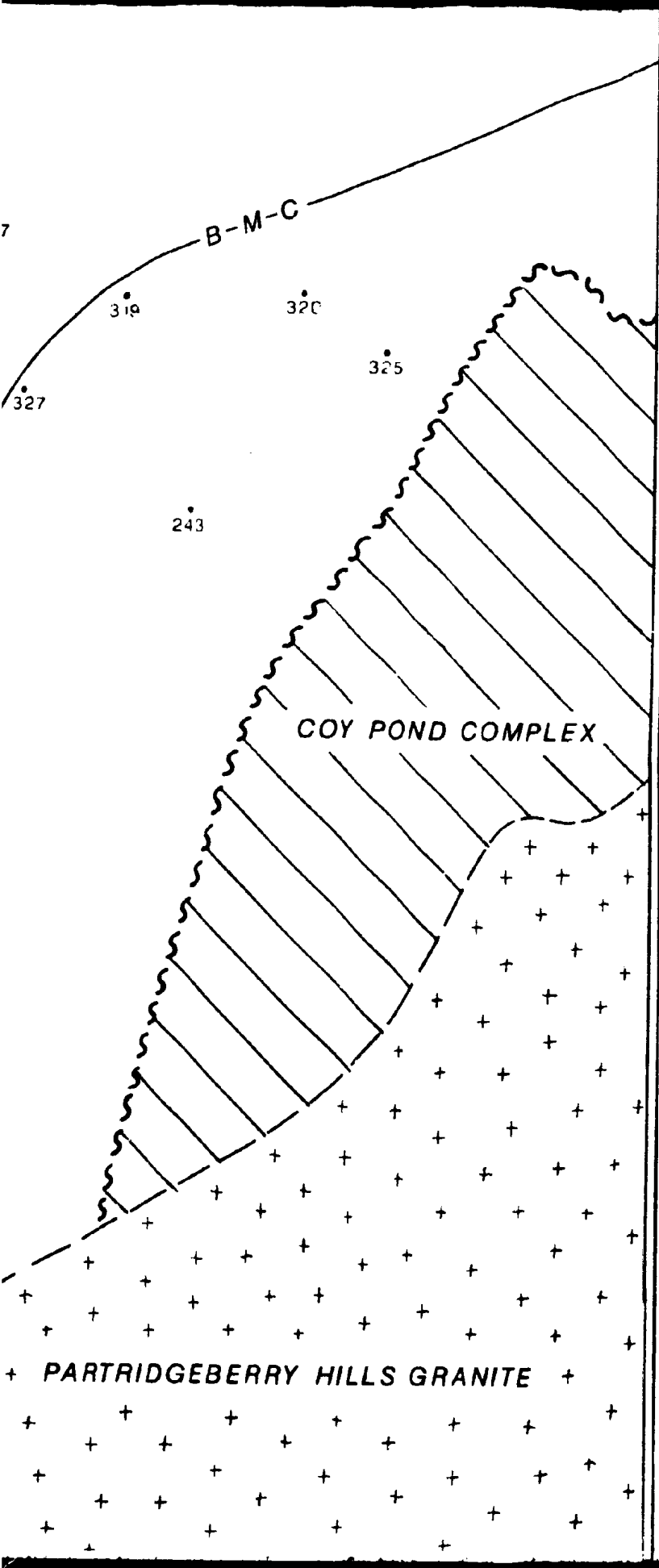
382

392

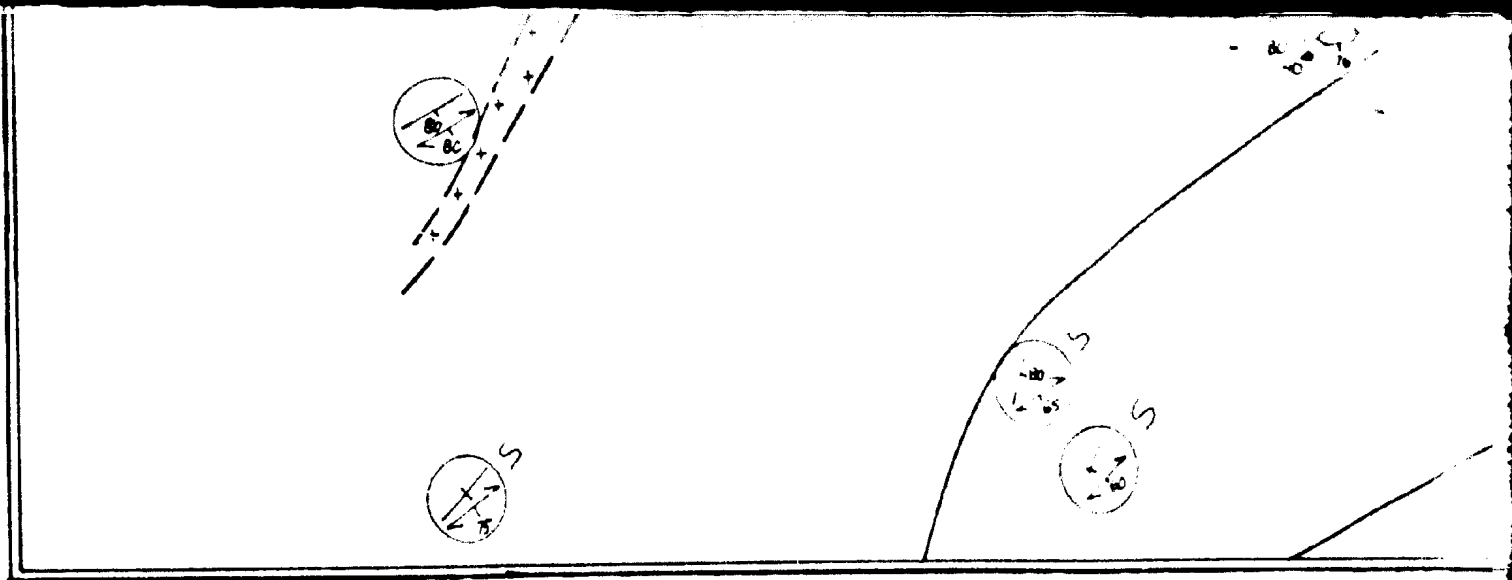
386, 7, 8

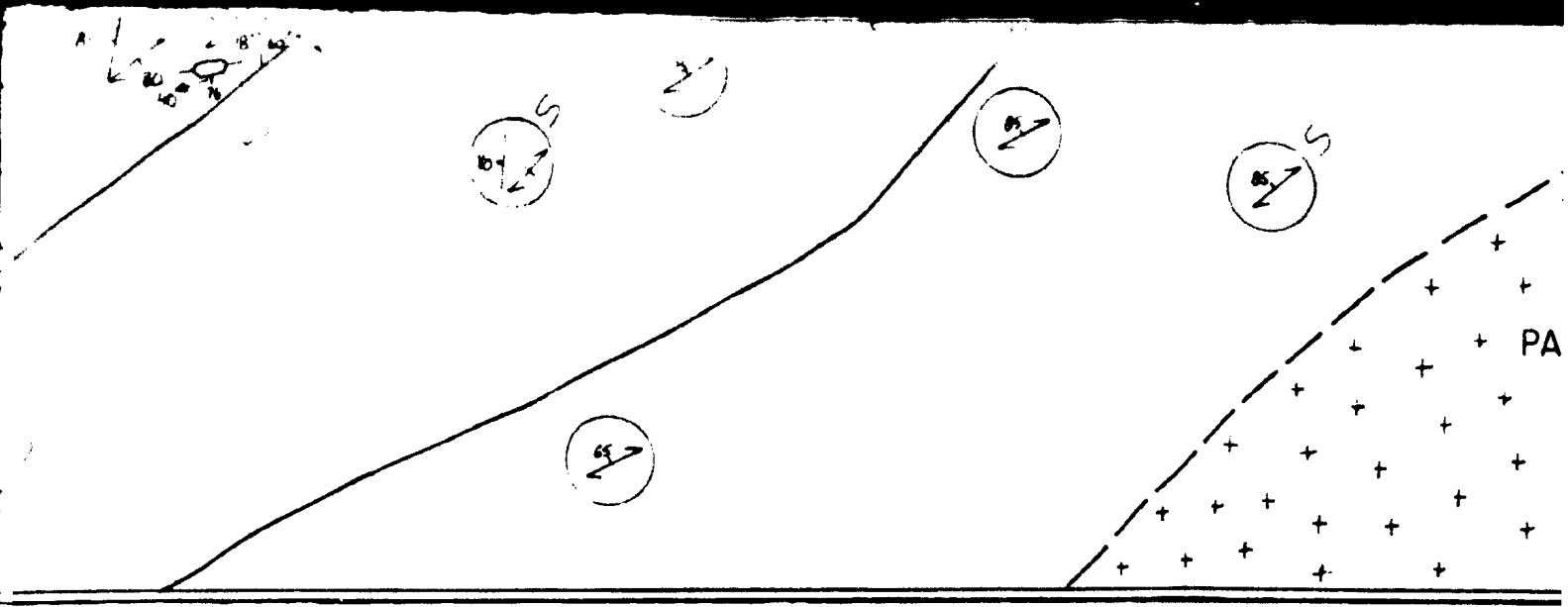
B-M-C

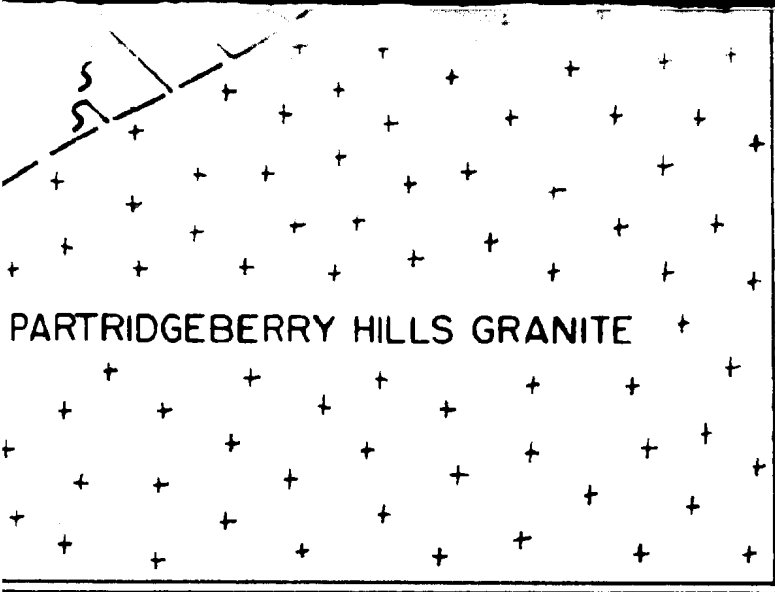
PART



WED

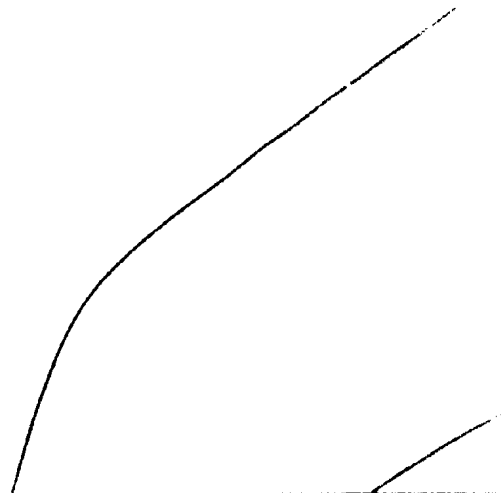
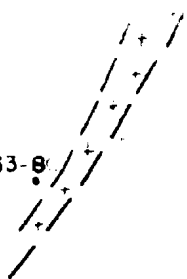


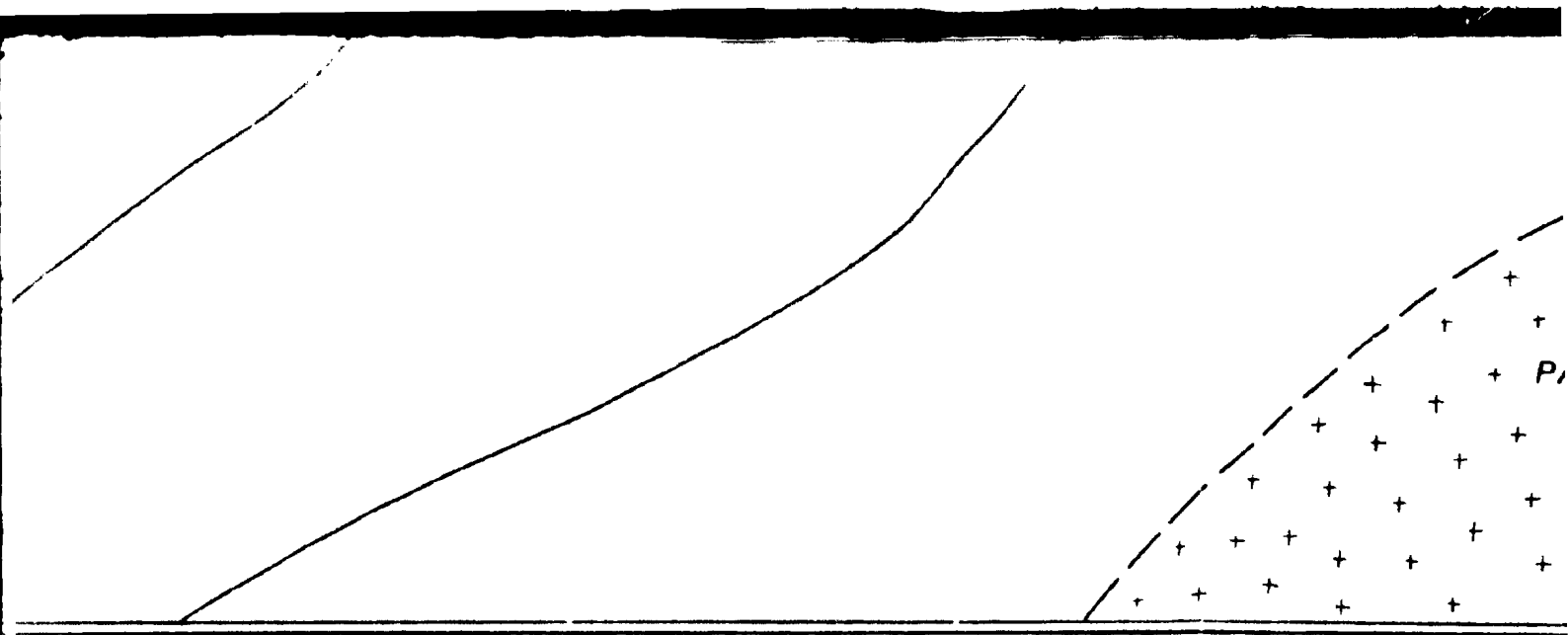


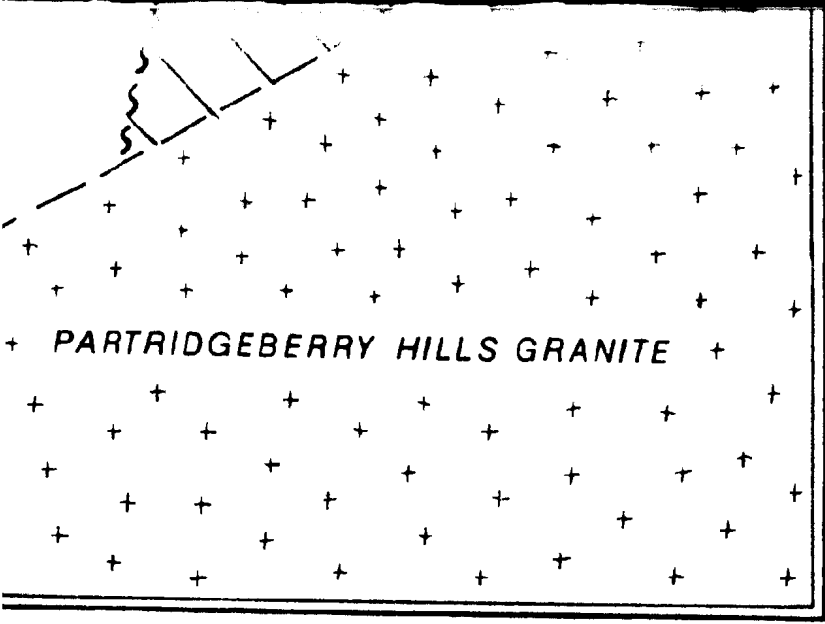


PARTRIDGEBERRY HILLS GRANITE

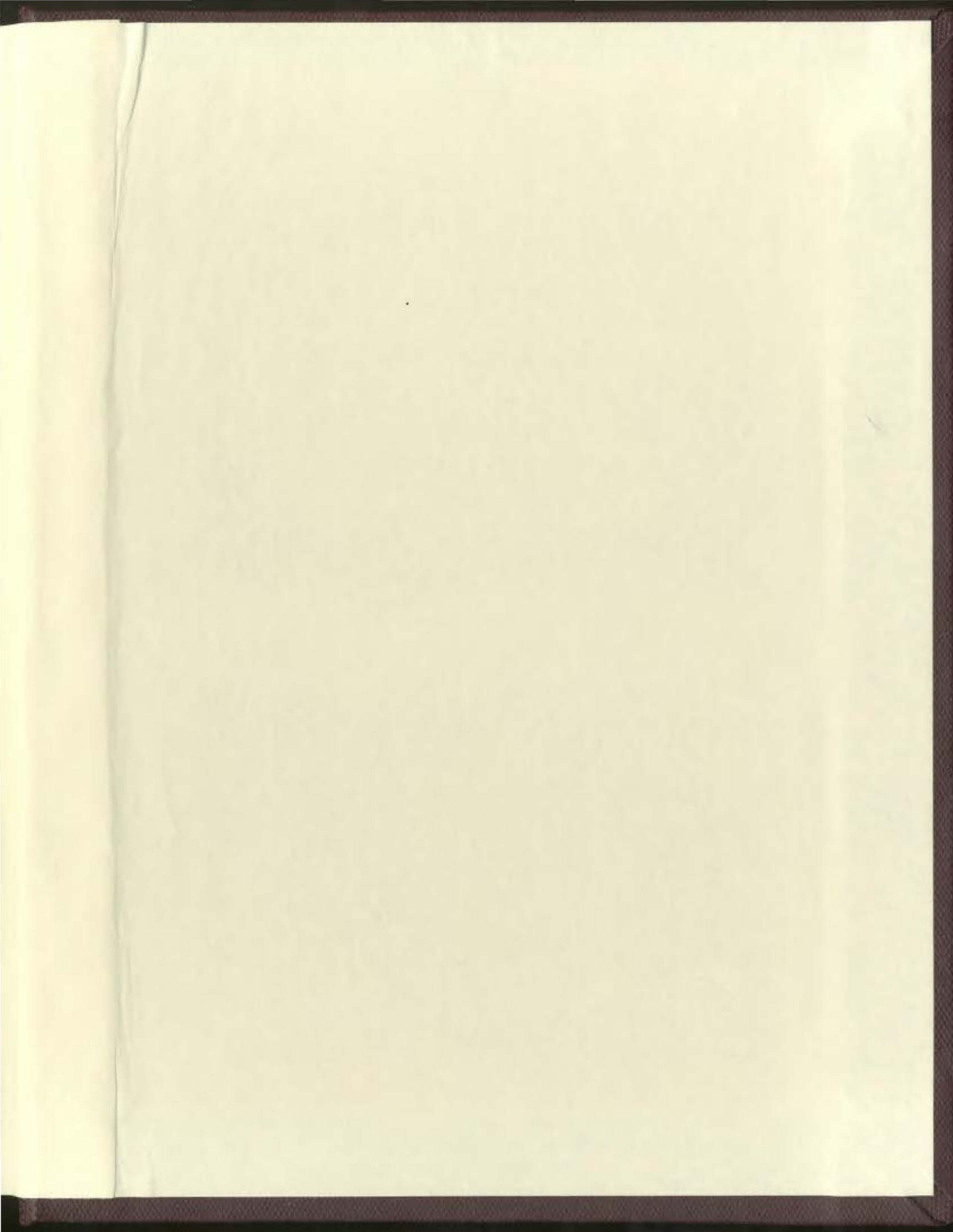
G-163-8







+ PARTRIDGEBERRY HILLS GRANITE +



CHAPTER 1

INTRODUCTION

1.1 Appalachian Orogen

The Appalachian Orogen, located on the east coast of North America from Alabama to Newfoundland, is a linear belt between ~ 100 and ~ 1000 kilometres in width, composed of rocks that were deformed during the Early and Middle Paleozoic. Its extension to the northeast is exposed in northwest Europe where it is termed the Caledonian Orogen. Most modern tectonic models of the Appalachian-Caledonian system explain the orogen in terms of a Wilson cycle involving opening and closing of an Early Paleozoic Iapetus Ocean (Williams, 1964; Wilson, 1966; Dewey and Bird, 1970).

The Appalachian Orogen in North America has been divided into five zones based on stratigraphic and structural contrasts between Cambrian-Ordovician and older rocks (Williams, 1978; Williams, 1979; Williams and Hatcher, 1982). These are, from west to east, the Humber Zone (ancient eastern margin of North America), Dunnage Zone (relics of Paleozoic ocean crust and associated arcs formed in Iapetus Ocean), Gander Zone (Early Paleozoic continental margin), Avalon Zone (terrane of older Precambrian crust welded on to North America) and Meguma Zone (Paleozoic